Luminescent Applications of Re(I) and Ir(III) Complexes for Cellular Imaging

Thesis submitted for the degree of
Doctor of Philosophy

by

Sarab Mahdi Salih Alazawi
Department of Chemistry
University of Leicester

at the
University of Leicester

May 2018

Abstract

Luminescent transition metal complexes are receiving great attention for use as bioimaging agents, in organic light-emitting devices (OLEDs), solar cells and sensors. They possess biological stability, low toxicity, large Stokes shifts, and long luminescence lifetimes. A new series of rhenium(I) and iridium(III), complexes incorporating polyamines were synthesized to use as dyes for cellular imaging in particular to replacement organic dyes such as FM1-43. Different probes were used in this study: click chemistry was used to prepare ancillary (N^N) ligands such as pyridyl triazoles and cyclometallated ligand (C^N) such as phenyltriazoles, whereas Stille coupling was used to synthesise ancillary ligand type (bipy) and cyclometallated type (phpy). In addition, Sonagashira coupling is used to synthesise ligands substituted with electron withdrawing groups in order to tune the emission of both complexes of rhenium (I) and iridium(III). Pyridine and triazole monodentate axial ligands were prepared by using reductive amination reactions containing either alkyl chains or polyamines. Their complexes with rhenium(I) and iridium(III) were synthesised using microwave methods and characterized by NMR spectroscopy and mass spectrometry and purified by HPLC. Luminescence properties, lifetime and quantum yield were studied in water solution at room temperature to investigate the effect of substituents in both the ancillary and cyclomelated ligands. Rhenium(I) and iridium(III) complexes substituted with electron withdrawing groups show broad emission in the green region with long lifetime and quantum yield. Rhenium(I) complexes bearing inverse pyridyltriazoles exhibit a high quantum and lifetime compared to corresponding complexes containing regular pyridyltriazoles. Rhenium(I) complexes containing triazole as a monodentate ligand exhibit better photophysical properties compared with analogoues pyridine complexes. It was found that substituent effects may tune and alter the optical and electronic properties of the complexes; their luminescence properties were studied in order to select which complexes would be suitable for use in fluorescence microscopy to image synaptic vesicles. Lipophilicity studies confirmed that the complexes substituted with long alkyl chains have high logP values and this would be promising to use as a bioimaging probe.

Dedication

Dedicated to the memory of my idol, my father.

Acknowledgements

First and foremost, I would like to thank my supervisor Dr Mark Lowe for giving me the opportunity to carry out this project, and his continued support, guidance, and help for all the duration of my PhD study.

I would like to thank Iraqi government to funding me during four years of my PhD study. I would also like to thank the University of Leicester who gave me this chance to and opportunity to use its facilities.

I must thank all the staff in the Department of Chemistry for their help, Dr Gerry Griffith for NMR spectroscopy, Dr Mick Lee running the mass spectrometry and Mr K. Singh for the X-ray structure and determinations also the staff in the stores and workshops.

I would also like to thank to Dr Andrew Hudson for help with measuring lifetimes. Many thanks for all people who help me through four years, Adil, Nada, Emad, Huda, Adit, Vicki, Raissa, and Nor.

The biggest thank you of all goes to my family, my husband Mohammed and my kids Mohand and Melak for all their support they have provided emotionally since I started this study. Without their support none of my recent achievements would have been possible. Special thanks to my mother for her loving support and the rest of my family: two sisters and my bother and friends for their support over recent years.

Sarab

Contents

Index

1 Rhenium(I) Complexes

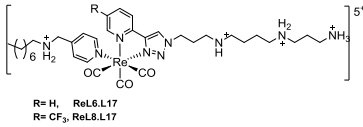

R= H, **ReL6.L17**
R= CF_3, **ReL8.L17**

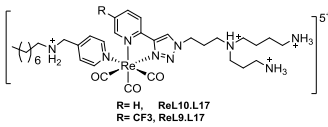

R= H, **ReL10.L17**
R= CF3, **ReL9.L17**

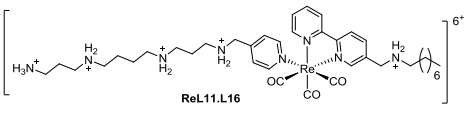

ReL11.L16

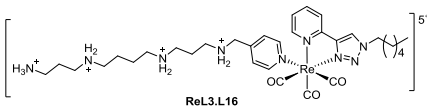

ReL3.L16

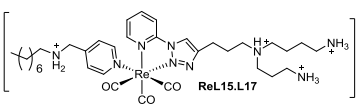

ReL15.L17

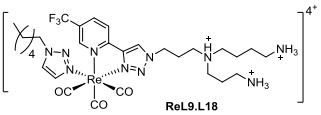

ReL9.L18

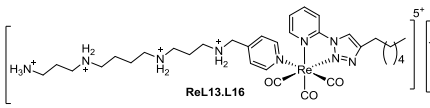

ReL13.L16

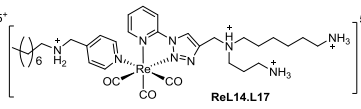

ReL14.L17

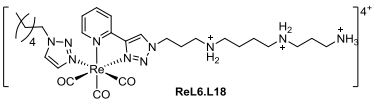

ReL6.L18

2 Iridium(III) Complexes

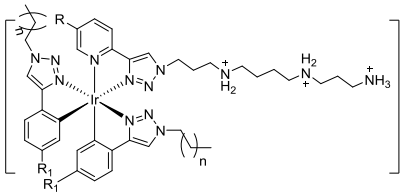

n= 2, R= H, R1= H, **Ir$(L1)_2$ L6**
n= 2, R= CF_3, R1= H, **Ir$(L1)_2$L8**
n= 4, R= H, R1= H, **Ir$(L2)_2$L6**
n= 4, R= CF_3, R1= H, **Ir$(L2)_2$L8**
n= 4, R= H, R1= OCH_3 **Ir$(L4)_2$L6**
n= 4, R= CF_3, R1= OCH_3 **Ir$(L4)_2$L8**

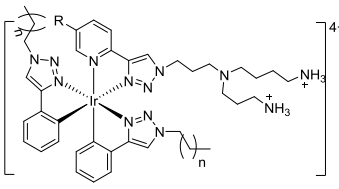

n= 2, R= H, R1= H, **Ir$(L1)_2$ L10**
n= 2, R= CF_3, R1= H, **Ir$(L1)_2$L9**
n= 4, R= H, R1= H, **Ir$(L2)_2$L10**
n= 4, R= CF_3, R1=H, **Ir$(L2)_2$L9**

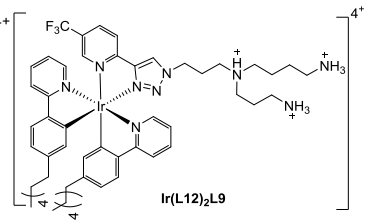

Ir$(L12)_2$L9

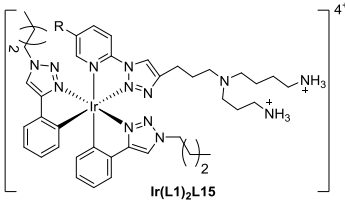

Ir$(L1)_2$L15

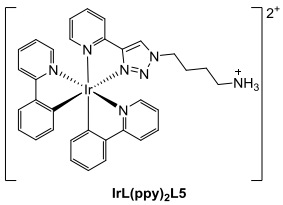

IrL$(ppy)_2$L5

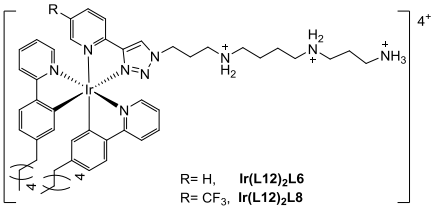

R= H, **Ir$(L12)_2$L6**
R= CF_3, **Ir$(L12)_2$L8**

Abbreviation

Bio

ABC	ATP binding cassette
AdoMetDC	S-Adenosyl methionine decarboxylase
ADP	Adenosine diphosphate
APAO	Acetyl polyamine oxidase
ATP	Adenosine triphosphate
ATPase	Adenosine triphosphatase
AZ	Antizyme
CME	Clathrin mediated endocytosis
CPP	Cell penetrating peptide
CvME	Caveolae mediated endocytosis
CHO-MG	Chinese hamster
DAM	Decarboxylated-S-Adenosyl Methionine
DNA	Deoxyribonucleic acid
E. coli	*Escherichia coli*
fAb	Antibody fragment
Gpc-1	Glypican-1
GTP	Guanosine-5'-triphosphate
GFP	Green Fluorescence protein
HDAC	Histone deacetylase
H. parainfluenzae	*Hemophilus parainflenzae*
HER2	Human epidermal growth factor receptor 2
HS	Heparan sulfate
HSPG	Heparan sulfate proteoglycan
Kir	Inwardly rectified potassium channel
mAb	Monoclonal antibody
MTA	5’-deoxy, 5’-methylthioadenosine
NCoR	Nuclear corepressor

NO	Nitric Oxide
ODC	Ornithine Decarboxylase
PTS	Polyamine transport system
PTD	Protein transduction domain
RNA	Ribonucleic acid
mRNA	Messenger ribonucleic acid
tRNA	Transfer ribonucleic acid
rRNA	Ribosomal ribonucleic acid
siRNA	Short interfering RNA
SAM	S-Adenosyl Methionine
SAMO	S-Adenosyl Methionine Decarboxylase
SLC	Solute carriers
SMO	Spermine oxidase
SMRT	Silencing mediator of retinoic acid & thyroid hormone receptor
SPDS	Spermidine synthase
SPECT	Single photon emission computed tomography
SPMS	Spermine synthase
SSAT	Spermine/Spermidine acetyl transferase
SV	Synaptic Vesicle

NMR

bd	broad doublet
bs	broad singlet
d	doublet
dd	doublet of doublets
ddd	doublet of doublet of doublets
dt	doublet of triplets
m	multiplet
s	singlet
q	quartet

quin	quintet
t	triplet
td	triplet of doublets
COSY	correlated spectroscopy
HMBC	heteronuclear multiple bond correlation
HSQC	heteronuclear single quantum correlation
NMR	nuclear magnetic resonance
NOE	nuclear Overhauser effect
NOESY	nuclear Overhauser effect spectroscopy
ppm	parts per million
δ	delta (NMR Chemical Shift)
J	coupling constant Hz

Chemical

acac	anion of pentane-2,4-dione
ACOH	Acetic acid
bipy	2,2'-bipyridine
bipy-tBu2	4,4'-di-tert-butyl-2,2'-bipyridine
Boc	tert-Butoxy carbonyl
Boc-ON	2-(tert-butoxycarbonyloxylimino)-2-phenylacetonitrile
DAB	Diaminobenzidine
DCM	dichloromethane
DMSO	dimethylsulfoxide
DMF	N,N-Dimethyl formamide
EtOAC	Ethyl Acetate
EtOH	Ethanol
iPr	isopropyl
MeCN	Acetonitrial
MeOH	Methanol
Phen	1, 10- phenanthroline

py	pyridine
pht	1,2,3-phenyltriazole
ppy	2-phenylpyridine
put	putrescine
spd	spermidine
spm	spermine
TFA	Trifluoroacetic acid
THF	Tetrahydrofuran
TMS	Tetramethylsilane

Techniques

CCD	Charge- Coupled Device
CuAAC	Copper(I)-catalysed Azide –Alkyne Cycloaddition
ECL	Electrochemiluminescence
HPLC	high performance liquid chromatography
IR	infra-red
MW	microwave
Mass	mass spectroscopy
MRI	Magnetic resonance imaging
NMR	nuclear magnetic resonance
ESMS	electrospray mass spectrometry

Others

Abs	Absorbance
au	Arbitrary Units
CFSE	Crystal Field Splitting Energy
eq	Equivalent
F	Fluorescence Intensity
fs	femtosecond
g	gram

HOMO	Highest Occupied Molecular Orbital
I	Intensity
I^o	Incident radiant power
IL	Intra Ligand
ISC	Inter System crossing
k	Rate of Non-Radiative Decay
M	Molar (mol dm^{-3})
m/z	mass to charge Ratio
MC	metal-Centred
mg	milligram
min	minute
mL	milliliter
MLCT	Metal to ligand charge transfer
mM	millimolar(mol dm^{-3})
mol	mole
nm	nanometer
P	Partition coefficient
s	second
$t_{1/2}$	half time
TCSPC	Time-Correlated Single Photon Counting
t_R	Retention Time
Γ	Rate of Radiative Decay
ε	Exctinction Coefficinent
η	Refractive Index
λ_{em}	Emission Wavelength
λ_{ex}	Excitation Wavelength
μM	Micromolar(μmol dm^{-3})
τ	Fluorescence life time
Φ	Fluorescence quantum yield

Chapter 1

1 Introduction

1.1 Polyamines

A polyamine is an organic compound which contains two or more primary amino groups. Examples of natural polyamines are spermidine, spermine and puterscine.[1]

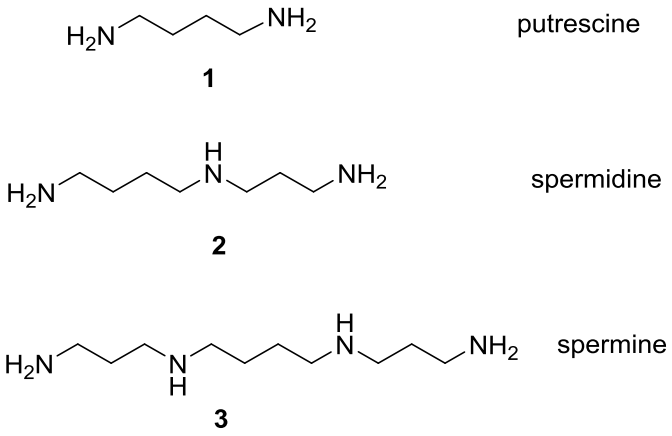

Figure 1.1: Structure of naturally occurring polyamines

Polyamines are known to be a positively charged at physiological pH. To be recognised by the Polyamine Transport System (PTS), a substrate must contain at least two cationic centres separated by a 4-carbon chain. Additional affinity is conferred by additional cationic centres spaced by carbon chains with a minimum of three carbons with most having a pK_{a1} of around 10.[2, 3]

The biosynthetic pathways of polyamines involves three main polyamines, the addition of aminopropyl groups derived from S-adenosylmethionine to L-ornithine to produce a putrescine core. For spermidine a single aminopropyl unit is added onto its end, whereas spermine has one aminopropyl group added onto each of its ends. Polyamines are either recycled back to smaller analogues, these aminopropyl groups are sequentially removed by spermidine/spermine-Nl-acetyltransferase (SAT) and polyamine oxidase (FAD-dependent) in two enzymatic steps, and can occur via two different enzymatic routes (Fig. 1.2).

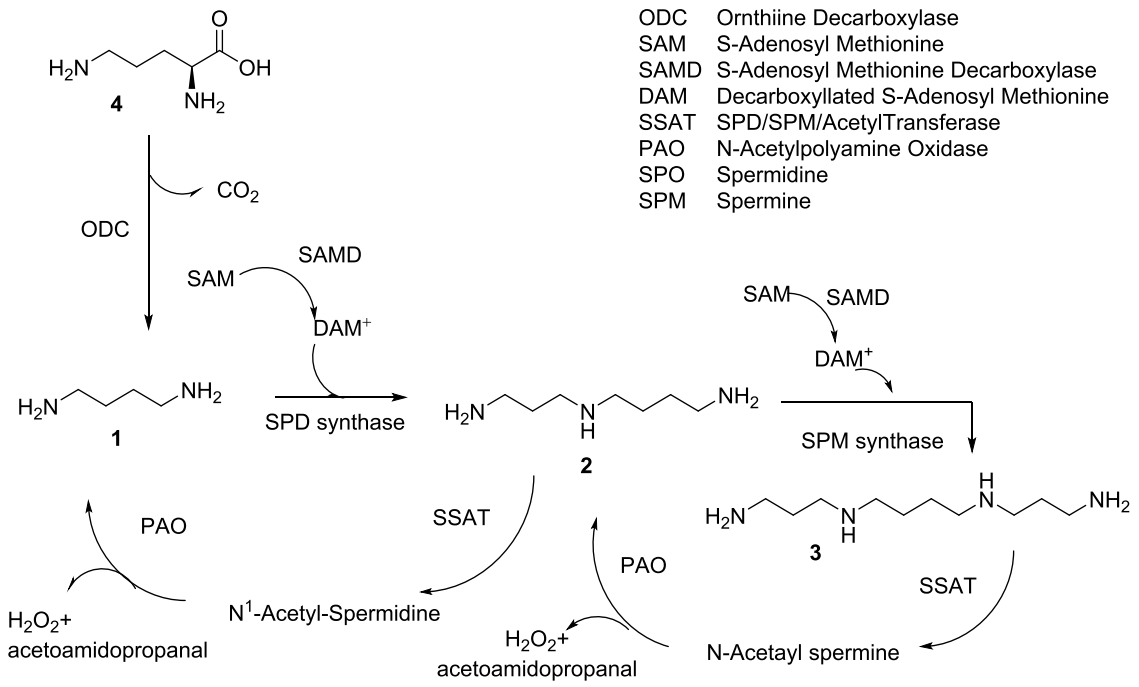

Figure1.2: Polyamine biosynthesis

1.2 Polyamine Analogues

In recent years many different types of analogues of polyamines have been investigated and used in the PTS to enter in cancer cells.[4] The first attempt at using a polyamine conjugate was spermidine –chlorambucil conjugate **5** (Fig. 1.3).[5] The function of this conjugated form is quite complex, it showed ca. 10,000-fold increase in DNA cross-linking ability compared with chlorambucil alone. It is suggested that the cationic nature of the polyamine brings about an affinity for polyanionic DNA at physiological pH and at the same time, the polyamine keeps a level of freedom of motion within a DNA-polyamine complex and allows the chlorambucil to reach and find the site for alkylation.

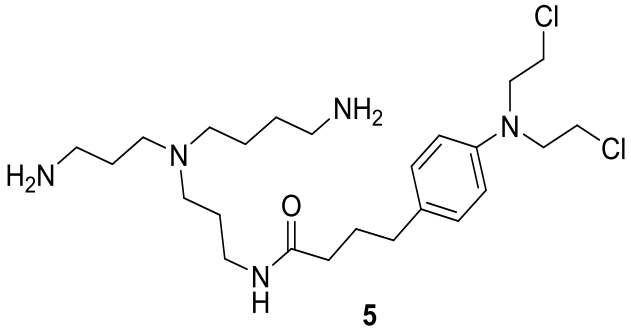

Figure 1.3: The structure of an early polyamine drug conjugate

Compound **5** possesses activity against cells both *in vitro* and *in vivo*. In α-difluoromethylornithine (DFMO) the PTS prefers the conjugate instead of spermidine uptake into the cell, cytotoxicity is increased in the absence of DFMO. This conjugate is considered as a delivery mechanism of cytotoxic agents. Other studies revealed that polyamine conjugate NPC-16, **6** (Fig. 1.4) is a polyamine-linked intercalator.[6] This type of polyamine is found to induce apoptosis and autophagy in cancer cells with high selectivity to the tumor, which is more toxic to cancer cells than uninfected cells during the upregulated PTS.[7]

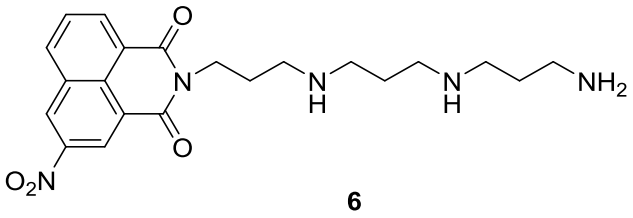

6

Figure1.4: The structure of NPC-16

Polyamine-anthracene conjugates **7, 8** and **9** as shown in Fig. 1.5 have attracted considerable interest from researchers. These types show high selectivity and cytotoxicity for cancer cells by coupling to an anthracene intercalator, the linear structure of polyamines is enhanced by the presence of three basic nitrogen atoms spaced between propylene and butylene chains.[8]

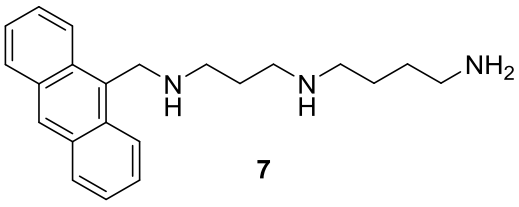

7

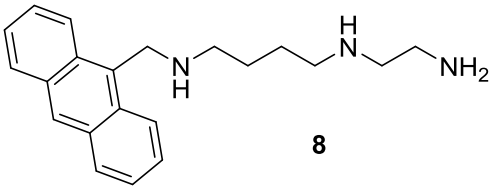

8

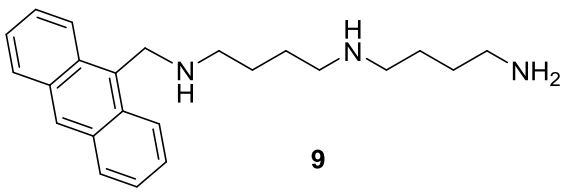

9

Figure 1.5: Structure of polyamine-anthracene conjugates

Recently, the report by Barret and co-authors reported novel analogues which have a highly potent spermine–etoposide conjugate(F 14512; Fig. 1.6).[9] In fact, this compound **10** (F 14512) has all the features hypothesised of the ideal polyamine drug conjugate, such as increased cytotoxicity and DNA-binding ability over its parent compound, uptake via the PTS and therefore, reduction in toxicity when used in *vivo*. Also it was found that the potent cytotoxicity of F14512 was 73 times greater in the wild type cell line when it was applied in an isogenic cell line with and without a PTS. However, focusing on the structural modification helps to examine the mechanism of the polyamine transport system and could potentially be exploited to develop a novel and selective anticancer drug delivery system. In this study new types of conjugated polyamine linker to the pyridyltriazole derivatives were prepared, details can be seen in Chapter 2.[10]

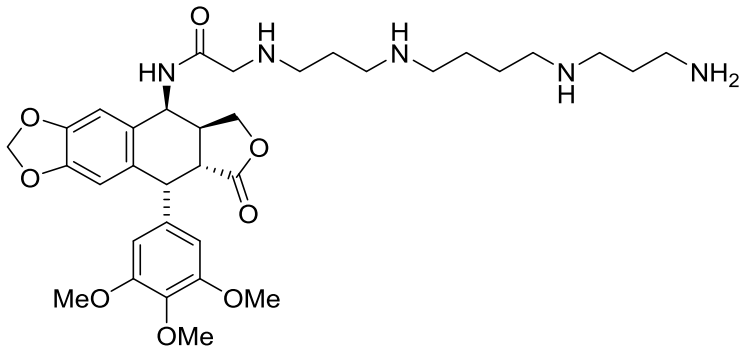

F14512 **10**

Figure 1.6: Structure of F14512

1.3 Polyamine Transport

De novo synthesis is the main source of polyamines. Polyamines are taken up by a system which exists in the cell, called the polyamine transport system (PTS).[11] In mammals, the PTS plays an important role in the biosynthesis of polyamines, assisting polyamine homeostasis by uptake of polyamines from exogenous sources. Characterization of the PTS in eukaryotes is limited.[12] In general, polyamines were of interest to many researchers as a transporter.[13] Ornithine decarboxylase (ODC) is one of the essential enzymes involved in polyamine biosynthesis. In cancer cells it often increases the intracellular pools of polyamines via ODC up-regulation in the biosynthetic pathway, ODC itself is considered a protooncogene.[14] Early studies demonstrated that genes associated with polyamine transport have been described in

lower organisms (e.g., *E. Coli* and *C. Elegans*), the genes involved in mammalian transport are only now being identified by Poulin, who suggested there are two models of mammalian polyamine transport, Caveolin-1, nitric oxide synthase (NOS2), and SLC3A2.[15, 16] Poulin proposed that the polyamines enter the cell through an active plasma membrane transporter, the next step is sequestration into polyamine-sequestering vesicles (PSVs), a vesicular H^+/polyamine carrier is important for polyamines to internalize within these PSVs to enable the import and escape from the PSV. On the other hand, Belting proposed a multistep endocytosis process where polyamines bind to heparan sulfate proteoglycans in caveolae. At the same time, the polyamines are then endocytosed via a caveolin-dependent process followed by the cleavage of their heparan sulfate chains with the polyamines being released by nitric oxide (NO)[13] as shown in Fig. 1.7.

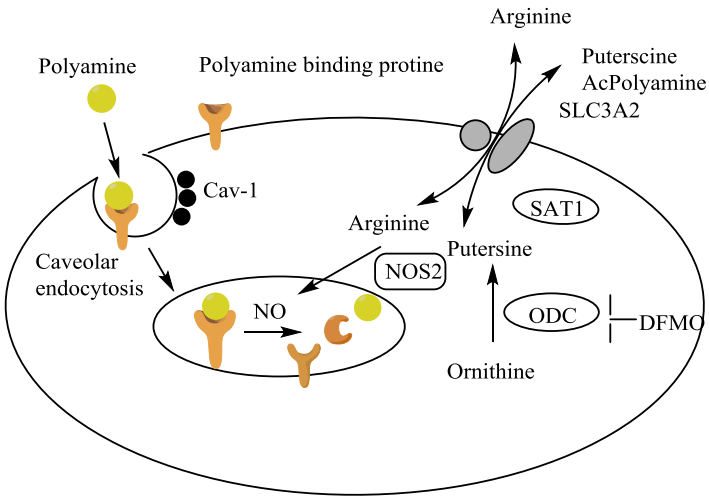

Figure 1.7: Model of polyamine transport in animal

There are two important models to maintain polyamine homeostasis. In general, a type of protein embedded in the membrane working as a pump is considered to be important in cellular transport; it transports a single species across the membrane against the concentration gradient, fuelled by ATP, such as ATP binding cassette (ABC) transporters.[17] There are two types of carrier proteins; antiporters, which transport substrates in opposite directions, whilst symporters transport both substances in the same direction. Endocytosis is another form of active transport, usually demonstrated by its inhibition at low temperatures. Endocytic processes can be classified based on their dependence on the GTPase dynamin.[18] The dynamin-dependent mechanisms can be further sub-divided into three categories; namely clathrin dependent, caveolin

dependent and clathrin and caveolin independent.[19] After the receptors bind to plasma membranes, a signal is sent through the membrane, and gives an order to the membrane to coat the receptors. It is required to fuse with other membranes proteins and is then recycled in cytoplasm to form the early endosome. This system becomes saturable and uptake decreases since the receptor is internalized, until receptors are recycled to the surface.[20] This is shown in Fig. 1.8.

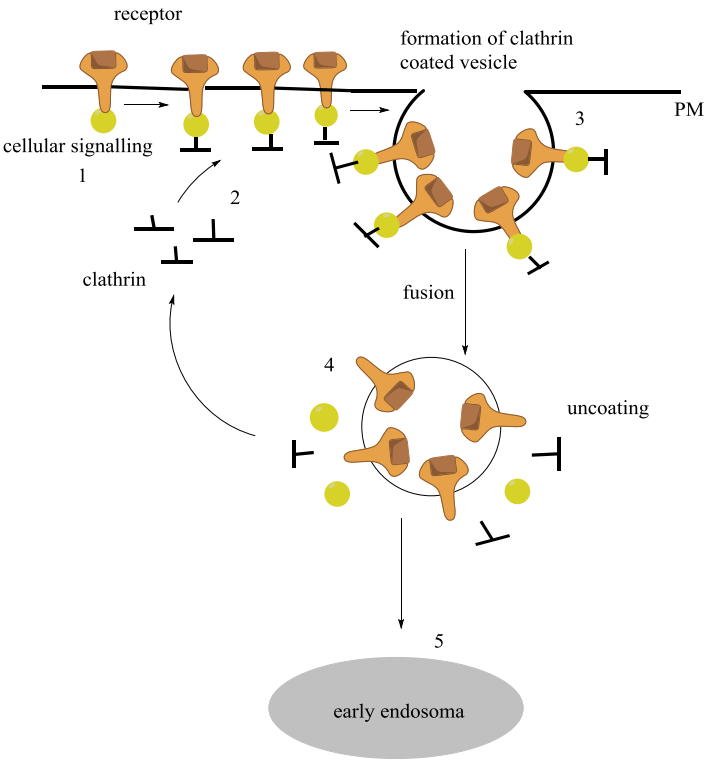

Figure 1.8: Clathrin dependent endocytosis

Adenosine triphosphatase (ATPase) pumps protons into the endosome to acidify early endosomes (to a pH of 6.1 to 6.8). When the endosome is acidified, there are two types of cargo: some cargoes are recycled and others remain in the endosome. The cargo that is not recycled remains in the endosome, while continued action of the ATPase proton pump reduces the pH to around 4.8 - 4.6. As it recycles back to extracellular environments, digestive degradation of the cargo at pH 4.5 takes place which leads to the late endosome fusing with a lysosome to form an endolysosome.[21]

Another endocytosis mechanism that plays an important role in polyamine uptake it is called caveolae-mediated endocytosis (CvME)[13], this mechanism is known to avoid the lysosomal degradation processes.[22] Therefore, understanding and modulating the

cellular entry pathways of the carriers is crucial for successful intracellular application. The first described report of caveolae was the continuous endothelium of the heart in 1953 by G.E. Palade as subcellular structures,[23] caveolae are considered subtypes of lipid rafts that form invaginations and are capable of endocytosis.[24, 25] Morphologically defined caveolae are flask-shaped invaginations of the plasma membrane with a diameter of 50 –100 nm. They have been implicated in endocytosis and signal transductions.[11] Caveolin-1 is a major structural protein of caveolae in nonmuscle cells and the stability of caveolae structure plays an important role in negatively regulating the caveolae-dependent endocytosis.[13] Caveolin-1 participates to form a hairpin structure that is embedded into the membrane through its N and C termini, the presence of which in the cytoplasm is used to stabilize extracellular protein. The mechanism of caveolar endocytosis is less understood than clathrin dependent endocytosis. Polyamine uptake in gastrointestinal tissues was mainly mediated by caveolar endocytosis and a NOS2-dependent mechanism. Caveolar endocytosis which consists of polyamine binds to polyamine binding protein(s) and is internalized by caveolar endocytosis, which is negatively regulated by caveolin-1 (Cav-1). The nitric oxide (NO) produced by NOS2 releases polyamine from polyamine binding protein(s). In certain putrscine concentration gradients, SLC3A2 can catalyze the uptake of dietary putrescine by a reverse reaction.[26]

Numerous studies carried out by Belting and co-workers have clarified that glypican-1 (Gpc-1) plays a pivotal role in the cellular uptake of polyamines.[27] As most mammalian cells express heparan sulfate proteoglycan (HSPG) at the cell surface, extracellular polyamines should be efficiently absorbed by the sulfated HS side chains of glypicans which localizes on lipid rafts and caveolae.[28] The affinity of spermine for HS is ten times more potent than for DNA. This high affinity binding is attributed to the formation of salt bridges between cationic polyamines and anionic sulphate groups of HS. A competitive inhibitor of polyamine uptake is exogenous HS, whilst cells deficient in proteoglycans show diminished uptake and increased sensitivity to DMFO.[29] In reaction to polyamine depletion, cells try to synthesise glypican HS chains and enhance affinity for spermine.[30]

A comprehensive study was carried out by Gerner *et al.* that clearly revealed the uptake of polyamines to be mediated by caveolar endocytosis and also provide a mechanism by the K-Ras oncogene which could enhance polyamine uptake. This study suggested that

polyamines are taken up by a dynamin-dependent mechanism which is involved when human colon cancer cells were treated with Brefeldin A, a known inhibitor of endocytosis; spermidine uptake was inhibited. Its uptake was also inhibited when cells were incubated at low temperature, referring to an endocytotic mechanism of uptake.[31]

1.4 Polyamines in Metal Complexes

There are limited studies using polyamines with metals as chemotherapeutic agents. Particularly, overcoming resistance is of more concern than transport. One of the important treatments for cancer is drugs based on platinum complexes. Cisplatin **11** is one of the most widely used anticancer drugs and it is estimated that today 50-70% of all cancer patients are treated with cisplatin.[32] Studies still continue to develop efficient platinum(II) drugs that are effective against cancers.[33] The latest discovery in platinum drugs, are multinuclear platinum complexes such as BBR346 which has potency against cisplatin resistant cancer, this discovery is associated with polyamine-linker platinum drugs. Di-nuclear platinum complexes with polyamines are more effective than mononuclear platinum (II) drugs in terms of developing these drugs. The electrostatic interaction between the BBR346 **12** and DNA via hydrogen bonding leads to an increase in its attraction for DNA and formation of adducts through each of its monofunctional terminal platinum chloride moieties.[34, 35]

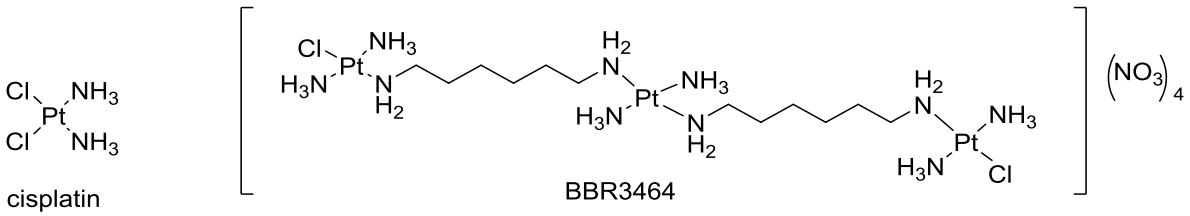

Figure 1.9: Structure of platinum complexes

There are few reports of polyamine containing rhenium complexes. Two polyamine rhenium tricarbonyl complexes **13, 14** have been reported as anticancer agents.[36] These types of complexes were evaluated as cytotoxic agents and found to have IC_{50} values in the low micromolar range and more effective than cisplatin when they were found to crosslink DNA.

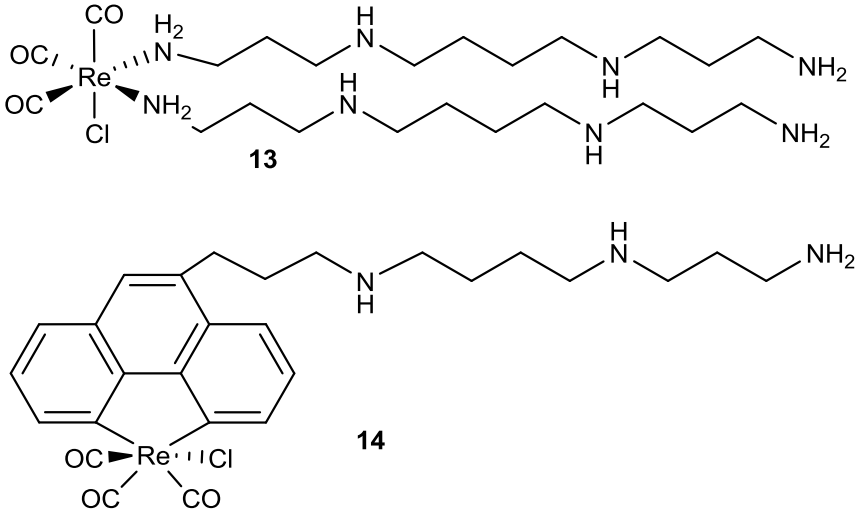

Figure 1.10: Structure of rhenium(I) complexes

Attempts still continue to find ways to new strategies for tumour therapy. Previous work in the Lowe group synthesised rhenium complexes bearing polyamines as a way to deliver drugs into cells and were also used as imaging agents.[37] The study in this thesis followed the same strategy with modification of the ligand properties by increasing the hydrophobicity and tuning of the photophysical properties of these complexes.

1.5 Synaptic Vesicles

In mammalian physiology the synaptic vesicles are considered as small and excretory organelles of axon terminals where the neurotransmitters are stored and release their content. These have diameter averages approximately 40-50 nm, the vesicles associated with the active zone (AZ) were found to be slightly smaller in diameter (23-49 nm) than the non-docked vesicles (20-60 nm).[38] The gab between a presynaptic terminal and postsynaptic compartment is called the synaptic cleft and is ~15-20 nm. Although there is limited evidence in direct measurements for the number of vesicles proteins, theoretical studies revealed that an individual vesicle contains 8,000-10,000 phospholipid molecules and proteins, with a combined molecular weight of no more than 3-10 milion, the number of proteins was limited in synaptic vesicles due to the fact a vesicle needs a protein to fit onto and be suitable for all synaptic vesicle functions.[39] Moreover, the vesicle membrane has a high degree of curvature which is required for asymmetric packing of both phospholipids and proteins. Generally, larger vesicles are

more stable and more fusogenic than liposomes.[40] This factor plays important roles in synaptic vesicle exocytosis. According to their function, these synaptic vesicle membrane proteins can be broadly classified into two types: proteins involved in neurotransmitter uptake and storage, and proteins included in membrane trafficking.[41]

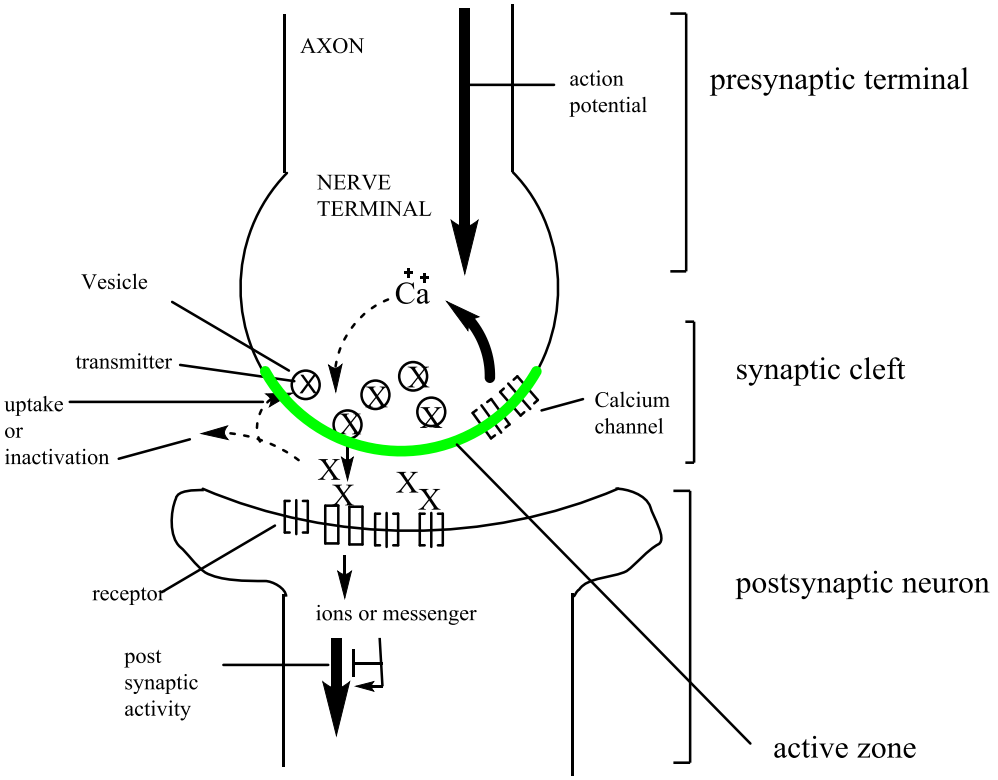

Figure 1.11: Synapse structure

1.6 Synaptic Vesicle Recycling

Interneuron communication can take place via electrical or chemical synapses. Nevertheless, the majority of communication in the mammalian CNS occurs via chemical synapses. This process consists of the calcium channels opening, following depolarization of a presynaptic neuron, leading to an increase in the rate of intracellular calcium, and the fusion between the synaptic vesicle (SV) membrane and the presynaptic plasma membrane and then release of neurotransmitter molecules into the synaptic cleft.[42] Earlier observations that synaptic vesicles recycle following their release was made in the frog neuromuscular junction using electrophysiology combined with electron microscopy to show that synaptic vesicles fuse with the membrane, release their neurotransmitter content and are subsequently reformed from the

presynaptic membrane and stored at the terminal.[43] The early studies on the synaptic vesicle cycle involved the entire process from docking of synaptic vesicle to its availability at the active zone following endocytosis roughly taking a minute to complete.[44] The exocytosis concluded two important steps: docking and priming. In general, there are two main steps in synaptic vesicle cycle: exocytosis – fusion of the SV with the plasma membrane and release of its neurotransmitter content, followed by endocytosis. Endocytosis is responsible for retrieving the synaptic vesicle membrane and protein components and recycling for additional rounds of release. Earlier in the 1970s Heuser and Reese proposed that the model of vesicle retrieval is via clathrin-mediated endocytosis, while later studies pointed towards another recycling mechanism, without the involvement of clathrin.

In this model the vesicles are thought to transiently fuse with the plasma membrane, release their content via a fusion pore and are recycled back into the terminal whilst retaining their identity.[43, 45] This mechanism was referred to as 'kiss and run'.[46] After that four modes of endocytosis have been described in hippocampal neurons: i) clathrin-mediated endocytosis (CME); ii) kiss-and-run endocytosis; iii) ultrafast endocytosis; iv) bulk endocytosis.

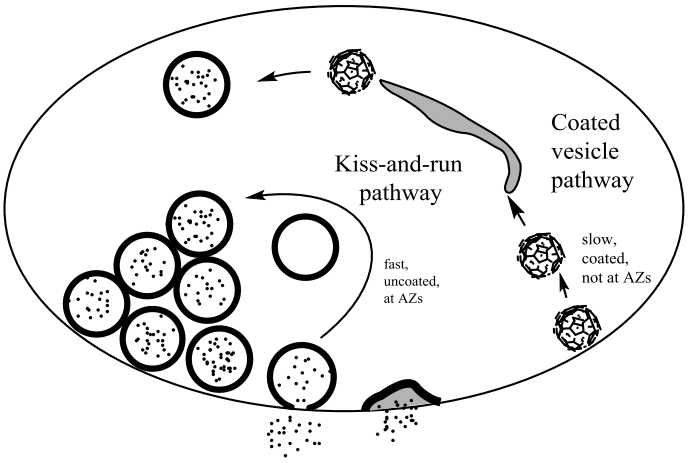

Figure 1.12: Two models for synaptic vesicle recycling in nerve terminals[47]

1.7 Imaging Synaptic Vesicle Recycling

Understanding the structure of synapses is an essential first step in understanding their function.[48] Since the late 19th century the structural basis of information transfer between nerve cells remained obscure until the revolutionary understanding of the

components of neurotransmission started in the mid-20th century; both electrical[49] and chemical.[50] Electron microscopy opened avenues for examining presynaptic function and structure. Although this method offered ultrastructural details in three dimensional reconstructions, it captures just a particular moment in the life of a synapse. Fluorescent probes were developed in the early 1990s, it allowed exploration and monitoring of presynaptic function to more directly study their behavior. This approach achieved high sensitivity, with high contrast, multi-color labeling and live imaging.[51] However, this approach is not suitable to investigate the tiny surface area of the central nerve terminal. Recently, optical techniques based on fluorescent dyes have been used to study recycling of synaptic vesicle membrane.[44] Fei Mao synthesized styryl dyes as membrane potential sensors that have become increasingly useful tools in the study of synaptic vesicle recycling, synaptic transmission and imaging synaptic vesicles in living preparations.[52, 53] FM dyes as a result of modifying styryl dyes have been used for many years as fluorescent probes of membrane potential. One important styryl dye is FM1-43, which was developed by Betz and colleagues in 1992. Styryl dyes like FM1-43 are amphiphilic which can divide their structure to three regions: the first region is the tail region, represented by aliphatic hydrocarbon chains which are lipophilic and cause the dye to penetrate into lipids and other hydrophobic domains; the second region is called the bridge region and is located in the middle of molecule and contains two aromatic rings that produce the fluorophore; the number of double bonds in the bridge linking the two rings determines the fluorescence properties of the dye for example FM1-43 has one double bond and can be excited with standard fluorescein optics whereas FM4-64 has three double bonds and its excitation and emission are both red-shifted;[54] the needed lipophilic tail determines the membrane penetration, the longer the tail, the longer washout time. (With a four-carbon tail, FM1-43 is more hydrophobic than FM2-10, which has a two-carbon tail). The third region is a head, including a positively charged group which preventes the dye from flipping across membranes.

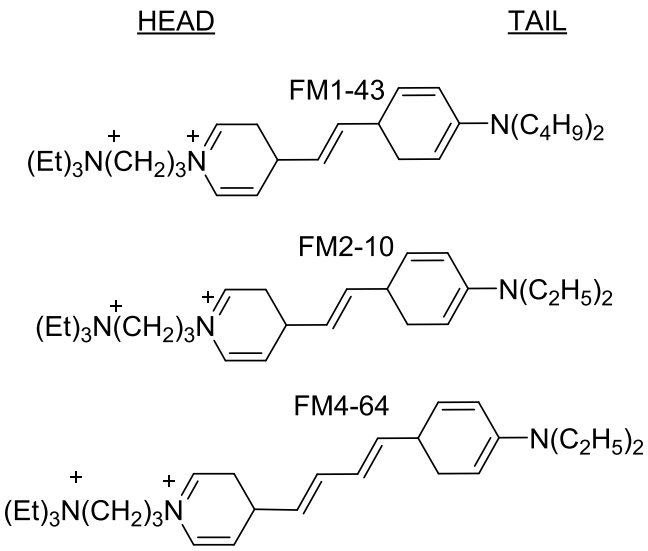

Figure 1.13: Structures of FM dyes

FM1-43 can be used as a dye to monitor the vesicle cycle in the following manner: FM1-43 stains the extracellular membrane, on stimulation, exocytosis causes the vesicular membrane to fuse with the cellular membrane and then the dye is incubated to exocytosing membrane. The stained membrane undergoes endocytosis, and excess dye from the superfusate can be removed by washing, after a second round of stimulation the endocytosed vesicles are destained.[52] Thus, the dye was adapted for use in several other synaptic preparations. These included motor nerve terminals in amphibia mammals[44] and Drosophila larvae,[55] cultured hippocampal neurons,[56] pituitary cells,[57] dictyostelium[56, 58] and yeast.[59]

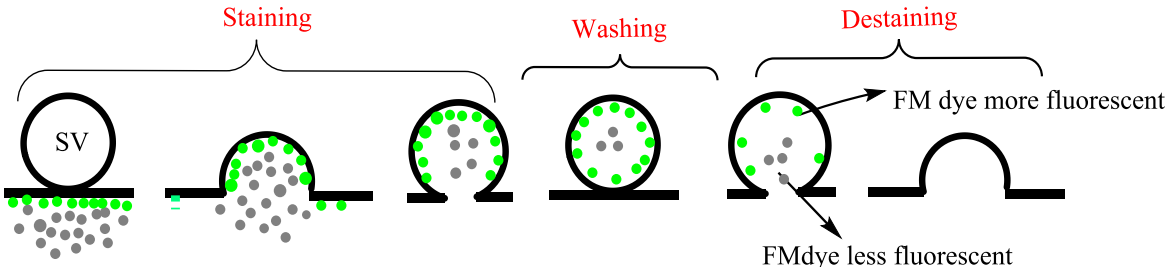

Figure 1.14: FM1-43 staining of Synaptic vesicles

In pituitary lactotrophs, only membranes were stained by FM dyes, due to the fact that the entire dense core secretory contains no lipid granule,[60] while other neuroendocrine cells do not stain with FM dyes. An alternative approach by Heuser and Reese (1973) used a combination between tracer techniques and electron microscopy to examine this limitation of the technique, this method revealed that following exocytosis, the synaptic

vesicle membrane is retrieved by endocytosis and then fused with an internal membrane compartment before ultimately reappearing as a synaptic vesicle. This approach obtained direct evidence in support of the concept of recycling for peripheral nervous system synapses, at the neuromuscular junction.[61] Recently, another technique is photoconversion of FM dyes, which allows for characterization of the path of endocytosed dense core granules at the ultrastructural level. Finally, some proteins are fluorescent; these features can be fused into dense core granules, and it may be possible to follow the route of a granule from biogenesis through exocytosis and subsequent recycling. To characterize the pore that forms when a vesicle fuses with the surface membrane by comparing the release of different size granule markers to the uptake of FM dye.[62] The illumination of a specimen is restricted to a layer above the substrate, it can be resolved by green fluorescent protein (GFP) that is fused to secreted peptides, and this probe can be used as a fluorescent marker for dense core secretory granules.[63] GFP coupled to peptides or proteins involved in cellular signaling is considered as one of several recent findings which turned out to be specific molecular markers with all the potential of targeting and modification offered by molecular biology.[64] FM dyes open the way to studies deeper inside the cell, these can be used with different protocols to explore diverse aspects of synaptic vesicle recycling and can also be used to evaluate SV recycling at ultrastructure level by correlating observations from light and electron microscopy. Finally, FM dyes provide a rich source of information relative to SV recycling and functions. This method has been successfully applied to small central synapses in native brain tissue.

An alternative method depends on transition metals especially, d^6 ones like Re(I) and Ir(III) that offer potential alternatives to fluorescent organic dyes in different photonic applications because these complexes have features that distinguish them from other molecules such as: strong spin-orbit coupling, long lifetime, high quantum yield, large Stokes shift and reduced photobleaching. These properties make these complexes candidates for bio- imaging agents for cellular applications. Iridium(III) complexes prepared by the Lowe group, suggested that iridium(III) conjugates substituted with polyamines can be used to image synaptic vesicles as alternatives to FM dyes, because the FM dyes are treated with OsO_4 and polymerized with diaminobenzidine (DAB) to enable the electron microscopy to give clear and bright images. These organic probes have drawbacks, e.g. they can't be removed by washing, undergo photobleaching and on the use of toxic OsO_4, plus the imaging is unclear. The new protocol by the Lowe group

succeeded in reducing the photobleaching and potentially eliminating the use of diaminobenzidine (DAB)(Fig. 1.15).[65]

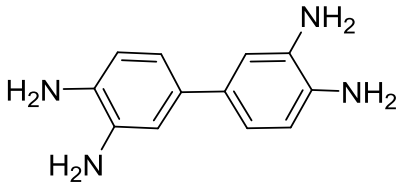

Figure 1.15: diaminobenzidine (DMB)

Previously, Lowe and co-workers used primary neuronal cultures which were stimulated by exposure to high potassium concentration, in the presence of iridium complexes as a dye and then attached to the membrane by the exocytosis process. Staining of the vesicle was imaged using a CCD camera as shown in Fig. 1.16

The important reason to use transition metal dyes, particularly d^6 metals such as rhenium(I) or iridium(III) is to provide electron microscopy with high electron density. Iridium(III) is next to osmium in the periodic table and is expected to offer enhanced electron density for electron microscopy.

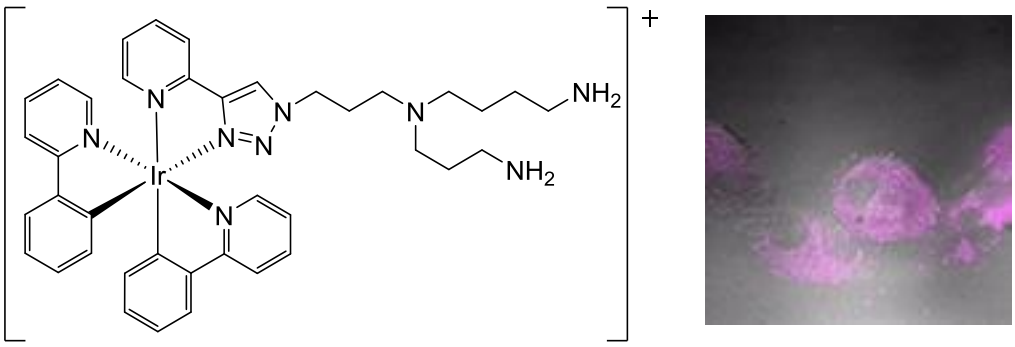

Figure 1.16: Image of primary neuronal cultures harvested from E17 rats incubated with iridium(III) complex showing incorporated into putative synaptic vesicle.

Thus, this method achieved bright and clear imaging of synaptic vesicles by using a new approach based on transition metals. In this study, the same probe was used but with changes in the cyclometalated and ancillary ligand of both rhenium(I) and iridium(III) complexes, by using more hydrophilic functional groups to tune the hydrophobicity to change the structure, from e.g. phenyltriazole to phenylpyridine, or add electron withdrawing groups to ancillary ligands, such as CF_3 group substituted in pyridyltriazole or electron donating such as OCH_3 substituted in phenylpyridine. These

changes enhanced the photophysical properties of these complexes and offer potential to obtain bright imaging of synaptic vesicles.

1.8 Luminescence

The emission of light from any substance is called luminescence, which occurs from electronically excited states. It is divided into two categories: fluorescence and phosphorescence, depending on the type of excited state from which the emission occurs. Fluorescence occurs when an electron in an excited state is paired anti–parallel with an electron in a ground state, so the return of this electron is spin allowed and occurs rapidly on a timescale 10^{-9} to 10^{-8} s^{-1}, so that a typical fluorescence lifetime is in the region of 10 ns (10×10^{-9} s). The average time between excitation and a return to the ground state is called the lifetime (τ) of a fluorophore (or the fluorescence lifetime). It is informative to consider a 1 ns lifetime within the context of the speed of light. Conversely, emission of light from triplet excited states to the ground state level, are formally spin forbidden and are referred to as phosphorescence. Here, the emission rates for e.g. purely organic compounds are slow (10^{-3} to 10^{2} s^{-1}), so that phosphorescence lifetimes are typically on the millisecond to second, minutes or hours. There are many deactivation processes such as non-radiative decay and quenching processes that compete with emission, and thus phosphorescence is usually not seen in fluid solutions at room temperature. Generally, emission spectra are used to present the fluorescence spectral data. A fluorescence emission spectrum is a plot of fluorescence intensity versus wavelength (nanometres) or wavenumber (cm^{-1}). A Jablonski diagram is used to illustrate the processes that occur between the absorption and emission of light, showing the singlet ground, and first and second excited electronic states, described by S_0, S_1, and S_2, respectively,[66] (Fig. 1.17).

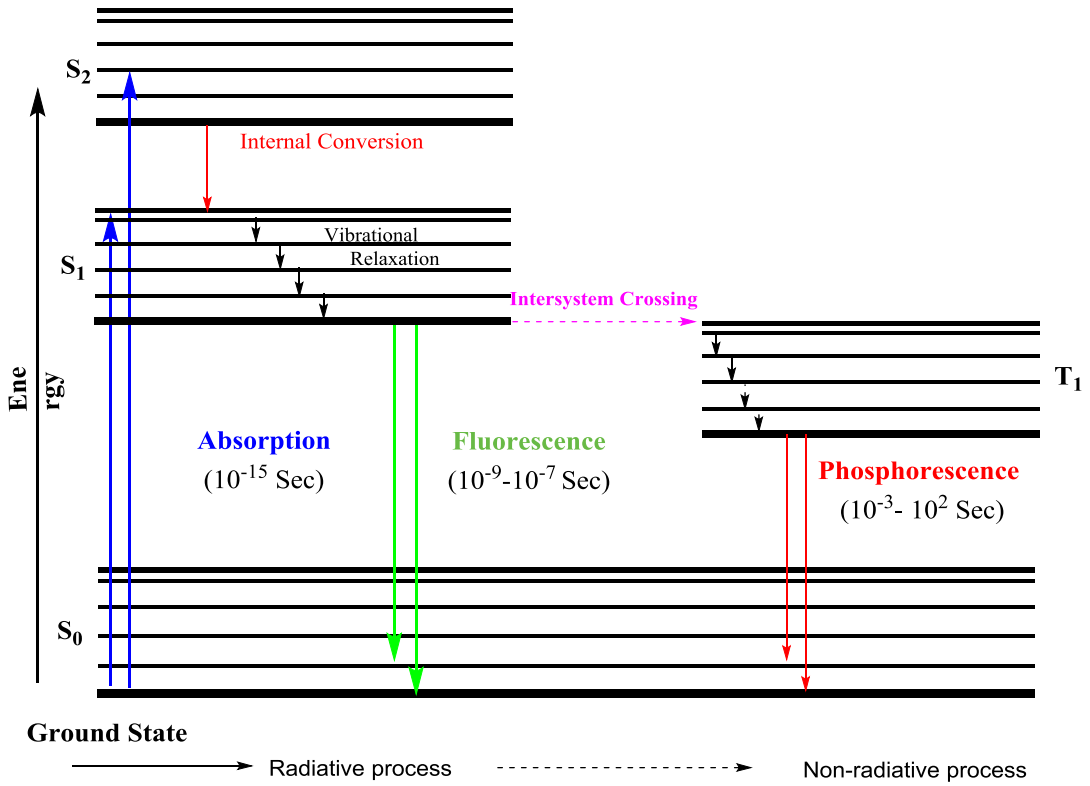

Figure 1.17: Jablonski diagram for photophysical processes of inorganic luminophore

In addition to fluorescence and phosphorescence, there are many other process that can occur, as illustrated by the Jablonski diagram. The molecules in the singlet excited state (S_1) can undergo a spin conversion to the triplet excited state (T_1) via Inter System Crossing (ISC). This process occurs through the conversion of the S_1 to T_1 state, for example. The transition from the T_1 state to the singlet ground state is formally spin forbidden. The most important terms regarding fluorescence are lifetime and quantum yield, which are used to determine the photophysical properties of a fluorophore.[66]

1.9 Luminescence of Transition Metals

Luminescent transition metal complexes are developed as alternatives to organic fluorophores as they possess luminescent properties that make them ideal for use as imaging probes.[67] The luminescence properties of complexes can be controlled by altering the ligand, geometry and metal ion. Transition metal complexes have *d*-orbitals which are split by the octahedral crystal field of the ligands into triply degenerate t_{2g} levels and doubly degenerate e_g levels. The splitting arises because the two e_g^* orbitals are directed toward the six ligands and the remaining t_{2g} orbitals are aligned between the

ligands. Fig. 1.18 shows the energetic consequences of this arrangement are attributable to the electrostatic interactions between the filled ligand orbitals and electrons placed in the different *d*-orbitals. Thus, an electron placed in an e_g orbital is of higher energy than one placed in a t_{2g} orbital. The magnitude of the splitting is given by the crystal field splitting Δ. This is a particularly important parameter whose size is determined by the ligand field strength and the central metal ion.[68] With strong ligand fields, the ground state for d^6 transition metals is t_{2g}^6 and all spins are paired, it is a singlet (S_0). The lowest excited states are derived from promoting an electron to one of the unoccupied orbitals. The magnitude of Δ affects the distribution of electrons between the t_{2g} and e_g* levels. If Δ is large (i.e., large splitting in a strong field), it is energetically more favourable to pair electrons in the t_{2g} level than to keep them unpaired by distributing them throughout the t_{2g} and e_g levels (Hund's rule). There are three types of excited states:

a) Metal-centred *d-d* states arise from promoting a bonding electron from the t_{2g} level to e_g^* level ($t_{2g}e_g^*$) and give rise to weak (Laporte forbidden) absorption bands (ε = ca. 100 $mol^{-1}dm^3cm^{-1}$). Thus, *d-d* emission is characterized by long radiative lifetimes and negligible quantum yields.

b) Ligand-based π-π* states derived from promoting a bonding π-electron to an antibonding π* level. These transitions are highly intense and are localized on the ligands.

c) Metal-to-ligand charge transfer (MLCT) by promoting an electron from a metal orbital to a ligand orbital ($t_{2g}\pi^*$) or ligand to metal charge transfer (LMCT) which involves promoting an electron from a ligand to a metal orbital (πe_g^*). These transitions have significant absorption bands in the visible region

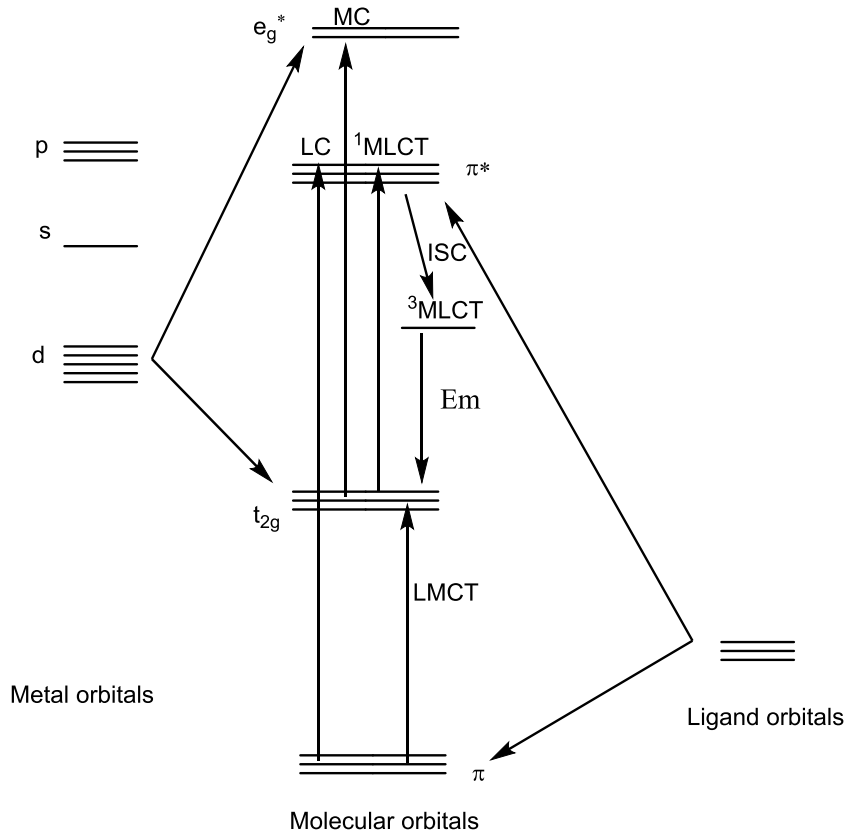

Figure 1.18: Simplified orbital and state diagrams for a d^6 metal in an octahedral environment[69]

The following important rules have been found to dictate the luminescent and photochemical properties of metal complexes:

(i) The lowest excited state must arise either through CT or ligand π-π*. This avoids the photochemical instability associated with unstable *d-d* excited states.

(ii) Spin-orbit coupling should be high to enhance the emission and permit radiative decay to compete more effectively with non-radiative decay, which precludes the first transition series complexes.

The crystal field should be strong enough to raise the *d–d* state above the MLCT state to avoid thermal excitation. For instance, the $[FeL_3]^{2+}$ complex is considered non-emissive because the *d-d* states are lower than the MLCT and are very close to the ground state, whilst the $[RuL_3]^{2+}$ complex is considered emissive as the *d-d* state is above the MLCT state and because it has a high energy gap between the MLCT state and ground state which indicates inefficient nonradiative decay. In the $[OsL_3]^{2+}$ complex the *d-d* state is well above the MLCT state which is the expected emitting state. However, the $[OsL_3]^{2+}$

complex is much less emissive than the Ru complex, due to the energy gap between MLCT state and ground state being less than in $[RuL_3]^{2+}$. This makes this complex weakly luminescent compared with $[RuL_3]^{2+}$ as per the energy gap law, which indicates that as the energy of the excited state approaches that of the ground state, the rate of non-radiative decay increases.[67]

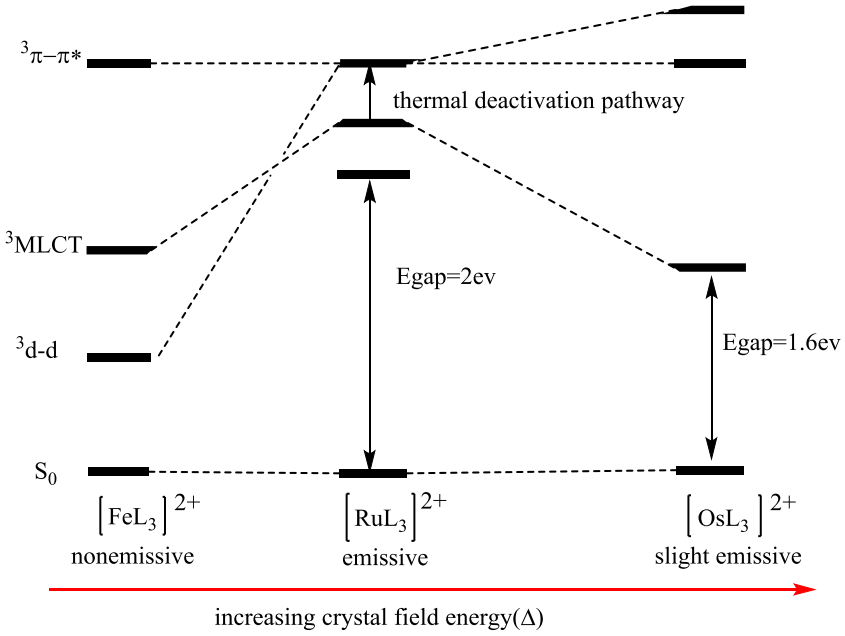

Figure 1.19: Lowest triplet-state orderings for different metal complexes with d and crystal field strength

1.10 Luminescence of Re(I) Complexes

The luminescence of organometallic compounds represents an important branch of coordination chemistry. This field considers fundamental aspects of organometallics, as well as their applications.[70] Most studies in photochemistry focus on transition metals in low oxidation states. Recently, a number of other studies have considered higher oxidation state metals. However, rhenium, one of transition metals, has a range of oxidation states extending from 0 (e.g., $Re_2(CO)_{10}$) to VII (e.g., CH_3ReO_3). In particular, Re(I) has a d^6 electron configuration and complexes such as Re(I) carbonyl halides $Re(CO)_5Cl$ were initiated by Wrigthon's pioneering studies.[71] Many other studies have considered the photochemical properties of theses complexes due to the various favourable features of Re(I) complexes such as their stability in air, their diamagnetism and their strong CO absorptions in IR spectroscopy, and that they are

often emissive in solution.[71] Researchers have found various uses for rhenium in biological systems as probes and spectroscopic tools; in addition, *fac*-tricarbonylrhenium(I) complexes serve as cold analogues for radioactive ^{99m}Tc(I) biological imaging agents. Recent studies have revealed that there is considerable interest in the use of rhenium in therapeutic agents due to the availability of beta – emitting ^{188}Re complexes.[72] *fac*-Tricarbonylchloro-bis (ligand) rhenium(I) complexes have long been studied because they are emissive in solution.[73] In particular, the chelate complex *fac*-[Re(CO)$_3$(N^N)(X)], where N^N is a diimine and X is a halide, is known to exhibit phosphorescent emission, and has photophysical properties that can be modified by varying the ancillary ligands. In these Re(I) complexes, the electronic states responsible for luminescence can then be assigned to a mixture of a metal-to-ligand charge transfer (MLCT) state and an intraligand charge-transfer state. Ranjan *et al.*[74] synthesized and characterized two related Re(I) complexes, [Re(CO)$_3$(N^N)(btpz)], where N^N = 2,2'-bipyridine (bpy) (**1**) and 1,10-phenanathroline (phen) (**2**), and btpz = 3,5-bis(trifluoromethyl)pyrazolate. This study revealed that complexes **15** and **16** (Fig. 1.20) show photoluminescent emission in both solution and the solid state at room temperature which arises from a MLCT transition with strongly overlapping intraligand π-π^* transitions. It was found that Re(I) metal complexes **15** and **16** exhibited strong phosphorescent emission with λ_{max} = 525 and 544 nm in solid-state samples, compared to the yellow-orange emission of **1** (λ_{max} = 571 nm) and **16** (λ_{max} = 568 nm) observed in solution. It was found that their parent halide complexes [Re(CO)$_3$(bpy)Br] and [Re(CO)$_3$(phen)Br], showed strong ^{3}MLCT emission bands in the range 620-640 nm in solutions of CH_2Cl_2 and CH_3CN. Comparison of complexes **15** and **16** showed that they exhibited a blue shifted of emission maximum on the replacement of bromide by 3,5-bis(trifluoromethyl)pyrazolate (btpz) consistent with the properties of their absorption spectra. The long excited state lifetimes of complexes **15** and **16**; (0.51 and 1.56 μs) for **15**, and (0.44 and 1.39 μs) for **16**, respectively. The complex **16** shows a four-time greater luminescence quantum yield in deaerated solution.[74, 75]

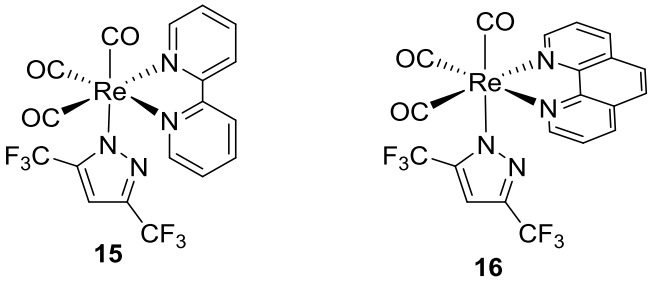

Figure 1.20: Rhenium(I) complexes **15** and **16**

A number of studies have considered the modification of the electronic structure of $[Re(CO)_3Cl(N\text{^}N)]$ by developing an ancillary ligand from bipy to pyt. For example Obata M.*et al*[76] synthesized 4-(2-pyridyl)-1,2,3-triazole (pyta) and derivatives as new α,α- diimines coordinated with Re(I) to produce $[Re(Cl)(CO)_3(R\text{-pyta})]$ where R= (Bn), AcGlc, Glc as shown in the figure below:

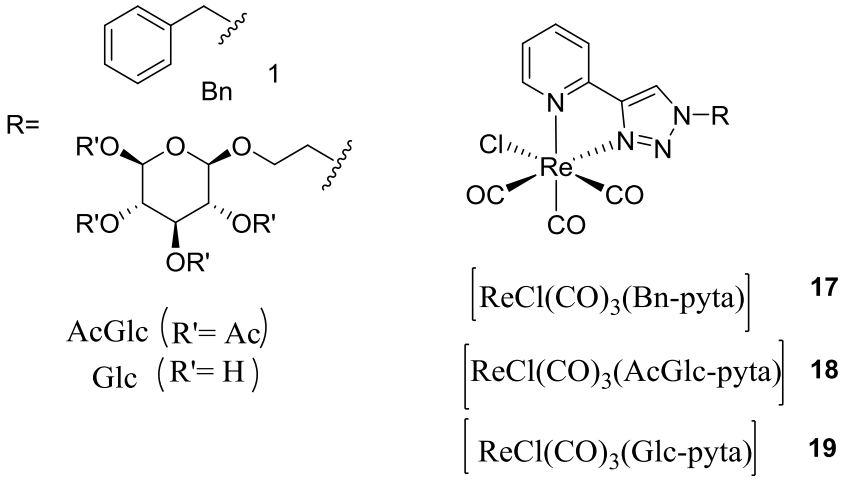

Figure 1.21: Rhenium(I) complexes **17**, **18** and **19**

This study indicated that $[ReCl(CO)_3(Bn\text{-pyta})]$ **17** exhibited blue-shifted luminescence spectrum compared to $[ReCl(CO)_3(bpy)]$. This was because the Bn-pyta ligand has the same function as an electron-donating group, such as bipyridine ligand; this study also revealed that the luminescence lifetime of $[ReCl(CO)_3(Bn\text{-pyta})]$ (8.90 μs) is almost three times longer than that of $[ReCl(CO)_3(bpy)]$ (3.17μs), affording a long-lived luminescence with a higher quantum yield. The complexes $[ReCl(CO)_3(AcGlc\text{-pyta})]$ **18** and $[ReCl(CO)_3(Glc\text{-pyta})]$ **19** exhibited similar photophysical properties to those of $[ReCl(CO)_3(Bn\text{-pyta})]$. DFT calculations demonstrated that the HOMO-1 orbitals of $[ReCl(CO)_3(Bn\text{-pyta})]$ and $[ReCl(CO)_3(bpy)]$ are localized over the Re(I) and Cl atoms which form π-antibonding orbitals, while the LUMOs are centred on the π* orbitals of

the pyta and bpy ligands. Hence the lowest energy electronic transition can clearly be assigned to mixed metal–ligand-to-ligand charge transfer (MLLCT) in both complexes.[76]

The study by Cle'de *et al.*[77] used a single rhenium tris-carbonyl moiety to design a new compound which was utilized as a Single Core Multimodal Probe for Imaging (SCoMPI) depending on the luminescent properties that this complex displayed.

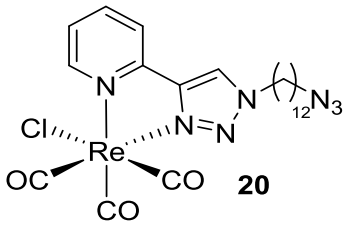

Figure 1.22: Structure Complex **20**

UV data revealed absorption bands at 300 nm which were assigned to intraligand π-π* transitions, whereas the broad 320–350 nm absorption band can be assigned to the MLCT transition; this band gives a large radiative emission band at ca. 510 nm, a quantum yield in water:ethanol (1:1) mixture at room temperature is 0.19%. The luminescent properties of $[(L)Re(CO)_3]$ and their SCoMPI probes show considerable potential with regards to studies in biological media.

Relative to this study, Wolff *et al.*[78] synthesized three complexes shown below:

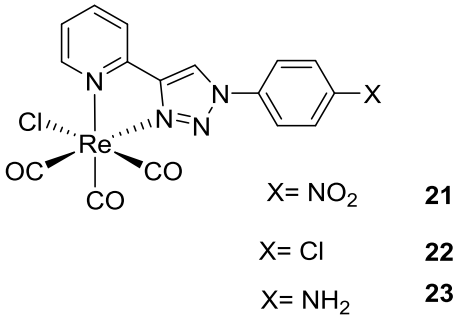

Figure 1.23: Structure of complexes **21**, **22** and **23**

This study revealed that photophysical properties are affected by the nature of the substituent group on the phenyl pendant arm (X = NO_2, NH_2 or Cl). DFT calculations confirmed these studies, where it was found that complexes **21** and **22**, incorporating the electron-withdrawing substituents –Cl and $–NO_2$, have the same HOMO and HOMO-1 which are involved of $5d_{yz}$ and $5d_{xz}$ rhenium orbitals and chlorine orbital *p*, HOMO-2

orbital composed carbonyl π* orbital while the HOMO-3 orbitals are mainly centred on the chelate ligand (pyta) and the substituents of the phenyl ring strongly effect the energies of this level. HOMO-3 energy level of **21** is low compared with **22**. Moreover, the HOMO-3 orbital of **23** is localized on the 4-aminophenyl part of the chelate ligand due to the strongly electron-donating NH_2 substituent on the phenyl ring. This study indicated the LUMO is localized on the $PhNO_2$ moiety, which is a part of the chelate ligand, whereas the LUMOs of **22** and **23** are localized on the pyta-like π* orbitals. In addition, the HOMO-LUMO energy gap decreases in the order **22** > **23** > **21**. The NO_2, Cl and NH_2 substituents have also direct effects on the composition of LUMO orbitals in **21-23**. Moreover, photophysical data revealed absorption bands at 300–325 nm, corresponding to the MLCT transition of each complex, and that complexes **22** and **23** exhibited large emission bands at 541 and 543 nm, respectively, while **21** is not luminescent, even when emission spectra were recorded at 77 K in methanolic solution, due to the high probability of nonradiative deactivation. The quantum yields were also investigated at room temperature and found as Φ = 0.21 for **22** and Φ = 0.10 for **23**.

Another attempt by Cle'd *et al.*[79] reported the synthesis of three neutral complexes derived from the *fac*-[$Re(CO)_3Cl(pyta)$] core. This study demonstrated that the effect of the pendant alkyl side chain on the photophysical properties that were as expected from a previous literature report.[77]

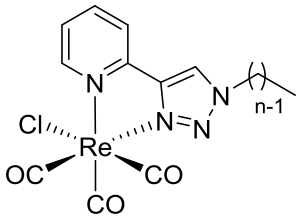

n = 4 **24**
n = 8 **25**
n =12 **26**

complex	λ_{ex}/ (nm)	λ_{em} /(nm)	Φ
24	335	527	0.0015
25	335	527	0.0014
26	335	527	0.0014

Figure 1.24: Structure of complexes **24**, **25** and **26**

Luminescence properties indicated that compounds **24**, **25**, and **26** exhibited the same absorption/emission properties in acetonitrile (MeCN) as typical $[Re(CO)_3(pyta)]^+$ emitters, whereas **24** and **25** displayed emission spectra that were blue shifted (527 nm) and enhanced in comparison with those observed in MeCN due to the effects of the solvent on the alkyl chain; in water, the metal core is shielded by this alkyl chain from

water molecules and this prevents the metal core from interacting with the water, whereas the alkyl chain in MeCN interacts strongly with the solvent and at the same time shields the metal core from solvent. Also, this study suggested compound **24** was not emissive in aqueous solution due to the alkyl chain being too short to prevent the solvent from interacting with the metal core.[79]

Recently, a new series of neutral Re complexes were synthesized and characterized by Ching *et al.*[80]

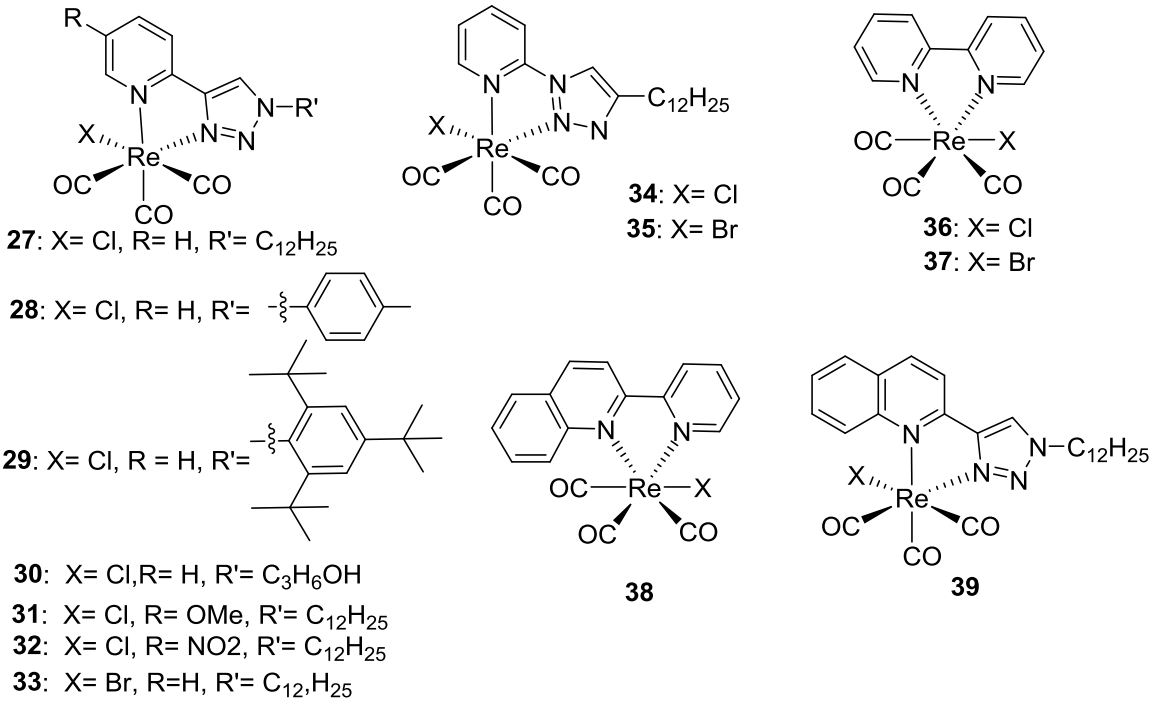

Figure 1.25: Rhenium complexes **27-39**

This study prepared different Re complexes bearing the pyta-ligand which have different alkyl and substituents at the N1 of the triazole (complexes **27**−**30**), different *para*- substituted pyridine moieties (complexes **27**, **28**, **29**), or different halide ligands (X = Cl or Br). Also, the tapy-based compounds all contain a dodecyl chain at the C4 of the triazole with different X (Cl or Br) ligands (complexes **34** and **35**). [Re(bpy)(X)$(CO)_3$] complex **36** and **37** with X = Cl and Br, respectively, were used for comparison. Also synthesized and studied as a reference was [Re(quinpy)(Cl)$(CO)_3$] **38**, where quinpy is a 2-(2-quinolyl)-pyridine ligand. All these complexes were used to investigate the abilities of this class of complexes to catalyse the electroreduction and photoreduction of CO_2. It was found that this class of Re pyta derivatives (**27**−**31**)

displayed a first reduction wave at ~1.7 V vs. SCE; a catalytic wave appeared in the presence of CO_2 and also indicated that electron-donating or electron-withdrawing groups on the pyridyl ring resulted in decreased activity. Thus, the functionalization of the pyridyl triazole provided the catalyst with a noteworthy stability.

Further studies concerning with cationic rhenium complexes that have wide utility across different aspects of bioimaging and photolumincence due to their many favourable features such as being non-toxic and large Stokes shift and high quantum yield compared with neutral species. A new class of cationic rhenium complexes $[Re(bpy)(CO)_3(\mathbf{Ta})]$ PF_6 were synthesised from $[Re(bpy)(CO)_3Cl]$ and characterized by Elliott *et al.*[81]

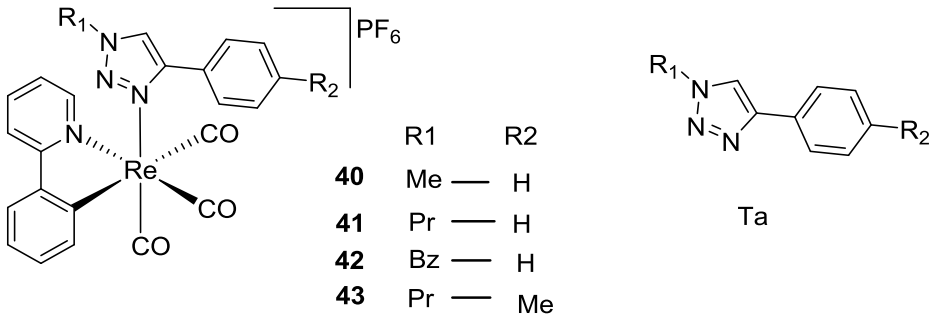

Figure 1.26: Synthesis rhenium complexes **40-43**

Their UV spectroscopy suggested that complexes **40-43** were luminescent due to absorption at 260 nm which corresponding to a π-π^* in aerated dichloromethane at room temperature and exhibited broad emission for the triazole complexes (542 to 552 nm) which are assigned to ^{3}MLCT states. These emission bands are significantly blue-shifted relative to that of the parent chloride complex $[Re(bpy)(CO)_3Cl]$ (612 nm) consistent with the replacement of a π-donor with a π-accepting ligand leading to stabilisation of the HOMO relative to the LUMO. The emission of **40-43** are similar to those measured for $[Re(bpy)(CO)_3(py)]^+$ under identical conditions (549 nm). However, it was found that when changing solvent from dichloromethane to acetonitrile there is very little difference observed in the position of emission maxima. Also this study revealed that the lifetime for complexes with triazole (475 ns) are slightly longer than those of complexes with pyridine $[Re(bpy)(CO)_3(py)]^+$ (466 ns) under identical condition.

In accord with this study, Boulay *et al.*[82] synthesized dimeric complexes of rhenium(I) bearing pyridytriazole with a –COOH arm, as expected it should obtain mononuclear. Surprisingly, due to the nature of the R group, different rhenium complexes were produced including a mixture of mononuclear **44**, **45** and dimeric **46** complexes.

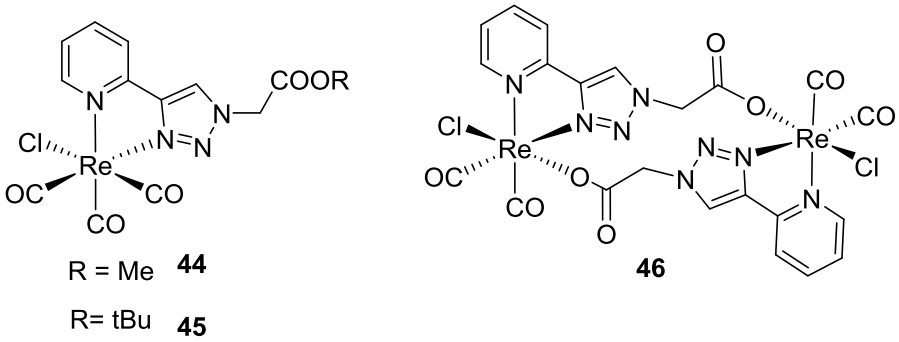

Figure 1.27: Mononuclear **44**, **45** and dimeric **46**

This study revealed the dimer **46** and monomers **44** and **45** exhibit absorbance at 260-318 nm and 320-380 nm at room temperature in MeOH/DMF solutions assigned to π-π* and MLCT transition respectively and the quantum yield of dimer (0.55%) is higher than that of the monomer. Recently, a new range of cationic rhenium complexes were synthesized by Connell *et al.*[83] It was found that the luminescence properties of the type $[Re(CO)_3(bpy)Br]$ when compared with $[Re(CO)_3L1(py)]OTf$ and $[Re(CO)_3L^{2a}(py)]OTf$, showed emission spectra in acetonitrile with significant blue shifts. Interestingly, $[Re(CO)_3L1(py)]OTf$ shows a blue shift in its emission maximum when compared with its halide analogue, $[Re(CO)_3L1Cl]$. While the luminescent quantum yields were calculated relative to $[Re(CO)_3(bpy)Br]$ and were found to be similar to other rhenium complexes containing 4-(2-pyridyl)-1, 2, 3-triazole ligands, these complexes are candidates for use as superior radiolabelling.

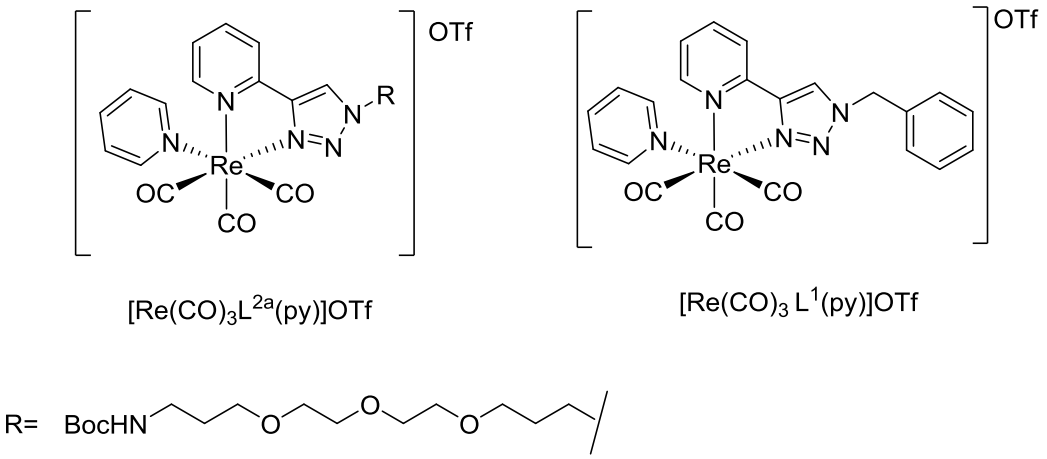

Figure 1.28: Structure of cationic rhenium complexes[84]

1.11 Luminescence of Ir(III) Complexes

The photophysical properties of d^6 transition metal complexes have received considerable attention due to their potential for use in a variety of applications such as oxygen sensors, biological probes and phosphorescent dopants in optoelectronic devices. In particular, cyclometallating complexes of iridium(III) have attracted interest because of the high tunability of their emission in terms of colour and efficiency.[85]

From the late 1980s to early 1990s, Watts and co-workers studied the photophysical and electrochemical properties of cationic heteroleptic iridium complexes of the form [Ir $(ppy)_2(bpy)]^+$, where Hppy is 2-phenylpyridine and bpy is 2,2'-bipyridine. Because of their large ligand field splitting and the strong spin-orbit coupling they offer the possibility for colour tuning in these phosphors.[86] The complex $[Ir(ppy)_2(bpy)]^+$ **47** has been used in light-emitting electrochemical cells.[87] However, the emission was enhanced when this complex substitued with fluorine on the cyclometallating ligand, as shown in Fig.1.29.

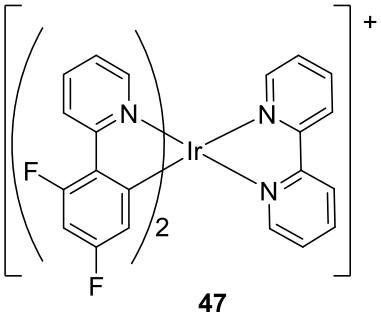

47

Figure 1.29: Structure of iridium complex **47**

This study revealed that this complex **47** displayed intense green (λ_{em} = 517 nm) photoluminescence with an emission lifetime of 0.90 μs. Such long emission lifetimes (on the microsecond scale) are indicative of the phosphorescent nature of the emissions. The HOMO mostly resides on the Ir atom and the phenyl ring of the ppy ligands, whereas the LUMO is mainly located on the bpy ligand alone. This study suggested that electron-withdrawing enhanced the photoluminescence properties.[88]

On the other hand, the study by Zysman-Colman *et al.*[89] indicated that a methoxy substituent on the phenyl ring of the C^N ligands could have an impact on the photoluminescence properties of cationic iridium complexes (Fig. 30). Optoelectronic data revealed that all these complexes exhibit an absorption band at ca. 308–312 nm. Compared to other heteroleptic iridium(III) cationic complexes, complexes **49**, **50** displayed red shifts (710 and 680 nm respectively) compared to $[Ir(ppy)_2(bpy)]PF_6$ (610 nm)[90] whereas **53, 54** are slightly blue-shifted, compared to **49** and **50**. This study also indicated that when three methoxy groups were present on the C^N ligand **54** and a further blue shift is exhibited by **50** and **51**. However**,** electron-donating substituents on the N^N ligands in **49**, **52**, **54** and **55** exhibited blue-shifted emissions compared to their respective analogues of **48**, **50**, **51** and **54**. The photoluminescence quantum yields (Φ_{PL}) for **48-55** were carried out in degassed acetonitrile, in which it was found that the Φ_{PL} values were exceedingly low, especially compared to other iridium complexes emitting in the same spectral region as **50** (5.7%) and **51** (15.4%).

		λ_{em}
48	1a R= 3-MeO, R'= H	710
49	1b R= 3-MeO, R'= H	680
50	2a R= 4-MeO, R'= H	618
51	2b R= 4-MeO, R'= tBu	595
52	3a R= 3,4-dMeO, R'=H	730
53	3b R= 3,4-dMeO, R'= tBu	700
54	4a R= 3,4,5-tMeO, R'= H	720
55	4b R= 3,4,5-tMeO, R'= tBu	685

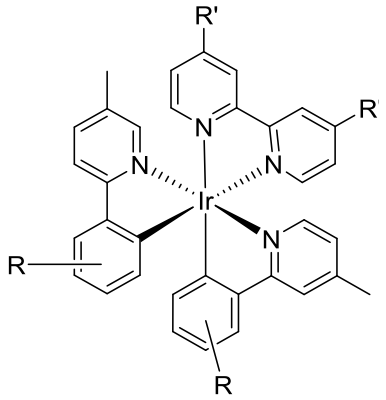

Figure 1.30: Structure of iridium complexes **48-55**

The DFT calculations confirmed this study, suggesting the HOMO is located on both the phenyl ring of the C^N ligands and the iridium atom, while the LUMO for each of the eight complexes is located on the diimine ligand. It was found that the LUMO orbitals were relatively invariant at around −2.48 eV for complexes **48**, **50**, **52** and **54.** Similarly, for **49**, **51**, **53** and **55**, the LUMO energies are destabilized due to the electron-donating effect of the *tert*-butyl substituents. Hence, the HOMO-LUMO energy gap is therefore smallest for **50**, at 2.90 eV, and largest for **51**, at 3.40 eV. It was found that electron-donating substituents on the cyclometallating ligands in cationic iridium complexes enhanced the photophysical properties for some complexes, namely **50** and **51**, but photoluminescence quantum yields and emission lifetimes were reduced compared to $[Ir(ppy)_2(bpy)]PF_6$.[91]

A similar study was reported by Lowry *et al.*,[92] demonstrated the effects of different substituents at the 3-position in $[Ir(C^N)_2(bipy)]^+$

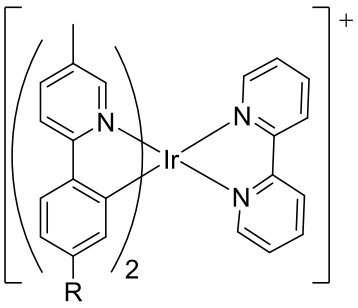

	λ_{em}	
R= H	587	**56**
F	558	**57**
Cl	553	**58**
Br	553	**59**
Ph	582	**60**
OMe	593	**61**

Figure 1.31: Iridium complexes **56-61**

This study revealed that electron withdrawing groups such as F, Cl, Br and Ph exhibit a blue shift, while –OMe exhibits a slight red shift. The emission maxima of these

complexes were associated with the ΔE between the HOMO and LUMO obtained from DFT calculations, and were found to be consistent with literature.[91, 92]

Recently, Zysman-Colman *et al.*[93] was successful in the synthesis of a new class of heteroleptic cationic Ir(III) complexes containing bis (triazole) as ancillary ligand with the formula $[Ir(C^N)(btl)]^+$, where btl = 1,1'-benzyl-4,4'-bi-1H-1,2,3-triazolyl as ancillary ligand N^Nand C^N = 2-phenylpyridine (phpy), 1-benzyl-4-phenyl-1H-1,2,3-triazole (phtl) and 1-benzyl-4-(2,4-difluorophenyl)-1H-1,2,3-triazole (dfphtl). All these complexes exhibit high intensity absorptions above 250 nm that can be assigned to π-π* transitions, whilst complex **58** showed emission at 481 nm, and complex **59** at 495 nm, while complex **64** did not show any emission at room temperature.

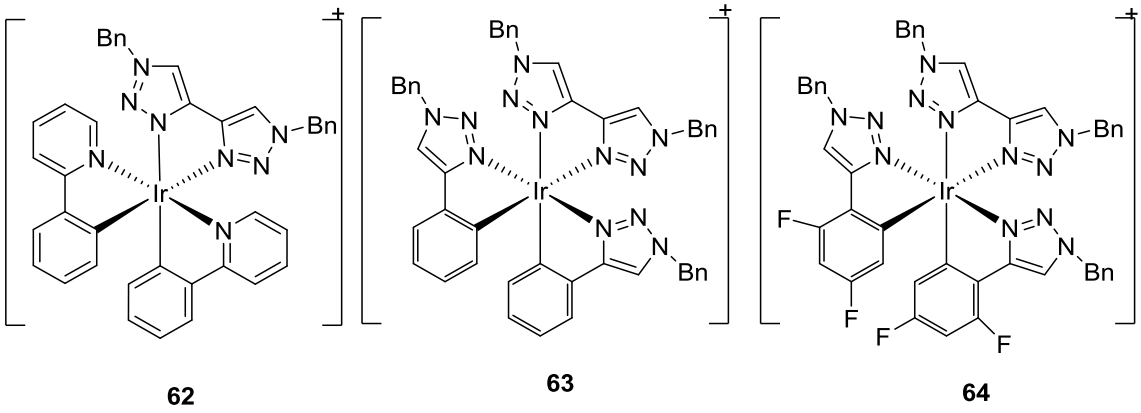

Figure 1.32: A new class of iridium complexes **62**-**64**

This study also included a DFT study, which illustrated that the HOMO is distributed between iridium and C^N for all three complexes, and also revealed that the replacement of phpy with phtl led to the destabilization of the LUMO in complex **63**, increasing the gap between the HOMO and LUMO in comparison with **62**, while the HOMO–LUMO gap increased in complex **64** compared to **63** due to the substitution of fluorine atoms onto the C^N ligands. This study indicated that photoluminescent quantum yields for **62** and **63** were moderate at ~3%. However, the lifetime for complex **62** was on the microsecond scale at 298 K, and approximately doubled at 77 K. Complex **63**, however, only showed a 48 ns lifetime at 298 K though the emission was very long-lived (15.8 μs) at 77 K. So, the radiative rate constant, k_r increased 44-fold. As expected, the non-radiative rate constant, k_{nr}, increased about 46-fold.[93]

Other attempts by Zysman-Colman and co-workers[86] were reported to develop the luminescence of cyclometallated iridium(III) complexes by using a phenyltriazole as cyclometallating ligands (C^N) due to have strong-field and wide HOMO–LUMO energy gaps that can be introduced to form Ir(III) complexes with high-energy emission.

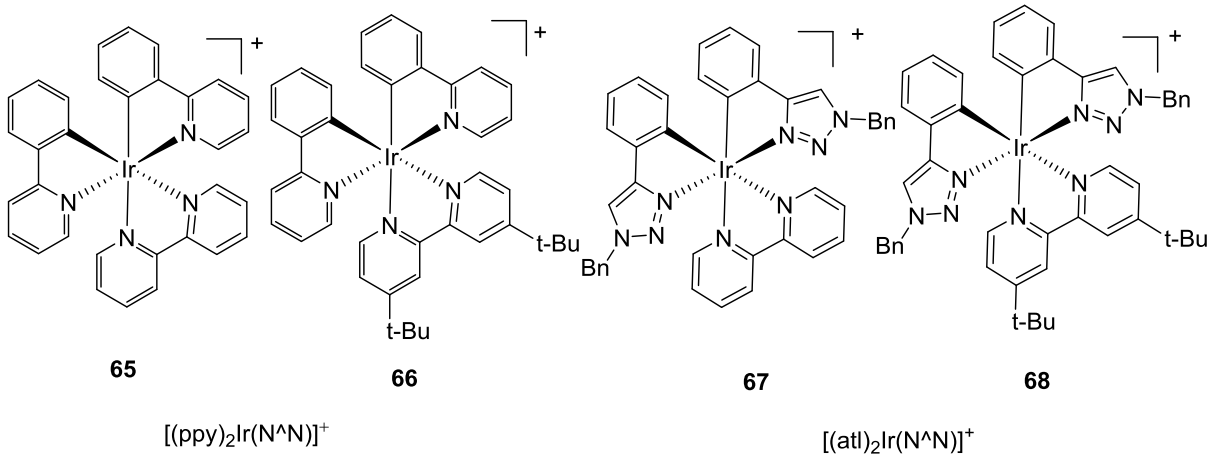

Figure 1.33: Structure of iridium complexes **65-68**

This study found that the LUMO orbitals for complexes **65** and **66** were centred only on the ancillary ligand, while the HOMOs for **65** and **68** were localized between the metal and/or the cyclometallating ligand. Also, it was revealed that the replacement ppy-type ligand (for the atl-type ligand) resulted in destabilization of both the HOMO and the LUMO energies, so complexes with pyt = C^N, 2.83-3.15 eV have larger energy gap than complexes with pph = C^N, 2.74-2.97 eV. UV data indicated that complexes **67** and **68** exhibited a blue shift (471 and 630 nm) compared to **65**, **66**. Also, the lifetimes of **67** and **68** are similar to those found for **65** and **66**, on the order of 4-6 μs. Quantum yields increased dramatically for pyt- complexes from 25 to 80%. This increase in quantum yield was due to a diminution of nonradiative rates with increasing emission energy; for example, **67** is about three times as bright as **65**.

A new trend is to synthesise new classes of cyclometallated iridium which have considerable potential in electrochemiluminescence (ECL) applications.[94] Connell *et al.*[95] used a 1,2,3- triazole containing ligand which induced a large hypsochromic shift in emission, compared to complexes prepared with 2,2-bipyridine, which enables multiple colour detection.[96]

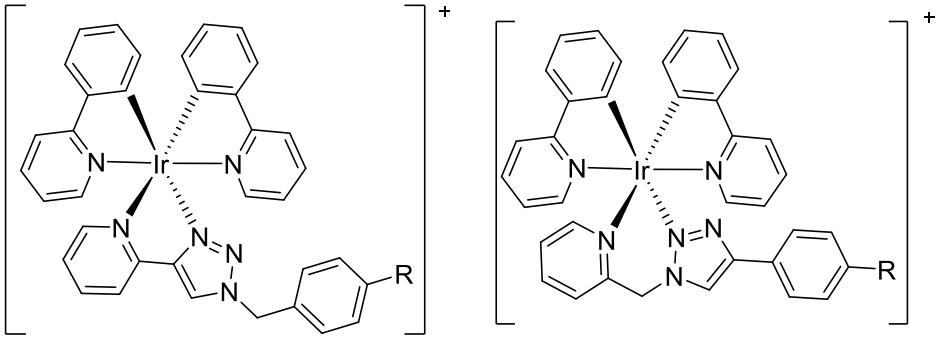

R= H $[Ir(ppy)_2L^{1a}]BF_4$ **69**
R= NO_2 $[Ir(ppy)_2L^{1b}]BF_4$ **70**
R= OCH_3 $[Ir(ppy)_2L^{1c}]BF_4$ **71**

R= H $[Ir(ppy)_2L^{2a}]BF_4$ **72**
R= NO_2 $[Ir(ppy)_2L^{2b}]BF_4$ **73**
R= OCH_3 $[Ir(ppy)_2L^{2c}]BF_4$ **74**

Figure 1.34: Series of iridium complexes **69-74**

A series of cyclometallated complexes were synthesized and characterized as shown in Fig. 1.31. This study revealed that all these complexes were luminescent at room temperature with the exception of the nitroaromatic-containing complexes $[Ir(ppy)_2L^{1b}]BF_4$ **70** and $[Ir(ppy)_2L^{2b}]BF_4$ **71**. It was also found that the complexes with L^{1x} as ancillary ligands had quantum yields between Φ_{em} = 0.2− 0.3 and lifetimes in the microsecond range, while complexes containing L^{2x} ancillary ligands showed lower magnitudes for the associated quantum yields and emission lifetimes. This study also revealed that the complex $[Ir(ppy)_2L^{2b}]BF_4$ **71** was essentially nonemissive in solution at room temperature, where only a weak featureless band was observed (λ_{em} = 513 nm) with a quantum yield of Φ_{em} < 0.001. Better emission quantum yields and longer emission lifetimes were obtained from the $[Ir(ppy)_2L^{1x}]BF_4$ complexes, which were also more stable to ligand substitution in solution and where emission was decreased due to the presence of the nitroaromatic group.

1.12 Luminescent Re(I) Complexes as Biomolecular Probes and Imaging Agents

The combination of a luminescent transition metal complex and biomolecules has attracted a great deal of attention due to the potential applications of these complexes for development as probes.[97, 98] However, the first dyes used were organic fluorophores and luminescent lanthanide chelates.[99] There were considerable limitations to using these reagents due to photodegradation rates, pH dependence, fluorescence lifetimes, and Stokes shifts. However, luminescent transition metal complexes such as rhenium(I),

ruthenium(II) and iridium(III) polypyridines were developed to overcome these limitations.[76] The selection of transition metals used can be attributed to the following factors: (1) most transition metal complexes are stable; (2) transition metal complexes have long-luminescent lifetimes (100 ns to μs) which are much greater than any organic luminophores; and (3) heavy metal complexes have large Stokes shifts which help to reduce possible self-quenching effects. These features make them suitable as sensing or imaging probes.[97] Recent studies have shown considerable attention to the use of a *fac*-tricarbonyl Re(I) fragment with a bisimine ligand such as 2,2'-bipyridine (bpy) or 2-pyridyltriazole (pyta) which show emission from a ^{3}MLCT excited state in various biomolecular applications.[100] Generally, there are two types of Re(I) complexes: neutral complexes of the form [ReX(bipy)$(CO)_3$] (X = Cl/Br) exhibit absorption at 350 nm and emission maxima at 500-600 nm, and lifetimes of about 100 ns and Φ in the order of 0.1%, while cationic derivatives with formulae of the type [Re(bipy)$(CO)_3$(L)]$^+$ have more attractive photophysical properties with long lifetimes and large magnitudes of Φ than neutral complexes. Thus, these cationic complexes have attracted the most attention in the imaging field, particularly those with axial pyridine ligands.[101] Also, these cationic complexes are kinetically inert in many different chemical and biological environments. The first application of a Re(I) diimine species was reported in 2007 by Coogan and co- workers[102] in a series of biological imaging experiments, as shown in Fig. 1.35.

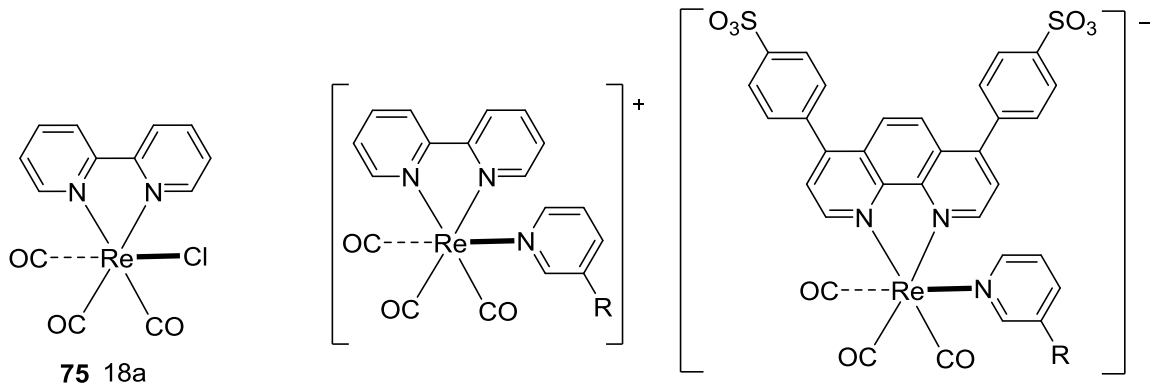

75 18a

76 18b R= CH_2OH
77 18c R= $CH_2O_2C(CH_2)_6CH_3$
78 18d R= $CH_2O_2C(CH_2)_{12}CH_3$
79 18e R= $CH_2O_2C(CH_2)_{16}CH_3$

80 18f R= H
81 18g R= CH_2OH

Figure 1.35: Series of rhenium complexes **75-81**

A wide range of rhenium(I) tricarbonyl complexes with the bisimine ligands phen, bipy and bathophenanthroline sulfonate, including lipophilic and hydrophilic complexes (both cationic and anionic) with axial chlorides, pyridine, 3-hydroxymethylpyridine and aliphatic esters of 3-hydroxymethylpyridine, were selected in order to study the toxicity and uptake for a variety of Re(I) species. This study revealed that the choice of ligand(s) is essential to controlling toxicity. It was found that **75** had high toxicity due to chloride release that allowed biomolecules to coordinate, whilst complex **79** also showed high toxicity because of its high concentration, while **76-78** have low toxicity with good uptake. This study also indicated that anionic complexes **80** and **81** were accumulated in digestive vacuoles by phagocytosis and also found low toxic than the **75** and **76-79** complex, while cationic complexes were localized in membranes and membrane structures in the cytoplasm.[101]

A recent study by Lo[97] was successful in modifying rhenium(I) polypyridine complexes to develop new probes for biological receptors depending on the advantages relating to their ease of emission and colour-tuning through the use of different diimine ligands with long-lived excited states. In this study, a new class of rhenium(I) complexes with the general formula $[Re(bpy\text{-}R1)(CO)_3(py\text{-}R_2)]^+$ were synthesized, including reactive functional groups. These complexes were classified either as a covalent label or noncovalent, and were used to label amine and sulfhydryl groups of biomolecules such as biotin, estradiol, and indole.

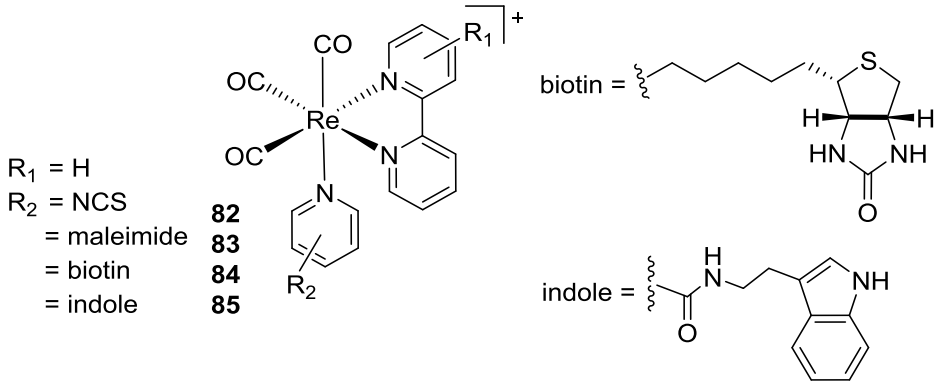

Figure 1.36: rhenium complexes **82-85**

This study revealed that Re(I) complexes $[Re(N\text{^}N)(CO)_3(py\text{-}NCS)]^+$ **82** $[Re(N\text{^}N)(CO)_3(py\text{-}maleimide)]^+$ **83** were used to label amine- and sulfhydryl-modified oligonucleotides (e.g., M13 sequencing primers)[103] amino acids (e.g., alanine)[104] peptides (e.g., glutathione) and proteins (e.g., serum albumins and avidin);[105] while the

complex $[Re(N^N)(CO)_3(py\text{-}biotin)]^+$ **84** displayed a higher emission intensity and longer emission lifetime after binding to avidin as a result of the decreased polarity of their local environment with good uptake. Recently, biotin Re conjugates have been applied in cell imaging, whereas the complex $[Re(N^N)(CO)_3(py\text{-}indole)]^+$ **85** has been used to examine the interactions between these complexes and with indole-binding proteins such as bovine serum albumin (BSA) and lysozyme.[97]

Boulay *et al.*[106] used the new trend of strategies by designing dual-imaging probes based on phosphorescence (Re core) and magnetic resonance imaging modalities. This report demonstrated the synthesis of a neutral heterobimetallic Re(I)–Gd(III) complex via functionalized 2,2'-bipyridine moiety (bpyCOOMe) **86**.

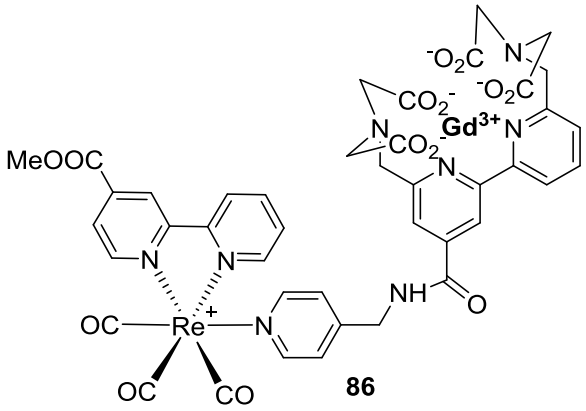

Figure 1.37: Structure of rhenium complex **86**

The photophysical study revealed that complex **86** exhibited excitation at 350 nm and emission at 578 nm which is assigned as originating from a ^{3}MLCT[dπ(Re)-π^* (bpyCOOMe ligand)] excited state on the basis of previous spectroscopic studies of $[Re(py)(CO_3)bpy]^+$complexes.[107] The quantum yield of complex **86** was about 1.4% which is sufficiently large for detection in fluorescence microscopy.[77] Also, the relaxometric properties of complex **86** were investigated at 0.01–60 MHz. It was found that complex **86** showed a high relaxivity for all magnetic fields and had the typical shape for a low-molecular-weight Gd complex. This probe should be useful for *in vivo* detection of pathologies via MRI and for supporting surgical guidance via intraoperative fluorescence imaging.[106] Another study used a rhenium tris-carbonyl core to design a new bimodal probe for imaging based on infrared and luminescent properties. This probe was called the Single Core Multimodal Probe for Imaging (SCoMPI). According to previous studies, rhenium tris-carbonyl complexes have two strong absorption bands in the IR-transparent carbonyl absorptions which allowed mapping inside MDAMB-231

breast cancer cells.[108] In addition, metal tris-carbonyl moieties (including Mn, Re, Os) have been used as IR-labels, thus Cle'de *et al.*[77] were successful in combining both spectroscopies; this study demonstrated that [$ReCl(CO)_3$-pyta-$C_{12}N_3$] **20** was synthesized using a ‘‘click-to-chelate’’ strategy, as shown in Fig. 1.22. This study revealed that an azide terminal function was added in order to compare infrared signals from the N_3 and CO groups, a long lipophilic alkyl side chain was introduced to encourage cellular uptake and demonstrated that MDA-MB-231 breast cancer cells were used in this study and incubated with complex **20** in the 10-micromolar range for 1h; UV properties show excitation about 330 nm and emission at around 520 nm that can be attributed to the MLCT transition.[109] The FTIR spectrum of compound **20** as a solid showed two bands at 1920 and 2025 cm^{-1} and a weak absorption at 2096 cm^{-1} corresponding to the azide. Thus, IR and luminescence spectroscopy were consistent with each other and showed a perinuclear location of **20** that assigned to the Golgi apparatus. This SCoMPI probe has great potential to development studies in biological media. In accordance with the previous study by Cle'de *et al.*[77] which used the $Re(CO)_3$ moiety containing the pyta ligand, new classes of $Re(CO)_3$ bearing a pyta link to alkyl chains of different lengths (C4, C8, and C12) were investigated in terms of lipophilicity and their uptake of the [$Re(CO)_3$(pyta)] core and cytotoxicity via SCoMPI (Fig. 1.24).[79] This study revealed that complexes **24**, **25** and **26** were synthesized according to a protocol previously described for a similar *fac*-[$Re(CO)_3Cl$(pyta)] compound with a -$C_{12}N_3$ side chain. This study revealed that complexes **24**, **25** and **26** were as expected in terms of lipophilicity, which increased with increasing length of the alkyl side chain from 4 to 12 carbons. Cytotoxicity was investigated using MDA-MB-231 breast cancer cells and evaluated after five days of exposure. The IC_{50} values were found to have the order **26** < **25** < **24,** whilst qualitative observation indicated cellular uptake. As a result, this study indicated that complex **26** was more lipophilic and had higher cytotoxicity due to its greater cell-penetration ability. Also, the ratio between the in-cell luminescence of cells incubated with **26** and **24** was about 1.7, which is almost consistent with IR spectroscopy. Hence, IR and luminescent spectroscopies of the bimodal SCoMPI unit are clearly consistent. This study suggested that the toxicity of the SCoMPI can be identified by an improvement of the cellular internalization.

To achieve good cellular localization and a cytotoxic effect, a new strategy was used by D’Alfonso and Licandro to functionalize the metal complexes with artificial peptide nucleic acids (PNAs).[110] This study found that complex **87** was photostable and

noncytotoxic, readily permeated living cells, and stained the cytoplasm and nucleus with different colours. Complex **87** has been exploited for cell imaging and DNA targeting.

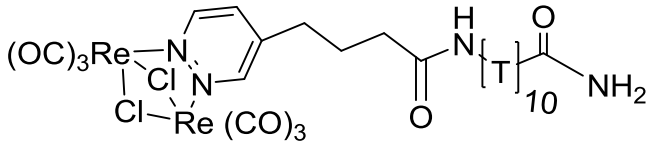

87

Figure 1.38: Structure of complex **87**

1.13 Re(I) Complexes with Potential for Use as Radiopharmaceutical Agents

For a long time, tricarbonyl technetium(I) and tricarbonyl rhenium(I) cores have been intensively studied in terms of their coordination chemistry for many reasons such easy as production of the hydrophilic air-stable *fac*-$[M(CO)_3(H_2O)_3]^+$ precursor from the corresponding permetallates MO_4^- (M = ^{99m}Tc or $^{186/188}$Re), and wide use of the ^{99m}Tc and $^{186/188}$Re radioisotopes in the development of diagnostic and therapeutic radiopharmaceuticals, respectively.[111] Interestingly, an alternative to technetium complexes, namely $^{185/187}Re(CO)_3$ complexes, are used for the macroscopic scale, because it is commonly used as luminescent probes. In the latter case, the tricarbonyl rhenium core was coordinated by a heteroaromatic amine, e.g., diquinolinylamine (dqa)[112], or an α, α′- diimine such as 2,2′-bipyridine; however, a significant challenge still remained in terms of finding a new strategy to functionalize bipyridines.[113] Recently, the study by Seridi *et al.*[114] attempted to design fluorescent rhenium(I) complexes from monofunctionalized 2-pyridyl-1,2,3-triazole derivatives (or pyta) as alternative ligands to 2,2′-bipyridines. The mild reaction via click approach allowed the synthesis of a large number of monofunctionalized pyta derivatives. ^{99m}Tc complexes were also synthesized with $[^{99m}Tc(CO)_3(2)Cl]$ where 2 = pyt-(2- methoxyphenyl) piperazine.

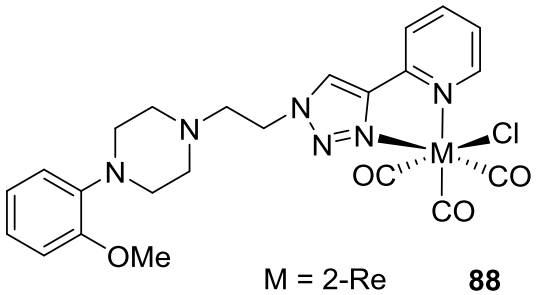

M = 2-Re **88**

= 2-^{99m}Tc **89**

Figure 1.39: Structure of complexes **88, 89**

According to the DFT study, the HOMO–LUMO gap is about 3.32 eV. The LUMO and LUMO+1 are localized on the 2-pyridyl-1,2,3-triazole fragment of the chelate ligand, while the higher virtual orbitals are delocalized over the carbonyls and Re atom or among carbonyls, Re and chelate ligand. The three HOMOs are centred on the (2-methoxyphenyl) piperazine part of the chelate ligand, complex **88** exhibited, as expected, an excitation at 330 nm and emission at 522 nm. The quantum yield was found to be Φ = 0.32% which is consistent with the values measured for other Re(I) complexes of the type [Re(α, α′-diimine)$(CO)_3$X] (α,α′-diimine = 2,2′-bipy or pyta, X = halide)[76] while complex **89** was prepared was an excellent yield (95%) using *fac*-[^{99m}Tc$(CO)_3(H_2O)_3]^+$ as a starting material. The lipophilic study was carried out in physiological conditions (0.1 M phosphate buffer, pH 7.4/n-octanol), $logP_{o/w}$ refer to the partition coefficient (P), and it was found about 2.34 for 2-^{99m}Tc complex which indicated that it is moderately lipophilic. It was in agreement with the value range for related radiocomplexes able to cross the blood brain barrier ($logP_{o/w}$ = 0.5–2.5).[115] Tc- or Re-tricarbonyl complexes with bidentate ligands were suitable for *in vivo* work and exhibited high stability against histidine and cysteine challenge experiments. Thus, these complexes are considered a good starting point for the preparation of novel ^{99m}Tc 5HT1A imaging probes and an alternative for 5HT1A imaging probes based on PET emitters.[114]

Recently, Yazdani *et al.*[116] synthesized complexes related to a previous study by Pitchumony *et al.*[117] (Fig.1.40),which used basic monodentate pyridine ligands, where M = Re(I), ^{99m}Tc these complexes were effective luminescent probes.

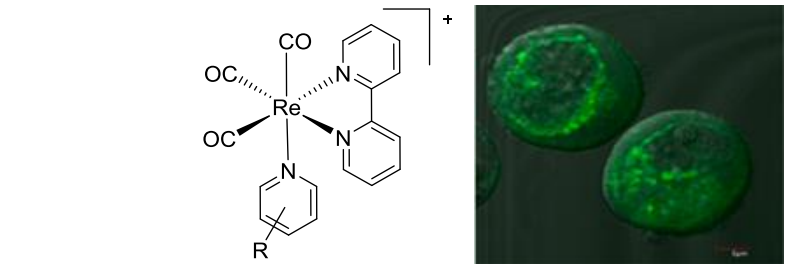

Figure 1.40: Images of $[^{99m}Tc(CO)_3(bipy)(DMAP)]^+$ 1a and Re (I) complex 1b incubated with MCF-7 cells for 1.5 h at room temperature (cyclohexyl)

While this study prepared a new series of Re and ^{99m}Tc complexes as [2+1] systems with imidazole as a monodentate ligand instead of pyridine with the general formula $[M(CO)_3(bipy)(L)]^+$ where L = *N*-alkyl imidazole ligands. The stability study was carried out by incubation of Tc(III) complexes in both isotonic saline and plasma, and revealed that complex **91** was stable after 6 h of incubation in 0.9% saline without any decomposition. While the *in vivo* imaging study using SPECT/CT images showed **97** applied to Balb/c mice as expected, showed high liver uptake which is likely associated with the binding of the reactive complex with serum proteins. So, data from the imaging and incubation in saline and plasma confirmed the stability of Tc complexes bearing imidazole derivatives for use as the basis for preparing targeted isostructural optical and nuclear probes.[116]

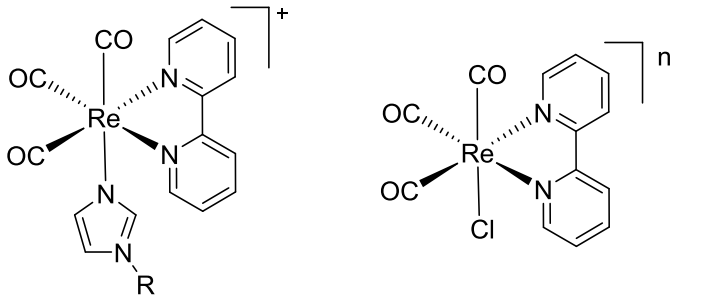

Figure 1.41: Re and ^{99m}Tc complexes **90-97**

An interesting study by Connell *et al.*[83] indicated how to synthesise a wide range of Re(I), ^{99m}Tc(I) bearing 1,4-substituted pyridyl-1,2,3-triazole ligands with the general formula $[M(CO)_3 L^x(py)]^+$, M = Re, Tc (Fig.1.42). All these complexes are luminescent with quantum yields consistent with $[Re(CO)_3(bipy)Br]^+$. It was found that the complex

linker to a cyclic-(RGDfK) peptide through a short methylene group have high affinity and specificity for $\alpha v\beta_3$ integrin receptors and superior radiolabelling with corresponding $[^{99m}TcL1(CO)_3X]^+$where X= py. These complexes are used specifically with the $\alpha v\beta_3$ integrin receptor, where in some cases it is found that it overexpresses resulting in the activation of endothelial cells of cancer neovasculature and some types of tumours. Thus, diagnostic imaging of integrin expression is one of the important roles in characterizing tumour-associated angiogenesis (Fig.1.42).

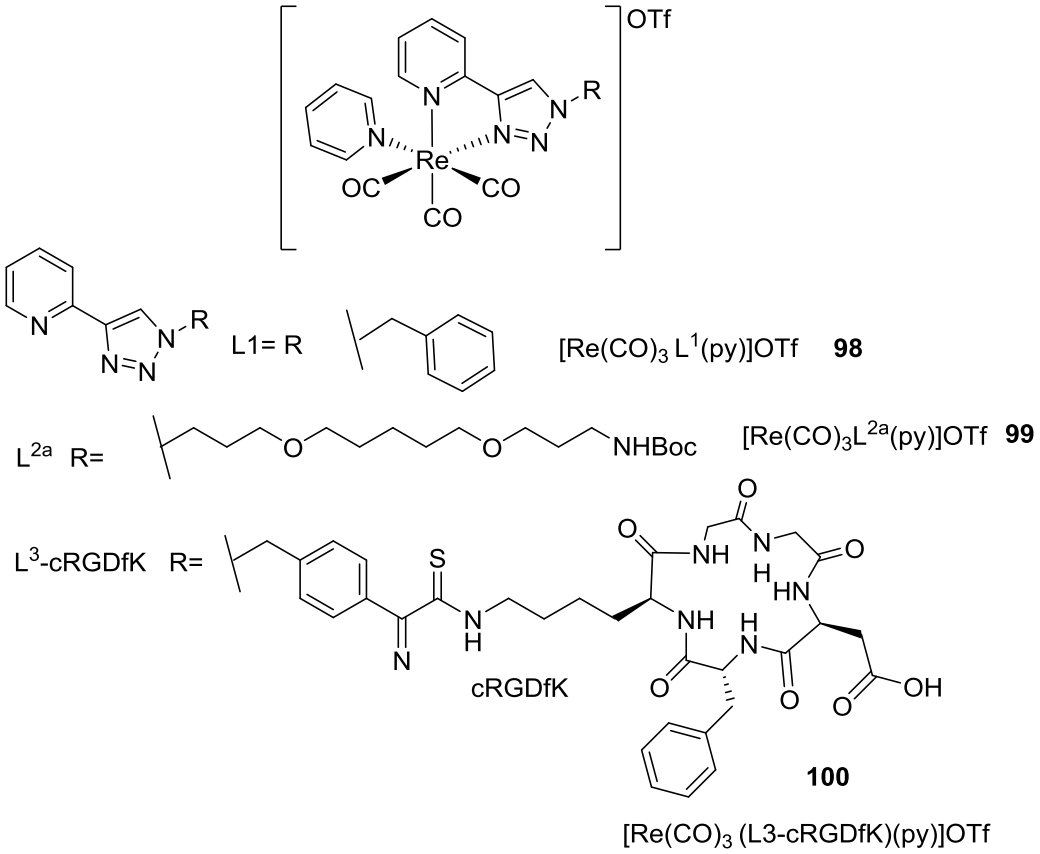

Figure 1.42: Re(I) complexes **98-100**

1.14 Luminescent Ir(III) Complexes as Biomolecular Probes and Imaging Agents

There are two types of cyclometallated Ir(III)complexes: homoleptic and heteroleptic. These are known to emit phosphorescence at ambient temperature and have high quantum yields. Various examples of heteroleptic cationic complexes, including a combination of two cyclometallated ligands and one diimine (e.g. bipyridine, phenanthroline or their derivatives), have been published, a study of how the electronic

excited state was effected by substitution into the diimine ligand was described.[118, 119] Heteroleptic complexes are readily tuned in terms of emission energy by changing the nature of the cyclometallated ligand C^N and the diimine ligand, or by adding electron withdrawing groups in order to have excitation at lower energy in the visible region.[120] Basically, 2-phenylpyridine (ppy) cyclometallated iridium(III) complexes and derivatives are highly emissive, and their photophysical properties and applications in sensing have been reported.[121] The family of complexes with the general formula $[Ir(ppy)_2(N^N)]^+$ (N^N = bpy) are the most widely utilized and are attractive for cell imaging purposes for many reasons: for instance, easy membrane uptake as they are monocationic. In addition, flexible tuning of their photophysical properties in both the cyclometallating and chelating ligands can be achieved as these contribute to the emission properties, allowing fine tuning across a wide range of wavelengths through a complex admixture of MLCT, ILCT, LLCT and sigma-bond-to-ligand charge-transfer (SBLCT).[122] Therefore, these features make iridium(III) complexes highly attractive candidates for biological imaging agents. The first attempt to use iridium complexes in fluorescent cell imaging and their application were begun in early 2008 by Li *et al.*[123] who found that **101** and **102** (Fig. 1.43) were showed good uptake by HeLa cells due to the fluorinated cyclometallates, which increase the lipophilicity and their cationic charge to internalize to the membrane and are localised in the cytoplasm rather than membrane or nucleus. Also, it was found that both complexes show low cytotoxicity.

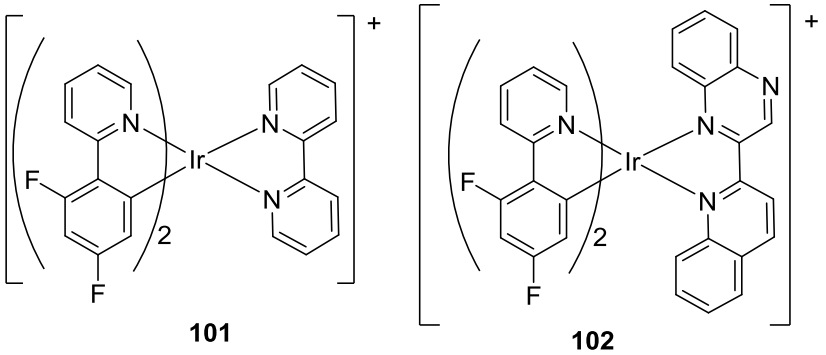

Figure 1.43: Iridium complexes **101** and **102**

Lo and co-workers reported a series of new luminescent iridium(III) polypyridine complexes bearing alkyl chains of varying lengths and studied the lipophilicity, cytotoxicity and cellular uptake properties of these complexes.[124] It was found that there was an increase in the magnitude of $\log P_{o/w}$ (**103c-105a**) (Fig.1.44) with increasing alkyl chain length, following the order C2 < C10 < C18, while cytotoxicity studies indicated

that the C10 complexes exhibited the highest cytotoxicity and the C18 complexes were non-cytotoxic. A flow cytometer was used to study the cellular uptake for all species **105a–c**; and whilst it revealed good uptake, there was a non-linear relationship between chain length and uptake according to the order **105b** > **105a** > **105c**. Confocal fluorescence microscopy showed that the distribution inside the cytoplasm after HeLa cells had been incubated with **105c** with a lesser amount of nuclear uptake. Thus, this study demonstrated that $logP_{o/w}$ measurements of lipophilicity are important factors in the design of imaging agents, and also that relatively small changes to the ligand structure can have significant effects in terms of cytotoxicity.

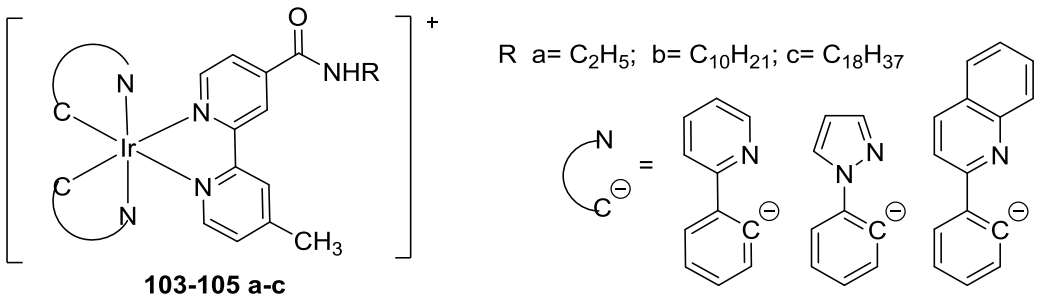

Figure 1.44: Synthesis Iridium **103-105 a-c**

Law *et al.*[125] investigated the lipophilicity, cellular uptake efficiency, and cytotoxicity of a series of cyclometallated iridium(III) polypyridine complexes appended with a β-D-glucose moiety with the general formula $[Ir(N^C)_2(bpy\text{-}TEG\text{-}ONCH_3\text{-}\beta\text{-}D\text{-}glc)]PF_6$ (Fig.1.45). This study indicated that the photophysical study for all complexes exhibited strong and long-lived green to yellow emission in solution under ambient conditions, while the lipophilicity of the iridium (III) complexes bt (**106**, **110** and **114**), pq (**108** and **112**), and bzq (**109** and **113**) complexes higher rather than their ppy (**107** and **109**) counterparts and cisplatin (−2.30).[126, 127]

Additionally, the cellular uptake of the complexes carried out by human cervix epithelioid carcinoma cells (HeLa) and measurement via ICP-MS experiments was undertaken, where it was found that there was a higher uptake of complex **114** compared with its less lipophilic sugar counterparts, complexes **106**.

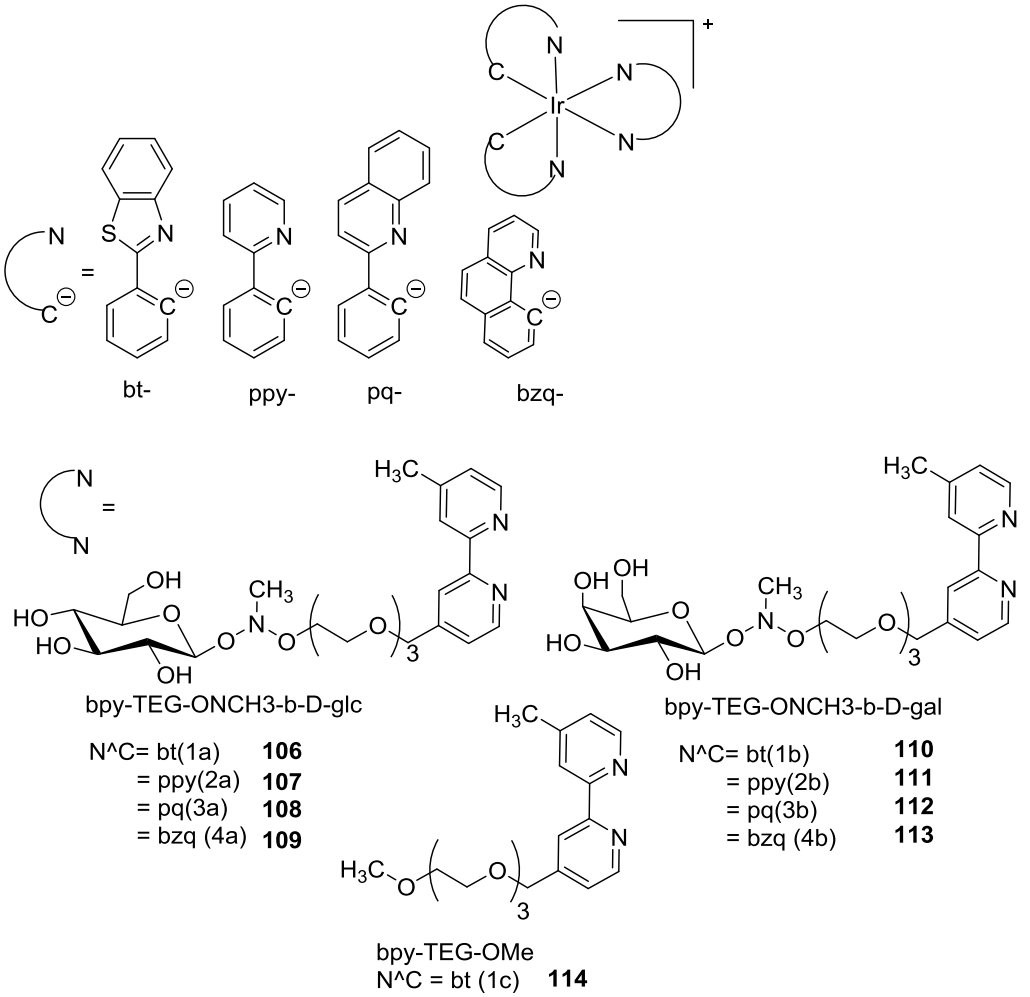

Figure 1.45: Series cyclometalated iridium (III) polypyridine complexes

It was noteworthy that the transport of bt−glucose complex **106** across the cell membrane through endocytosis was facilitated by different glucose transporters (GLUTs). Confocal microscopy indicated that complex **106** was localized in the mitochondria, which was a result of its cationic and lipophilic nature. In addition, complex **106** showed considerable photostability, which is much higher than the fluorescent organic compound 2-NBDG and low photobleaching. The cytotoxicity was evaluated by MTT assay toward HeLa cells by incubation for 48 h, from which it was revealed that all complexes had smaller IC_{50} values than that of cisplatin (22.3 μM). Thus, this study suggested that the iridium(III) glucose complexes with high photostability are excellent candidates for time-lapse cellular imaging applications.[125]

It has been confirmed that strong-field cyclometallating ligands (C^N) have wide HOMO-LUMO energy gaps that can result in iridium(III) complexes with high-energy emission and the same effect when used as ancillary ligand. Felici *et al.*[128] synthesized

new classes of iridium(III) complexes appended to the phenylpyridine (ppy) ligands as cyclometallating and pyt-Bcd resulting $[Ir(ppy)_2(R)]Cl$(R = methyl adamantane(ada), β-cyclodextrine) (Fig. 1.46), adamantane and derivatives have been widely applied as supramolecular building blocks in various areas including photoactivated electron transfer processes.[129]

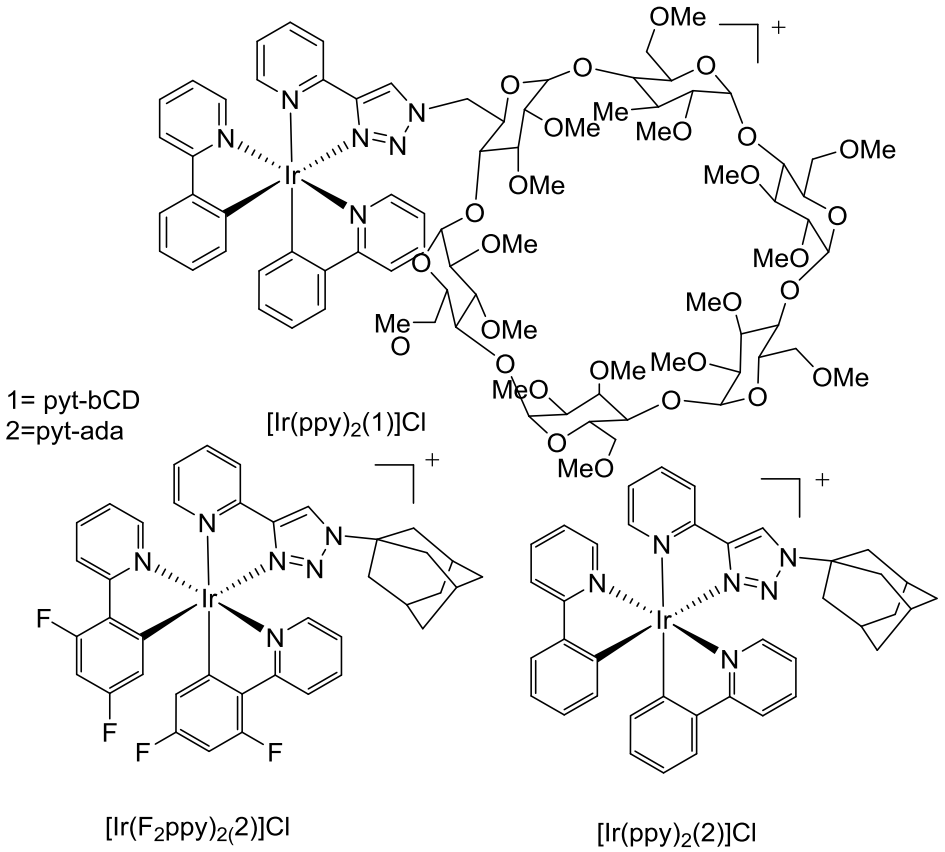

Figure 1.46: Structure of Iridium complexes

The photophysical properties showed that the cyclometallated Ir(III) complexes exhibit long lifetimes and have very high emission quantum yields. $[Ir(ppy)_2(ppy)]Cl$ has an emission quantum yield and lifetime of $\Phi = 0.54$, $\tau = 2800$ ns whilst the identical values for the complex $[Ir(ppy)_2(ada)]Cl$ are $\Phi = 0.23$, $\tau = 1000$ ns; the quantum yield and lifetime are enhanced in these complexes due to their increased rigidity for a metal complex. Iridium complexes exhibit higher luminescence, where the emission intensity is enhanced on going from the adamantane-appended $[Ir(ppy)_2(2)]Cl$ to the cyclodextrin-appended derivative $[Ir(ppy)_2(1)]Cl$. While the luminescence of $[Ir(F_2ppy)_2(2)]Cl$ (Fig. 1.46), which has a substituted fluorine on the phenyl ring, produces a bright blue emitting compound (450 nm), because it lowers the energy of the HOMO

orbital. Iridium(III) complexes appended to β-cyclodextrin enhanced luminescence properties, which allows their use in electrochemiluminescent devices with highly improved efficiencies.

To improve emission performances and sensing capabilities, Baschieri *et al.*[130] synthesized a new series of iridium complexes bearing pyridyltriazole appended to biotin $[(C\text{^}N)_2\ Ir(N\text{^}N\text{-spacer-X-CO-biotin})]^+$, where HC^N is 2-phenylpyridine, N^N is the neutral chelating (2-pyridyl)-1,2,3-triazole ligand, the term "spacer" refers to alkyl (−C11H22) or aromatic (p-phenyl- or 4,4-biphenyl-) chains, and X is NH or O (Fig.1.47).

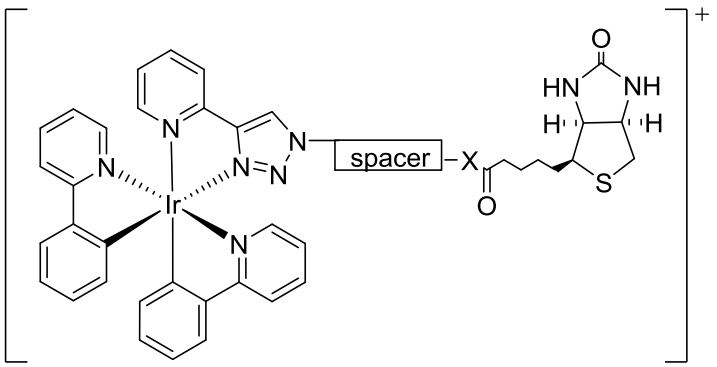

115 X=NH,spacer= $C_{11}H_{22}$ X= NH, spacer= C_6H_4 **117**
116 X=O, spacer= $C_{11}H_{22}$ X= O, spacer= C_6H_4 **118**

X= NH, spacer= C_6H_4-C_6H_4 **119**
X= O, spacer= C_6H_4-C_6H_4 **120**

Figure 1.47: Structure of iridium complexes **115-120**

This study revealed all six new Ir(III) complexes in both CH_2Cl_2 and aqueous solutions at room temperature displayed a bright blue-green colour. The emission profiles for these complexes exhibited an intense band centred at 480 nm and another intense band at 508 nm with quantum yields as high as 0.60 (complex **116**), all of which were quite long-lived. While the interactions of these new biotinylated complexes with avidin carried out by 4-hydroxyazobenzene-2-carboxylic acid (HABA) assays and emission titrations. Basically, the increase in emission intensity of the Ir(III) complexes indicated their interaction with the avidin. This study confirmed that the replacement of bpy-based biotin with other types of diimine ligand, such as pyridyl-1,2,3-triazole derivatives, in the structure of biotinylated Ir(III) could lead to enhanced luminescent properties which that might allow their use as intracellular sensors and bioimaging reagents.

Recently, Connell *et al.*[131] attempted to improve imaging probes by using a d^6 transition metal complexes as a labelling reagent for proteins as an alternative to certain organic compounds. A series of iridium(III) complexes (Fig.1.48) were synthesized with the general formula $[Ir(ppy)_2L1]PF_6$ and $[Ir(pq)_2L1]PF_6$. This study indicated that the electronic properties of the metal complex were not affected by changing the functional group of the ligand $L^{2\text{-}4}$ when compared with both complexes containing L1, which displayed emission at 506 nm for the $[Ir(ppy)_2L1]PF_6$ complexes, while the $[Ir(pq)_2L1]PF_6$ complexes exhibited a bathochromic shift in emission (λ_{em} = 559 nm) due to extending the conjugation of the cyclometallated ligand. Conjugation reactions were carried out by electrospray ionisation liquid chromatography mass spectrometry (ESI-LCMS) and SDS-PAGE under a UV source (λ_{ex} = 365 nm). All the metal complex conjugates migrated through the gel at the same speed as the native protein. The SDS-PAGE results revealed that the $[Ir(ppy)_2L4]^+$ complexes were less emissive than complexes with L2 or L3, with mass spectrometry confirmed this result, while L1 metal complex–protein conjugates showed the same emission spectra as complexes prepared with L2.

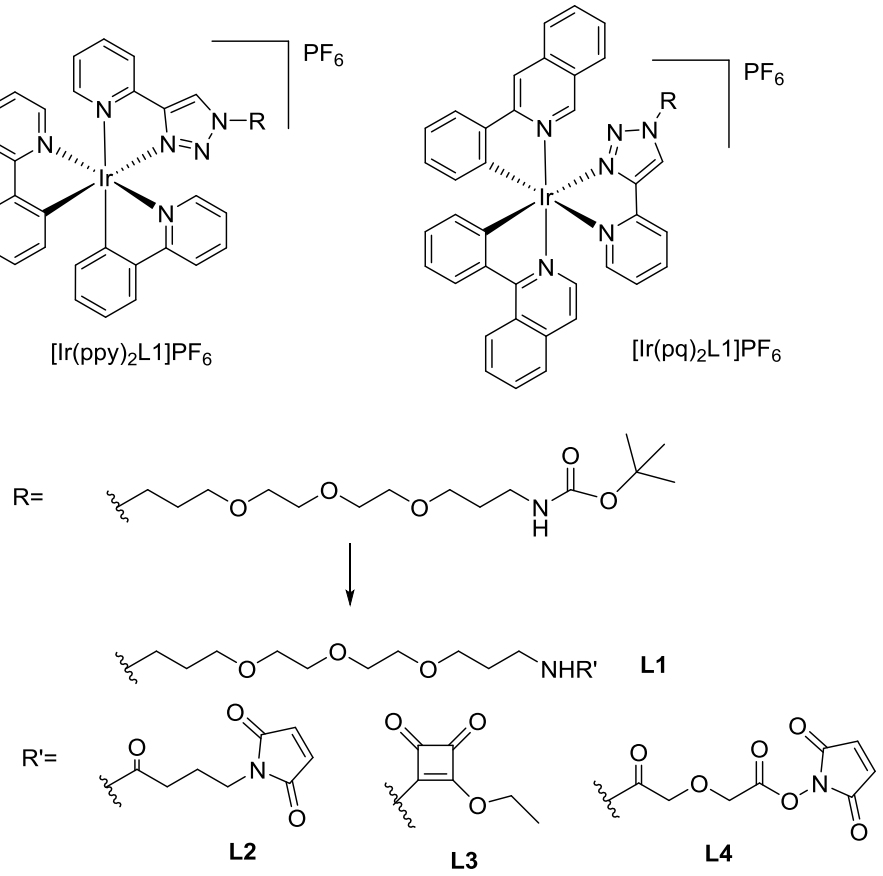

Figure 1.48: Series of Iridium (III) complexes

The study demonstrated that L1, which has a pendant amine, was further used to introduce functional groups, which were suitable for reaction with either cysteine residues, such as the maleimide derivative L2, or lysine residues of proteins, the squarate ethyl ester L3 and the *N*-hydroxysuccinimide activated ester L4. These new derivatives were conjugated to the metalloprotein Fe2Tf, this leads to continual visualization of the labelled protein in a cancer cell line. Thus, these complexes can be widely applied to other proteins and biomolecules and are also well suited to live cell imaging in protein trafficking.[132]

1.15 Aim of Thesis

The aim of this study to design new dyes based on rhenium(I) and iridium(III) complexes. The studies carried out by a previous group member suggested that the iridium/rhenium polyamine complexes were too hydrophilic to be of use in imaging synaptic vesicles and needed to be more ambiphlic like FM dyes. A hydrophilic complex is needed to internalize into the cell and a more hydrophobic one to interact with the surface of the neuronal cells. These complexes (Fig. 1.49) have features that resemble FM1-43FX dye in term of structure and function. A hydrophobic groups represented by cyclometallated ligands bearing phenyltriazole substituted with alkyl chain can be synthesized by using Click Chemistry or using phenylpyridine as cyclometallated ligands. Hydrophilicity is another requirement that needs to be achieved in order to deliver molecules into the cell; this can be carried out by using pyridyltriazoles appended with a polyamine. Combining the hydrophilic and hydrophobic features with Ir(III) or Re(I) should yield Ir(III), Re(I) complexes suitable as dyes for staining synaptic vesicles by both light and electron microscopy. Cationic rhenium(I) complexes are not toxic, an important requirement for complexes to be used as bioimaging probes. This is achieved by using a monodentate 4-substituted pyridine ligand with variable substitution, either a polyamine or hydrocarbon chain via replacement of the chloride in the natural rhenium(I) complexes. Also a triazole can be used instead of pyridine as a mono axial ligand. The important requirement these complexes should be excitation in a safe region of spectrum this can be achieved be adding electron withdrawing groups in the ancillary ligand or adding electron donating group in the cyclometaled ligand or adding both in some cases.

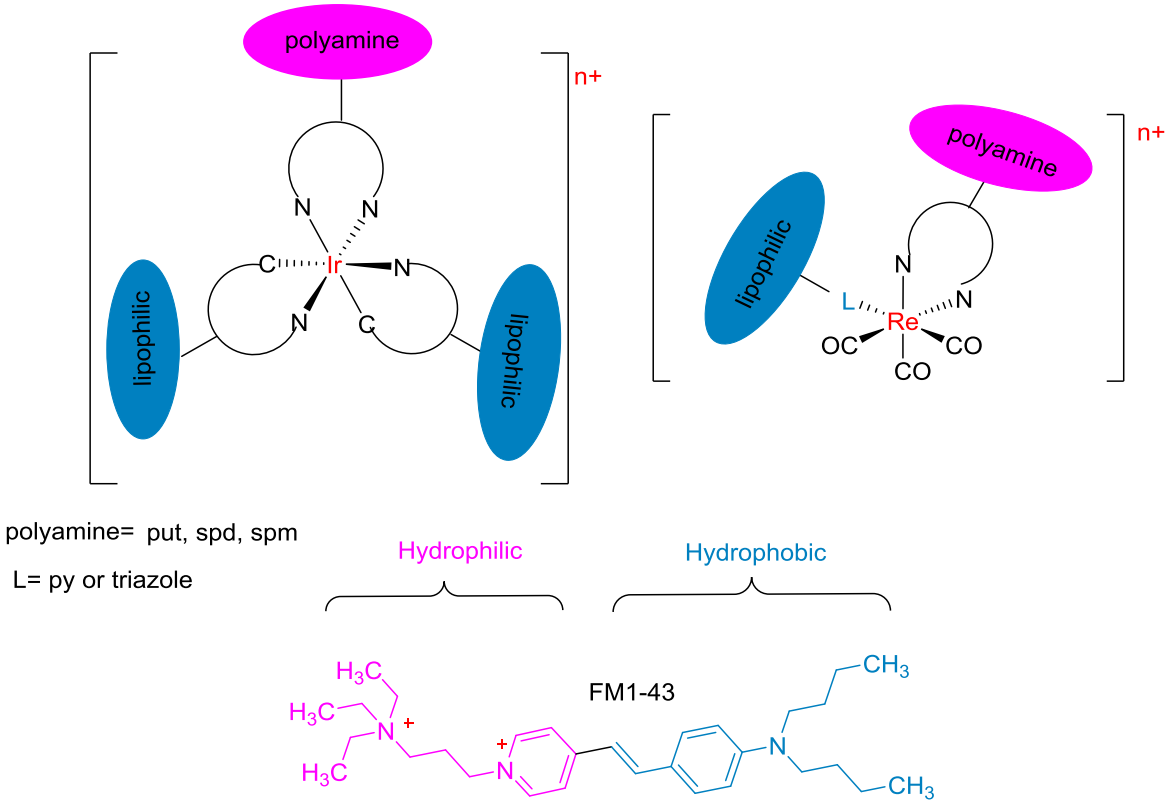

Figure 1.49: Design of new styryl dye

1.16 Thesis outline

Chapter **1** presents an introduction to polyamines and luminescent of transition metals as both rhenium and iridium complexes and an overview about their application. Chapter **2** discusses the synthesis of the three types of ligands involved ancillary ligands, cyclometllated ligand precursors and monodentate ligands by different types of reaction such as click reaction, Stille reaction and also Sonogashira reaction in order to prepare alkynes that contain electron withdrawing groups.

Chapter **3** describes the synthesis of rhenium(I) complexes with three different types of ancillary ligand: pyridyltriazole, bipyridine and inverse pyridyltriazole derivatives with two types of axial monodentate ligand 4-pyridine and triazole substituted with alkyl chain or polyamine. This chapter also involves the synthesis of cyclometalated iridium(III) complexes based on phenyltriazole or phenylpyridine, where the ancillary ligand is a pyridyltriazole-containing polyamine. Chapter **4** discusses the photophysical properties of rhenium(I) complexes and presents comparison in terms of effect of the

change in the structure of the ancillary ligand or in terms of the effect of the electron withdrawing or electron donating group on the photophysical properties. The photophysical properties of iridium(III) complexes were also investigated and comparison is made in terms of changes to the cycolmetalated ligand from phenyltriazole to phenylpyridine. Chapter **5** gives some outlook to the whole thesis and Chapter **6** presents the experimental part for all ligand and complexes synthesis. Finally Chapter 7 presents the appendix for HPLC and X-ray crystallography.

Chapter 2

2 Synthesis of Ligands

2.1 Chemistry of Conjugation

Polyamines are considered one of the most important molecules in many cellular processes.[133] As mentioned in the Section **1.1**, there are three natural polyamines: putrscine, spermidine and spermine.[1] Polyamine transporters are able to recognize these polyamines and other polyamine analogues; indeed, there is a relationship between this transporter and the polyamine structures.[134] For recognition it is necessary to have at least two positive charges and four methylene or propylene groups. Spermine is readily recognized by the PTS, while putrscine and spermidine with less positive charge show less uptake. In addition, the hydrophobicity of polyamines is another important factor that modulates their interaction with other macromolecules.[135] Previous work has shown the relationship between the charge and the binding to the polyamine transporter to be one of more charge allowing tighter binding.[5] This study uses natural polyamines such as spermine, spermidine, and putrscine as commercially available starting materials to which a protection group was added to protect one NH_2 on putrscine, two amino groups on spermidine and three on spermine; each reaction requires different conditions and reagents the synthesis of protected polyamine in this thesis are shown in the Scheme 2.1.

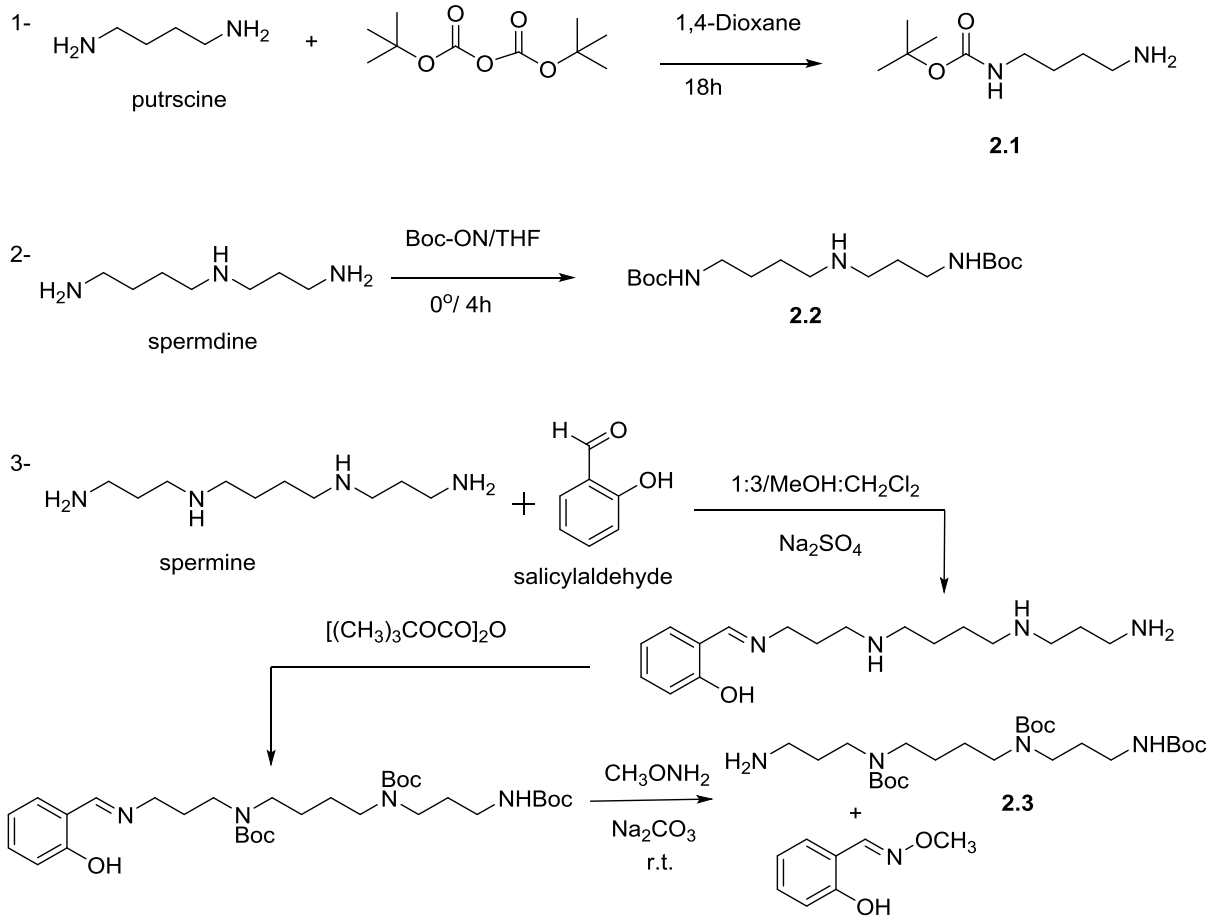

Scheme 2.1: Synthesis of Boc-protected polyamines

In route 1 and 3 reactions, di-*tert*-butyl dicarbonate was used to protect the amino group for puterscine and spermine, Boc-protection was achieved using 1,4-dioxane as a solvent, a high yield of **2.1** was obtained without any further purification due to the side products being dissolved in water during the extraction. Spermidine has a different selectivity for its protected primary amines, where Boc-ON was used as a reagent to get these primary amines to give **2.2** other reactions; this reagent is inert towards reaction with the secondary amino group.[136] Spermine has four amino groups, three of which required Boc-protection, leaving one terminal free NH_2, di-*tert*-butyl dicarbonate was used to this purpose. *Tert*-butyl dicarbonate (Boc) group is widely used for amine protection because it is both easy to introduce and is easily and cleanly removed,[137, 138] furthermore, it is generally stable to a wide range of difficult reaction conditions. A different strategy was used to synthesise **2.3**. The first step was to protect one primary amine using 2-hydroxybenzaldehyde to produce a salicylimine, after which di-*tert*-butyl

dicarbonate was added to protect the three amine centres of spermine *in situ.* Methoxyamine was added to hydrolyse the imine *via* imine exchange giving the primary amine with the desired Boc-protection **2.3**. The three Boc-protected polyamines were characterized by ^{1}H NMR spectroscopy, though the 3.33-1.44 ppm region. A slow rotation was obtained on the NMR experimental timescale around the carbon-nitrogen bond for these Boc groups; the two rotamers (E/Z) are seen to cause a broad signal in this region (Scheme 2.3). It was found that three different *tert*-Bu signals were in an essentially identical region of the spectrum with one signal integration, rather than a separate integration for each. To address this problem, VT-NMR was used by increasing the temperature from 298 K to 323 K, the rate of rotation is increased, hence increasing the resolution of the peaks, potentially allowing the individual signals to be distinguished. Despite this increased resolution, however, it was still difficult to entirely separate the multiplicities of these peaks due to the continued presence of the rotamers.

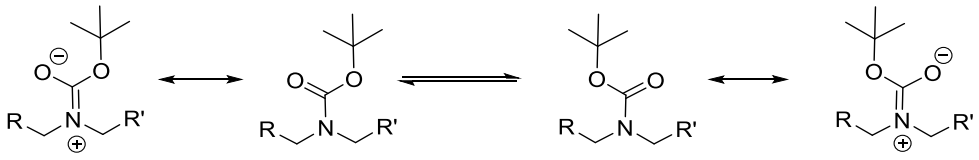

Scheme 2.2: Rotamers of Boc groups in polyamines

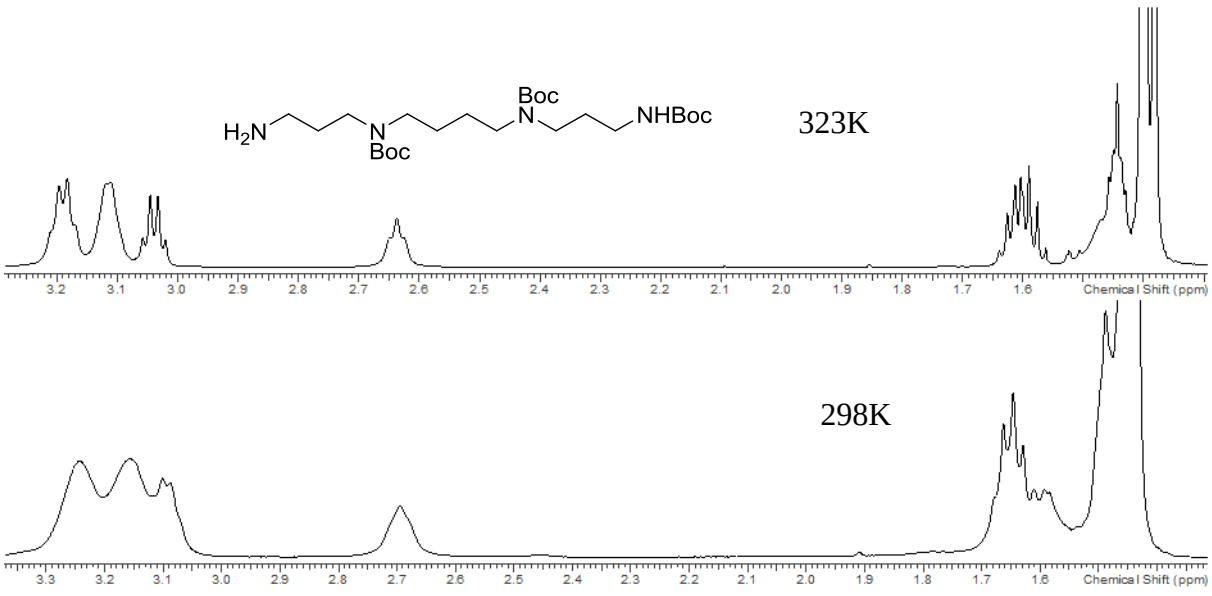

Scheme 2.3: ^{1}H NMR spectra of **2.3** at 323K and 298 K

2.2 Click Chemistry

The concept of "Click Chemistry", as developed by K. B. Sharpless in 2001, can be characterized by a high yielding, stereospecific and simple to perform reaction. This reaction involves small units being joined together with heteroatomic links (C-X-C) in a manner producing few or no by-products; those that are, can be removed without chromatography, which can usually be completed in easily removable or benign solvents. In 2002, the research groups of Fokin and Sharpless[139, 140] and Meldal *et al*. described the Huisgen Reaction, which is an azide/alkyne cycloaddition that produces a mixture of 1,4 - and 1,5-disubstitution products, while the CuAAC reaction of terminal alkynes is completely selective towards the formation of 1,4-disubstituted triazoles. The reaction is easily carried out under ambient or mild conditions in organic or aqueous solvents, or even in water.

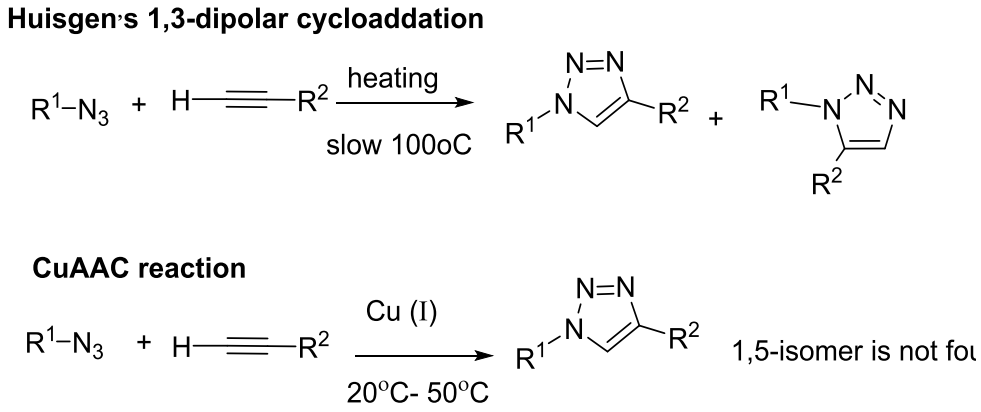

Scheme 2.4: Huisgen reaction

A variety of Cu(I) catalysts are used in the CuAAC reaction to produce a 1,2,3-triazole ring.[139] Cu(I)-catalysed azide/alkyne cycloaddition (CuAAC) is an important branch of the "click" reactions.[141] Since the CuAAC reaction was known, it has been very popular as a "click" reaction due to the fact that it is so easy to carry out and widely applicable as shown in Scheme 2.4. A wide variety of copper catalysts are used in CuAAC reactions as Cu(I) species, which are generated during the reaction itself.[140] A Cu(II) salt (usually $CuSO_4$) is used as the pre-catalyst and is subsequently reduced to Cu(I) by a reducing agent (usually sodium ascorbate). The mechanism of the CuAAC reaction was determined using kinetic studies and DFT calculations.[142, 143] It was suggested that

the pH of the reaction should be at pH 9.8 which leads to deprotonation of the alkyne and then coordination to Cu(I) to form an alkynyl-Cu(I) species as the intermediate.[144] The azide then attaches to the same Cu centre bearing the alkynyl ligand, as shown in scheme 2.4.[145]

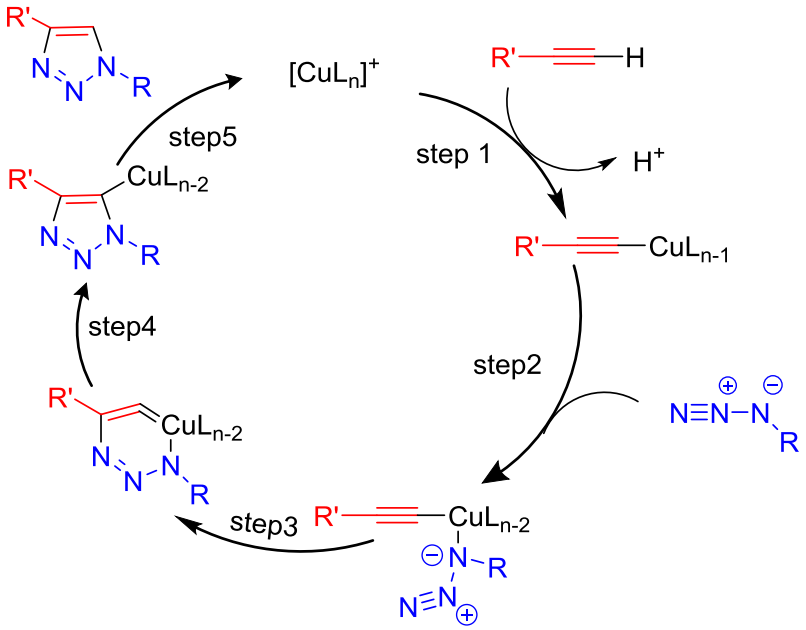

Scheme 2.5: Proposed mechanism of CuAAC reaction[146]

This cycle can be summarised as follows: the first step is the formation of Cu(I) acetylide; the second step requires the addition of an azide derivative; the third step sees the formation of a metallaheterocycle; and the last step a copper triazoide derivative is obtained, which is protonated to yield a 1,2,3-triazole.[146]

Over the last decade there have been many attempts to enhance the click reaction via non-conventional energy sources like microwave heating, ultrasound and photo-induced reactions being used rather than conventional chemical reaction. This method is considered a powerful technique by which to enhance the reaction rate of various chemical transformations. Recently, a few microwave-Cu(I)-coupled click chemical methods have been reported.[139] Microwave activation was applied with Cu(I) catalysis to enhance the 1,3-dipolar cycloaddition between azide and terminal alkynes under solvent-free conditions to afford the corresponding 4-substituted 1,2,3-triazole.[147] Appukkuttan *et al.*[148] were able to successfully decrease the associated reaction time from hours to minutes and enhance the product yield when using different alkyl halides and alkynes containing various functionalities when irradiated with microwave

radiation. In this study, the azide is generated *in situ* from the corresponding halides (Scheme 2.6), whereupon they are captured by copper(I) acetylides, forming the corresponding 1,4-disubstituted 1,2,3-triazoles. Performing both steps of this process under microwave irradiation significantly reduces the reaction time. Simple filtration was used to isolate the products.[149]

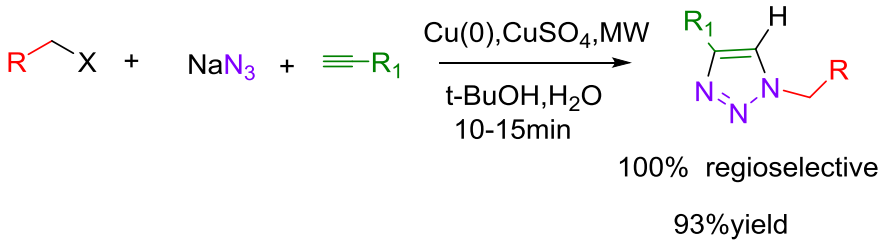

Scheme 2.6: 1,4-Disubstituted 1,2,3-triazoles

It was found that this approach could reduce the reaction time with efficient production of the 1,4-disubstituted-1,2,3-triazoles in a completely regioselective manner, which often crystallize out from the reaction mixture and do not require any additional purification. This method could avoid isolation and handling of potentially unstable small organic azide and provides a method of obtaining triazole products in their pure form.[148]

In the same way, Beckmann and Wittmann used microwave irradiation to generate 1,4-disubstituted-1,2,3-triazoles from amines.[150] This reaction is a one-pot procedure for diazo transfer and subsequent azide–alkyne cycloaddition using trifluoromethanesulfonyl azide to convert the amine group to an azide.[151] (Scheme 2.7)

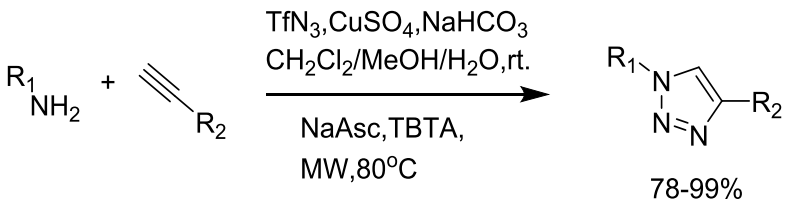

Scheme 2.7: Microwave irradiation to synthesise 1,4-disubstituted-1,2,3-triazoles

2.2.1 Synthesis of Phenyl/Pyridyltriazole Ligands Bearing Alkyl Chains

In this study, both classical and non-classical conventional reactions are considered appropriate base steps for the preparation of different types of 1,4-disubstuted-1,2,3-triazoles which can be used as linkers between metals and polyamines or to bear an

alkyl chain to enable the complex to interact with the cell membrane; in this latter case, three ligands, **L1**, **L2,** and **L3** were prepared in a conventional reaction with yields of 76%, 73%, and 81%, respectively. The preparation of these three ligands was based on CuAAC reactions which involved the reaction between a bromoalkane and sodium azide. This step was carried out *in situ* for 24 hr and required a co-solvent to ensure the solubility of more hydrophobic reactants.[152] Sodium azide should be added in excess in the first step to ensure full conversion; after heating at 90ºC for 24 hr, TLC analysis showed the reaction had gone to completion, and all the starting material had been converted to azide. The azide products are not be isolated as, due to their low molecular weight, they could potentially be explosive, particularly when the total number of carbon (C) plus oxygen (O) atoms is less than the total number of nitrogen atoms (N) by a ratio of three.[153] The aryl acetylenes were added followed by sodium ascorbate, the latter acting as a reducing agent to generate Cu(I) species from $CuSO_4.5H_2O$, which then produced the desired product with good yield; these results are quantitatively similar to whose previous result reported in the literature.[148] However, the yield was increased to about 90% when microwave irradition was used for the same reaction. The microwave method reduces both the reaction time and number of by-products; in this case, there were no by-products, so the main products in these three reactions do not require any further purification, as shown in Scheme 2.8.

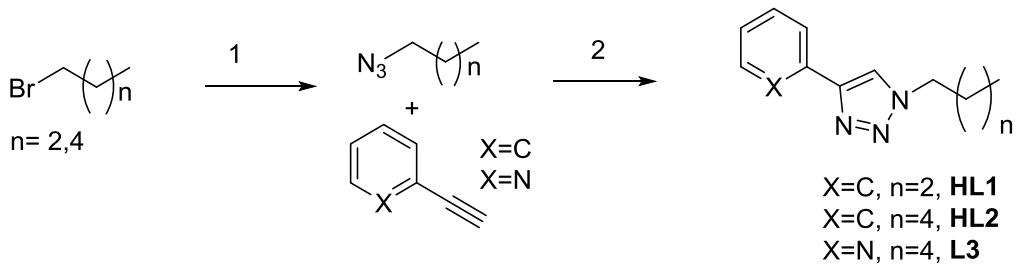

Scheme 2.8: Synthesis **L1-3** ligand, 1) NaN_3, $EtOH/H_2O$ (7:3) at 90º for 18h 2) $CuSO_4.5H_2O$, Na-ascorbate at 60º

The ^1H NMR characterization of the products confirms that the triazoles were successfully synthesised, with a characterisatic singlet peak seen at 7.74 ppm for **HL1** and **HL2** and 8.12 pm for **L3**, corresponding to the CH of the triazole in each case. No peak is seen for the alkyne, which confirms that all of the starting materials were used in the reaction. A characterisation triplet resonance is also noted at 4.39, 4.36 and 4.41 pm for **HL1**, **HL2** and **L3**, respectively, corresponding to the methylene group nearest to the

triazole ring. **HL4** was prepared by following the CuAAC reaction which starts with the synthesis of the azide compound followed by cycloaddition of the alkyne (4-ethynyl anisole). This alkyne is substituted with electron donating-OMe group in *para* position as shown in the Scheme 2.9. It was found that the addition of donating groups like Me, OCH_3 in the phenyl ring could be increase the electron density that donate to metals during the coordination which results in stabilising the HOMO and increasing the HOMO-LUMO energy gap (more details in Chapter 4).

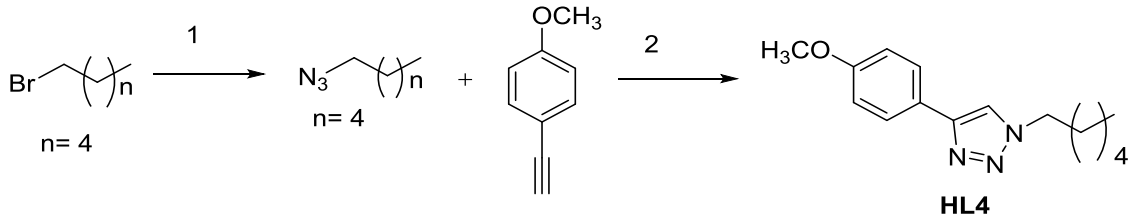

Scheme 2.9: Synthesis of **HL4**, 1) NaN_3, $EtOH/H_2O$ (7:3) at 90º for 24h; 2) $CuSO_4.5H_2O$, Na-ascorbate at 60º

^{1}H NMR spectroscopy of **HL4** shows a singlet signal at 7.6 ppm corresponding to proton of triazole ring and two doublet signals were observed at 7.7 and 6.9 ppm assigned to proton of phenyl ring and also singlet signal was observed at 3.8 ppm attributed to the protons of OCH_3 group. The triplet signal was observed at 4.36 corresponding to the protons of the methylene adjacent to triazole ring which confirmed that reaction was successful.

2.2.2 Synthesis of Pyridyl Triazole Ligands Bearing Polyamines

The click reaction was also used to synthesise a series of ligands which contain polyamines; however, these types of reaction require diazo-transfer to create the azido compound; this route starts with amine compounds represented by protected polyamines such as **2.1**, **2.2** and **2.3** instead of a bromoalkane. The reagent used to convert the amine group to an azide via diazo-transfer reaction is imidazole sulfonylazide. The reagent that was commonly used in the diazo-transfer reaction was trifluoromethanesulfonyl azide, but this reagent is high cost and unstable in the absence of a solvent.[154] Thus, methanesulfonyl azide has been used as an alternative to trifluoromethanesulfonyl azide due to it being more stable and cheaper as a start material.[155] However, it is less reactive as this reagent is oily and it needed to be freshly prepared before each reaction. Recently, imidazole-1-sulfonyl azide hydrochloride

(ISA-HCl), was found to act as an inexpensive and effective diazotransfer reagent, but is itself sensitive and of a limited shelf life and decomposed when left for a long time.[156] Imidazole-1-sulfonyl azide hydrogen sulphate ($ISA.H_2SO_4$) is typically the best reagent in this instance due to it being easier and less expensive to prepare than the hydrochloride salt (ISA-HCl), and it can be stored with the exclusion of moisture to prolong its shelf life. It is significantly safer to handle than ISA-HCl, which makes it the recommended alternative to the hydrochloride, ISA-HCl.[154]

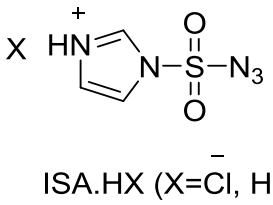

ISA.HX (X=$\bar{Cl}$, $H\bar{S}O_4$)

Scheme 2.10: Structure of imidazole-1-sulfonyl azide

The diazo-transfer reaction involves the conversion of a primary amine into an organic azide by the action of a powerful diazo donor represented by imidazole-1-sulfonyl azide as a salt, followed by the CuAAC reaction to produce triazole derivatives. This route was used to prepare the ligands **L5.Boc** and **L6.Boc**. As shown in Scheme 2.11:

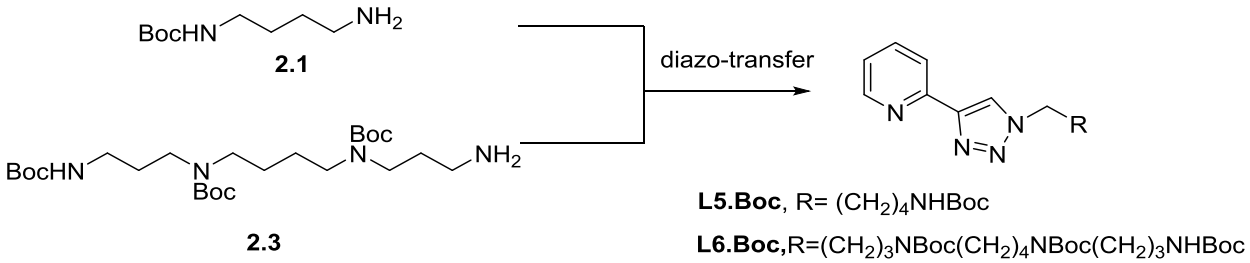

L5.Boc, R= $(CH_2)_4NHBoc$

L6.Boc,R=$(CH_2)_3NBoc(CH_2)_4NBoc(CH_2)_3NHBoc$

Scheme 2.11: Synthesis of **L5.Boc** and **L6.Boc**: $ISA.H_2SO_4$, $NaHCO_3$, $CuSO_4.5H_2O$, Na-ascorbate and aryl acetylene at r.t.

The catalysis for both the diazotransfer and the cycloaddition is achieved via the same metal, but in different oxidation states. With regards to the previously proposed mechanism of the diazo-transfer reaction by Fischer and Anselme, it was suggested that the amine compound complexes to the copper catalyst, and then azide undergoes nucleophilic attack by the amine owing to its high electrophilicity, followed by deprotonation, which might form the copper-stabilized mixed tetrazene. The tetrazene ring is then broken down to produce the azide product via a reverse reaction.[157]

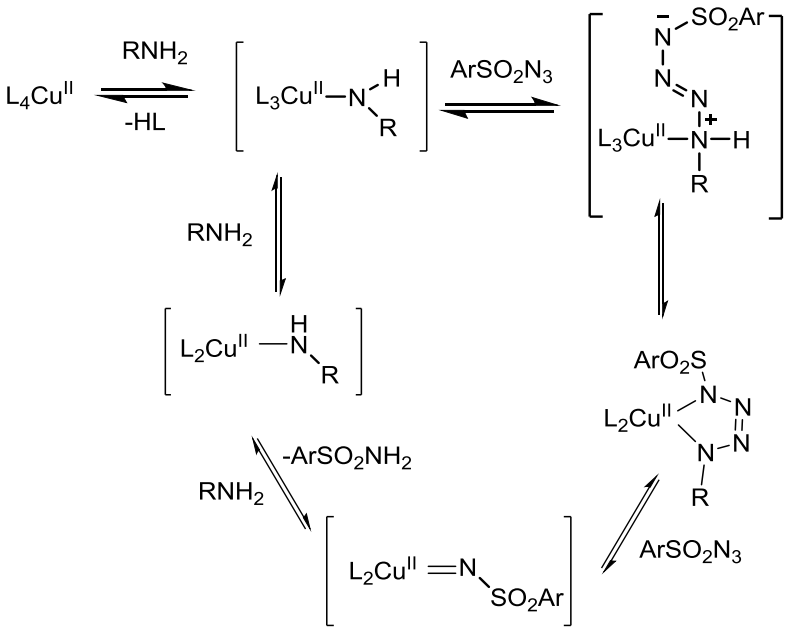

Scheme 2.12: Proposed mechanism of diazo-transfer[157]

Compelling evidence was presented by Pandiakumar *et al.*[158] that the diazo-transfer reaction involves the transfer of the two terminal nitrogen atoms of the azidating agent to the amine to form the azide. This study was carried out using labelled amino acids such as L-valine and L-isoleucine, and also confirmed the metal catalyst has no effect on the site of the amino attack. This study was confirmed by a previous study by Anselme.[159]

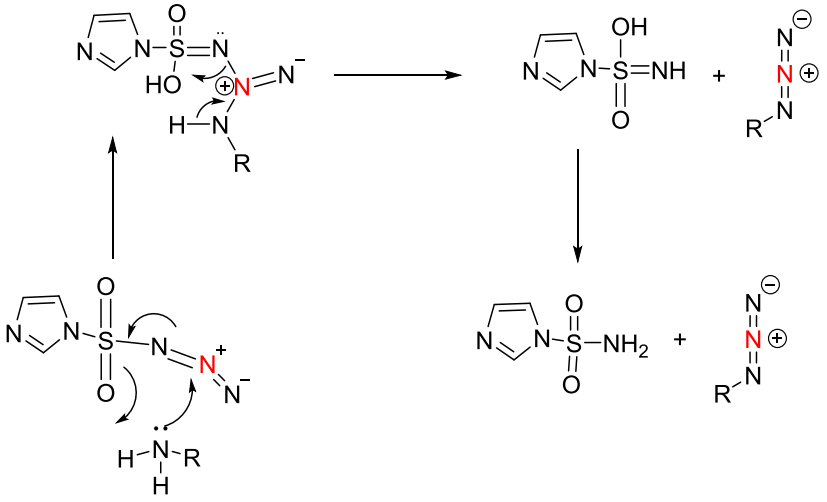

Scheme 2.13: Mechanism of diazo-transfer

The ligands **L5.Boc** and **L6.Boc** were prepared by diazo-transfer (Scheme 2.13). This route started with the Boc-protected polyamine, which contained the primary amine,

and then imidazole sulfonyl azide was added carefully in small batches to prevent any possibility of explosion. This reaction should be carried out at pH ~8, so $NaHCO_3$ is added in a 10-fold equivalent to the spermine, which leads to deprotonation by the copper catalyst, which gives convincing evidence as to the mechanism of diazo-transfer, as mentioned previously. The copper catalyst represented by $CuSO_4.5H_2O$ and sodium ascorbate play a key role in this reaction. TLC analysis showed that all amine converted to the azide after that sodium ascorbate and 2-ethynyl pyridine were added and the colour of solution changes from blue to yellow and then to brown as reduction of Cu(II) to Cu(I) occurs . The conventional reaction has a yield of 76%, while the highest yield is obtained when the reaction was performed in a microwave, at about 95%. After workup, further purification is needed for both products. All products were characterized via COSY, HSQC and HMBC NMR spectroscopy.

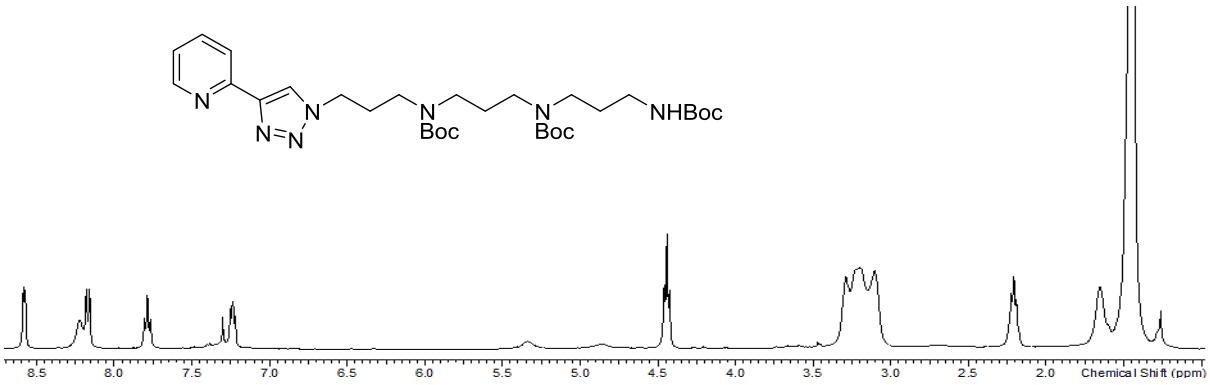

Scheme 2.14: ^{1}H NMR spectrum of **L6.Boc** at 298 K in ($CDCl_3$, 400 MHz)

2.3 Palladium-catalyzed Cross-couplings

Palladium is considered one of the more important transition metal catalysts which is used to synthesise a varity of compounds contain C-C bonds by generating Pd(0) active species in *situ*. This catalytic metal is applied to different synthetic reactions such as Heck,[160] Stille,[161] Negishi,[162] SuzukieMiyaura[163] and Hiyama.[164]

2.3.1 Sonogashira Reaction

The Sonogashira reaction is one of the most effective methods to form new carbon-carbon bonds.[165, 166] This study uses this reaction to react terminal alkynes with aryl halides to produce only one alkyne, **2.4** (Scheme 2.20) that is required for the synthesis

of another ligand. Since this reaction was independently discovered by Heck,[167] Cassar[168] and Sonogashira,[163] the Sonogashira reaction has been widely used in the synthesis of substituted alkynes and conjugated alkynes (Scheme 2.15).[169, 170] Usually, this reaction is carried out in the presence of catalytic amounts of palladium(II) complexes as well as copper(I) iodide in an amine as solvent.[171]

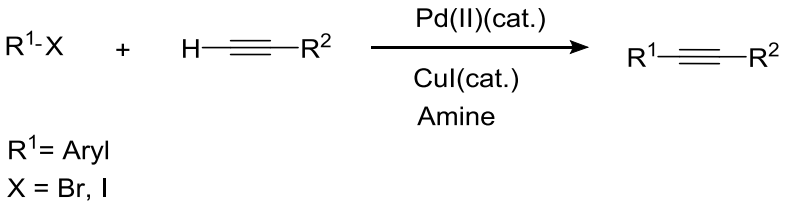

Scheme 2.15: Sonogashira reaction to synthesise alkynes

There are many problems with this reaction, one of which is that the aryl bromide is less reactive, so this reaction needs to run in harsh conditions. In this reaction homocoupling also occurs when oxygen is not excluded completely.[172] After many studies of Sonogashira reactions considerable research has been conducted in the attempt to overcome the obstacles presented by this reaction. One of these attempts, by Stephan *et al.*, found that when used in varying reaction conditions, good to excellent yields are obtained when the coupling is carried out with THF as a solvent instead of an amine (Scheme 2.16). Furthermore, it has been found that homocoupling is reduced by slow addition of the alkyne.

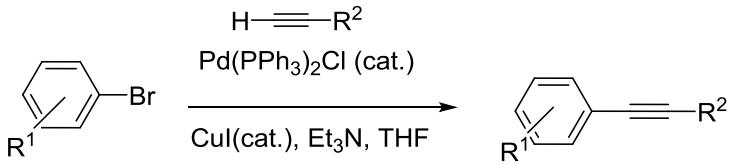

Scheme 2.16: Sonogashira reaction to synthesise aromatic alkynes

It was found that this method achieved a 92% yield when using R^1 = 4-COMe, R^2 = Me_3Si at 25ºC for 1 hr, comparable with literature when using only Et_3N as a solvent.[173] For many years the microwave irradiation of organic reactions has proved to be popular cf. other techniques, a new methodology was suggested by Pagni *et al.*(Scheme 2.17),[174] this method is based on coupling microwave irradiation with a solid-state, solvent-free synthesis. This involves the use of a solvent-free mixture of potassium fluoride on alumina under conditions of microwave irradiation. A green reaction was gained via this

reaction with high yields of the desired aryl alkynes, also this study indicated that electron-donating and withdrawing groups enhanced the yield.

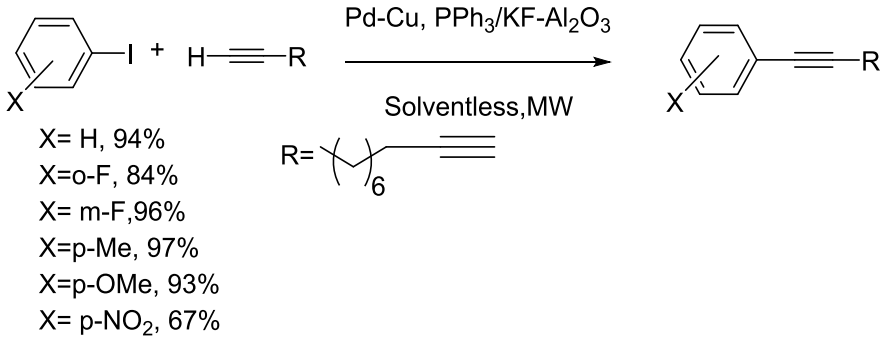

Scheme 2.17: Sonogashira reaction to synthesis alkynes in microwave

A successful study by Gogoll *et al.* reported that the reaction conditions provide good to excellent yields in the region of 80-97% within a few minutes in a microwave (Scheme 2.18), as compared to hours or days when conventional literature conditions and different aryl halides are used.[175]

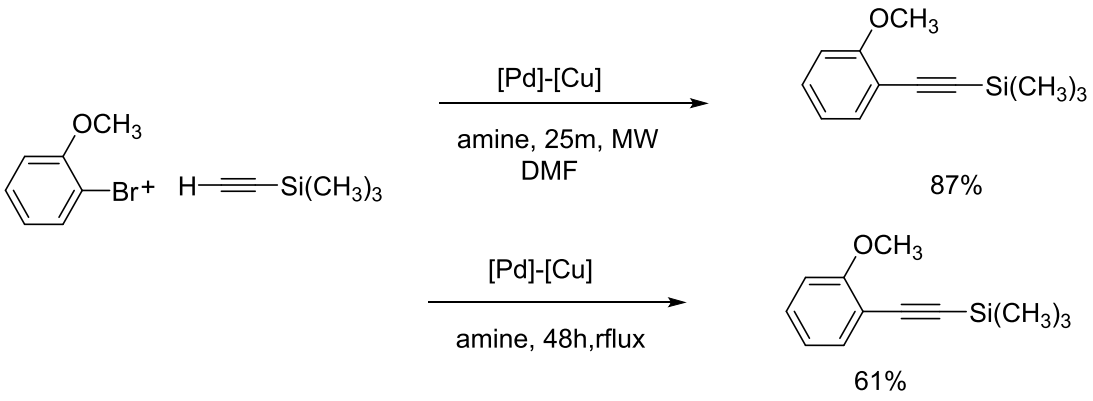

Scheme 2.18: Sonogashira reaction to synthesise alkynes using microwave and conventional methods

The Sonogashira reaction mechanism is still not fully understood, even though there are many studies that have been reviewed, due to the difficulties in explaining the combined action of the two metal catalysts present. As shown in (Scheme 2.19), there are two cycles, the first of which is a palladium cycle, as started by the catalytically active species $Pd(0)L_2$ which is formed from $Pd(PPh_3)_2Cl_2$, and where the first step in this cycle is oxidative addition of the aryl halide (considered to be the rate-limiting step of the Sonogashira reaction).

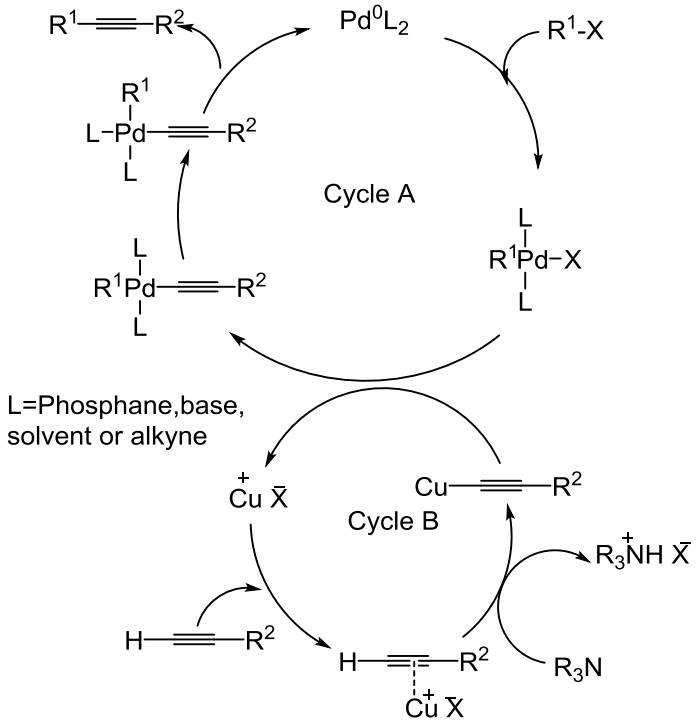

Scheme 2.19: Proposed mechanism of Sonogashira reaction[176]

The next step is the formation of [Pd(II)R^1L2X] which is then transformed into a [Pd(II)L2R^1($CR{\equiv}CR_2$] species after transmetallation with a copper acetylide formed in the 'copper cycle' (cycle B). This adduct suffers reductive elimination, after cis/trans-isomerization to produce the final alkyne and regenerate the catalyst, [Pd(0)L2]. The role of the amine in this cycle is a scavenger for excess hydrogen halide.[176] This method was applied in the preparation of **2.4** (Scheme 2.20), many attempts have been tried to improve the yield, the first attempt to prepare this ligand resulted in a low yield (74%) when using 2-bromo-5-(trifluoromethyl)pyridine with trimethylsilylacetylene and in presence of $Pd(PPh_3)_2Cl_2$ with CuI as a catalyst, PPh_3 and triethyamine as both a solvent and base. This reaction was carried out in dry conditions as the palladium catalyst is sensitive to moisture, and is heated at 50ºC for 1 hr under N_2. A (74%) yield was obtained by this method after purification by column chromatography due to the presence of a degree of homocoupling it assumed that using an excess of trimethylsilylacetylene, which causes this homocoupling. In terms of reaction time, this yield compares well with that reported (5h, 80%) in the literature.[175] The second attempt to prepare **2.4** showed an improvement in yield from good to excellent (90%) when carried out in a Schlenk tube with the same starting materials, in addition to toluene as a solvent and a reduced quantity of trimethylsilylacetylene from 4 to 1.1 equivalents with slow addition of TMS to the mixture reaction to minimize side reactions such as

homocoupling.[177] This reaction required dry equipment and an inert environment. The solution was heated at 110ºC to ensure that all starting materials were consumed, as confirmed by TLC analysis in a reaction that takes about 1 hr. This is shown in the scheme below:

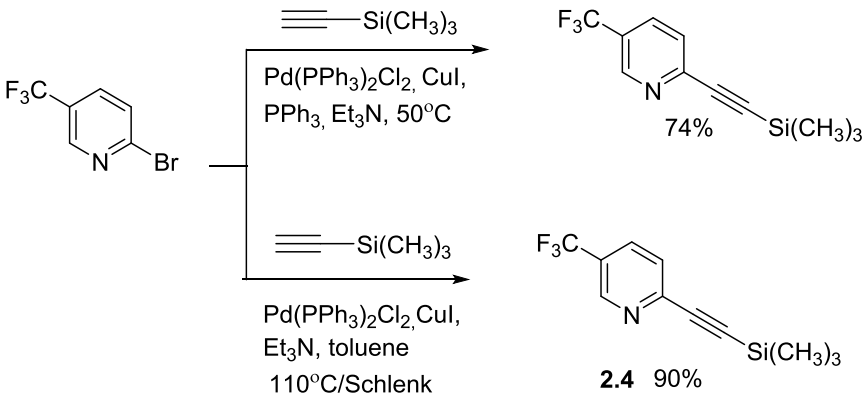

Scheme 2.20: Synthesis of **2.4**

This compound was characterized using NMR techniques such as COSY, HSQC, HMBC, and also mass spectroscopy. This product was synthesised for use in the click reaction to prepare a pyridytriazole was substituted with an electron withdrawing group (**L7.Boc, L8.Boc**) (Scheme 2.21) to see if this substituent had any effect on the photophysical properties of the complex after coordinating with the ligand. More details are shown in Chapter 4.

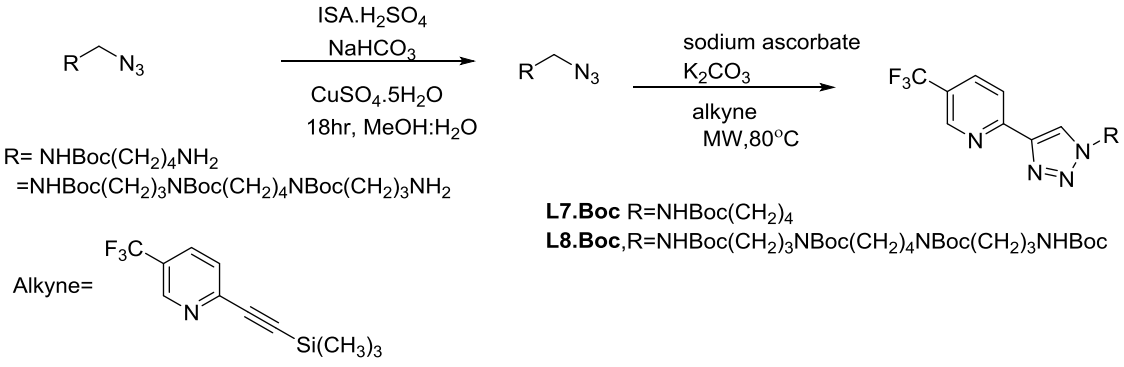

Scheme 2.21: Synthesis of **L7.Boc** and **L8.Boc**

Another group of ligands were synthesised using **2.4**, but starting with 3-bromopropanol instead of polyamines, resulting in pyridyltriazole substituted with a CF_3 group bearing a propanol which is then converted to the chloride required to react with Boc-Spermdine

(as a branched polyamine) to produce the pyridyltriazole linker to this branched polyamine, as shown in Scheme 2.22.

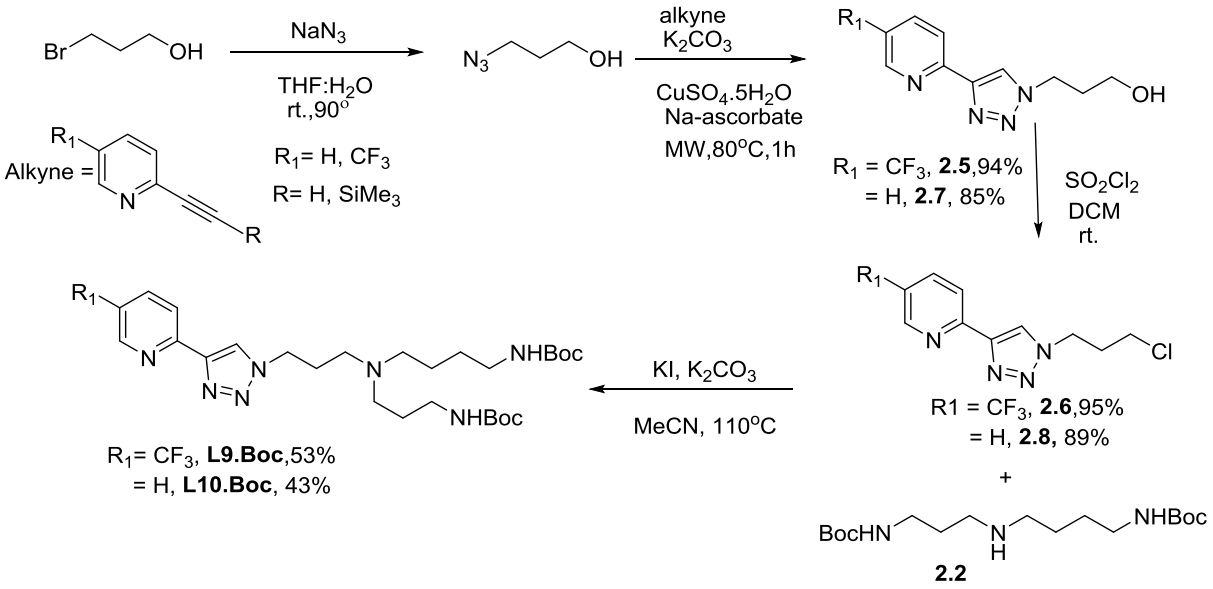

Scheme 2.22: Synthesis of **L9.Boc** and **L10.Boc**

L9.Boc was prepared via an S_N2 mechanism, as shown in the scheme 2.23.

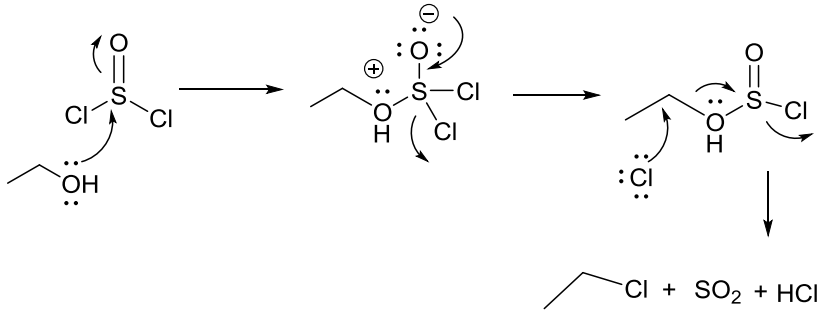

Scheme 2.23: Mechanism of S_N2

This reaction gave a high yield with less impurity because the side products are gases and thus are easy to remove from the reaction mixture. ^{1}H NMR spectroscopy of **2.5** shows a singlet signal at 8.28 ppm corresponding to proton of triazole ring, and also shows two triplet signals, one at 4.61 ppm assigned to protons of methylene group close to triazole ring and another triplet at 3.80 ppm assigned to protons adjacent to OH group. The product **2.5** is used for another reaction to synthesise **2.6** via an S_N2 nucleophilic substitution.

Initiate attempts to synthesise **L9.Boc** using K_2CO_3 gave low yields. However, an improvement in yield was gained when using both K_2CO_3 and KI because the iodide replaces the chloride in the presence of an aprotic solvent such as MeCN leading to an increase in the interaction between the nucleophile and carboncation, making the reaction proceed faster. Also, the addition of a base is required for this reaction because the amine used is a secondary amine, and the associated rate order is 1^o-x > 2^o-x > 3^o-x, so to increase the rate of the reaction a base will be needed. ^{1}H NMR spectroscopy of **2.6** (Fig. 2.1) shows all protons of pyridine was shifted downfield due to changing from OH compound to Cl compound, also the signal of the methylene group adjacent to triazole ring was shifted from 4.52 ppm in **2.5** to 4.76 ppm in **2.6,** a triplet signal assigned to the proton of OH was observed at 1.88 ppm in **2.5** disappears in **2.6** as shown in Fig. 2.1. ^{19}F NMR for **2.5** and **2.6** show a singlet at - 62.3 ppm attributed to CF_3.

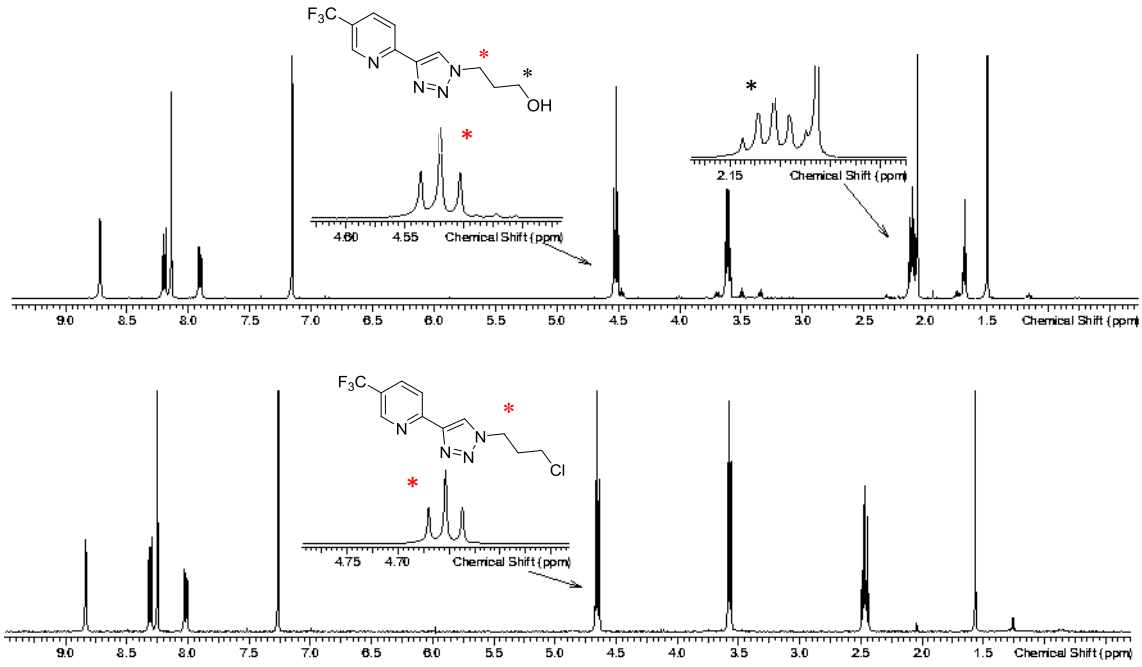

Figure 2.1: ^{1}H NMR spectra of **2.5** and **2.6** in ($CDCl_3$, 400MHz)

A series of ligands were synthesised to give pyridyltriazole bearing Boc-Spermdine, but without any substitution.

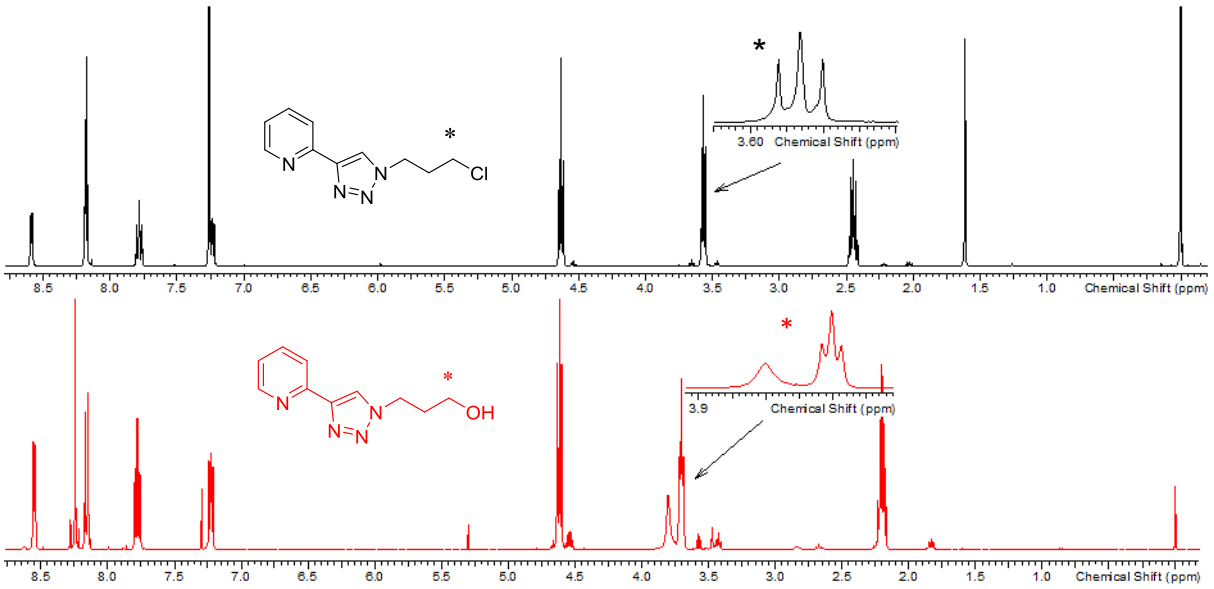

Figure 2.2: ^{1}H NMR spectra of **2.7** and **2.8**

The yields for both **L9.Boc** and **L10.Boc** were different, as explained previously, because when potassium carbonate was used the yield became lower than when potassium iodide was used. The ^{1}H NMR spectrum of **L9.Boc** shows a triplet signal at 4.51 ppm assigned to protons of methylene adjacent to the triazole ring that was shifted upfield compared with **2.6**, indicating the formation of **L9.Boc**. Also, the triplet signal was observed at 2.43 ppm for **L9.Boc** and shifted up field compared with **2.6**. Similarly, the ^{1}H NMR spectrum of **2.7** shows two singlet signals, one at 8.24 ppm corresponding to proton of triazole ring and other one at 3.80 ppm assigned to proton of hydroxyl group, and also shows triplet signal at 4.61ppm corresponding to protons of methylene group adjacent to triazole ring. The protons of methylene adjacent to OH group were observed at 3.70 ppm (Fig.2.2). While the ^{1}H NMR of **2.8** shows a singlet signal at 8.18 ppm corresponding to the proton of triazole ring also the signal was observed at 3.55 ppm corresponding to protons of methylene groups adjacent to chlorine which is shifted upfield compared with **2.7** due to convertion from hydroxyl group to chloride. Mass spectrometry confirmed the structure of compound **2.8** by showing peak *m/z* 223 assigned to $[M+H]^{+}$.

2.3.2 Stille Coupling Reaction

The Stille reaction was used for efficient carbon-carbon bond formation reactions, Kosugi first described the Stille reaction as a Pd-coupling in the late 1970s[178] and was

afterward developed as a significant tool in organic synthesis by Stille.[179] Stille coupling is considered to be a powerful intermolecular carbon-carbon (C-C) bond formation process due to the generation of different types of carbocyclic and heterocyclic rings, especially five- and six-membered rings. This reaction is shown in the Scheme 2.24.

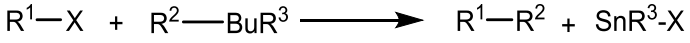

Scheme 2.24: Stille coupling

The mechanism of the Stille reaction was proposed by Stille, who first described this mechanism as being based primarily on data obtained from the coupling of benzoyl chloride and tributyl(phenyl)stannane.[180] The first step is started through the active catalytic species, [PdL_2] (L = PPh_3) which reacts with the organic electrophile R-X to form complex 1 (Scheme 2.25). Transmetallation is the second step, which leads to formation of complex 2, which then undergoes *cis-trans* isomerization to give 3, which is a very fast step. The final step was reductive elimination to give the organic species required for the product R-R'.

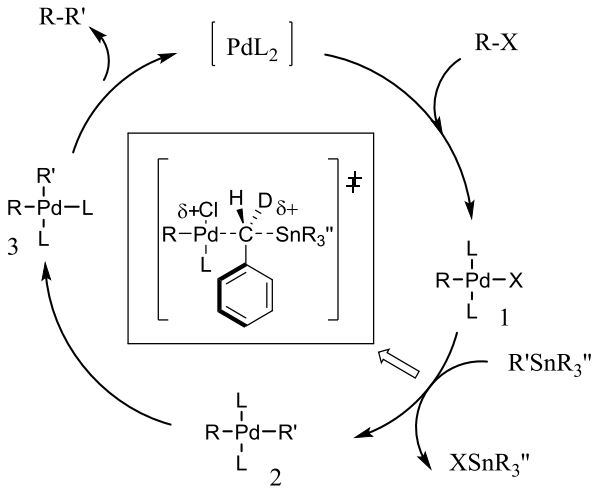

Scheme 2.25: the original proposal for the Stille Mechanism[180]

Currently, this mechanism is acceptable in terms of the oxidative addition and the reductive elimination steps but the mechanism of the transmetallation step is still unknown.[181] One of the important reagents in the Stille reaction is pyridyl stannanes (1), which were among the first azine organometallics to be used successfully in palladium-catalysed cross-couplings and are still commonly employed in spite of their toxicity due to the tin reagents. Pyridyl stannanes are more stable than other pyridyl organometallics, and there are three methods by which to prepare this compound(Scheme 2.26).[182]

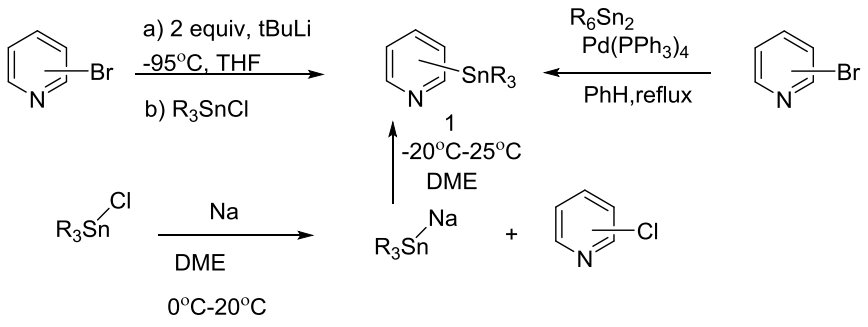

Scheme 2.26: Preparation of stannyl pyridines

Different types of pyridine organometallics are used in the Stille reaction. In 1986, Yamamoto and co-workers reported one of the first uses of trimethylstannyl pyridines and quinolines in various palladium-catalysed Stille reactions.[183] In 1995, Ogura and co-workers reported the use of $PdCl_2(PPh_3)_2$/LiCl in the Stille coupling of 4-trimethylstannylpyridine with aryl bromides (Scheme 2.27).[184]

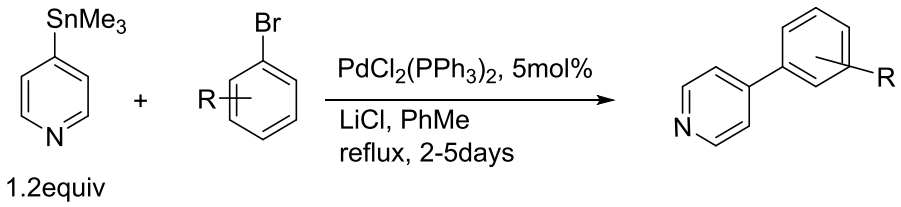

Scheme 2.27: Ogura and co-workers prepared phenypyridine derivatives

The study by Gronowitz and co-workers was found that Stille cross-couplings between 2-stannylpyridines with aryl iodides and some aryl bromides (Scheme 2.28) are more likely to be stable and the reaction occur in much faster and give higher yields than other derivatives.[185]

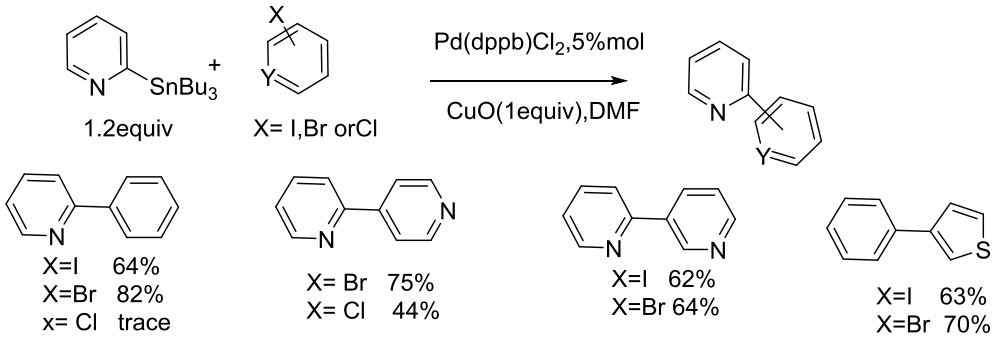

Scheme 2.28: Synthesis different types of bipyridine via Stille coupling

There are three isomers of pyridyl organometallics (2, 3 and 4), which are less nucleophilic, lead to the transmetallation of the arylPdX complex at slower rates.[186] 2-

tributylstannylpyridine is used in this study in the presence of the tetrakis(triphenylphosphine)palladium(0) complex,[187] which was used in this study because it is commercially available, and because bulky and electron-rich species like phosphine ligands PPh_3 with palladium increase the stability of Pd(0) complexes. However, $Pd(PPh_3)_4$ is light-sensitive and unstable in air.[188]

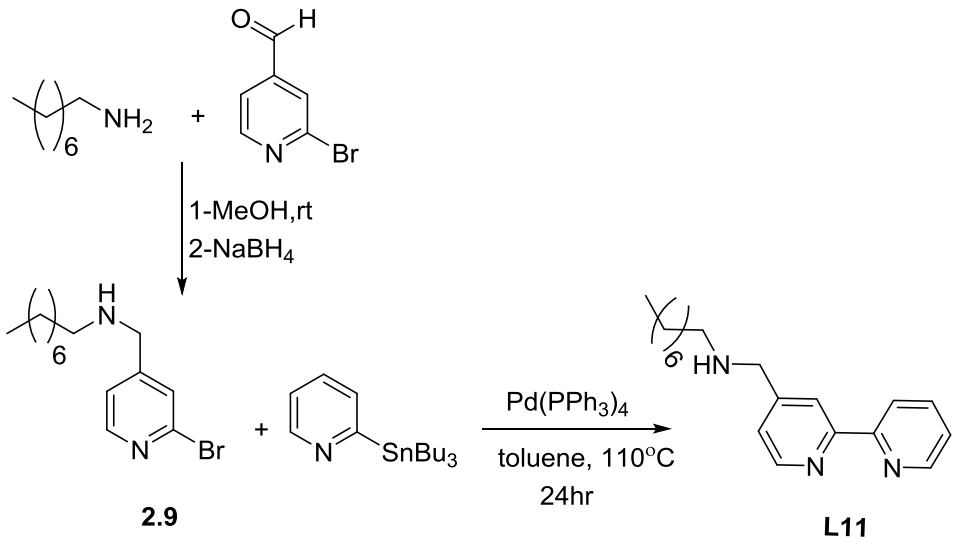

Scheme 2.29: Synthesis of **L11** via Stille coupling

The initial step was to prepare aryl halide **2.9** (Scheme 2.29) by reaction between 2-bromo-4-caroxylaldhyde pyridine and alkyl amine, this reaction involved conversion of the aldehyde group to an amine via reductive amination.[189] This reaction is used to form an N-C bond which involves transforming the amine into an imine and then reducing the imine.[190] Generally, this reaction involves two steps, the first being to form the imine by the reaction between the amine and aldehyde (with TLC analysis used to monitor the reaction that confirm all the starting material had been convert to the imine), and then without isolation it is directly used in the second step, where the reaction mixture is cooled to 0ºC to prevent any effervescence after adding the reagent. This reagent needs to be added in small batches, and stirring maintained overnight. TLC analysis confirmed all the imine was consumed and converted to the amine. The yield gained here was 88%. The ^1H NMR spectrum of **2.9** shows the disappearance of the proton of aldehyde at 10.0 ppm and a new signal at 3.78 ppm assigned to the CH_2 near the aromatic ring and three signals were observed in aromatic region (Fig. 2.3).

The next step forms **L11** via the reaction between the tin reagent and aryl halide, it was carried out in harsh conditions, so a Schlenk tube is used in this reaction, under nitrogen

and in the dark; $Pd(PPh_3)_4$ is light-sensitive and unstable in air so all equipment used in this reaction needs to be very dry before use. TLC analysis was used to monitor this reaction. Compound **L11** was purified by column chromatography to yield 49% of product. The ^1H NMR spectrum of **L11** shows seven signals in aromatic region between 8.68-7.31 ppm with a singlet signal at 3.96 ppm corresponding to protons of the methylene group adjacent to pyridine ring which is shifted downfield compared with **2.9** due to ring current from pyridine, this confirmed the formation of product.

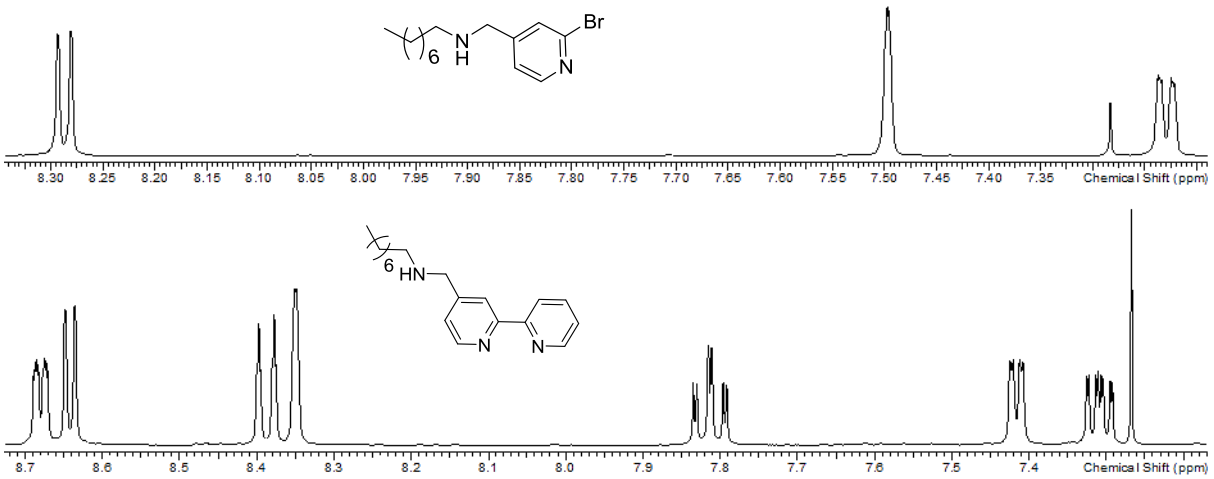

Figure 2.3: ^1H NMR Spectra of **2.9** and **L11** show the aromatic region

A suggested mechanism for this reaction was shown in the Scheme 2.30.

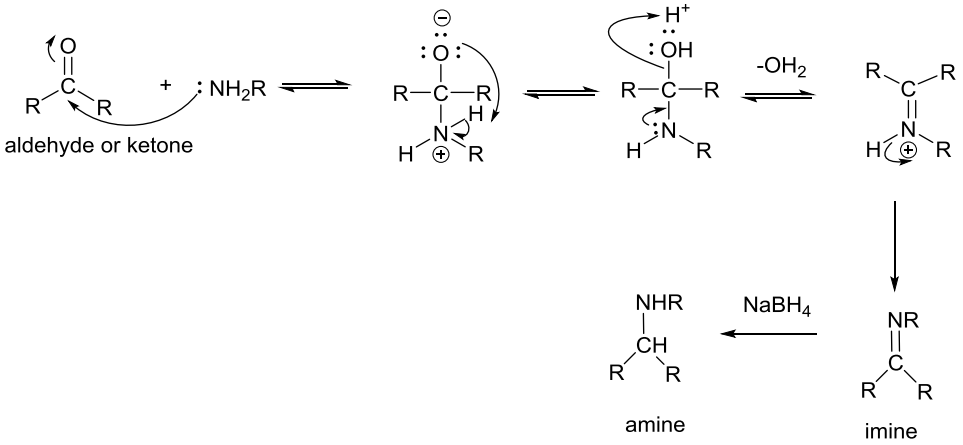

Scheme 2.30: Mechanisum of reductive amination

According to this scheme, the first step is the nucleophilic addition of the amine to the carbonyl carbon followed by deprotonation of the nitrogen atom. The resulting carbon

in amine loses water to convert to the imine. $NaBH_4$ was added to reaction as a reducing reagent to reduce the imine to amine.[191] This route was also used to synthesise a monodentate ligand, which will be discussed later.

Two types of ligands were synthesised via Stille coupling reaction; a bipyridine ligand containing an alkyl chain where the alkyl chain was used to change the lipophilicity of rhenium(I) complexes; phenylpyridine ligands containing an alkyl chain to be used as a cyclometalating ligand was synthesised for iridium(III) complexes.

A phenylpyridine derivative was also prepared via Stille coupling with a yield of 61% (conventional heating) and 38% (microwave heating) after purification by column chromatography, the phenyl pyridine substituent with the alkyl chain was required for interaction with cell membranes. This reaction starts with 4-hexylbromobenzene that couples with the tin reagent to produce **HL12** as a final product as shown in the Scheme 2.31.

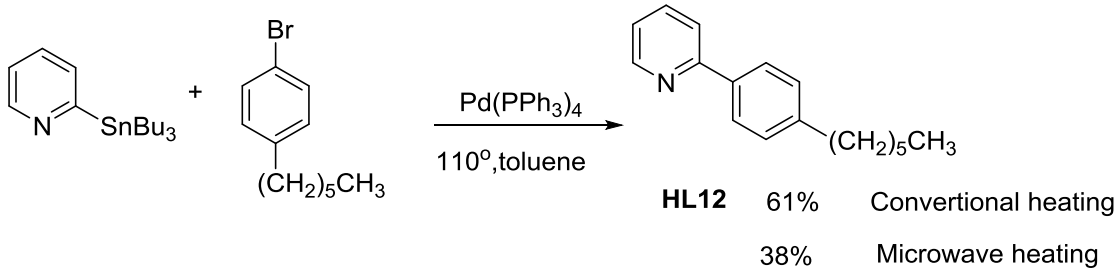

Scheme 2.31: Stille coupling to synthesise **HL12**

This ligand was characterized by NMR spectroscopy including COSY, HSQC and HMBC in addition to mass spectrometry. The ^{1}H NMR spectrum of **HL12** shows two doublet signals with 2H integral were observed at 7.9 and 7.2 ppm corresponding to protons of the phenyl ring. Also, one signal with one proton integral was observed at 8.66 ppm corresponding to proton of the CH adjacent to the nitrogen in the pyridine ring and signals at 7.70 ppm and 7.18 ppm attributed to the remaining protons of pyridine ring. Mass spectrometry showed a peak at *m/z* 240 assinged to $[M+H]^+$.

2.4 Reverse Click Reaction

1,2,3-Triazoles are important units in terms of biological fields.[192, 193] Particularly, several derivatives of pyridyltriazoles are interesting as they exhibit a variety of

biological properties, including control of arthropod pests, substance-related disorders, ATP-competitive inhibition of vascular endothelial growth factor receptors I and II, and antibacterial and antimicrobacterial activity.[194, 195] These compounds were synthesized either by base-promoted substitution between 1,2,3-triazole and 2-halopyridine or by thermal 1,3-dipolar cycloaddition.[196] The discovery of the Cu-catalysed click chemistry of azides with alkynes by Sharpless *et al*. until now represents the most efficient way to assemble the 1,2,3-triazole ring (A).[196] However, the method used to prepare pyridotriazole is not straightforward because these azides exist in an equilibrium between their closed (tetrazole **A**) and open forms (azide **B**) as shown in Scheme 2.32.

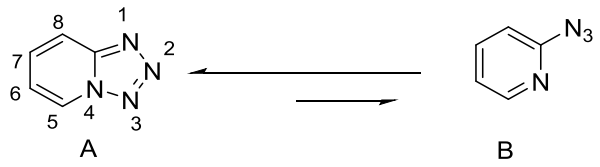

Scheme 2.32: Structure of azidopyridine in the closed (tetrazole **A**) and open forms (azide **B**)[197]

Previous studies have indicated that the preparation of the two forms is determined by the temperature. At room temperature, the azide exists as a closed form (A), while at high temperature, the azide takes the (B) open form.[198]

Other studies ignored this idea and demonstrated that the equilibrium form depends on the type of substitution and its position on the pyridine ring. While electron-withdrawing groups at the C-6 position of the pyridine take the open form B; in contrast, the azide compound prefers the closed form A when withdrawing groups NO_2, COOH, and Cl are substituted at the C-8 position and the unsubstituted tetrazole mainly exist.[199] The study by Chattopadhyay *et al.*[193] confirmed that pyridotetrazoles exist in an open/closed form equilibrium (between **A** and **B**) depending on the substituent. It was also found that pyridotetrazoles in closed form are inert to the click reaction under standard conditions.[200] So, no product was obtained, but when the reaction was performed in the presence of $Cu(OTf)_2$ instead of $CuSO_4$, it afforded a good yield.[201] Thus, several derivatives of pyridotriazoles have been synthesized over the last decade according to the role of this compound in different areas. Sun *et al.* developed an efficient new design for the catalytic system CuCl/2-$PyCH_2N{=}P^tBu_3$ for the synthesis of 1-(pyridin-2-yl)-1,2,3-triazole derivatives in the Cu(I)-catalysed azide–alkyne cycloaddition (CuAAC) reaction (Scheme 2.33), which was successful in moderating

the yield from good to excellent (46–98%). This study found the main form of tetrazole is in the closed form even with C8-position such as 8-chlorotetrazolo.[198]

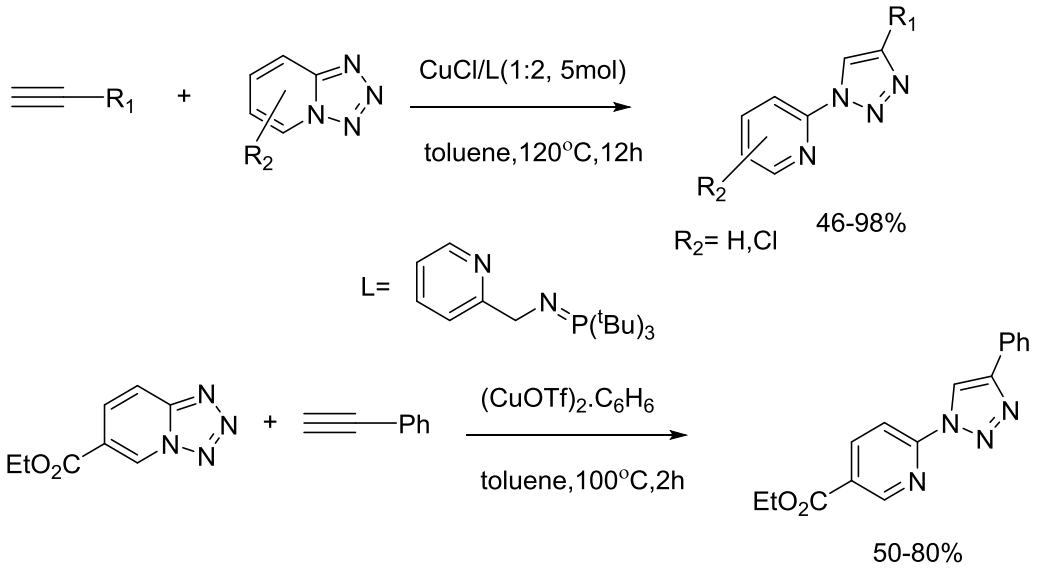

Scheme 2.33: Synthesis of pyridotriazole derivatives

As mentioned earlier, the tetrazolo compound is expected to be found in solution in equilibrium between the closed (A) and open (B) forms. However, the study by Jindabot *et al.* demonstrated that the tetrazolo compound in its closed form only in the solid state.[202] Therefore, this explains why harsh conditions are needed for the click reactions. A mixture of $Cu^{II}(OTf)_2$ and Cu^0 was used in toluene at 120ºC under an inert atmosphere to afford the corresponding pyridineetriazole products L1-L3 in moderate yields (54-79%) (Scheme 2.34).

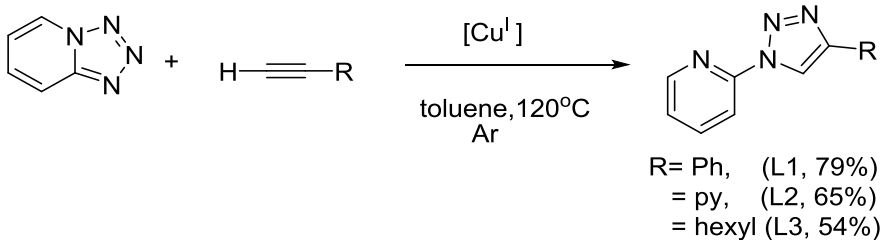

Scheme 2.34: Synthesis of L1-L3

Kolarovic *et al.*[203] developed a tandem practical protocol for the synthesis of 1,4-disubstituted triazoles from aryl halides and alkynoic acids via 1,3-dipolar cycloaddition involving decarboxylative coupling (Scheme 2.35).

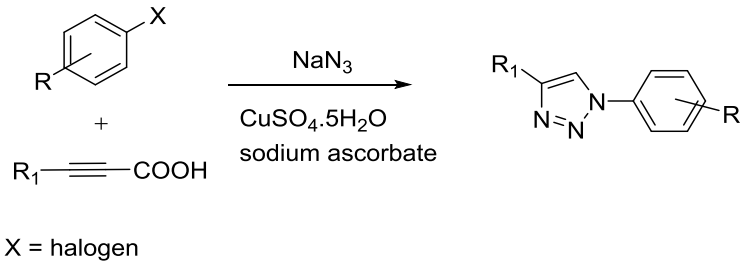

Scheme 2.35: Synthesis of 1, 4-disubstituted triazoles

A different type of route was used by Hu and co-worker to synthesise 1-(pyridin-2-yl)-1,2,3-triazoles from 6-substituted electron-withdrawing tetrazolo-[1,5-a]pyridines via copper(I)-(CuAAC) using copper(I) acetate as a catalyst(Scheme 2.36).[204]

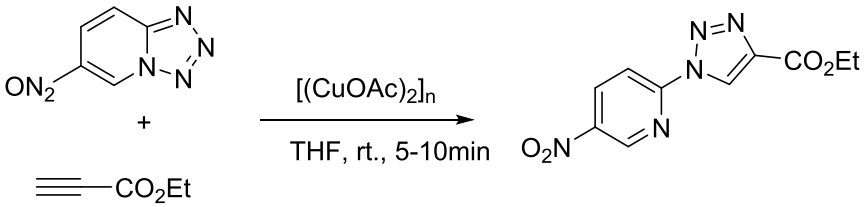

Scheme 2.36: Synthesis of 1-(pyridin-2-yl)-1, 2, 3-triazoles by Hu *et al*

This catalyst formed HOAc *in situ* and may play a dual role of promoting the protonation of complex 1 and preventing the formation of complex 2 (Scheme 2.37). So, this study can improve the efficiency for CuAAC when using 6-substituted tetrazolo-[1, 5-a]pyridines.

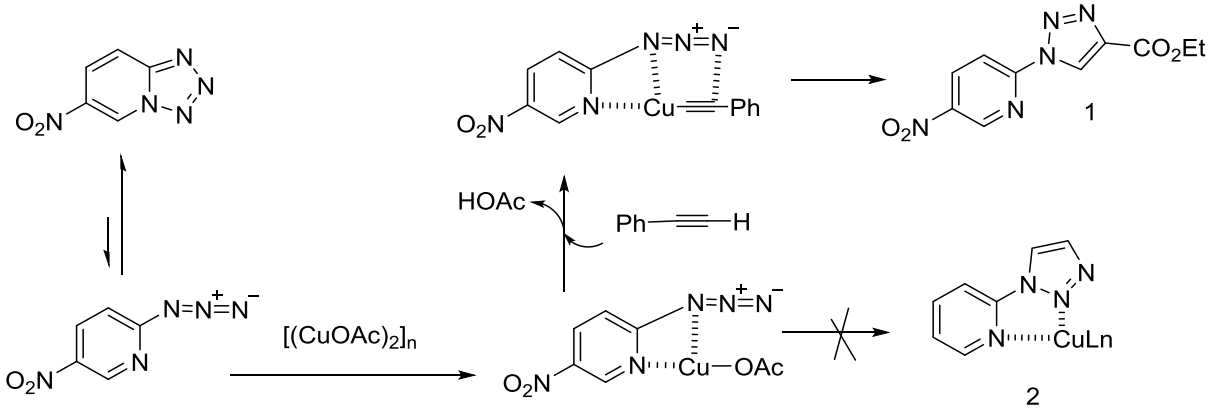

Scheme 2.37: Mechanism of inverse CuAAC reaction

Inverse click reactions can be considered a new strategy to improve the CuAAC efficiency. On the other hand, this reaction is efficient with a wide variety of alkynes in producing *N*-heterocyclic derivatives of 1,4-disubstituted triazoles. Thus, this route plays an important part in this study in terms of the synthesis of novel ligands which

were required for the preparation of its rhenium(I) complexes and to allow for comparison with regular complexes in terms of photophysical properties and stability, one of which would be chosen as a candidate for imaging synaptic vesicles. **L13, 2.11** and **2.12** ligands were synthesised by this method. This reaction was started with the conversion of 2-bromopyridine to 2-azidopyridine using NaN_3 in the presence Cu(OAc) as a catalyst in a co-solvent ($EtOH/H_2O$, 7:3), which was then heated using microwave condition for 1hr.[205] The reaction time was reduced from 24h to 1h by this approach. The azide compound can be isolated, and further characterized by NMR and mass spectrometry. The next step was the synthesis of 2-pyridyltriazolo starting from the relevant alkyne, which was added to 2-azidopyridine in the presence of CuI as a catalyst in CuAAC and sodium ascorbate to ensure reduction was complete, the solvent system was $EtOH/H_2O$ and it was microwave heated for 12hr. Column chromatography was needed in order to get pure products in good yield.

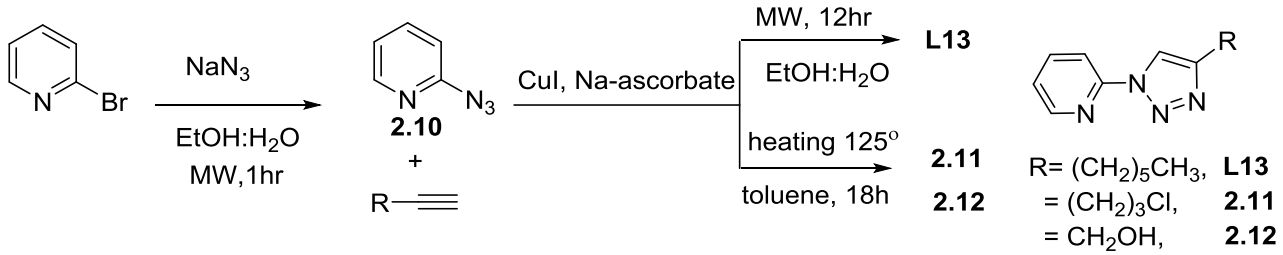

Scheme 2.38: Synthesis of **L13**, **2.11** and **2.12**

All these compounds were characterized by NMR spectroscopy, namely through ^1H NMR, COSY, HSQC and HMBC. The ^1H NMR sprctra shows characteristic a singlet at 8.30 ppm, 8.37 ppm, and 8.56 ppm for **L13, 2.11** and **2.12** representing to the triazole CH. This signal cannot be found in the azido compound, thus giving further evidence as to the formation of these ligands. ^1H NMR spectra show another signals at 2.80 ppm, 3.63 ppm and 4.90 ppm attributed to methylene group that is closest to the triazole ring, for **L13**, **2.11** and **2.12**, respectively. The **2.12** ligand was then converted to the chloride via reaction with $SOCl_2$ in dichloromethane (Scheme 2.39).

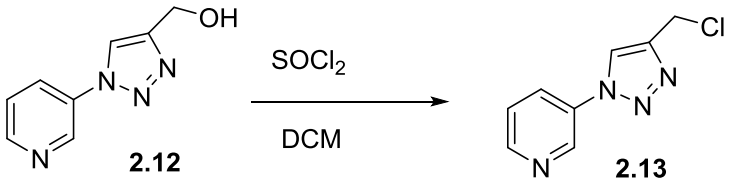

Scheme 2.39: Synthesis of **2.13**

2.13 was characterized by NMR and IR spectroscopy. ^{1}H NMR spectra shows that protons of the CH_2 group close to the triazole ring of compound **2.12** was shifted from 4.90 ppm upfield to 4.80 ppm (Fig.2.4); the signal also changed from a doublet to a singlet, confirming conversion of OH to Cl. The IR spectrum also confirmed that the broad peak at 3500 cm^{-1} for **2.12** was absent in **2.13**. **L13** was synthesised in order to moderate the lipophilicity and to tune the photophysical properties of rhenium(I) complexes, while **2.11** and **2.13** were used to react with Boc-Spermdine via an S_N2 mechanism to synthesise **L14.Boc** and **L15.Boc** (Scheme 2.40). The presence of polyamines in complexes enables the complex to undergo easy internalization in the cell.

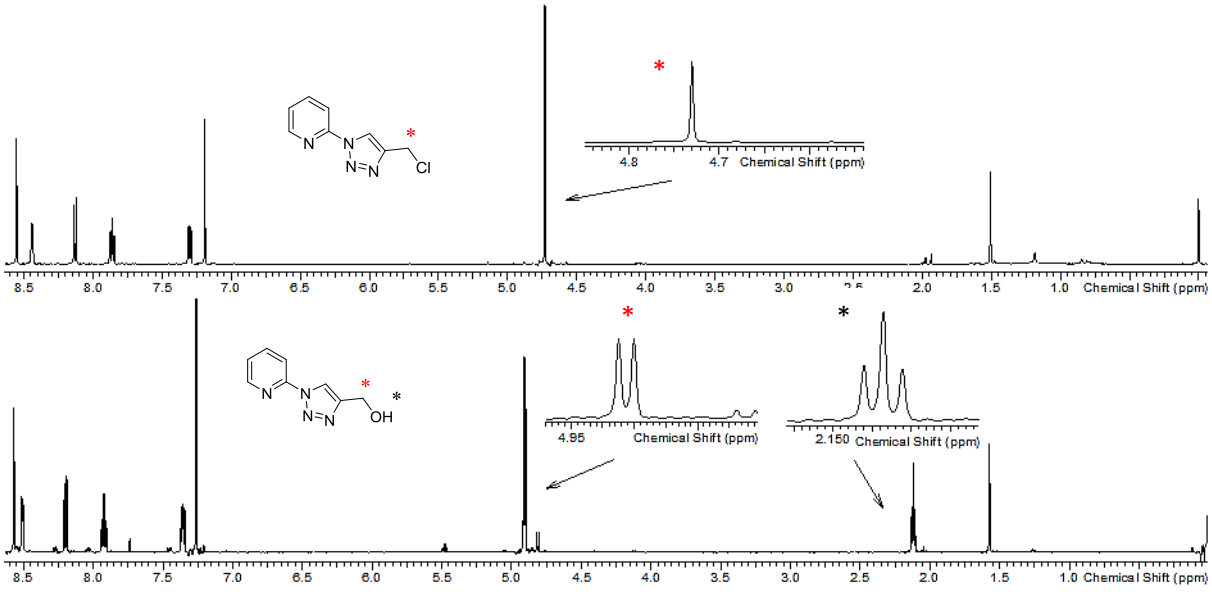

Figure 2.4: ^{1}H NMR spectra of **2.12** and **2.13** **L14.Boc** in $CDCl_3$ in 500 MHz

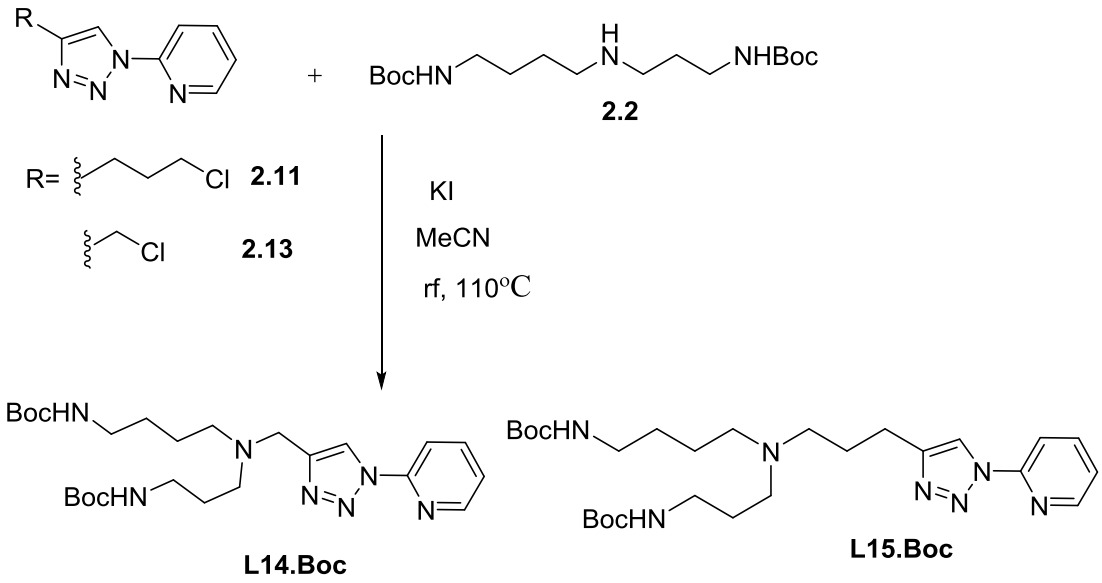

Scheme 2.40: Synthesis of **L14.Boc** and **L15.Boc**

These two compounds were synthesised via an S_N2 mechanism as mentioned previously in the synthesis of **L14.Boc**. ^{1}H NMR spectra of **L14.Boc** and **L15.Boc** show the proton of the triazole ring shifted to upfield at 8.50 and 8.45 ppm respectively compared with corresponding halide compound as a result of linking with **2.2**, additionally, the protons of the CH_2 group were more heavily influenced as a result of connecting with Boc-spermdine, which shifted from 3.63 ppm in **2.11** to 2.20 ppm in **L15.Boc** due to a change in the coordination from the chlorine atom to the nitrogen atom, which has a lower electronegativity than chlorine according to the electronegativity order F > O > Cl > N.

2.5 Synthesis of Monodentate Ligands

This section will address two classes of monodentate ligand, one is pyridine derivatives whilst the other is triazole derivatives; it will also discuss the synthesis types of ligand, their structures and the active position in both compounds. These can be used to introduce alkyl chains or polyamines to rhenium(I) complexes via substitution of the chloride in $[Re(N\text{^}N)(CO)_3Cl]$. Pyridine is considered an important aromatic organic ligand as it has one lone pair of electrons, and can even be found as a salt. It is weakly basic, with a pK_a of ~5.2 in H_2O. It is liquid at room temperature. There are various methods by which pyridine can be prepared and a wide variety of compounds can be prepared from pyridine such as quinolines, isoquinoline and its derivatives.[206] These ligand were coordinated with transition metals via this electron ion pair in the nitrogen

atoms. Re(I), Os(II), and Ru(III) complexes bearing pyridine have been widely used in biological applications such as sensors[207] and bioimaging agents.[208] In the last decade, it has been found that the polypyridine link with a reactive functional group such as isothiocyanate, aldehyde, maleimide, and iodoacetamide can modify the luminescence properties of d^6 complexes for bioconjugation purposes, as explained previously in Chapter 1. Rhenium(I) complexes with the form $[Re(N\hat{}N)(CO)_3Cl]$, are used in different biological applications such as drugs due to presence of the chloride.[102] Various research groups have taken advantage of the addition of pyridine to these complexes to render them more stable, reduce their toxicity and moderlying their charge such as with pyridine-indole and pyridine-biotin, which discussed in Chapter 1. It is clear that simple rhenium(I) complexes of the type $[Re(CO)_3(bipy)(py)]^+$ show good uptake into a variety of cell types, even without conjugation with uptake vectors. It was also found that additional axial ligands enhanced the photophysical properties. Pyridine derivatives were prepared with either an alkyl chain or polyamine substituted in the 4-position because it is considered one of the requirements of this study. As mentioned previously, the monodentate ligand can be prepared via a reductive amination mechanism, as shown in Scheme 2.41.

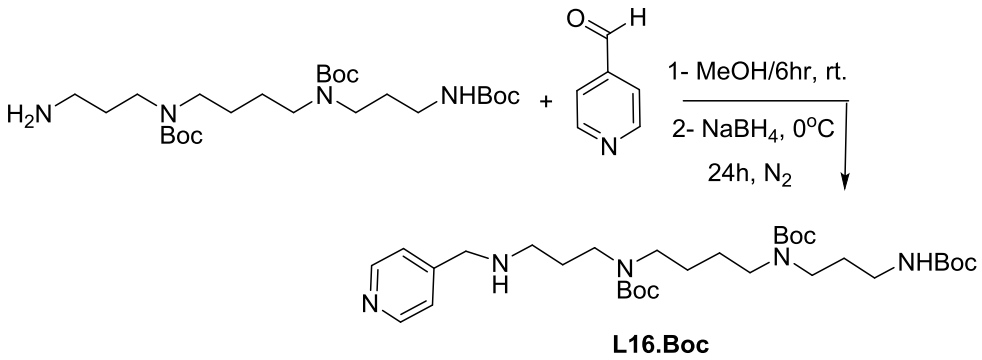

Scheme 2.41: Synthesis of a monodentate pyridine ligand **L16.Boc**

This route involves the reaction between aldehyde (4-caboxylahdehyde pyridine) and Boc-Spermine **2.3** in MeOH. The reaction is started by attaching the amine group of the Boc-protected **2.3** to the carbon atom of aldehyde followed by water abstraction to produce an imine. $NaBH_4$ is then used as a reducing reagent to form a C-N bond, as pure **L16.Boc,** with a yield of 76%. NMR spectroscopy and mass spectrometry were used to characterize this ligand. The ^1H NMR spectrum shows two signals with integral of two into aromatic region at 8.53 and 7.20 ppm corresponding to protons of pyridine

ring, and a characteric singlet signal was also observed at 3.75 ppm with an integral two protons attributed to the protons of methylene group adjacent to pyridine ring. This product of 4-pyridine substituted with the polyamine is used as an axial ligand replacement with the chlorine of rhenium(I) chloride complexes to produce cationic rhenium(I) complexes (see Chapter 3). 4-Pyridine substituted with an alkyl chain can also be prepared via this route (Scheme 2.42), but octylamine is used instead of Boc-Spermine.

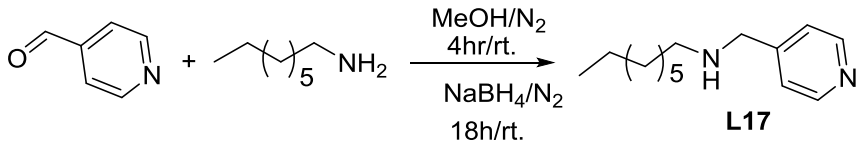

Scheme 2.42: Synthesis of **L17** via reductive amination reaction

L17 has been characterized by ^{1}H NMR spectroscopy and 2D COSY, HSQC and HMBC NMR spectroscopy. The ^{1}H NMR spectra shows the proton of the aldehyde was disappeared and a new peak at 3.95 ppm had appeared as a singlet, indicative of the CH_2 group close to the pyridine ring. This route gives a good yield without need for further purification. To date, pyridine is the most commonly used ligand for the axial position; recently, click chemistry has found widespread application including the biological and materials sciences, this approach formed 1, 4-disubstituted-1,2, 3-triazole with functional molecule synthesis in a wide range of fields, due to its reliability, mild reaction conditions and wide substrate scope.[196] The structure of 1,2,3-triazole allows for various interactions with other molecules via hydrogen bonding; triazole can also coordinate with metals via an anionic, neutral or cationic nitrogen donor,[209] as shown in Scheme 2.43.

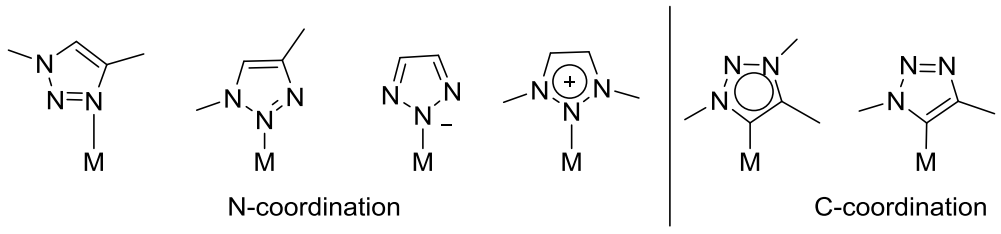

Scheme 2.43: Selected super molecular interactions of 1,2,3-triazole[210]

1,2,3-triazole has two nucleophilic positions, one at the 1-postion and the other in the 3-position due to that the presence of an electrophilic atom, having an electron sextet and

a formal positive charge, as well as a nucleophile atom, having an electron octet and a formal negative charge as shown in Scheme 2.44.

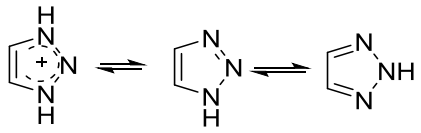

Scheme 2.44: tautomerism of 1,2,3-triazole compound

The triazole ring has three nitrogen atoms and has features similar to both pyrrole and pyridine: the N1 atom in the isomer 1H- 1,2,3-triazole, like pyrrole, is acidic and σ-accepting and π-donating, and the N2, like pyridine, is basic and σ-donating and π-accepting. Triazole is considered in the first aromatic compounds because the three nitrogen atoms cause strong aromaticity due to polarization of the aromatic π system and the σ framework. The isomer 2H-1,2,3-triazole is more aromatic than pyridine or pyrrole.[211]

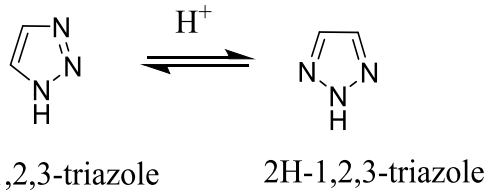

Scheme 2.45: Structural isomers of triazole

There are many studies in the literature about the coordination of the triazole with metal atoms, as mention in Chapter 1, which find that triazole coordination, is via the N2 or N3 atoms, with the majority of studies indicating that N3 coordination forms more stable complex than N2 coordination. DFT calculations demonstrate that the electron density in N3 is greater than that in N2.[212] Indeed, there is a recent, and highly interesting, study about triazole being used as a mono- or polydentate ligand using three different triazole ligands, as shown in the Fig. 2.5.

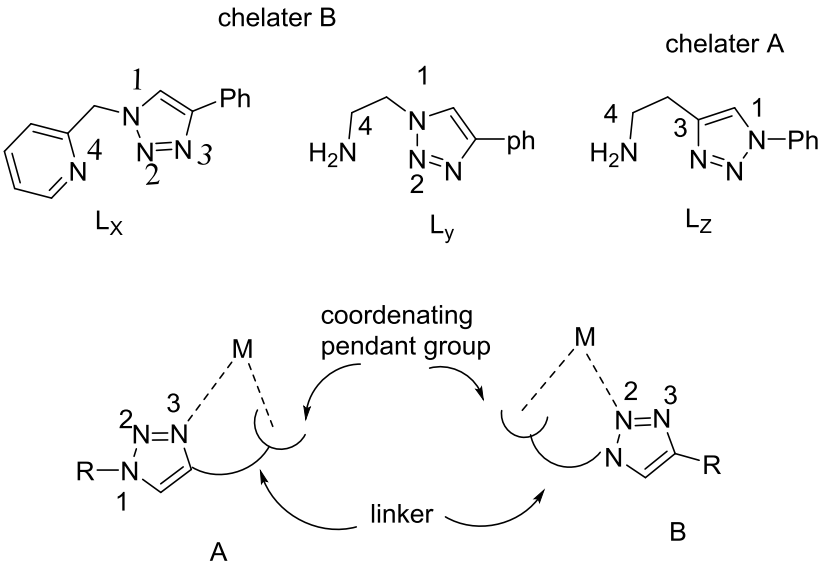

Figure 2.5: the coordination of triazole as a mono and di dentate ligand

This study demonstrated that Lx as shown in Fig. 2.5 can form stable a coordination complex with Pt(II), Pd(II), Cu(II), and Ru(II) where the 1,2,3-triazole coordinates via the N2 nitrogen atom, as assisted by a pendant pyridine group. The structures of the chelates were confirmed by X-ray diffraction, showing that Ly failed to form a complex with Pt(II), as was also the case for Lz.[213] Click chemistry is used to synthesise 1, 4-disubstituted-1, 2, 3-triazoles, and there are several reports of its synthesis in the literature. Monosubstituted 1, 2, 3-triazole is synthesised via two steps in one pot by converting the alkylbromide to an azide through the addition of NaN_3, followed by trimethylsilylacetylene in aqueous solution.[214] It was found that the reaction conditions were suitable for both alkyl and aryl azide reactants, including analogues with electron-donating and electron-withdrawing functionalities.

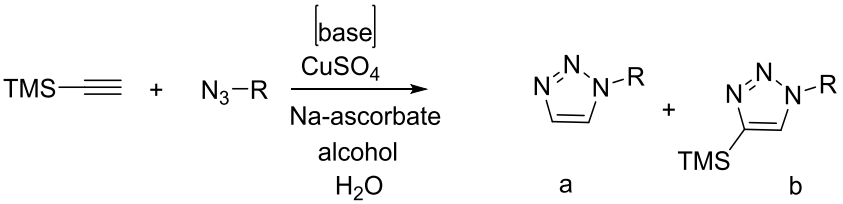

Scheme 2.46: Monosubstituted 1, 2, 3-triazole

The best results were found when using K_2CO_3 or KOH as the base and MeOH as the solvent, with one product showing a yield of 50-69%. This method is used in this study to synthesise 1-hexyl-1,2,3-triazole **L18** as a monodentate ligand, which is then used to replace the chloro-rhenium(I) complexes to form cationic complexes and to make

comparison with rhenium complexes that contain pyridine as a monodentate ligand (in terms of its photophysical properties).

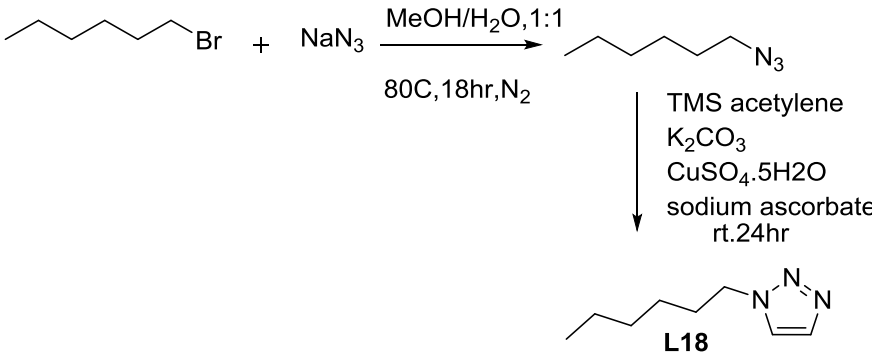

Scheme 2.47: Synthesis of **L18**

In this reaction, the alkyl azide intermediates were never isolated.[215] ^{1}H NMR spectroscopy was used to characterize this ligand, which was found to be in accord with the literature.[214]

2.6 Conclusion

In conclusion, in this study three types of ligands were synthesized that will be able to coordinate with transition metals to synthesise the complexes which are considered as the main aim in this work. The first type is the ancillary ligands which are prepared by click probe such as **L3**, **L6.Boc** and **L10.Boc**. **L11** was prepared by Stille coupling while **L8.Boc** and **L9.Boc** by Sonogashira reaction. Inverse click reaction is also has a part of this study by preparing ancillary ligands like **L13, L14.Boc** and **L15.Boc**. The second type of ligands is cyclometalated ligands which are also prepared by the click reaction, such as **HL1**, **HL2** and **HL4** and Stille reaction for **HL12**. The third ligands are monodonate axial ligands which were prepared by reductive amination reactions such as **L16.Boc, L17** and **L18**, a click approach is used to prepare either mono or bidentate sites. All these ligand were purified by column chromotoghraphy and characterized by NMR spectroscopy and mass spectrometry.

Chapter 3

3 Synthesis of Re(I) and Ir(III) complexes

3.1 Introduction

Complexes of d^6 transition metals such as rhenium(I) and iridium(III) have received a lot of attention over the past four decades due to their specific photophysical properties such as: long life time, large Stoke shift, high quantum yield and reduced photobleaching. These properties make them suitable for many application such as luminescence live-cell imaging,[216] photoinitiated anticancer agents and singlet oxygen sensitization for photodynamic therapy[217] and molecular sensors.[218] Imaging agents are one of the important biological applications, currently organic dyes are used for this purpose particularly, for example FM1-43 which is used for imaging of synaptic vesicles in neuroscience application.[62] FM1-43 has ambiphilic properties, both hydrophilic and lipophilic regions are found in its structure as mentioned in Section 1.7. However, this technique has drawbacks such as photobleaching and the use of toxic OsO_4 associated with FM1-43 in electon microscopy. Interesting studies have been reviewed relating to the use rhenium(I) for cellular imaging.[71, 219] This study is an attempt to synthesis rhenium(I) complexes for use as imaging agents in neuroscience as a replacement for FM1-43. The rhenium incorporates a pyridyltriazole ligand bearing a hydrophilic part such as a polyamine represented by **L6** or **L10** the other part of the complex should contain a lipophilic group represented by axial ligands such as **L17** and **L18** to enable intraction with vesicle membrane as shown in (Scheme 3.1). This can also be reversed for example, pyridyltriazole bearing a lipophilic alkyl chain represented by **L3** or **L11** and with hydrophilic **L16** to complete the ambiphilic picture. Iridium(III) complexes can also be made ambiphilic, by functionalising the cyclometalated ligand with alkyl chains such as **HL1, HL2, HL4** and **HL12** with the ancillary ligand containing a polyamine as the rhenium(I) complexes.

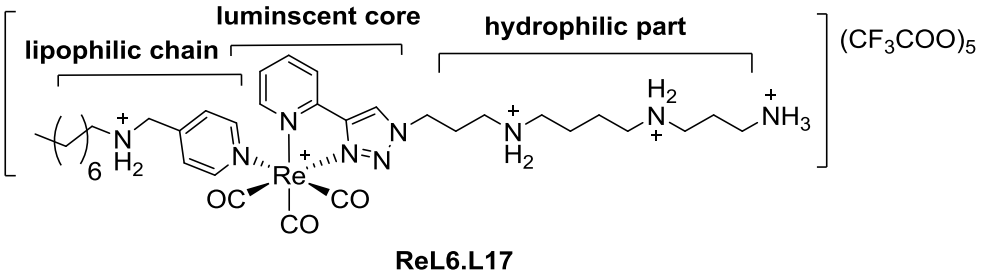

Scheme 3.1: Ambiphilic rhenium(I) complex

3.2 Synthesis of Rhenium(I) Complexes

Different types of rhenium(I) complexes prepared in this chapter are shown in scheme 3.2.

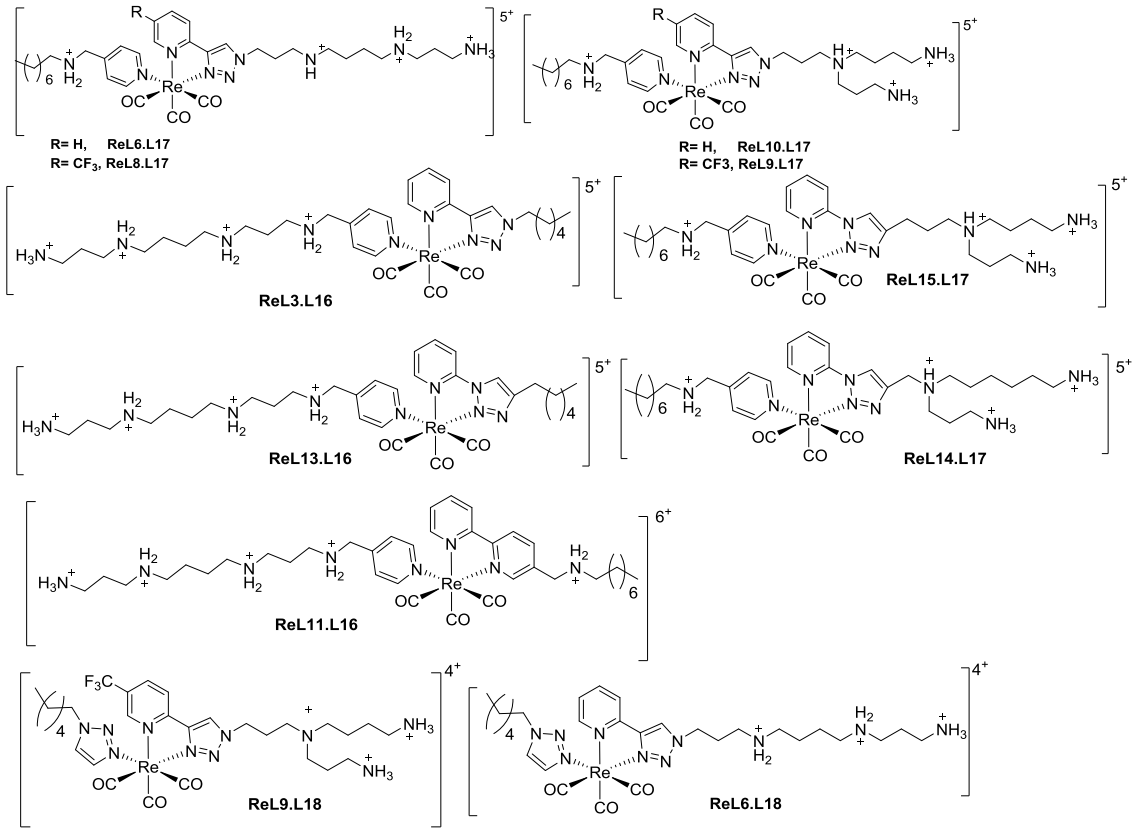

Scheme 3.2: The structure of rhenium(I) complexes prepared in this work

3.2.1 Rhenium(I) Complexes with Pyridyl Triazole

Recent studies show the pyridyltriazole moiety as an important common donor chelating ligand which is formed by the CuAAC reaction.[153] This reaction offers significant advantage to allow ligand design enabling access to a rich coordination chemistry that can be applied to different biological applications.[196] Rhenium(I)-based

pyridyltriazole chloride complexes $ReL(CO)_3Cl$ have been reviewed.[209, 220] The target molecules are rhenium(I) complexes which were synthesised via microwave irradiation, as this tool reduces reaction time, increases the yield and gives fewer impurities. The first step is to synthesise the rhenium(I) chloride complex by reacting $[Re(CO)_5Cl]$ with **L6.Boc** in dry THF (Scheme 3.3).

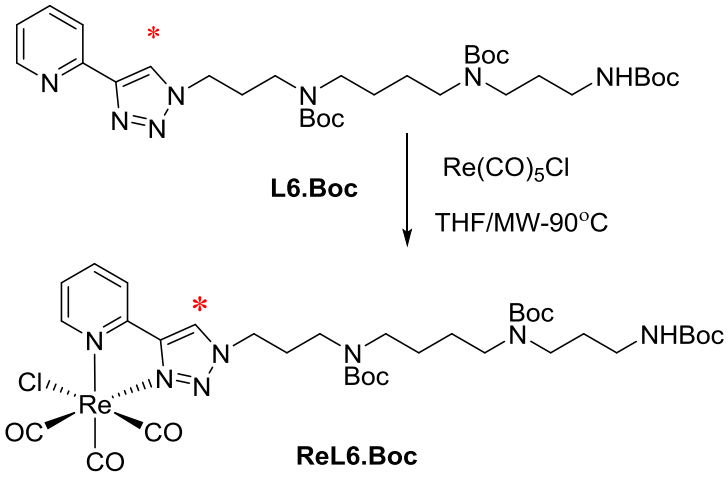

Scheme 3.3: Synthesis of **ReL6.Boc**

This step proceeded smoothly and an excellent yield was obtained (87%), this result is better than typical reactions using conventional heating in MeOH which give yields of (53%)[76] and (68%).[114] This complex was characterized by ^1H, HSQC and HMBC NMR spectroscopy. Coordination of the ligand to rhenium(I) results in a downfield shift of ^1H NMR signals of the pyridyl-rings and triazolyl-rings when compared with the uncomplexed ligand. This downfield shift is particularly evident in the triazole proton (*). It was shifted from 8.18 ppm in the free ligand **L6.Boc** to 8.79 ppm in the complex (Fig. 3.1).

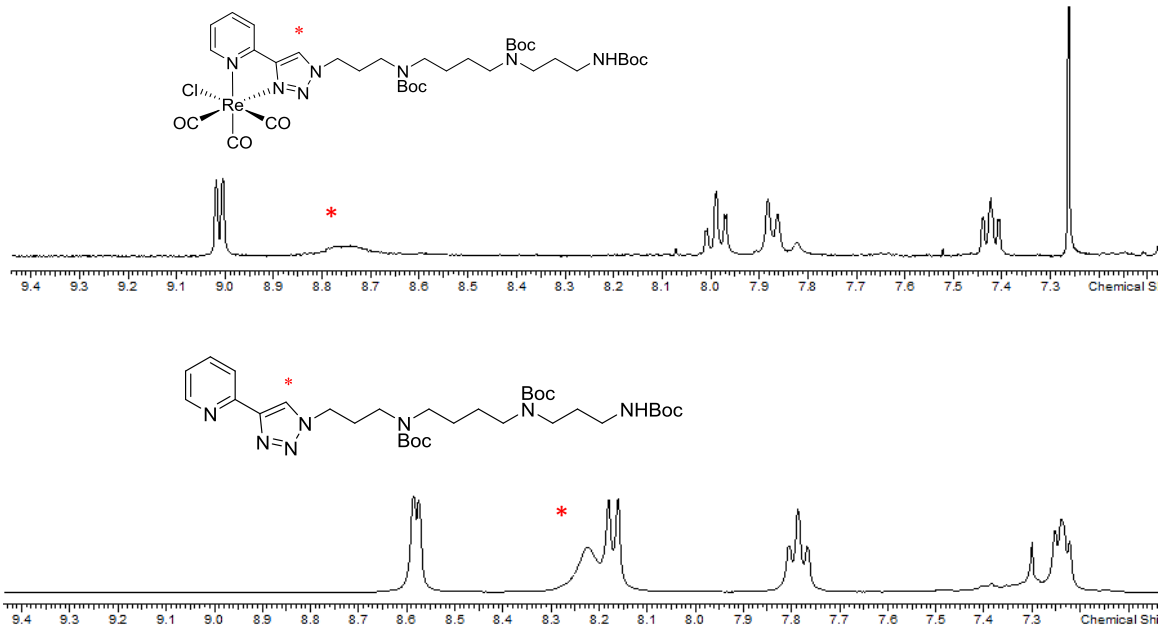

Figure 3.1: ^{1}H NMR spectra of **L6.Boc** and **ReL6.Boc** showing the aromatic region (in $CDCl_3$, 400 MHz)

While the methylene protons adjacent to the triazole ring also affected by coordination with metal, it changes from triplet signal at 4.44 ppm to non-first order as shown in Fig. 3.2. ^{13}C NMR shows three signal at 198.5, 197 and 190.3 corresponding to the three carbonyl groups.

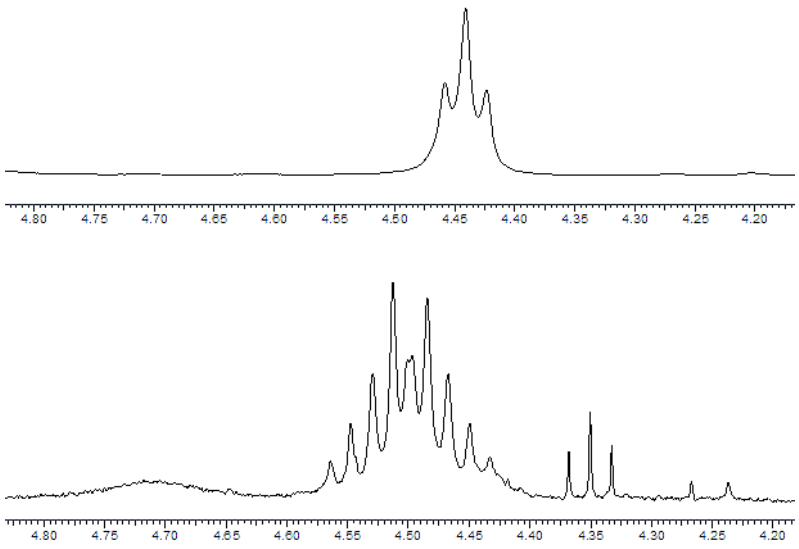

Figure 3.2: ^{1}H NMR spectra of **L6.Boc** and **ReL6.Boc** showing the CH_2 triazole signal (in $CDCl_3$, 400 MHz)

Addition of an axial pyridine ligand has been show to effect the emission of the complexes.[72] The next step was to synthesize the cationic rhenium complex in order to introduce a lipophilic component. These cationic rhenium(I) tricarbonyl diimine complexes are known to be emissive and less stable than their natural chloride complexes;[221, 222] to complete the picture of bio-imaging, a pyridine substituted with an alkyl chain **L17** in the para position was used to generate **ReL6.Boc.L17**. This reaction involved the addition of **L17** after abstraction the chloride using $AgBF_4$ in presence of MeCN (Scheme 3.4).

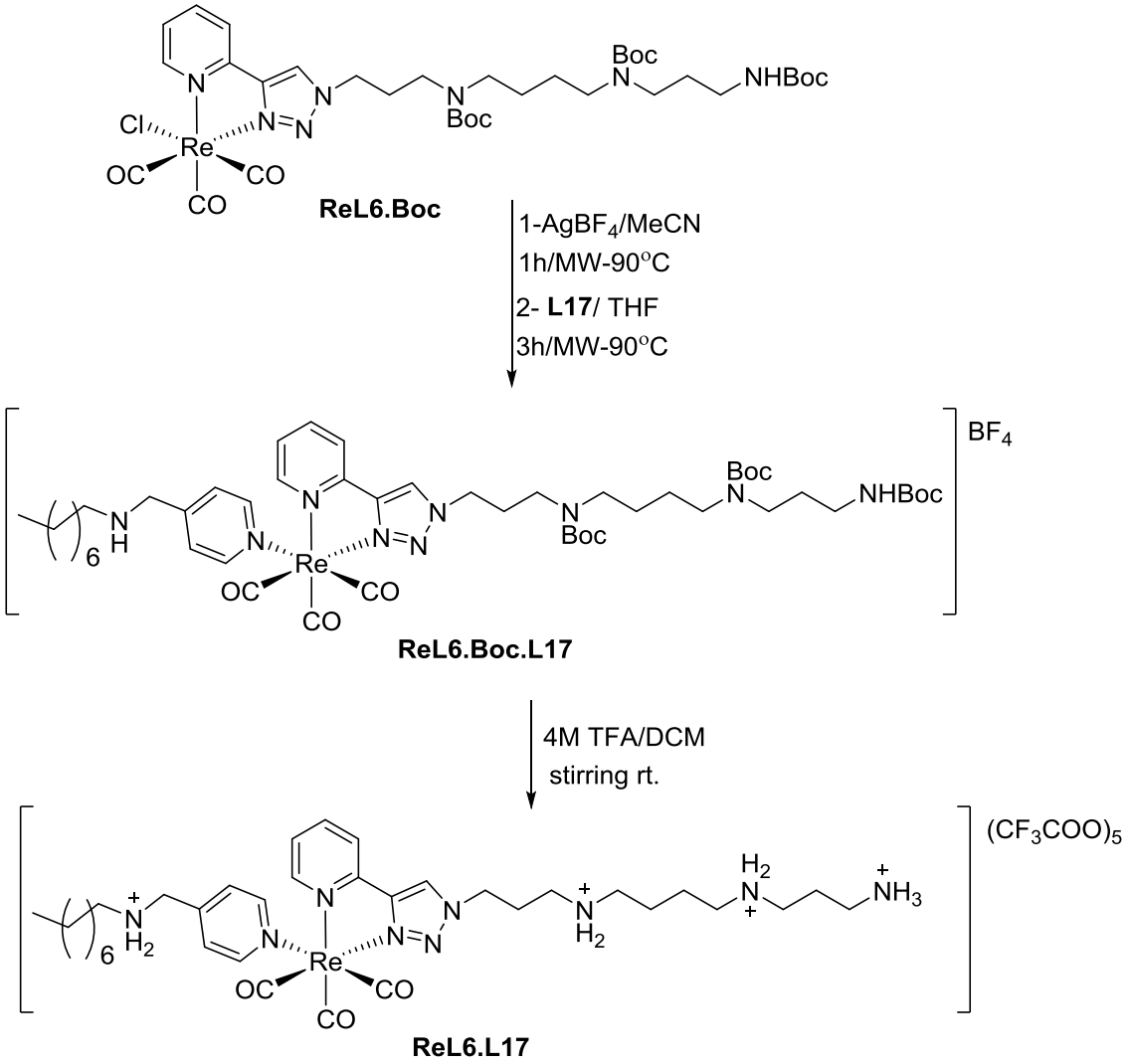

Scheme 3.4: Synthesis of **ReL6.Boc.L17**

The rhenium(I) chloride complex **ReL6.Boc** was dissolved in MeCN. Chloride abstraction is more easily achieved in polar solvents to form $[Re(CO)_3(\textbf{L6.Boc})(MeCN)]^+$ after which pyridine is used to replace the coordinated MeCN.[102, 223] Purification was attempted by column chromatography; however, some

starting material of the pyridine ligand remained. Purification was achieved using reverse phase high performance liquid chromatography (RP-HPLC). ^{1}H NMR spectroscopy in combination with 2D HSQC, HMBC and COSY NMR allowed characterization of the product. The ^{1}H NMR spectrum shows two doublets each with an integral to 2H in the aromatic region in addition to the signals of the pyridyltriazole (Fig. 3.3). These doublets corresponded to protons of the pyridine **L17** at 8.54 ppm, 7.53 ppm respectively.

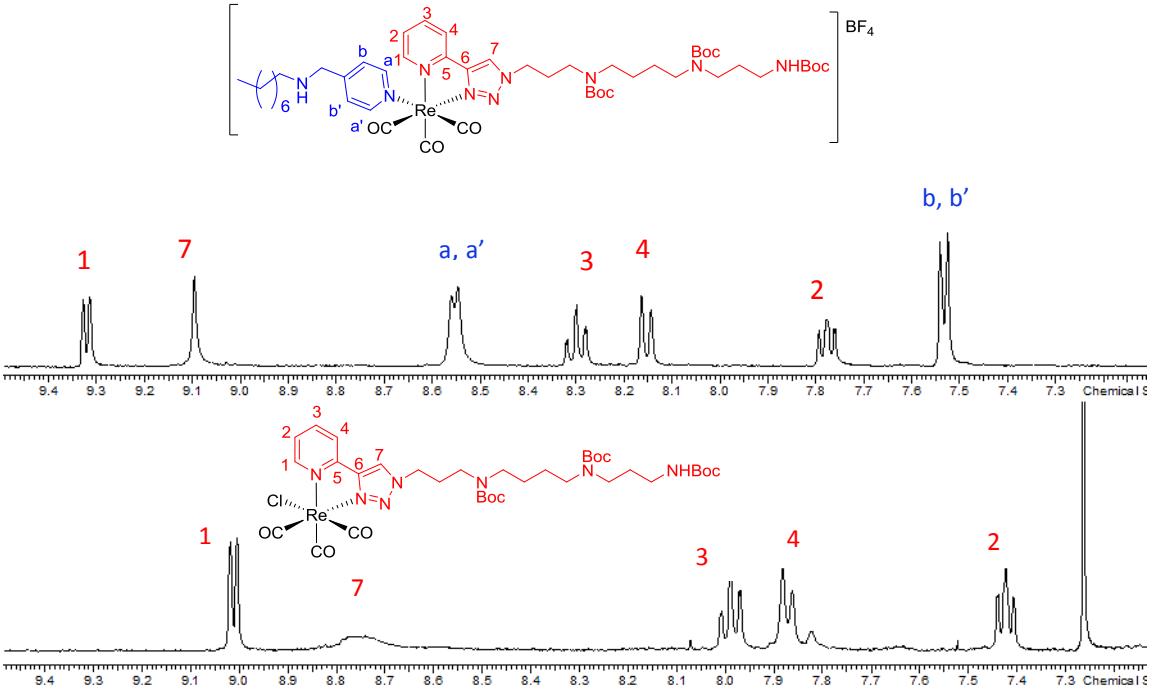

Figure 3.3: ^{1}H NMR spectra of **ReL6.Boc** and **ReL6.Boc.L17** showing the aromatic region (in MeOD, 400MHz)

The ^{1}H NMR spectrum shows a multiplet observed at 4.70 ppm attributed to the methylene close to the triazole ring, also a singlet with two integrals signal was observed at 4.24 ppm corresponding to methylene close to pyridine ring of the **L17.** **ReL6.Boc.L17** containing Boc protecting groups is insoluble in water, so in order to get the target molecule and gain more water solubility these need to be removed. This was achieved by adding 4M solution of TFA in DCM. The ^{1}H NMR spectrum of **ReL6.L17** shows similar signals to **ReL6.Boc.L17** except the protons of the Boc group are absent. Mass spectrometry also confirms the successful synthesis, with a peak containing the characteristic rhenium isotope pattern observe at *m/z* 822. When reporting ESMS data, the complexes will be refered to in their non-protonated form, e.g. ReL6.L17 is a cationic Re(I) complex, therefore its corresponding peak in the mass spectrum is refered

to as $[M]^+$. RF-HPLC uses 0.1% TFA, it is therefore assumed that the complexes in this thesis are isolated as their TFA salt ($CF_3CO_2^-$) with amines protonated.

The pyridyltriazole bearing a Boc-protected **L10.Boc** is another N^N ligand containing branched polyamine. A similar synthesis route to **ReL6.Boc** is used to synthesize **ReL10.L17** via **ReL10.Boc** and **ReL10.Boc.L17** (Scheme 3.5).

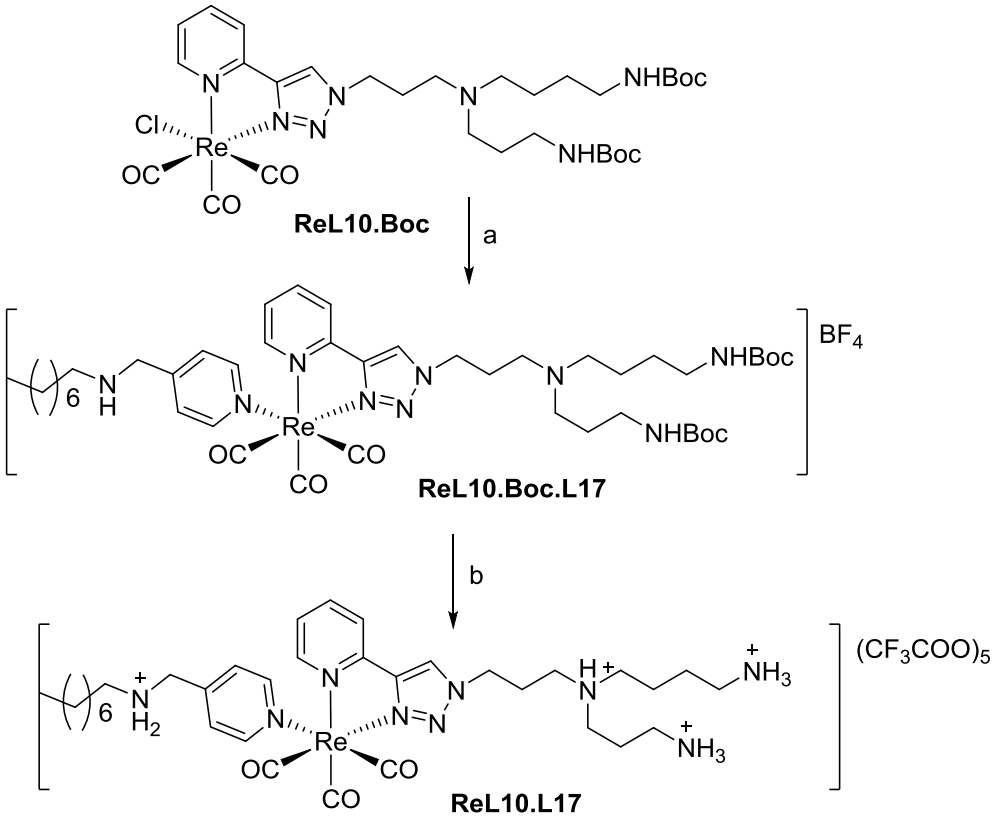

Scheme 3.5: Synthesis of **ReL10.L17** a) $AgBF_4$, MeCN, 1h, MW-90; **L17**, THF, 3h, MW b) 4M, TFA, DCM,18h

Once again, these complexes were characterized by NMR spectroscopy involving COSY, HSQC and HMBC in addition to mass spectrometry. The ^1H NMR spectrum shows all protons of pyridine ring were shifted down field and also the signal of triazole CH shifted from 8.17 to 9.10 ppm compared with free ligand. Also the signals of pyridine slightly shifted downfield.

The third type of rhenium(I) complex is **ReL3**. This type contains pyridyltriazole linked to an alkyl chain, while the axial pyridine ligand is linked to a polyamine. This complex was prepared by following the previous procedures (Scheme 3.6). All these complexes were characterized by NMR spectroscopy including COSY, HSQC and HMBC in addition to mass spectrometry.

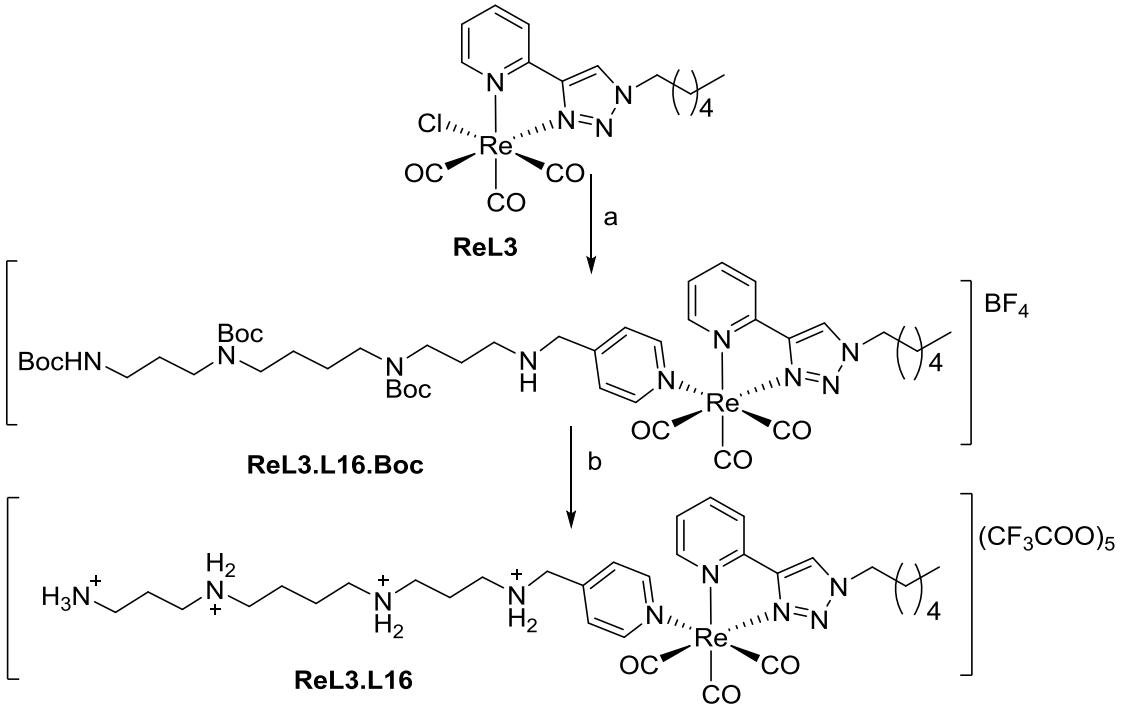

Scheme 3.6: Synthesis of **ReL3.L16** a**)** $AgBF_4$, MeCN, 1h, MW-90; **L16.Boc**, THF, 3h, MW b) 4M, TFA, DCM, 18h

The ^1H NMR spectrum of **ReL3** shows all protons of the pyridine ring were shifted downfield and also the signal of triazole shows a large shift from 8.17 to 9.10 ppm compared with free ligand. Also the signals of triazole ligand shifted downfield from 8.17 to 8.35 ppm compared with uncomplexed ligand. The signal of methylene protons adjacent to the triazole ring region change from a triplet (*) to non-first order multiplet (*) upon coordination of the pyta to rhenium as shown in Fig. 3.4.

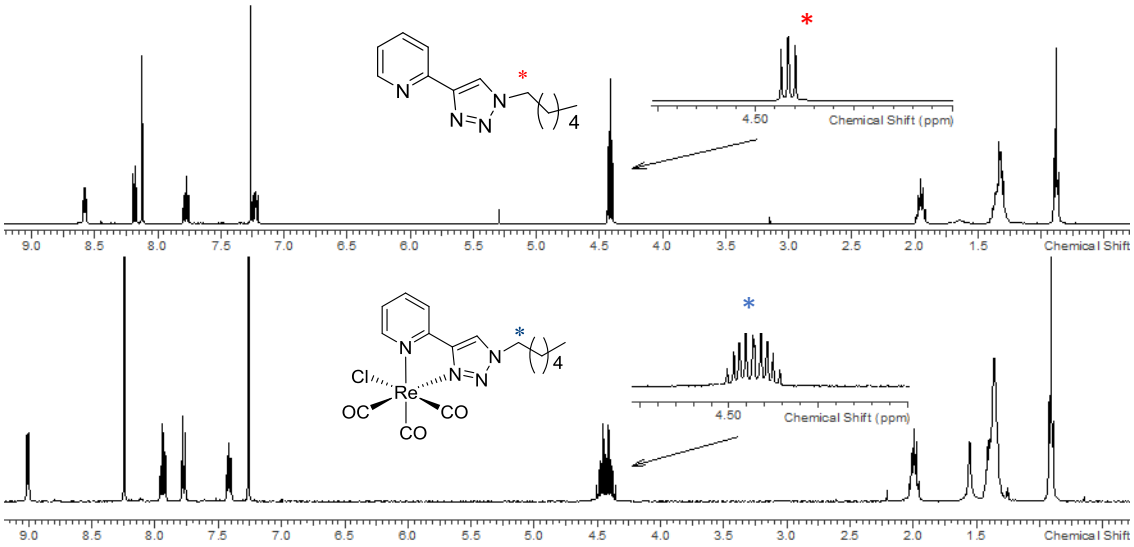

Figure 3.4: ^{1}H NMR spectra of **L3** and **ReL3** in ($CDCl_3$, 400MHz)

The ^{1}H NMR spectrum of **ReL3.L16.Boc** complex shows that pyridine signals are slightly shifted downfield compared with **ReL3**. The aromatic region of the spectrum has two additional signals corresponding to the pyridine ligand in **L16.Boc**, which are slightly shifted downfield compared to free ligand. The ^{1}H NMR spectrum also shows a large shifted downfield of triazole signal (*) compared to **ReL3** (*) due to electron density from pyridine ring and upon coordination to metal (Fig. 3.5). The ^{13}C NMR spectrum shows identical signal at 28.7 ppm corresponding to the methyl groups of the Boc groups and at 81.7, 80.9 and 79.9 assigned to quaternary carbon of Boc groups.

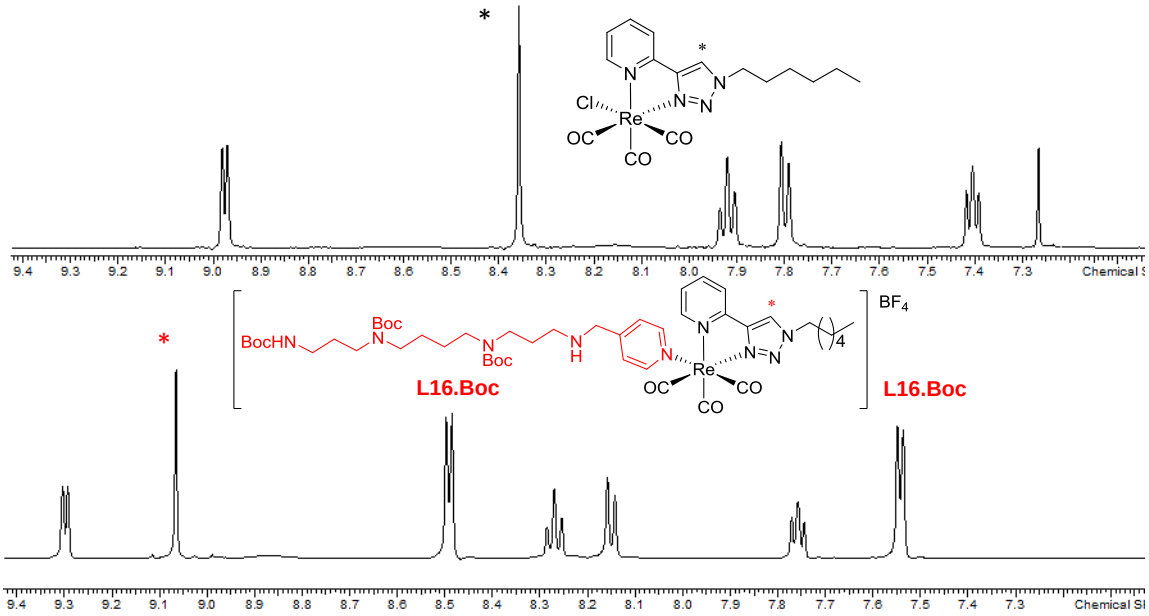

Figure 3.5: ^{1}H NMR spectra of **ReL3** and **ReL3.L16.Boc** showing the aromatic region in (MeOD, 500MHz)

After removing the Boc groups, the ^{1}H NMR spectrum of **ReL3.L16** shows the signals of the Boc groups are absent from the spectrum, indicating successful removal from the complex. It also shows that all signals of the protons of pyridine in **L16** or **L3** are shifted downfield in addition to the signal of triazole ring. The signal of the axial pyridine ligand has slightly shifted downfield compared with free ligand.

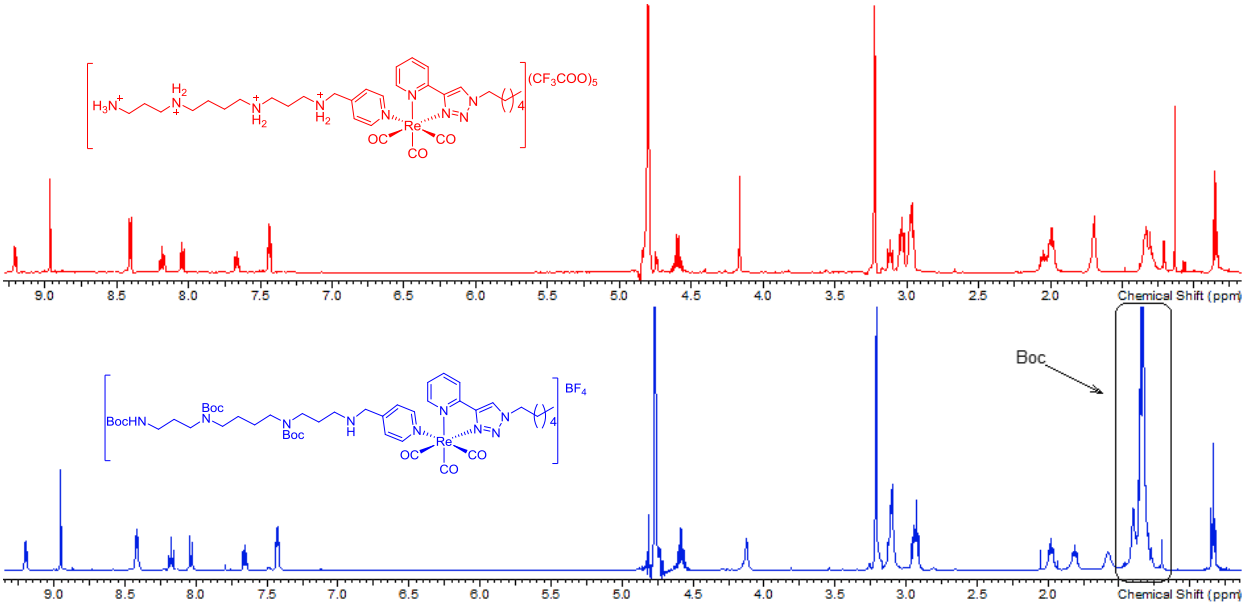

Figure 3.6: ^{1}H NMR spectra of **Re3.L16.Boc** (blue) and **Re3.L16** (red) in (MeOD, 500MHz)

The ^{13}C NMR spectrum shows that there are three signals observed at 196.5, 195.0 and 191.9 ppm assigned to three (C≡O) ligands. The ^{19}F NMR spectrum shows a singlet at -77.25 ppm corresponding to conuter ($CF_3CO_2^-$).

3.2.2 Rhenium(I) Complexes of Pyridyltriazoles Containing an Electron Withdrawing Group

Recently, it was found that the photophysical properties of rhenium(I) complexes can be tuned by modified the diimine ligand by adding electron withdrawing groups.[72] According to DFT studies by Xiao-Zhu *et al*. the introduction of electron-withdrawing groups (-NO_2 and -CN) can decrease the energy of the LUMO resulting in a narrower energy gap, which leads to red-shifting of the lowest energy absorption and emission bands in comparison with non-substituted ligands.[224] In order to apply this photophysical tuning in this study, two complexes were synthesised using **L8.Boc** or **L9.Boc** which are pyridyltriazole ligand substituted with –CF_3 in the 5-position of pyridine ring. Reaction of these with [$Re(CO)_5Cl$] in THF, under microwave heating allowed **ReL8.Boc** or **ReL9.Boc** complexes to be produced (Scheme 3.7). These complexes did not require any purification, ^1H NMR spectroscopy and 2D include COSY, HSQC and HMBC were used to characterize these complexes. The ^1H NMR spectrum of **ReL8.Boc** shows that three signals of pyridine are observed and shifted downfield, also the signal of the triazole has a large downfield shift compared with free ligand from 8.21 to 8.95 ppm due to the effect of the electron density of the pyridine ring (Fig. 3.7).

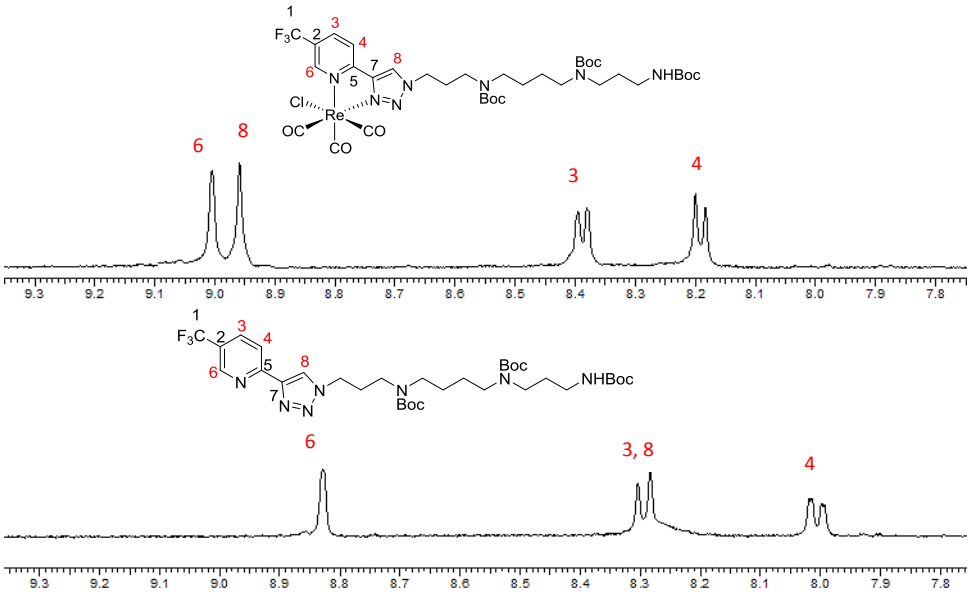

Figure 3.7: ^{1}H NMR spectrum of **L8.Boc** and **ReL8.Boc** showing the aromatic region

ReL8.L17 and ReL9.L17 were prepared by following the previous procedure for synthesis of **ReL6.L17**, (Scheme 3.7) starting with rhenium(I) chloride and then adding the axial pyridine ligand to synthesise Boc-protected complexes and then, the final form with the Boc groups removed. NMR spectroscopy and mass spectrometry confirmed the structures of these complexes.

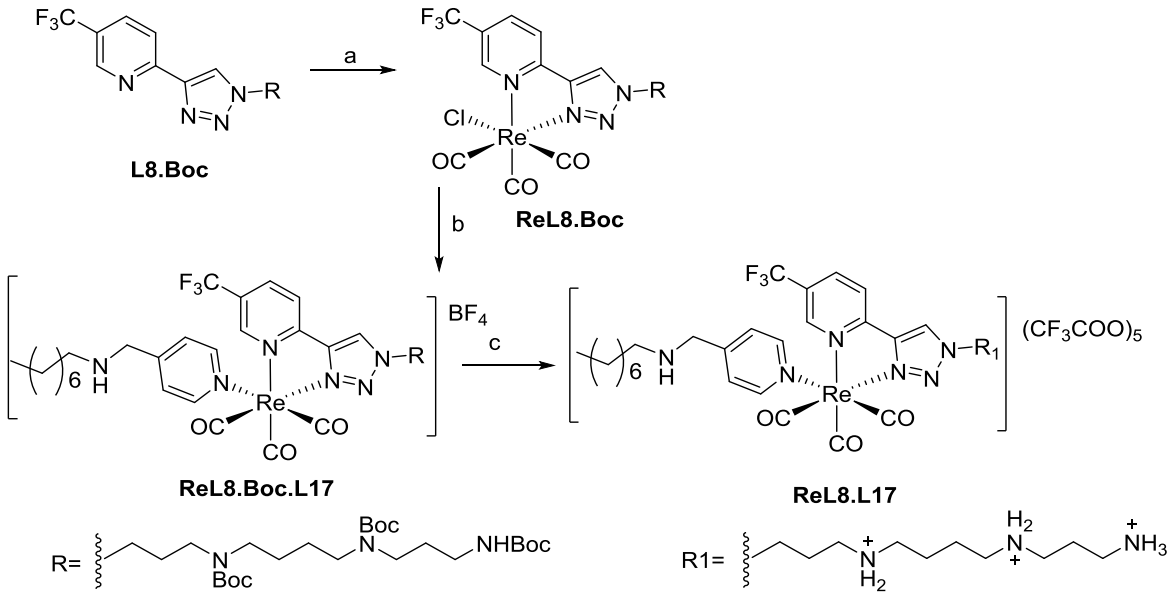

Scheme 3.7: Synthesis of **ReL8.L17** a) $Re(CO)_5Cl$,THF, MW-90, 3h ; b) $AgBF_4$, MeCN for 1h in MW-100; **L17**, THF for 3h MW-90ºC, c) 4M TFA/DCM, 18h.

The ^{1}H NMR spectrum of **ReL8.Boc.L17** shows two signals at 8.30 and 7.61ppm assigned to the protons of pyridine axial ligand, and also shows that the signal for the methylene protons adjacent to triazole ring changes from a triplet to non-first order multiplet upon coordination of the pyta to rhenium as shown in Fig. 3.8.

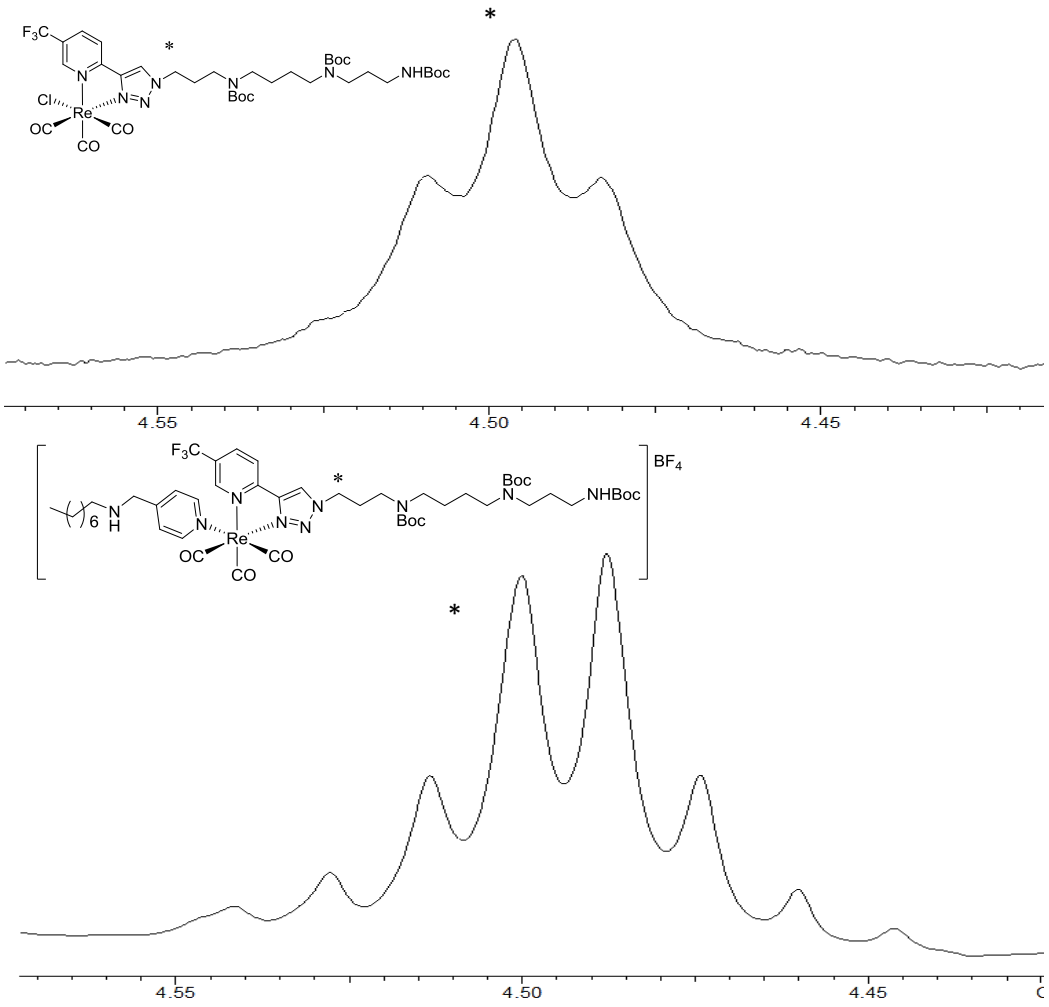

Figure 3.8: ^{1}H NMR spectra of **ReL8.Boc** and **ReL8.Boc.L17** shows methylene group

The ^{1}H NMR spectrum of **ReL8.L17** shows the signals of Boc groups disappear compared with spectrum of **ReL8.Boc.L17** and also shows all protons of pyridine shifted downfield due to metalation with rhenium(I), in addition to the proton of the triazole also shifted downfield affected by the ring current of the pyridine.[83] The ^{19}F NMR spectrum shows two peaks at -64ppm and one -77ppm assigned to CF_3 substituent and $CF_3CO_2^-$ respectively. COSY NMR spectroscopy shows that a doublet signal at 8.54 ppm adjacent to a doublet signal at 7.55 ppm for the axial pyridine ring and TOCSY

confirmed these connections. Mass spectrometry shows a peak at *m/z* 890 corresponding to the $[M]^+$.

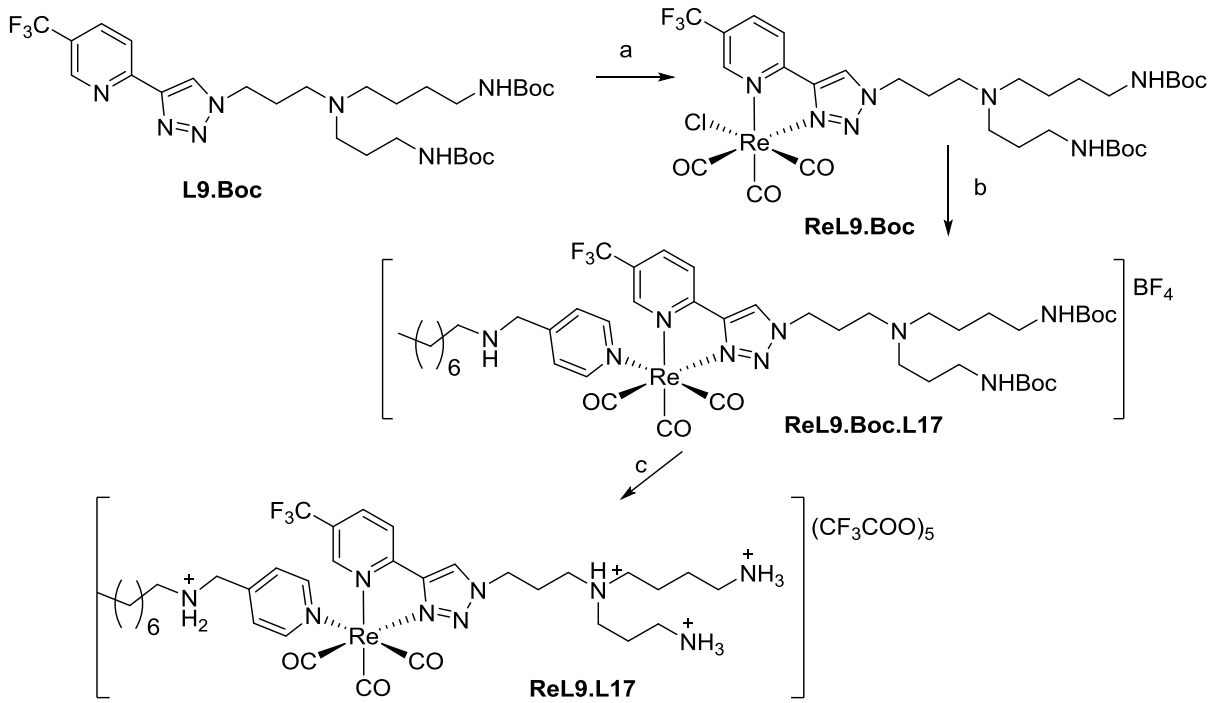

Scheme 3.8: Synthesis of **ReL9.L17** a) $Re(CO)_5Cl$,THF, MW-90,3h; b)AgBF4, in MeCN for 1h in MW-100; **L17**,in THF for 3h MW-90ºC; C) 4M TFA/DCM, 18h.

The ^1H NMR spectrum of **ReL9.Boc.L17** does not show a signal for the methylene protons adjacent to triazole ring because it overlaps with MeOD; this can be observed by changing the solvent to the CD_3CN, leading to the appearance of this signal at 4.71ppm. It can also be confirmed by HSQC NMR, showing the peak at 51.9 ppm corresponding to the carbon of the methylene adjacent to the triazole ring and also at 50.1 ppm to carbon of methylene adjacent to axial pyridine ring (Fig.3.9).

The ^{19}F NMR spectrum shows one peak at -63.1 ppm assigned to $-CF_3$ and is at -76.2 ppm assigned to $CF_3CO_2^-$, the integration signal of CF_3 group is used as a reference to determine the number of $CF_3CO_2^-$counter ions. **ReL9.L17** is the final product and the NMR shows similar signals to **ReL9.Boc.L17** except that the protons of Boc group are absent. Mass spectrometry shows a peak at *m/z* 890 attributed to $[M]^+$

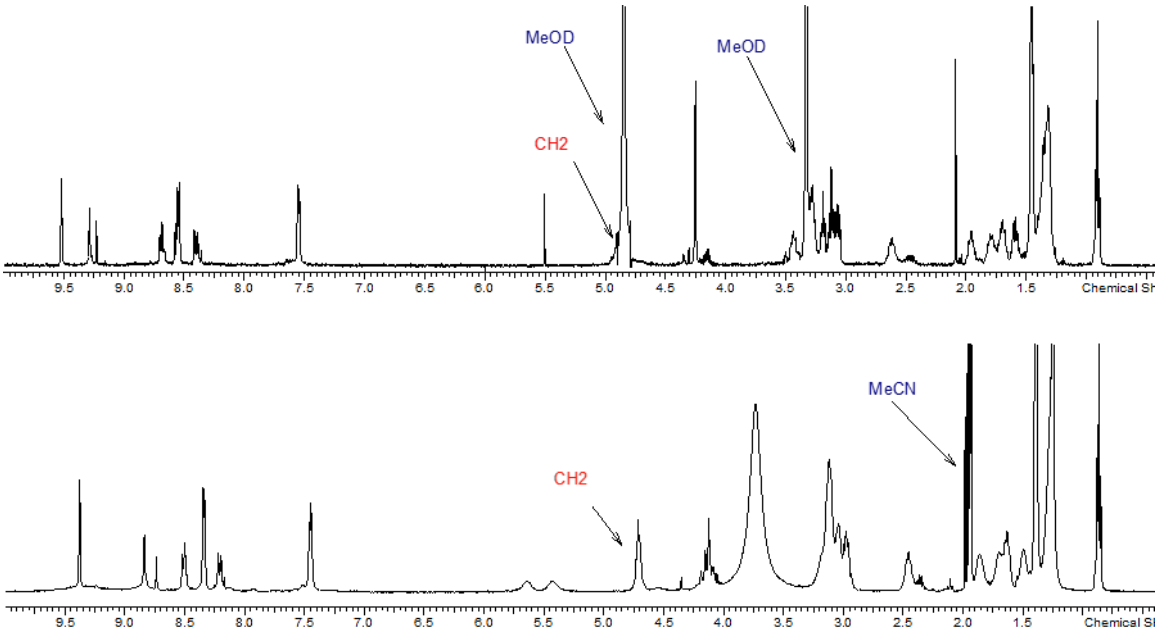

Figure 3.9: ^{1}H NMR spectra of **ReL9.Boc.L17** complex in different solvent

3.2.3 Rhenium(I) Complexes Based on a Bipyridine Ligand

Bipyridine ligands and their complexes became attractive since they were recognized in the 1970s,[103] particularly, rhenium(I) tricarbonyl complexes of the type *fac*[Re(CO)$_3$(N^N)L] where N^N = 2,2'-bipyridine. Their spectroscopic, photochemical and photophysical properties have continued to attract much attention ever since.[225] These complexes have strong spin-orbit coupling, resulting in enhanced singlet–triplet mixing, This class of chelated metal carbonyl complex are strong phosphorescent emitters possessing long-lived excited states.[74]

Furthermore, it has been shown that rhenium(I) complexes of this type can display two-photon excitation.[113] These complexes are luminescent at room temperature with excitation and emission in the visible region and exhibit long-lived emission which potentially can overcome the major drawback of organic fluorophores.[106] It was shown that the excited state properties of the Re carbonyl–diimine complexes can be controlled by a reasonable choice of the axial and diimine ligands and by the medium. These relations can be employed to design new functional molecular photonic materials. In this study new bipyridine derivative ligand was prepared via Stille coupling (as mentioned in the Chapter 2) and then coordinated with Re(CO)$_5$Cl to give **ReL11**(Scheme 3.9).

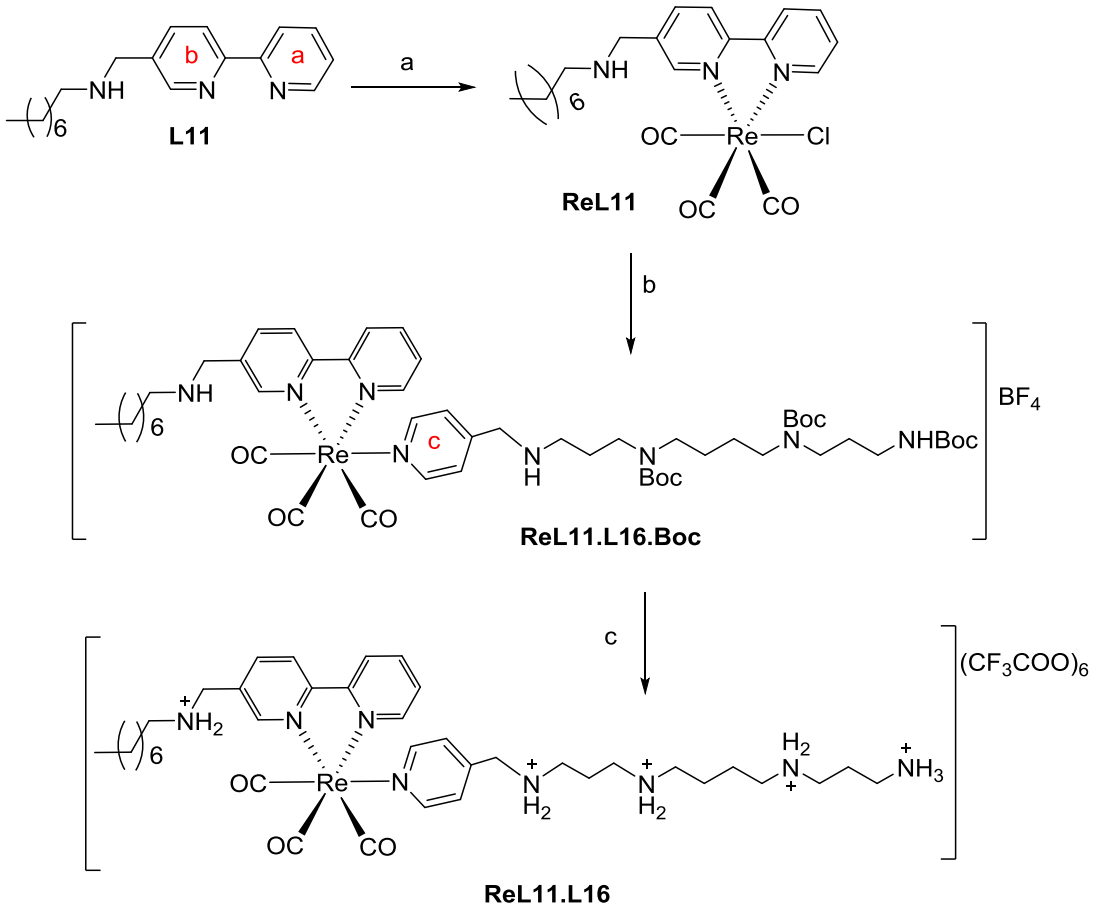

Scheme 3.9: Synthesis of **ReL11.L16** a) $Re(CO)_5Cl$ in THF for 3h, MW-90ºC b) $AgBF_4$, MeCN, 1h, MW-90ºC; **L16.Boc**, THF, 3h, MW-90ºC c) 4M TFA/DCM, 18h.

This route consisted of reaction between $[Re(CO)_5Cl]$ and **L11**, a bipyridne substituted with an alkyl chain, designed to interact with synaptic vesicles. This reaction was heated in microwave at 90ºC in the presence of THF. The product **ReL11** was obtained after 3h, column chromatography was used to purify this complex with a yield of 60%, and this yield is acceptable compared with literature.[226] This complex was characterized by ^1H NMR spectroscopy which showed that the protons of the bipyridine ring were shifted downfield compared with free ligands due to upon coordination to rhenium(I), especially the proton closest to the rhenium(I) metal which is observed at 8.71 ppm and significantly shifted compared with the free ligand 8.35 ppm for pyridine ring b. The protons of pyridine ring c also shifted from 8.39 to 8.60 ppm compared with free ligand. A singlet observed at 4.40 ppm was assigned to methylene protons adjacent to ring b, it is also shifted downfield compared to the free ligand due to the effect of the ring current of the pyridine. **ReL11** is not the final product for target molecules; it needs to be converted to the cationic complex which can be produced by coordination of **ReL11** with an axial pyridine; this ligand should also contain a polyamine because **ReL11**

contains an alkyl chain. **L16.Boc** was added to **ReL11** after abstracting the chloride using $AgBF_4$ to produce **ReL11.L16.Boc**. The product was purified by RP-HPLC method A. ^1H NMR spectroscopy, and 2D NMR spectroscopy including COSY, HSQC and HMBC were used to characterize this complex. **ReL11.L16** was obtained after adding 4M solution of TFA in dichloromethane. The ^1H NMR spectrum of **ReL11.L16** shows most of the signals of the bipyridine are shifted upfield affected by the ring current from the axial pyrindine ligand **L16.Boc** compared with **ReL11.L16.Boc**. Two doublet signals were observed at 8.49 and 7.52 ppm corresponding to the protons of **L16.Boc** has slightly shifted compared with **ReL11.L16.Boc** and two singlet signals were observed at 4.50 ppm and 4.25 ppm corresponding to protons methylene adjacent to the bipyridine ring and pyridine ring respectively. COSY NMR spectroscopy shows a doublet signal was observed at 9.39 ppm connected with 2H and also shows 1H with 3H as shown in Fig. 3.10.

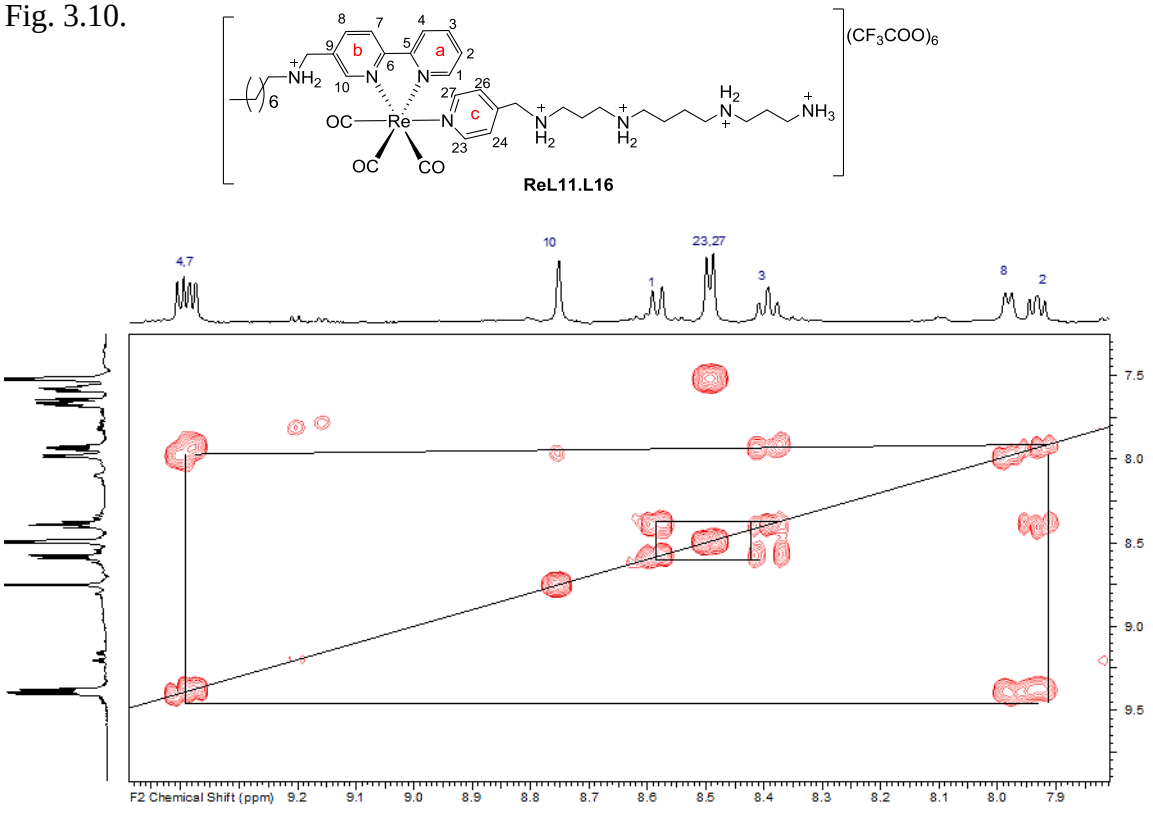

Figure 3.10: COSY NMR spectrum of the complex **ReL11.L16**

3.2.4 Rhenium(I) Complexes Based on an Inverse Pyridyltriazole

4-(2-pyridyl)-1,2,3-triazole (pyta) has been a widely used tool for the preparation of luminescent Re(I) complexes. Many functionalized derivatives have been developed with a pendant side chain of an alkyl or aromatic group, or a functionalization as a

biomolecule.[227] However, these complexes have some weaknesses such as a very low luminescence quantum yield in aqueous medium (typically around 0.7%). The preparation rhenium complexes based on 'inverse click' pyridytriazole have been studied in the last decade.[228] Inverse click refers to swapping the reaction of the azide and alkyne i.e. a 2-azidopyridine is reacted with an alkyne, while the regular reaction involves a 2-ethynylpyridine with an azide. These complexes show a high increase in luminescence intensity and quantum yield in aqueous solution in comparison to the corresponding pyridyltriazole complexes. Imaging studies showed a strong luminescence intensity enhancement in incubated breast cancer MDA-MB-231 cells.[229] Other studies demonstrated that the properties of these "inverse click" complexes have been compared with regular compounds by using a variety of techniques. X-ray crystallographic analysis shows that the regular and inverse complexes have the similar structure. The absorption spectra of the inverse rhenium(I) complexes are red-shifted compared to the regular compounds.[228] The 2-(1-R-1H-1,2,3-triazol-4-yl) pyridine ligands have been termed regular click chelators as they coordinate through the more electron rich N3 nitrogen atom of the 1,2,3-triazole unit. Inverse 2-pyridyl-1,2,3-triazole (inv-pyta) click chelators coordinate through the N2 nitrogen atom (Scheme 3.10).

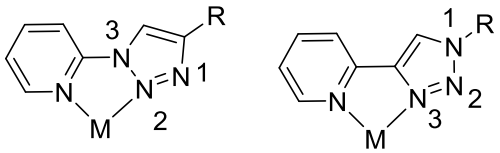

Scheme 3.10: Coordination of regular and inverse pyridyltriazole derivatives

This study takes advantage of this type of complex, inverse ligands were synthesised as the initial step to reach the final complexes. As mentioned in the Chapter 3, three type of inverse click ligand were synthesised: **L13, L14.Boc** and **L15.Boc,** these three ligands were reacted with $[Re(CO)_5Cl]$ to form three complexes: **ReL13**, **ReL14.Boc** and **ReL15.Boc** respectively.

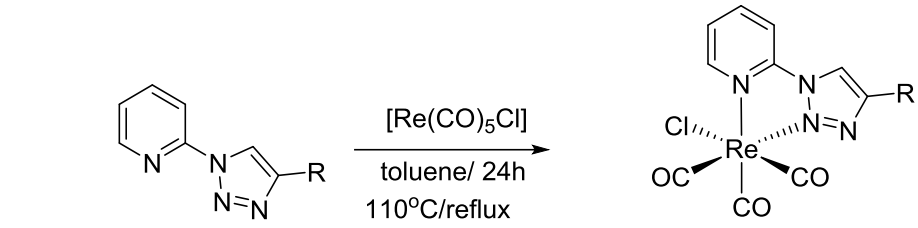

L13, R = $(CH_2)_5CH_3$
L14.Boc, R = $NHBoc(CH_2)_3NCH_2(CH_2)_4NHBoc$
L15.Boc, R = $NHBoc(CH_2)_3N(CH_2)_3(CH_2)_4NHBoc$

ReL13, R = $(CH_2)_5CH_3$
ReL14.Boc, R= $NHBoc(CH_2)_3NCH_2(CH_2)_4NHBoc$
ReL15.Boc, R = $NHBoc(CH_2)_3N(CH_2)_3(CH_2)_4NHBoc$

Scheme 3.11: Synthesis of inverse rhenium(I) complexes

ReL13 was synthesised by reaction between **L13** and $[Re(CO)_5Cl]$ in the dry toluene and heated at for 18h (Scheme 3.11). This reaction needs an inert atmospher because the ligand is sensitive to moisture, the reaction is carried out at high temperature, thus toluene is suitable solvent. After purification by column chromatography a bright yellow precipitate with a good yield was obtained in agreement with the literature.[229] **ReL14.Boc** and **ReL15.Boc** were prepared by reacting **L14.Boc** and **L15.Boc** respectively with $[Re(CO)_5Cl]$ and following the same strategy of synthesis **ReL13**. ^1H NMR spectroscopy confirmed that the reaction was completed, showing there is a downfield shift in the protons of pyridine and triazole rings of complex compared with free ligand. On coordination, the protons of the CH_2 close to the triazole ring were influenced as well, changing from a triplet to non-first order multiplet signal upon coordination with Re(I).

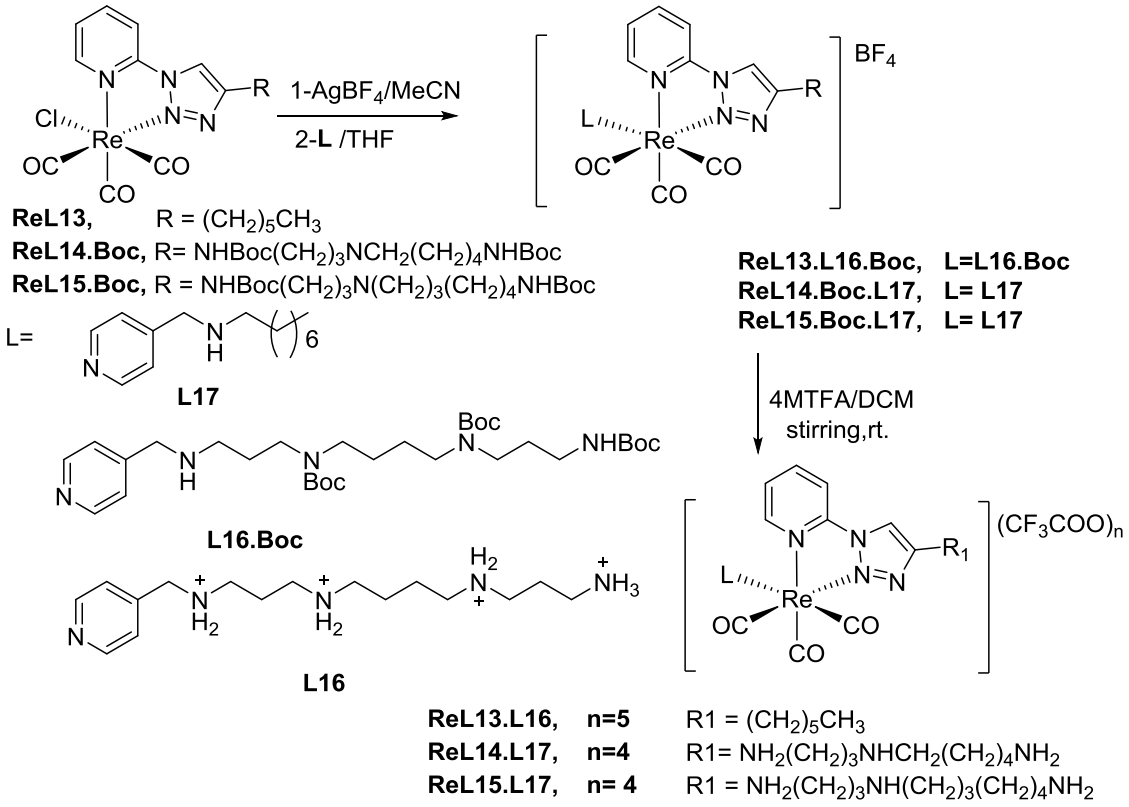

Scheme 3.12: Synthesis of rhenium complexes with inverse pyridyltriazole

These rhenium chloride complexes **ReL13, ReL14.Boc** and **ReL15.Boc** were heated in MeCN in presence of $AgBF_4$, then heated in THF in presence of an excess of substituted pyridine (Scheme 3.12). A pyridine substituted with a polyamine **L16.Boc** was used to obtain the protected form of the rhenium tricarbonyl pyridine complex **ReL13.L16.Boc,** while pyridine substituted with alkyl chain was used to form **ReL14.Boc.L17** and **ReL15.Boc**.**L17** and then purified by HPLC. **ReL13.L16, ReL14.L17** and **ReL15.L17** were produced as crude after adding 4M TFA/DCM. NMR spectroscopy confirmed that these complexes were formed along with mass spectrometry at *m/z* 794 for **ReL13.L16, ReL14.L17** and *m/z* 822 for **ReL15.L17** assigned to $[M]^+$. These complexes showed improved photophysical properties which are discussed in detail in the Chapter 4. ^{1}H NMR spectra of inverse complexes are similar to the regular complexes, except the position of the signal of methylene close to triazole ring was shifted (e.g. 4.68 ppm in **ReL3.Boc.L16**(*) to 2.96 ppm in the **ReL13.Boc**.**L16** (*) as shown in Fig. 3.11.

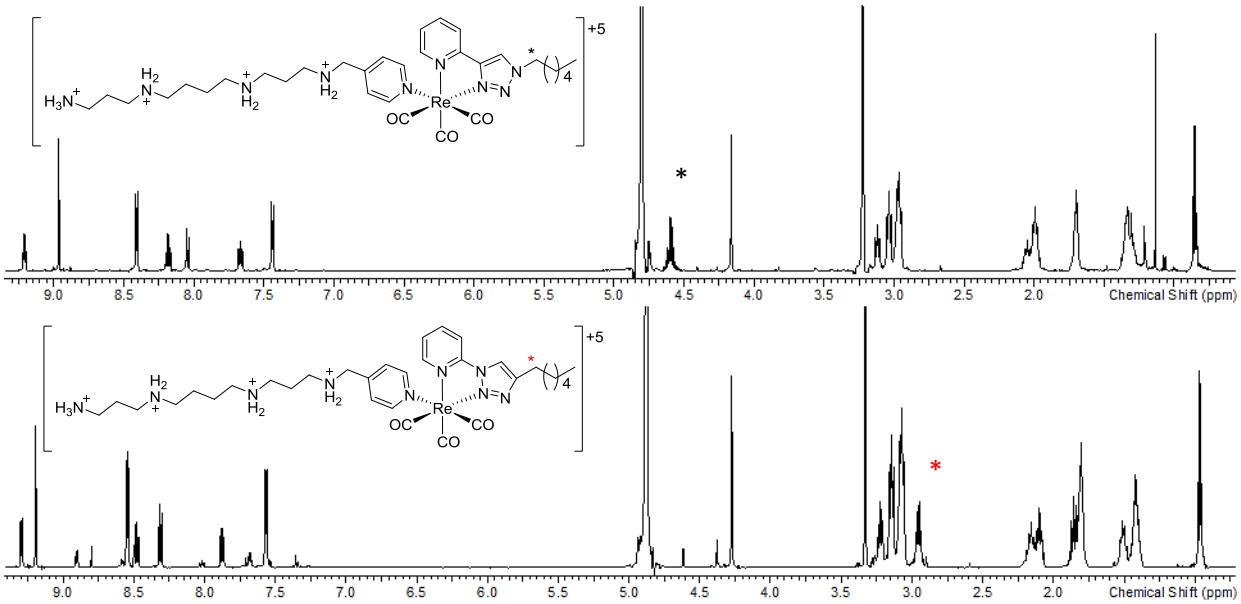

Figure 3.11: ^{1}H NMR spectra of **ReL3.L16** and **ReL13.L16** showing the methylene close to the triazole ring (MeOD, 500MHz)

3.2.5 Rhenium(I) Complexes Coordinated with an Axial Monodentate 1, 2, 3-triazole

A review of the use of 1,2,3-triazole ligands as monodentate ligand was reported by Suijkerbuijk *et al.*[230] who reported the coordination properties of cationic NCN-pincer palladium(II) and platinum(II) complexes (Scheme 3.13). Competition experiments with a range of other Lewis bases showed that these ligands are more strongly coordinating than H_2O, DMSO, MeCN and Et_2S, much weaker than PPh_3 and *N*-methylimidazole and comparable to pyridine.

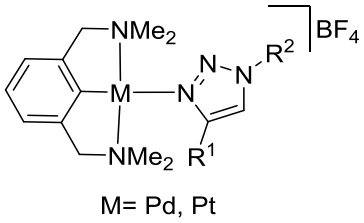

Scheme 3.13: Palladium(II) and platinum(II) complexes with axial monodentate 1,2,3-triazole ligands

Uppal. *et al.*[81] prepared a series of cationic bipyridyltricarbonylrhenium(I) complexes **40-43** with axial monodentate 1,2,3-triazole ligands and fully characterized these complexes shown in Scheme 3.13. This study revealed that these complexes are

luminescent in aerated dichloromethane at room temperature with emission maxima at 542 to 552 nm comparable to that of the pyridine analogue (549 nm) and blue shifted relative to the parent chloride complex. Long luminescent lifetimes are observed for the triazole complexes (475 to 513 ns) in aerated dichloromethane solutions at room temperature. This study found that these ligands are slightly better donors than pyridine.

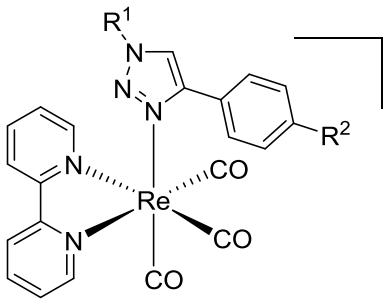

	X=	R^1	R^2
40	I	Me	H
41	Br	Pr	H
42	Br	Bz	H
43	Br	Pr	Me

Scheme 3.14: Rhemium(I) complexes bearing axial monodentate 1,2,3-triazole ligands

New rhenium(I) complexes were prepared with axially coordinated 1,2,3-triazole ligands, in order to investigate which ligand, pyridine or triazole gives, better luminescent properties when coordinated to rhenium(I) complexes in place of chloride (Scheme 3.15).

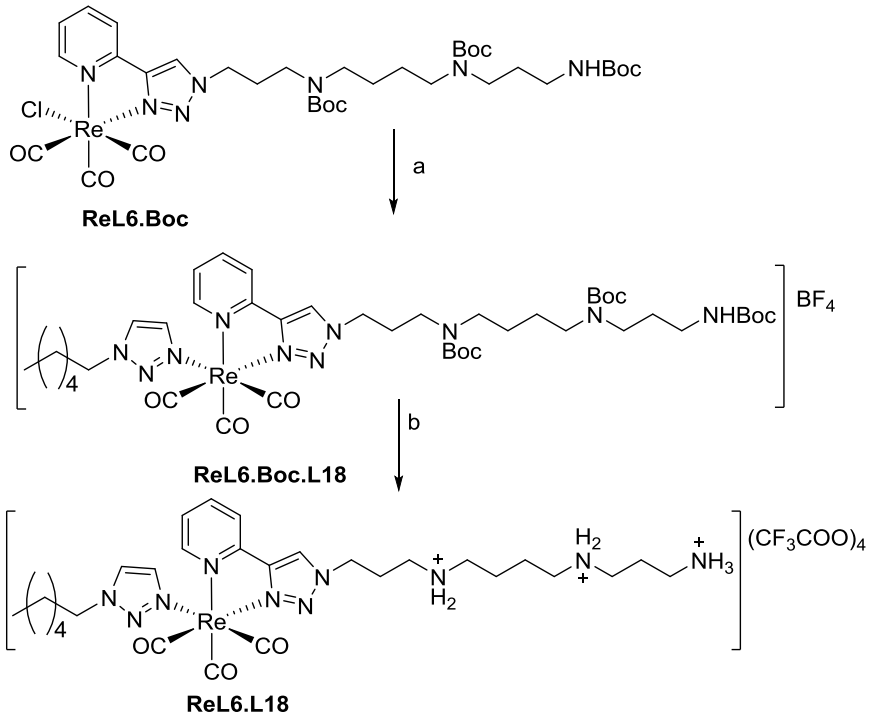

Scheme 3.15: Synthesis of **ReL6.L18** a) $AgBF_4$, MeCN, 1h in MW-90ºC; **L18**, THF, 3h, MW-90ºC b) 4M TFA/DCM, 24h

ReL6.L18 was prepared by following the procedure reported earlier for corresponding of rhenium(I) complex **ReL6.Boc** bearing an axial chloride ligands. **L18** was prepared as mentioned in Chapter 2, this ligand was used to replace pyridine as a ligand, because the triazole moiety in this complex leads to a destabilization of the ligand-based LUMO of their complex resulting in a blue-shifting in optical absorption and emission maxima. ^{1}H NMR spectroscopy was confirmed that the rhenium(I) complex coordinates with the triazole though the N3 giving the same two signals for protons of triazole ring at 8.06 and 7.79 ppm which are shifted downfield compared with free ligand.[81] The triazole ligand was also used as a monodentate axial ligand instead of pyridine in a complex containing CF_3 substituted pyridine **ReL9.L18** (Scheme 3.16). The impact on the photophysical properties of the rhenium(I) complex when using triazole as axial ligand are discussed in Chapter 4.

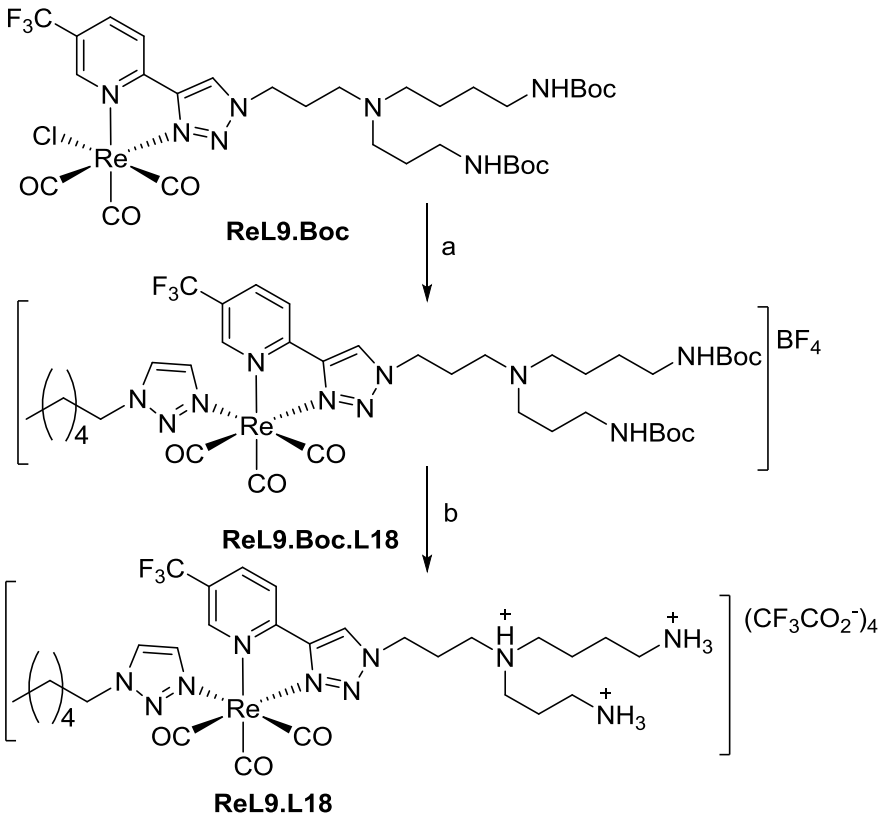

Scheme 3.16: Synthesis of **Re5-dL18** a) $AgBF_4$, MeCN, 1h in MW-90ºC; **L18**, THF, 3h, MW-90ºC b) 4M TFA/DCM, 24h

ReL9.L18 was prepared according to the previous procedure as mentioned in earlier sections. RP-HPLC was used to purify this complex. ^{1}H NMR spectroscopy of **ReL9.L18** shows that there are two protons in the aromatic region attributed to triazole axially

ligand at different location compared axial ligand of **ReL9.L17** (Fig. 3.12). Mass spectrometry shows a peak at m/z 823 corresponding to $[M]^+$.

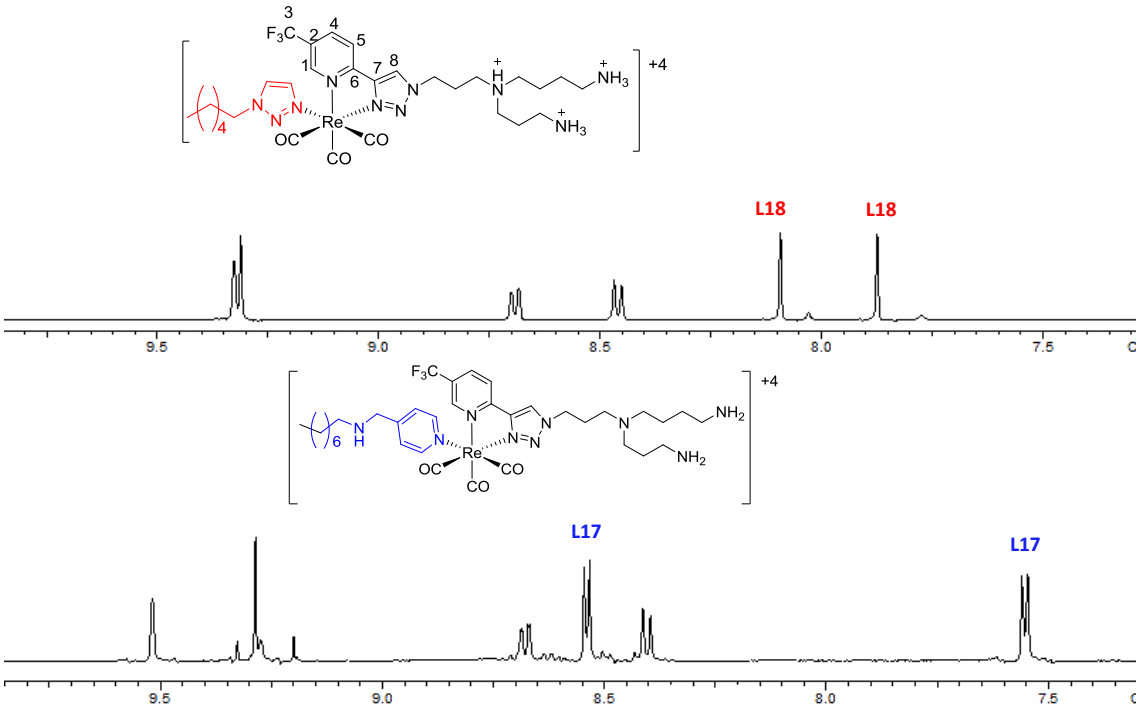

Figure 3.12: ^{1}H NMR spectra showing of the aromatic region of **ReL9.L18** and **ReL9.L17** in (MeOD, 500MHz)

3.3 Synthesis of Iridium(III) Complexes

Different types of ambiphilc iridium(III) complexes prepared in this chapter are shown in scheme 3.17.

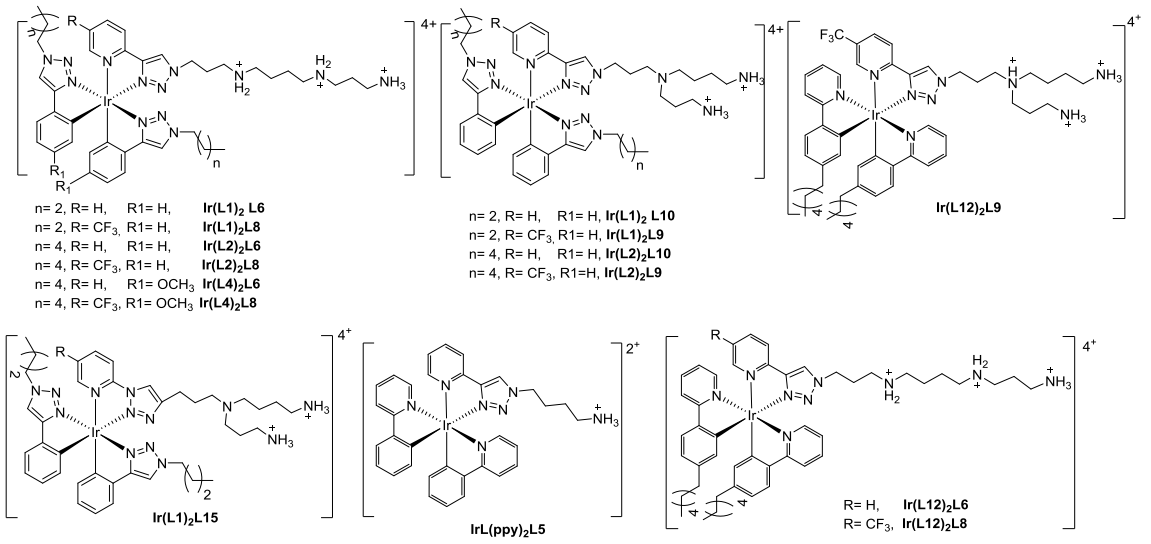

Scheme 3.17: The structure of iridium(III) complexes prepared in this work

3.3.1 Ortho-metallation

The process of cleavage of *ortho* C-H bonds of aryl groups by metals is called ortho-metallation reactions. Metal-carbon (M-C) bonds are the result of this reaction. The reaction is usually between aryl groups bound to coordinated donor atoms such as nitrogen or phosphorus and with electron-rich metals in low oxidation states, which are able to undergo oxidative additions. Examples of *ortho*-metalating ligands include; 2-phenylpyridine (ppy), benzo[h]-quinoline (bzq) and 2-(2-thienyl)pyridine (thpy), Fig. 3.13. The vast majority of these coordinate to the Ir, forming a 5-membered metallacycle through activation of the *ortho* C-H bond of a phenyl ring that is adjacent to the heterocycle.[231]

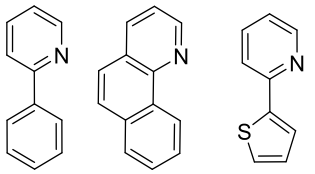

Figure 3.13: Common *ortho*-metalation ligands precurors

The mechanism of the formation metallacycles involves the metal connected to donor atoms forming an intramolecular five-membered ring (2) (Scheme 3.18) the ligand loses the proton and coordination to the metal ion though activation of the *ortho* C–H bond adjacent heteroatoms such as N atom in phenylpyridine and then metallacycle compound (3) is formed.

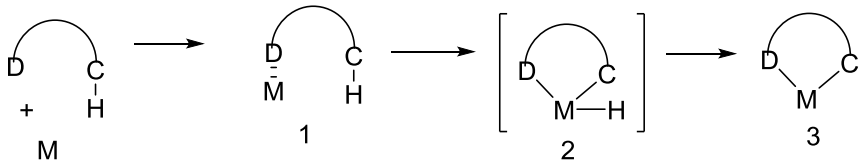

Scheme 3.18: Mechansium of ortho C-H

Symbol D is used to represent the donor group of aromatic heteroatoms adjacent to C-H activation. This mechanism is widely used to form metal-carbon σ-bound with Pd(II) and Pt(II) as well as Ir(III), Rh(III).[232]

In 1984 the first reaction using this mechanism to prepare dichloro-bridged Ir(III) dimers was reported by Watts *et al.* The first procedure gave a 72% yield using ppy or benzo[*h*] quinoline as *N,C*-cyclometallating ligands, and heating at reflux iridium trichloride hydrate with the ligand in 2-ethoxyethanol–water for one day (Fig.3.14, a).[233, 234]

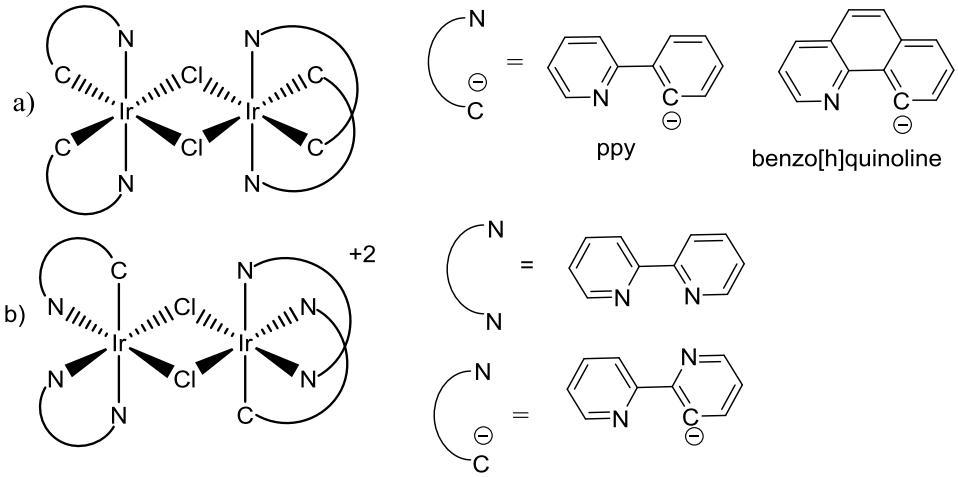

Figure 3.14: Representation of cyclometallated dichloro-bridged dimers

A few years later, the same group found another procedure to prepare a dichloro-bridged dimer and the iridium centre is surround by one *N,N*-coordinated bpy and one *N,C*-coordinated bpy by reacting potassium hexachloroiridium(IV) and potassium hexachloroiridium(III) with bpy in EtOH–H_2O, (Fig. 3.14).[235] Different types of bridged iridium dimer complexes were synthesized based on phenylpyridine, these chloro-

bridged diiridium species are very poorly emissive at room temperature and also have low quantum yield.[236] In this study, a number of dichloro-bridged iridium dimers were synthesised, their structures are shown in Scheme 3.19 and 3.20.

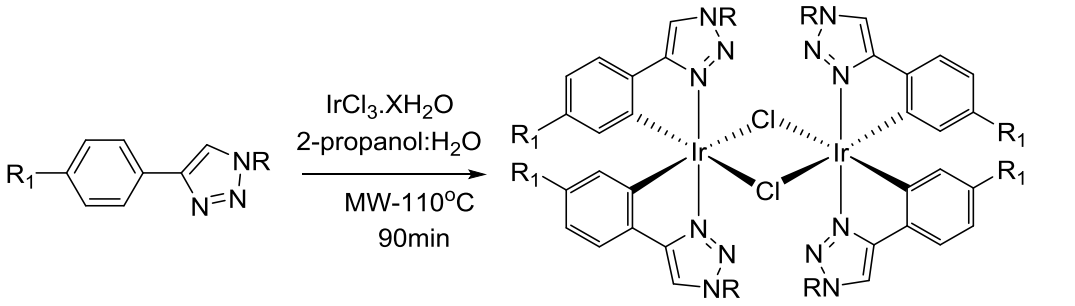

R1 = H, R = $(CH_2)_3CH_3$, **HL1**
R1= H, R = $(CH_2)_5CH_3$, **HL2**
R1= OCH_3,R = $(CH_2)_5CH_3$, **HL4**

R1=H, R= $(CH_2)_3CH_3$, **$[Ir(L1)_2Cl]_2$**
R1=H, R= $(CH_2)_5CH_3$, **$[Ir(L2)_2Cl]_2$**
R1=OCH_3,R= $(CH_2)_5CH_3$, **$[Ir(L4)_2Cl]_2$**

Scheme 3.19: Synthesis of iridium(III) dimer bearing pyridyltriazoles ligands

Also another series of iridium dimers bearing phenylpyridines as a cyclometalating ligand were synthesised (Scheme 3.20).

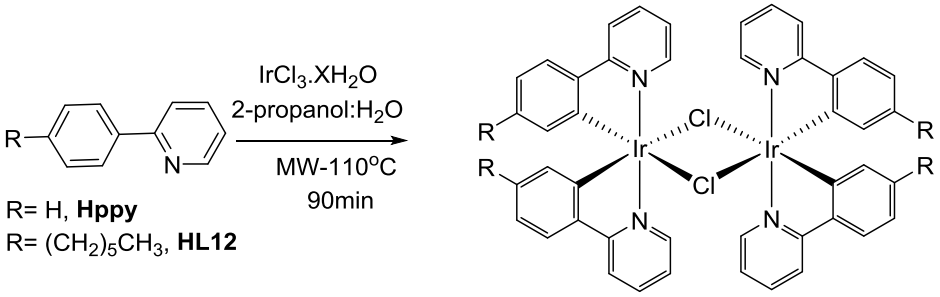

R= H, **Hppy**
R= $(CH_2)_5CH_3$, **HL12**

R = H, **$[Ir(ppy)_2Cl]_2$**
R = $(CH_2)_5CH_3$ **$[Ir(L12)_2Cl]_2$**

Scheme 3.20: Synthesis of iridium(III) dimer bearing phenylpyridines ligands

Phenyltriazole based iridium dimers **$[Ir(L1)_2Cl]_2$** and **$[Ir(L2)_2Cl]_2$** were characterized only by mass spectrometry because the NMR spectra were fluxional a similar observation was reported by Schubert *et al.*[237] when phenyltriazole were used for cyclometalation due to that the choride could be coordinate with lone pair of nitrogen in triazole ring. While **$[Ir(ppy)_2Cl]_2$** and **$[Ir(L12)_2Cl]_2$** were charactarized by NMR spectroscopy and mass spectrometry, the phenylpyridines complexes exhibit more rigid NMR behaviour.

3.3.2 Iridium(III) Complexes Bearing Pyridyltriazoles

Ortho-metallated chloride bridged dimer complexes were weakly emissive at room temperature according to the literature.[236] So, they were considered unsuitable for bioimaging probes, as the important requirement in this project that the complexes should be emissive; this is the initial requirement for these complexes. So it is important to convert these complexes to cationic mononuclear iridium(III), complexes which have been widely used for a variety of bioimaging applications,[123] Thus, the first requirement to be usefully applied in the biological field is: good photophysical properties and also a low toxicity in cells, more solubility and finally large Stokes shift. The first target can be achieved by enhancing the emission of the bridged iridium(III) complexes through breaking these iridium(III) dimers with a bidentate diimine ligand which is refered to as the ancillary ligand (N^N). These complexes were synthesized according to a literature procedure.[234] This procedure consists of the formation of a dichloro-bridged iridium(III) intermediate with the form $[Ir(C\hat{}N)_2Cl]_2$ where C^N is a cyclometalating ligand such as the commonly used 2-phenylpyridine. In this work, pyridyltriazole was used to break the iridium(III) dimer. These ligands can be modified by adding electron withdrawing groups such as ($-CF_3$) in order to stabilise the LUMO and red shift the emission by decreasing the gap between the LUMO and HOMO.[123] The second target in this study, was that the complexes should be amphiphilic molecules, this can achieved by adding alkyl chains. **$Ir[(L1)_2Cl]_2$**, **$[Ir(L2)_2Cl]_2$** and **$[Ir(L12)_2Cl]_2$** were synthesized for this purpose. The third target is to get good solubility and internalize into synaptic vesicles, this can be achieved by using polyamines which link to ancillary ligands such as **L6.Boc, L8.Boc** as shown in Scheme 3.21.

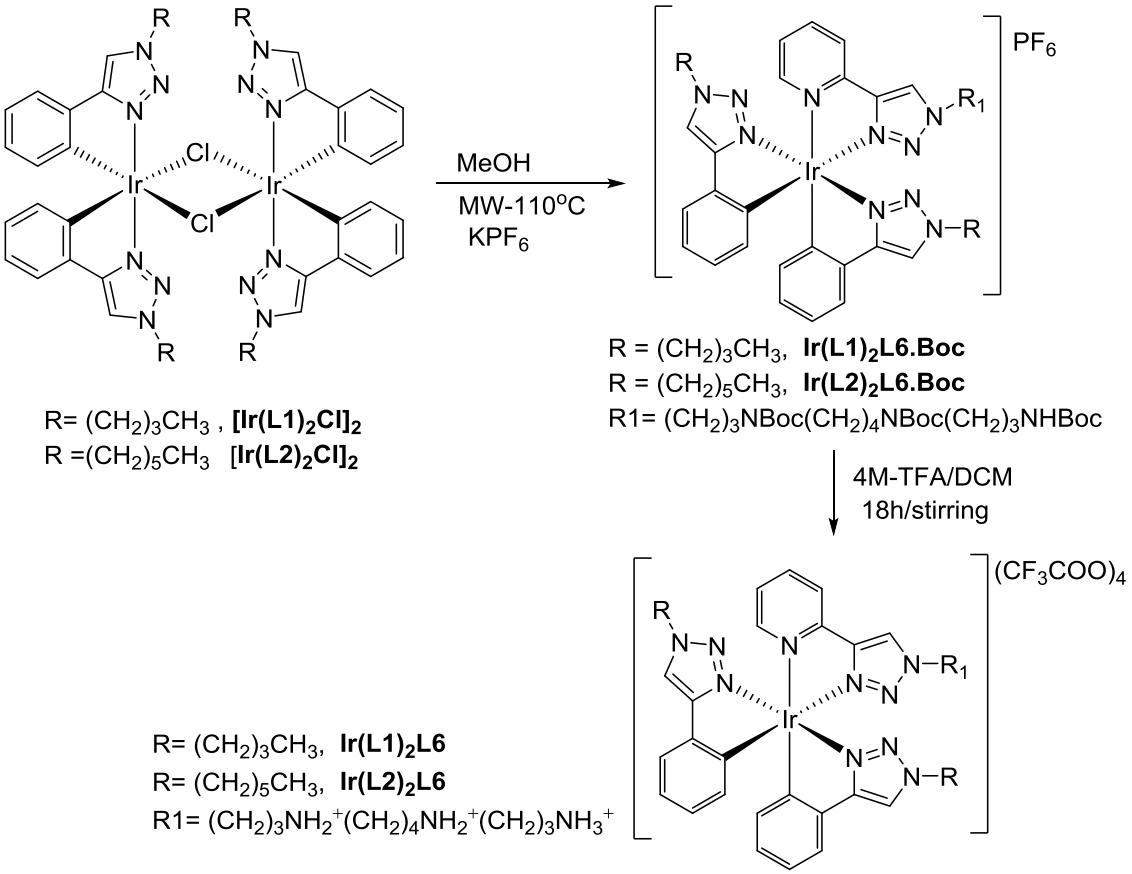

Scheme 3.21: Synthesis of **Ir(L1)$_2$L6** and **Ir(L2)$_2$L6**

All iridium(III) complexes were prepared in two steps, the first step being preparation of a chloride-bridged iridium dimer according to the Nonoyama reaction and second step breaking the dimer with ancillary ligand, with KPF_6 added in order to change the counter anion to PF_6^-. This route yielded **Ir(L1)$_2$L6.Boc** and **Ir(L2)$_2$L6.Boc** in good yield, consistent with literature reports of related complexes.[85] All the complexes were obtained by reacting the corresponding iridium(III) dimer with a bidentate ligand such as pyridyltriazole ligand linked to a Boc-protected polyamine in MeOH and then heating under microwave at 110ºC for 90 min at pressure 150 psi and power 50 W. TLC analysis was used to monitor the reactions and typically showed only one new spot, characterized by a bright luminescence under 365 nm illumination. All the complexes were purified by alumina column chromatography. NMR spectroscopy was used to characterize these complexes including: ^{1}H NMR, COSY, HSQC and HMBC in addition to NOESY and TOCSY. The ^{1}H NMR spectrum of **Ir(L1)$_2$L6.Boc** shows all protons of the phenyl after cyclometallation typically shifted upfield due to the ring current from the cyclometalation with the proton of the triazole shifted downfield. The protons of the ancillary ligand were shifted upfield except for the proton of the triazole

which was shifted downfield due to the effect of the ring current of the cyclometalated ligand comparing to free ligand. ^{1}H NMR spectra of **Ir(L2)$_2$L6.Boc** showed similar shifting pattern for **Ir(L1)$_2$L6.Boc.** Mass spectrometry shows a peak at 1280.67 assinged to $[M]^+$. The ^{19}F NMR shows a doublet at -74.6 ppm corresponding to fluorine in a counter PF_6^- as shown in Fig. 3.15.

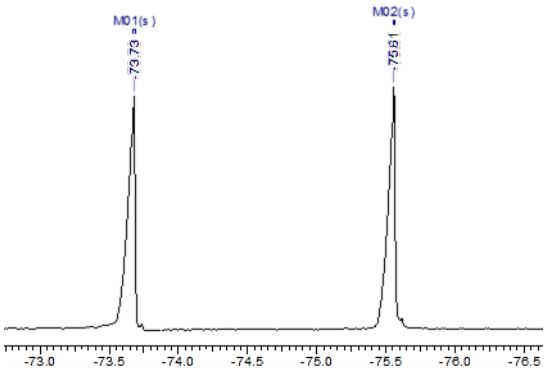

Figure 3.15: ^{19}F NMR spectrum of **Ir(L2)$_2$L6.Boc**

These complexes are insoluble in water. Solublility is one of the requirements for an imaging agent. The Boc-protecting groups need to be removed from the amines by adding a 4M solution of TFA in dichloromethane and stirring for 18h. Brown and sticky products were obtained that could be purified by RP-HPLC at t_R = 23.8 min, using method A.

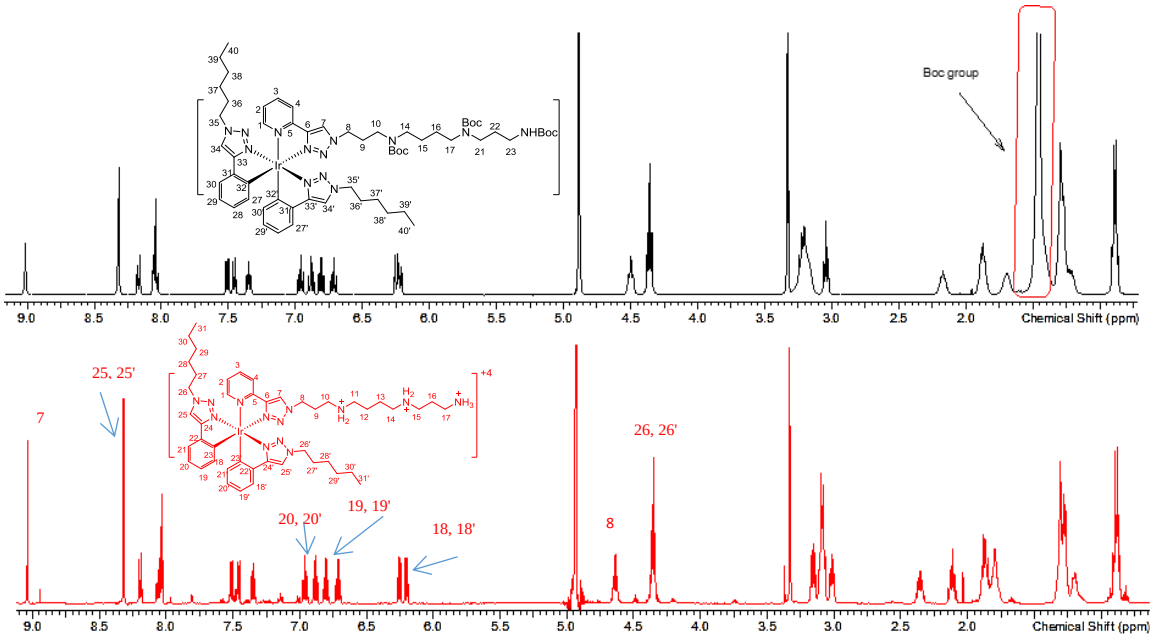

Figure 3.16: ^{1}H NMR spectrum of **Ir(L2)$_2$L6.Boc** (black) and **Ir(L2)$_2$L6** (red)(MeOD, 500MHz)

NMR spectroscopy and mass spectrometry were used to characterize these complexes. ^{1}H NMR of **Ir(L1)$_2$L6** or **Ir(L2)$_2$L6** showed similar signals to the spectrum of **Ir(L1)$_2$L6.Boc** or **Ir(L2)$_2$L6.Boc** except the signal for the Boc groups were missing. The ^{19}F NMR spectra of **Ir(L2)$_2$L6** shows singlet at -77.3 ppm (Fig. 3.17) attributed to fluorine in the counter anion $(CF_3CO_2)^-$ while that of **Ir(L1)$_2$L8** shows two signals due to the CF_3 substituent on the pyridine which was used as a reference to determine the number of counter anions by calculating the integral for both peaks.

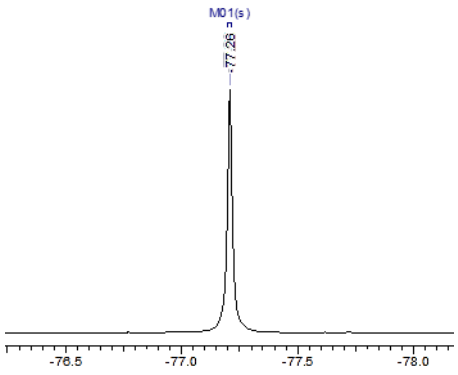

Figure 3.17: ^{19}F NMR spectrum of **Ir(L2)$_2$-L6**

The NOESY spectrum of **Ir(L1)$_2$L6** is an important tool to distinguish between two protons in different cyclometating rings, it shows that there is a correlation between

(7H, 21'H) and also NOESY shows there is nOe correlation between (25H, 26H) and also correlation between (26H, 27H). It also nOe shows that 7H has a correlation with (20'H) and (18'H). Also there are nOe between (25H, 21'H) and (8H, 10H) as shown in Fig.3.18. This enables assignment of the two inequivalent phenyltriazole ligands.

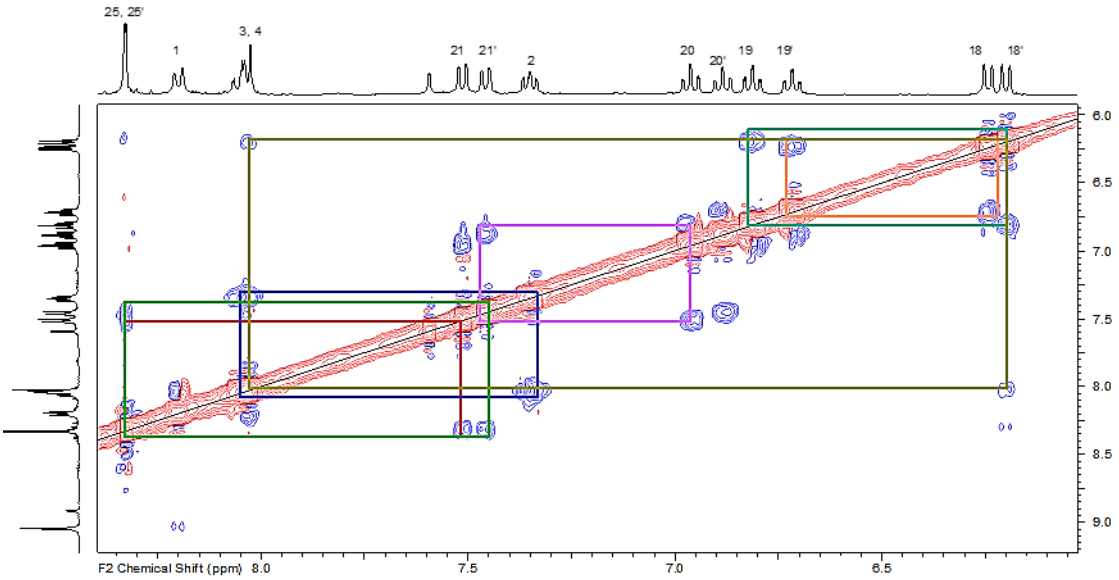

Figure 3.18: NOESY spectrum of **Ir(L1)$_2$L6** (MeOD, AV-400MHz)

In the TOCSY NMR spectrum (Fig. 3.19), the orange circle shows connections between proton 1 and 3,4 and 2 protons, the pink circle shows the connection between proton 21 and 20, 19, and 18 and the blue circle shows the connection between 21' with 20', 19'and 18'. This technique allows all protons in a given ring system to be identified.

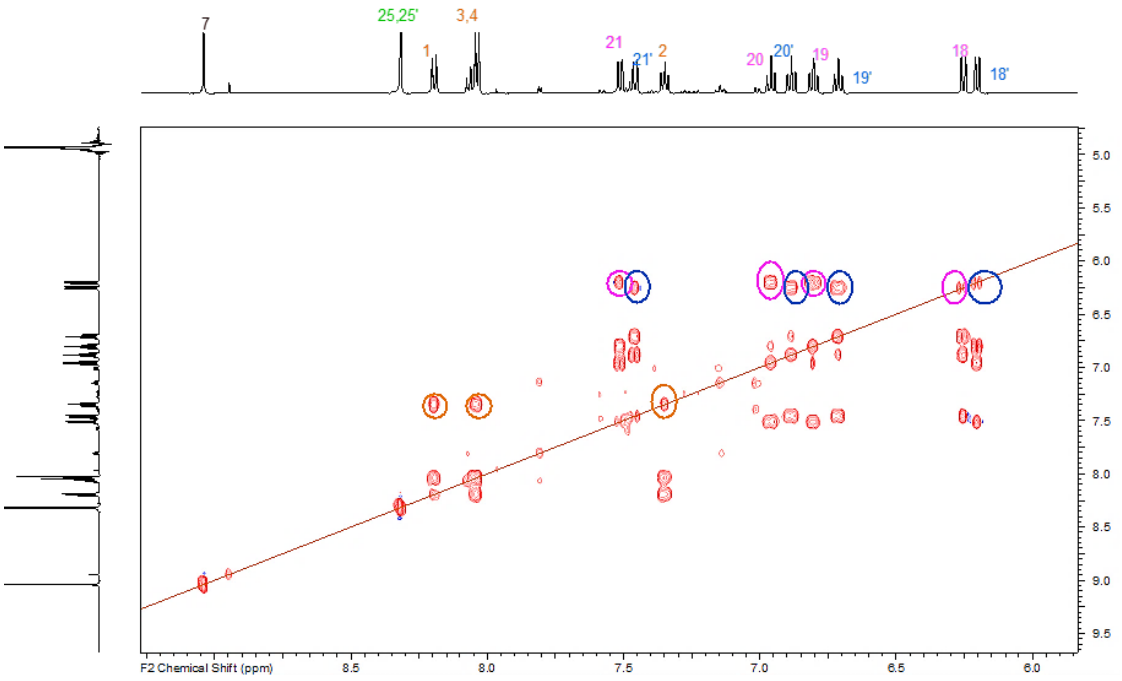

Figure 3.19: TOCSY NMR spectrum of **Ir(L1)$_2$L6** (MeOD, AV-400MHz)

3.3.3 Enhancing the Emission of Iridium(III) Complexes

In order to enhance the photophysical properties of the iridium(III) complexes to be suitable for use as imaging agents, it is necessary to tune the excitation and emission to longer wavelength.[238, 239] One important strategy is to attach electron withdrawing or releasing groups to the phenyl ring of the cyclometalated ligand or the substituted pyridine in the ancillary ligand.[240-243] In this study, an electron withdrawing -CF_3 is substituted in the *meta* position of the pyridine moiety of the ancillary ligand (Scheme 3.22). It was found that the photophysical properties for these complexes exhibited long wavelength emission at (575 nm) compared to the corresponding complex without –CF_3 group (more details in Chapter 4).

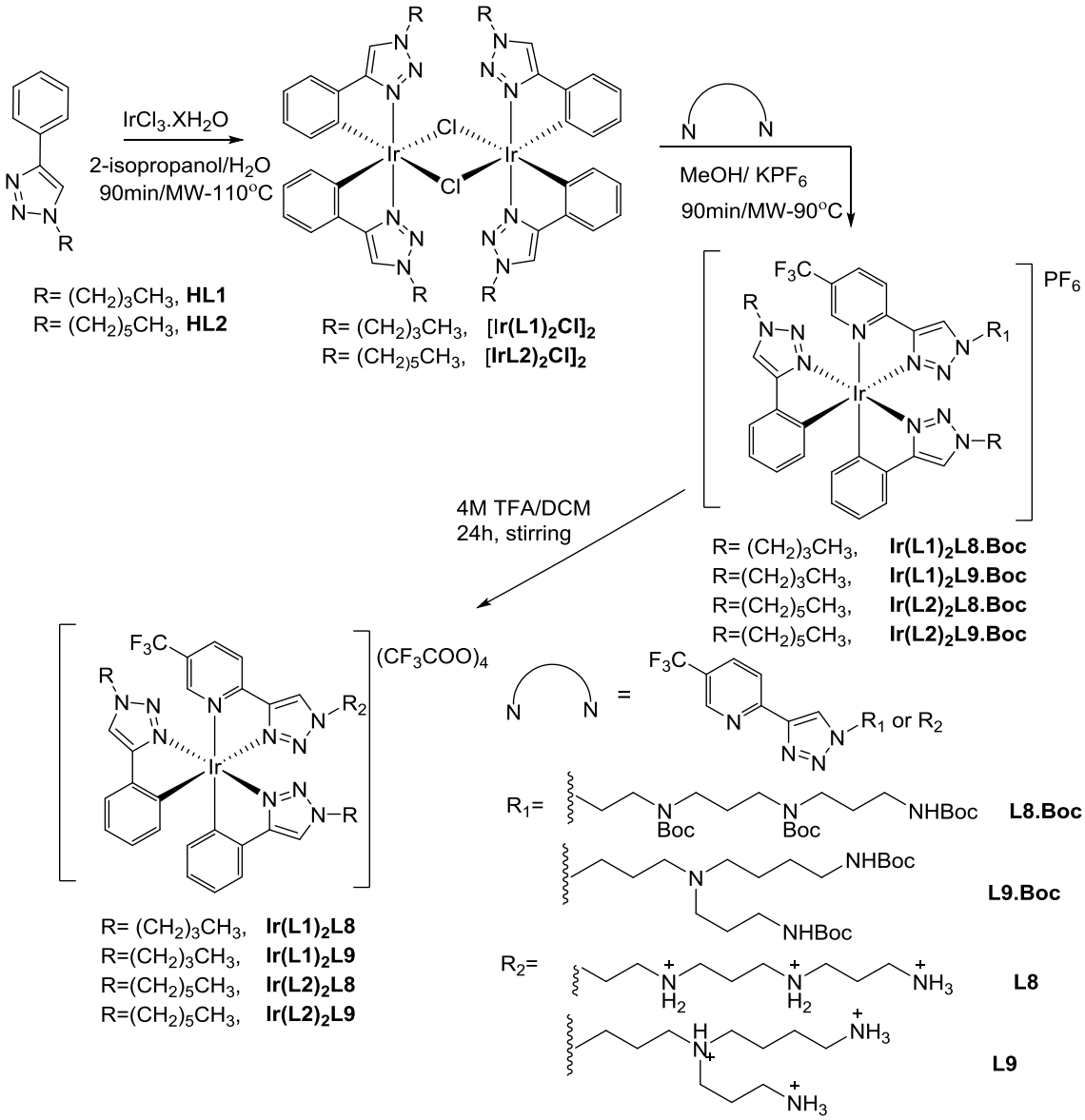

Scheme 3.22: Synthesis of iridium(III) complexes bearing an electron withdrawing group

Microwave heating was used to synthesise the **[Ir(L1)$_2$Cl]$_2$** and **[Ir(L2)$_2$Cl]$_2$** dimers according to the procedure described in the literature[234] and from these, corresponding cyclometalated iridium(III) complexes **Ir(L1)$_2$L8.Boc** and **Ir(L1)$_2$L9.Boc** were prepared and purified by RP-HPLC. The ^{1}H NMR spectrum of **Ir(L1)$_2$L8.Boc** shows the most significant shifts belonged to the protons close to iridium, leading to proton deshielding and a downfield shift. The ^{1}H NMR spectrum also shows the signal of the proton of triazole was observed at 8.28 ppm and shifted upfield compared with the free ligand due to the influence of the ring current of another cyclometalated ligand at the same metal. The ^{1}H NMR spectrum shows all signals of ancillary ligand pyridine ring were shifted

downfield compared with the free ligand except the signal of triazole ring which was observed at 8.21 ppm was shifted upfield compared with free ligand 8.14 ppm due to the effect of the ring current from the phenyltriazole ligand as shown in Fig. 3.20

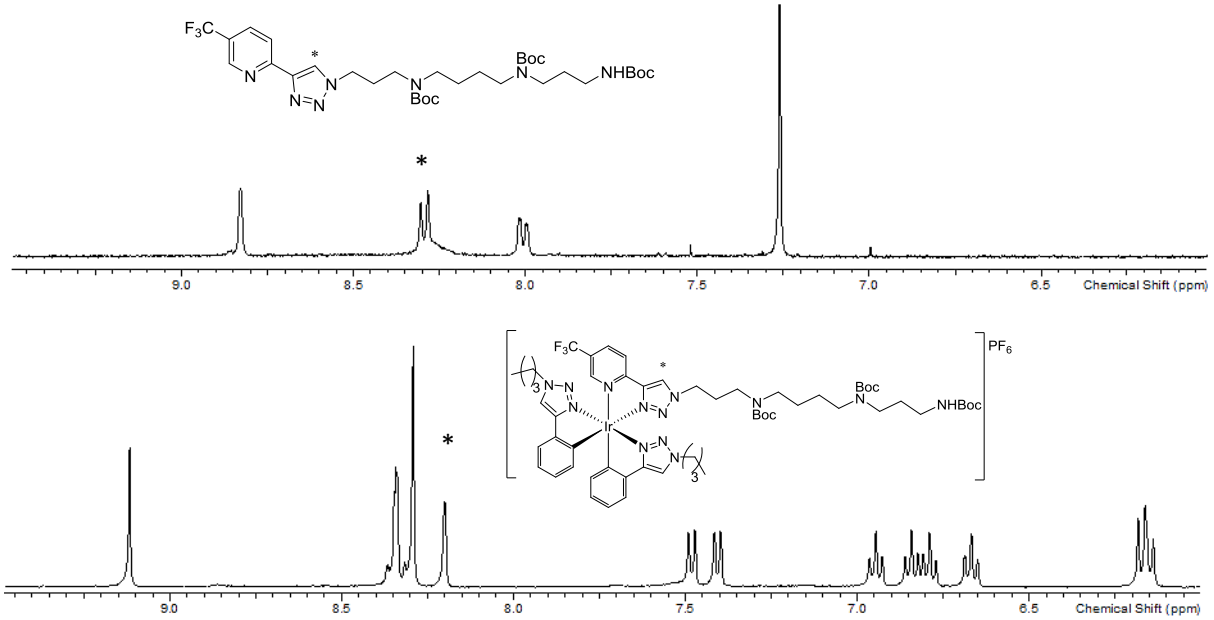

Figure 3.20: ^{1}H NMR spectrum of **L8.Boc** and **Ir(L1)$_2$L8.Boc** (400MHz)

The ^{1}H NMR spectrum shows two triplet signals attributed to the protons of methylene for the ancillary ligand and other signal with four integral corresponding to the protons of methylene close to triazole ring in cyclometallated ligand. The COSY NMR spectrum confirmed that 36H or 36'H were adjcent to 37H or 37' and also 9H adjacent to the 10H proton (Fig. 3.14). NOESY NMR shows correlation between (1H) with (4 or 5H) and (31H) with (36H) similarly (31'H) with (36'H) also show a nOe between (31H, 30H) similarly (31'H, 30'H), (29, 28H) and (29', 28'H) as shown in Fig. 3.21.

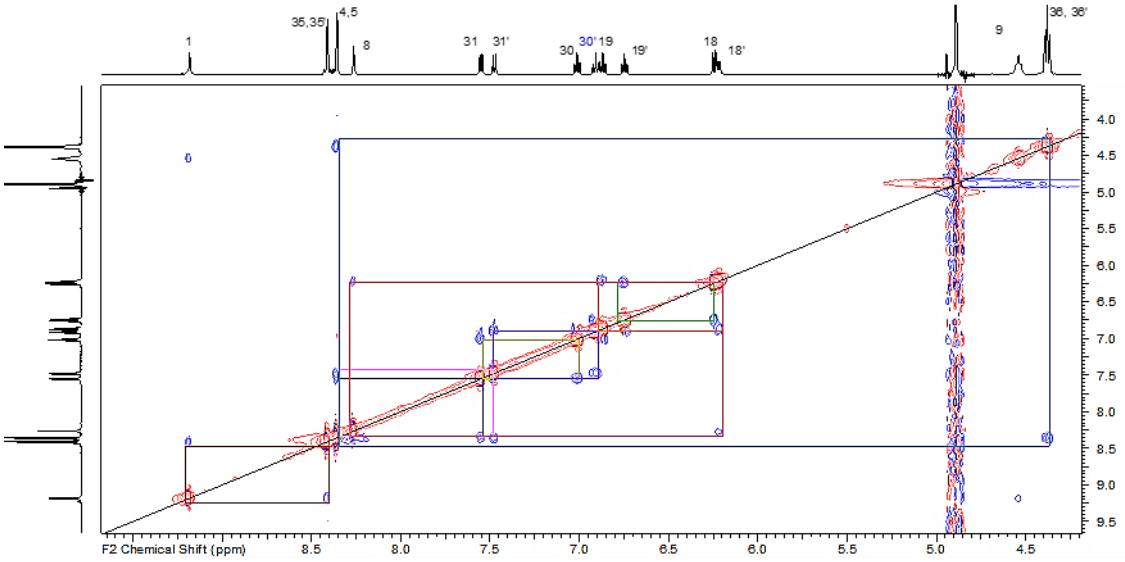

Figure 3.21: NOESY NMR spectrum of **Ir(L1)$_2$L8.Boc**(MeOD, AV-400MHz)

The ^{1}H NMR spectrum of **Ir(L1)$_2$L9.Boc** shows similar shifts comparing with **Ir(L1)$_2$L8.Boc**. **Ir(L1)$_2$L8.Boc** and **Ir(L1)$_2$L9.Boc** were converted to their de-protected form **Ir(L1)$_2$L8** and **Ir(L1)$_2$L9** by adding 4M solution of TFA in dichloromethane. RP-HPLC method A was used to collect the product **Ir(L1)$_2$L8** and **Ir(L1)$_2$L9** at R_t = 24.9 min as pure solid. The ^{1}H NMR spectrum shows that the signal of the Boc groups is absent from both spectra of **Ir(L1)$_2$L8** and **Ir(L1)$_2$L9,** it also shows some slight downfield shifts of some of the protons of the cyclometalted and ancillary ligands compared with **Ir(L1)$_2$L8.Boc** and **Ir(L1)$_2$L9.Boc**.

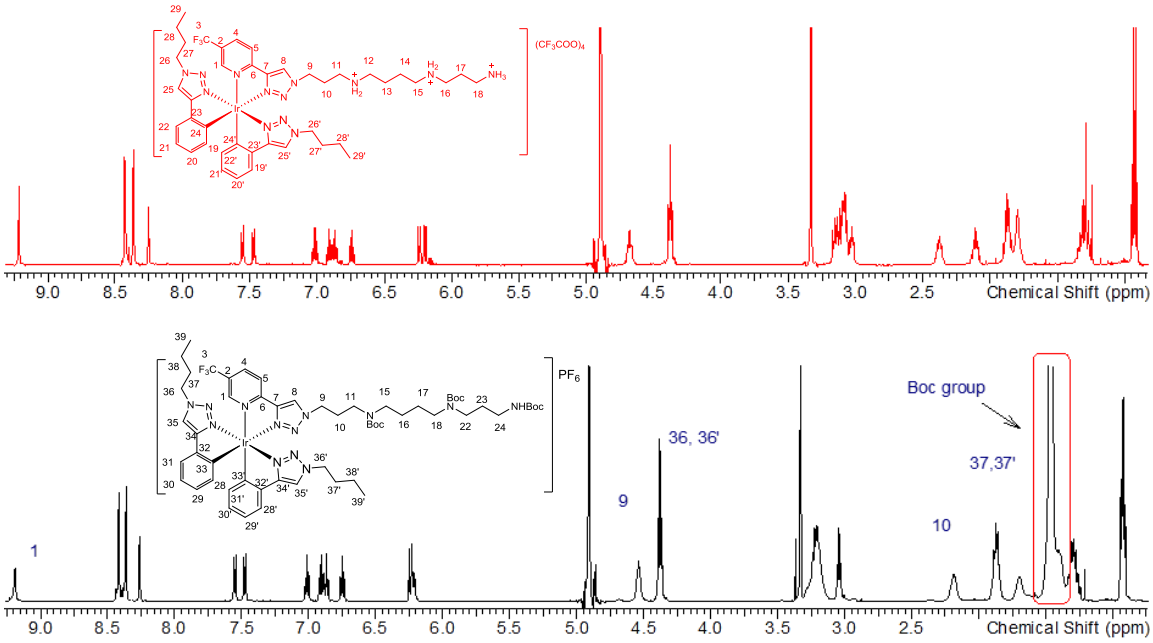

Figure 3.22: ^{1}H NMR spectra of **Ir(L1)$_2$L8.Boc** (black) and **Ir(L1)$_2$L8** (red)(MeOD, 500MHz)

Also the complexes **Ir(L2)$_2$L8.Boc** and **Ir(L2)$_2$L9.Boc** were synthesised according to procedure mentioned in (Scheme 3.22).[234, 244] The ^{1}H NMR spectrum of **Ir(L2)$_2$L8.Boc** and **Ir(L2)$_2$L9.Boc** show similar signals compared with **Ir(L1)$_2$L8.Boc** and **Ir(L1)$_2$L9.Boc**. Mass spectrometry of **Ir(L2)$_2$L8.Boc** and **Ir(L1)$_2$L9.Boc** show peaks at *m/z* 1348 and 1248 respectively corresponding to $[M]^{+}$. **Ir(L2)$_2$L8** and **Ir(L2)$_2$L9** were prepared via similar route as mentioned before. RP-HPLC was used to purify these complexes. ^{1}H NMR spectrum of **Ir(L2)$_2$L8** and **Ir(L2)$_2$L9** show similar signals to that of **Ir(L1)$_2$L8** and **Ir(L1)$_2$L9**. Mass spectrometry shows peak at *m/z* 1048 and 939 respectively corresponding to $[M]^{+}$. The ^{19}F NMR spectrum of both complexes show two signals observed at -64.5 ppm corresponding to fluorine in $-CF_3$ and at -76.8 ppm attributed to the counter anion ($CF_3CO_2^-$) and the integral suggests four ($CF_3CO_2^-$) counter anion using $-CF_3$ as an internal reference (Fig. 3.23).

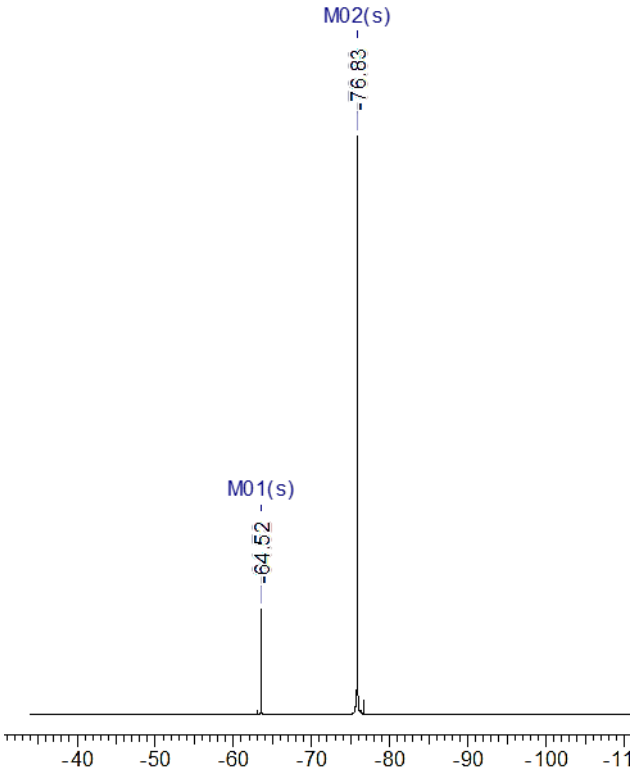

Figure 3.23: ^{19}F NMR spectrum of **Ir(L2)$_2$L8** in (MeOD, 400 MHz)

The NOESY spectrum of **Ir(L2)$_2$L8** shows that the proton (26H) correlates with (27H) and (23H) while the proton (23H) shows correlation with (22H) and (26H) also the proton (27H) shows correlation with (28H) and (29H). It was shows a nOe correlation between (21H) and (20H) and also another nOe between (31H, 32H). TOCSY and COSY NMR confirmed this correlation.

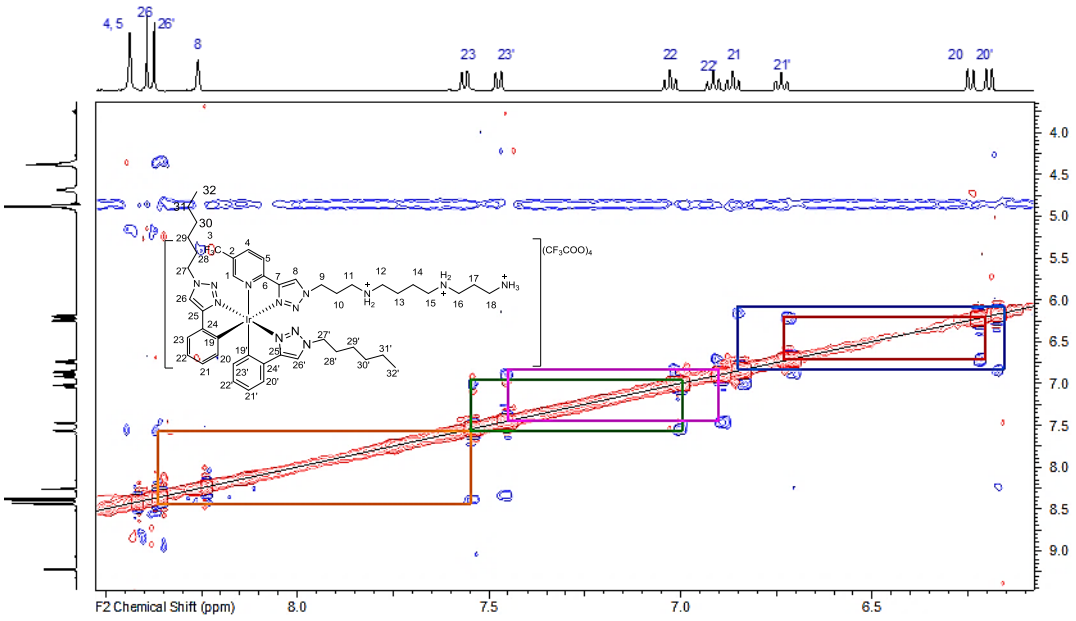

Figure 3.24: NOESY spectra of the **Ir(L2)$_2$L8** (MeOD, AV-400MHz)

3.3.4 Cyclometalated Iridium(III) Substituted with Electron Donating Groups

The luminescence can be tuned by altering the substituents on the cyclometallated phenyl. In the case of phenyl ligands the 4-substituted position has been used, resulting in only one complex of cyclometallation being obtained as shown in (Scheme 3.23).[244]

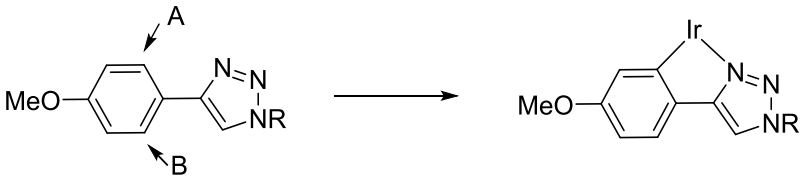

Scheme 3.23: Possible sites (A and B) for cyclometallation of 4-subsituted phenyls

It was found that incorporating methoxy group as a substituent on the ppy rings has an primarily influence on the HOMO and/or the LUMO level, as well as the ^{3}MLCT state of the complex.[245] In this study two types of iridium(III) complexes were prepared (Scheme 3.24), each complex was substituted with the electron donor group –OMe in the 4-position (e.g. **Ir(L4)$_2$L6.Boc)**. **Ir(L4)$_2$L6.Boc** was prepared from the corresponding [**Ir(L4)$_2$Cl]$_2$** dimer and ancillary ligand (**L6.Boc** or **L8.Boc**) was added to break the dimer followed by KPF_6.[244] Purification of this complex was carried out by RP-HPLC method A to obtain the desired fraction at R_t = 35 min.

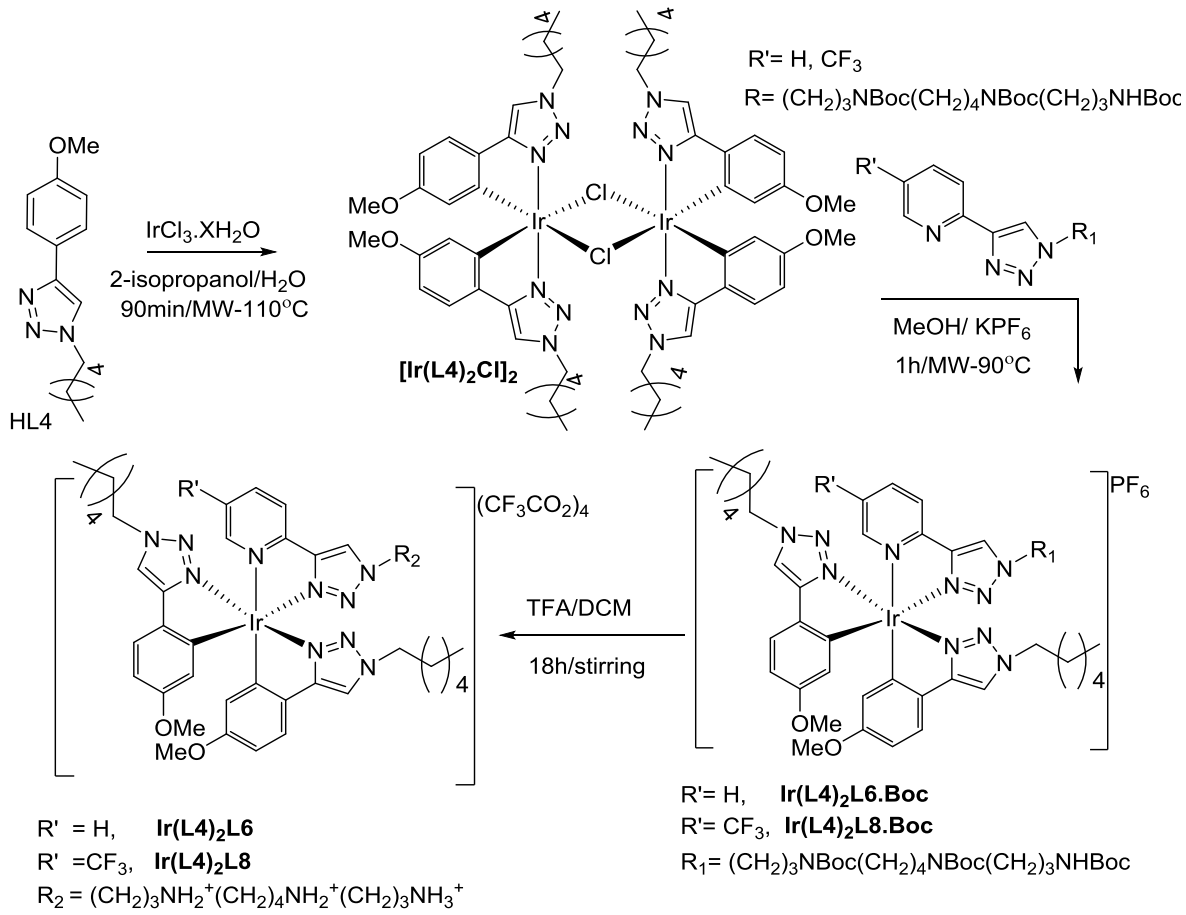

Scheme 3.24: Synthesis of **Ir(L4)$_2$L6** and **Ir(L4)$_2$L8**

The ^{1}H NMR spectrum of **Ir(L4)$_2$L6.Boc** is similar to **Ir(L2)$_2$L6.Boc** except the presence of two new singlet signals observed at 3.60 and 3.57 ppm corresponding to the protons of the -OMe group which shifted upfield upon coordination.[244] The proton of the triazole ring has a large shift to the downfield. The ^{1}H NMR spectrum shows that the protons of the pyridine in the ancillary ligand shifted upfield and the proton of the triazole ring shifted downfield due to the influence of the ring current of other the triazole ring.[89] Mass spectrometry shows a peak at *m/z* 1340.68 assinged to $[M]^+$.

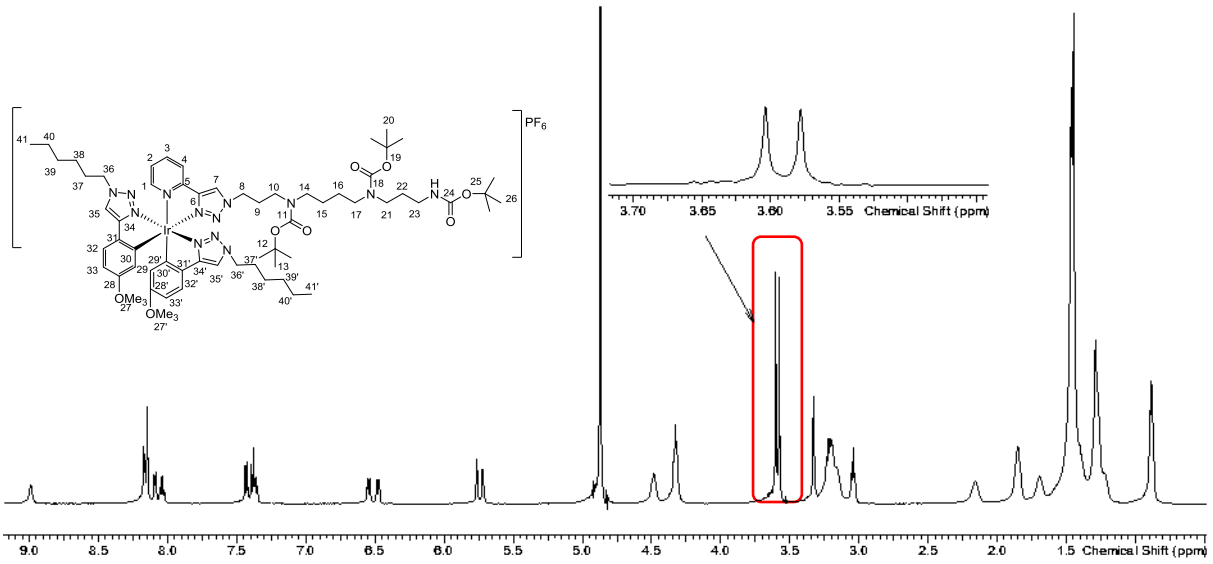

Figure 3.25: ^{1}H NMR spectra of **Ir(L4)$_2$L6.Boc** showing the OMe group (MeOD, 500MHz)

The NOESY NMR spectrum of **Ir(L4)$_2$L6.Boc** shows a correlation between (7H, 8H), (33H, 27H) and similarly (33'H, 27'H) and the proton (35H) with (32H). There is a nOe between (1H, 8H) and (27H, 29H) it was also found that there is a nOe correlation between (22H, 23H), (36H, 37H) and (37H, 38H) and similarly (36'H, 37'H) and (37'H, 38'H) (Fig. 3.27-1,2). COSY NMR spectrum confirmed this correlation as shown in Fig. 3.26.

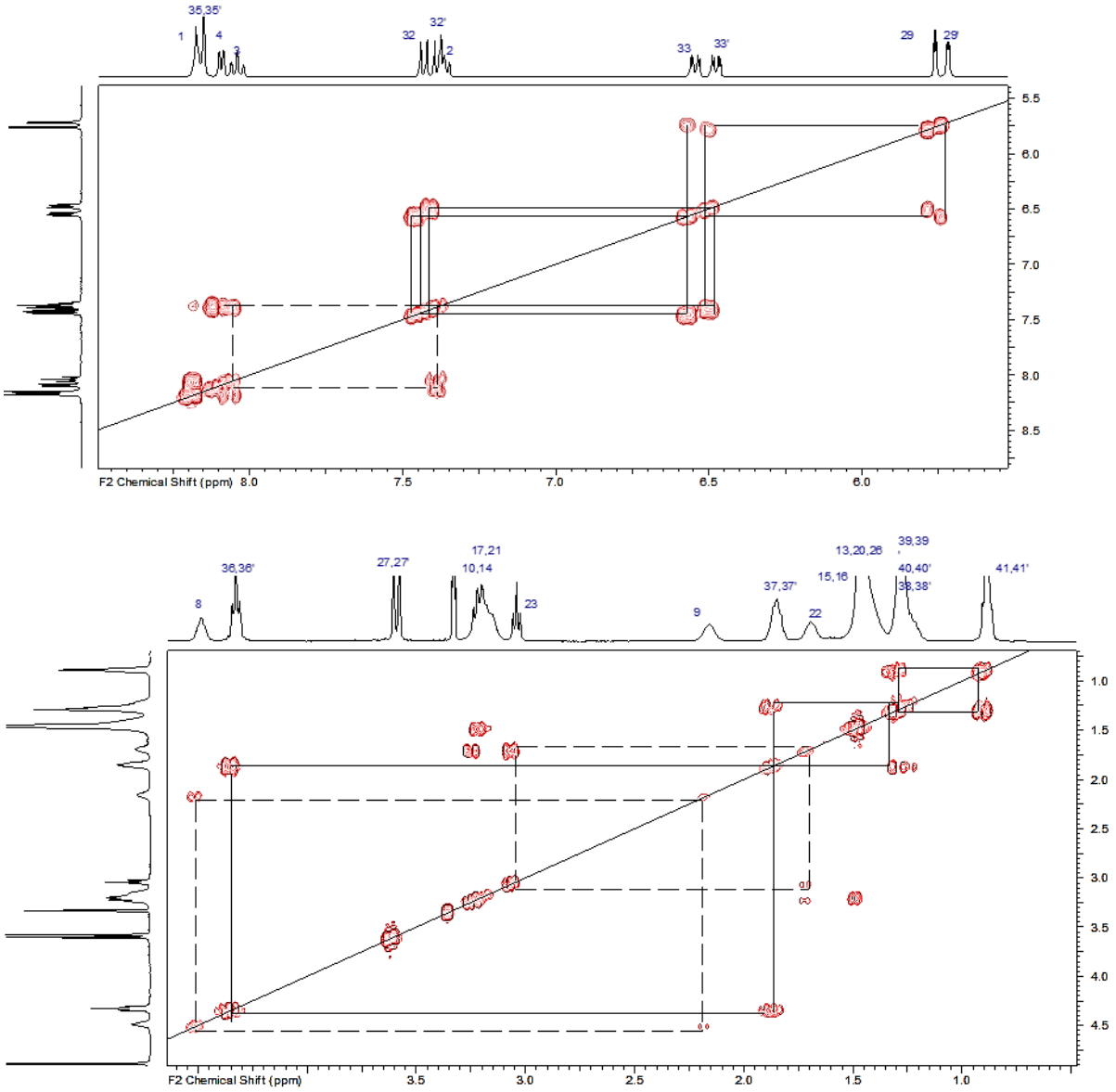

Figure 3.26: COSY spectrum of **Ir(L4)$_2$L6.Boc** shows (----) representing the cyclometalated ligand and (——) representing ancillary ligand

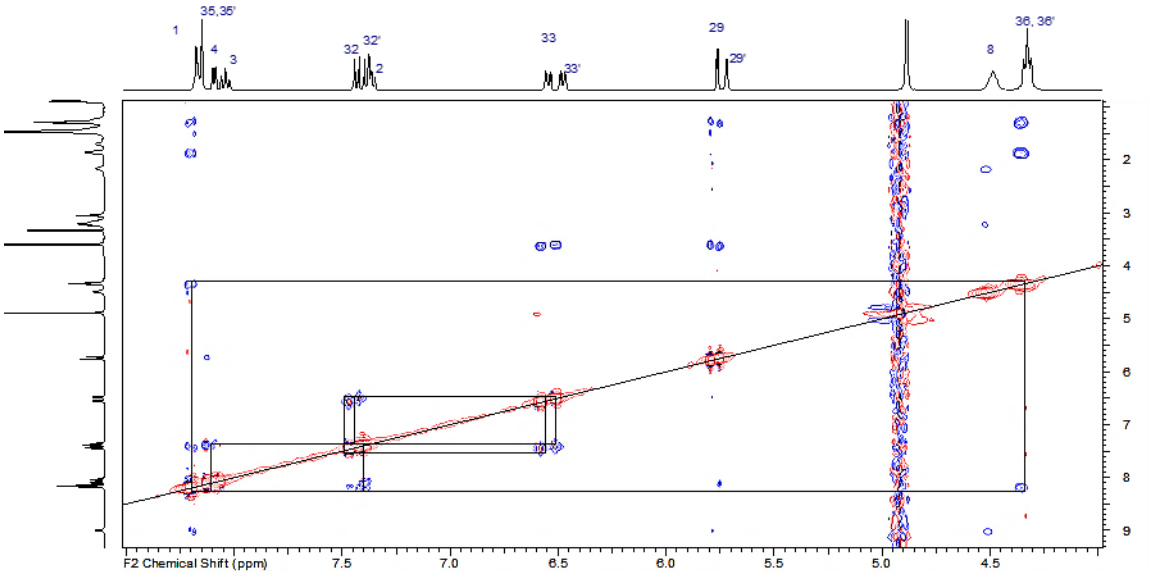

Figure 3.27(1): NOESY spectrum of **Ir(L4)$_2$L6.Boc**(MeOD, AV-400MHz)

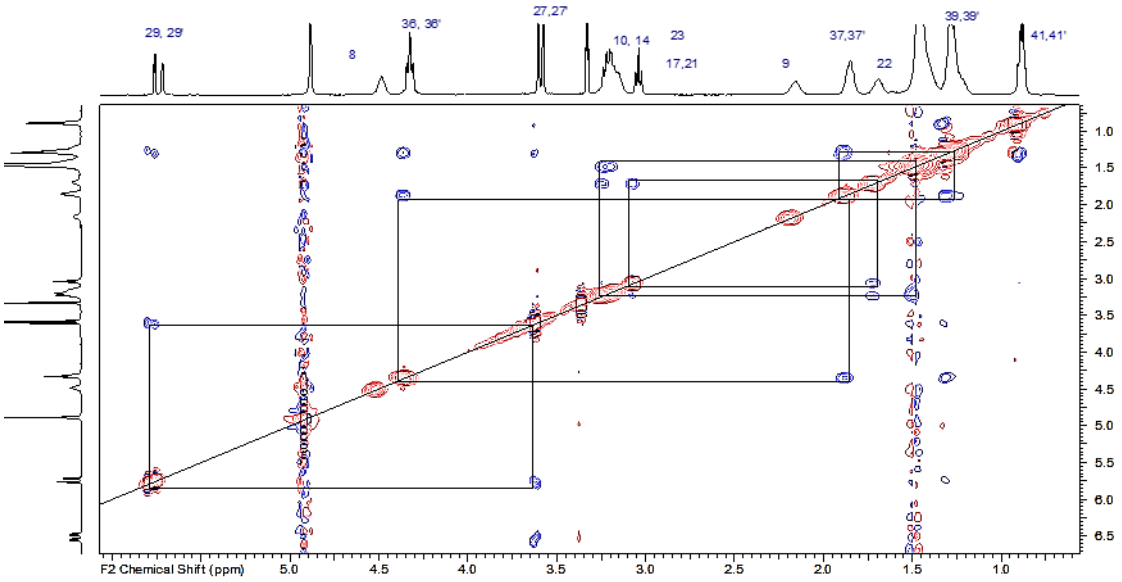

Figure 3.27(2): NOESY spectrum of **Ir(L4)$_2$L6.Boc**(MeOD, AV-400MHz)

The ^{1}H NMR spectrum of **Ir(L4)$_2$L6** is similar spectrum to that of **Ir(L4)$_2$L6.Boc** except the protons of the Boc group were absent. Also the COSY (Fig. 3.38-1,2) and NOESY spectra are similar.

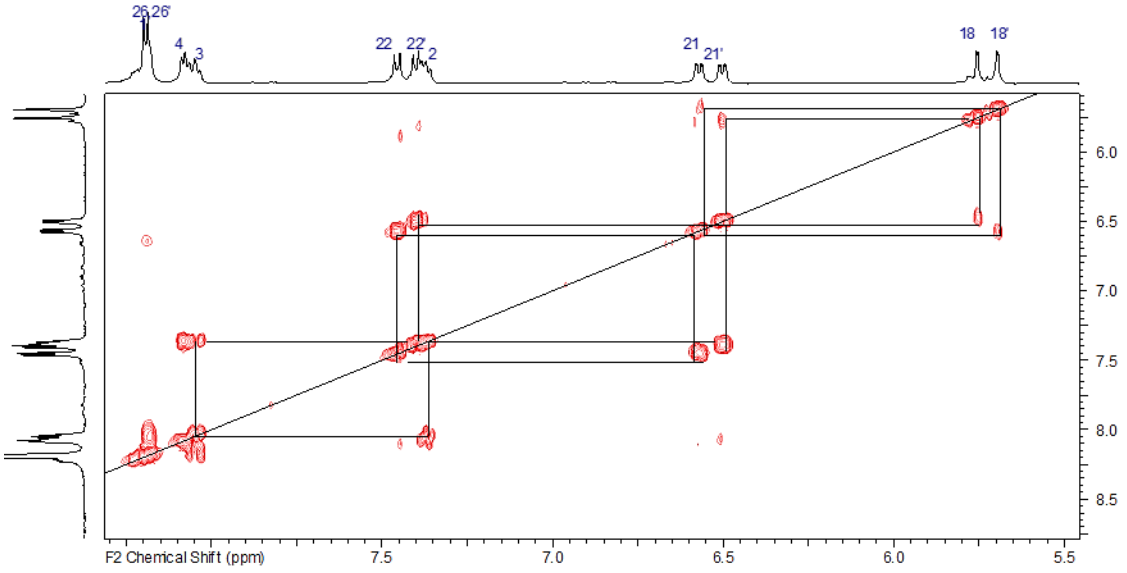

Figure 3.28(1): COSY spectra of **Ir(L4)$_2$L6** (MeOD,500MHz)

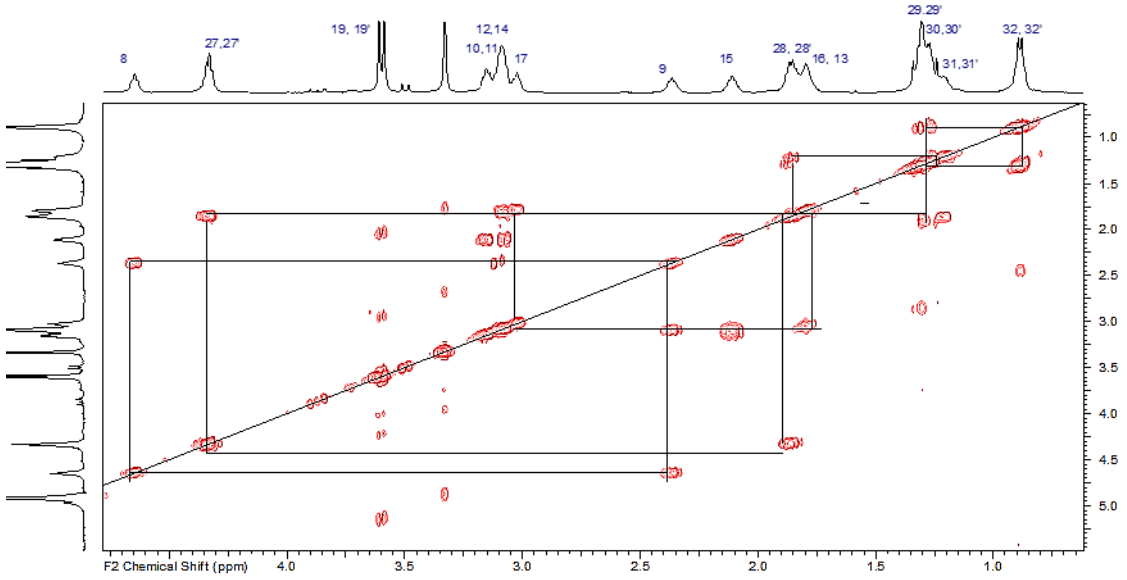

Figure 3.28(2): COSY spectra of **Ir(L4)$_2$L6** (MeOD,500MHz)

^{1}H and ^{13}C NMR spectra of **Ir(L4)$_2$L8** are similar to **Ir(L4)$_2$L6** except the aromatic region due to the presence of CF_3 substitutent in the ancillary ligand.

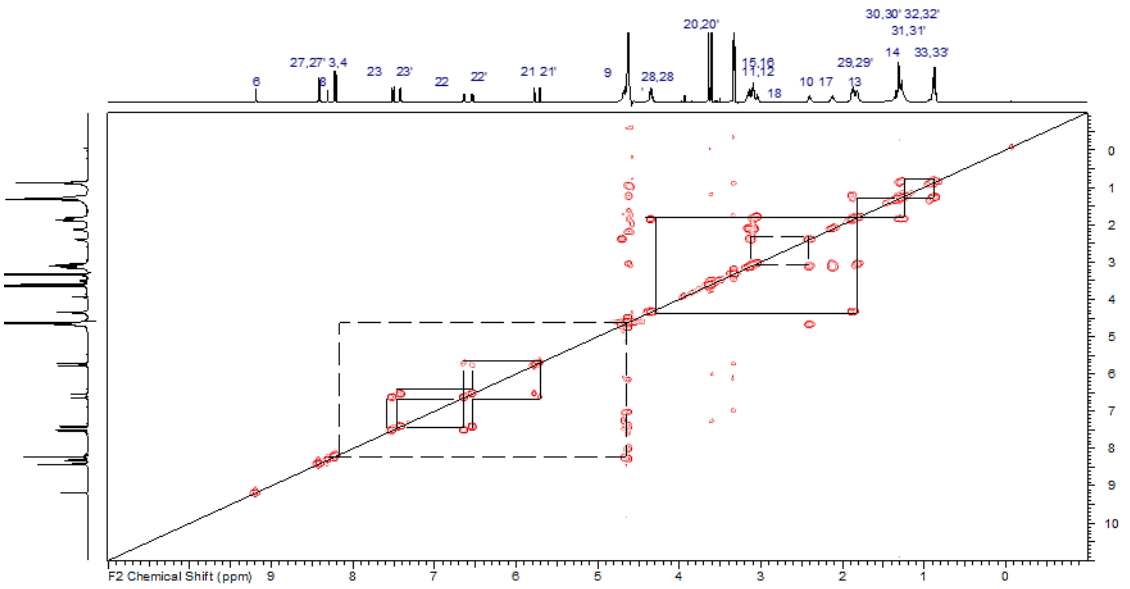

Figure 3.29: COSY NMR of **Ir(L4)$_2$L8** shows (——) representing the cyclometalated ligand and (----) representing the ancillary ligand

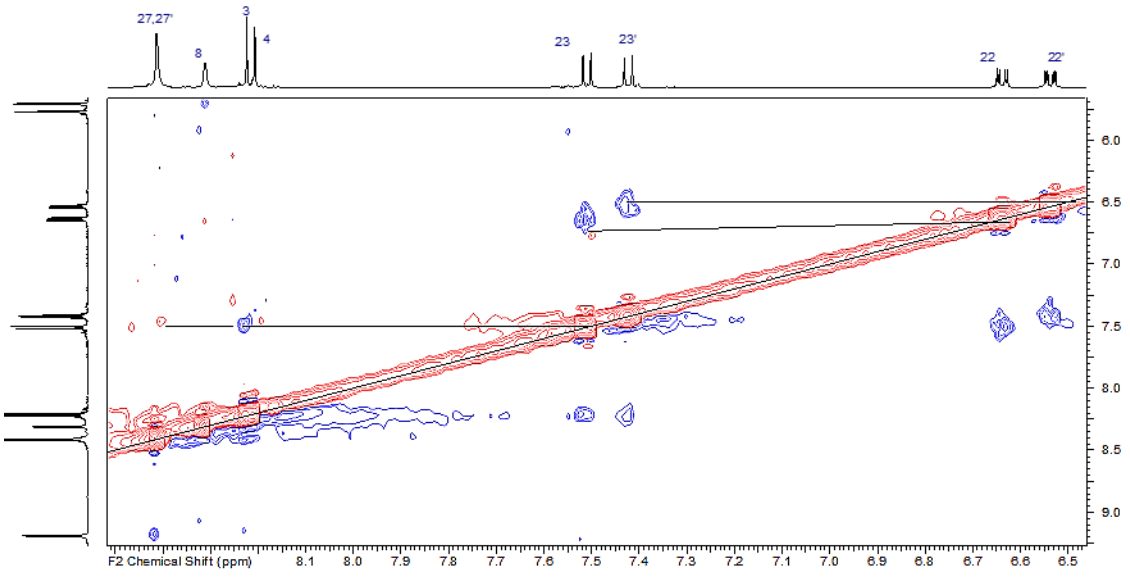

Figure 3.30: NOESY NMR of **Ir(L4)$_2$L8** (MeOD, AV-400MHz)

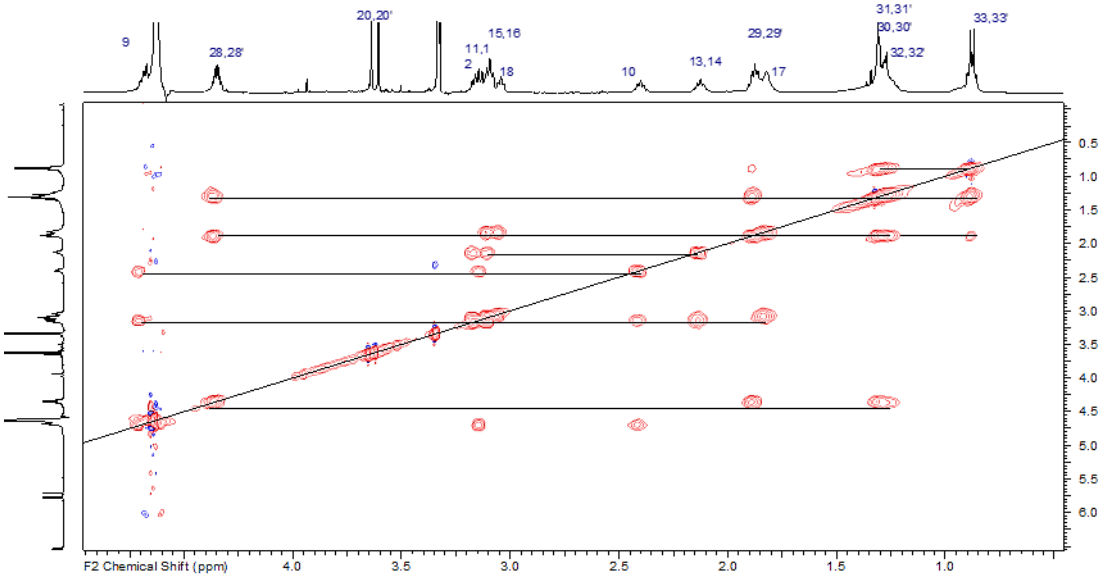

Figure 3.31: TOCSY NMR of **Ir(L4)$_2$L8**(MeOD, 500MHz)

3.3.5 Iridium Complexes Bearing a Non –Substituted Phenylpyridine

Since the synthesis of the first iridium(III) complexes with 2-phenyl pyridine were described in 1984, iridium(III) phenylpyridine based complexes are becoming increasingly important in applications such as light emitting devices and luminescent biological labels.[246, 247] Thompson *et al.* have extensively studied these complexes as multiple color emission labelling agents for biological applications and as sensors.[248, 249] This is due to photophysical properties such as good photochemical stability and high photoluminescence (PL) quantum yield, and short triplet lifetimes.[231, 250] So, numerous studies have used this complex or related ones by tuning the emission color by varying the ligand structure or incorporation of ancillary ligands.[248] In this work, a series of iridium(III) complexes with phenylpyridine were prepared by following the procedure in the literature.[234] This involved two steps: the first step is synthesis of the bridged iridium dimer then breaking the dimer with the ancillary ligand (Scheme 3.25).

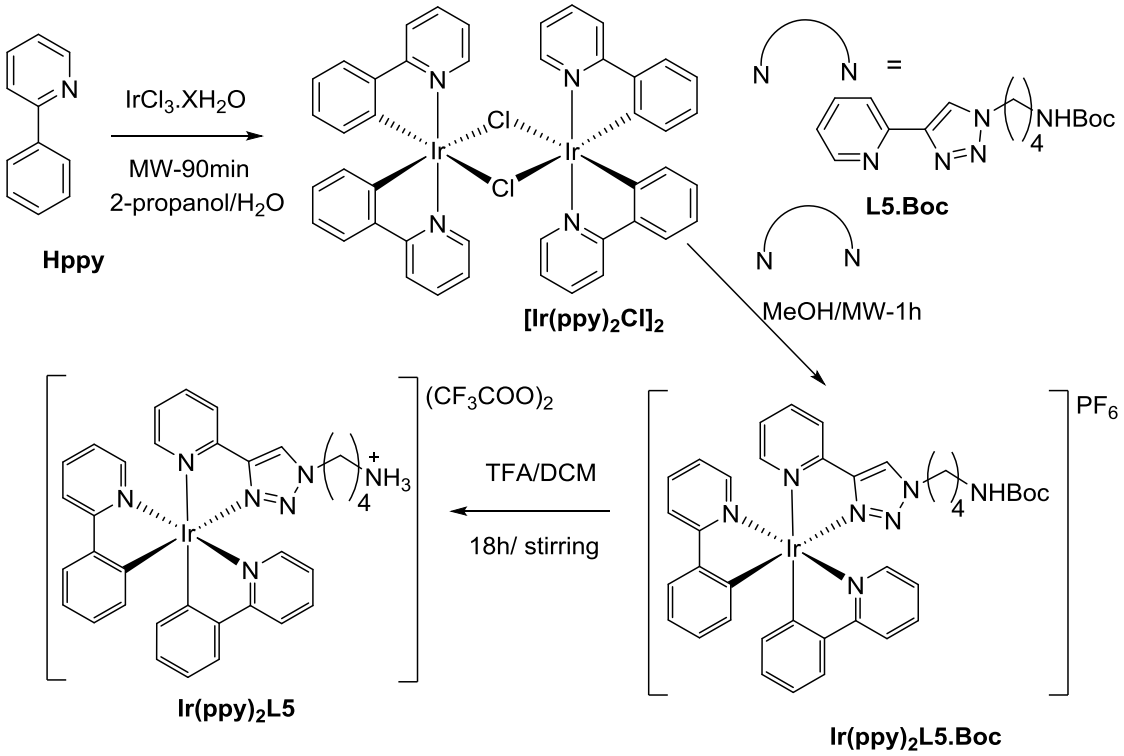

Scheme 3.25: Synthesis of **Ir(ppy)$_2$L5**

Ir(ppy)$_2$L5 was prepared by a previous group member[37]; this complex was synthesised in this study in order to make a comparison with other complexes containing alkyl chains in term of lipophilicity and photophysical properties. Good yields were obtained when the reaction was carried out under microwave heating and compared with conventional reaction.[251] This complex was characterized by NMR spectroscopy including: ^{1}H NMR, COSY, HSQC and HMBC. As mentioned before the main goal of this study to prepare amphiphilic complexes, so in order to achieve this goal, new cyclometalated iridium complexes based on phenylpyridine linked to an alkyl chain were prepared with formula $[Ir(C\text{^}N)_2(N\text{^}N)]^+$ Where N^N is the pyridyltriazole ancillary ligand bearing a polyamine, as shown in Scheme 3.26.

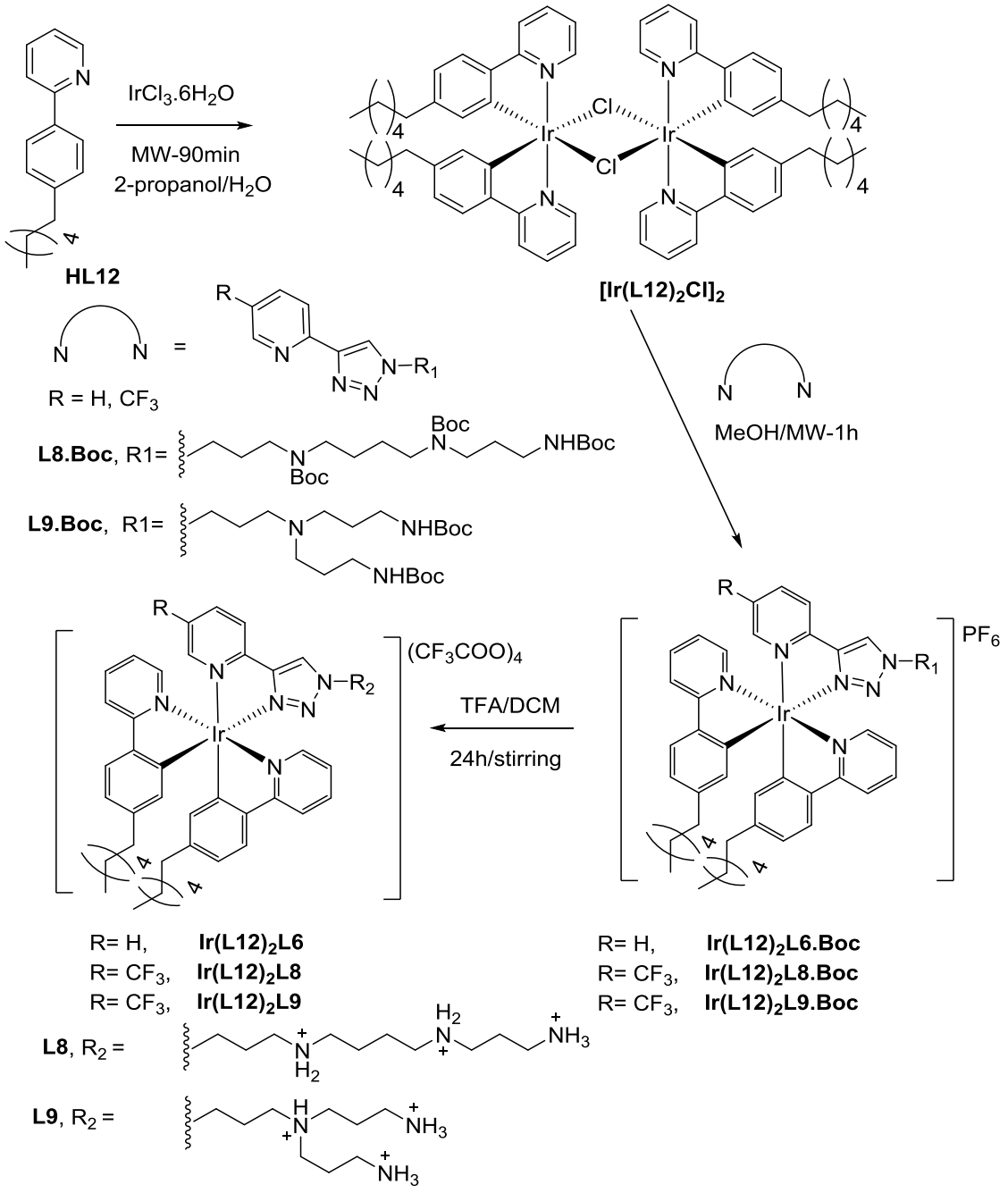

Scheme 3.26: Synthesis of **Ir(L12)$_2$L6**, **Ir(L12)$_2$L8** and **Ir(L12)$_2$L9**

Ir(L12)$_2$L6.Boc, **Ir(L12)$_2$L8.Boc** and **Ir(L12)$_2$L9.Boc** complexes were synthesized in two steps according to previous method, **HL12,** the cyclometalating ligand was prepared as mentioned in Chapter 2 and the ancillary ligand were **L6.Boc, L8.Boc** and **L9.Boc.** Microwave irradiation was used to prepare these complexes. The final products **Ir(L12)$_2$L6**, **Ir(L12)$_2$L8** and **Ir(L12)$_2$L9** were obtained after purification by the RP-HPLC as a pure product. ^{1}H NMR spectrum of these complexes are similar to each other, a singlet signal at 9.28 ppm was assigned to 1H and also 28H was found as a doublet

signal in the upfield at 6.11 ppm (Fig. 3.32) has a nOe correlation between 22H and similarly (22'H, 28'H) also a nOe was observed between 20H and (21H, 5H, 25H). The COSY spectrum shows connections between (25H, 26H) and (22H, 21H) and the TOCSY confirmed these connection. HMBC spectra identity the quaternary carbon signals at 169 ppm and 168 ppm assigned to (24-C), (24'-C) and also at 154.5 ppm assigned to (23-C, 23'-C). ^{19}F NMR shows two peaks was appeared at -62.8 ppm (CF_3) and at -76.5 ppm ($CF_3CO_2^-$). ESMS shows a molecular ion at *m/z* 1066 corresponding to $[M]^+$. The NOESY spectrum of **Ir(L12)$_2$L9** is similar to **Ir(L12)$_2$L8**.

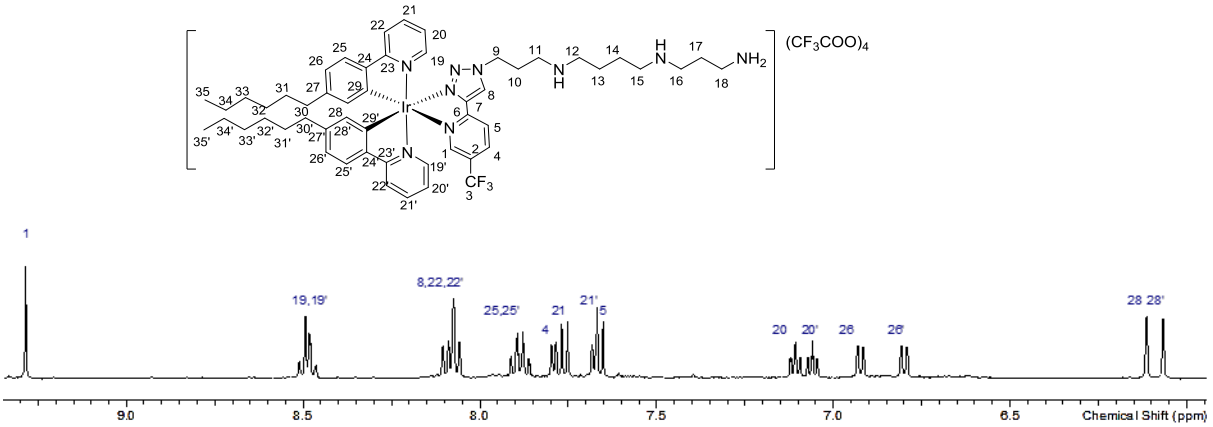

Figure 3.32: ^1H NMR spectrum of **Ir(L12)$_2$L8** showing the aromatic region (MeOD, 500MHz)

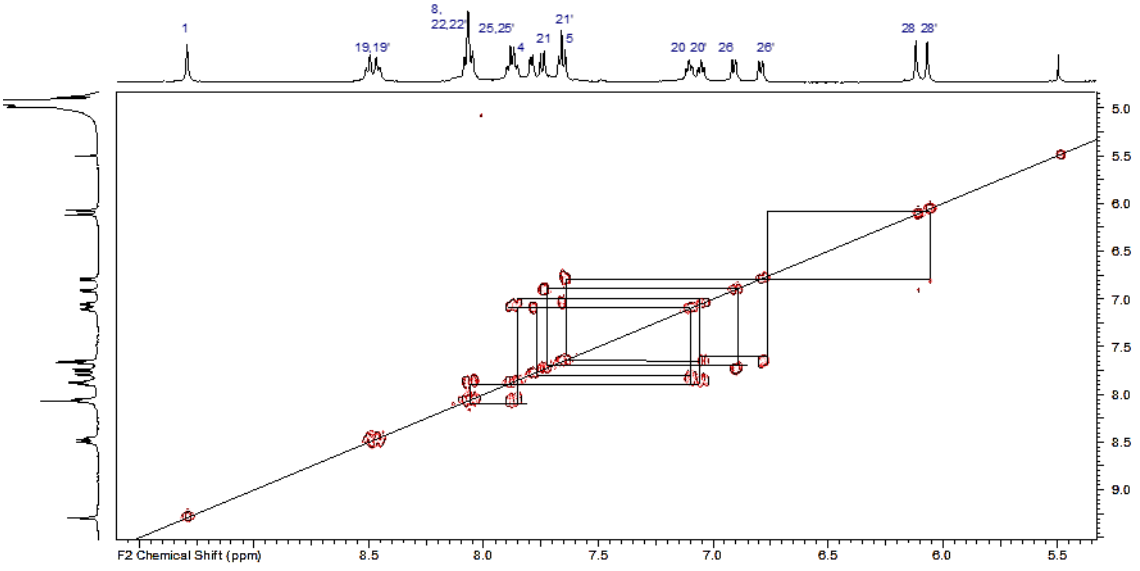

Figure 3.33: COSY NMR spectrum of **Ir(L12)$_2$L8** (MeOD, 500MHz)

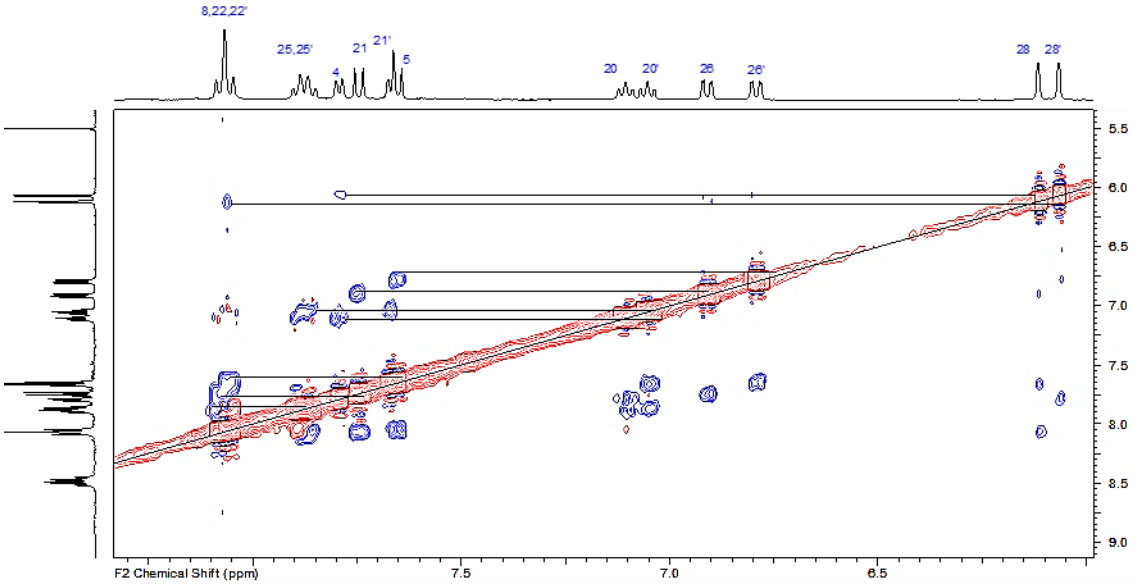

Figure 3.34: NOESY spectrum of **Ir(L12)$_2$L8** (MeOD, AV-400MHz)

3.3.6 Iridium(III) Complexes Contain Inverse Pyridyltriazole as an Ancillary Ligand

There are many strategies to obtain longer wavelength emission by decorating the N^N ligand with electron-withdrawing groups or adorning electron-donating groups on the C^N ligand as mentioned before. However, this study found that replacement of the pyridine ring of the C^N ligand with a 1,2,3-triazole promotes a blue-shift in emission and found some enhancement in the emission when using a phenylpyridine ligand such as C^N. A new strategy was used by using the inverse click ligand as ancillary ligand to investigate if this ligand will tune the emission, or could be used to increase the quantum yield, as in previous studies when this ligand was used with heavy metals such as rhenium(I) and iridium(III).[95, 229] In this study, the iridium(III) complex was prepared as shown in Scheme 3.27.

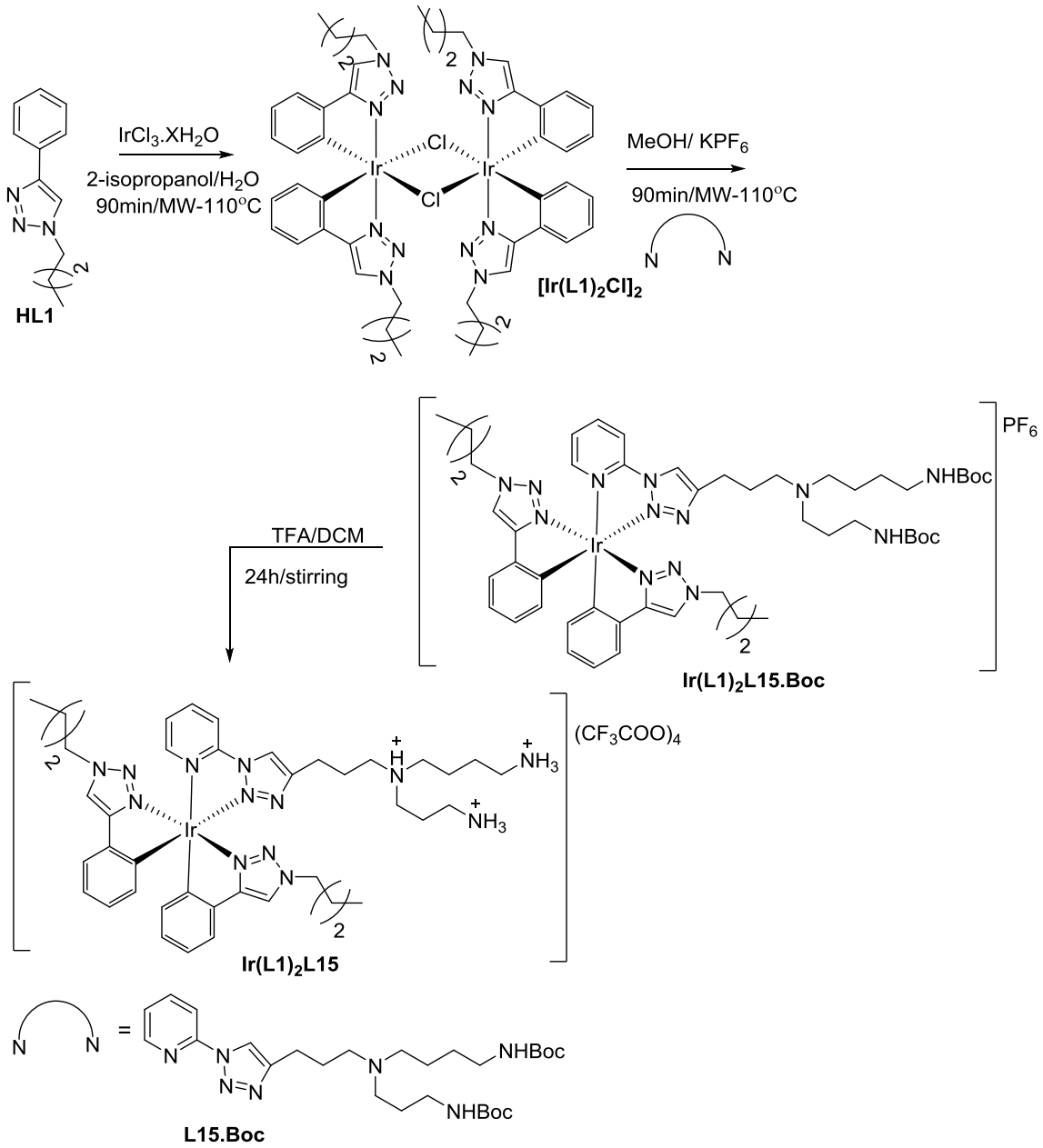

Scheme 3.27: Synthesis of **Ir(L1)$_2$L15** complex

Ir(L1)$_2$L15.Boc was synthesised by microwave technique as described in the literature.[251] RP-HPLC was used to purify this complex. The ^{1}H NMR spectrum shows a singlet signal at 9.05 ppm assigned to triazole ring of ancillary ligand and shifted downfield compared to the free ligand at 8.45 ppm. Three signals for the phenyl ring of the cyclometalated ligand are observed at 6.26-6.96 ppm and are shifted downfield compared with the free ligand except one signal for the phenyl ring shifted upfield due coordination to the metal. The signal for the triazole ring of the cyclometalated ligand was also observed at 8.34 ppm and shifted upfield, affected by the electron density from

the other cyclometalating ligand.[237] ESMS shows a peak at *m/z* 924 for **Ir(L1)$_2$L15** was obtained after adding 4M solution of TFA. RP-HPLC was used to purify this complex. The ^{1}H NMR spectrum of **Ir(L1)$_2$L15** shows that there three signals of the phenyl in the ancillary ligand were observed at 7.44, 8.19 and 7.93 ppm as shifted upfield, also multiplet signals were observed at 3.06 ppm assigned to methylene proton (8H) close to triazole ring in the ancillary ligand. The COSY spectrum shows connections between 8H and 9H and also shows connection between 1H and 2H. Protons of the triazole in the ancillary ligand shifted downfield from 8.45 in the free ligand to 9.12 ppm in the complex. The ^{1}H NMR also shows all the protons of the phenyl of the cyclometalated ligand was shifted upfield and the protons of the triazole shifted upfield due to the ring current from the ancillary ligand,[244] which has a nOe with 26H and 21H similarly (25'H, 26'H) (25'H, 21'H) and also 27H has a correlation with 26H and 28H. The NOESY spectrum (Fig. 3.35) shows correlation between (20H, 21H) and (18H, 19H) similarly (20'H, 21'H) and (18'H, 19'H)

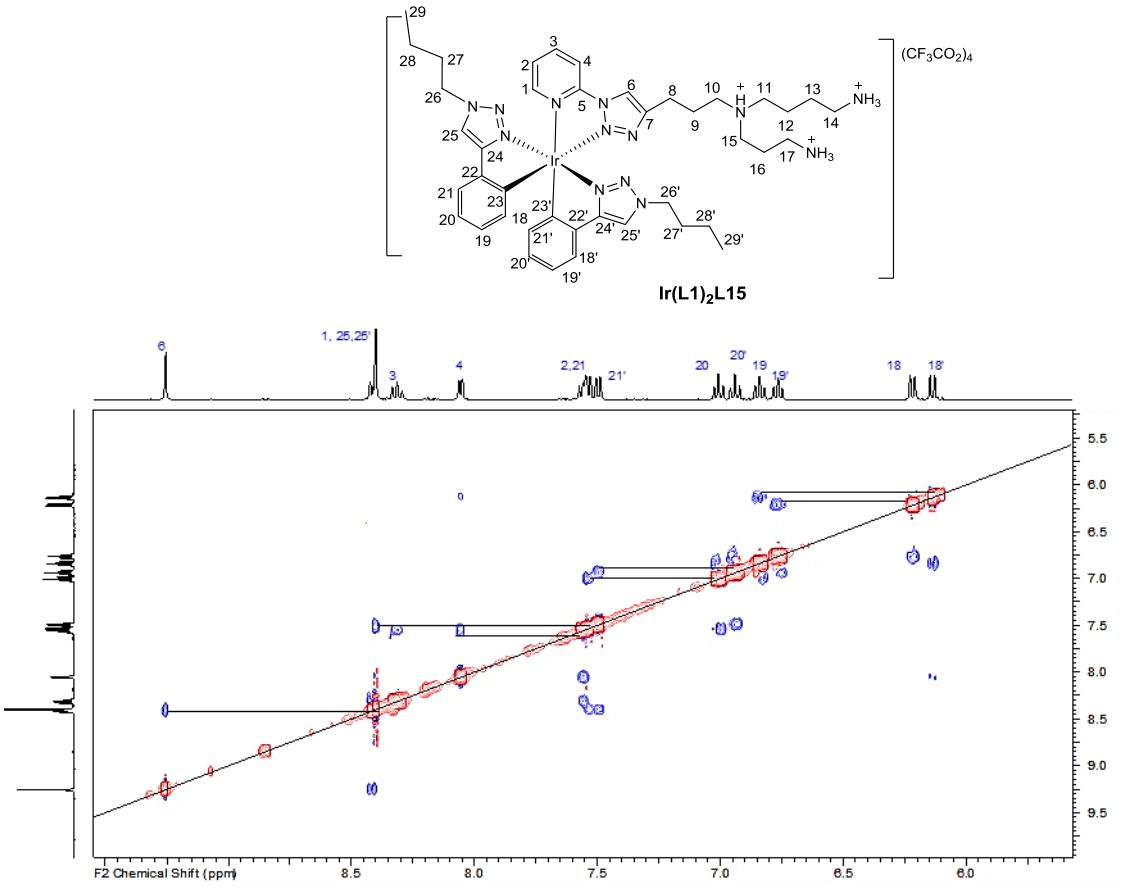

Figure 3.35: NOESY NMR spectrum of **Ir(L1)$_2$L15** (MeOD, AV-400MHz)

3.4 Conclusion

A series of cationic pyridyltriazolecarbonylrhenium(I) complexes **ReL6.L17, ReL10.L17** and **ReL3.L16,** containing 4-pyridine substituted with either alkyl chains or polyamines as axial monodentate ligands were synthesised by using microwave techniques. These complexes were fully characterizated. A new class of rhenium(I) complexes bearing pyridyltriazoles substituted with an electron withdrawing CF_3 group in the 5-position such as **ReL8.L17** and **ReL8.L17** and another rhenium(I) complexes based on bipyridine link to alkyl chain also were synthesised and characterized like **ReL11.L16**. Variations of these rhenium complexes, bearing 'inverse' pyridyltriazoles were also synthesized and characterized such as **ReL13.L16**, **ReL14.L17** and **ReL15.L17**. A monodentate triazole ligand instead of an axial pyridine ligand was also reported in the synthesis of new rhenium complexes **ReL6.L18** and **ReL9.L18**. All these complexes were characterized by 1D and 2D NMR spectroscopic techniques including ^{1}H NMR, COSY, HSQC and HMBC spectroscopy in addition to mass spectrometry. A new class of amphiphilic iridium(III) complexes were synthesized with different cyclometalating ligands. The first class of cyclometalated ligand is phenyltriazoles containing alkyl chains (**$[Ir(L1)_2Cl]_2$** and **$[Ir(L2)_2Cl]_2$** and also phenytriazoles substituted in 4-position with -OMe groups to enhance the photophysical properties such as **$[Ir(L4)_2Cl]_2$**. The ancillary ligand in these complexes is pyridyltriazole and also pyridyltriazole substituted in the *meta* position with a -CF_3 group in addition to inverse pyridyltriazole ligand linkers to polyamines such as **$Ir(L1)_2L8$** and **$Ir(L1)_2L9$**. The second type of cycolmetalated ligands of phenylpyridines linked to alkyl chains and the ancillary ligand is pyridytriazole bearing polyamines such as **$Ir(L12)_2L6$**, **$Ir(L12)_2L8$** and **$Ir(L12)_2L9$**. All these complexes were characterized by NMR spectroscopy and high resolution mass spectrometry. All of these complexes reported were obtained in a good yield and the purity was confirmed by analytical RP-HPLC technique.

Chapter 4

4 Photophysical Properties of Re(I) and Ir(III) Complexes

4.1 Introduction

Transition metal complexes, particularly those metals with d^6 electronic configurations, have been the subject of much attention, mostly because of their unique photophysical and photochemical properties.[252-254] Complexes of Re(I), Ru(II), Os(II) and Ir(III) have been widely studied over the last three decades as possible candidates for biological probes for imaging or therapeutic purposes. Generally, d^6 metal complexes display an octahedral geometry; the ligands around the metal split the *d*-orbitals into three lower and two higher levels. In octahedral complexes there are different types of electronic transition as mentioned before in Chapter 1. MLCT transitions are essential for emission in the d^6 metal complexes and also are responsible for luminescent properties, especially when the metal is Re(I), Ru(II), Os(II) and Ir(III). MLCT consists of an electron from the ground state undergoing MLCT to a chelating ligand, which is then transformed into the emissive excited triplet state through inter system crossing (ISC). Energy of excitation is lost through long-lived phosphorescence. MLCT transitions are affected by ligand field, so if the ligand is strong field, it raises the *d-d* excited state above the MLCT state, thereby resulting in emissive complexes. These complexes with MLCT make them suitable for biological studies.[255] This chapter presents the photophysical properties for rhenium(I) and iridium(III) complexes including the absorption, excitation and emission, also this chapter reports quantum yield and lifetime studies for both metals. Finally, this chapter also includes a lipophilicity study and *in vitro* imaging study.

4.2 Photophysical Properties of Rhenium(I) Complexes

Rhenium(I) tricarbonyl complexes have been extensively studied, as typically, complexes are good MLCT emitters and giving broad emission bands dependent on the ligands incorporated into the complex.[76, 254] This study presents the absorption, excitation and emission of rhenium(I) complexes. This study is carried out to evaluate the photophysical properties of these complexes. The electronic absorption and emission spectra for all complexes were measured at room temperature in water solution.

The two main absorption characteristics that is observed for the complex **ReL6.L17**. The first band is assigned to the spin allowed intraligand π- π* transition of the coordinated ligand. It is generally observed at higher energies 260 nm, the second broad band is metal-to-ligand charge transfer ^{1}MLCT bands (formally Re (dπ)-bisimine (π*)) appearing at around 350 nm this is similar to the absorption properties observed in related rhenium(I) carbonyl complexes.[76, 256, 257]

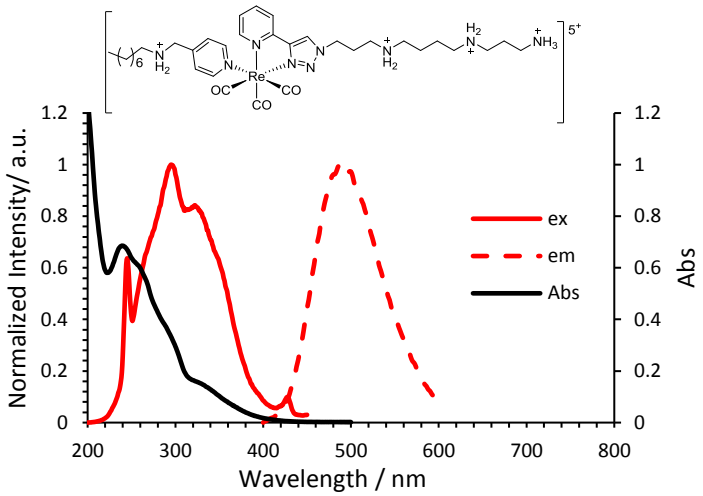

Figure 4.1: Absorption, excitation and emission spectra of **ReL6.L17** (100μM) in H_2O (λ_{ex}= 350 nm, λ_{em}= 500 nm)

The emission spectrum of this complex at (λ_{ex}= 350 nm) exhibits a broad emission profile with a maximum at (λ_{em}= 500 nm) giving a large Stokes shift of 150 nm (Figure 4.1). The MLCT absorption bands of this complex exhibited a blue shift in absorption in comparison with the corresponding rhenium halide (**ReL6.Boc**) due to replacement of the π-donor chloride ligand with the π-accepting pyridine ligand, this leads to a decrease

in the energy of the HOMO which is localized on Re(I) with respect to the LUMO which is localized on the pyridyltriazole, resulting in higher energy MLCT transitions.[81] Luminescence measurements were recorded at room temperature in water solution and with a standard conc. of 100 μM with an excitation wavelength of 350 nm (Table 4.1). Fig.4.1 shows the normalised emission spectra for the **ReL6.L17**. The luminescent properties for both **ReL10.L17** and **ReL3.L16** do not differ much from **ReL6.L17**, both exhibit broad excitation maxima around (350 nm , 330 nm) respectively and also a broad emission centred around 520 nm in total agreement with data already reported for complexes containing bisimines or others of the family.[229]

Complexes	**N^N**	**Axial ligand**	**Excitation/(nm)**	**Emission/(nm)**
ReL6.L17	pyta	py	350	500
Re10.L17	pyta	py	350	500
ReL3.L16	pyta	py	330	500
ReL8.L17	CF_3-pyta	py	350	540
ReL11.L16	bipy	py	350	570
ReL13.L16	Inv-pyta	py	390	580
ReL6.L18	pyta	triazole	350	510
ReL9.L18	CF3-pyta	triazole	350	540
ReL15.L17	Inv-pyta	py	390	540

Table 4.1: Photophysical properties of rhenium(I) complexes (100μM) in H_2O

These complexes have a large Stokes shift around 150 nm, this value is large in comparison with organic molecules, so it is easy to avoid interference from scattered light and autofluorescence. The slight difference in the excitation and emission maxima values is probably due to the small electronic effect from changes in the pyridinetriazole and pyridine axial ligand at the metal centre.[77]

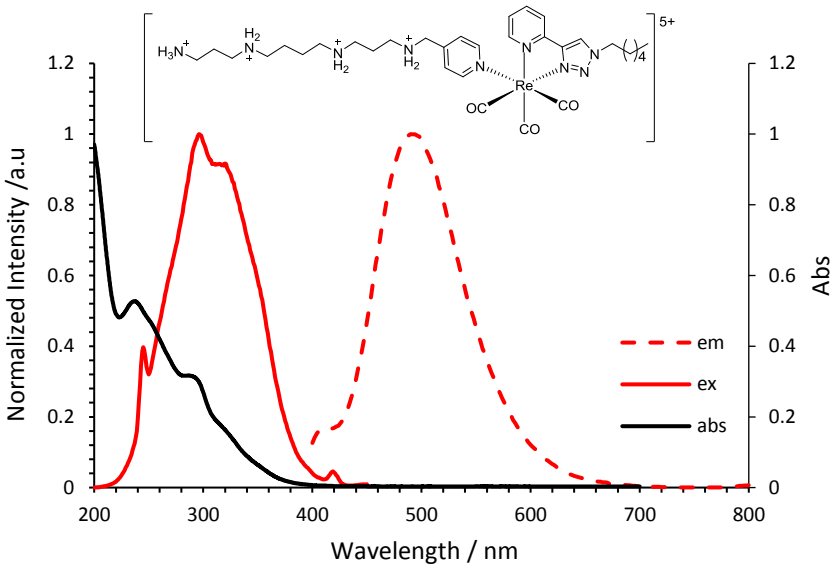

Figure 4.2: Absorption, excitation and emission of **ReL3.L16** in H_2O (λ_{ex}= 330 nm, λ_{em}= 500 nm)

As discussed in Section 3.2.2 the photophysical properties luminescent complexes are affected by the nature of the ligand or their environment, and if one of these factors is changed, the luminescence can be tuned. The rhenium(I) complexes of the type *fac*-$[Re(CO)_3(N^N)L]$ where N^N = diimine and L= py should ideally emit in visble region of the spectrum.[258] It was found that modification of the diimine directly effects the luminescent properties. Modifications were made to the ancillary ligand through the techniques mentioned in Chapter 2, by creating the ligand with the required substituent using the Sonogashira reaction. In this study **ReL6.L17** and **ReL8.L17** were synthesised and designed for this purpose. Both complexes **ReL6.L17** and **ReL3.L16** exhibited blue shifts compared with **ReL8.L17** which is involving a broad excitation around 350 nm and broad emission around 540 nm. **ReL6.L17** and **ReL3.L16** have almost identical areas of maximum excitation with a similar profile while for **ReL8.L17** the excitation wavelength was shifted to longer wavelength as was the emission wavelength which is suitable to excite around 405 nm (405 nm is one of the light source of confocal microscopy). It is suggested that the inductive electron withdrawing -CF_3 affects the HOMO-LUMO energy gap[259] as shown in Fig. 4.3.

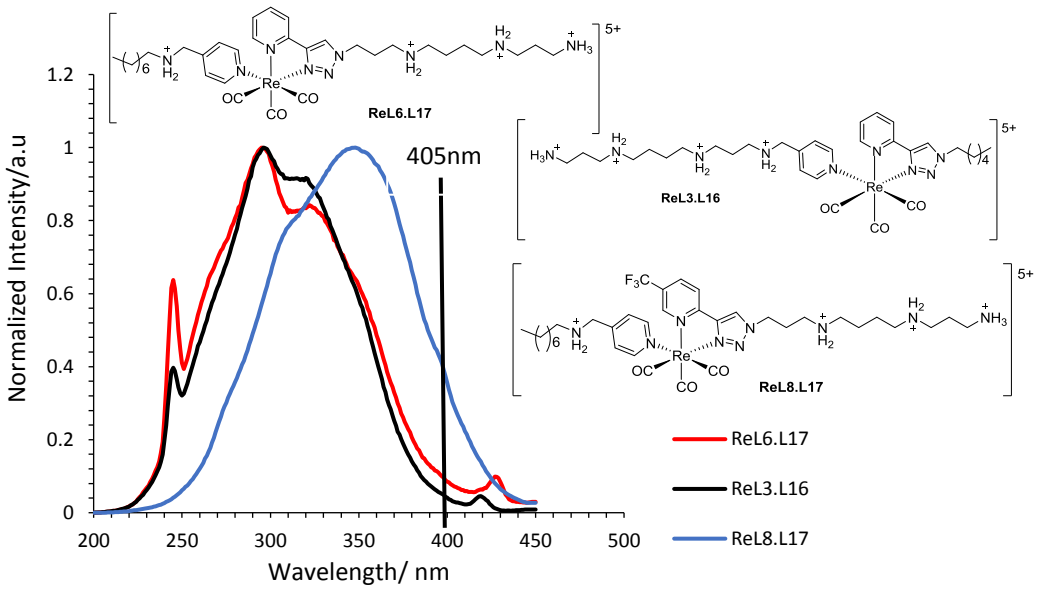

Figure 4.3: Excitation data for rhenium(I) complexes with modified ancillary ligands (100μM) in H_2O

Emission of complex **ReL8.L17** is red shifted (to longer emission wavelengths) compared to complexes **ReL6.L17** and **ReL3.L16** which showed similar emission profiles indicating that the electron withdrawing group are affecting the antibonding orbital, leading to a lowing energy of the LUMO, this therefore decreases the HOMO-LUMO gap, increasing the wavelength of emission when an excited electron returns to its ground orbital (Fig. 4.4).[259, 260]

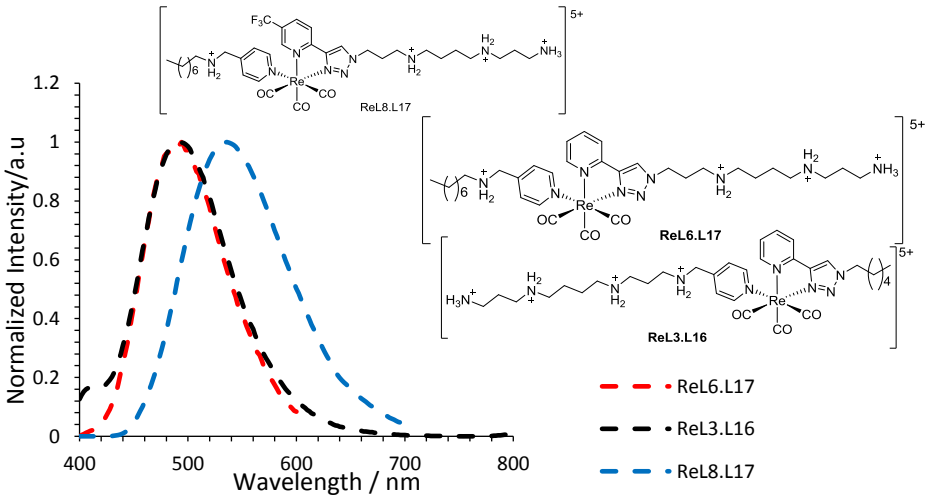

Figure 4.4: Emission spectra for rhenium(I) complexes with modified ancillary ligands (100μM) in H_2O

The UV-vis absorption spectrum of a rhenium(I) complex based on bipyridine ligand, was recorded in water solution at room temperature.

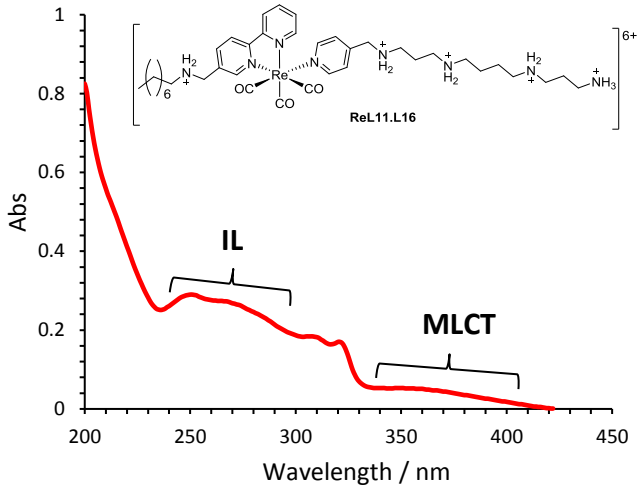

Figure 4.5: UV-vis absorption spectra for **ReL11.L16** (100μM) in H_2O solution

This complex shows absorption bands in the shorter wavelength region at 250-270 nm which are assigned to the intraligand π-π* transitions and the low energy broad bands at approximately 350-400 nm attributed to the metal to ligand charge-transfer (^{1}MLCT) dπ(Re) -π*(bpy) transitions. This result is similar to those observed in related Re(I) carbonyl complexes.[81] Luminescence measurements were recorded at room temperature in water with an excitation wavelength of 350 nm. Fig. 4.6 shows a comparison between the normalised excitation and emission spectra of the rhenium complex containing a bipy ligand and rhenium(I) complex based on a pyridyltriazole.

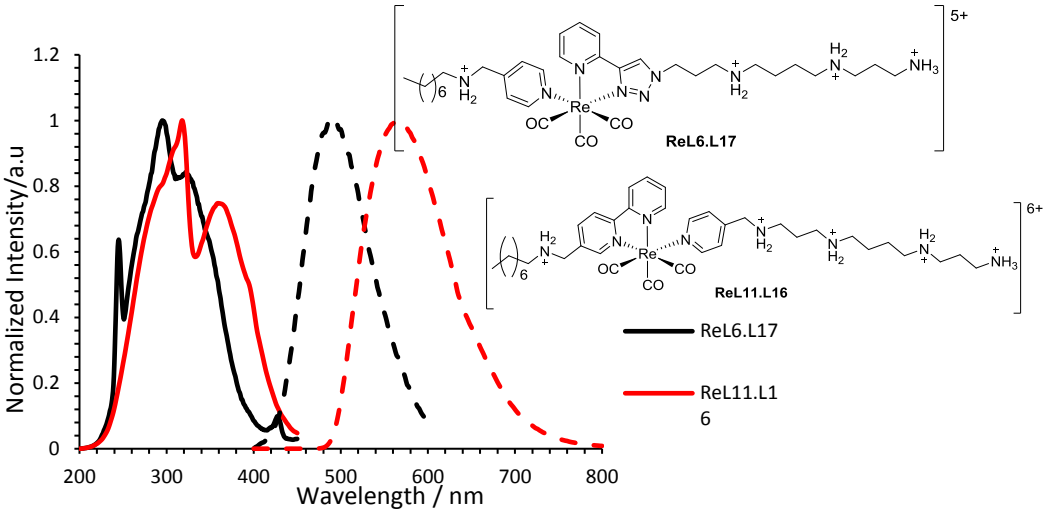

Figure 4.6: Excitation and emission spectra for **ReL6.L17** (λ_{ex} = 350, λ_{em} = 500) and **ReL11.L16** (λ_{ex} = 350, λ_{em} = 570) (100 μM) in H_2O

Complexes **ReL6.L17** and **ReL11.L16** exhibit broad emission with maxima at 500 nm and 570 nm respectively assigned as arising from phosphorescent emission from ^{3}MLCT states. The bpy ligand is less electron-rich than the triazole moiety leading to destabilization of the pyridine-based LUMO in the triazole complexes relative to that of bipyridine complexes thus leading to higher energy ^{1}MLCT and ^{3}MLCT states for **ReL6.L17**. The LUMO orbital in **ReL11.L16** is centered on the bipyridine and the HOMO is located on the metal. **ReL6.L17** exhibits blue emission compared to **ReL11.L16** due to the LUMO orbital of pyridyltriazole being higher in energy than bipyridine which leads to an increase in the HOMO-LUMO gap relative to bpy, resulting in blue emission consistent with literatures examples.[76]

An important strategy that was reported by the group of Crowley, is to change the structure of the N^N from 'regular' triazole form to the 'inverse' triazole form in order to tune the emission to longer wavelength.[228] UV-visible spectroscopy in water at room temperature, showed each complex has intense bands in the near UV region between 230 and 300 nm corresponding to the π-π* transitions of the ligands. Whilst the broad

metal-to-ligand charge transfer ^{1}MLCT band (formally Re(dπ)-bisimine(π*)) for complexes **ReL3.L16** and **ReL13.L16** were observed around 330-370 nm consistent with related rhenium(I) complexes.[261] It was found there are slight differences in the absorption profile for the three complexes as shown in the Fig. 4.7.

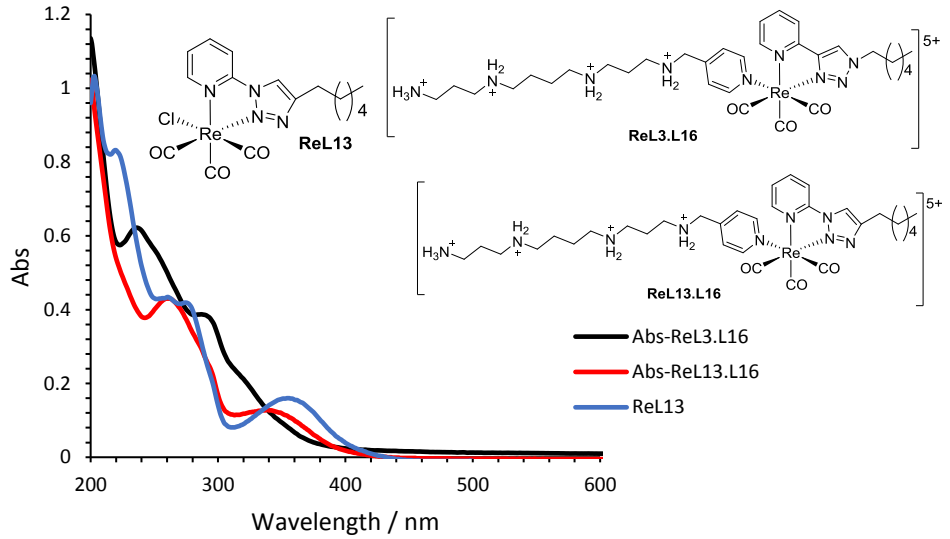

Figure 4.7: Electronic absorption spectra for **ReL13**, **ReL3.L16** and **ReL13.L16** (100μM) in H_2O

Luminescence measurements were recorded at room temperature in water with an excitation wavelength of 370 nm. Fig. 4.8 shows the normalised emission and excitation spectra for **ReL13**, **ReL3.L16** and **ReL13.L16**.

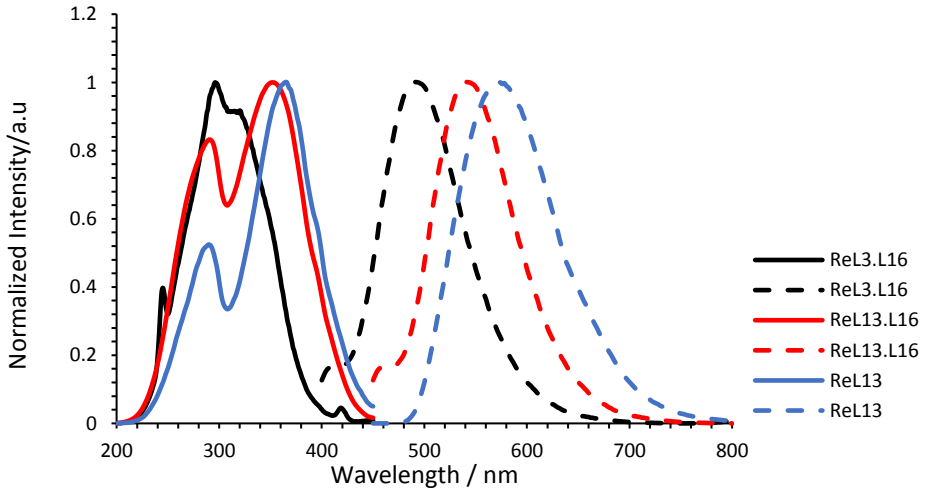

Figure 4.8: Excitation and emission for **ReL13**, **ReL3.L16** (λ_{ex} = 330, λ_{em} = 500) and **ReL13.L16** (λ_{ex} = 390, λ_{em} = 570) (100μM) in H_2O

Broad emission bands are observed with λ_{max}= 570 nm for **ReL13.L16** and 500 nm for **ReL3.L16** in water. These bands are assigned to phosphorescent emission from triplet metal to ligand charge-transfer (^{3}MLCT) excited states. These emission bands are significantly blue-shifted relative to that of the parent chloride complex **ReL13.L16** (570

nm) consistent with the replacement of a π-donor with a moderately π-accepting ligand leading to stabilization of the HOMO relative to the LUMO. Rhenium(I) with the 'inverse' ligand exhibits a ~ 70 nm red shift compared to the rhenium(I) complex containing 'regular' ligand due to inversion of the bridge between the triazole ring and pyridine make the pyridine excellent an electron withdrawing which reduces the energy of the py-centerd LUMO leading to reduced HOMO-LUMO gap resulting a red shift.[229] The complex with the long chain in the inverse pyridyltriazole shows an impressive enhancement in emission compared with corresponding complexes without alkyl chain, as mentioned in Chapter 1. The effect of the side chains can be explained by the alkyl chain wrapping or folding back onto the luminescent Re core in polar solution, isolating it from the solvent environment, so the excited state is shielded from the solvent quenching effect.[262] The UV-visible spectra of **ReL10.L17** and **ReL15.L17** show absorption bands in the shorter wavelength region at 250-270 nm assigned to the intraligand π-π* transitions. The low energy broad bands at approximately 390 nm are attributed to the metal to ligand charge-transfer (^{1}MLCT) dπ(Re) - π*(**L8**) transitions. All the MLCT absorption bands of both complexes are similar to those observed in related Re(I) carbonyl complexes.[213, 228]

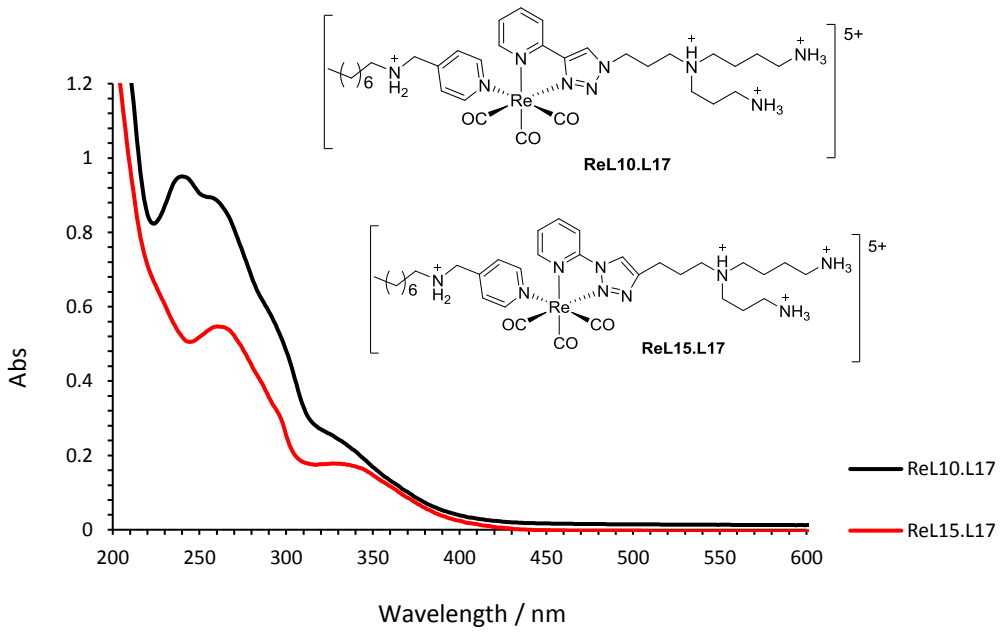

Figure 4.9: Absorption spectra of **ReL10.L17** and **ReL15.L17** (100μM) in H_2O

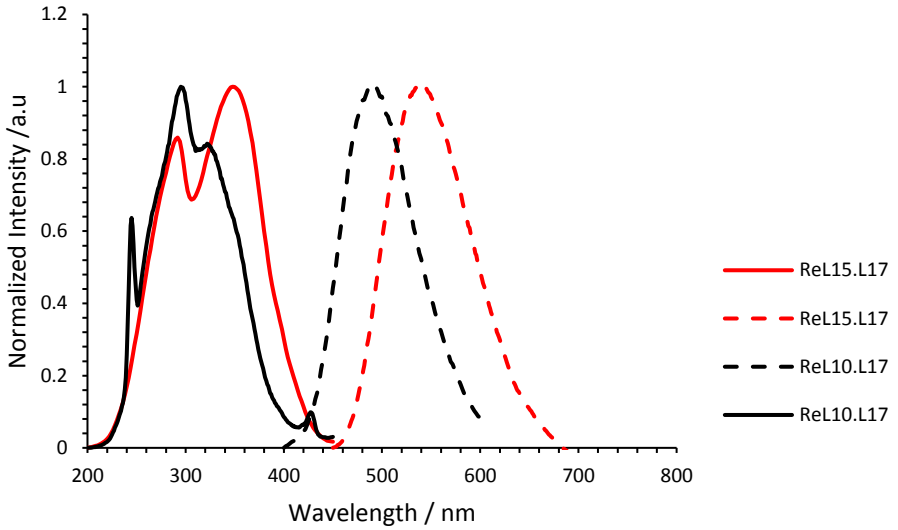

Figure 4.10: Excitation and emission spectra for both **ReL15.L17** (λ_{ex}= 390, λ_{em}= 570) and **ReL10.L17** (λ_{ex} = 350, λ_{em} = 500) (100μM) in H_2O

ReL15.L17 exhibted broad emission at (570 nm) and red shift was obtained with increase excited at ~40 nm compared with requlare complex **ReL10.L17** (350, 500 nm) due to that nitrogen atom of the triazole now banded to the pyridine expect an electron withdrawing effect through the σ- bond which reduces the energy of py-centred (LUMO) leading to reduced HOMO-LUMO gap and resulting a red shift (Fig. 4.10). The UV-visible absorption spectra for complexes **ReL6.L17** and **ReL6.L18** were recorded in water and show identical absorption profiles as shown in Fig. 4.11.

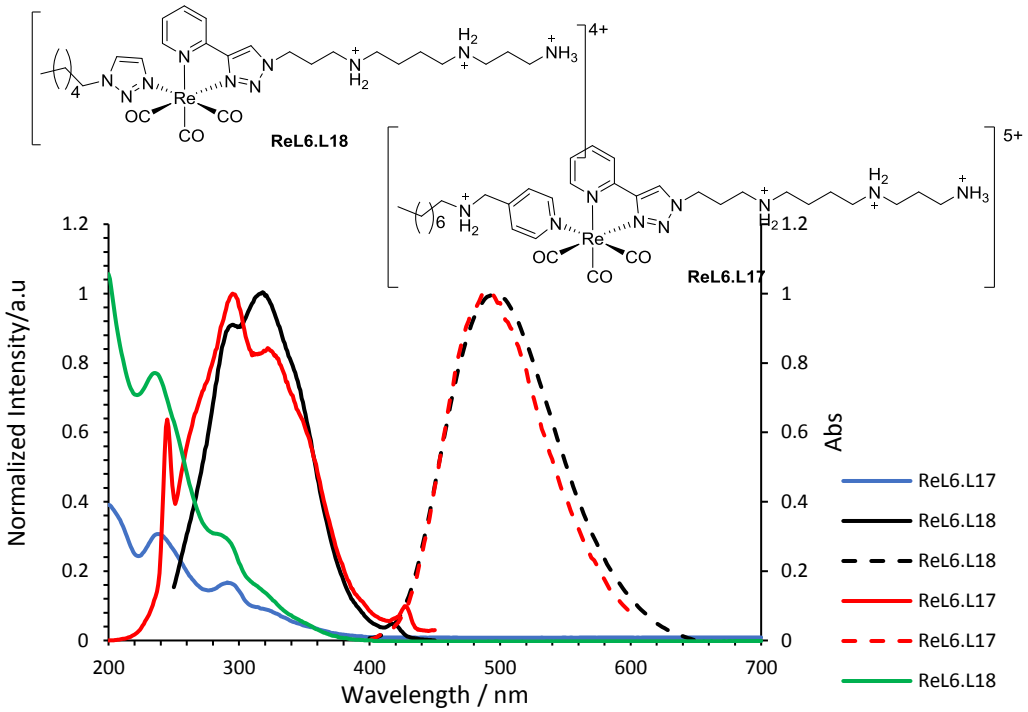

Figure 4.11: Electronic absorption, excitation and emission spectra for **ReL6.L17** (λ_{ex} = 350, λ_{em} = 500) and **ReL6.L18** (λ_{ex} = 350, λ_{em} = 510) (100μM) in H_2O

UV-visible spectra of complexes **ReL6.L17** and **ReL6.L18** show absorption bands between 250-260 nm attributed to ligand centred (LC) π-π* transitions. The next region between 300-350 nm shows weaker transitions of charge transfer character ^{1}MLCT attributed to electron transfer from metal to ligand. Broad bands were observed at longer wavelengths between 400-600 nm assigned to excitation state ^{3}MLCT and broad emission was obtained for both complexes centred at 500 nm. Both complexes show identical excitation and emission profiles as shown in Fig. 4.11, it is clear that the replacement of the pyridine axial ligand with a triazole axial ligand has no effect on the photophysical properties under the same conditions as observed by Uppal *et al.*[81] UV-vis spectra for both complexes **ReL9.L17** and **ReL9.L18** have the similar absorption profile.

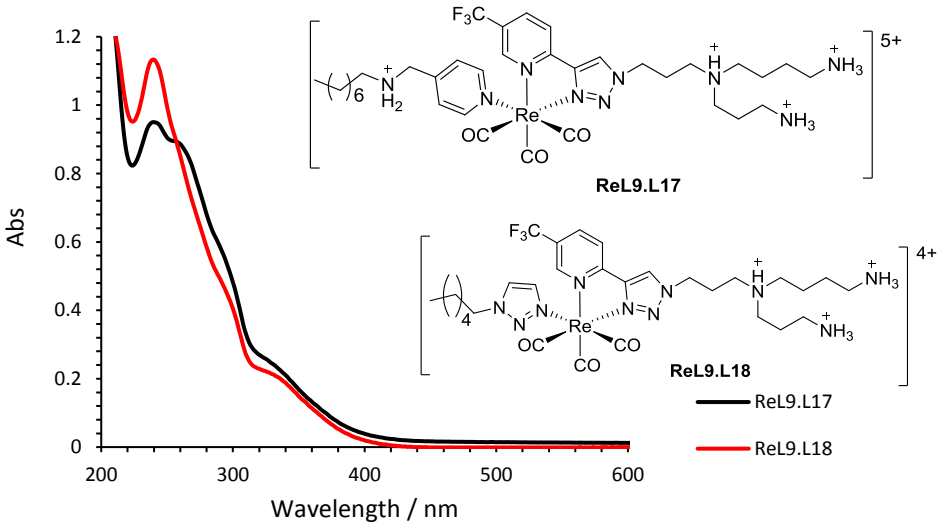

Figure 4.12: Electronic absorption spectra of **ReL9.L17** and **ReL9.L18** (100μM) in H_2O

Both **ReL9.L17** and **ReL9.L18** exhibit absorption bands in the UV region at 260 nm that are assigned to π-π* transitions. The lower energy broad bands above approximately 350 nm are attributed to the dπ(Re)- π*(pyt) metal to ligand charge-transfer ^{1}MLCT with intralingand (IL)

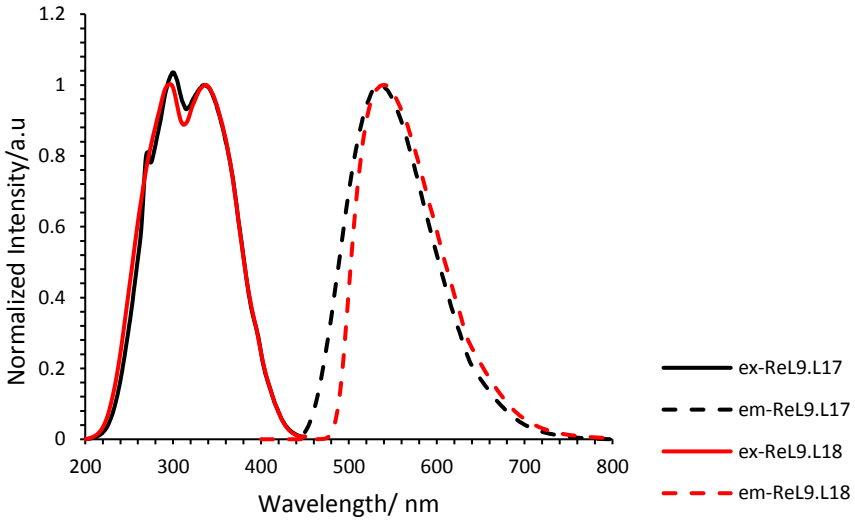

Figure 4.13: Excitation and emission spectra for both **ReL9.L17** (λ_{ex}= 350, λ_{em}= 540) and **ReL9.L18** (λ_{ex} = 350, λ_{em} = 540) (100μM) in H_2O

Luminescence measurements were conducted at room temperature in water with an excitation wavelength of 350 nm. Fig. 4.13 displays normalized emission spectra for both complexes **ReL9.L17** and **ReL9.L18**. A broad emission band is observed at 540 nm for the triazole complexes and was only slightly different to the pyridine complex, with

an observed emission band at 545 nm assigned to phosphorescent emission metal to-ligand charge-transfer ^{3}MLCT. It was found there is little difference in the position of emission maxima when changing from a triazole axial ligand to a pyridine axial ligand. The triazole ligand is a slightly better a donor than pyridine, and the LUMO energy of triazole is suggested to be higher than pyridine, increasing HOMO-LUMO gap.[81]

4.3 Photophysical Properties of Iridium(III) Complexes

Luminescent probes are crucial tools in cell biology, physiology and related areas of the biomedical sciences. The organometallic complexes which are most commonly applied in cell imaging are based on d^6 complexes.[122] Being among the best class of phosphorescent heavy-metal complexes, iridium(III) complexes exhibit high luminescent quantum yield (Φ = 0.7 in organic solvents), tunable luminescent color (from blue to red), and remarkable structure–function relationships, and have been used as highly efficient emitters in organic light-emitting diodes,[246] biolabeling[263] and phosphorescent chemosensing systems.[264] To take advantage from these complexes, different types of iridium(III) complexes were synthesized and characterized as mentioned in Chapter 3, the measurement of photophysical properties is discussed in this chapter. This chapter presents the absorption, excitation and emission properties along with quantum yield and lifetime determinations that allows comparisons to be made between species at different functional groups. UV-vis data was carried out in water solution at room temperature with 100 μM conc. Iridium(III) complexes **Ir(L1)$_2$L6**, **Ir(L2)$_2$L6** and **Ir(L2)$_2$L8** have identical UV-vis spectra and shows absorption bands in the UV region at 260 nm which is assigned to intraligand π-π* transitions. The lower energy broad band at 350 nm is attributed to the dπ(Ir) - π*(pyt) metal to ligand charge-transfer (^{1}MLCT) and ligand-to-ligand (^{1}LLCT) (Table 4.2).[119]

Complexes	C^N	N^N	Exitation/ nm	Emission /nm
Ir(L1)$_2$L6	pht	pyta	350	510
Ir(L2)$_2$L6	pht	pyta	350	510
Ir(L2)$_2$L8	pht	CF_3-pyta	350	550
Ir(L1)$_2$L10	pht	pyta	350	510
Ir(L4)$_2$L6	MeO-pht	pyta	350	510
Ir(L4)$_2$L8	MeO-pht	CF_3-pyta	350	560
Ir(L12)$_2$L8	ppy	CF_3-pyta	400	590
Ir(L1)$_2$L15	pht	Inv-pyta	350	545

Table 4.2: The photophysical propreties of iridium(III) complexes in H_2O (100Mm)

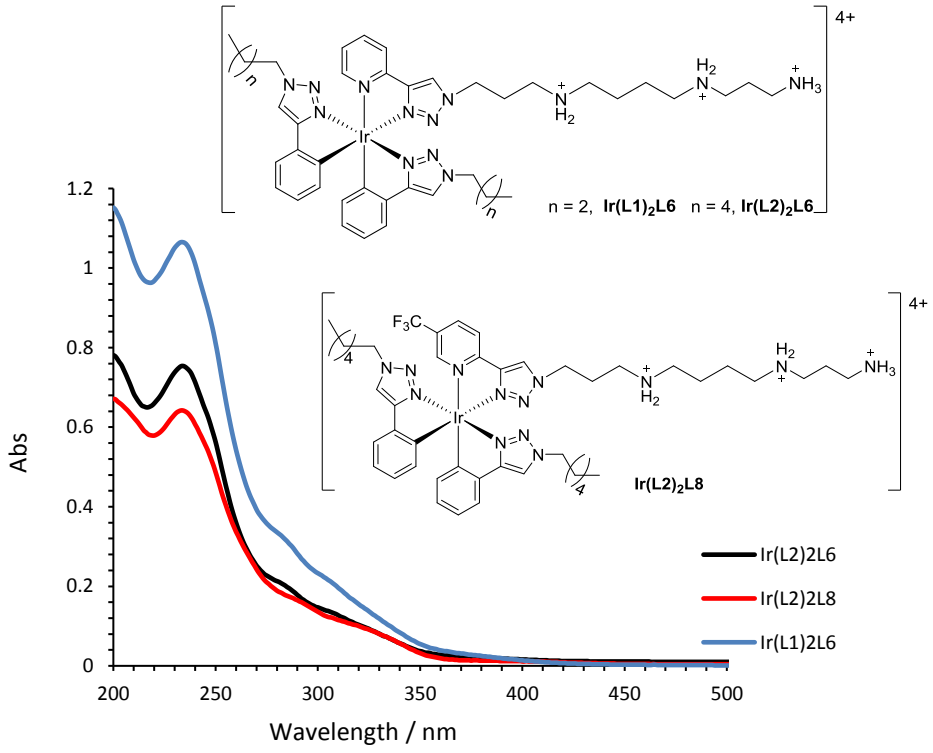

Figure 4.14: UV-vis absorption spectra for **Ir(L1)$_2$L6**, **Ir(L2)$_2$L6** and **Ir(L2)$_2$L8** in H_2O

The broad emission band observed at 510 nm is assigned to phosphorescent emission of metal to-ligand charge-transfer ^{3}MLCT character. It is noteworthy that the different alkyl chains are attached to these complexes have no impact on excitation or

emission.[265] When comparing these complexes with corresponding iridium(III) complexes substituted with an electron withdrawing group **Ir(L2)$_2$L8**, it was found that emission measuring increase by ~ 20-40 nm. This can be explained in terms of the electron withdrawing effect leading to stabilization of the N^N ligand based LUMO, leading to lowering the energy of LUMO and decreasing the HOMO-LUMO energy gap leading to the red shifted emission (Fig. 4.15).[266]

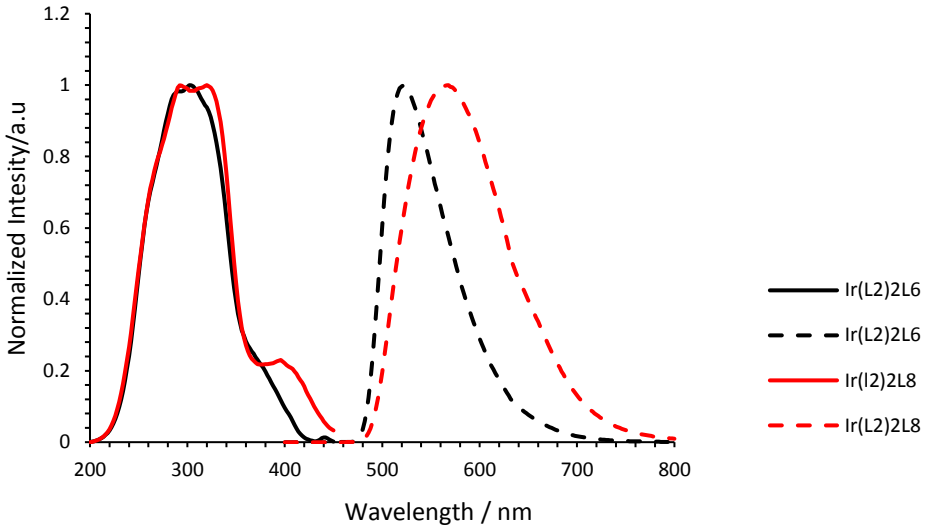

Figure 4.15: Excitation and emission spectra for **Ir(L2)$_2$L6** (λ_{ex} = 350 , λ_{em} = 510) and **Ir(L2)$_2$L8** (λ_{ex}= 350 , λ_{em}= 550) in H_2O

UV-vis absorption spectra of **Ir(L2)$_2$L6**, **Ir(L4)$_2$L6** and **Ir(L4)$_2$L8** in water at 298K display bands in the UV and the visible region resulting from intraligand π-π* between 200-250 nm and metal-to-ligand charge-transfer transitions ^{1}MLCT between 240-340 nm respectively. It was found that **Ir(L4)$_2$L8** absorbs at higher energy compared with **Ir(L2)$_2$L6** and **Ir(L4)$_2$L6**, while **Ir(L2)$_2$L6** absorption is higher energy compared with **Ir(L4)$_2$L6** as shown in Fig. 4.16.

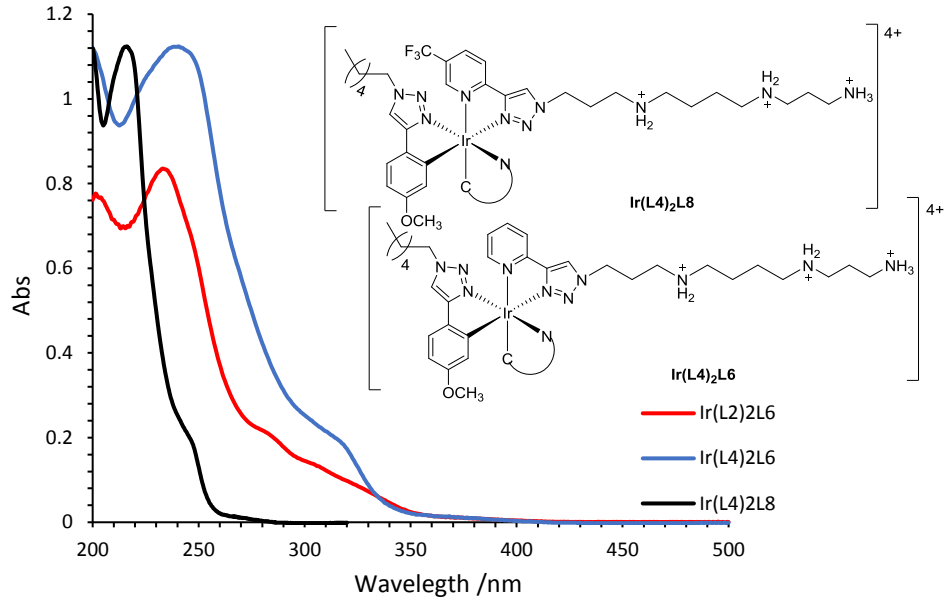

Figure 4.16: UV-vis absorption spectra for **Ir(L2)$_2$L6**, **Ir(L4)$_2$L6** and **Ir(L4)$_2$L8** complexes (100 µM) in H_2O

Excitation of these complexes **Ir(L2)$_2$L6** and **Ir(L4)$_2$L6** at 350 nm leads to broad emission at 490, 510 nm for **Ir(L2)$_2$L6** and **Ir(L4)$_2$L6** respectively while **Ir(L4)$_2$L8** exhibits a broad emission at a longer wavelength of 560 nm when excited at 350 nm which attributed to the metal to ligand charge transfer ^{3}MLCT.

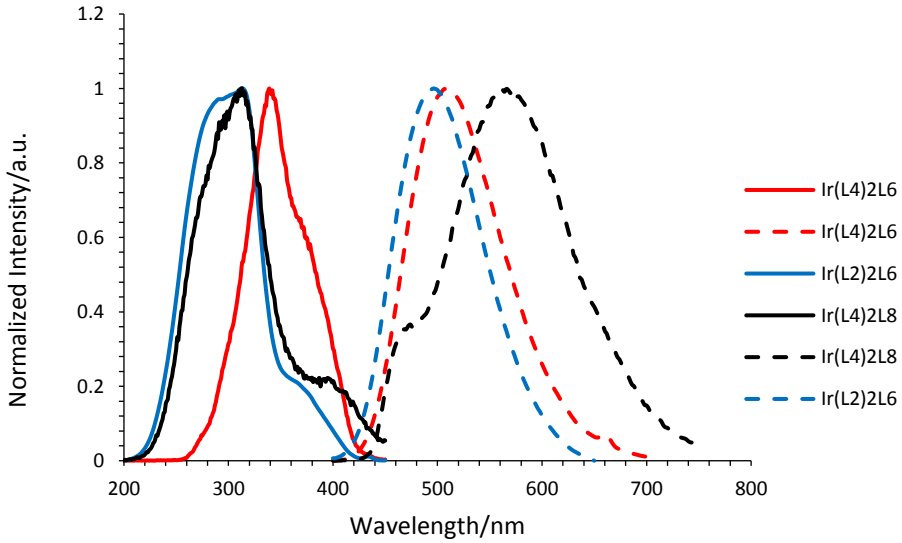

Figure 4.17: Excitation and emission spectra for **Ir(L2)$_2$L6**, **Ir(L4)$_2$L6** (λ_{ex} = 350 , λ_{em} = 480-510) and **Ir(L4)$_2$L8** (λ_{ex} = 350 , λ_{em} = 560) (100 µM) in H_2O

The emission of **Ir(L4)$_2$L8** complex is red shifted compared with **Ir(L2)$_2$L6** and **Ir(L4)$_2$L6** complexes due to the attachment of electron donating group in 4-position in phenyl triazole ligand resulting in stabilizing the HOMO by donating the electron to the metal at the same time electron withdrawing substituted in the ancillary ligand has a high effect on the stabilization of the LUMO which lead to low energy and a resulting decrease in the energy gap between HOMO and LUMO leading to a red shift.[266, 267] Complex **Ir(L4)$_2$L6** exhibits a red shift compared with **Ir(L2)$_2$L6** due to the decrease of the energy gap of HOMO-LUMO because the electron donating substitutent in the cyclometalted leads to destabilization of the LUMO, decreasing its energy, resulting in a red shift compared to the corresponding complex without substituted **Ir(L2)$_2$L6** (Fig. 4.17).[89, 245, 268]

The UV-vis spectra of complexes **Ir(L1)$_2$L6** and **Ir(L1)$_2$L15** were carried out in the water solution at room temperature. Both complexes exhibited a band at 250 nm assigned to π-π* transition of phenyltriazole and pyridyltiazole which is spin allowed, while at long wavelength shows a band 300-330 nm for both complexes which is assigned to metal to ligand charge transfer ^{1}MLCT (Fig. 4.18). These results were consistent with other reported iridium (III) complexes.[128, 269]

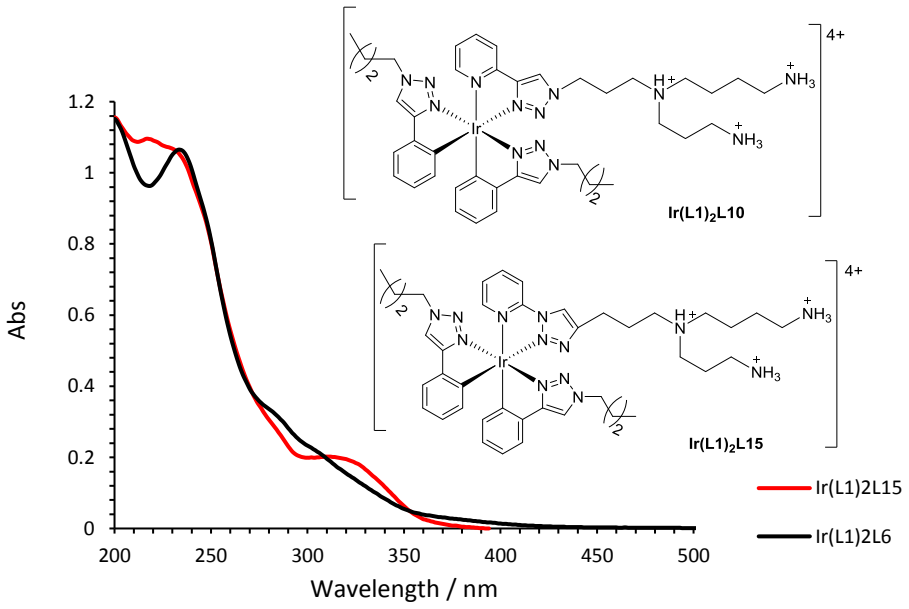

Figure 4.18: Absorption spectra of **Ir(L1)$_2$L6** and **Ir(L1)$_2$L15** (100μM) in H_2O

The luminescence spectra of **Ir(L1)$_2$L6** and **Ir(L1)$_2$L15** show a broad band centred around 510, 540 nm respectively, the excitation maximum of these complexes accur at 350 nm.

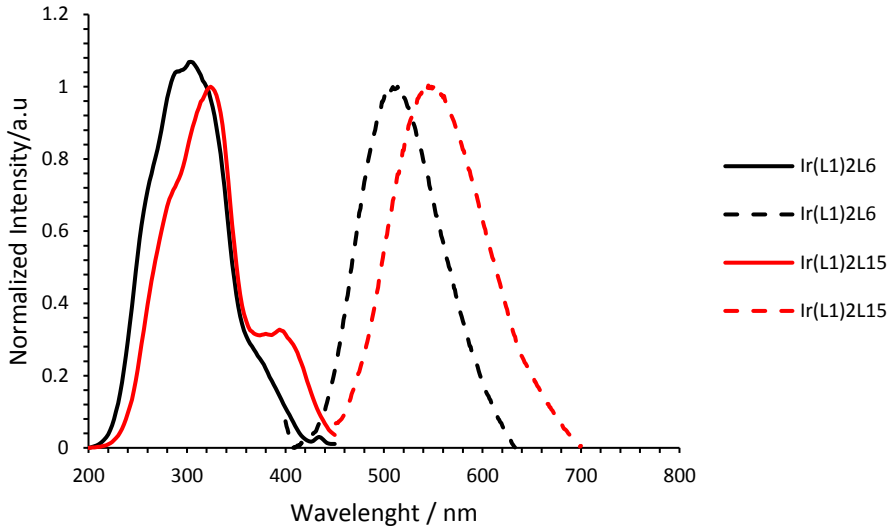

Figure 4.19: Excitation and emission spectra for **Ir(L1)$_2$L6** (λ_{ex} = 350, λ_{em} = 510) and **Ir(L1)$_2$L15** (λ_{ex} = 350, λ_{em} = 540) (100 μM) in H_2O

Changing the structure of ancillary ligand from the regular pyridyltriazole to inverse pyridyltriazole which involves the change of the bridge between the pyridine and triazole, resulted in the hoped for shift in the maximum of the emission by ~ 40 nm, this is consistent with other iridium complexes reported in the literature.[95] It was clear that the change in the structure of ancillary ligand from regular to inverse triazole leads to improvement of the photophysical properties by exhibiting emission at longer wavelength.[237] More importantly there is also a significant change in the excitation spectrum, with an increase in absorbance at 405 nm. Despite these positive results, the cyclometalted phenyltriazole ligands still don't absorb well at 405 nm, a common light source for confocal fluorescence microscopy.

The next strategy used was to tune the excitation wavelength by changing the cyclometalted ligand from phenyl triazole to phenyl pyridine. The UV-vis region shows absorbance bands at 230-250 nm belong to the interligand allowed π–π* transitions of the phenytriazole for the complexes **Ir(L2)$_2$L6** and **Ir(L2)$_2$L8** while absorption was observed for complexes **Ir(L12)$_2$L8** and **Ir(L12)$_2$L9** in the region 250-300 nm, belonging to the interligand allowed π–π* transitions of phenylpyridine and pyridyltriazole. The spectra show that there is some difference in the UV profile between iridium complexes based phenyltriazole and iridium(III) complexes based bipyridine.[128, 246] All the complexes display the typical metal-to-ligand chargetransfer singlet ^{1}MLCT band

between 400 and 500 nm; however, crucially, that of **Ir(L12)$_2$L8** shows significantly higher absorption at 405 nm.

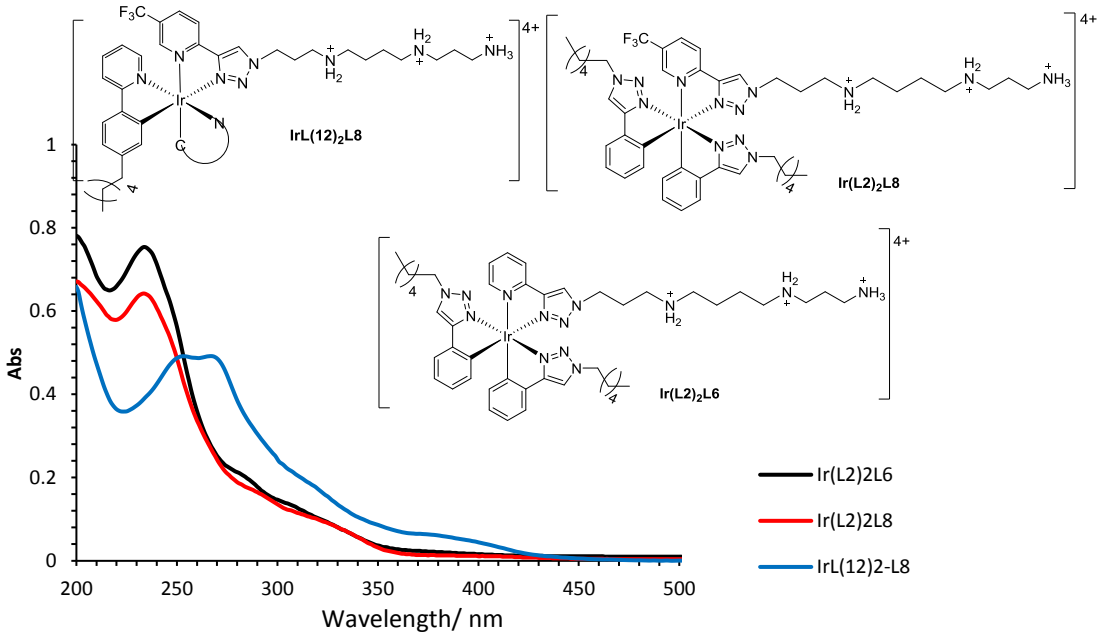

Figure 4.20: Absorption spectra for **Ir(L2)$_2$L6**, **Ir(L2)$_2$L8** and **Ir(L12)$_2$L8** in H_2O

The luminescence spectra of the iridium(III) complexes **Ir(L12)$_2$L8** and **Ir(L12)$_2$L9** show a broad band centered on 590 nm at longer wavelength compared with **Ir(L2)$_2$L6** and **Ir(L2)$_2$L8** which is assigned to metal to ligand charge transfer ^{3}MLCT state due to that changing from phenyltriazole to the phenylpyridine, resulting in a shift in the excitation and emission due to that phenylpyridine is a stronger field ligand than phenyltriazole. On the other hand, phenylpyridine has a lower energy LUMO than phenyltriazole due to is better π accepter than triazole.[270] This result makes the **Ir(L12)$_2$L8** complex sutiable for excitation at 405 nm and more sutiable to be used as a dye for bioimaging more details in Section 4.6.3.

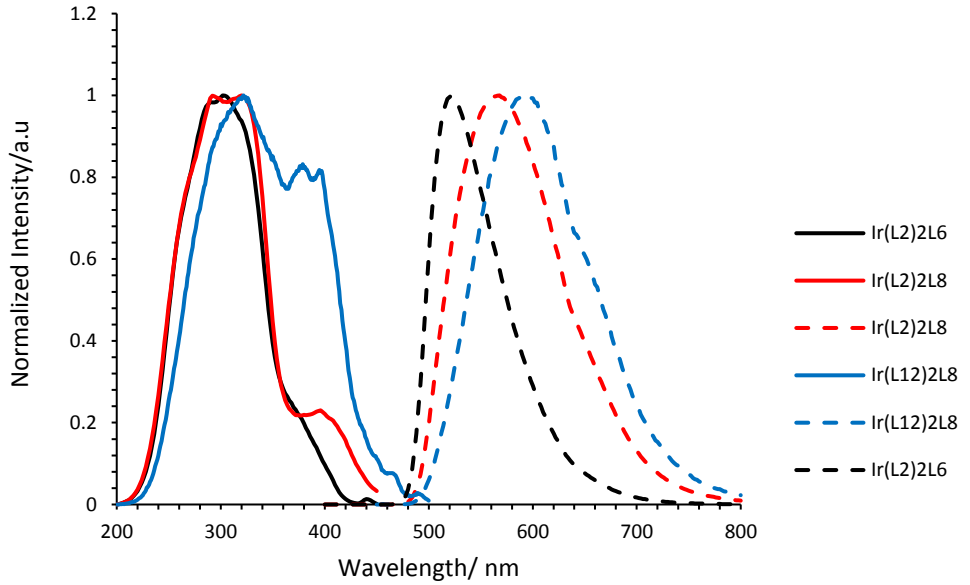

Figure 4.21: Excitation and emission spectra for iridium(III) complexes based phenylpyridine (**L12**) (λ_{ex} = 400 , λ_{em} = 590) and pyridyltriazole (**L2**) (λ_{ex} = 350 , λ_{em} = 510) in H_2O

According to previous studies, replacement of the phenylpyridine with phenyltriazole leads to destabilization of both HOMO/LUMO orbitals in comparison with ppy-type analogues resulting in a red shift of the emission spectrum.[86, 268] While **Ir(L2)$_2$L8** exhibits a red shift compared with **Ir(L2)$_2$L6,** due to the presence of an electron withdrawing group in the ancillary ligand as earlier mentioned.[245]

4.4 Luminescence Quantum Yields and Lifetime Measurement

Quantum yield is the number of emitted photons relative to the number of absorbed photons. Substances with the largest quantum yields, such as the rhodamines, display the brightest emission. The fluorescence quantum yield is, specifically, the ratio of the number of photons emitted to the number absorbed.[271]

The emissive rate of the fluorophore (Γ) and rate of nonradiative decay to S_0 (k_{nr}) both depopulate the excited state. The fraction of fluorophores that decay through emission, and hence the quantum yield is given by:

$$\Phi = \frac{\Gamma}{\Gamma + k_{nr}} \qquad (4.1)$$

Luminescence quantum yields were recorded by using dilute solutions. There are two methods to calculate the quantum yield, the gradient and single-point comparative methods. These methods involve comparing the analyte to a standard. In this study the gradient method is slightly more accurate.[272] This method included plotting absorbance *versus* integrated fluorescence intensity for a range of concentrations to give a slope proportional to the quantum yield and absolute values can be calculated using Equation (4.2) through comparison to a standard.

$$\Phi x = \Phi s \left(\frac{\text{Gradx}}{\text{Grads}}\right)\left(\frac{\eta x}{\eta s}\right)^2 \qquad (4.2)$$

Φ_x is quantum yield for sample and Φs is quantum yield for reference.

This method gives more a reliable value for quantum yield of both rhenium and iridium complexes compared to values reported in the literature.[271, 273] The lifetime (τ) can be defined the average time that the molecule spends in the excited state before returning to the ground state. Generally, phosphorescence lifetimes are near 10 ns.

$$\tau = \frac{1}{\Gamma + k_{nr}} \qquad (4.3)$$

The decay rate of luminescence as a function of time is given by:

$$I_t = I_\circ e^{-t/\tau} \qquad (4.4)$$

Where the luminescence intensity at *t* time is I_t, at time = 0 the luminescence intensity is I_0.[66]

4.4.1 Quantum Yield and Lifetime of Rhenium(I) Complexes

The quantum yield and life time for all rhenium(I) complexes were measured in aerated water solution at room temperature. The quantum yield method included preparation of five solution for both standard and complexes.[274] Under the same conditions the lifetimes measured by TCSPC fitted to a single exponential decay, it was found that **ReL3.L16** displayed a short-lived excited state with high quantum compared to **ReL6.L17**, due to effect of the structue. It is possible that effective shielding by **L16** tail of **ReL3.L16** is stronger compared to **L17** tial of **ReL6.L17**.

Complexes	N^N	Axial ligand	Φ(air)	τ (ns)	Emission/(nm)
ReL6.L17	pyta	py	0.002	103	500
Re10.L17	pyta	py	-	-	500
ReL3.L16	pyta	py	0.014	78	500
ReL8.L17	CF_3-pyta	py	0.076	529	540
ReL11.L16	bipy	py	0.011	546	570
ReL13.L16	Inv-pyta	py	0.024	904	580
ReL6.L18	pyta	triazole	0.022	112	510
ReL15.L17	Inv-pyta	py	0.045	1128	540

Table 4.3: Luminescence lifetimes and emission quantum yields of rhenium(I) complexes

The quantum yield of complexes **ReL6.L17** and **ReL8.L17** and standard $[Ru(bpy)_3]Cl_2$ were carried out in water at 350 nm excitation wavelength. The introduction of electron-withdrawing substituents into the 5-position of the N^N pyridyl rings leads to an improvment and increases the quantum yield and life time for **ReL8.L17** complex (0.076, 529 ns) compared with **ReL6.L17** complex (0.002, 103 ns). This is attributed to the lowering of the LUMO and subsequent increase of the stability of ^{3}MLCT resulting in increased energy separation between the ^{3}MLCT and the ^{3}MC by lowing energy of ^{3}MLCT caused by the electron withdrawing group, which leads to an increase in the value of quantum yield and lifetime consistent with relevant rhenium(I) complexes.[259]

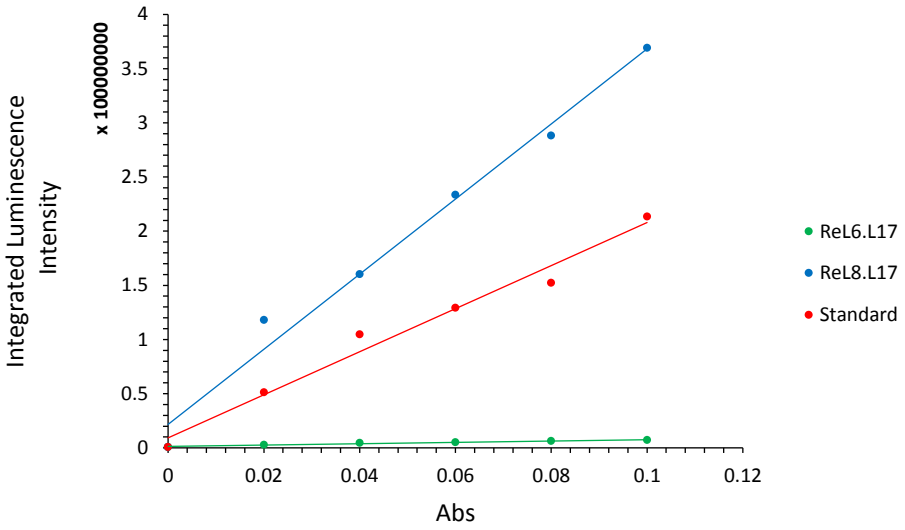

Figure 4.22: Integrated Fluorescence Intensity-Absorbance for **ReL6.L17 and ReL8.L17** and **[Ru(bpy)$_3$]Cl$_2$** as a standard at (λ_{ex} = 350 nm λ_{em} = 530 nm)

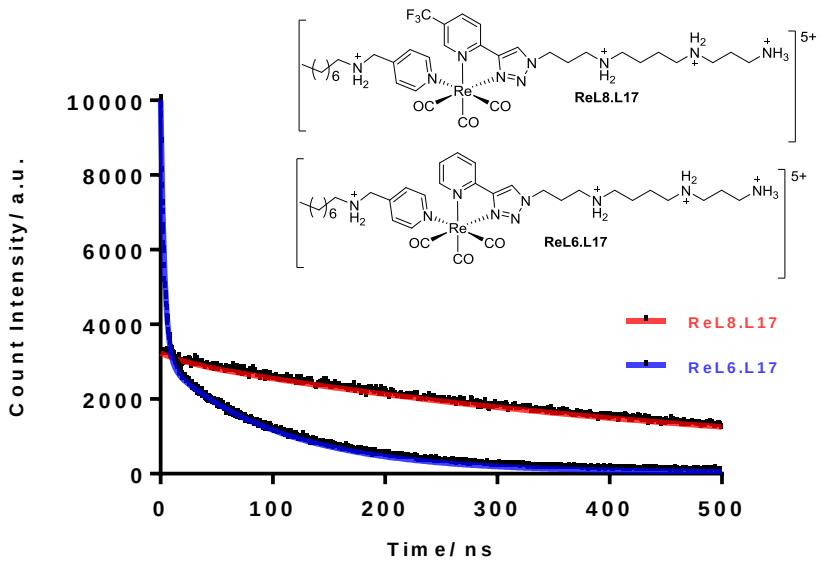

Figure 4.23: TCSPC luminescence exponential decay plot for **ReL8.L17** and **ReL6.L17** at (λ_{ex} = 350 nm, λ_{em} = 530 nm) (100µM in aerated water)

Also the complex **ReL11.L16** displayed better emission quantum yield (0.017) compared with **ReL6.L17** (0.002) in term of structure both complexes have different structure, **ReL11.L16** containg bipyridine being a strong field ligand and its LUMO level localized lower than pyridyltriazole, also the delocalized electron density from electron donating substitutents in the bipyridine compared with pyridyltriazole.[100, 275] As a result the

emission shifted to longer wavelength, also the alkyl chain shields the metal core from solvent leading to increase in the quantum yield and lifetime, the non-radiative decay rate depends on the structure of the diimine ligand, and these observed results were similar to those reported in the literature (Fig. 4.24).[102, 274]

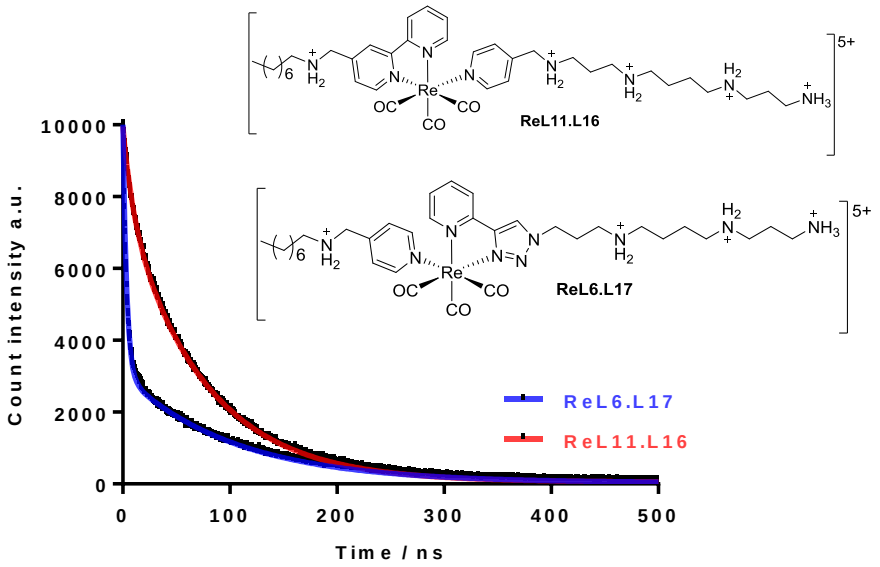

Figure 4.24: TCSPC luminescence exponential decay plot for **ReL11.L16** and **ReL6.L17** at λ_{ex} = 350 nm, λ_{em} = 570 nm, 530 nm (100µM in aerated water)

The complex bearing the inverse pyridyltriazole linker alkyl chain **ReL13.L16** shows an impressive enhancement in emission and quantum yield and lifetime (0.024, 904 ns) compared with corresponding regular complexes **ReL3.L16** (0.014, 78 ns) due to the effect of the different bridge between triazole and pyridine allowing slow relaxation to the ground state.[228] In addition, the effect of the side chains can be explained such that the chain is wrapping or folding back onto the luminescent Re core in polar solutions, isolating it from the solvent environment (as mention before in Chapter 1), so the excited state is shielded from the solvent quenching effect.[262] The complex containing the inverse pyridytiazole linker to spermidine **ReL15.L17** displayed interesting luminescent quantum yields (0.045, 1128 ns) compared with corresponding regular rhenium complex **ReL6.L17** (0.0068, 102.7 ns) due to effect of different bridge between triazole and pyridine.

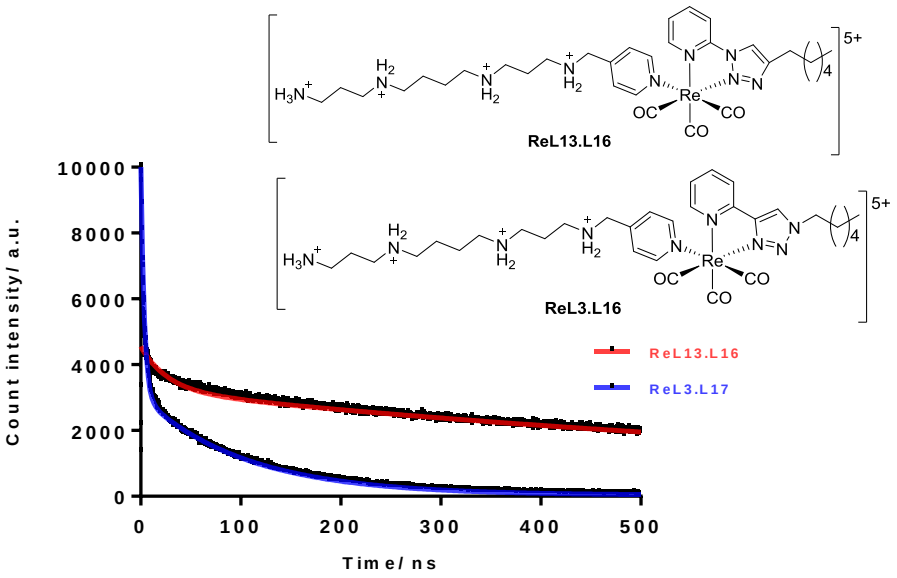

Figure 4.25: TCSPC luminescence exponential decay plot for **ReL13.L16** and **ReL3.L16** at λ_{ex} = 390, 330 nm λ_{em} = 500, 550 nm (100 μM) in aerated water

ReL6.L18 exhibited a quantum yield slightly greater with slightly longer lifetime (0.022, 111 ns) compared with **ReL6.L17** (0.002, 103 ns) due to effect of the different charge as a result to alter the axial ligand structure from pyridine to triazole and leading to the different solvent intraction and then resulting an increase in the longer-lived excited states and higher emission quantum yield.[276] This result is consistent with observations of other cationic rhenium tricarbonyl complexes diimine complexes where nature of the axial N-donor ligand is changed (Fig. 4.26).[81, 260]

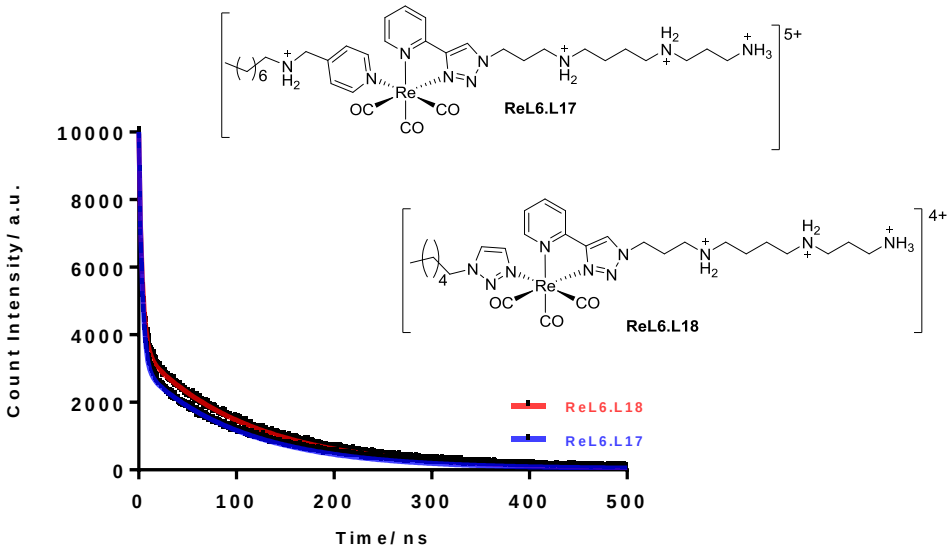

Figure 4.26: TCSPC luminescence exponential decay plot for **ReL6.L18** and **ReL6.L17** at λ_{ex} = 350 nm λ_{em} = 520 nm (100μM in aerated water)

4.4.2 Quantum Yield and Lifetime of Iridium(III) Complexes

Luminescence lifetime measurements and quantum yield were recorded for all iridium(III) complexes in aereated solution at room temperature; quantum yield was calculated for all complexes by using the gradient method and lifetime were measured by time-correlated single photon counting spectroscopy. According to the literature,[277] the luminescence properties were enhanced by adding alkyl groups. It was found that both complexes **Ir(L1)$_2$L6** and **Ir(L2)$_2$L6** exhibited the same quantum yield (0.02) but the lifetime increase depends on the long alkyl group substitution in the cyclometalated ligand (Table 4.4). The excited state lifetime **Ir(L2)$_2$L6** (448 ns) is longer lived compared with **Ir(L1)$_2$L6** (52 ns) attributed to the shielding effect of the long alkyl chain which plays a protecting role from quenching by oxygen molecules in the solvent and through solvent intraction as well.[259, 278]

Complexes	C^N	N^N	Φ(air)	τ(ns)	Emission/nm
Ir(L1)$_2$L6	pht	pyta	0.02	52	510
Ir(L2)$_2$L6	pht	pyta	0.02	448	510
Ir(L2)$_2$L8	pht	CF_3-pyta	0.03	519	550
Ir(L1)$_2$L10	pht	pyta	0.02	103	510
Ir(L4)$_2$L6	MeO-pht	pyta	0.05	-	510
Ir(L4)$_2$L8	MeO-pht	CF_3-pyta	0.03	98	560
Ir(L12)$_2$L8	ppy	CF_3-pyta	0.04	224	590
Ir(L1)$_2$L15	pht	Inv-pyta	0.01	54	545

Table 4.4: Luminescence lifetimes and emission quantum yields of iridium(III) complexes

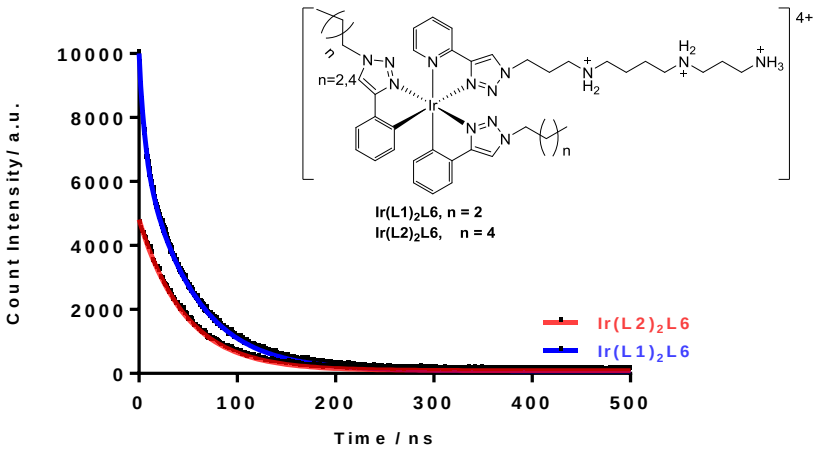

Figure 4.27: TCSPC luminescence exponential decay plot for **Ir(L1)$_2$L6** and **Ir(L2)$_2$L6** at λ_{ex} = 350 nm λ_{em} = 510 nm (100μM) in aerated water

On the other hand, one strategy to increase the quantum yields of iridium(III) complexes is to introduce electron withdrawing such as CF_3 substituents. This leads to a decrease of the HOMO-LUMO gap, also the additional electron withdrawing group in the ancillary ligand improves the quantum yield and lifetime.[279] It was found that **Ir(L2)$_2$L8** shows slightly higher quantum yield and slightly longer lifetime (0.03, 519 ns) compared to the **Ir(L2)$_2$L6** (0.02, 448 ns), the increase is due to the electron withdrawing group that enhances the close-lying π-π* and MLCT states, leading to an increase of the radiative rate constant and decrease of the nonradiative rate constant.[128, 280-282] Complex **Ir(L4)$_2$L8** shows an increase in quantum yield compared to **Ir(L2)$_2$L6** for similar reasons, but exhibits a shorter lifetime compared to **Ir(L2)$_2$L6**, attributed to a lowering of the

metal centered triplet states (^{3}MC) and subsequent depopulation of the ^{3}MLCT state through these efficient non-radiative pathway,[259] or maybe due to the introduction of sterically hindered spacers.[245] The decay traces for the emission for iridium(III) complexes are shown in Fig. 4.28.

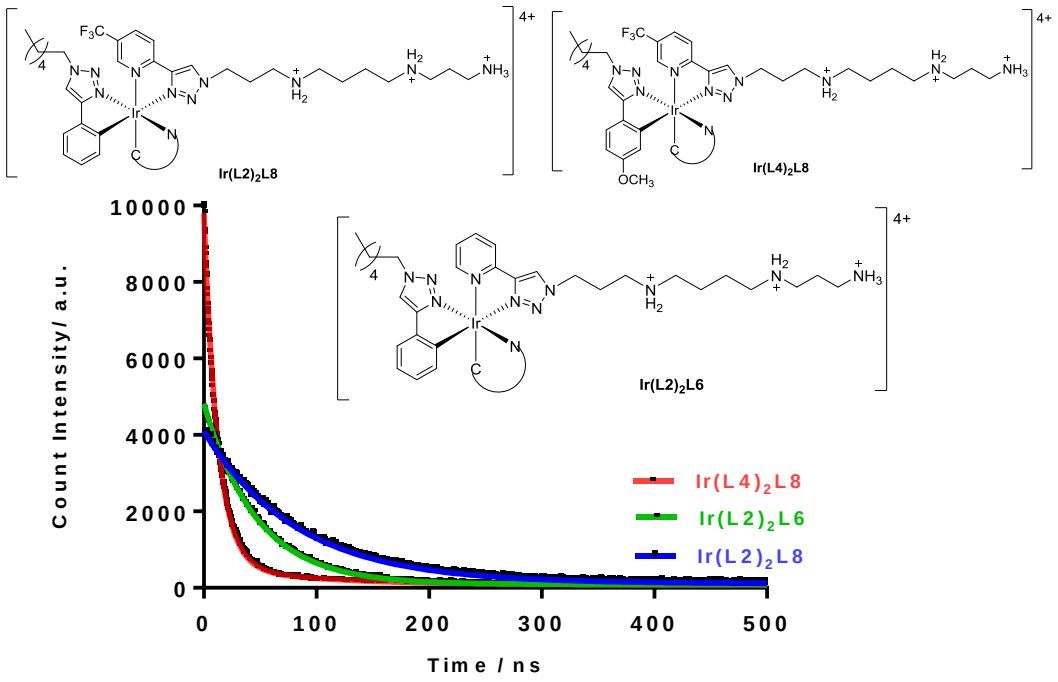

Figure 4.28: TCSPC luminescence exponential decay plot for **Ir(L4)$_2$L8, Ir(L2)$_2$L8** and **Ir(L2)$_2$L6** at λ_{ex} = 350 nm λ_{em} = 550, 510 nm (100 μM in aerated water)

Iridium(III) complexes substituted with a methoxy group on the phenyltriazole rings has an influence on the HOMO level, as well as the ^{3}MLCT state of the complex. Substitution with an electron donating group exhibited an increased quantum yield, it was found that **Ir(L4)$_2$L6** shows higher quantum yield (0.05) compared to the **Ir(L2)$_2$L6** complex (0.03) due to that the introduction of the donor substituents on the phenyl, leading to the increasing HOMO destabilization, subsequently lowering MLCT energy and then decreasing the non-radiative deactivation processes.[277, 283]

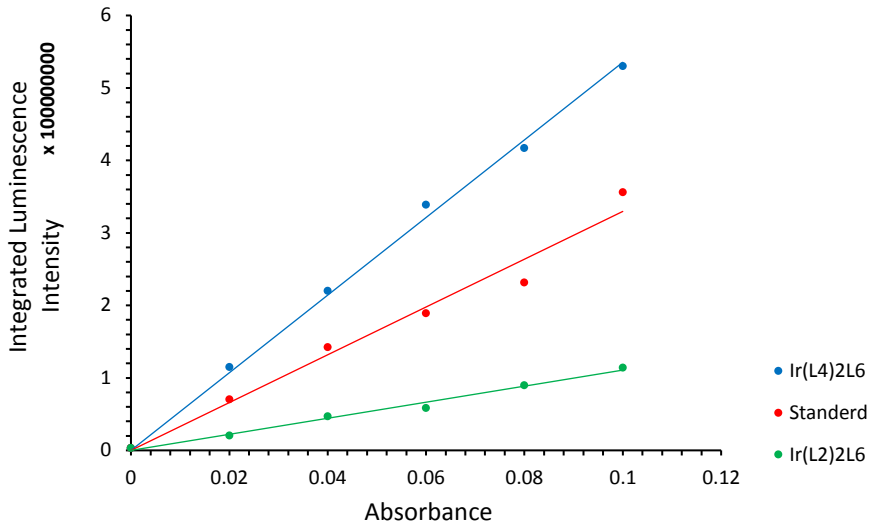

Figure 4.29: Integrated Fluorescence Intensity-Absorbance for **Ir(L4)$_2$L6 and Ir(L2)$_2$L6** and **[Ru(bpy)$_3$]Cl$_2$** as a standard at λ_{ex} = 330 nm λ_{em} = 510 nm

The replacement of phenylpyridine as the cyclometalating ligand with phenyltriazoles had been reported.[237, 284] These types of complexes show a bluer emission compared to complexes based phenylpyridine due to the triazole having a considerably higher LUMO energy than that of pyridine. In this study, it was found that complex **Ir(L2)$_2$L8** shows a blue shift compared to the **Ir(L12)$_2$L8** as discussed in Section 4.2, it was also found that the complex **Ir(L2)$_2$L8** displays smaller quantum (0.03) compared to complex **Ir(L12)$_2$L8** (0.04) due to the lowering of the LUMO and subsequent increased mixing of the ^{3}MLCT and ^{3}LLCT states. The more the LLCT excited state, is lowered in energy, the longer the lifetime (519 ns) for **Ir(L2)$_2$L8** to (224 ns) for **Ir(L12)$_2$L8** while thermal population mainly affects the non-radiative decay pathways, reducing the emission quantum yield.[232, 259]

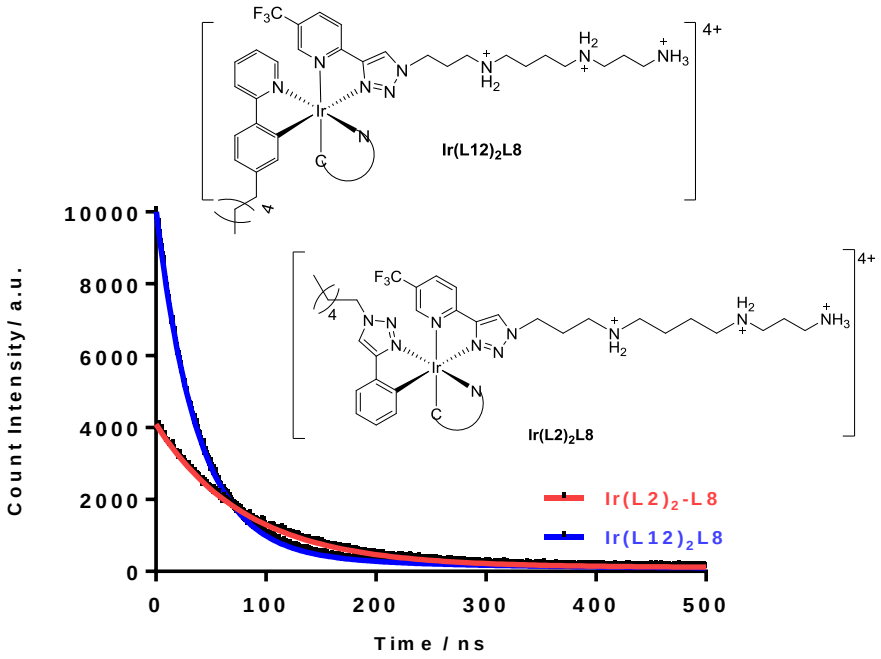

Figure 4.30: TCSPC luminescence exponential decay plot for **Ir(L2)$_2$L8 and Ir(L12)$_2$L8** at λ_{ex} =350, 405 nm λ_{em} = 550, 590 nm (100 µM in aerated water)

The effect of the 'inverse'-type triazolepyridine ligands in iridium(III) complexes have been reported.[95]

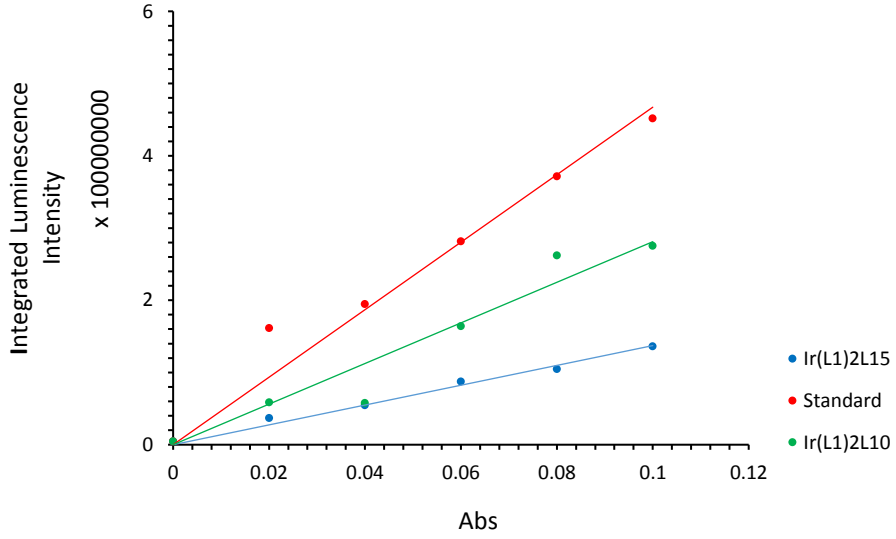

Figure 4.31: Integrated Fluorescence Intensity-Absorbance for **Ir(L1)$_2$L10 and Ir(L1)$_2$L15** and **[Ru(bpy)$_3$]Cl$_2$** as a standard at λ_{ex} = 350 nm λ_{em} = 520 nm (100µM in aerated water)

This study found that **Ir(L1)$_2$L15** (0.008, 54 ns) shows a reduced quantum yield and shorter lifetime compared to corresponding iridium(III) complex **Ir(L1)$_2$L10** (0.02, 103 ns). This may be attributed to an increase in nonradiative paths of decay due to the change of the bridge between triazole and pyridine of the **L15** ligands relative to **L10**.[95, 237]

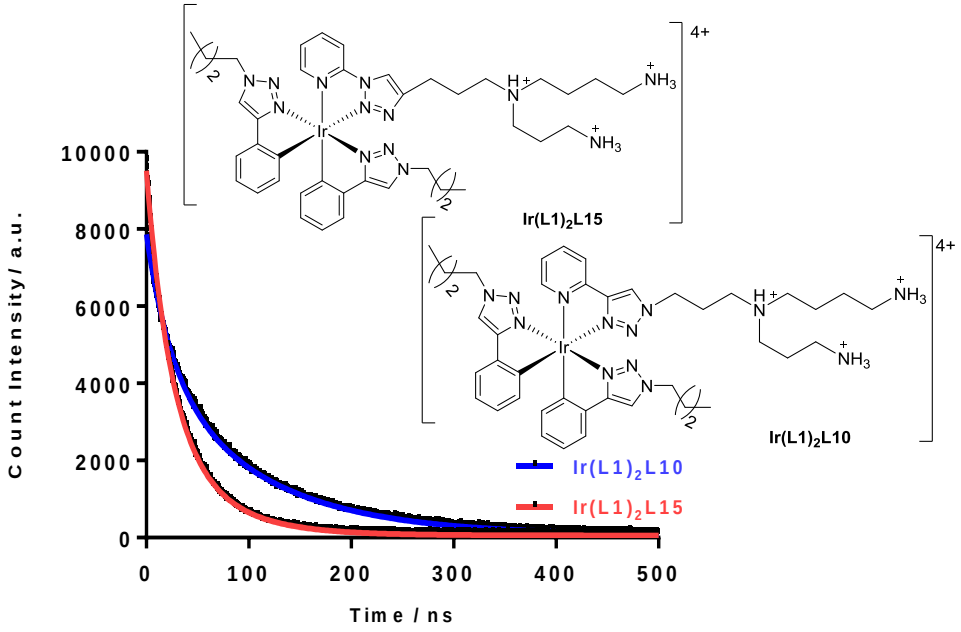

Figure 4.32: TCSPC luminescence exponential decay plot for **Ir(L1)$_2$L10** and **Ir(L1)$_2$L15** (100 μM in aerated water)

4.5 Lipophilicity

Lipophilicity is described as the permeability of molecules across biological membranes, it is considered a pivotal physiological parameter for compounds in describing both pharmacodynamic and pharmacokinetic aspects of drug action.[285-287] This quantitative descriptor of lipophilicity, the partition coefficient (P) often expressed in its logarithmic form of logP, can be defined as the ratio of the equilibrium concentrations of a dissolved substance in a two-phase system consisting of two largely immiscible solvents. In the case n-octanol and water.[288]

$$P = \frac{C_\circ - C_w}{C_w} \qquad (4.5)$$

C_o the concentration of the sample in octanol layer and C_w is the concentration of sample in water layer. As described earlier, lipophilicity is the affinity of a molecule for a lipophilic environment whilst hydrophobicity is the association of non-polar groups or molecules in an aqueous environment.[289] The study the lipophilicity of different compounds is of interest due to the physicochemical properties that are required for quantitative modeling of *in vitro* and *in vivo* biological data, for example, the oral route of drug delivery is the most desirable, therefore, much research has focused on optimizing the absorption and bioavailability of drugs following the oral route.[290] Following on from absorption, lipophilic molecules can easily pass through the cell membrane (intercellular pathway) or cytoplasm (intracellular pathway) to reach the blood stream and from there the target site. Lipophilicity is an established property that influences the distribution of drugs through drug-plasma protein interactions, consequently influencing pharmacokinetic and pharmacodynamic behaviour.[291] Recently, Halbach found that lipophilicity may affect the toxicological properties of compounds.[292] Thus, it is important to know the lipophilicity for compound when using these compounds as bioimaging agents or relevant in order to know how much interaction or absorption by the membrane cell. There are many ways to estimate the partition coefficients logP for a compound such as the shake flask method and RP-HPLC method.

4.5.1 Shake Flask Method

This method is also called octanol–water partition coefficients, this method is widely used as a measure of lipophilicity and one of the most commonly reported physicochemical properties of drugs and industrial chemicals.[293, 294] Octanol was chosen as the organic solvent due to the presence of hydrophobic chains with a polar head group in its structure which correlates well with biological activity, the hydroxyl group in the n-octanol molecule has a hydrogen bonding capability both as a donor, and an acceptor, similar to a membrane, and a receptor's hydrogen bond property. Although the amphiphilic properties of octanol- water system, the octanol-water system does not reveal the real biological partitioning for highly lipophilic or hydrophilic species.[295] Thus, alternative systems are used instead to the octanol- water.

Octanol–water partition coefficients method involves preparation of two solutions one for octanol and other for water; each solution should contain an equal number of moles

of sample and these solution are mixed in a plastic tube (25 mL) with cap and then shaken at rt. for 48 hr by a shaker machine. This solution is transferred to a separating funnel and allowed to separate into two layers, octanol and water. After separation both C_o and C_w were measured by spectrophotometry at λ= 330 nm or 350 nm. The octanol/water partition coefficient, namely, logP, is calculated by the following equation (4.6)[288]

$$\mathrm{L}ogP = \log(C_\circ/C_w) \qquad (4.6)$$

The concentration of each complex in the water phase (*Cw*) and organic phase (*Co*) of solution were determined separately using UV-spectrophotometry.[296]

In this study, the shake-flask method was used to calculate the logP. So, in order to calculate the extension coefficient of the solution, was used a prepared solution of complex of known concentration in both water and octanol, and the extinction coefficient was calculated by using beer lambert law at the same wavelength.

$$A = \varepsilon cl \qquad (4.7)$$

After separation, the extinction coefficient was substituted in equation (4.7) to determine the concentration in both phases and this conc. is then substituted in equation (4.6). This method is used to calculate the logP for some rhenium(I) complexes to investigate which complexes are suitable to candidates for imaging agents. It was found the logP for **ReL11.L16** complex is (0.28) this value is less than the range for related complexes able to cross the blood brain barrier (logP = 0.5–2.5),[115] **ReL8.L17** complex exhibited high lipophilicity with logP = 0.62 compared with **ReL11.L16** due to presence of fluorine, leading to an increase in the lipophilicity.[101] This method was used to measure the logP for iridium(III) complexes, it was found **Ir(L2)$_2$L8** shows high lipophilicity (0.53) compared to **Ir(L1)$_2$L8** (0.18). As expected,[108] the logP increases with the length of the alkyl side chain from 4 to 6 carbons which is consistent with previous report, as a result the complex with higher lipophilicity is expected to have better uptake.[79] **Ir(L12)$_2$L8** exhibited a high logP (0.19) compared to corresponding complex without alky chain (0.08) (Table 4.5). In conclusion, the *fac* rhenium(I) complexes synthesised have been shown to have higher logP compared with the iridium(III) complexes, making them promising candidates for the design of specific cell imaging

agents. Howerever, the complexes contain polyamine with low logP can take advantage of active transport to passing through the cell membrane.

Complexes	logP
ReL8.L17	0.28
ReL11.L16	0.62
Ir(L1)$_2$L8	0.18
Ir(L2)$_2$L8	0.53
Ir(L12)$_2$L8	0.19
Ir(phpy)L6	0.08

Table 4.5: Lipophilicity of rhenium(I) and iridium(III) complexes

4.6 In Vitro imaging study

4.6.1 Luminescence Cell Imaging

The cellular imaging method is optical imaging, or more specifically; fluorescence cell imaging. This technique based on physical principles of excitation by a light source with subsequent detection of the fluorescence emission. Fluorescence microscopy is a relatively modern approach and its oncological application has much increased interest in the field of photochemistry.[297] Operation of fluorescence microscopy can be successful if the fluorophore has a number of essential properties.[298] It must more soluble in buffer and growth media and be photostable. It must be able to penetrate tissue (assisted by high lipophilicity) and localization at a target site is preferred, and be nontoxic. In addition to this, there is a photophysical criterion that the lumophore must adhere to. It must be able to exite and emit at long wavelength in order to be in safe region and non-damaging to the cell. It should show a large Stokes shift to prevent self-quenching of the fluorophore, and have a long lifetime. A successful imaging agent should have a balance of lipophilicity and solubility in polar media.[122] These are the criteria under scrutiny when determining the suitability of a lumophore in luminescent studies. When species do not exhibit these characteristics, it should pose an obvious limitation.

4.6.2 Confocal Fluorescence Microscopy

Confocal fluorescence microscopy is considered as a powerful tool, a high resolution technique in biological imaging with specific fluorescent staining techniques. This technique is used for diagnostic investigations of tissue samples. It can image the slices of tissue when only light which comes from the focal point gets to the detector, or some time with light from above or below rejected to get 3D imaging *cf.* cells.[299] The technique has much greater sensitivity than normal microscopy due to the fact that only emitted light is observed rather than reflected or transmitted. Fluorescence emitted from the sample in this technique is refocused by the objective lens and transmitted by the dichroic mirror before being collected in a detector though a pinhole. The light from the regions out of the plane of focus of the spotlight is also out of focus at the pinhole detector and thus rejected. The emitted light is monochromated before image acquisition, so it is possible to differentiate between emission from distinct luminescent components within the cell, provided they have a significant difference in emission wavelengths. Similarly, excitation is usually done with a scanning laser, with a typical microscope having a variety of laser lines available covering the visible spectrum.[122]

4.6.3 Synaptic Imaging

FM1-43FX is a common dye that is used to stain synaptic vesicles. The dye can bind to the membrane and be internalized upon induction of endocytosis. This process requires addition of 3,3'- diaminobenzidine (DAB) which it is polymerized with FM1-43 and then a precipitate is formed, OsO_4 is another material was used in this process to provide the electron density for the electron microscope.[65] An alternative approach used by a previous researcher with the Lowe group based on using d^6 heavy metals such as Re(I), Ir(III) complexes, as these metals possess many of the features as mentioned before. Previousy the Lowe group was able to image synaptic vesicles by using iridium(III) conjugated with a polyamine. This tail makes interaction with cell membrane through the electrostatic interaction and also provides water solubility, so it is easy to remove the excess of dye by washing it. Iridium(III) itself being electron dense was postulated to be an alternative to OsO_4, it can provide the contrast in electron microscopy by virtue of this electron density. It was hoped the replacement OsO_4 with iridium(III) complex would eliminate the need for treatment with DAB before

performing the electron microscopy, as well as avoiding the use of toxic OsO_4. An aim of this study was to prepare complexes that have similar features to FM1-43, it was found that the results of photophysical studies for some of the complexes shared them to be suitable as a dye for imaging synaptic vesicle. In this study **Ir(L12)$_2$L8** complex was the candidate used as a dye image neurons. A two photon microscope was used, this technique has deeper penetration and intrinsic three-dimensional resolution and includes high resolution imaging of structures.[300, 301] Mouse cerebral cortex was used in this method. After cutting from the brain of a mouse as a 300 μm acute slice and then treating with a solution containing higher potassium concentration to induce vesicle release, the iridium complex was added for ~30 seconds (137 mM NaCl, 40 mM KCl, 2.5 mM $CaCl_2$, 1 mM $MgCl_2$, 10 mM d-Glucose, 5 mM HEPES, 10 μM **Ir(L12)$_2$L8** and then in EBS and 10 uM **Ir(L12)$_2$L8** for 2 minutes to allow endocytosis(Fig. 4.33). The potential of the membrane was altered in order to enable the vesicle to internalize via endocytosis. A CCD camera was used to image the samples with a multiphoton system. It was found that the images look unclear. It was suggested that there is an excess of dye that was not internalized due to a strong electrostatic interaction between the polyamine and the cell surface, as a result it was found not easy to wash the dye from surface.

In conclusion, it is likely that a multiphoton system able to excite **Ir(L12)$_2$L8** and promising for future studies with MLC conjugates; as this complex is more stable also it was found this approach will avoid the use of potentially damaging UV irradiation and would be interesting to see if multiphoton excitation is possible with the rhenium(I)-polyamine conjugates. This result opens up a new direction in developing new probes to study the synaptic vesicle function in deeper detail.

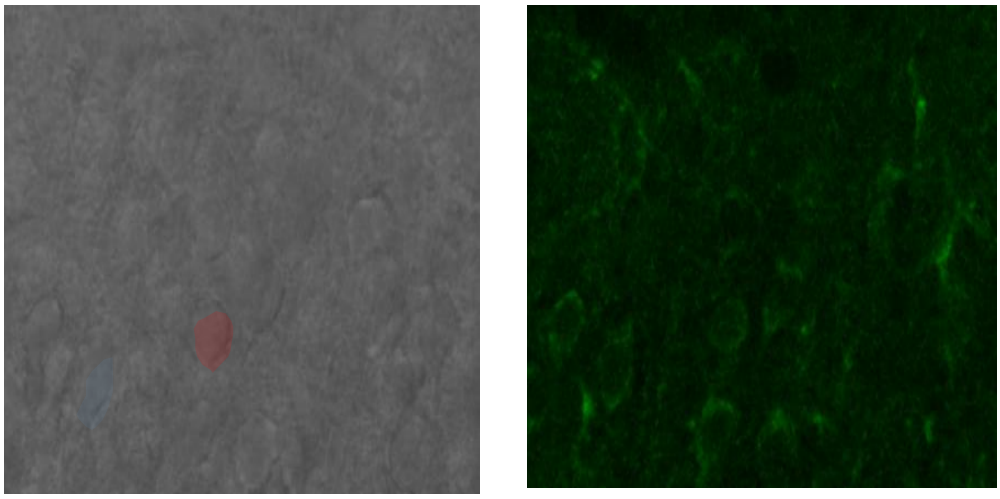

Figure 4.33: Complex **Ir(L12)$_2$L8** pressure injected in mouse cerebral cortex. Both transmitted light (left) and epifluorescence image (right) obtained using a multiphoton microscope (Zeiss LSM 720) equipped with a Ti: Sapphire laser at 720 nm and emission light was collected at 530/20 nm. Complex **Ir(L12)$_2$L8** emission allows clear identification of individual neurons (nerve cells).

When compared this complex with previous study (Fig. 4.34),[37] it was found that the **Ir(L12)$_2$L8** gives better uptake and bright image and also more intraction with cell membrane due to presence the alkyl chain in the cyclometating.

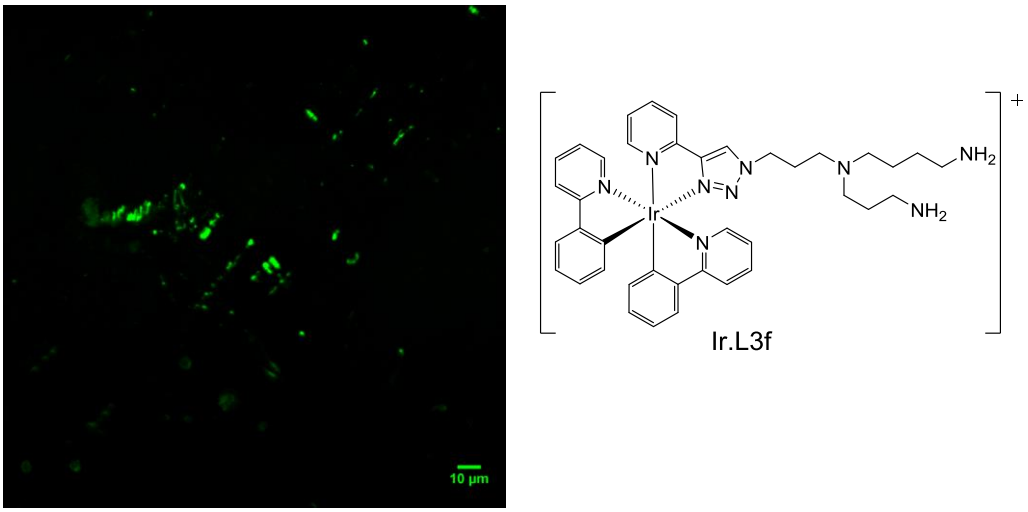

Figure 4.34: Multiphoton image of primary neuronal cultures harvested from E17 rats incubated with Ir.L3f showing incorporation into putative terminal synaptic vesicles.Excitation at 710 nm with a 500-550 nm emission filter.

4.7 Conclusion

In conclusion this study is successful in the synthesis and characterisation a varity of ligands.These ligands were preapered by click chemisty and other prepared by stille coupling. Rhenium(I) beased on 1,2,3- pyridyltriazole and bipyridine derivatives linked to polyamine or alkyl chain. Iridium(III) complexes also were synthesised based on phenyltriazole and phenylpyridine. Photophysical studies was carried in water solution and shows that **ReL13.L16** exhibited red shift and broad emission at longer wavelength (580 nm) with high quantum yield and long lifetime (0.024, 904 ns) compared with corresponding regular complexes also **ReL15.L17** shows longer lifetime (1128 ns) while **ReL8.L17** exhibited larger quantum yield (0.076) compared with other rhenium(I) and iridium(III) complexes. Photophysical studies of **Ir(L12)$_2$L8** exhibit greater luminescent and give red shift (590 nm) compared with **Ir(L2)$_2$L6** while **Ir(L2)$_2$L8** shows longer lifetime compared with other iridium(III) complexes. Lipophilcity shows that iridium complexes with long alkyl chain have a higher logP than short one. **Ir(L12)$_2$L8** shows bright and clear image and to provide a promsing probe to study the synaptic vesicles in deeper detial.

Chapter 5

5 Conclusions and Future Work

5.1 General Conclusions

The thesis presented the synthesis of new ambiphilic rhenium(I) and iridium(III) complexes in order to be used as a dye to replace the FM1-43 dye for imaging synaptic vesicles. Three types of rhenium complexes were synthesised depending on the type of ancillary ligand; the first type with pyridyltriazoles, some with electron withdrawing subsitutents or the second type with bipyridine substituted with alkyl chains and the last type with 'inverse' pyridyltriazoles. These complexes contain pyridine substituted in the 4-position and other rhenium(I) complexes containing triazole as a monodentate ligand. It was found that the rhenium complex with the inverse pyridyltriazole ligand exhibited the highest quantum yields and longer lifetimes between the three types. New cationic iridium(III) complexes incorporating different types of cylometalating ligand were synthesized, represented by phenyltriazole substituted with different types of alkyl chain, in addition electron donating substitutents in some complexes or phenylpyridine substituted with an alkyl chain as a cyclometalating ligand, while the ancillary ligand is a pyridyltriazole bearing polyamine (with or without substituted electron withdrawing group). It was found that iridium(III) complexes cyclometalated with phenylpyridines have the highest quantum yield and longer lifetime, with red emission, compared to the phenyltriazole as a cyclometalating ligand. Photophysical properties of iridium(III) complexes have higher quantum and longer lifetime than rhenium(I) complexes. Lipophilicity studies found that rhenium(I) complexes containing the CF_3 group display high logP values while iridium(III) complexes with long chains have higher logP value than the short ones. Complexes were characterized by NMR spectroscopy and mass spectrometry. Based on the luminescence properties, iridium(III) complex **Ir(L12)$_2$L8** is a candidate for imaging synaptic vesicles. Multiphoton fluorescence microscopy imaging was used with **Ir(L12)$_2$L8** complex to image acute cerebral mouse brian slices.

5.2 Future work

5.2.1 Modifying the Ancillary Ligand

This thesis found that CuAAC chemistry offers significant advantages as a tool in ligand design and has enabled access to rich coordination chemistry particularly the pyridyltriazole moiety. However, this ligand was found gave bluer emission as an ancillary ligand when coordination with rhenium(I) metal. This considered as drawback for using pyridyltriazole as a ligand. Efficient ligand design can be successful when their complexes display tuning of electronic and photophysical properties. Thus to take advantage of a previous study that suggested when adding electron withdrawing subsituents in the ancillary ligand will lower the LUMO energy leading to decrease HOMO-LUMO energy gap resulting red shift.[280, 302] So, it is worth designing a ligand containing electron withdrawing subsitutent in bipyridine as shown in Scheme 5.1

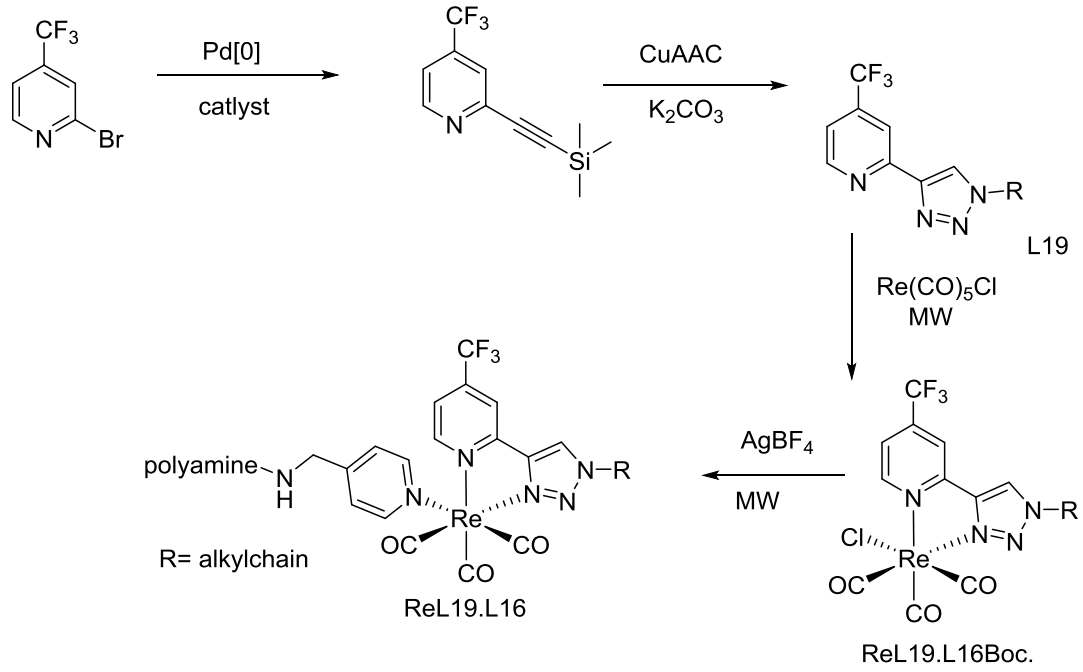

Scheme 5.1: Syntheis of rhenium(I) complexes

Also it was found that if the ancillary ligand such as a pyridyltriazole contains a bromo subsitutent in the pyridine ring, it could be functionalised by Sonogashira reaction to form different compounds. The addition conjucation in the ancillary ligand lead to lower LUMO energy and resulting to decrease the HOMO-LUMO energy gap and red shift.

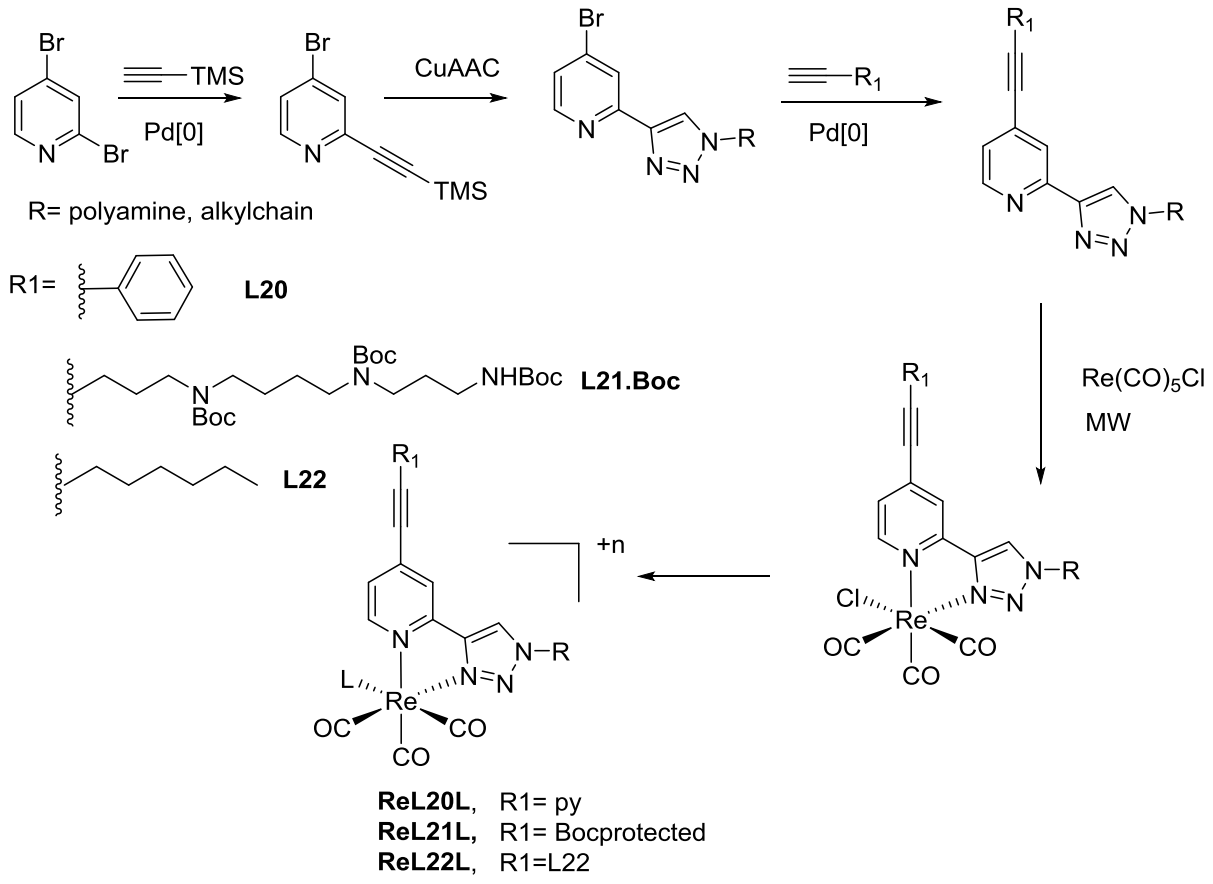

Scheme 5.2: Syntheis of rhenium(I) complexes

Similary, it was suggested that for iridium(III) complexes based phenylpyridine or phenyl triazole the same ancillray ligand can also be used such as **L20, L21Boc and L22** as shown in Scheme 5.3.

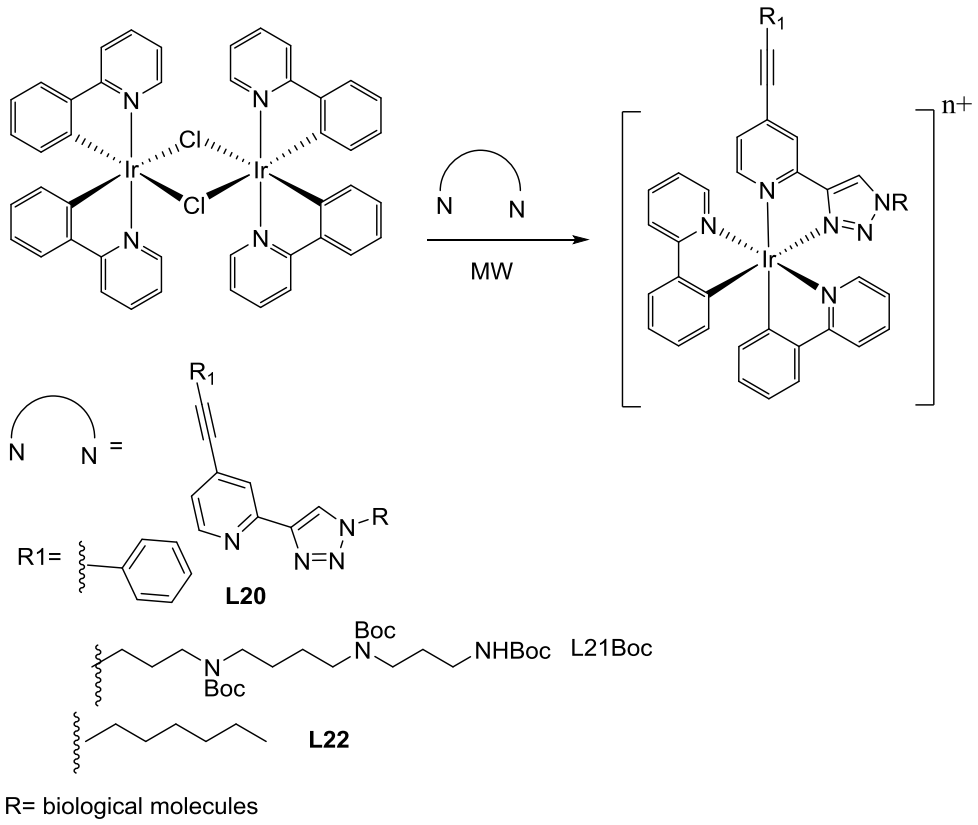

Scheme 5.3: Synthesis of iridium(III) complexes

5.2.2 Cytotoxicity

One of the important requirements of imaging agents to is have low toxicity. Although the study by Lo *et al.*[101] found that the cell proliflation of cationic iridium complexes showed low cytotoxicity comparing with organic dyes and also found the cytotoxicity of phosphorescent heavy-metal complexes is dependent on their chemical structures, it was important to control the toxicity of the complexes by preparing complexes with shorter alkyl chains because the complexes with high lipophilicity are highly cytotoxic.

5.2.3 The Potential Rhenium(I) Complexes as Radiolabelling

Technetium-99m is the most widely used radionuclide in diagnostic nuclear medicine. Many complexes of Technetium-99m were synthesised and used in applications diagnostic nuclear medicine, rhenium and techetium have the same chemistry coordination.[83] It noteworthy that the rhenium complexes based on pyridyltriazole that were prepared in this study can be used as labile agent due to some of these complexes have high quantum yield, long lifetime and large Stokes shift and suitable for single

photo excitation, in addition to their ambiphlic propeties these complexes and air-stable making these complexes as candidates for use in radiolablling. It suggests that The ligands prepared in this study could be used to prepare ^{99m}Tc complexes as a previous study by Connell *et at.*,[83] the synthesis of these complexes can be started with [^{99m}Tc(CO)$_3$(H$_2$O)$_3$] and then adding pyridyl triazole contianing polyamine and 4-pyridyl as axial ligand to form [^{99m}Tc(CO)$_3$(pyta)$_3$py]$^+$and then inject these compexes to the brain of the mouse for 30min.(connel2014) and then take imaging.

Chapter 6

6 Experimental

6.1 Material and instrument

All reagents and solvents were obtained commercially from Aldrich or Alfa Aesar and used without further purification with the exception of: triethylamine which was distilled over potassium hydroxide; prior to use; dichloromethane, tetrahydrofuran, toluene and acetonitrile which were dried using a PureSolve solvent drying system from Innovative Technologies, $[Ir(ppy)_2Cl]_2$ was synthesized using adapted literature methods[87] and imidazole 1-sulfonyl azide hydrogensulfate were prepared by a previous worker in the Lowe group.[154]

Analytical TLC was run on aluminum-backed silica or neutral alumina plates with a fluorescence indicator at 254 nm, preparative flash column chromatography was performed with silica gel 60 (230-400 mesh) or neutral activated Brockmann I grade alumina (150 mesh).

Analytical and preparative HPLC was performed on a ThermoFisher Ultimate 3000 system with Chromeleon software on Phenomenex Luna C18 columns. Methods employed are as follows: **Method A** (A = 0.1% TFA in H_2O, B = 0.1%TFA in MeCN) 10% B for 5 min, 10-100% B over 30 min, 100% B for 5 min, 100-10% B for 2 min, 10% B for 3 min. **Method B** (A = 25 mM NH_4HCO_3 in H_2O, pH 7, B = MeCN) 10% B for 5 min, 10-100% B over 30 min, 100% B for 5 min, 100-10% B for 2 min, 10% B for 3 min.

NMR spectra were recorded on Bruker AV500, DRX400 or AV400 spectrometers at 298 K unless otherwise stated. Chemical shifts are quoted in ppm relative to tetramethylsilane (TMS). All coupling constants are quoted in Hz and were calculated from spectra directly with TOPSPIN v3.5.

Electronic absorption spectra were recorded on a Shimadzu UV 180 spectrometer using a 10 × 10 mm quartz Hellma cuvette with 2 nm slit width and are recorded in nm. Luminescence data was recorded using a Jobin Yvon Horiba FluoroMax-P spectrometer in a 10 × 10 mm quartz Hellma cuvette. Excitation and emission maxima are limited in accuracy to the monochromator slit width of 3 nm and are recorded in nm.

Quantum yield was measured following comparative methods.[271] 0.1 M $[Ru(bpy)_3Cl_2]$ was used as a standard for photoluminescence quantum yield. Five dilute solutions from both the standard and the sample were prepared depending on the absorbance wavelengths (0.1, 0.08, 0.06, 0.04 and 0.02). After determining the integrated fluorescence intensity at the same λ_{ex} and solvent for all samples, a graph of the integrated fluorescence intensity *vs*. absorbance was plotted.

Lifetimes were measured using a Jobin Yvon Horiba FluoroLog 3 exciting at 372 nm monitoring the emission 500-570 nm with a bandwidth of 10 nm (Re) or 1.5 nm (Ir). The bandwidth of the excitation laser was determined by Rayleigh scattered light from a suspension of Ludox. The data was binned into channels of 1.95 ns/ch and 0.24 ns/ch. All plots were created and analysed using GraphPad Prism 7.

The numbering of compounds is arbitrary from left to right and is purely to aid the assignment of spectra; it does not reflect any IUPAC nomenclature or substitution pattern. Primes indicate the same atom in a different ligand. All methods reported are for the best yield obtained.

Infra-red spectra were recorded on a Perkin Elmer Spectrum one FTRIR instrument and stretches are quoted in reciprocal centimeters (cm^{-1}).

A Micromass Quatro LC Spectrometer was used to record mass spectra, measured in *m/z*, with analytes in methanol. High resolution mass spectra were recorded on a Water Aquity XEVO QT of machine and also measured in *m/z*.

Lipophilicity was recorded by using a shaker machine type IKA VORTEX GENIUS3 the sample was dissolved in both octanol and water to prepare solution and then both

solutions were mixted in a plastic vial screw lad. After shaking for 24h the solution was transfered to a separation funnel. A UV-vis spectrometer was used to calculate the concentration of sample in both layers.

All rhenium(I) and iridium(III) complexes and some ligand synthesis were carried out using Microwave irradiation using a CEM asset ID: SYN24 by using vial size 10mL or 50mL with septum.

6.2 Ligand Synthesis

6.2.1 Tert-butyl (4-aminobutyl) carbamate (2.1)[303]

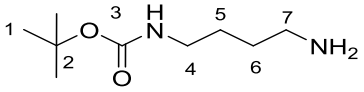

Di-tertbutyl dicarbonate (0.882 g, 1.0 mmol) was dissolved in 1,4-dioxane (30 mL) and added dropwise over 2 hours via an addition funnel to a rapidly stirring solution of 1,4-diaminobutane (0.760 g, 1.0 mmol) in dioxane (20 mL) under dry N_2 at 0 ^{0}C. After addition was completed, the mixture was allowed to warm to room temperature and left to stir overnight. The solvent was removed in *vacuo* and the residue was dissolved H_2O (50 mL) and filtered. The filtrate was extracted with dichloromethane (3 x 20 mL), dried over Na_2SO_4 and the solvent removed under reduced pressure to afford a colorless oil (0.341g, 52%) which was used without further purification. ^{1}H NMR (400 MHz, $CDCl_3$), δ 4.58 (s br, 1H, NH), 3.05 (q, J = 6.3 Hz, 2H, 4-CH_2), 2.64 (t, J = 6.8 Hz, 2H, 7-CH_2), 1.48-1.39 (m, 4H, 5, 6-CH_2), 1.37 (s, 9H, 1-$(CH_3)_3$), 1.14 (sbr, 2H, NH_2); ^{13}C NMR (100 MHz, $CDCl_3$), δ 156.1 (3-C), 79.0 (2-C), 41.7 (4-C), 40.4 (7-C), 30.7 (6-C), 28.4 (1-C), 27.5 (5-C); MS (ES+) 189 $[M+H]^+$; HRMS (ES+) $C_9H_{21}N_2O_2$ $[M+H]^+$ requires 189.1601 found 189.1603.

6.2.2 *N*1, *N*8-bis-Boc-spermidine (2.2)[304]

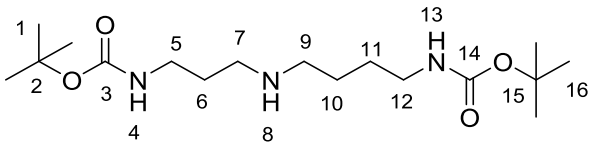

Spermidine (0.500g, 3.44 mmol) was dissolved in dry THF (25 mL) and cooled to 0 °C where upon Boc-ON (1.69 g, 6.88 mmol) was added and the resulting solution stirred for 4 hr at 0 °C (by use maintenance of chiller), TLC was used to monitor the reaction. After that the solvent was removed, the product was taken up in Et_2O (50 mL) and washed with 1 M NaOH until the yellow color was removed. The solvent was dried

over Na_2SO_4, filtered and removed under reduced pressure. The title compound was obtained as a white solid without further purification (1.0309 g, 86%); ^{1}H NMR (400 MHz, $CDCl_3$, 298 K), δ 5.17 (s br, 1H, 4-NH), 4.87 (s br, 1H, 13-NH), 3.21-3.15 (m, 2H, 12-CH_2), 3.22-3.11 (m, 2H, 5-CH_2), 2.65 (t, 2H, *J* = 6.6Hz, 7-CH_2), 2.59 (t, 2H, *J* = 6.8Hz, 9-CH_2), 1.63 (quint, 2H, *J* = 6.5Hz, 6-CH_2), 1.57-1.54 (m, 4H, 10- and 11-CH_2), 1.44 (s, 18H, 1- and 16-$(CH_3)_3$); ^{13}C NMR (100 MHz, $CDCl_3$), δ 156.2 (one of 3- or 14-C), 156.1 (one of 3- or 14-C), 79.0 (one of 2- or 15-C), 68.0 (one of 2- or 15-C), 49.4 (9-C), 47.66 (7-C), 40.5 (5-C), 39.2 (12-C), 29.9 (6-C), 28.5 (1- and 16-C), 27.6 (10-C), 25.6 (11-C); MS (ES+) 346 $[M+H]^+$, 290 $[M-t\text{Bu}+2H]^+$, 246 $[M\text{-Boc}+H]^+$, 234 $[M-2(t\text{Bu})+3H]^+$, 190 $[M\text{-Boc-}t\text{Bu}+3H]^+$, 146 $[M-2(\text{Boc})+3H]^+$; HRMS (ES+) $C_{17}H_{36}N_3O_4$ $[M+H]^+$ requires 346.2715 found 346.2706.

6.2.3 Tert- butyl (4-((3-aminopropyl) (tert-butoxycarbonyl) amino)butyl)(3-((tert-butoxycarbonyl)amino)propyl)carbamate (2.3)[137]

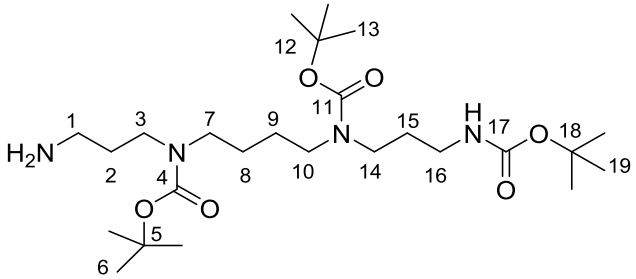

To a stirring solution N_1, N_1'-(butane-1, 4-diyl) bis (propane-1,3-diamine) (1.00 g, 5.10 mmol) in 25% MeOH/CH_2Cl_2) (200 mL) and 2-hydroxybenzaldehyde (0.63 g, 5.1 mmol) was added drop wise. Anhydrous Na_2SO_4 (5.7 g: 40.2 mmol) was added and the reaction was stirred overnight at rt. The imine product was used in the next step without purification. The reaction mixture was cooled to 0 °C, and di-tertbutyldicarbonate (3.40 g, 15.6 mmol) was added. After stirring for 18h at rt., the solvent was removed under *vacuo* to provide the tri-Boc protected imine which was used in the next step without purification. The imine was cleaved by addition of CH_3ONH_2 (1.60 g, 18.7 mmol) and Na_2CO_3 (2.00 g, 18.7 mmol). The reaction changed to a cloudy white solution in which was stirred for 2 h. The solvent was removed under *vacuo* and the residue dissolved in CH_2Cl_2 (50 mL). The organic layer was washed with an aqueous solution of Na_2CO_3 (~10 wt %), separated, filtered and concentrated to yield 5.08 g of crude product. Column Chromatography (SiO_2) was used, eluted with (75% CH_2Cl_2: 25% hexane) to remove the oxime (R_f = 0.4). The solvent system was then changed to 1% NH_4OH: 5% MeOH in DCM to elute the product (R_f = 0.3). The product was obtained as a sticky oil

in a yield about (1.0 g, 41%); ^{1}H NMR (400 MHz, $CDCl_3$), δ 3.41-3.04 (m, 10H, 3, 7, 10, 14, 16-CH), 2.71(t, *J* = 6.10, 2H, 1-CH), 2.09-2.06 (m, 4H, 2, 15-CH), 1.52-1.41 (m, 31H, 6, 8, 9, 13, 19-CH); ^{13}C NMR (100 MHz, $CDCl_3$): δ 156 (4, 11, 17-C), 79.5 (5-C), 79.3 (11-C), 78.9 (17-C), 46.7 (7-C), 43.9 (10-C), 39.3 (3-C), 37.4 (14-C), 28.5 (1-C), 28.4 (6, 13, 19-C), 26.0 (2, 15-C), 25.6 (8, 9-C); MS (ES+) 504 $[M+H]^+$, 404 $[M\text{-Boc} +2H]^+$; HRMS (ES+) $C_{25}H_{51}N_4O_6$ $[M]^+$ requires 503.3805 found 503.3809.

6.2.4 5-(trifluoromethyl)-2-((trimethylsilyl)ethynyl)pyridine (2.4)

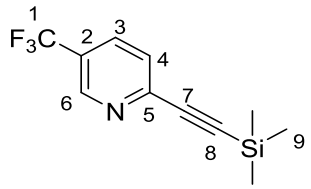

2-bromo-5-(trifluoromethyl) pyridine (0.59g, 2.61mmol), bis (triphenylphosphine) palladium(II) dichloride (0.09 g, 0.13mmol) and CuI (0.03g, 0.13mmol) were added under N_2. Triethyl amine (20mL) and ethynyltrimethylsilane (1.48mL, 10.40mmol) were added by using syringe though a septum sealed the RBF. Solution was stirred and heated to 50°C under N_2 for 1hr and allowed to cool to room temperature. The consumption of arylhailde was monitored by TLC analysis in 100% EA, followed by $KMnO_4$ stain. The reaction mixture extracts by Diethyl ether (20mL) and then washed with saturated aqueous ammonium chloride (3 x 25mL). Organic layers were combined, dried over Na_2SO_4 and filtered and then the solvent was removed under *vacuo*. Product was purified by column chromatography starting with 100% hexane to collect the first fraction containing start material and then using 95:5 hexane: ethyl acetate to collect fraction of product and then the solvent was removed and yielding a white flaky solid (469mg, 74%); ^{1}H NMR (400MHz, $CDCl_3$): δ 8.82 (d, *J* = 2.1 Hz, 1H 6-CH), 7.87 (dd, *J* = 8.1, 2.1 Hz, 1H, 3-CH), 7.55 (d, *J* = 8.3 Hz, 1H, 4-CH), 0.28 (s, 9H, 9-$(CH_3)_3$); ^{13}C NMR (100MHz, $CDCl_3$), δ 147.2 (6-C): 146.8 (5-C), 133.7 (3-C), 127.2 (4-C), 125.7 (2-C), 123.6 (1-C), 102.8 (7-C), 98.6 (8-C), 0.42 (9-C);^{19}F NMR (400MHz, $CDCl_3$) 62.4(s, 3F-py); MS(ES+) m/z 244 $[M+H]^+$; HRMS (ES+) $C_{11}H_{13}NF_3{}^{28}Si$ requires 244.0760 found 244.0769.

6.2.5 3-(4-(5-(trifluoromethyl) pyridin-2-yl)-1H-1, 2, 3-triazol-1-yl) propan-1-ol (2.5)

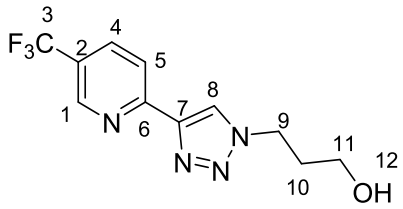

A solution of sodium azide (0.39 g, 0.61 mmol) and 3-bromo-1-propanol (0.08g, 0.56mmol) in THF: H_2O (1:1, 20 ml) was refluxed for 24 hours at 90°C. Upon cooling, alkyne (0.13g, 0.51mmol), sodium ascorbate (0.02 g, 0.102 mmol) and $CuSO_4.5H_2O$ (0.013g, 0.051 mmol) were added (in order) and the mixture was sealed and placed in microwave reactor at 80ºC for 1hr. the solvent was removed after microwave and the EDTA saturated solution at pH =10 was added by adding NH_4OH and then extract with dichloromethane (5 x 30 mL) .The organic layer was collected and dried over $MgSO_4$. The dry organic layer was filtered and solvent removed under vacuum affording crude product (0.13 g, 94%) which was used without further purification; ^{1}H NMR (400MHz, $CDCl_3$), δ 8.83(s, 1H, 1-CH), 8.30 (d, *J* = 8.4 Hz, 1H, 4-CH), 8.24 (s, 1H, 8-CH), 8.01 (dd, *J* = 8.0, 2.0 Hz, 1H, 5-CH), 4.65 (t, *J* = 6.6 Hz, 2H, 9-CH_2), 3.57 (t, *J* = 5.9 Hz, 2H, 11-CH_2), 2.46 (p, *J* = 6.4 Hz, 2H, 10-CH_2); ^{13}C NMR (100 MHz, $CDCl_3$), δ 153.5(6-C), 146.4(7-C), 134 (4-C), 123.5 (3, 8-C), 119.6 (2, 5-C), 58.7 (11-C), 47.2 (9-C), 32.4(10-C); IR (neat): 3310, 2927 (C-H), 1611, 1331, 1123; ^{19}F NMR (400MHz, MeOD), δ -62.0; MS (ES+): 273 $[M+H]^+$, 295$[M+Na]^+$; HRMS (ES+) $C_{11}H_{12}N_4OF_3$ $[M+H]^+$ requires 273.0955 found 273.0963.

6.2.6 2-(1-(3-chloropropyl)-1H-1, 2, 3-triazol-4-yl)-5-(trifluoromethyl) pyridine (2.6)

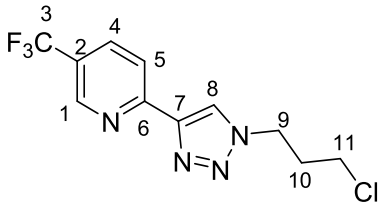

A solution of **2.5** (0.27 g, 0.98 mmol) was dissolved in DCM (20 mL) and $SOCl_2$ (1.8ml, 25mmol) was added by syringe and heated for 24 hours at 40°C under N_2. TLC was run 100% EtOAc and show all starting material was consumed, solution of $NaHCO_3$ was added as a dropwise and then extracted with dichloromethane (5 x 30 mL) and dried over $MgSO_4$. The dry layer was filtered and then the solvent was removed under vacuum

affording crude product (0.27 g, 95%); ^{1}H NMR (400MHz, $CDCl_3$), δ 8.84 (s, 1H, 1-CH), 8.31 (d, *J* = 8.4 Hz, 1H, 4-CH), 8.25 (s, 1H, 8-CH), 8.01 (dd, *J* = 8.3, 1.9 Hz, 1H, 5-CH), 4.65 (t, *J* = 6.7 Hz, 2H, 9-CH_2), 3.57 (t, *J* = 5.9 Hz, 2H, 10-CH_2), 2.47 (quint, *J* = 6.3 Hz, 2H, 11-CH_2);^{13}C NMR (100 MHz, $CDCl_3$), δ 150.0 (1-C), 146.4(6-C), 143(4-C), 134.0 (2-C), 123.5 (3, 8-C), 122 (5,7-C), 48.0 (9-C), 41.0 (11-C), 32.4 (10-C); IR (neat): 1611, 1330, 1117, 817, 774; ^{19}F NMR (400MHz, MeOD), δ -62.3 MS (ES+): 291 $[M+H]^+$; HRMS (ES+) $C_{11}H_{11}N_4F_3Cl$ $[M+H]^+$ requires 291.0630 found 291.0624.

6.2.7 3-(4-(pyridin-2-yl)-1H-1, 2, 3-triazol-1-yl) propan-1-ol (2.7)

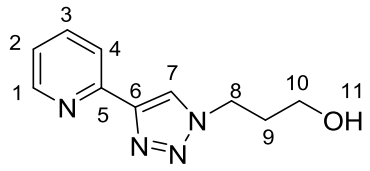

A solution of sodium azide (0.8321 g, 12.8 mmol) and 3-bromo-1-propanol (1.49g, 10.66 mmol) in THF: H_2O (1:1, 20 ml) was refluxed for 24 hours at 90°C. Upon cooling, 2- ethynylpyridine (1g, 9.69mmol), sodium ascorbate (0.11 g, 0.08 mmol) and $CuSO_4.5H_2O$ (0.09g, 0.15 mmol) were added (in order) and the solution heated to 65°C under N2 for 24 hours, forming a dark brown solution. Upon cooling, NH_4OH (15 ml) was added. Two layers formed. The organic layer was collected after extracted with Dichloromethane (5 x 30 ml) and dried over $MgSO_4$. The dry organic layer was filtered and solvent removed under vacuum affording crude product (1.67g). Crude product was purified by using column chromatography over silica gel using ethyl acetate/hexane (50:50) as eluent and change to 100% ethyl acetate to afford a white product (1.29 g, 85%); ^{1}H NMR (400MHz, $CDCl_3$), δ 8.54 (d, *J* = 4.9 Hz, 1H, 1-CH), 8.24 (s, 1H, 7-CH), 8.16 (dd, *J* = 7.9, 1.0 Hz, 1H, 4-CH), 7.77 (ddd, *J* = 8.5, 7.7, 1.7 Hz, 1H, 3-CH), 7.22 (ddd, *J* = 7.5, 6.3, 1.2 Hz, 1H, 2- CH), 4.61 (t, 2H, *J* = 6.8, 8-CH_2), 3.80 (bs, 1H, 11-OH), 3.70(t, *J* = 5.7 Hz, 2H, 10-CH_2), 2.19 (quint, 2H, *J* = 6.6 Hz, 9-CH_2); ^{13}C NMR (100 MHz, $CDCl_3$), δ 150.2 (5-C), 149.9 (1-C), 148.4 (6-C), 137.1 (3-C), 123.0 (7-C), 122.9 (2-C), 120.3 (4-C), 59.1 (10-C), 47.2 (8-C), 32.2 (9-C); MS (ES+): 273$[M+H]^+$ 295 $[M+Na]^+$; HRMS (ES+) $C_{11}H_{12}N_4O$ $[M+H]^+$ requires 273.0955 found 273.0963.

6.2.8 2-(1-(3-chloropropyl)-1H-1, 2, 3-triazol-4-yl) pyridine (2.8)

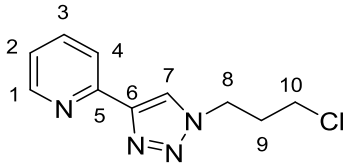

A solution of compound **2.7** (0.5g, 2.45mmol) in DCM (10 ml) was cooled to 0°C and thionyl chloride (2 ml, 3.28g, 27.57mmol) was added as a drop-wise via a self-equalising funnel with stirring under N_2. The pale yellow solution was refluxing at 40°C, TLC analysis (100% EtOAc) was used to monitoring the reaction. Aqueous solution of $NaHCO_3$ (10 ml) was added as a drop-wise and resulting solution was extracted with DCM (3 x 25 ml). The organic layer was dried over $MgSO_4$, filtered and solvents removed under *vacuo* to afford a white precipitate (0.48g, 89%) without further purification; ^{1}H NMR (400MHz, $CDCl_3$), δ 8.58 (d, *J* = 4.9 Hz, 1H, 1-CH), 8.18 (s, 1H, 7-CH), 8.17 (dd, *J* = 7.9, 1.0 Hz, 1H, 3-CH), 7.78 (ddd, *J* = 8.1, 7.8, 1.8 Hz, 1H, 4- CH), 7.23 (ddd, *J* = 7.9, 6.1, 1.2 Hz, 1H, 2-CH), 4.63 (t, *J* = 6.6 Hz, 2H, 8-CH_2), 3.55 (t, 2H, *J* = 5.9 Hz, 10-CH_2), 2.44 (q, *J* = 6.5 Hz, 2H, 9-CH_2); ^{13}C NMR (100 MHz, $CDCl_3$), δ 150.2 (1-C), 149.4 (6-C), 140.5 (5-C), 136.9 (3-C), 122.9 (2-C), 122.5 (7-C), 120.0 (4-C), 47.2 (10-C), 41.0 (8- C), 32.5 (9-C); MS (ES+): 245 $[M+ Na]^+$, 223 $[M+H]^+$. HRMS (ES+) $C_{10}H_{12}N_4Cl$ $[M+H]^+$ requires 223.0739 found 223.0750.

6.2.9 *N*-[(2-bromopyridin-4-yl) methyl] octan-1-amine (2.9)

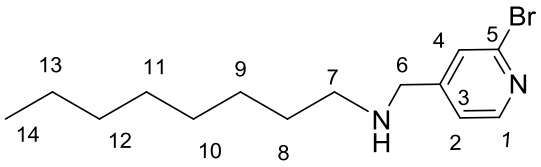

A solution of 2-bromo-4-pyridincarboxaldehyde (0.1g, 0.53 mmol) in MeOH (10 mL) was added to a stirring solution of octylamine (0.06g, 0.53 mmol). The reaction was then stirred at room temperature under N_2 for 18hr. TLC (5:5) EtOAc/DCM was confirmed all starting material was consumed. $NaBH_4$ (0.04g, 1.06 mmol) was added in small portions to the solution after cooling to 0 °C, and the mixture was stirred at room temperature under N_2 for overnight. The volatiles were then removed under reduced pressure, $NaHCO_3$ saturated solution (15mL) was added to the residue and then extracted with CH_3Cl (3x15mL). The organic layer was separated, dried over Na_2SO_4, filtered, and concentrated yielding a colorless oily product (0.135, 88%); ^{1}H NMR

(400MHz, $CDCl_3$), δ 8.28 (d, *J* = 5.0 Hz, 1H, 1-CH), 7.50 (s, 1H, 4-CH), 7.22 (d, *J* = 4.9 Hz, 1H, 2-CH), 3.78 (s, 2H, 6-CH_2), 2.61 (t, *J* = 7.1Hz, 7-CH), 1.54-1.47 (m, 2H, 8 -CH), 1.32-1.28 (m, 10H, 9, 10, 11, 12, 13-CH), 0.88 (t, *J* = 6.7Hz, 3H, 14-CH_3); ^{13}C NMR (100MHz, $CDCl_3$), δ 153.2 (5-C), 150.0 (1-C), 142.5 (3-C), 127.1 (4-C), 122.1 (2-C), 52.2 (6-C), 50.0 (7-C), 31.8 (9-C), 30.1 (10-C), 30.0 (11-C), 27.3 (12- C), 22.7 (13-C), 14.1 (14-C); MS (ES+): 299 $[M+H]^+$, HRMS (ES+) $C_{14}H_{23}N_2Br$ $[M+H]^+$ requires 299.1123 found 299.2319.

6.2.10 2-azidopyridine (2.10)

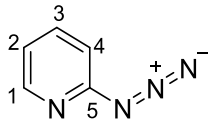

A solution of 2-bromopyridine (0.49 g, 3.14mmol) in (EtOH:H_2O/7:3) (10mL) and NaN_3 (0.24, 3.77mmol) was added and followed by CuOAc (0.0388g, 0.314mmol) and placed in microwave at 125°C for 1hr. TLC was run 100% EtOAc and show all starting material was consumed. Saturated solution of EDTA at pH=10 was added after remove the solvent and then extracted with ethyl acetate (3×20mL). Organic layers were combined and dried over $MgSO_4$ and filtrated and then the solvent was removed in *vacuo*. The residue was purified by column chromatography, eluting with ethyl acetate to give the title compound as white solid (0.2947, 78%). ^1H NMR (400MHz, $CDCl_3$), δ 8.84 (dd, *J* = 6.90, 1.11 Hz, 1H, 1-CH), 8.06 (dd, 9.0,1.1 Hz, 1H, 4-CH), 7.68 (ddd, *J* = 9.0, 7.9, 1.1 Hz, 1H, 3-CH), 7.23 (ddd, *J* = 7.3, 6.8, 1.1 Hz, 1H, 2-CH), ^{13}C NMR (100 MHz, $CDCl_3$), δ 148.6 (5-C), 131.8 (1-C), 125.5 (3-C), 116.5 (2-C), 116.1 (4-C); MS (ES+): 121 $[M+H]^+$, HRMS (ES+) $C_5H_5N_4$ $[M+H]^+$ requires 121.0510 found 121.0514.

6.2.11 2-(4-(3-chloropropyl)-1H-1, 2, 3-triazol-1-yl) pyridine (2.11)

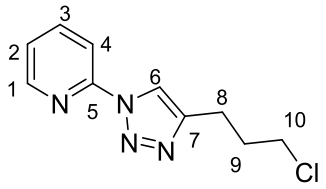

A solution of **2.10** (0.26g, 2.17mmol) in toluene (10mL) and 5-chloro-1-pentyne (0.44, 4.3mmol) was added and followed by CuI (0.04g, 0.21mmol) and sodium ascorbate (0.042g, 0.21 mmol) and then heated at 125°C for 18hr. TLC was run 100% EtOAc to monitoring the reaction and then the solvent was remove in *vacuo*. The residue was

purified by column chromatography, eluting with 100% EtOAc to yield (0.31g, 50%) of product. ^{1}H NMR (500MHz, $CDCl_3$), δ 8.49 (d, *J* = 4.6 Hz, 1H, 1-CH), 8.37 (s, 1H, 6-CH), 8.18 (d, *J* = 8.2 Hz, 1H, 4-CH), 7.91 (ddd, *J* = 8.6, 7.9, 1.5 Hz, 1H, 3-CH), 7.33 (ddd, *J* = 7.4, 6.1, 1.0 Hz, 1H, 2-CH), 3.63 (t, *J* = 6.5 Hz, 2H, 8-CH2), 2.99 (t, *J* = 7.3 Hz, 2H, 10-CH_2), 2.24 (p, *J* = 7.9 Hz, 2H, 9-CH_2); ^{13}C NMR (125 MHz, $CDCl_3$), δ 149.3 (5-C), 148.5 (1-C), 146.9 (7-C), 139.1 (3-C), 123.4 (2-C), 118.6 (6-C), 113.7 (4-C), 44.1 (8- C), 31.8 (9-C), 22.7 (10-C); MS (ES+): 223 $[M+H]^+$, HRMS (ES+) $C_{10}H_{12}N_4Cl$ $[M+H]^+$ requires 223.0757 found 223.0750.

6.2.121-(pyridin-2-yl)-1*H*-1, 2, 3-triazol-4-yl] methanol (2.12)

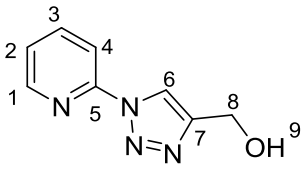

A solution of **2.10** (0.38 g, 3.27mmol) in toluene (10mL) and 1-propagyelalcohol (0.22g , 3.8mmol) was added and followed by CuI (0.05g, 0.32mmol) and sodium ascorbate (0.06g, 0.32mmol) and then heating at 125°C for 18hr and then TLC was used to monitoring the reaction in 100% EtOAc. Saturated solution of EDTA at pH=10 was added after remove the solvent and then extracted with ethyl acetate (3×20mL). Organic layers were combined and dried over $MgSO_4$ and filtrated and then the solvent was removed in *vacuo*. The residue was purified by column chromatography, eluting with 100% EtOAc and then to give the title compound as yellow solid (0.20g, 80%). ^{1}H NMR (500MHz, $CDCl_3$), δ 8.56 (s, 1H, 6-CH), 8.50 (d, *J* = 4.8 Hz, 1H, 1-CH), 8.20 (d, 8.1 Hz, 1H, 4-CH), 7.92 (ddd, *J* = 8.5, 7.4, 1.5 Hz, 1H, 3-CH), 7.36 (ddd, *J* = 7.4, 6.3, 2.4 Hz, 1H, 2-CH), 4.90 (d, *J* = 6.1 Hz, 2H, 8-CH_2), 2.11 (t, *J* = 6.1 Hz, 1H, 9-H); ^{13}C NMR (125 MHz, $CDCl_3$, Me_4Si): 149.8 (5-C), 148.6 (1-C), 147.8 (7-C), 139.2 (3-C), 123.4 (2-C), 119.2 (6-C), 113.8 (4-C), 56.8 (8-C); MS (ES+): 177 $[M+H]^+$, HRMS (ES+) $C_8H_9N_4O$ $[M+H]^+$ requires 177.0780 found 177.0776.

6.2.132-[4-(chloromethyl)-1*H*-1, 2, 3-triazol-1-yl] pyridine (2.13)

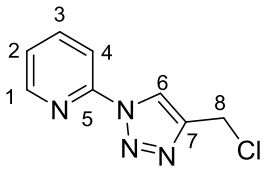

Compound **2.12** (0.1 g, 0.56mmol) was dissolved in DCM (20ml) and $SOCl_2$ (1.98gm, 16.8mmol) was added gradually to the solution and then stirred at rt. for 18hr under N_2.

TLC was run in 100% EtOAc and then $NaHCO_3$ was added and then extracted with DCM (3×20ml). Organic layers were combined and dried over $MgSO_4$ and filtrated and then the solvent was removed under *vacuo*. The residue was purified by column chromatography using 100% EtOAc to give the title compound as white solid (0.09g, 90%); ^{1}H NMR (500MHz, $CDCl_3$), δ 8.63 (s, 1H, 6-CH), 8.51 (d, *J* = 5.1 Hz, 1H, 1-CH), 8.20 (d, *J* = 8.1 Hz, 1H, 4-CH), 7.93 (ddd, *J* = 8.3, 7.7, 1.8 Hz, 1H, 3-CH), 7.37 (ddd, *J* = 7.4, 6.1, 0.8 Hz, 1H, 2-CH), 4.80 (s, 2H, 8-CH_2), ^{13}C NMR (125MHz, $CDCl_3$), δ 148.98 (5-C), 148.6 (1-C), 145.1 (7-C), 139. 2 (3-C), 123.81 (2-C), 120.0 (6-C), 113.8 (4-C), 36.1 (8-C); MS (ES+): 195 $[M+H]^+$, HRMS (ES+) $C_8H_8N_4$ ^{35}Cl $[M+H]^+$ requires 195.0441 found 195.0437.

6.2.14 1-butyl-4-phenyl-1H-1, 2, 3-triazole (HL1)

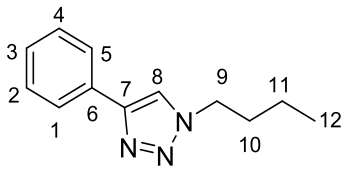

Asolution of 1-Bromobutane (0.37 g, 2.69 mmol) and NaN_3 (0.19 g, 2.96 mmol) were dissolved in EtOH/H_2O (7:3 ratio, 15 mL) was heated at 90°C for 18 hr. On cooling to rt. phenyl acetylene (0.25 g, 2.45 mmol), sodium ascorbate (0.73 g, 0.36 mmol) and $CuSO_4.5H_2O$ (0.611 g, 0.245 mmol) were added, followed by heated for 18hr at 60ºC. The reaction mixture consisted of two layers; on cooling to rt, the reaction mixture was washed with a saturated EDTA solution (10 mL made basic ~ pH 10 with NH_4OH). The solid was extracted with EtOAc (3 × 50 mL). The organic layer was dried with $MgSO_4$, filtered and the solvent removed under vacuum, yielding the product as light yellow powder with yield (0.37 g, 76 %), Melting point 49ºC; ^{1}H NMR (500 MHz, $CDCl_3$), δ 7.83 (d, *J* = 7.9 Hz, 2H, 1, 5-CH), 7.74 (s, 1H, 8-CH), 7.41 (t, *J* = 7.5 Hz, 2H, 2, 4-CH), 7.32 (ddd, *J* = 8.1, 7.4, 1.0 Hz, 1H, 3-CH), 4.39 (t, *J* = 7.3 Hz, 2H, 9-CH_2), 1.93 (p, *J* = 7.3 Hz, 2H, 10-CH_2), 1.43-1.35 (m, 2H, 11-CH_2), 0.97 (t, *J* = 7.3 Hz, 3H, 12-CH_3); ^{13}C NMR (125 MHz, $CDCl_3$), δ 147.7(6-C), 130.7 (7-C), 128.8 (2, 4-C), 128.1 (3-C), 125.7 (1, 5-C), 119.4 (8-C), 50.1 (9-C), 32.3 (10-C), 19.7 (11-C), 13.4 (12-C); MS (ESI+) *m/z* 202.13 $[M+H]^+$, HRMS (ES+) $C_{12}H_{16}N_3$ requires 202.1336 found 202.1344.

6.2.15 1-hexyl-4-phenyl-1H-1, 2, 3-triazole (HL2)

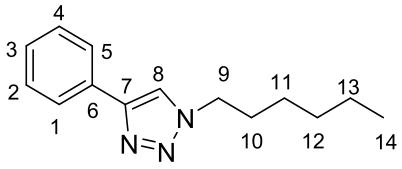

A solution of 1-Bromohexane (0.44 g, 2.69 mmole) and NaN_3 (0.19 g, 2.96 mmol) in (7:3, EtOH/H_2O) (20mL) was heated at 90ºC for 18hr. After cooling to rt phenyl acetylene (0.25 g, 2.45 mmol), sodium ascorbate (0.09 g, 0.49 mmol) and $CuSO_4.5H_2O$ (0.06 g, 0.24 mmol) were added the mixture was heated at 60ºC for 18 hr. After work up the title compound **HL2** was obtained (0.82 g, 73%) m.p (63ºC). ^{1}H NMR (500 MHz, $CDCl_3$), δ 7.82 (d, *J* = 7.5 Hz, 2H, 1, 5-CH), 7.74 (s, 1H, 8-CH), 7.40 (t, *J* = 7.6 Hz, 2H, 2, 4-CH), 7.31 (t, *J* = 7.4 Hz, 1H, 3-CH), 4.36 (t, *J* = 7.2 Hz, 2H, 9-CH_2), 1.92 (m 2H, 10-CH_2), 1.33-1.30 (m, 6H, 11, 12, 13-CH_2), 0.97 (t, *J* = 7.3Hz, 3H, 14-CH_3); ^{13}C NMR (125 MHz, $CDCl_3$), δ 147.7 (6-C), 130.7 (7-C), 128.8 (2, 4-C), 128.1 (3-C), 125.6 (1, 5-C), 119.4 (8-C), 50.4 (9-C), 31.2 (10-C), 30.3 (11-C), 26.1 (12-C), 22.4 (13-C) 13.9 (14-C); MS (ESI+) *m/z* 230 $[M + H]^+$; HRMS (ES+) $C_{14}H_{20}N_3$ $[M + H]^+$; requires 230.1651 found 230.1657.

6.2.16 1-hexayl-4-pyridyl-1H-[1, 2, 3] triazole (HL3)

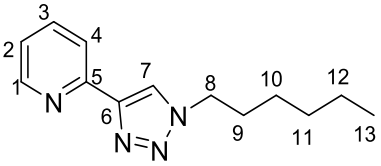

A solution of 1-Bromohexane (0.44 g, 2.7 mmol), NaN_3 (0.19g, 2.92 mmol) were refluxed at 90 °C in a THF: H_2O (4:1) solution (20 mL) for 18h. On cooling to rt. ethynyl pyridine (0.25 g, 2.42 mmol), sodium ascorbate (0.09 g, 0.48 mmol) and $CuSO_4.5H_2O$ (0.04g, 0.24 mmol) were added to the mixture. After heating at 60ºC for 4h the reaction mixture was cooled to room temperature and the solid was extracted by ethyl acetate and a saturated EDTA solution (10 mL made basic ~ pH 10 with NH_4OH). Organic layers were combined and dried over $MgSO_4$, filtrated the solvent removed under vacuum, yielding the product as brown solid (0. 456g, 81%); ^{1}H NMR ($CDCl_3$, 400 MHz), δ 8.58 (d, *J* = 4.9 Hz, 1H, 1-CH), 8.18 (d, *J* = 7.9 Hz, 1H, 4-CH) , 8.12 (s, 1H, 7-CH), 7.77 (ddd, *J* = 8.3, 7.7, 1.8 Hz, 1H, 3-CH), 7.22 (ddd, *J* = 7.5, 6.2 Hz, 1H, 2-CH), 4.41 (t, *J* = 7.2 Hz , 2H, 8-CH_2), 1.95 (quin, *J* = 7.2 Hz, 2H, 9-CH_2), 1.33 (m, 6H, 10, 11, 12-CH_2), 0.88 (t, *J* = 6.9 Hz, 3H, 13-CH_3);^{13}C NMR ($CDCl_3$,

100MHz), δ 147.4 (1-C), 135.3 (7-C), 121, 120 (2, 4-C), 98 (3-C), 48.8 (8-C), 29.4 (9-C), 28.4 (10-C), 24.4 (11-C), 20 (12-C), 12.2 (13-C); MS (ESI^+) *m/z*: 231 $[M+H]^+$, 253 $[M+Na]^+$; HRMS (ES+) $C_{13}H_{19}N_4$ $[M+H]^+$ requires 231.1602 found 231.1610.

6.2.17 4-(4-methoxyphenyl)-1-pentyl-1H-1, 2, 3-triazole (HL4)

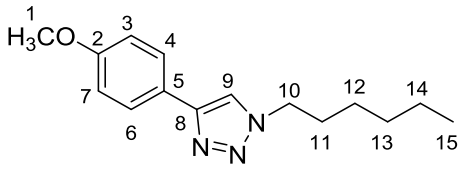

Sodium azide (0.29g, 4.57 mmol) was added to a solution of 1-bromohexane (0.68 g, 4.16 mmol) in EtOHl/H_2O (70:30,10mL). The solution was refluxed overnight at 90ºC. After cooling to rt. 4-ethynyl anisole was added (0.50g, 3.78 mmol) followed by $CuSO_4$ (0.09g, 0.1 mmol) and sodium ascorbate (0.13g, 0.2 mmol). The resulting mixture was heated overnight at 78 °C. The volatiles were removed and saturated EDTA (10 mL, at pH=10) was added and the aqueous mixture was extracted with EtOAc (3 x 25 mL). The combined organics were dried $MgSO_4$, filtered and concentrated. The crude residue was crystallised from EtOAc/Hexan to the title compound as white crystals (0.61g, 62 %) and melting point (98ºC); ^1H NMR (400 MHz, $CDCl_3$), δ 7.7 (d, *J* = 8.7 Hz, 2H, 4, 6-CH),7.6 (s, 1H, 9-CH), 6.9 (d, *J* = 8.9 Hz, 2H, 3, 7-CH), 4.36 (t, *J* = 7.15 Hz, 2H, 10-CH), 3.8 (s, 3H, 1-CH), 1.96-1.88 (m, 2H, 11-CH_2),1.37-1.29 (m, 6H, 12, 13, 14-CH_2), 0.88 (t, *J* = 6.7Hz, 3H, 15-CH_3); ^{13}C NMR (100 MHz, $CDCl_3$), δ 159.5 (2-C), 147.5 (8-C), 126.9 (4, 6-C), 123.5 (9-C), 118.6 (5-C), 114.0 (3,7-C), 55 (1-C), 50 (10-C), 31 (11-C), 30 (12-C), 26 (13-C), 22 (14-C), 13 (15-C); MS (ES+): 260 $[M+H]^+$; HRMS (ES+) $C_{15}H_{22}N_3O$ $[M+H]^+$ requires 260.1751 found 260.1763.

6.2.18 *tert*-butyl (4-(4-(pyridin-2-yl)-1H-1, 2, 3-triazol-1-yl) butyl)carbamate (L5.Boc)

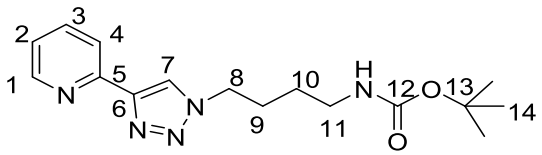

Boc-pu **2.1** (0.18 g, 1 mmol) and $NaHCO_3$ (0.29 g, 3.5 mmol) were dissolved in MeOH/H_2O (3:1, 4 mL) $CuSO_4.5H_2O$ (2 M (aq); 50 µL, 0.1 mmol) were added to the mixture reaction. After ISA.HSO_4 (0.325 g, 1.2 mmol) was added the reaction mixture was stirred at room temperature for 1 hr. TLC was run in (1 % NH_4OH: 9 % MeOH: 90 % DCM) to confirm the consumption of the amine. After sodium ascorbate (0.39 g, 0.2

mmol) was added followed by 2-ethynylpyridine (101 μL, 1 mmol) and the mixture was stirred at 60 ºC for overnight under N_2. After the solvent was removed, the residue was washed by EtOAc (30 mL) and water (30 mL) and separated. The organic layer was washed with water (30 mL), saturated $NaHCO_3$ (30mL), saturated brine (30 mL), dried over $MgSO_4$, filtered and concentrated. The residue was purified with EtOAc/hexane to give the title compound as light brown (0.17 g, 55 %). ^{1}H NMR (400 MHz, $CDCl_3$,), δ 8.50 (d, *J* = 4.3 Hz, 1H, 1-CH), 8.09 (d, *J* = 7.9 Hz, 1H, 4-CH), 8.06 (s, 1H, 7-CH), 7.70 (ddd, , *J* = 8.1, 7.8, 1.8 Hz, 1H, 3-CH), 7.15 (ddd, *J* = 7.5, 6.0, 1.6 Hz, 1H, 2-CH), 4.38 (t, *J* = 7.9 Hz, 2H, 8-CH_2), 3.09 (q, *J* = 6.4 Hz, 2H, 11-CH_2), 1.92 (m, 2H, 9-CH_2), 1.47 (m, 2H, 10-CH_2), 1.36 (s, 9H, 14-CH_3); ^{13}C NMR (100 MHz, $CDCl_3$, 323 K), δ 155.9 (12-C) 150.34 (5-C), 149.4 (1-C), 148.4 (3-C), 136.8 (7-C), 122.8 (4-C), 122.9 (2-C), 120.0 (6-C), 50.02 (13-C), 39.17 (11-C), 28.3 (14-C), 27.4 (10-C), 27.16 (9-C). MS (ESI+): 340 $[M+Na]^+$, 318 $[M+H]^+$, 262 $[M-C(CH_3)_3]^+$. HRMS (ES+) $C_{16}H_{23}N_5O_2Na$ $[M+Na]^+$ requires 340.1749 found 340.1749.

6.2.19 *tert*-butyl (4-((tert-butoxycarbonyl) (3-((tert butoxycarbonyl) amino) propyl) amino) butyl) (3-(4-(pyridin-2-yl) -1H-1,2,3-triazol-1-yl) propyl) carbamate (L6.Boc)

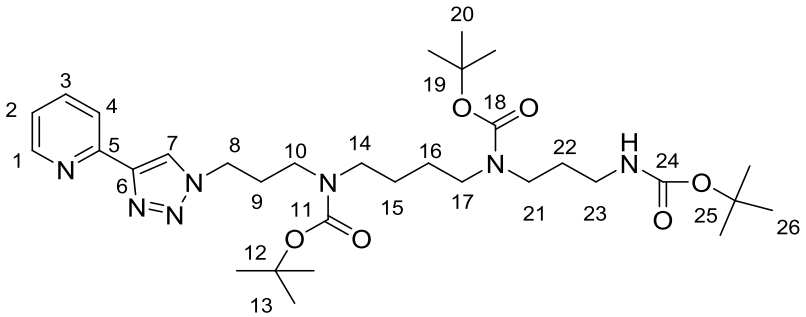

Tert- butyl (4-((3-aminopropyl) (tert-butoxycarbonyl) amino) butyl) (3-((tert-butoxycarbonyl) amino)propyl)carbamate **2.3** (0.25 g, 0.49 mmol), $NaHCO_3$ (0.85 g, 5mmol), $CuSO_4.5H_2O$ (12.6mg, 0.05mmol) ISA.H_2SO_4 (0.149 g, 0.55 mmol) were dissolved in MeOH/H_2O (2:1, 9mL) and stirred overnight at rt. The consumption of amine was monitored by TLC analytical (1% NH_4OH: 9% MeOH: 90 %DCM). Sodium ascorbate (0.19g, 0.1mmol) was added followed by 2-Ethynylpyridine (51μL, 0.5mmol). The reaction mixture was heated in microwave reactor at 80ºC for 1hr. Saturated EDTA solution (adjusted to pH =10 with NH_4OH) was added and the mixture stirred for 15 min. The reaction mixture was extracted with EtOAc (3 x 30 mL) and the organic layer separated and dried over $MgSO_4$, solvent was evaporated to dryness. The

residue was purified by column chromatography, eluting with MeOH /DCM (5:95) to afford brown oily product with yield (0.28g, 91%); ^{1}H NMR (500 MHz, $CDCl_3$, 323K), δ 8.51 (d, *J* = 4.3 Hz, 1H, 1-CH), 8.18 (s, 1H, 7-CH), 8.15 (d, *J* = 7.9 Hz, 1H, 4-CH), 7.75 (ddd, *J* = 8.03, 7.7, 1.8 Hz, 1H, 3-CH), 7.20 (ddd, *J* = 7.5, 6.2, 0.9 Hz, 1H, 2-CH), 4.43 (t, *J* = 7.06 Hz, 2H, 8-CH_2), 3.29 (t, *J* = 6.8 Hz, 2H, 10-CH_2), 3.19 (t, *J* = 7.0, 14,17, 6H, 21-CH_2), 3.10 (q, *J* = 6.4, 2H, 23-CH_2), 2.20 (q, *J* = 6.8 Hz, 2H, 9-CH_2), 1.66 (q, *J* = 6.2 Hz, 2H, 15-CH_2), 1.44 (s, 31H, 16, 22, 3(CH_3)); ^{13}C NMR (125 MHz, $CDCl_3$, 323K), δ 155.9 (18-C), 155.4 (11-C), 150.3 (5-C), 149.3 (1-C), 148.4 (6-C), 136.6 (3-C), 122.6 (2-C), 122.0 (7-C), 120.0 (4-C), 79.7 (12-C), 79.4 (19-C), 78.8 (25-C), 48.1 (8-C), 47.1 (14-C), 46.6 (10-C), 44.1 (17-C), 44.3 (21-C),44.1 (23-C), 37.7 (22-C), 29.3 (9-C), 28.5 (13, 20 and 26-C), 26.3 (16-C), 25.8 (15-C); MS (ES+): 632 $[M+H]^+$, 532 $[M\text{-}Boc]^+$; HRMS (ES+) $C_{32}H_{54}N_7O_6$ requires 632.4157 found 632.4136.

6.2.20 *tert*-butyl (4-(4-(5-(trifluoromethyl) pyridin-2-yl)-1H-1,2,3-triazol-1yl)butyl)carbamate (L7.Boc)

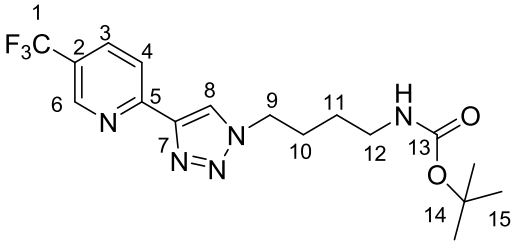

Mixture of Boc-put **2.1** (0.05 g, 0.26 mmol), $NaHCO_3$ (0.08 g, 0.93 mmol), and $CuSO_4.5H_2O$ (0.03g, 0.1mmol) were dissolved in MeOH/H_2O (3:1, 4 mL) followed by ISA.H_2SO_4 (0.08g, 0.31mmol) and stirred for overnight at r.t. sodium ascorbate and potassium carbonate (0.04g, 0.26mmol) were added to reaction mixture followed by alkyne **2.4** (0.06g, 0.26 mmol), stirred under N_2 for two days. The consumption of amine was monitored by TLC analysis in 100% EtOAc. The reaction mixture wash with EtOAc (15mL) and NaCl solution (15mL) was added, and then $NaHCO_3$ solution (15mL) and water (15mL). Aqueous layers combined and extracted with EtOAc (3 x 15mL). Organic layers combined and dried over $MgSO_4$. The solvent was removed under *vacuo* to yielding a brown solid product (0.07g, 72%); ^{1}H NMR (500MHz, $CDCl_3$), δ 8.25 (s, 1H , 5-CH), 8.30 (d, *J* = 8.7 Hz, 1H, 4-CH), 8.21 (s, 1H, 8-CH) 8.0 (d, *J* = 8.06 Hz, 1H, 3-CH), 4.55 (br s, 1H, NH), 4.48 (t, *J* = 7.06 Hz, 2H, 9-CH_2), 3.18 (q, *J* = 5.9 Hz, 2H, 12-CH_2), 2.07-1.97 (m, 2H, 10-CH_2), 1.60-1.51 (m, 2H, 11-CH_2), 1.43 (9H, s, 14-CH_3); ^{13}C NMR (125MHz, $CDCl_3$), δ 156.0 (13-C), 153.2 (6-C), 146.5 (7-C), 145.6 (5-C), 134.0 (3-C), 123.1 (1-C), 122.8 (2-C), 122.5 (8-C), 120 (4-C), 79.4 (14-C), 50.1 (9-C), 39.6 (12-C), 28

(15-C), 27.4 (10-C), 27.1 (11-C); ^{19}F NMR (500MHz, $CDCl_3$), δ -62.2 (s, 3F-py); MS m/z (ES+): 386$[M+H]^+$, 409 $[M+Na]^+$; HRMS (ES+) $C_{17}H_{23}N_5O_2F_3$ requires 386.1810 found 386.1807.

6.2.21 *tert*-butyl (4-((tert-butoxycarbonyl) (3-((tert- butoxycarbonyl) amino) propyl) amino) butyl) (3-(4-(5-(trifluoromethyl)pyridin-2-yl)-1H-1,2,3-triazol-1-yl) propyl) carbamate (L8.Boc)

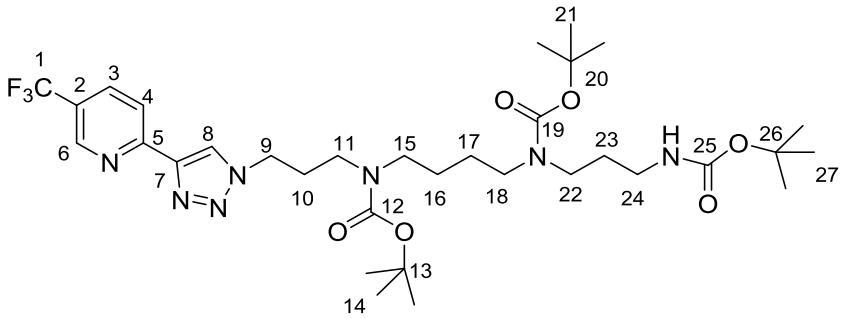

A mixture of Tert- butyl (4-((3-aminopropyl)(tert-butoxycarbonyl)amino)butyl)(3-((tert-butoxycarbonyl)amino)propyl)carbamate **2.3** (0.25g, 0.49mmol), $NaHCO_3$ (0.42g, 4.9mmol) and $CuSO_4.5H_2O$ (0.01g, 0.05mmol) were dissolved in MeOH/H_2O (2:1), (9mL) followed by ISA.H_2SO_4 (0.16g, 0.58mmol) and stirred for overnight at r.t. TLC analysis was used to monitoring the reaction mixture (80:20, DCM/MeOH , 3 drops NH_4OH) and then dipped in Ninhydrin to detect the amine, sodium ascorbate (0.09g, 0.5 mmol) and K_2CO_3 (0.06g, 0.49mmol) were added to reaction mixture followed by alkyne **2.4** (0.12g, 0.49mmol), stirred under N_2 for two days. TLC analysis in 100 % ethyl acetate confirmed all alkyne was reacted. (15mL) of EtOAc was added to the reaction mixture and washed with aqueous sodium chloride solution (15mL), aqueous sodium hydrogen carbonate solution (15mL) and water (15mL). Aqueous layers were combined and extracted with EtOAc (3 x 15mL). Organic layers combined and dried over $MgSO_4$. After that solvent was removed yielding a brown solid (0.322g, 93%); ^{1}H NMR (400MHz, $CDCl_3$), δ 8.82 (s, 1H, 6-CH), 8.29 (d, *J* = 8.5 Hz, 1H, 3-CH), 8.21(s, 1H, 8-CH) 8.01 (dd, *J* = 8.3, 1.8 Hz, 1H, 4-CH), 4.45 (t, *J* = 7.0 Hz, 2H, 9-CH_2), 3.3-3.08 (m, 10H, 11, 15, 18, 22, 24-CH_2), 2.25-2.18 (m, 2H, 10-CH_2), 1.71-1.50 (m, 2H, 23-CH_2), 1.58-1.53 (m, 31H, 16, 17-CH, 3(CH_3)); ^{13}C NMR (100MHz, $CDCl_3$), δ 155.6 (5-C), 153.5 (7-C), 146.7 (6-C), 136.2 (3-C), 123.1 (1-C), 122.5(2-C), 119.7 (4-C), 82.3 (13-C), 79.9 (20-C), 79.6 (26-C), 48.3 (9-C), 48.2 (11-C), 44.0 (15, 18-C), 37.3 (22, 24-C), 29.3 (19-C), 26.0 (23-C), 28.9 (14, 21, 27-C); ^{19}F NMR (400MHz, $CDCl_3$), δ -62.3

(s, 3F-py); MS(ES+) m/z 701 $[M+H]^+$, 601$[M\text{-}Boc]^+$; HRMS (ES+) $C_{33}H_{53}N_7O_6F_3$ requires 700.4033 found 700.4009.

6.2.22 di-tert-butyl (((3-(4-(5-(trifluoromethyl)pyridin-2-yl)-1H-1,2,3-triazol-1-yl)propyl)azanediyl)bis(propane-3,1-diyl))dicarbamate (L9.Boc)

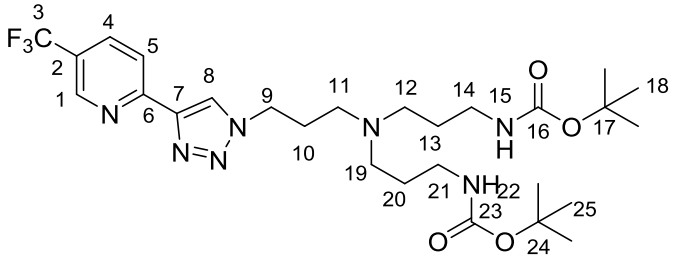

A solution of **2.3** (0.16, 0.45mmol), **2.6** (0.13g, 0.45mmol) and KI (0.38g, 2.27mmol) in MeCN (25mL) were stirred and refluxed at 110°C under N_2 for 48hr, TLC analysis (DCM: MeOH 9:1) was used to monitoring the reaction. The solution was allowed to cool, and then (30ml) of water was added and extracted with DCM (3x 25ml). The organic layer was dried over $MgSO_4$, filtered and solvent removed under *vacuo* to yield crude product (0.31g) the crude was purified by column chromatography (50%DCM: 50%EtOAc) on silica gel to afford the desired product (0.15g, 53% yield); ^{1}H NMR (400MHz, $CDCl_3$,), δ 8.84 (s, 1H, 1-CH), 8.30 (d, *J* = 8.3 Hz, 1H, 4-CH), 8.25 (s, 1H, 8-CH), 8.01 (dd, *J* = 8.3,1.9 Hz, 1H, 5-CH), 5.30 (broad s, 1H, 22-NH), 4.86 (s broad, 1H, 15-NH), 4.51 (t, *J* = 6.9 Hz, 2H, 9-CH_2), 3.19 (m, 2H, 21- CH_2), 3.15-3.12 (m, 2H, 14-CH_2), 2.47-2.43 (m, 6H, 11-CH_2, 12-CH_2, 19-CH_2), 2.16-2.13 (m, 2H, 10-CH_2), 1.68-1.58 (m, 2H, 13-CH_2), 1.52-1.44 (m, 20H, 20-CH_2 and 2x (Boc); ^{13}C NMR (100 MHz, $CDCl_3$), δ 156.1 (16, 23-C), 153.5 (1-C), 146.7 (7-C), 134.0 (4-C), 124.9 (3-C), 123.5 (2, 8-C), 119.6 (5-C), 79.0 (17, 24-C), 53.4 (19-C), 52.1 (11-C,), 50.5 (12- C), 48.4 (9-C), 40.3 (21-C), 39.9 (14-C), 28.4 (18-C), 28.0 (10-C), 27.8 (13-C), 27.1 (20- C), 24.1 (25-C); ^{19}F NMR (400MHz, $CDCl_3$), δ -62.4 (s, 3F-py); MS (ES+): 601 $[M+H]^+$, HRMS (ES+) $C_{28}H_{45}N_7O_4F_3$ $[M+H]^+$ requires 600.3515 found 600.3485.

6.2.23 di-tert-butyl (((3-(4-(pyridin-2-yl)-1H-1,2,3-triazol-1- yl) propyl) azanediyl) bis(propane-3,1-diyl)) dicarbamate (L10.Boc)

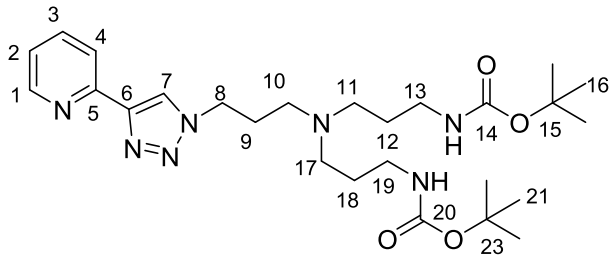

A solution of **2.2** (0.18g, 5.34 mmol), **2.8** (0.16g, 4.95 mmol) and K_2CO_3 (0.18 g, 13.34 mmol) in acetonitrile (25mL) was stirred and refluxed at 110°C under N_2. After 48 hours, TLC analysis (DCM: MeOH 9:1) was used to monitoring the reaction. The solution was allowed to cool, and then solvent was evaporated and then water was added (30ml) and product was extracted with DCM (5 x 30ml). The organic layer was companied and then dried over $MgSO_4$, filtered and solvent removed under vacuum to yield crude product (0.13g). Crud product was purified with column chromatography (DCM: MeOH: (95:5) with 3drops of NH_4OH) and then changing to (80% DCM: 20%MeOH) affording the purified product (0.06 g, 43% yield); ^{1}H NMR (400MHz, $CDCl_3$), δ 8.59 (dd, *J* = 4.9, 0.8 Hz, 1H, 1-CH), 8.17 (m, 2H, 7, 4-CH), 7.78 (ddd, *J* = 8.1, 7.8, 1.8 Hz, 1H, 3-CH), 7.23 (ddd, *J* = 7.5, 4.9, 1.1 Hz, 1H, 2-CH), 5.33 (broad s, 1H, NH), 4.89 (s broad, 1H, NH), 4.49 (t, *J* = 6.7 Hz, 2H, 8-CH_2), 3.22-3.09 (m, 4H, 13, 19-CH_2), 2.43-2.51 (m, 6H, 10-CH_2, 11-CH_2, 17-CH_2), 2.13 (quintet, *J* = 6.6 Hz, 2H, 9-CH_2), 1.70-1.63 (m, 2H, 12-CH_2), 1.43 (s, 20H, 13, 18, 16, 21-CH_3); ^{13}C NMR (100 MHz, $CDCl_3$), δ 156.1 (14-C and 20-C), 150.3 (5-C) 149.4 (1-C), 148.2 (6-C), 136.9 (3-C), 122.8 (2-C), 122.3 (7-C), 120.2 (4-C), 78.9 (15, 23-C), 53.4 (17-C), 52.1(10-C), 50.5 (11-C), 48.3 (8-C), 40.3 (13-C), 39.5 (19-C), 28.5 (18-C), 27.9 (9-C), 27.7 (12-C), 26.9 (16-C), 24.02 (21-C); MS (ES+): 555 $[M+Na]^+$, 533 $[M+H]^+$, 433 [M-Boc+2H]+.; HRMS (ES+) $C_{27}H_{45}N_7O_4Na$ $[M+Na]^+$ requires 554.3426 found 554.3431.

6.2.24 *N*-([2, 2'-bipyridin]-5-ylmethyl) octan-1-amine (L11)

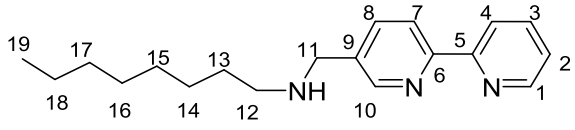

2-(tributylstannyl) pyridine[184, 305] (0.26 g, 0.7 mmol) was added to a degassed solution of 2-bromo-4-octyamin pyridine **2.9** (0.18 g, 0.6 mmol) and $Pd(PPh_3)_4$ (0.04 g, 0.03 mmol) in toluene (10 mL). The mixture was refluxed under an inert atmosphere for 18h,

the solvent was evaporated and the resulting solid residue was purified by column chromatography (EtOAc/hexane: 60/40 → 60/40 DCM/EtOH) yielded (0.07 g, 49%) of product; ^{1}H NMR (400MHz, $CDCl_3$), δ 8.68 (d, *J* = 4.8 Hz, 1H, 4-CH), 8.64 (d, *J* = 4.8 Hz, 1H, 7-CH), 8.39 (dt, *J* = 8.0, 0.9 Hz, 1H, 1-CH), 8.35 (s, 1H, 10-CH), 7.81(ddd, *J* = 8.3, 7.8, 1.8 Hz, 1H, 3-CH), 7.42 (dd, *J* = 5.1, 1.6 Hz, 1H, 2-CH), 7.31 (ddd, *J* = 7.5, 4.7, 1.1 Hz, 8-CH), 3.96 (s, 2H, 11-CH_2), 2.69 (t, *J* = 7.3 Hz, 12-CH_2), 1.72-1.56 (m, 2H, 13-CH_2), 1.30-1.24 (m, 10H, 14, 15, 16, 17, 18-CH_2), 0.86 (t, *J* = 6.8 Hz, 3H, 19-CH_3); ^{13}C NMR (100MHz, $CDCl_3$), δ 156.3 (5-C), 156.0 (6-C), 149.5 (4-C), 149.2 (7-C), 148.6 (9-C), 139.9 (3-C), 123.7 (2-C), 123.3 (8-C), 121.3 (10-C), 120.7 (1-C), 52.3 (11-C), 49.0 (12-C), 31.8 (13-C), 29.3 (14-C), 29.2 (15,16-C), 27.6 (17-C), 22.6 (18-C), 14.1 (19-C); MS (ES+): 298 $[M+H]^+$, HRMS (ES+) $C_{19}H_{28}N_3$ $[M+H]^+$ requires 298.2289 found 298.2283.

6.2.25 2-(4-hexylphenyl) pyridine (HL12)

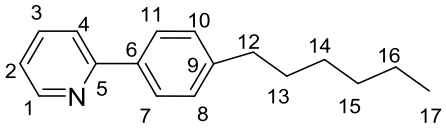

2-(tributylstannyl) pyridine was prepared according to literature[305] (0.90 g, 2.5 mmol) and added to a degassed solution of **2.9** (0.50 g, 2.08 mmol) and Pd $(PPh_3)_4$ (0.12 g, 0.10 mmol) in toluene (10 mL) in schlenk tube. The mixture was refluxed at 110°C under an inert atmosphere for 48h. TLC was used to monitoring the reaction for two days and then the solvent evaporated and the residue was extracted with 6 M aq HCl (3 ×10 mL) provided an aqueous layer, which was carefully neutralized with 10% aq ammonia, then extracted with EtOAc (3 × 25mL). The combined organic layers were washed with water and dried over anhydrous $MgSO_4$. The solvent was evaporated and the resulting liquid residue was purified by column chromatography (diethyl ether /hexane: 20/80) and (0.34 g, 61%) was obtained as a brown liquid; ^{1}H NMR ($CDCl_3$, 400 MHz), δ 8.66 (dd, 4.9,1.4 Hz, 1H, 1-CH); 7.90 (d, *J* = 8.3 Hz, 2H, 7,11-CH); 7.70 (m, 2H, 3, 4-CH); 7.21 (d, *J* = 8.4 Hz, 2H, 8, 10-CH); 7.18 (ddd, *J* = 5.9, 5.6, 2.6 Hz, 1H, 2-CH), 2.65 (t, *J* = 7.6 Hz, 2H, 12-CH_2), 1.64 (p, *J* = 7.6 Hz, 4H, 13,14-CH_3), 1.31 (m, 4H, 15, 16-CH_2), 0.91(t, *J* = 7.3 Hz, 3H, 17-CH_3); ^{13}C NMR (100 MHz, $CDCl_3$), δ 157.5 (5-C), 149.6 (1-C), 145.0 (9-C), 136.8 (6-C), 136.6 (3, 4-C), 128.8 (8, 10- C), 126.7 (7, 11-C), 121.7 (4-C), 120.3 (2-C), 35.7 (12-C), 31.4 (13-C), 28.9 (14-C), 22.6

(15-C), 16.5 (16-C), 14.1 (17-C); MS (ES+): 240 $[M+H]^+$, HRMS (ES+) $C_{17}H_{22}N$ $[M+H]^+$ requires 240.1752 found 240.1752.

6.2.26 2-(4-hexyl-1*H*-1, 2, 3-triazol-1-yl) pyridine (L13)

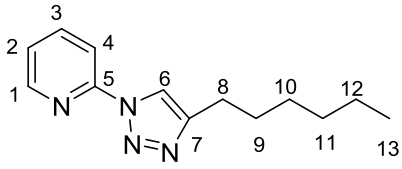

A solution of 2-azidopyridine **2.10** (0.36 g, 3.03 mmol) in (EtOH:H_2O,1:1) (10mL) and 1-octyne (0.40, 3.6 mmol) was added and followed by CuI (0.05g, 0.30 mmol) and sodium ascorbate (0.06g, 0.30mmol) and then placed in microwave at 125°C for 12hr. TLC was run 100% EtOAc and show all starting material was consumed. Saturated solution of EDTA at pH = 10 was added after remove the solvent and then extracted with EtOAc (3×20ml). Organic layers were combined and dried over $MgSO_4$ and filtrated and then the solvent was removed under *vacuo*. The residue was purified by column chromatography, eluting with EtOAc: hexane) (40:60) to give the title compound as white solid (0.30g, 43%). ^{1}H NMR (400MHz, $CDCl_3$), δ 8.84 (d, *J* = 5.0 Hz, 1H, 1-CH), 8.30 (s,1H, 6-CH), 8.18 (dd, 8.2, 0.9 Hz, 1H, 4-CH), 7.89 (ddd, *J* = 8.4, 7.9, 1.8 Hz, 1H, 3-CH), 7.31 (ddd, *J* = 7.5, 6.2, 1.0 Hz, 1H, 2-CH), 2.80 (t, *J* = 7.4 Hz, 2H, 8-CH_2), 1.69-1.80 (m, 2H, 9-CH_2),1.37-1.46 (m, 2H, 10-CH_2), 1.27-1.35 (m, 4H, 11, 12-CH_2), 0.89 (t, *J* = 6.8 Hz, 2H, 13-CH_3); ^{13}C NMR (100 MHz, $CDCl_3$), δ 149.5 (5-C), 148.9 (7-C), 148.4 (1-C), 139.0 (3-C), 123.2 (2-C), 118.0 (6-C), 113.7 (4- C), 31.6 (11- C), 29.3 (9-C), 28.9 (10-C), 25.7 (8-C), 22.6 (12-C), 14.1 (13- C); MS (ES+): 231 [M+H]+, HRMS (ES+) $C_{13}H_{19}N_4$ $[M+H]^+$ requires 231.1612 found 231.1610.

6.2.26 tert-butyl(4-((3-((tert-butoxycarbonyl)amino)propyl)((1-(pyridin-2-yl)-1H-1,2,3-triazol-4-yl)methyl)amino)butyl)carbamate (L14.Boc)

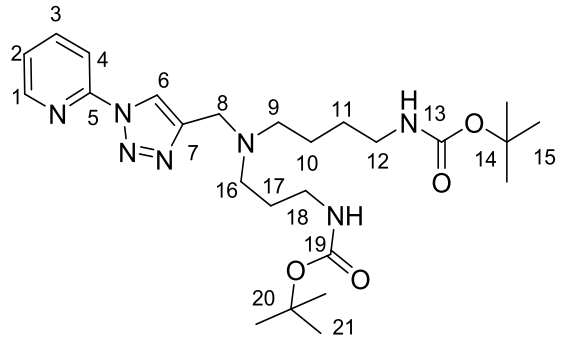

A solution of Bocspd **2.2** (0.17, 0.5mmol), **2.13** (0.09g, 0.5mmol) and KI (0.25g, 1.5mmol) in MeCN (25mL) were stirred and refluxed at 110°C under N_2. For 24 hr. TLC analysis (DCM: MeOH 9:1) was indicated that the majority of **2.13** in the pale yellow solution was consumed. The solution was allowed to cool, water added (15ml) and product extracted with DCM (3x 25ml). The organic layer was dried over $MgSO_4$, filtered and solvent removed under *vacuo* and then the crude was purified by column chromatography (90% DCM: 10% MeOH) on silica gel to afford the desired product (0.10g, 40 % yield). ^{1}H NMR (500MHz, $CDCl_3$), δ 8.50 (broad s, 2H, 1, 6-CH), 8.19 (d, *J* = 8.2 Hz, 1H, 4-CH), 7.91 (ddd, *J* = 8.5, 8.2, 1.5 Hz, 1H, 3-CH), 7.35 (ddd, *J* = 7.4, 6.2, 2.4 Hz, 1H, 2-CH), 5.43 (s br, 1H, 1-NH), 4.89 (s br, 1H, 2-NH), 3.88 (s, 2H, 8-CH_2), 3.41-3.27 (m, 2H, 12- CH_2), 3.14-3.10 (m, 2H, 18-CH_2), 2.57 (t, *J* = 6.1 Hz, 2H, 9-CH_2), 2.50 (t, *J* = 6.1 Hz, 2H, 16-CH_2), 1.73 (t, *J* = 6.3 Hz, 2H, 17-CH_2) 1.60-1.57 (m, 2H, 10-CH_2), 1.55-1.51 (m, 2H, 11-CH_2), 1.47-1.43 (m, 18H, 2x (NHBoc); ^{13}C NMR (125 MHz, $CDCl_3$), δ 156.8 (5-C), 149.2 (7-C), 148.5 (1- C), 139.1 (3- C), 123.5 (2-C), 120.0(6-C), 113.8 (4-C), 77.2, 77.0 (14, 20-C), 53.1 (9-C), 52.2 (8-C,), 48.3 (12-C), 39.7 (18-C), 28.4 (15, 21-C), 27.7 (17-C), 26.7 (10-C), 24.2 (11-C); MS (ES+): 504 [M+H]+, HRMS (ES+) $C_{25}H_{42}N_7O_4$ $[M+H]^+$ requires 504.33323 found 504.3298.

6.2.27 tert-butyl(4-((3-((tert-butoxycarbonyl)amino)propyl)(3-(1-(pyridin-2-yl)-1H-1,2,3-triazol-4-yl)propyl)amino)butyl)carbamate (L15.Boc)

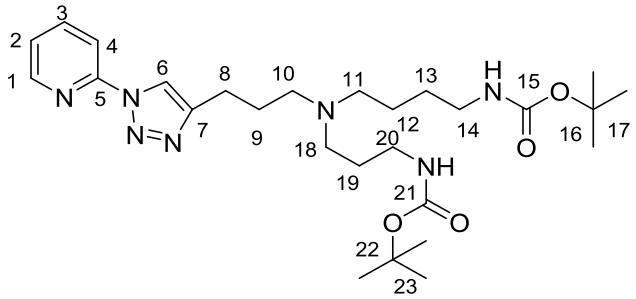

A solution of **2.2** (0.14g, 0.4 mmol), **2.11** (0.09g, 0.4 mmol) and potassium iodide (0.20g, 1.2mmol) in MeCN (25mL) were stirred and refluxed at 110°C under N_2 for 18 h, TLC analysis (DCM: MeOH 9:1) indicated the majority of **2.11** in the pale yellow solution was consumed. The solution was allowed to cool, and then solvent was removed and then water was added (15ml) and product extracted with DCM (3x 25mL). The organic layer was dried over $MgSO_4$, filtered and solvent removed under *vacuo* and then the crude was purified by column chromatography (90%DCM: MeOH) on silica gel to afford the desired product (0.13 g, 60% yield); ^{1}H NMR (500MHz, $CDCl_3$), δ 8.51 (d, *J* = 4.1 Hz, 1H, 1-CH), 8.45 (s, 1H, 6-CH), 8.16 (d, *J* = 8.2 Hz, 1H, 4-CH), 7.93 (ddd, *J* = 9.0, 7.6, 1.5 Hz,1H, 3-CH), 7.36 (ddd, *J* = 7.6, 6.3, 2.3 Hz, 2-CH), 3.36-3.32 (m, 2H, 11-CH_2), 3.25 (m, 6H, 8, 10, 18-CH_2), 3.17-2.98 (m, 2H, 14-CH_2), 2.20-2.15 (m, 2H, 20-CH_2), 1.97-1.91(m, 2H, 19-CH_2), 1.68-1.64 (m, 6H, 9, 12, 13-CH_2) 1.44 (d, *J* = 4.4 Hz, 18H, 17, 23-(CHBoc); ^{13}C NMR (125 MHz, $CDCl_3$), δ 155.5 (5-C), 149.1 (7-C), 148.6 (1-C), 139.2 (3-C), 133.4 (6-C), 123.6 (2-C), 114.9 (4-C), 77.2, 77.0 (16, 22-C), 47.9 (10-C), 46.5 (8-C), 45.1 (18-C), 36.4 (11-C), 27.4 (9, 12,13-C), 27.0(20-C), 26.8 (17, 23-C), 26.0 (12-C), 23.7 (19-C); MS (ES+): 532 [M+H]+, HRMS (ES+) $C_{25}H_{42}N_7O_4$ $[M+H]^+$ requires 532.3698 found 532.3611.

6.2.28 *tert*-butyl (4-((tert-butoxycarbonyl) (3-((pyridin-4-ylmethyl) amino) propyl) amino) butyl) (3-((tert-butoxycarbonyl) amino)propyl)carbamate (L16.Boc)

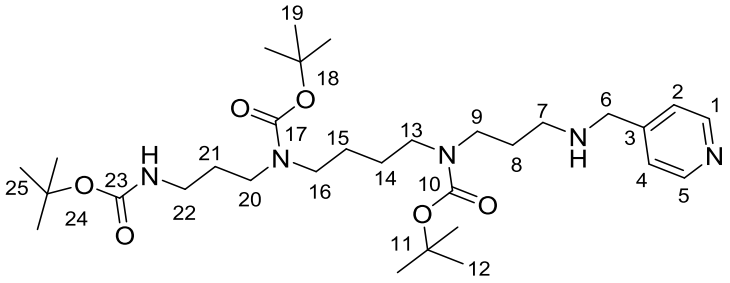

A solution of 4-pyridincarboxaldehyde (0.05g, 0.49 mmol) in MeOH (10 mL) was added to a stirred solution of **2.3** (0.25g, 0.49 mmol). The reaction was then stirred at rt. under N_2 for 4 hrs. TLC (5% MeOH: 95% DCM) was use to monitoring the reaction. $NaBH_4$ (0.02g, 0.49 mmol) was added in small portions to the solution after cooling to 0 °C, and then the mixture reaction was stirred at rt. under N_2 for overnight. The volatiles were then removed under reduced pressure, and the residue was re-dissolved (15mL) in water. 1N HCl was added to make pH = 8 of solution and extracted with DCM (3x15mL). The organic layer was separated, dried over Na_2SO_4, filtered, and concentrated to yield a colorless oily product (0.22g, 76%);^{1}H NMR (400MHz, $CDCl_3$), δ 8.53 (d, *J* = 4.6 Hz, 2H, 1, 5-CH), 7.20 (d, *J* = 7.04 Hz, 2H, 2, 4-CH), 3.70 (s, 2H, 6-CH_2), 3.30-3.10 (m, 10H, 9, 13, 16, 20, 22-CH_2), 2.59 (t, *J* = 6.09 Hz, 2H, 7-CH_2), 1.90 (m, 2H, 8–CH_2), 1.70 (m, 4H, 14, 15-CH_2), 1.51 (s, 27H, 3(CH_3)): ^{13}C NMR (100MHz, $CDCl_3$), δ 206.9 (10, 17, 23-C), 149.6 (1, 5-C), 121 (2, 4-C), 63.2 (6-C), 30.8 (7-C), 28.4 (12, 19, 25-C); MS (ESI+): 595 $[M+H]^+$, 495 $[M\text{-}BOC+2H)]^+$; HRMS (ES+) $C_{31}H_{56}N_5$ requires 594.4246 found 594.4231.

6.2.29 N-(pyridine-4-ylmethyl) octan-1-amine (L17)

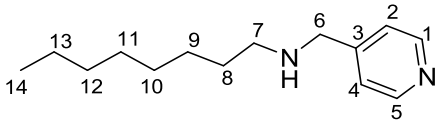

A solution of 4-pyridincarboxaldehyde (0.50 g, 3.86 mmol) in MeOH (15 mL) was added to a stirred solution of octylamine (0.41 g, 3.86 mmol). The reaction was then stirred at rt. under N_2 for 4hr. TLC analytical was indicated all the aldehyde was consumed. ^{1}H NMR was confirmed that the imine compound was formed, the solution was cooled to 0 °C and then $NaBH_4$ (0.146 g, 3.86 mmol) was added slowly in small portions and stirred at rt. under N_2 for 18h. The volatiles were removed under reduced

pressure. The residue was re-dissolved in water (15mL), and the solution was extracted three times with DCM. The organic layer was separated, dried over Na_2SO_4, filtered and then the solvent was removed by *vacuo* yielding a pale yellow product (0.56 g, 65 %); ^{1}H NMR (400 MHz, $CDCl_3$), δ 8.60 (d, *J* = 5.9 Hz, 2H, 1, 5-CH), 7.45 (d, *J* = 5.98 Hz, 2H, 2, 4-CH), 3.95 (s, 2H, 6-CH_2), 2.71 (t , *J* = 7.6 Hz, 2H,7-CH_2), 1.78-1.67 (m, 2H, 8-CH_2), 1.21 (s, 10H, 9, 10, 11, 12, 13-CH_2), 0.86 (t, *J* = 7.1 Hz, 3H, 14-CH_3); ^{13}C NMR (100 MHz, $CDCl_3$), δ 150 (1, 5-C), 144 (3-C), 121 (2, 4-C), 52 (6-C), 49 (7-C), 32 (12-C), 30 (8-C), 28 (10, 11-C), 27 (9-C), 22 (13-C), 12 (14-C); MS (ESI+) *m/z*; 221 $[M+H]^+$; HRMS (ES+) $C_{14}H_{25}N_2$ requires 221.2018 found 221.2018.

6.2.30 1-hexyl-1H-1, 2, 3-triazole (L18)[214]

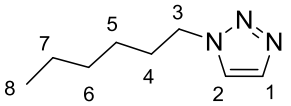

A mixture of 1-Bromohexane (0.17 g, 1 mmol), NaN_3 (0.08 g, 1.2 mmol) were dissolved in MeOH/H_2O (1:1, 10 mL) and then refluxed at 80ºC for 18h. TLC analysis (20 % MeOH in DCM) was used to monitoring the reaction. Ethynyltrimethylsilane (0.12 g, 1.2 mmole), K_2CO_3 (0.13 g, 1.2 mmole), $CuSO_4.5H_2O$ (0.12 g, 0.5 mmole) and sodium ascorbate (0.19 g, 1mmole) were added to the reaction mixture and stirred at rt. for overnight under N_2. Reaction mixture was washed with aqueous 5% NH_4OH solution (10 mL) and extracted with DCM (3 x 15 mL). Organic layers were combined and dried over $MgSO_4$. After that solvent was removed yielding a brown oily product (0.07 g, 47%); ^{1}H NMR (400 MHz, $CDCl_3$), δ 7.71 (s, 1H, 1-CH), 7.50 (s, 1H, 2-CH), 4.38 (t, *J* = 7.2 Hz, 2H, 3-CH_2), 1.91 (m, 2H, 4-CH_2), 1.48-1.40 (m, 6H, 5, 6, 7-CH_2), 0.86 (t, *J* = 6.8 Hz, 3H, 8-CH_3); ^{13}C NMR (100 MHz, $CDCl_3$), δ 133.5 (1-C), 123 (2-C), 50.2 (3-C), 31(6-C), 30.2 (4-C), 26 (5-C), 22 (7-C), 13.9 (8-C); MS (ESI+) m/z: 154 $[M+H]^+$; HRMS (ES+) $C_8H_{16}N_3$ requires 154.1341 found 154.1344.

6.3 Synthesis of Rhenium(I) Complexes

6.3.1 $[Re(CO)_5(L6.Boc)Cl]$ (ReL6.Boc)

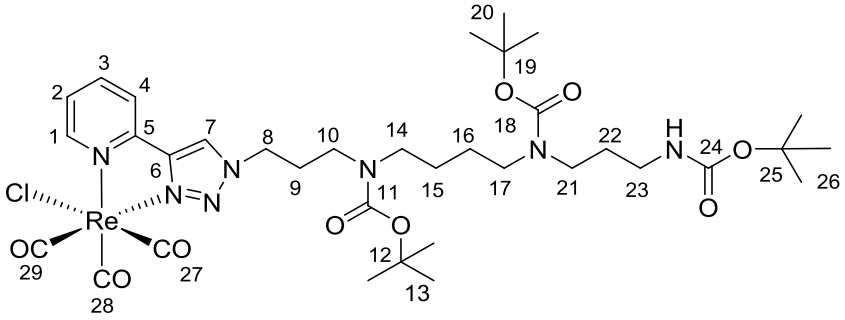

Pentacarbonylchlororhenium (0.05 g, 0.138 mmol), **L6.Boc** (0.087g, 0.138 mmol) and THF (4 mL) were added to a microwave tube. The suspension was heated in a microwave reactor at 90°C for 3 hr with power 50 and pressure 150, yielding a clear yellow solution. The solvent was removed in *vacuo* yielding a brown oily product (0.113 g, 87 %); ^{1}H NMR (400MHz, $CDCl_3$), δ 9.01 (d, *J* = 5.6 Hz, 1H, 1-CH), 8.75 (s br, 1H, 7-CH), 7.98 (ddd, *J* = 7.8, 1.4 Hz, 1H, 3-CH), 7.87 (d, *J* = 7.9 Hz, 1H, 4-CH), 7.42 (ddd, *J* = 6.4, 1.0 Hz, 1H, 2-CH), 4.56 (t, *J* = 6.2 Hz, 2H, 8-CH_2), 3.20 (q, 10H, 10, 14, 17, 21 and 23-CH_2), 2.2 (q, *J* = 6.6 Hz, 2H, 9-CH_2), 1.67-1.55 (m, 6H, 15, 16 and 22-CH_2), 1.47 (s, 27H, 13, 20, 26-$(CH_3)_3$); ^{13}C NMR (100 MHz, $CDCl_3$), δ 198.5 (27-C), 197.1 (28-C), 190.3 (29-C), 158.4 (5-C), 154.3 (1-C), 150.9 (6-C), 141.4 (3-C), 127.2 (2-C), 126.3 (7-C), 123.6 (4-C), 81.3 (12-C), 80.9 (19-C), 79.9 (25-C), 51.1(8-C), 47.8 (10-C), 46.1 (14, 23-C), 45.6 (17-C), 38.9 (21-C), 36.7 (22-C), 30.7 (9-C), 28.8 (13, 20, 26-C), 26.9 (15-C), 26.5 (16-C); MS *m/z* (ES+): 902 $[M-Cl]^+$; HRMS (ES+) $C_{35}H_{54}N_7O_9{}^{187}Re$ $[M-Cl]^+$ requires 902.3422 found 902.3456.

6.3.2 $[Re(CO)_3(L6.Boc)(L17)]BF_4$ (ReL6.Boc.L17)

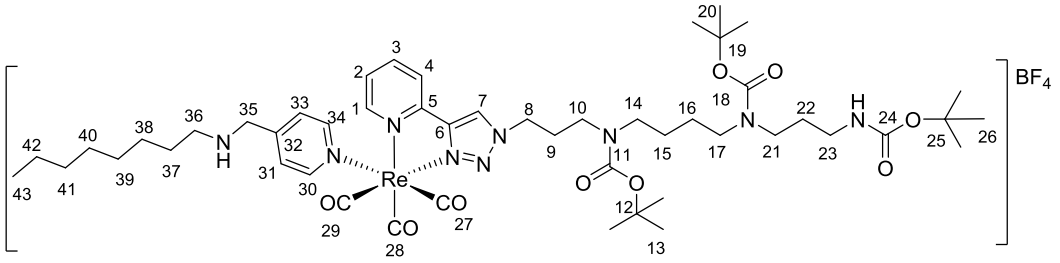

ReL6.Boc (0.11 g, 0.12 mmol) was dissolved in MeCN and followed by $AgBF_4$ (0.03 g, 0.175 mmol) and heated at 90°C for 1hr in microwave. The solution was filtered through celite and then solvent was removed in *vacuo*. After that the residue was dissolved in THF and then **L17** (0.0.51g, 0.23 mmol) was added and then heated in microwave at 90°C for 3hr. On cooling the solution was filtered through celite and then solvent was removed in *vaccuo* to produce (0.19 g) of crude. The crude was purified by RP-HPLC method A, R_t = 31.2 min to give (46 mg) of pure product as an oil. ^{1}H NMR (400 MHz, MeOD), δ 9.31 (d, *J* = 5.2 Hz, 1H, 1-CH), 9.09 (s, 1H, 7-CH), 8.54 (d, *J* = 5.4 Hz, 2H, 30, 34-CH), 8.29 (ddd, *J* = 8.4, 7.8, 1.2Hz, 1H, 3-CH), 8.15 (d, *J* = 7.8 Hz, 1H, 4-CH), 7.77 (ddd, *J* = 7.9, 6.5, 1.1 Hz, 2-CH), 7.53 (d, *J* = 6.4 Hz, 2H, 31, 33-CH), 4.71-4.65 (m, 2H, 8-CH_2), 4.23 (s, 2H, 35-CH_2), 3.46-3.35 (m, 2H, 23-CH_2), 3.25 (t, *J* = 6.6 Hz, 4H, 10, 14-CH_2), 3.05 (m, 4H, 17, 21-CH_2), 2.36 (m, 2H, 9-CH_2), 1.69 (m, 4H, 36, 22-CH_2), 1.57 (s br, 4H, 15, 16-CH_2), 1.47 (s, 29H, 37, 13, 20, 26-CH_3), 1.29 (bs, 10H, 38, 39, 40, 41, 42-CH_2), 0.90 (t, *J* = 6.5 Hz, 3H, 43-CH_3); ^{13}C NMR (100 MHz, MeOD), δ 196.5, 195.1, 192.2 (27, 28, 29-C), 155.5 (5-C), 153.4 (1-C), 152.6 (6-C), 151.4 (24, 30-C), 143.0 (3-C), 141.9 (32-C), 127.4 (2-C), 125.6 (31, 33-C), 124.6 (7-C) 124.2 (4-C), 82.4, 81.9, 80.2 (12, 20, 25-C), 51.1 (35-C), 50.1 (8-C), 50.0 (9-C), 48.0 (17-C), 47.3 (10, 14-C), 44.8 (23-C), 40.8 (36-C), 36.4 (21-C), 32.8 (38-C), 30.1 (22-C), 29.4 (39, 40-C), 28.8 (13, 20, 26-C), 28.0 (41-C), 27.6 (37-C), 24.3 (15, 16-C), 23.6 (42-C), 14.3 (43-C); ^{19}F NMR (400MHz, MeOD) δ -77.2 (s, 3F-CF_3CO_2); MS (ES+) 1122 $[M]^+$; HRMS (ES+) $C_{49}H_{77}N_9O_9{}^{187}Re$ $[M]^+$ requires 1122.4957 found 1122.5405.

6.3.3 $[Re(CO)_3(L6)(L17)](CF_3CO_2)_5$ (ReL6.L17)

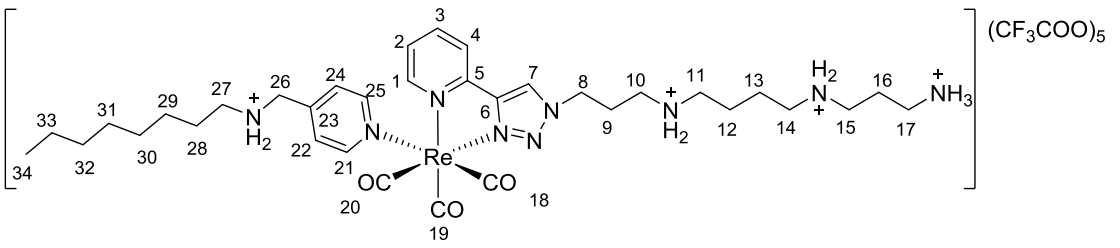

ReL6.Boc.L17 (0.02 g, 0.016 mmol) was dissolved in 4M TFA in DCM and stirred at rt. for 18hr. The volatiles were removed to produce the product (0.022g) without further purification. ^{1}H NMR (500 MHz, MeOD), δ 9.21 (d, *J* = 5.3 Hz, 1H, 1-CH), 9.01 (s, 1H, 7-CH), 8.40 (d, *J* = 5.4 Hz, 2H, 21, 25-CH), 8.19 (t, *J* = 8.1 Hz, 1H, 3-CH), 8.07 (d, *J* = 7.9Hz, 1H, 4-CH), 7.67 (t, *J* = 6.6 Hz, 2-CH), 7.43 (d, *J* = 5.6 Hz, 2H, 22, 24-CH), 4.70 (t, *J* = 6.6 Hz, 2H, 8-CH_2), 4.13 (s, 2H, 26-CH_2), 3.15 (t, *J* = 6.1 Hz, 2H, 17-CH_2), 3.08-3.04 (m, 8H, 10, 11, 14, 15, 27-CH_2), 3.00-2.95 (m, 4H, 9, 16-CH_2), 2.46-2.42 (m, 4H, 12, 14-CH_2), 2.20-1.88 (m, 2H, 28-CH_2), 1.74 (bs, 2H, 29-CH_2), 1.58 (s, 2H, 30-CH_3), 1.22 (s br, 6H, 31, 32, 33-CH_2), 0.83-078 (m, 3H, 34-CH_3); ^{13}C NMR (125 MHz, MeOD), δ 196.4, 194.3, 191.9 (18, 19, 20-C), 161.8 (q, *J* = 39.1 Hz, $CF_3CO_2^-$), 156.3 (5-C), 155.1 (1-C), 153.9 (21, 24-C), 150.8 (6-C), 145.1 (23-C), 143.0 (3-C), 128.8 (2-C), 128.1 (22, 24-C), 124.4 (4-C), 122.6 (7-C), 50.6 (26-C), 50.1 (8-C), 48.2 (10, 11-C), 45.8 (14, 17-C), 45.7 (15-C), 37.8 (9, 16-C), 32.8 (29-C), 30.1 (31-C), 26.8 (12, 13-C), 24.2 (28-C), 24.2 (32-C), 23.6 (33-C), 14.3 (34-C); ^{19}F NMR (500MHz, MeOD), δ -76.8 (s, 3F-CF_3CO_2); MS (ES+) 822 $[M]^+$; HRMS (ES+) $C_{34}H_{53}N_9O_3{}^{187}Re$ $[M]^+$ requires 822.3845 found 822.3829.

6.3.4 $[Re(CO)_3Cl(L3)]$ (ReL3)

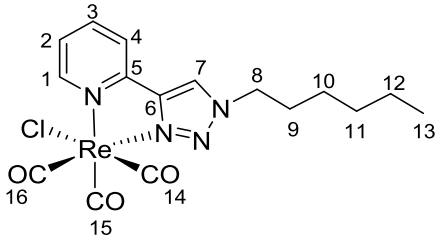

L3 (0.05 g, 0.21 mmol), and $Re(CO)_5Cl$ (0.08 g, 0.21 mmol) were dissolved in THF and then heated in microwave at 90 °C for 3hr. The solution was filtrated though the celite and solvent was removed under *vacuo* to produce (0.102 g, 88%) without need to purification. ^{1}H NMR (500 MHz, $CDCl_3$), δ 8.97 (d, 1H, *J* = 5.5 Hz, 1-CH), 8.35 (s, 1H,

7-CH), 7.91 (ddd, *J* = 8.3, 7.8 Hz, 1H, 3-CH), 7.79 (d, *J* = 7.8 Hz, 1H, 4-CH), 7.40 (ddd, *J* = 7.9, 6.6 Hz, 1H, 2-CH), 4.46-4.33 (m, 2H, 8-CH_2), 1.99-1.93 (m, 2H, 9-CH_2), 1.35-1.32 (m, 6H, 10, 11, 12-CH_2), 0.90 (t, *J* = 6.7Hz, 3H, 14-CH_3); ^{13}C NMR (125 MHz, $CDCl_3$), δ 197.20, 195.58, 189.02 (14, 15, & 16-CO), 153.1 (1-C), 149.3 (5-C), 148.6 (6-C), 139.3 (3-C), 125.7 (2-C), 123.4 (7-C), 122.1 (4-C), 52.4 (8-C), 31.0 (10-C), 30.0 (9-C), 25.9 (11-C), 22.4 (12-C); MS (ES+) 542 $[(M-Cl)+MeCN]^+$, 501 $[M-Cl]^+$; HRMS (ES+) $C_{18}H_{21}N_5O_3{}^{187}Re$ $[M-Cl+MeCN]^+$ requires 542.1202 found 542.1202.

6.3.5 $[Re(CO)_3(L3)(L16.Boc)]BF_4$ (ReL3.L16.Boc)

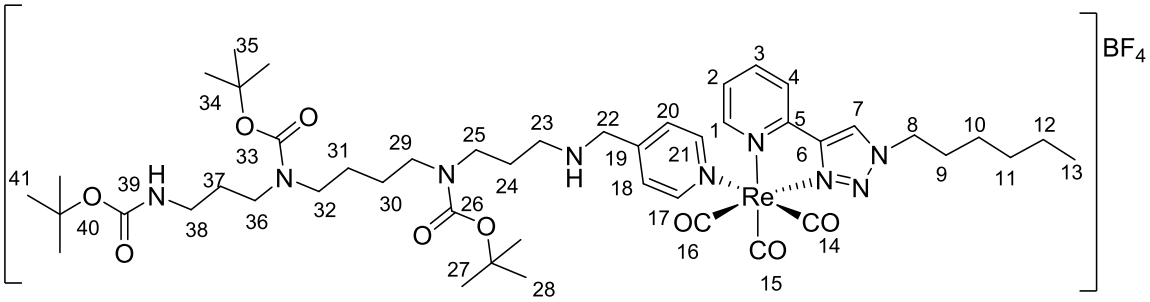

ReL3 (0.05g, 0.09 mmol) was dissolved in MeCN and $AgBF_4$ (0.05, 0.23 mmol) was added and the heated for 1hr in microwave and then the solution was filtered through celite and then solvent was removed in *vacuo.* Residue was dissolved in THF and then **L16.Boc** (0.011g, 0.18mmol) was added to the solution and then heated in microwave at 90° C for 3hr. after that the solution was filtrated though the celite and then solvent was removed to offered crude (0.09 g). Product was purification by RP-HPLC method A, tR = 31 min, (0.04 g). ^{1}H NMR (500 MHz, MeOD), δ 9.31 (d, *J* = 5.6 Hz, 1H, 1-CH), 9.09 (s, 1H, 7-CH), 8.51 (s, 2H, 17, 21-CH), 8.29 (ddd, *J* = 7.8, 8.8 Hz, 1H, 3-CH), 8.16 (d, *J* = 7.8 Hz, 1H, 4-CH), 7.77 (ddd, *J* = 7.7, 6.7, 0.9 Hz, 1H, 2-CH), 7.55 (d, *J* = 5.7 Hz, 2H, 18, 20-CH), 4.70-4.63 (m, 2H, 8-CH_2), 4.24 (s, 2H, 22-CH_2), 3.33-3.32 (m, 4H, 25, 29-CH_2), 3.24-3.21 (m, 6H, 32, 36, 38-CH_2), 3.08-3.03 (m, 2H, 23, 24-CH_2), 2.13-2.07 (m, 2H, 37-CH_2), 1.95-1.92 (m, 2H, 30-CH_2),1.69 (s br, 2H, 31-CH_2), 1.52-1.50 (m, 4H, 9, 10-CH_2), 1.46 (d, *J* = 8.8 Hz, 31H, 28, 35, 41-CH_3, 11, 12-CH_2), 1.35-0.95 (t, *J* = 7.0 Hz, 3H, 13-CH_3); ^{13}C NMR (125MHz, MeOD), δ 196.5, 195.1, 192.03 (14, 15, 16-C), 158.4 (5-C), 155.1 (1-C), 154.0 (17, 21-C), 150.7 (6-C), 146.1 (19-C), 142.8 (3-C), 135.6 (4-C), 128.2 (2-C), 128.7 (19, 20-C), 124.3 (7-C), 81.3, 80.9, 79.9 (27, 34, 40-C), 53.8 (8-C), 50.2 (22-C), 47.7 (23-C), 46.8 (32-C), 46.1 (36-C), 45.6 (38-C), 44.4 (25, 29-C), 38.9 (24-C), 32.1 (10-C), 30.7 (9, 37-C), 28.83, 28.80, 28.7 (28, 35, 41-C), 27.04 (30, 31-C), 23.5 (11, 12-C), 14.3 (13-C); MS (ES+) 1094.5 $[M]^+$; HRMS (ES+) $C_{47}H_{73}N_9O_9{}^{187}Re$ $[M]^+$ requires 1094.5127 found 1094.5089

6.3.6 $[Re(CO)_3(L3)(L16)](CF_3CO_2)_5$ (ReL3.L16)

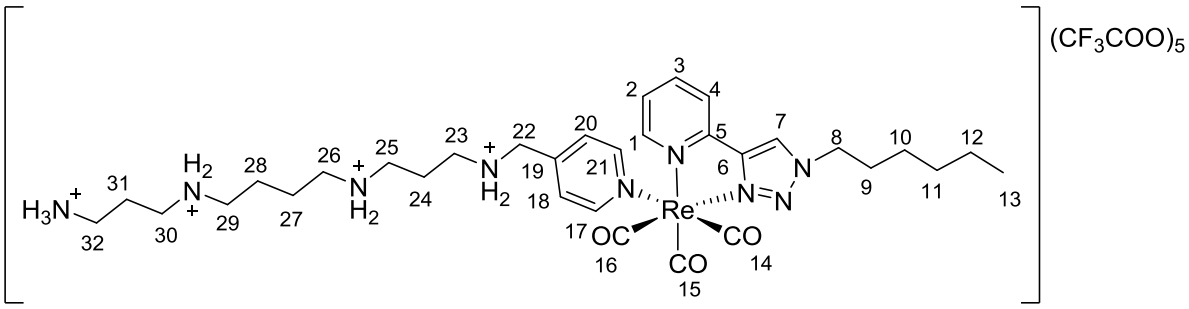

ReL3.L16.Boc (0.03g, 0.02mmol) was dissolved in 4M TFA in DCM and stirred at rt. for 18hr. The volatiles were removed to produce the product (0.03g) without further purification ^{1}HNMR (500 MHz, MeOD), δ 9.20 (d, *J* = 5.3 Hz, 1H, 1-CH), 8.96 (s, 1H, 7-CH), 8.41 (d, *J* = 6.5 Hz, 2H, 17, 21-CH), 8.18 (ddd, *J* = 8.4, 7.9, 1.2 Hz, 1H, 3-CH), 8.04 (d, *J* = 7.9 Hz, 1H, 4-CH), 7.67 (ddd, *J* = 7.8, 6.5, 1.3 Hz, 1H, 2-CH), 7.44 (d, *J* = 6.6 Hz, 2H, 19, 20-CH), 4.64-4.56 (m, 2H, 8-CH_2), 4.16 (s, 2H, 22-CH_2), 3.12 (t, *J* = 7.5 Hz, 2H, 32-CH_2), 3.04 (t, *J* = 7.7 Hz, 4H, 25, 26-CH_2), 3.01-2.94 (m, 6H, 23, 29, 30-CH_2), 2.08-2.04 (m, 2H, 24-CH_2), 2.07-1.90 (m, 4H, 27, 28-CH_2), 1.70-1.68 (m, 4H, 29, 31-CH_2), 1.34-1.32 (m, 6H, 10, 11, 12-CH_2), 0.85 (t, *J* = 6.8 Hz, 3H, 13-CH_3);); ^{13}C NMR (125 MHz, MeOD), δ 196.5 (16-C), 195.0 (15-C), 192.0 (14-C), 161.4 (q, *J* = 38.1 Hz, $CF_3CO_2^-$), 155.1 (1-C), 153.8 (17, 21-C), 150.7 (5-C), 145.5 (6, 19-C), 142.7 (3-C), 128.6 (2-C), 128.2 (18, 20-C), 127.3 (4-C), 124.3 (7-C), 53.8 (8-C), 50.3 (22-C), 48.2 (23-C), 46.3 (32-C),45.3 (25-C),45.8 (26-C), 37.8 (29-C), 32.1 (10-C), 30.7 (27, 28-C), 27.0 (11-C), 25.3 (24-C), 24.1 (30-C), 24.0 (12-C), 23.4 (9, 31-C), 14.2 (13-C); ^{19}F NMR (500MHz, MeOD), δ -77.3 (s, 3F-CF_3CO_2); MS (ES+) 795 $[M]^+$; HRMS (ES+) $C_{32}H_{49}N_9O_3{}^{187}Re$ $[M]^+$ requires 794.3541 found 794.3516.

6.3.7 $[Re(CO)_3(L8.Boc)(Cl)]$ (ReL8.Boc)

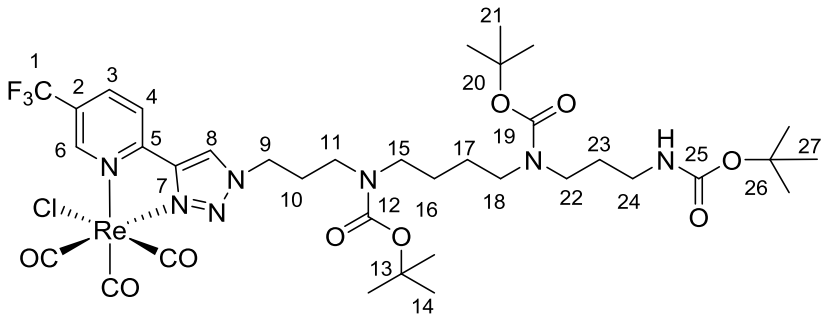

Pentacarbonylchlororhenium (0.03g, 0.07 mmol), **L8.Boc** (0.05 g, 0.07 mmol) and THF (4ml) all were added to a microwave tube. The suspension was heated in a microwave reactor at 90°C for 3hr, yielding a clear yellow solution, solvent was removed in *vacuo*

to yielding yellow solid. (0.05 g, 81%) ^{1}H NMR (500MHz, MeOD), δ 9.00 (s, 1H, 6-CH), 8.95 (bs, 1H, 8-CH), 8.38 (d, *J* = 7.9 Hz, 1H, 4-CH), 8.19 (d, *J* = 8.4 Hz, 3-CH), 4.49 (t, *J* = 6.5 Hz, 2H, 9-CH), 3.08-3.04 (m, 6H, 11,15, 24-CH_2), 2.86 (t, *J* = 6.7Hz, 2H, 18-CH_2), 2.15 (t, *J* = 6.2 Hz, 2H, 22-CH_2), 1.51 (s br, 2H, 10-CH_2), 1.35 (s br, 4H, 16, 23-CH_2), 1.30-1.27 (m, 29H, 17-CH_2, 14, 21, 27-$(CH_3)_3$); ^{13}C NMR (125 MHz, MeOD), δ 153.5 (5-C), 150.9 (6-C), 148.1 (2-C), 138.9 (3-C), 138.2 (4-C), 128.0 (8-C), 124.2(1-C), 81.7 (13-C), 79.4 (20-C), 78.9 (26-C), 51.2 (9-C), 47.6 (11-C), 47.3 (15-C), 38.8 (18-C), 38.1 (17-C), 29.5 (10-C), 28.7 (14, 21, 27-C), 28.1 (22-C), 25.6 (16, 23-C);^{19}F NMR(500MHz, MeOD), δ 64.1 (s, 3F-py); MS(ES+) *m/z* 970 $[M-Cl]^+$, HRMS (ES+) $C_{36}H_{52}N_7O_9F_3{}^{187}Re$ $[M-Cl]^+$ requires 970.3370 found 970.3336.

6.3.8 $[Re(CO)_3(L8.Boc)(L17)]BF_4$ (ReL8.Boc.L17)

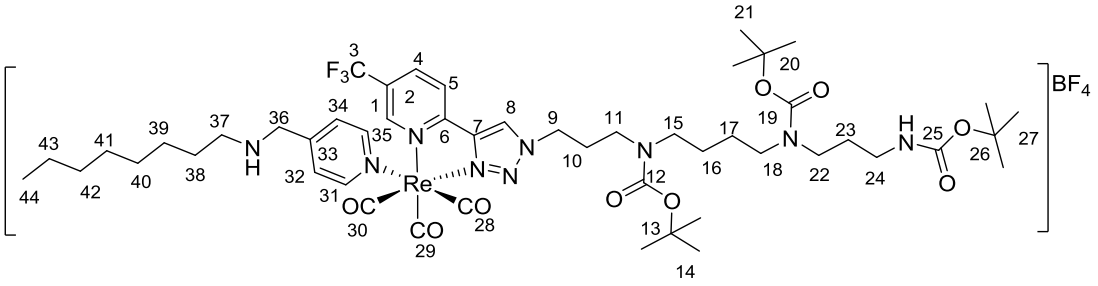

ReL8.Boc (0.15 g, 0.13 mmol) was dissolved in MeCN and followed by $AgBF_4$ (0.07, 0.34 mmol) and heated at 90 °C in microwave for 1hr and then the solution was filtered through celite and then solvent was removed in *vacuo*. The crude was dissolved in THF and then **L17** (0.06, 0.27 mmol) was added to reaction mixture and then heated at 90 °C in microwave for 3hr. The solution was filtered through celite and then solvent was removed in *vacuo* to produce (0.22 g) of product as crude. The product was purification by RP-HPLC method A, tR = 33 min, (0.049 g). ^{1}H NMR (500 MHz, MeOD), δ 8.87 (s, 1H, 1-CH), 8.62 (dd, *J* = 8.2, 1.8 Hz, 5-CH), 8.62 (s, 1H, 8-CH), 8.30 (d, *J* = 5.9 Hz, 2H, 31, 35-CH), 8.15 (d, *J* = 8.3 Hz, 1H, 4-CH), 7.61 (d, *J* = 6.2 Hz, 2H, 32, 34-CH), 4.52-4.46 (m, 2H, 9-CH_2), 4.34 (s, 2H, 36-CH_2), 3.30 (t, *J* = 6.5 Hz, 2H, 24-CH_2), 3.25-3.22 (m, 6H, 11, 15, 18-CH_2), 3.09 (t, *J* = 8.1 Hz, 2H, 22-CH_2), 3.05 (t, *J* = 6.7 Hz, 37-CH_2), 2.20 (m, 2H, 10-CH_2), 1.77-1.68 (m, 4H, 16, 17-CH_2), 1.54-1.50 (m, 4H, 23, 38-CH_2), 1.46 (d, *J* = 8.3 Hz, 27H, 14, 21, 27-CH_3), 1.36-1.32 (m, 10H, 39-43-CH_2), 0.91(t, *J* = 6.8 Hz, 3H, 44-CH_3); ^{13}C NMR (125 MHz, MeOD), δ 196.2, 194.7& 194.2 (28, 29, 30-CO), 163.2 (q *J* = 38.1Hz, CF_3CO_2),159.0 (6-C), 158.1 (33-C), 156.2 (31, 35-C), 153.9 (1-C), 149.2 (7-C), 141.3 (2-C), 140.1 (5-C), 130.7 (4-C), 128.7 (33, 34-C), 126.5

(8-C),124.2(3-C), 81.9, 81.5 & 81.0 (13, 20, & 26-C), 51.8 (9-C), 50.8 (36, 22-C), 48.8 (11-C), 48.6 (15-C), 46.4 (18-C), 45.7 (24-C), 39.7 (37-C), 33.3 (23, 38-C), 30.6 (10, 39-C), 29.4 (14, 21, 27-C), 28.1(16, 17, 40-C), 27.6 (41,42-C), 24.1 (43-C), 14.8 (44-C);^{19}F NMR (500MHz, MeOD), δ -64.1(s,3F-py), -77.1 (s, F-BF_4); MS (ES+) 1190 $[M]^+$; HRMS (ES+) $C_{50}H_{76}N_9O_9F_3{}^{187}Re$ $[M]^+$ requires 1190.5248 found 1190.5276.

6.3.9 $[Re(CO)_3(L8)(L16)](CF_3CO_2)_5$ (ReL8.L17)

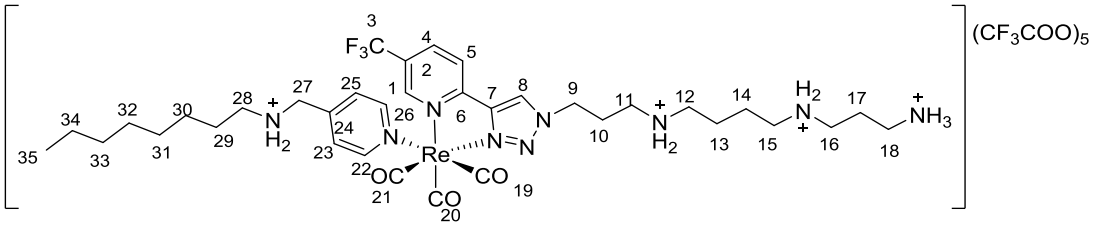

ReL8.Boc.L17 (0.04 g) was dissolved in 4M TFA in DCM and stirred at rt. for 18hr. The volatiles were removed to produce the product (0.05g) without further purification. ^{1}H NMR (500 MHz, MeOD), δ 9.52 (s, 1H, 1-CH), 9.28 (s, 1H, 8-CH), 8.68 (d, *J* = 7.6 Hz, 1H, 5-CH), 8.54 (d, *J* = 6.4 Hz, 2H, 22, 26-CH), 8.41 (ddd, *J* = 8.2, 8.9 Hz, 1H, 4-CH), 7.55 (d, *J* = 6.5 Hz , 2H, 23, 25-CH), 4.80 (m, 2H, 9-CH_2), 4.24 (s, 2H, 27-CH_2), 3.28-3.25 (m, 2H, 18-CH_2), 3.17-3.04 (m, 8H, 11, 12, 15, 16-CH_2), 2.29 (t, *J* = 7.6 Hz, 2H, 28-CH_2), 2.58-2.55 (m, 2H, 10-CH_2), 2.13-2.06 (m, 2H, 17-CH_2), 1.85-1.83 (m, 4H, 13, 14-CH_2), 1.71-1.63 (m, 4H, 29, 30-CH_2), 1.38-1.30 (m, 8H, 31, 32, 33, 34-CH_2), 0.94-0.89 (m, 35-CH_3); ^{13}C NMR (125 MHz, MeOD), δ 196.2, 194.6, 193.1 (19, 20, 21-C), 163.0 (q, *J* = 34.1 Hz, CF_3CO_2), 154.1 (22, 26-C), 153.7 (6-C), 153.5 (2-C), 151.8 (1-C), 149.8 (7-C), 146.3 (24-C), 140.3 (5-C), 129.5 (4-C), 128.3 (23, 25-C), 125.8 (8-C), 124.2(3-C), 50.2 (9-C), 48.2 (27-C), 45.8 (11, 12-C), 45.7 (18-C), 40.7 (28-C), 37.8 (15, 16-C), 32.8 (31-C), 30.2 (32-C), 27.4 (29, 30-C), 27.3 (10-C), 27.1(33-C), 25.3 (17-C), 24.2 (13, 14-C), 23.6 (34-C), 14.4 (35-C); ^{19}F NMR(500MHz, MeOD) δ -62.4 (s, 3F-py), -76.8 (s, 3F-CF_3CO_2); MS (ES+) 890 $[M]^+$; HRMS (ES+) $C_{35}H_{52}N_9O_3F_3{}^{187}Re$ $[M]^+$ requires 890.3726 found 888.3703.

6.3.10 $[Re(CO)_3(L10)(L17)](CF_3CO_2)_5$ (ReL10.L17)

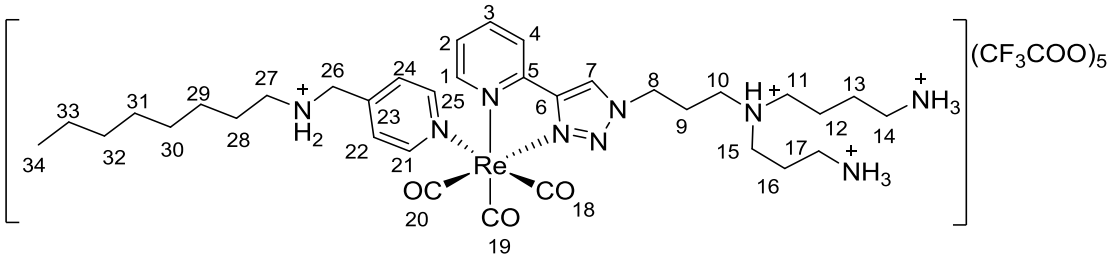

(ReL10.Boc.L17) (0.02 g, 0.018 mmol) was dissolved in 4M TFA in DCM and stirred at rt. for 18hr. The volatiles were removed to produce the product (0.025 g) without further purification. ^{1}H NMR (500 MHz, MeOD), δ 9.32 (d, *J* = 5.1 Hz, 1H, 1-CH), 9.10 (s, 1H, 7-CH), 8.53 (d, *J* = 6.4 Hz, 2H, 21, 25-CH), 8.30 (ddd, *J* = 8.7, 7.2, 1.0 Hz, 1H, 3-CH), 8.16 (d, *J* = 8.1 Hz, 1H, 4-CH), 7.78 (ddd, *J* = 7.7, 5.8, 1.1 Hz, 1H, 2-CH), 7.53 (d, *J* = 6.4 Hz, 2H, 22, 24-CH), 4.90 (t, *J* = 6.6 Hz, 2H, 8-CH_2), 4.24 (s, 2H, 26-CH_2), 3.77-3.68 (m, 2H, 10-CH_2), 3.11 (t, *J* = 7.7 Hz, 2H, 14-CH_2), 3.05 (t, *J* = 7.7 Hz, 2H, 17-CH_2), 2.61-2.56 (m, 2H, 11-CH_2), 1.78-1.74 (m, 2H, 15-CH_2), 1.72-1.66 (m, 2H, 27-CH_2), 2.34-2.29 (m, 6H, 9, 12, 16-CH_2), 1.45 (bs, 4H, 13, 28-CH_2), 1.33-1.31 (m, 14H, 29, 30, 31, 32, 33-CH_2), 0.91 (t, *J* = 6.9 Hz, 3H, 34-CH_3); ^{13}C NMR (125 MHz, MeOD), δ 196.12, 195.2, 192.6 (18, 19, 20-C), 161.7 (q, *J* = 35.1 Hz, $CF_3CO_2^-$), 157.6 (5-C), 155.1 (1-C), 154.0 (21, 25-C), 150.8 (6-C), 147.9 (23-C), 142.8 (3-C), 128.7 (2-C), 128.1 (22, 25-C), 125.8 (7-C), 124.3 (4-C), 50.8 (8-C), 50.1 (26-C), 47.8 (10-C), 47.6 (11-C), 44.6 (14-C), 44.0 (15-C), 42.2 (17-C), 33.2 (9-C), 32.8 (16-C), 31.7 (28-C), 30.1 (29-C), 27.4 (31-C), 27.1 (32-C), 25.9 (12-C), 25.2 (13, 30-C), 23.6 (33-C), 14.3 (34-C);^{19}F(500MHz, MeOD) δ -62.4 (s, 3F-py), -76.3 (s, 3F-CF_3CO_2); MS (ES+) 822 $[M]^+$; HRMS (ES+) $C_{34}H_{53}N_9O_3{}^{187}Re$ $[M]^+$ requires 822.3752 found 822.3745.

6.3.11 $[Re(CO)_3(L9.Boc)\ (L17)]BF_4$ (ReL9.Boc.L17)

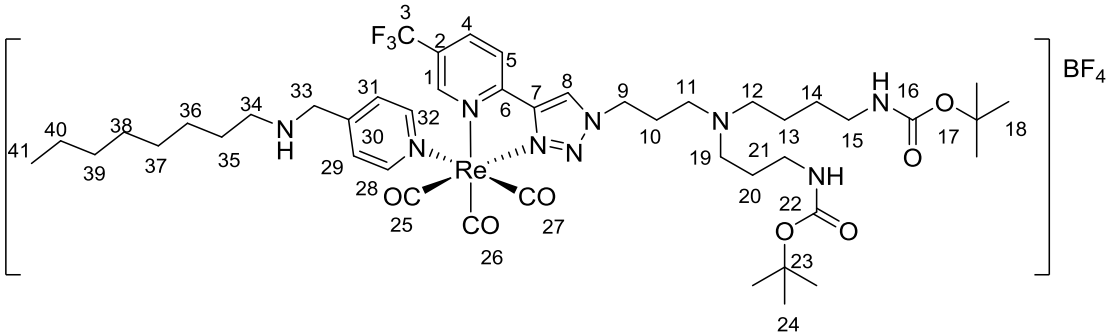

ReL9.Boc (0.11g, 0.13 mmol) was dissolved in MeCN and followed by $AgBF_4$ (0.03 g, 0.14 mmol) and then the solution was heated in microwave at 90°C for 1hr. and then the solution was filtered through the celite and then the solution was evaporated to produce

precipitate and the residue was dissolved in THF and then followed by **L17** (0.03g, 0.14 mmol) and then heated in microwave at 90°C for 3hr.The solution was filtered through celite and then solvent was removed in *vacuo* to give as brown oily product (0.12 g). The crude was purified by RP-HPLC method A, tR = 32 min to give (0.05g) of a pure product; ^{1}H NMR (500 MHz, MeOD), δ 9.52 (s, 1H, 1-CH), 9.28 (s, 1H, 8-CH), 8.68 (ddd, *J* = 8.2, 8.0, 1.2 Hz, 1H, 4-CH), 8.55 (d, *J* = 6.1 Hz, 2H, 28, 32-CH), 8.40 (d, *J* = 8.4 Hz, 1H, 5-CH), 7.55 (d, *J* = 5.8 Hz, 2H, 29, 31-CH), 4.71 (t, *J* = 6.7 Hz, 2H, 9-CH_2), 4.25 (s, 2H, 33-CH_2), 3.45-3.41 (m, 2H, 11-CH_2), 3.27 (t, *J* = 6.3 Hz, 2H, 15-CH_2), 3.18 (t, *J* = 6.3 Hz, 2H, 21-CH_2), 3.12 (t, *J* = 6.5 Hz, 2H, 12-CH_2), 3.06 (t, *J* = 8.1Hz, 2H, 19-CH_2), 2.63-2.61(m, 2H, 10-CH_2), 1.97-1.94 (m, 2H, 20-CH_2), 1.79-1.77 (m, 2H, 13-CH_2), 1.73-1.67 (m, 2H, 14-CH_2), 1.59 (t, *J* = 7.1 Hz, 2H, 34-CH_2), 1.45 (d, *J* = 1.4 Hz, 18H, 18, 24-$(CH_3)_3$), 1.35-1.30 (m, 12H, 35, 36, 37, 38, 39, 40-CH_2), 0.90 (t, *J* = 6.8 Hz, 3H, 41-CH_3); ^{13}C NMR (125 MHz, MeOD), δ 196.0, 194.6 & 190.9 (25, 26, 27-C), 156.0 (6-C), 152.3 (28, 32-C), 150.6 (1-C), 146.7 (7-C), 138.5 (4-C), 127.6 (8-C), 126.4 (29, 31-C), 124.1(3-C), 123.2 (5-C), 82.4, 81.3 (16, 22-C), 50.7 (9-C), 47.9 (33-C), 46.9 (21-C), 44.1(15-C), 40.8 (12-C), 37.4 (19-C), 31.0 (10-C), 28.3 (35, 36-C), 27.3 (18, 24-C), 26.4 (20-C), 25.2 (13, 37, 38-C), 21.9 (14, 39, 40-C), 13.0 (41-C); ^{19}F NMR (500 MHz, MeOD), δ -62.3 (s, 3F-py); MS (ES+) m/z 1090 $[M]^+$, HRMS (ES+); 1090 $[M]^+$ $C_{45}H_{68}N_9O_7F_3{}^{187}Re$ requires 1090.4771 found 1090.4751.

6.3.12 $[Re(CO)_3(L9)\ (L17)](CF_3CO_2)_5$ (ReL9.L17)

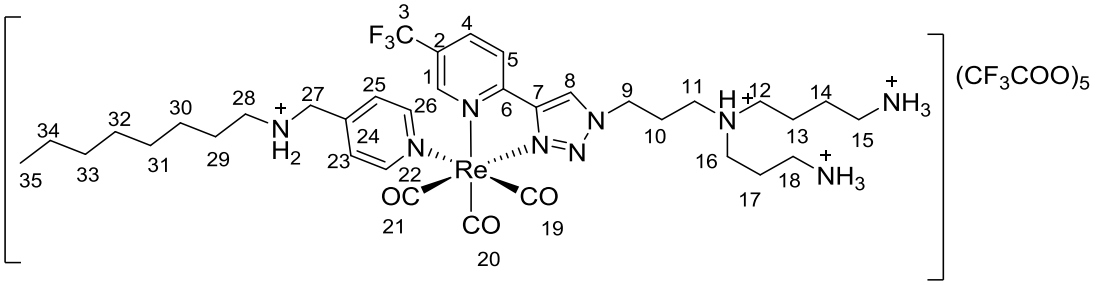

ReL9.Boc.L17 (0.03 g, 0.03 mmol) was dissolved in 4M TFA in DCM and stirred at rt. for 18hr. The volatiles were removed to produce the product (0.035g) without further purification ^{1}H NMR (500 MHz, MeOD), δ 9.50 (s, 1H, 1-CH), 9.30 (s, 1H, 8-CH), 8.66 (d, *J* = 6.4 Hz, 1H, 4-CH), 8.52 (d, *J* = 5.8 Hz, 2H, 22, 26-CH), 8.40 (m, 1H, 5-CH), 7.55 (d, *J* = 5.3 Hz, 2H, 23, 25-CH), 4.84 (t, *J* = 6.9 Hz, 2H, 9-CH_2), 4.24 (s, 2H, 27-CH_2), 3.43 (t, *J* = 7.2 Hz, 2H, 15-CH_2), 3.41-3.37 (m, 2H, 18-CH_2), 3.10-3.01(m, 6H, 11, 12, 16-CH_2), 2.64 (bs, 2H, 28-CH_2), 2.21 (s br, 2H, 10-CH_2), 1.92-1.87 (m, 2H, 17-CH_2), 1.82-1.76 (m, 2H, 13-CH_2), 1.72-1.65 (m, 2H, 14-CH_2), 1.34-1.30 (m, 12H,

29, 30, 31, 32, 33, 34-CH_2), 0.89 (t, *J* = 6.8 Hz, 3H, 35-CH_3); ^{13}C NMR (125 MHz, MeOD), δ 195.4, 194.5, 191.9 (19, 20, 21-C), 158.5 (24-C), 156.9(6-C), 154.0 (22, 26-C), 151.7 (1-C), 149.1 (2-C), 145.2 (7-C), 140.2 (4-C), 129.5 (8-C), 128.3 (23, 25-C), 124.8 (3, 5-C), 53.7 (9-C), 51.1 (15-C), 50.8 (18-C), 50.1 (27-C), 49.6 (11, 12-C), 39.9 (16-C), 37.8 (28-C), 32.8 (29-C), 30.1 (30, 31-C), 27.4 (33-C), 25.5 (32-C), 25.1 (14-C), 23.6 (10-C), 23.1 (17-C), 21.9 (13, 34-C), 14.3 (35-C); ^{19}F NMR (500MHz, MeOD), δ -62.4 (s, 3F-py), -77.1 (s, 3F-CF_3CO_2); MS(ES+) m/z 890 $[M]^+$, HRMS (ES+); $C_{35}H_{52}N_9O_3F_3{}^{187}Re$ requires 890.3734 found 890.3703

6.3.13 [Re(CO)$_3$(L11)(Cl)] (ReL11)

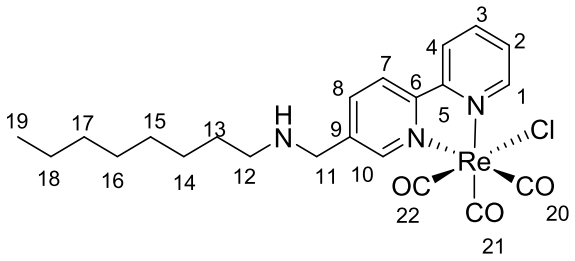

Pentacarbonylchlororhenium (0.09 g, 0.26 mmol), **L11** (0.09 g, 0.26 mmol) and THF (10ml) all were added into the microwave tube and suspension was heated in a microwave reactor at 90°C for 3hr, yielding a clear yellow solution, solvent was removed under *vacuo* to yielding brown oily product (0.15g), crude was purified by column chromatography using (DCM/ MeOH: 80:20%) to produce (0.09 g, 60%) of product. ^{1}H NMR (500 MHz, MeOD), δ 9.11 (d, 1H, *J* = 5.8 Hz, 4-CH), 9.09 (d, *J* = 4.1 Hz, 1H, 7-CH), 8.71 (s, 1H, 10-CH), 8.60 (d, *J* = 8.8 Hz, 1H, 1-CH), 8.33 (ddd, *J* = 8.5, 7.0, 1.0Hz, 1H, 3-CH), 8.30 (d, *J* = 8.2 Hz, 8-CH), 7.77-7.75 (m, 1H, 2-CH), 4.40 (s, 1H, 11-CH_2), 3.09 (t, *J* = 7.6 Hz, 2H, 12-CH_2),1.79-1.74 (m, 4H, 13, 14-CH_2), 1.70-1.65 (m, 8H, 15, 16, 17, 18-CH_2), 0.93-0.91 (m, 3H, 19-CH_3); ^{13}C NMR (125 MHz, MeOD), δ 197.3, 194.2, 190.6 (20, 21, 22-C), 157.1 (6-C), 153.7(5-C), 152.5 (4, 7-C), 147.2 (9-C), 140.7 (3-C), 130.1 (2-C), 128.6 (8-C), 125.3 (1-C), 124.5 (10-C), 50.9 (11-C), 46.3 (12-C), 32.9 (15-C), 30.2 (13, 14-C), 29.2 (16-C), 23.6 (18-C), 14.4 (19-C); MS (ES+) *m/z* 569 $[M-Cl]^+$, 609 $[M-Cl+MeCN]^+$ HRMS (ES+); $[M-Cl+MeCN]^+$ $C_{24}H_{30}N_4O_3{}^{187}Re$ requires 609.1894 found 609.1876.

6.3.14 $[Re(CO)_3(L11)(L16.Boc)]BF_4$ (ReL11.L16.Boc)

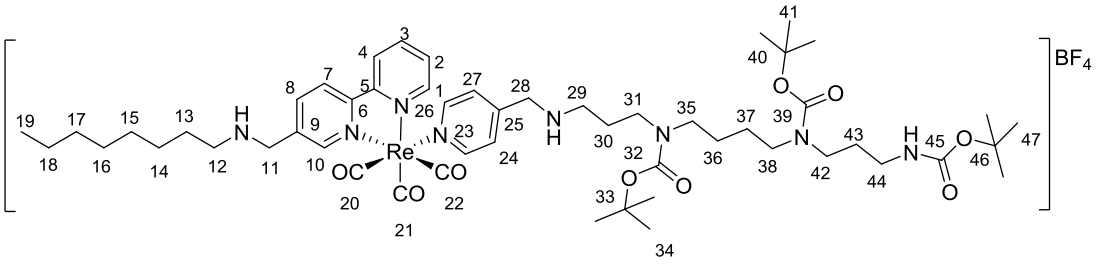

ReL11 (0.07 g, 0.12 mmol) was dissolved in MeCN and then $AgBF_4$ was added to the rhenium solution and heated in microwave at 90ºC for 1hr. The solution was filtered through celite and then solvent was removed in *vacuo* to yield sold precipitate and then dissolved in THF and followed by **L16.Boc** (0.07, 0.12 mmol) was added to the solution and heated in microwave at 90ºC for 3hr. Solution was filtered through celite and then the solvent were evaporated in *vacuo* to produce orange solid (0.11g). Product was purification by RP-HPLC method A, tR = 30 min, (0.05g). ^{1}H NMR (500 MHz, MeOD), δ 9.41 (d, 1H, *J* = 5.6 Hz, 4-CH), 9.38 (d, *J* = 5.3 Hz, 1H, 7-CH), 8.74 (s, 1H, 10-CH), 8.58 (d, *J* = 8.2 Hz, 1H, 1-CH), 8.52 (d, *J* = 5.2 Hz, 2H, 23, 26-CH), 8.40 (ddd, *J* = 8.9, 7.9, 1.3 Hz, 1H, 3-CH), 7.97 (d, *J* = 5.2 Hz, 8-CH), 7.94 (t, *J* = 6.4 Hz, 1H, 2-CH), 7.52 (d, *J* = 5.9 Hz, 2H, 24, 27-CH), 4.51 (s, 1H, 11-CH_2), 4.22 (s, 2H, 28-CH), 3.04 (q, *J* = 6.9 Hz, 8H, 31, 35, 38, 42-CH_2), 3.07-3.03 (m, 4H, 44, 29-CH_2), 1.90 (m, 2H, 30-CH_2), 1.81-1.77 (m, 2H, 43-CH_2), 1.72-1.69 (m, 2H, 12-CH_2), 1.53-1.48 (m, 6H, 13, 36, 37-CH_2), 1.49-1.44 (m, 31H, 14, 15-CH_2, 34, 41, 47-CH_3), 1.35-1.30 (m, 6H, 16, 17, 18-CH_2), 0.92 (t, *J* = 6.8 Hz, 2H, 19-CH_3); ^{13}C NMR (125 MHz, MeOD), δ 196.0 (20-C), 194.5 (21-C), 192.2 (22-C), 146.9 (3-C), 146.5 (9-C), 132.5 (2, 8-C), 129.4 (10-C), 127.6 (24, 27-C),82.8, 80.2, 79.8 (33, 40, 46-C), 52.4 (31-C), 49.7 (35-C), 49.0 (11-C), 48.4 (38, 42-C), 48.2 (28-C), 38.1 (29, 44-C), 32.1 (30-C), 27.6 (34, 41, 47-C), 29.3 (43-C), 26.7 (12-C), 26.5 (13, 36, 37-C), 22.8 (16, 17, 18-C), 13.6 (19-C); MS (ES+) 1161$[M]^+$; HRMS (ES+) $C_{53}H_{82}N_8O_9{}^{187}Re$ $[M]^+$ requires 1161.5814 found 1161.5762.

6.3.15 [Re(CO)$_3$(L11) (L16)](CF$_3$CO$_2$)$_6$ (ReL11.L16)

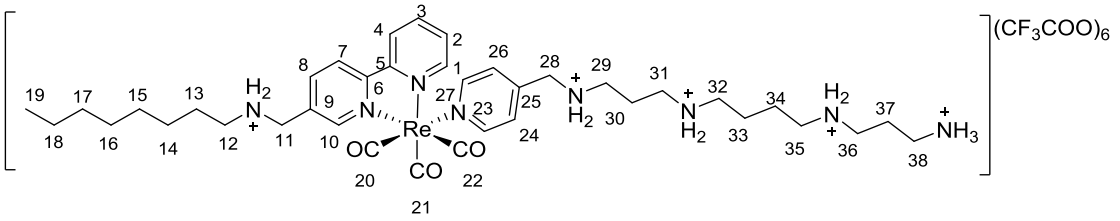

ReL11.L16.Boc (0.40 g, 0.03 mmol) was dissolved in 4M TFA in DCM and stirred at rt. for 18hr. The volatiles were removed to produce the product (0.05g) without further purification. ^{1}H NMR (500 MHz, MeOD), δ 9.39 (d, *J* = 5.6 Hz, 1H, 4-CH), 9.37 (d, *J* = 4.9 Hz, 1H, 7-CH), 8.75 (s, 1H, 10-CH), 8.58 (d, 8.1 Hz, 1H, 1-CH), 8.49 (d, *J* = 6.1 Hz, 2H, 23, 27-CH), 8.39 (ddd, *J* = 8.3, 7.7, 1.1Hz, 1H, 3-CH), 7.98 (d, *J* = 5.4 Hz, 1H, 8-CH), 7.93 (ddd, *J* = 7.6, 6.3, 0.8 Hz, 1H, 2-CH), 7.52 (d, *J* = 5.9 Hz, 2H, 24, 26-CH), 4.50 (s, 2H, 11-CH$_2$), 4.25 (s, 2H, 28-CH$_2$), 3.21 (t, *J* = 7.3 Hz, 4H, 29, 38-CH$_2$), 3.14 (t, *J* = 7.5 Hz, 6H, 31, 32, 36-CH$_2$), 3.09-3.05 (m, 8H, 12, 30, 35, 37-CH$_2$), 2.16-2.08 (m, 4H, 33, 34-CH$_2$), 1.82-1.76 (m, 6H, 13, 14, 15-CH$_2$), 1.37-1.33 (m, 6H, 16, 17, 18-CH$_2$), 0.92 (t, *J* = 6.1 Hz, 3H, 19-CH$_3$); ^{13}C NMR (125 MHz, MeOD), δ 196.3 (20-C), 194.3 (21-C), 192.2 (22-C), 161.6 (q, *J* = 36.5 Hz, CF$_3$COO$^-$), 157.9 (6-C), 156.8 (5-C), 155.5 (4-C), 155.4 (7-C) 153.9 (23, 27-C), 147.8 (9-C), 146.1 (25-C), 142.7 (3-C), 130.6 (8-C), 130.1 (2-C), 128.4 (24, 26-C), 126.4 (10-C), 126.2 (1-C), 50.5 (11-C), 50.3 (28-C), 48.3 (29-C), 46.4 (38-C), 45.9 (31, 32-C), 45.8 (12-C), 37.9 (35, 36-C), 32.9 (15-C), 30.2 (16-C), 30.2 (17-C), 27.6 (13-C), 27.3 (14-C), 25.4 (37-C), 24.3 (33-C), 24.2 (34-C), 23.7 (18-C), 14.5 (19-C); MS (ES+) 861[M]$^+$; HRMS (ES+) $C_{38}H_{58}N_8O_3{}^{187}Re$ [M]$^+$ requires 861.4200 found 861.4189.

6.3.16 [Re(CO)$_3$(L13)(Cl)] (ReL13)

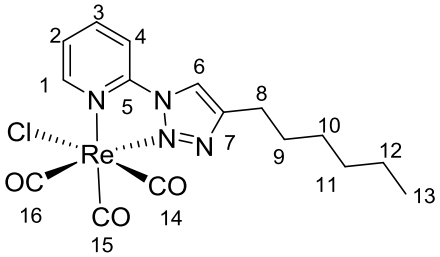

Pentacarbonylchlororhenium (0.16 g, 0.45 mmole) and **L13** (0.11 g, 0.45 mmol) were dissolved in toluene (25 mL) and refluxed at 110 °C for 18hr. The solution was filtered through celite and then the solvent was removed to give crude and then separated by column chromatography eluted with DCM: EtOAc (90:10) to afford complex (0.15 g,

86%); ^{1}H NMR (400MHz, $CDCl_3$), δ 8.94 (d, *J* = 5.5 Hz, 1H, 1-CH), 8.25 (bs, 1H, 6-CH), 8.16 (ddd, *J* = 8.7,7.9,1.7 Hz, 1H, 3-CH), 7.84 (d, *J* = 8.2 Hz,1H, 4-CH), 7.53 (ddd, *J* = 7.6, 5.6, 1.08 Hz, 1H, 2-CH), 2.90-2.73 (m, 2H, 8-CH_2), 1.7 (q, *J* = 7.8 Hz, 2H, 9-CH_2), 1.45-1.38 (m, 2H, 10-CH_2), 1.36-1.31 (m, 4H, 11, 12-CH_2), 0.91 (t, *J* = 6.9 Hz, 3H, 13-CH_3); ^{13}C NMR (100 MHz, CDCl3), δ 158.0 (5-C), 152.9 (1-C), 147.5 (7-C), 141.7 (3-C), 125.6 (2-C), 120.0 (6-C), 113.2 (4-C), 31.3 (9-C), 28.8 (10-C), 28.5 (12-C), 25.5 (8-C), 22.5 (11-C), 14.0 (13-C) m/z (ES+) 501 $[M\text{-}Cl]^+$, 542 $[M\text{-}Cl+MeCN]^+$; HRMS (ES+) $C_{18}H_{21}N_5O_3{}^{187}Re$ $[M\text{-}Cl+MeCN]^+$ requires 542.1186 found 540.1202.

6.3.17 $[Re(CO)_3(L13)(L16.Boc)]BF_4$ (ReL13.L16.Boc)

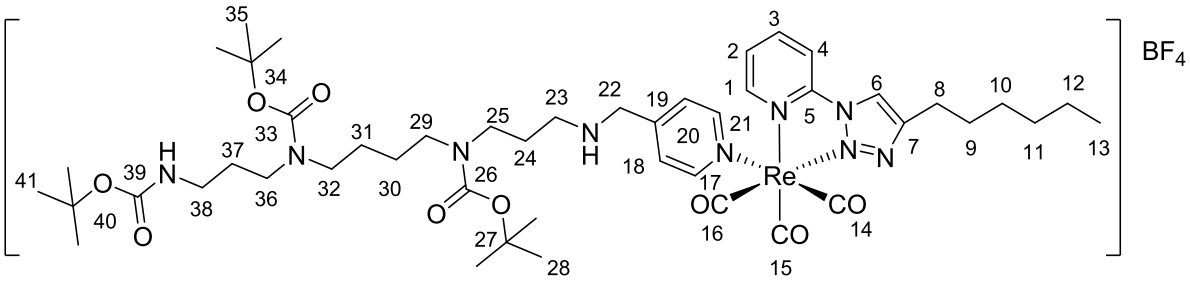

ReL13 (0.13 g, 0.23 mmole) and $AgBF_4$ (0.07g, 0.34 mmol) were dissolved in MeCN (10ml) and heated in microwave at 90 °C for 1hr and then solvent was filtered through celite and then evaporated to give crude and then dissolved in THF and then **L16.Boc** (0.21 g, 0.35 mmol) was added and placed heated in microwave at 90°C for 4hr. Solution was filtered through the celite and then evaporated in *vacuo* to give brown sticky product as crude (0.25 g) and then purified by RF-HPLC at 30.4 min to give (0.06g); ^{1}H NMR (400 MHz, MeOD), δ 9.29 (d, *J* = 5.7 Hz, 1H, 1-CH), 9.19 (s, 1H, 6-CH) 8.57 (d, *J* = 6.5 Hz, 2H, 17, 21-CH), 8.49 (ddd, *J* = 8.6, 8.1, 1.6Hz, 1H, 3-CH), 8.31 (d, *J* = 8.4 Hz, 1H, 4-CH), 7.87 (ddd, *J* = 7.7, 5.6, 1.0 Hz, 1H, 2-CH), 7.56 (d, *J* = 6.5 Hz, 2H, 18, 19-CH), 4.25 (s br, 2H, 22-CH), 3.25-3.20 (m, 10H, 25, 29, 32, 36, 38-CH_2), 3.08-3.03 (m, 4H, 23, 24-CH_2), 3.01-2.93 (m, 2H, 8-CH_2), 1.96-1.93 (m, 2H, 30-CH_2), 1.88-1.84 (m, 2H, 31-CH), 1.69 (s br, 2H, 37-CH), 1.50 (s br, 18H, 9, 10, 11, 12-CH_2), 1.45 (m, 27H, 28, 35, 41-3$(CH_3)_3$, 0.96(t, *J* = 7.0 Hz, 3H, 13-CH_3); ^{13}C NMR (100 MHz, MeOD), δ 195.7 (14-C), 194.5 (15-C), 191.3 (16-C), 159.1 (5-C), 155.0 (1-C), 154.0 (17, 21-C), 145.4 (7-C), 145.3 (3-C), 128.6 (2-C), 128.1 (18, 20-C),126.6 (19-C), 120.1 (6-C), 115.3 (4-C) 81.4, 81.2, 81.0 (27, 34, 40-C), 50.2 (38-C), 49.2 (25, 29-C), 48.5 (32, 36-C),45.5 (23-C), 36.5 (9, 37-C), 32.5 (24-C), 29.7 (8-C), 26.5 (12,

30, 31-C), 23.5 (10-C), 22.5 (11-C), 14.4 (13-C); MS (ES+) *m/z* 1095 $[M]^+$; HRMS (ES+) $C_{47}H_{73}N_9O_9{}^{187}Re$ $[M]^+$ requires 1094.5123 found 1094.5089.

6.3.18 $[Re(CO)_3(L13)(L16)](CF_3CO_2)_5$ (ReL13.L16)

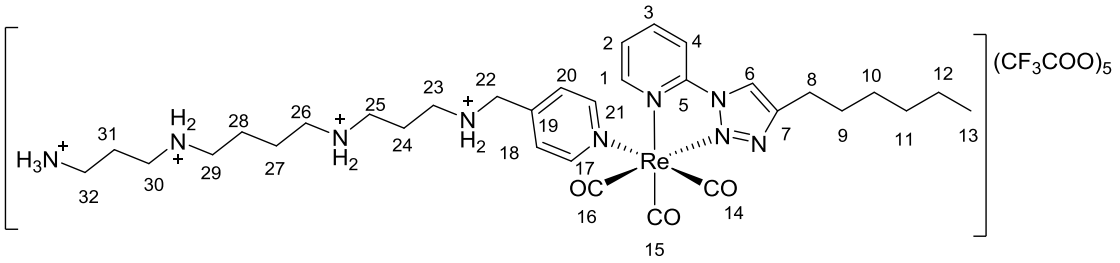

ReL13.L16.Boc (0.06 g, 0.05 mmol) was dissolved in 4M TFA and stirred at rt. for 18hr. and then the solvent was removed under *vacuo* to produce the product (0.04 g) without further purification. ^{1}H NMR (500 MHz, MeOD), δ 9.29 (d, *J* = 5.7 Hz,1H, 1-CH), 9.19 (s, 1H, 6-C), 8.54 (d, *J* = 6.5 Hz, 2H, 17, 21-CH), 8.48 (ddd, *J* = 8.7, 8.1, 1.4 Hz, 1H, 3-CH), 8.31 (d, *J* = 8.3 Hz, 1H, 4-CH), 7.87 (ddd, *J* = 7.9, 6.6, 0.8 Hz, 1H, 2-CH), 7.56 (d, *J* = 6.5 Hz, 2H, 18, 20-CH), 4.27 (s, 2H, 22-CH_2), 3.22 (t, *J* = 7.5 Hz, 2H, 32-CH_2), 3.14 (t, *J* = 7.6 Hz, 4H, 23, 25-CH_2), 3.07 (t, *J* = 7.5 Hz, 6H, 26, 29, 30-CH_2), 2.97-2.93 (m, 2H, 8-CH_2), 2.18-2.14 (m, 2H, 24-CH_2), 2.11-2.06 (m, 2H, 31-CH), 1.81-1.79 (m, 4H, 28, 27-CH_2), 1.53-1.48 (m, 2H, 9-CH_2), 1.44-1.38 (m, 6H, 10, 11, 12-CH_2), 0.96 (t, *J* = 6.9 Hz, 3H, 13-CH_3); ^{13}C NMR (125 MHz, MeOD), δ 196.6, 195.7, 194.1(14, 15, 16-C), 154.9 (5-C), 154.4 (1-C), 153.8 (17, 21-C), 149.4 (7-C), 146.1 (19-C), 145.2 (3-C), 128.6 (2-C), 128.2 (18, 20-C), 125.1 (6-C), 116.3 (4-C), 50.3 (22-C), 48.1 (32-C), 46.3 (23-C), 45.8 (30-C), 37.8 (25, 26-C), 32.6 (31-C), 29.8 (27-C), 29.6 (28-C), 26.4 (8-C), 25.3 (24-C), 24.1 (9, 10-C), 23.5 (11, 12-C), 14.3 (13-C); MS (ES+) *m/z* 794 $[M-5(CF_3COO)]^+$; HRMS (ES+) $C_{32}H_{49}N_9O_3{}^{187}Re$ $[M]^+$ requires 794.3555 found 794.3516.

6.3.19 $[Re(CO)_3(L14.Boc)\ (L17)]BF_4$ (ReL14.Boc.L17)

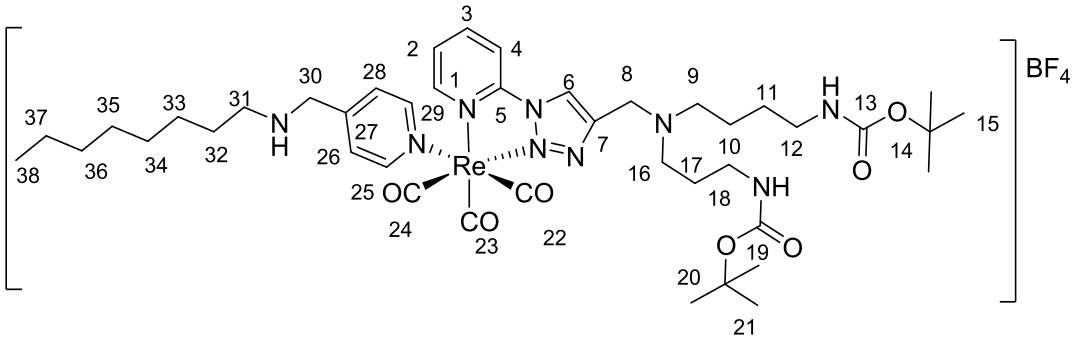

ReL14.Boc.L17 was prepared by dissolved $Re(CO)_5Cl$ (0.03 g, 0.08 mmol) and **L14.Boc** (0.04 g, 0.08 mmol) in toluene and then the solution was refluxed under nitrogen at 110ºC for 18hr. the solvent was removed in *vacuo* to give (0.06 g) of product. The product was purified by column chromatography to yield **ReL14.Boc**. This product was dissolved in MeCN and then $AgBF_4$ (0.02g, 0.10 mmol) was added and heated in microwave at 90ºC for 30min The solution was filtered through celite and then solvent was removed to give yellow precipitate. This product was dissolved in THF and then **L17** (0.02 g, 0.10 mmol) was added and heated in microwave for 4hr. The solution was filtered through celite and then the solvent was removed under *vacuo* to produce (0.08 g) of crude and then the crude was purified by RP-HPLC at 25 min to produce (0.03g) of **ReL14.Boc.L17**. ^{1}H NMR (500MHz, MeOD), δ 9.77 (bs, 1H, 6-CH), 9.35 (d, *J* = 5.3 Hz, 1H, 1-CH), 8.45 (d, *J* = 6.1 Hz, 2H, 25, 29-CH), 8.45 (d, *J* = 8.3 Hz, 1H, 4-CH), 8.12 (ddd, *J* = 8.4, 7.7, 1.5 Hz, 1H, 3-CH), 7.96 (ddd, *J* = 7.8, 6.2 Hz,1H, 2-CH), 7.57 (d, *J* = 6.3 Hz, 2H, 26, 28-CH), 4.88 (s br, 2H, 8-CH_2), 4.26 (s, 2H, 30-CH_2), 3.21-3.17 (m, 2H, 12-CH_2), 3.15-3.12 (m, 2H, 18-CH_2), 3.07 (t, *J* = 7.8 Hz, 2H, 9-CH_2), 2.10-2.02 (m, 2H, 16-CH_2), 1.94-1.90 (m, 2H, 17-CH_2) 1.73-1.67 (m, 2H, 10), 1.63-1.56 (m, 2H, 11-CH_2), 1.44 (m, 18H, 2x (NHBoc), 1.36-1.30 (m, 10H, 33, 34 , 35, 36, 37-CH_2), 0.90 (t. *J* = 6.7Hz, 3H, 38-CH_3); ^{13}C NMR (125 MHz, MeOD), δ 195.3, 193.9, 192.0 (22, 23, 24-C), 154.4 (27-C), 154.0 (25, 29-C), 149.9 (5-C), 146.1 (7- C), 141.1 (3- C),128.8 (2-C), 128.4 (26, 28-C),126.6 (6-C), 117.8 (4-C), 80.5, 8.1 (14, 20-C), 52.4 (12-C), 52.2 (18-C,), 47.6 (8-C), 47.3 (9-C), 40.3 (16-C), 38.1 (31-C), 32.8 (33, 34-C), 28.7 (15, 21-C), 28.1 (35-C), 25.9 (17-C), 25.8 (32-C), 23.6 (10, 11-C), 22.3 (36, 37-C); MS (ES+): 994 $[M]^+$, HRMS (ES+) $C_{42}H_{65}N_9O_7{}^{187}Re$ $[M]^+$ requires 994.4574 found 994.4565.

6.3.20 $[Re(CO)_3(L14)(L17)](CF_3COO)_4$ (ReL14.L17)

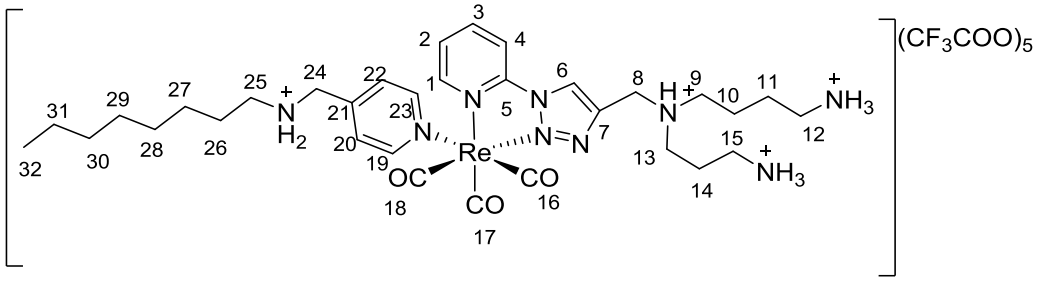

ReL14.Boc.L17 (0.03g, 0.02 mmol) was dissolved in (4M) TFA/DCM and stirred at rt. for 18hr. The solvent was removed under *vacuo* to produce (0.036 g) of product without further purification. ^{1}H NMR (500MHz, MeOD), δ 9.62 (s br, 1H, 6-CH), 9.17 (d, *J* = 5.4 Hz, 1H,1-CH), 8.93 (d, *J* = 6.0 Hz, 2H, 19, 23-CH), 8.04 (d, *J* = 8.2 Hz, 1H, 4-CH), 7.94 (ddd, *J* = 8.4, 8.2, 1.4Hz, 1H, 3-CH), 7.77(ddd, *J* = 7.6, 6.5 Hz, 1H, 2-CH), 7.39 (d, *J* = 5.1 Hz, 2H, 20, 22-CH), 4.53 (s br, 2H, 24-CH_2), 4.38 (s, 2H, 8-CH_2), 3.28 (t, *J* = 7.6 Hz, 2H, 12 -CH_2), 3.23-3.18 (m, 2H, 15-CH_2), 2.19-2.85 (m, 4H, 9, 13-CH_2), 2.16-2.10 (m, 2H, 25-CH_2), 1.88-1.82 (m, 2H, 14-CH_2), 1.67-1.59 (m, 4H, 10, 11-CH_2), 1.55-1.48 (m, 2H, 26-CH_2), 1.16-1.12 (m, 10H, 27, 28 , 29, 30, 31-CH_2), 0.70 (t. *J* = 7.2 Hz, 3H, 32-CH_3); ^{13}C NMR (125 MHz, MeOD), δ 194.0, 193.5, 190.4 (16, 17, 18-CO), 161.7 (q, *J* = 38.1 Hz,$CF_3CO_2^-$), 154.6, 154.0 (19, 23-C), 150.1 (1-C), 149.1 (21-C), 146.4 (5-C), 142.6 (7-C), 141.1 (3-C), 129.3 (6-C), 128.3 (2-C), 125.8 (20-C), 125.4 (22-C), 115.0 (4-C), 51.1 (24-C), 50.5 (12-C), 47.3 (8, 13-C), 40.0 (9-C), 37.8 (15-C), 32.8 (27-C), 30.1 (28-C), 27.5 (29-C), 27.1 (30-C), 25.6 (11-C), 23.6 (10-C), 22.1 (14, 25, 31-C), 14.4 (32-C) ; ^{19}F NMR (500MHz, MeOD) δ -76.8 (s, 3F-CF_3CO_2); MS (ES+) *m/z*: 794 $[M]^+$, HRMS (ES+) $C_{32}H_{49}N_9O_3{}^{187}Re$ $[M]^+$ requires 794.3643 found 794.3516.

6.3.21 $[Re(CO)_3(L15.Boc)(L17)]BF_4$ (ReL15.Boc.L17)

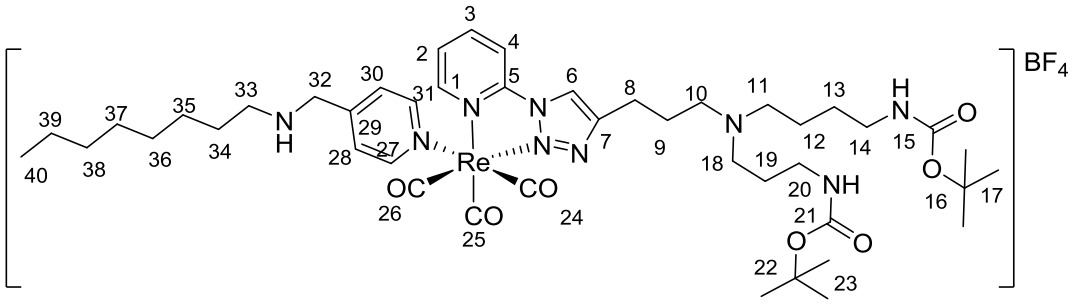

ReL15.Boc (0.05 g, 0.06 mmol) was dissolved in MeCN and then $AgBF_4$ (0.02 g, 0.08 mmol) was added and heated in microwave at 90ºC for 30 min and then white precipitate was formed. The solution was filtered through celite and then solvent was removed to give precipitate residue. This residue was dissolved in THF and then **L17**

(0.02 g, 0.07 mmol) was added and then heated in microwave for 4hr after that the solution was filtered through celite and then the solvent was removed under *vacuo* to produce (0.06g) of crude and then the crude was purified by RP-HPLC at 25 min to produce (0.03g) of product. ^{1}H NMR (500MHz, MeOD), δ 9.31 (d, *J* = 5.8 Hz, 1H,1-CH), 9.29 (s br, 1H, 6-CH), 8.55 (d, *J* = 6.4 Hz, 2H, 27, 31-CH), 8.51 (ddd, *J* = 8.6, 7.2 Hz, 1H, 3-CH), 8.34 (d, *J* = 8.3 Hz, 1H, 4-CH), 7.89 (ddd, *J* = 7.0, 6.4 Hz, 1H, 2-CH), 7.56 (d, *J* = 6.4 Hz, 2H, 28, 30-CH), 4.25 (s broad, 2H, 32-CH_2), 3.40-3.38 (m, 2H, 18-CH_2), 3.33 (m, 2H, 20-CH_2), 3.27 (t, *J* = 7.6 Hz, 4H, 8, 10 -CH_2), 3.19 (t, *J* = 6.4 Hz, 2H, 11-CH_2), 3.13 (t, *J* = 6.7 Hz, 2H, 14-CH_2), 3.07 (t, *J* = 7.1 Hz, 2H, 32-CH_2), 2.32 (m, 2H, 9-CH_2), 1.99-1.93 (m, 2H, 19-CH_2), 1.83-1.77 (m, 2H, 12-CH_2), 1.72-1.66 (m, 2H, 13-CH_2), 1.62-1.56 (m, 2H, 34-CH_2), 1.45 (s, 18H, 17, 23-$(CH_3)_3$), 1.34-1.30 (m, 12H, 34, 35, 36, 37, 38, 39-CH_2), 0.90 (t, *J* = 6.7 Hz, 3H, 40-CH_3); ^{13}C NMR (125 MHz, MeOD), δ 195.5, 194.3, 190.9 (24, 25, 26-CO), 154.7 (1-C), 154.0 (27, 31-C), 152.7 (7-C), 149.4 (5-C), 146.5 (29-C), 128.9 (2-C), 128.4 (28, 30-C), 125.9 (6-C), 116.6 (4-C), 81.2, 80.7 (16, 22-C), 53.3 (18-C), 52.1 (20-C), 50.2 (11, 32-C), 40.4 (8-C), 38.4 (10-C), 32.9 (39-C), 30.2 (37, 38-C), 28.93, 28.90 (17, 23-C), 28.2 (36-C), 27.5 (13-C), 27.3 (12-C), 25.8 (9-C), 23.8 (35-C), 23.7 (33, 34-C), 23.5 (14-C), 22.2 (19-C), 14.5 (40-C). MS (ES+): 1022 $[M]^+$, HRMS (ES+) $C_{44}H_{69}N_9O_7{}^{187}Re$ $[M]^+$ requires 1022.4919 found 1022.4878.

6. 3.22$[Re(CO)_3(L15)(L17)](CF_3CO_2)_5$ (ReL15.L17)

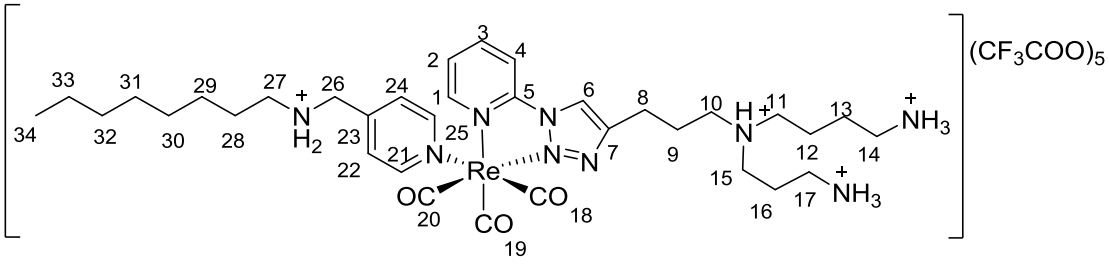

ReL15.Boc.L17 (0.03g, 0.027 mmol) was dissolved in (4M) TFA and stirred at rt for 18hr and then solvent was removed in *vacuo* to produce (0.035 g) of product without further purification. ^{1}H NMR (500MHz, MeOD), δ 9.19 (d, *J* = 5.4 Hz, 2H,1, 6-CH), 8.43 (d, *J* = 5.5 Hz, 2H, 21, 25-CH), 8.38 (dd, *J* = 7.3, 6.8 Hz, 1H, 3-CH), 8.23 (dd, *J* = 9.7, 7.9 Hz, 1H, 4-CH), 7.78 (ddd, *J* = 7.5, 6.6 Hz, 1H, 2-CH), 7.44 (d, *J* = 5.6 Hz, 2H, 22, 24-CH), 4.1 (s br, 2H, 26-CH_2), 3.32-3.25 (m, 4H, 15,17-CH_2), 3.00-2.88 (m, 8H, 8, 10, 11, 14-CH_2), 2.23 (t, *J* = 6.8 Hz, 2H, 27-CH_2), 2.10-2.07 (m, 2H, 9-CH_2), 1.85-1.76 (m, 2H, 16-CH_2), 1.67-1.64 (m, 2H, 12-CH_2), 1.60-1.54 (m, 2H, 13-CH_2), 1.22-1.19 (m,

12H, 27-33-CH_2), 0.78 (t, *J* = 6.8 Hz, 3H, 34-CH_3); ^{13}C NMR (125 MHz, MeOD), δ 196.1, 194.3, 191.3 (18, 19, & 20), 154.5 (1-C), 153.9 (21, 25-C), 152.6 (7-C), 149.6 (5-C), 146.4 (23-C), 145.4 (3-C), 128.8 (2-C), 128.3 (22, 24-C), 125.8 (6-C), 116.5 (4-C), 53.7 (15-C), 53.5 (17-C), 51.1 (10-C), 50.1 (26-C), 40.0 (11-C), 37.8 (8-C), 32.8 (28-C), 30.1 (29, 30-C), 29.4 (31-C), 27.4 (12-C), 27.1 (12-C), 25.6 (32-C), 23.2 (27-C), 23.6 (9-C), 22.9 (28-C), 21.6 (14, 33-C), 21.4 (16-C), 14.3 (34-C); MS(ES$^+$) 822 $[M]^+$, HRMS (ES+) $C_{34}H_{53}N_9O_3{}^{187}Re$ $[M]^+$ requires 822.3832 found 822.3829.

6.3. 23[Re(CO)$_3$(L6.Boc)(L18)] BF_4 (ReL6.Boc.L18)

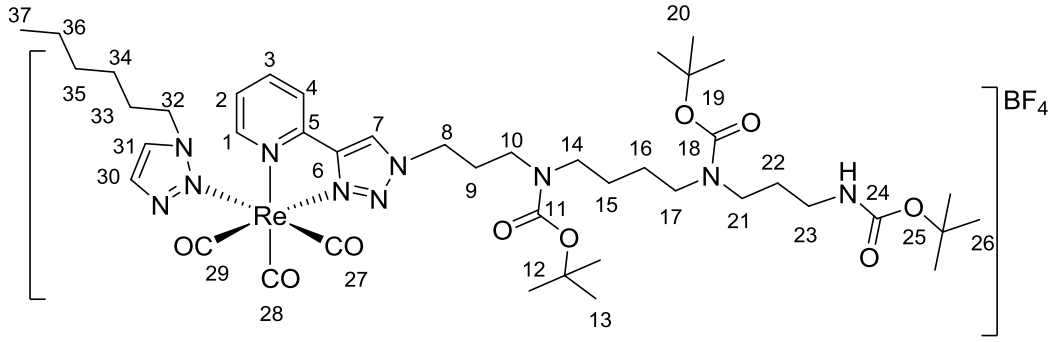

ReL6.Boc (0.05 g, 0.05 mmol) was dissolved in MeCN and followed by $AgBF_4$ (0.02g, 0.08mmol) and heated in microwave at 90ºC for 1hr. the solution was filtered through celite and then the solvent was removed in *vacuo*. The residue precipitate was dissolved in THF and **L18** (0.012 g, 0.08 mmol) was added to the solution and heated in microwave at 90ºC for 3hr. and then solution was filtered through celite and then solvent was removed in *vacuo* to obtain oily crude (0.08 g). This crude was purified by RP-HPLC method A, at tR = 35 min the product was obtained (0.03 g) as a pure product. ^{1}H NMR (500 MHz, MeOD), δ 9.13 (d, *J* = 5.4 Hz, 1 H,1-CH), 9.10 (br s, 1 H, 7-CH), 8.28 (ddd, *J* = 8.5, 7.2, 1.0Hz, 1 H, 3-CH), 8.20 (d, *J* =7.9 Hz, 1 H, 4-CH), 8.06 (s br, 1 H, 30-CH), 7.83 (s, 1 H, 31-CH), 7.67 (ddd, *J* = 7.6, 6.2, 0.9 Hz, 1 H, 2-CH), 4.68 (t, *J* = 6.4 Hz, 2 H, 8-CH), 4.23 (ddd, *J* = 7.3, 6.9, 2.3 Hz, 2 H, 32-CH_2), 3.30-3.26 (m, 2 H, 23-CH_2), 3.26-3.22 (m, 4 H, 10, 14-CH_2), 3.07-3.03 (m, , 2 H, 17-CH_2), 2.30-2.31 (m, 2 H, 21-CH_2), 1.62 - 1.74 (m, 4H 9, 22-CH_2), 1.58-1.53 (m, 4 H, 15, 16-CH_2), 1.44 - 1.49 (m, 27 H, 13, 20, 26(CH_3)$_3$), 1.27 - 1.35 (m, 4H, 33, 34-CH_2), 0.95 - 1.01 (m, 4 H, 35, 36-CH_2), 0.86 - 0.90 (m, 3H, 37-CH_3); ^{13}C NMR (125 MHz, MeOD), δ 196.8 (27-C), 193.9 (28-C), 192.3 (29-C), 157.2 (5-C), 155.1 (1-C), 151.1 (6-C), 142.4 (3-C), 137.8 (30-C), 125.1 (31-C), 128.0 (2-C), 123.8 (7-C), 123.5 (4-C), 81.3, 81.0, 80.0 (12, 19, 25-C), 52.6 (32-C), 50.0 (8-C), 47.4 (10, 14-C), 45.9 (17, 21-C), 38.7 (23-C), 34.8 (9, 22-C), 30.9 (15-C), 30.4 (16-C), 28.8 (13, 20, 26), 27.1 (33-C), 26.7 (34-C),

23.5, 23.4 (36, 37-C), 14.3 (37-C). MS (ES+) 1055 $[M]^+$; HRMS (ES+) $C_{43}H_{68}N_{10}O_9{}^{187}Re$ $[M]^+$ requires 1055.4760 found 1055.4728.

6.3.24 $[Re(CO)_3(L6)(L18)]$ $(CF_3CO_2)_4$ (ReL6.L18)

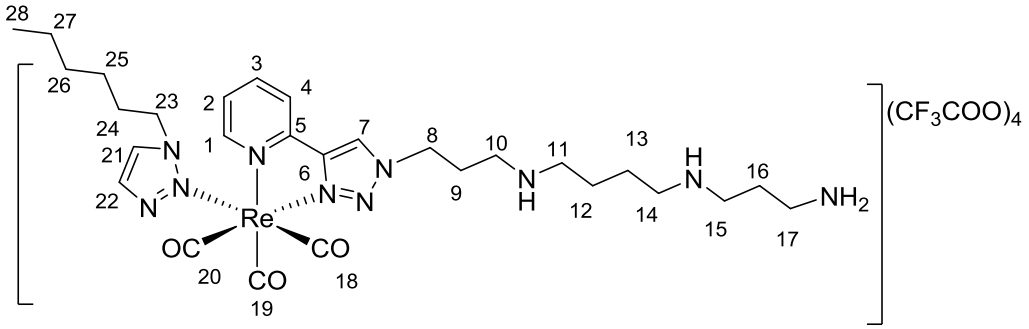

ReL6.L18 (0.03 g, 0.026 mmol) was dissolved in 4M TFA in DCM and stirred at rt. for 18hr. The volatiles were removed to produce the product (0.035g) without further purification. ^{1}H NMR (AV-400 MHz, MeOD), δ 9.13 (d, *J* = 5.9 Hz, 1 H, 1-CH), 9.12 (s, 1 H, 7-CH), 8.29 (ddd, *J* = 8.3, 7.3, 0.9 Hz, 1 H, 3-CH), 8.22 (d, *J* = 8.7 Hz, 1 H, 4-CH), 8.06 (d, *J* = 1.2 Hz, 1 H, 21-CH), 7.79 (d, *J* = 1.2 Hz, 1 H, 22-CH), 7.67 (ddd, *J* = 7.8, 6.5, 0.9 Hz, 1 H, 2-CH), 4.83-4.77 (m, 2 H, 8-CH), 4.26-4.16 (m, 2 H, 23-CH_2), 3.23 (t, *J* = 7.5 Hz, 2 H, 17-CH_2), 3.17-3.05 (m, 8H, 10, 11, 14, 15-CH_2), 2.55-2.46 (m, 2 H, 9-CH_2), 2.13-2.06 (m, 2 H, 16-CH_2), 1.85-1.83 (m, 6H, 12, 13, 24-CH_2), 1.69-1.61 (m, 25, 26 -CH_2), 0.90-0.85 (m, 5H, 27, 28- (CH_3). ^{13}C NMR (100 MHz, MeOD), δ 195.5 (18-C), 194.9 (19-C), 192.9 (20-C),169.0 (q, *J* = 34.17, CF_3CO_2), 153.2 (1-C), 151.2 (5-C), 151.1 (6-C), 142.6 (3-C), 138.6 (22-C), 128.7 (2-C), 128.2 (21-C),127.4 (7-C), 124.1 (4-C), 52.7 (23-C), 50.7 (8-C), 48.4 (11-C), 46.0 (10, 17-C), 37.9 (14, 15-C), 32.1 (27-C), 31.0 (24-C), 27.5 (9-C), 27.1 (26-C), 25.5 (16-C), 24.4 (12-C), 24.3 (13-C), 23.6 (25-C), 14.4 (28-C); ^{19}F NMR (400MHz, MeOD), δ -77.2 (s, 3F-CF_3CO_2); MS (ES+) 755 $[M\text{-}4(CF_3COO)]^+$; HRMS (ES+) $C_{28}H_{44}N_{10}O_3{}^{187}Re$ $[M]^+$ requires 755.3188 found 755.3156.

6.3.25 [Re (CO) $_3$(L9.Boc) (L18)]BF_4 (ReL9.Boc.L18)

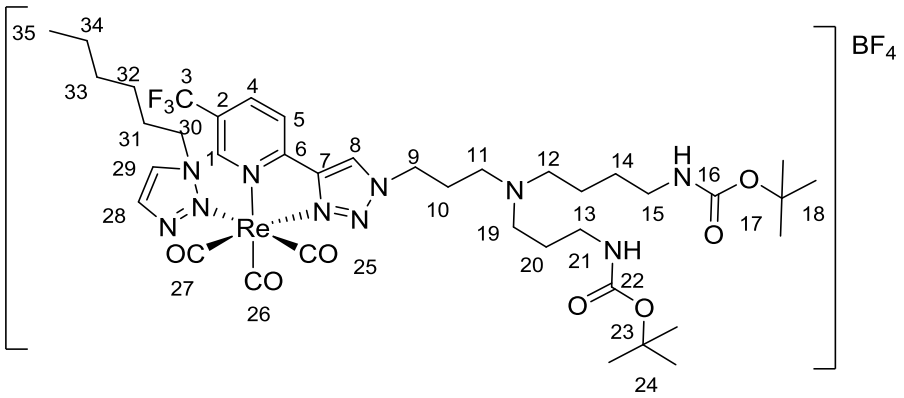

ReL9.Boc (0.06 g, 0.06 mmol) was dissolved in MeCN and $AgBF_4$ (0.017 g, 0.09 mmol) was added to the solution and then heated in microwave at 90ºC for 1hr. The suspension was filtered through celite. Solvent was removed in *vacuo* to form a yellow precipitate. The product was dissolved in THF and **L18** (0.018 g, 0.09 mmol) was added to the solution and heated in microwave at 90ºC for 3hr. The solution was filtered through celite and then the solvent was removed in *vacuo* to produce (0.13g) as a crude of product. The crude was purified by RP-HPLC method A, t_R = 28 min to produce (0.09 g) of pure product. ^{1}H NMR (500 MHz, MeOD), δ 9.32 (s, 2 H, 1-CH), 9.31 (s, 1H, 8-C), 8.68 (d, *J* = 7.6 HZ, 1H, 4-CH), 8. 46 (d, *J* = 8.4 Hz, 1 H, 5-CH), 8.10 (s, 1 H, 28-CH), 7.87 (s, 1 H, 29-CH), 4.84-4.78 (m, 2H, 8-CH_2), 4.28-4.17 (m, 2H, 30-CH_2), 3.41 (t, *J* = 7.1 Hz, 2 H, 15-CH), 3.28-3.24 (m, 4 H, 11, 21-CH_2), 3.17 (t, *J* = 6.4 Hz, 2 H, 12-CH_2), 3.11 (t, 6.7 Hz, 2H, 19-CH), 2.58-2.56 (m, 2H, 10-CH_2), 1.81-1.74 (m, 2 H, 20-CH_2), 1.67-1.63 (m, 2H, 13-CH_2), 1.60-1.55 (m, 2H, 14- CH_2), 1.45 (s, 18H, 18, 24-2(CH_3)$_3$), 1.35-1.33 (m, 6H, 31, 32, 33-CH_2), 1.24-1.20 (m, 2H, 34-CH_2), 1.01-0.89 (m, 3H, 35-CH_3). ^{13}C NMR (125 MHz, MeOD), δ 196.21 (25-C), 194.91 (26-C), 192.15 (27-C), 154.5 (2,6-C), 151.24 (1-C), 150.01 (7-C), 139.97 (4, 5-C), 138.85 (29-C), 129.01 (8-C), 128.28 (28-C), 124.3 (3-C), 52.7 (30-C), 51.4 (11, 21-C), 50.8 (15-C), 50.6 (8-C), 40.3 (19-C), 38.3 (12-C), 32.3 (10-C), 31.3 (32, 33-C), 30.3 (13-C), 28.8 (18, 24-C), 26.6 (14-C), 25.6 (34-C), 23.5 (31-C), 22.1 (20-C), 14.3 (35-C); ^{19}F NMR (500MHz, MeOD), δ -64.1 (s, 3F-py); MS (ES+) 1023 $[M\text{-}BF_4]^+$; HRMS (ES+) $C_{39}H_{59}N_{10}O_7F_3{}^{187}Re$ $[M]^+$ requires 1023.4078 found 1023.4078.

6.3.26 [Re(CO)$_3$(L9)(L18)](CF$_3$CO$_2$)$_4$ (ReL9.L18)

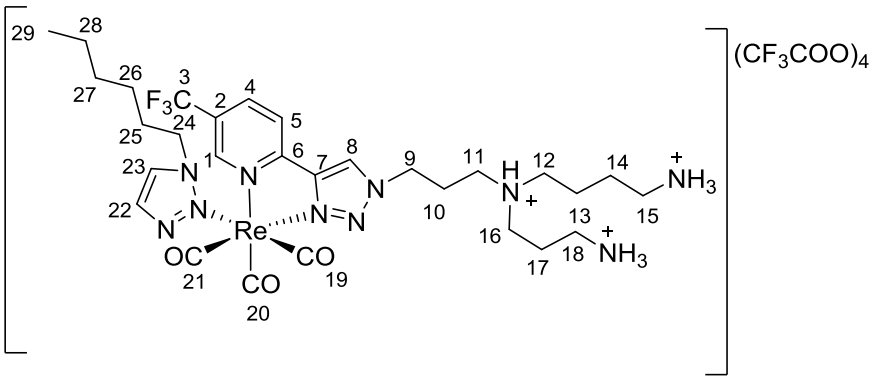

ReL9.Boc.L18 (0.03 g, 0.027 mmol) was dissolved in 4M TFA in DCM and stirred at rt. for 18h. The volatiles were removed to produce the product (0.04 g) without further purification. ^{1}H NMR (500 MHz, MeOD), δ 9.32 (s, 1H, 1-CH), 9.31 (s, 1H, 8-CH), 8.69 (d, *J* = 8.3 HZ, 1H, 4-CH), 8.46 (d, *J* = 8.4 Hz, 1 H, 5-CH), 8.1 (s, 1 H, 22-CH), 7.87 (s, 1 H, 23-CH), 4.85-4.78 (m, 2H, 9-CH), 4.27-4.16 (m, 2 H, 24-CH$_2$), 3.45 (t, *J* = 7.9 Hz, 2 H, 15-CH$_2$), 3.37 (t, *J* = 8.2 Hz, 2 H, 18-CH$_2$), 3.31- 3.30 (m, 2H, 11-CH$_2$), 3.08 (t, *J* = 7.3 Hz, 2H, 12-CH$_2$), 3.02 (t, *J* = 7.5 Hz, 16-CH$_2$), 2.6 (p, *J* = 7.4 Hz, 10-CH$_2$), 2.19 (p, *J* = 7.9 Hz, 17-CH$_2$), 1.92-1.89 (m, 2 H, 13-CH$_2$), 1.80-1.74 (m, 2 H, 14-CH$_2$), 1.66-1.61 (m, 2H, 25-CH$_2$), 1.60-1.55 (m, 2H, 31 -CH$_2$), 1.25-1.13 (m, 26, 27-CH$_2$), 0.99-0.95 (m, 2H, 28-CH$_2$), 0.87 (t, *J* = 6.8 Hz, 3H, 29-CH$_3$). ^{13}C NMR (125 MHz, MeOD), δ 196.2, 195.0, 192.2 (19, 20, 21-CO), 160.9 (q, *J* = 38.2 Hz, CF$_3$CO$_2$), 155.5 (6-C), 154.5 (2-C), 151.7 (1-C), 149.9 (7-C), 139.9 (4-C), 138.8 (23-C), 129.0 (22-C), 128.7 (8-C), 124.3 (3, 5-C), 52.6 (11-C), 51.5 (24-C), 51.3 (15-C), 51.1 (18-C), 50.6 (9-C), 39.9 (16-C), 37.8 (12-C), 31.9 (27-C), 31.2 (13, 14-C), 30.3 (26-C), 25.5 (28-C), 25.1 (25-C), 23.5 (10-C), 21.9 (17-C), 14.3 (29-C); ^{19}F NMR (500MHz, MeOD), δ -64.2 (s, 3F-py), -77.2 (s, 3F-CF$_3$CO$_2$); MS (ES+) 823 [M]$^+$; HRMS (ES+) $C_{29}H_{43}N_{10}O_3F_3{}^{187}Re$ [M]$^+$ requires 823.3053 found 823.3029.

6.4 Synthesis of Iridium(III) Complexes

6.4.1 General procedure to synthesise of [Ir(HCN)$_2$Cl]$_2$ dimer (Method A)[87]

IrCl$_3$. 6H$_2$O (1 eq) and cyclometalated ligand (2.2 eq) were placed in a microwave tube and 2-propanol/water (3:1, 4mL) was added. N$_2$ was bubbled for 2 min through the

solution and then tube sealed with septum cap and heating in microwave at 110ºC for 90 min with power 100 w at pressure 150 psi a yellow solution was obtained. After that the solvent was removed in *vacuo* leaving behind a solid which was dissolved in DCM (15 mL) and passed through celite. The filtrate was reduced in volume and hexane was added slowly to induce precipitation a pale yellow solid which was wash with EtOAc and then the solid was isolated by filtering to yield a desired product.

6.4.2 Synthesis of $[Ir(HL1)_2Cl]_2$ dimer $[Ir\ (L1)_2Cl]_2$

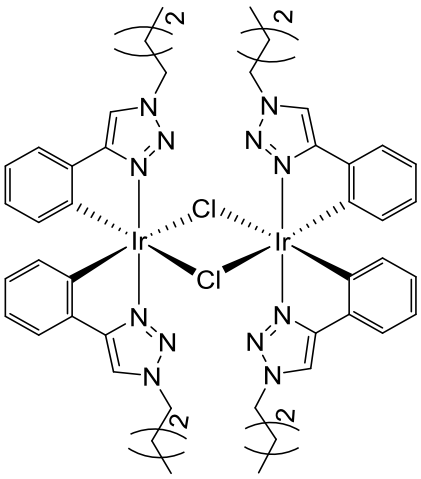

This was prepared from $IrCl_3.\ 6H_2O$ (0.10 g, 0.28 mmol) and 1- butan-4-phenyl 1,2,3-triazol (**HL1**) (0.13 g, 0.62 mmol) according to general procedure (method A) and after work up gave a pale yellow solid with yield (0.81 g, 92 %). ^1H NMR (400MHz, CD_2Cl_2) is unclear. MS (ES+) *m/z* 593 $[M/2\text{-}Cl]^+$; HRMS (ES+) $[M/2\text{-}Cl]^+$ $C_{24}H_{28}N_{12}{}^{193}Ir$ require 593.1996 found 593.2005.

6.4.3 Synthesis of $[Ir(HL2)_2Cl]_2$ dimer $[Ir\ (L2)_2Cl]_2$

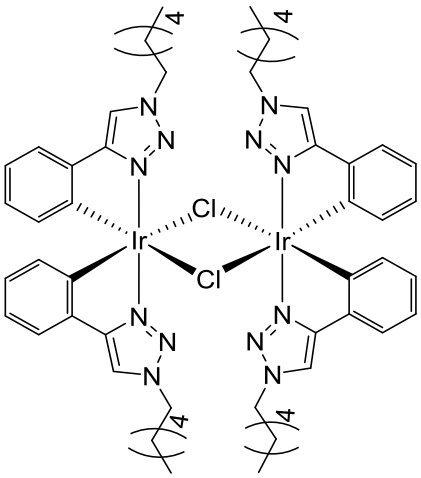

This was prepared from $IrCl_3.6H_2O$ (0.05 g, 0.14 mmol) and **HL2** (0.071 g, 0.31 mmol) after work up gave as a pale yellow solid with yield (0.05 g, 54%). MS (ES+) *m/z*: 732 $[(M/2\text{-}Cl) + 2MeCN]^+$; HRMS (ES+) $[M/2\text{-}Cl]^+$ $C_{32}H_{42}N_8{}^{191}Ir$ require 731.3163 found 731.3206.

6.4.4 Synthesis of $[Ir(HL4)_2Cl]_2$ dimer $[Ir(L4)_2Cl]_2$

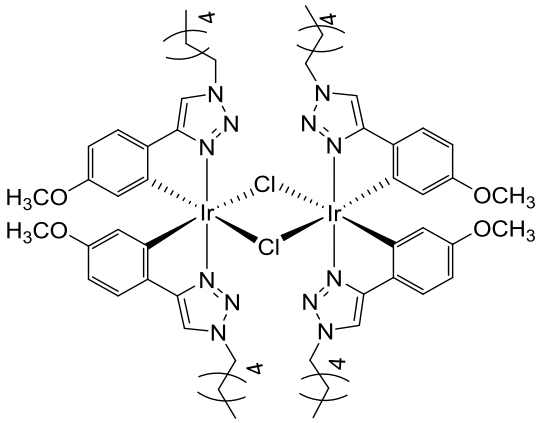

This was prepared from $IrCl_3.6H_2O$ (0.1 g, 0.28 mmol) and 4-(4-methoxyphenyl)-1-pentyl-1H-1, 2, 3-triazole **L4** (0.1618g, 0.60 mmol) according to general procedure (method A) and after work up gave as a yellow solid (0.209g, 73%); ^{1}HNMR was unclear; MS (ES) *m/z* 709 HRMS (ES+) $[M/2\text{-}Cl]^+$ $C_{30}H_{40}N_6O_2{}^{191}Ir$ require 709.2883 found 709.2885.

6.4.5 Synthesis of $[Ir(ppy)_2Cl]_2$ dimer[87, 231] $[Ir(ppy)_2Cl]_2$

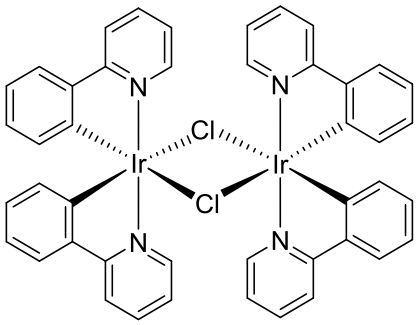

$IrCl_3.6H_2O$ (0.100 g, 0.28 mmol) and phenylpyridin **Hppy** (0.968 g, 0.623 mmol) were placed in a microwave vial and 2-propanol/water (4 mL) was added. Nitrogen was bubbled through the solution for 2 min the vial was then sealed with a septum cap and heated in a microwave reactor to 110°C for 90 min. Yellow precipitate was induced after removing the solvent in *vaccuo*. Precipitate was then passed through celite, solution was washed with dilute HCl (3X10 ml). After extracting the organic layer was

dried over Mg_2SO_4 and then filtered to resulting the desired product and isolated as a yellow solid (0.09 g, 63 %). ^{1}H NMR (400MHz, $CDCl_3$), δ 9.17 (d, *J* = 5.8 Hz, 4H, 1-CH), 7.79 (d, *J* = 7.9 Hz, 4H, 7-CH), 7.66 (ddd, *J* = 7.9, 7.8, 1.5 Hz, 4H, 4-CH) 7.41 (d, *J* = 7.7 Hz, 4H, 10-CH), 6.68 (m , 8H, 8, 9-CH), 6.48 (ddd, *J* = 8.3, 8.1, 3.4 Hz, 4H, 3-CH), 5.85 (d, *J* = 7.6 Hz, 4H, 2-CH).^{13}C NMR (100MHz, $CDCl_3$), δ 168.46 (1-C), 151.91 (2-C), 145.28 (3-C), 144.4 (4-C), 137.08 (5-C), 130.8 (8-C), 129.50 (7-C) , 124.08 (6-C); MS (ES) *m/z*, 1072 $[M]^+$, 1002 $[M+2Cl]^{+\cdot}$, 501 $[Ir(\mathbf{ppy})_2+H]^+$, 533 $[Ir(\mathbf{ppy})_2+H+MeOH]^+$.

6.4.6 Synthesis of $[Ir(HL12)_2Cl]_2$ dimer $[Ir(L12)_2Cl]_2$

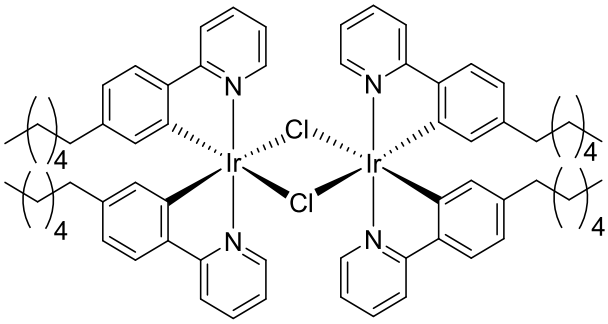

This was prepared from $IrCl_3.6H_2O$ (0.05 g, 0.14 mmol) and 2-(4-hexylphenyl) pyridine **HL12** (0.07g, 0.31 mmol) according to general procedure (method A) after work up gave as a brown solid as a brown solid with yield (0.11 g, 68%). MS (ES) *m/z*: 751 [(M/2-Cl) + 2MeCN]$^+$; HRMS (ES+) [M/2-Cl] $^+$ $C_{32}H_{42}N_8{}^{193}Ir$ require 751.3378 found 751.3352.

6.5 Synthesis of Cationic Iridium(III) Complexes

6.5.1 General Procedure to Synthesise Cationic Iridium(III) Complexes (Method B)

The iridium dimer (1 equiv), bipy (2.2 equiv) and KPF_6 (2.2 equiv) were placed in a microwave vial and methanol (4 ml) was added. Nitrogen was bubbled through the solution for 2 mins and the vial was then sealed with a septum cap and heated in the microwave reactor at 110°C for 90 min at pressure of 150 psi and power 50 W. After this time, the solvent was removed *in vacuo* leaving behind a solid which was dissolved in DCM (15 ml) and passed through celite. The solvent was removed in *vacuo* to yield a solid precipitate and then washed with EtOAc. The solid was isolated by simple filtered.

6.5.2 Synthesis of $[Ir(L1)_2L6.Boc]PF_6$ $Ir(L1)_2L6.Boc$

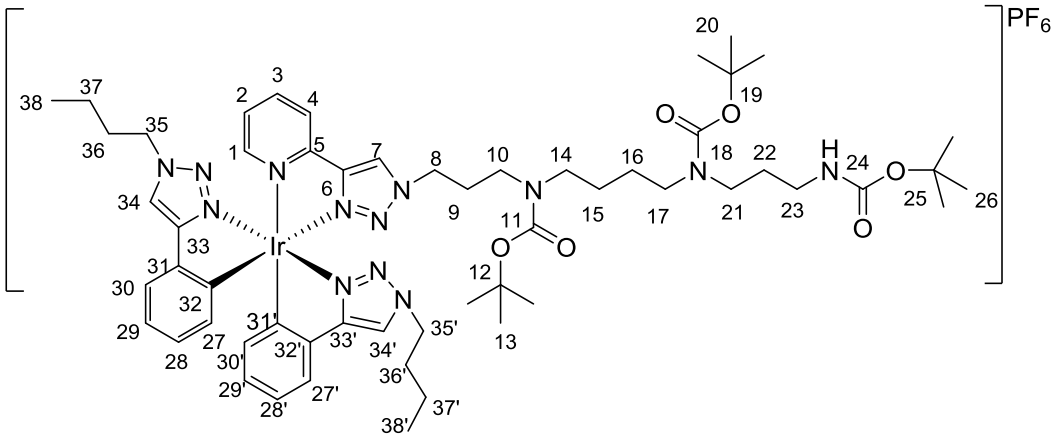

This was prepared from $[Ir(L1)_2Cl]_2$ dimer (0.06 mg, 0.05 mmol) **L6.Boc** (0.07 mg, 0.11 mmol) and KPF_6 (0.02mg, 0.11 mmol) according to method B and after work up gave a light green sold. The residue was purified through alumina, eluting with 5% MeOH in DCM (0.09 g, 69 %); ^{1}H NMR (500MHz, MeOD), δ 8.87 (s br,1H, 7-CH), 8.20 (d, *J* = 4.8 Hz, 2H, 34, 34'-CH), 8.04 (d, *J* = 7.9 Hz, 1-CH), 7.93 (ddd, *J* = 6.2, 6.1, 0.9 Hz, 2H, 3, 4-CH), 7.39 (d, *J* = 6.5 Hz, 1H, 30-CH), 7.35 (d, *J* = 6.5 Hz, 1H, 30`-CH),7.23 (m, 1H, 2-CH), 6.96 (ddd, *J* = 8.1, 7.5, 0.9 Hz, 1H, 29-CH), 6.88 (ddd, *J* = 8.2, 7.3, 1.0 Hz, 1H, 29'-CH), 6.81 (ddd, *J* = 8.1, 7.5, 1.0Hz, 1H, 28-CH), 6.72 (ddd, *J* = 8.1, 7.5, 1.0 Hz, 1H, 28'-CH), 6.24 (d, *J* = 7.6Hz, 1H, 27-CH), 6.21(d, *J* = 7.6Hz, 1H, 27'-CH), 4.50 (t, *J* = 6.5 Hz, 2H, 8-CH_2), 4.36 (t, *J* = 7.1 Hz, 4H, 35, 35'-CH_2), 3.23-3.19 (m, 8H, 10, 14, 17, 21-CH_2), 3.04 (t, *J* = 6.7 Hz, 2H, 23-CH_2), 2.18-2.16 (m, 2H, 9-CH_2), 1.76-1.74 (m, 4H, 36, 36`-CH_2), 1.57-1.55 (m, 2H, 15-CH_2), 1.42-1.38 (m, 4H, 16, 22-CH_2), 1.34 (d, *J* = 8.5 Hz, 27H, 13, 20, 26-$(CH_3)_3$), 1.18-1.15 (m, 4Hz, 37, 37'-CH2), 0.80-0.77 (m, 6H, 38, 38'-CH_3); ^{13}C NMR (125 MHz, MeOD), δ 155.2 (5-C), 152.2 (3-C), 151.8 (34, 34'-C) 142 (4-C), 139.7 (4-C),134.1 (27-C), 128.4 (28-C), 128.2 (28`-C), 126.6 (2-C),123.6 (7-C),123.4 (29-C), 123.2 (29`-C), 122.8 (30-C), 122.3 (30`-C), 120.5 (34-C), 120.3 (1, 34`-C), 50.6 (8-C), 52.5 (35,35`-C), 47.1 (10-C), 45.5 (14-C), 45.2 (17-C), 44.4 (21-C), 37.5 (23-C), 32.9 (36, 36`-C), 28.8 (13, 15, 20, 26-C) 28.5 (9-C), 26.1 (16, 22-C), 20.5 (37, 37`-C), 13.8 (38, 38`-C); ^{19}F NMR (500MHz, MeOD), δ -74.6 (d, 6F-PF_6); MS (ES+) 1224 $[M]^+$, HRMS (ES+) $C_{56}H_{81}N_{13}O_6{}^{193}Ir$ requires 1224.6105 found 1224.6062.

6.5.2 Synthesis of $[Ir(L1)_2L6](CF_3CO_2)_4$ $Ir(L1)_2L6$

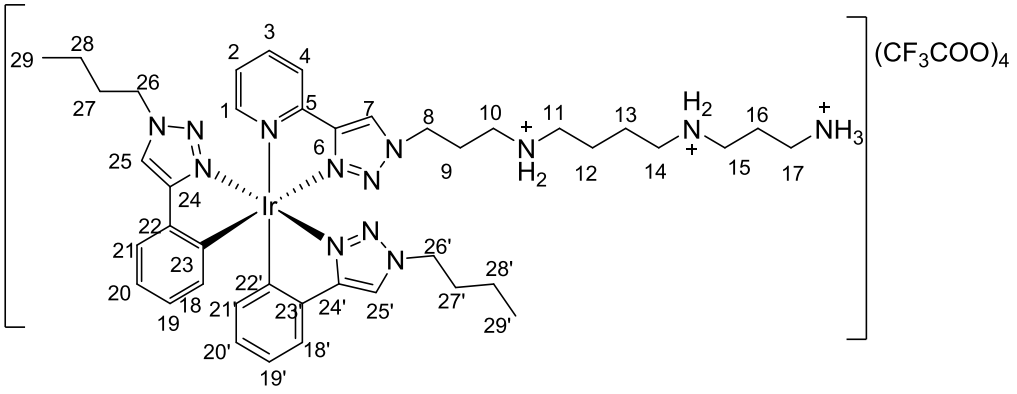

$Ir(L1)_2L6.Boc$ (0.09 g, 0.06 mmol) was dissolved in 4M TFA in DCM and stirred at rt. for 18hr. The volatiles were removed and the product was obtained and purified by RP-HPLC method A, R_t = 24 min to produced (0.05 g) of a pure product. ^{1}H NMR (AV-400MHz, MeOD), δ 9.02 (s, 1 H,7-CH), 8.31 (d, *J* = 3.0 Hz, 2 H, 25, 25'-CH), 8.19 (d, *J* = 7.6 Hz, 1 H, 1-CH), 8.03 (d, *J* = 7.2 Hz, 2 H, 3, 4-CH), 7.51 (d, *J* = 7.4 Hz, 1 H, 21-CH), 7.45 (d, *J* = 7.6 Hz, 1 H, 21'-CH), 7.34 (ddd, *J* = 7.5, 5.7, 0.7 Hz, 1 H, 2-CH), 6.95 (ddd, *J* = 8.3, 7.6, 0.7 Hz, 1 H, 20-CH), 6.88 (ddd, *J* = 7.7, 7.5, 0.7 Hz, 1 H, 20'-CH), 6.81 (ddd, *J* = 8.5, 7.4, 1.1 Hz, 1 H, 19-CH), 6.71 (ddd, *J* = 8.2, 7.6, 1.1 Hz, 1 H, 19'-CH), 6.25 (d, *J* = 7.6 Hz, 1 H, 18-CH), 6.20 (d, *J* = 7.6 Hz ,1 H,18'-CH), 4.63 (t, *J* = 6.5 Hz, 2 H, 8-CH_2), 4.35 (t, *J* = 7.0 Hz, 4 H, 26, 26'-CH_2), 3.15 (t, *J* = 7.7 Hz, 2 H, 17-CH_2), 3.08 (m, 8 H, 10, 11, 14, 15-CH_2), 3.01 (t, *J* = 7.0 Hz, 2 H, 9-CH_2), 2.35 (quin, *J* = 7.3 Hz, 2H, 16-CH_2), 2.06 - 2.16 (m, 4H, 12, 13- CH_2), 1.74 - 1.91 (m, 8H, 27, 27', 28, 28'-CH_2), 0.87 - 0.96 (m, 6 H, 29, 29'-CH_3); ^{13}C NMR (100MHz, MeOD), δ 162.9, 162.6 (q, *J* = 34.9 Hz, CF_3CO_2), 159.0 (22-C), 158.5 (22'-C), 152.3 (4-C), 151.8 (5-C), 150.9 (6-C), 146.7 (24-C), 143.2 (24'-C), 140.4 (3-C), 137.3 (23-C, 23'-C), 134.3 (18-C), 133.5 (18'-C), 129.3 (19-C), 128.5 (19'-C), 126.9 (2-C), 126.6 (7-C), 123.8 (1-C), 123.5 (21-C), 123.3 (21'-C), 123.1 (20-C),122.9 (20'-C), 120.6 (21-C), 120.4 (21'-C), 52.8, 52.7 (26, 26'-C), 50.0 (8-C), 48.2 (9, 10, 11-C), 46.0 (14, 17-C), 37.9 (15-C), 33.1 (27-C), 27.7 (16-C), 25.5 (12, 13-C), 24.3 (27'-C), 20.6 (28, 28'-C),13.7 (29, 29'-C); ^{19}F NMR (400MHz, MeOD), δ -77.3 (s, 3F- CF_3CO_2); MS (ES+) 924 $[M]^+$, HRMS (ES+) $C_{41}H_{57}N_{13}{}^{193}Ir$ requires 924.4515 found 924.4489.

6.5.3 Synthesis of $[Ir(L2)_2L6.Boc]PF_6$ Ir(L2)₂L6.Boc

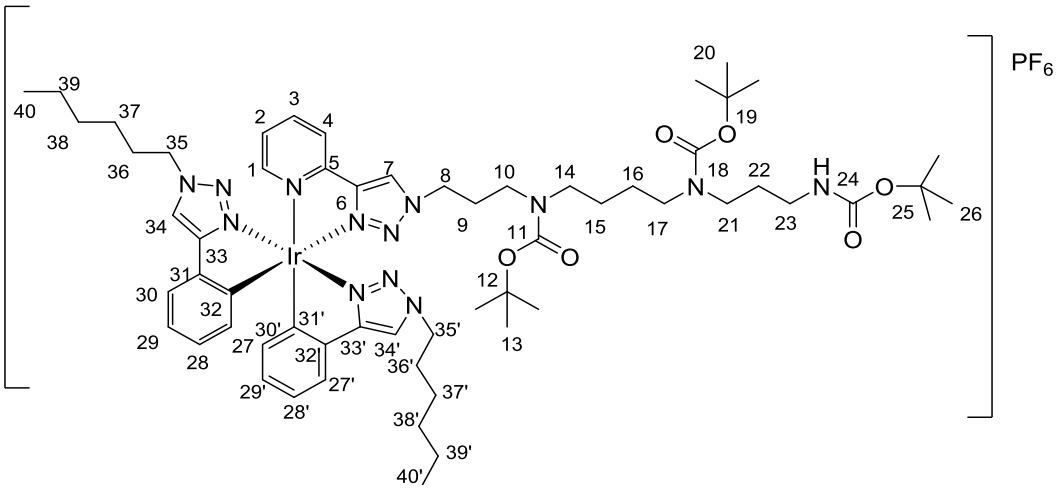

This was prepared from **$[Ir(L2)_2Cl]_2$** dimer (0.12 g, 0.08 mmol) and **L6.Boc** (0.12 g, 0.19 mmol) and KPF_6 (0.03 g, 0.19 mmol) according to method B and after work up gave light yellow sold as a crude. The residue was purified through alumina, eluting with 5% MeOH in DCM (0.18 g, 78%). ^{1}H NMR (AV_400MHz, MeOD), δ 9.01 (bs,1H, 7-CH), 8.32 (d, *J* = 2.8 Hz, 2H, 34, 34'-CH), 8.16 (d, *J* = 8.5 Hz, 1-CH), 8.06 (d, *J* = 1.5 Hz, 1H, 4-CH), 8.04 (ddd, *J* = 6.9, 5.9, 1.8 Hz, 1H, 3-CH), 7.50 (dd, *J* = 7.5, 0.9 Hz, 1H, 30-CH),7.45 (dd, *J* = 7.6, 1.0 Hz, 1H, 30'-CH), 7.34 (ddd, *J* = 7.4, 7.3, 1.2 Hz, 1H, 2-CH), 6.96 (ddd, *J* = 7.9, 7.5, 1.0 Hz, 1H, 29-CH), 6.88 (ddd, *J* = 7.8, 7.5, 1.1 Hz, 1H, 29'-CH), 6.80 (ddd, *J* = 7.8, 7.6, 1.4 Hz, 1H, 28-CH), 6.71 (ddd, *J* = 7.9, 7.5, 1.3 Hz, 1H, 28'-CH), 6.24 (d, *J* = 7.1 Hz, 1H, 27-CH), 6.22 (d, *J* = 7.5 Hz, 1H, 27'-CH), 4.49 (t, *J* = 6.7 Hz, 2H, 8-CH_2), 4.35 (t, *J* = 6.8 Hz, 4H, 35, 35'-CH_2), 3.24-3.18 (m, 8H, 10, 14, 17, 21), 3.04 (t, *J* = 6.8 Hz, 2H, 23-CH_2), 2.16 (m, 2H, 9-CH_2), 1.90-1.83 (m, 4H, 36, 36'-CH_2), 1.70-1.68 (m, 2H, 22-CH_2), 1.45 (d, *J* = 6.5 Hz, 31H, 15, 16-CH_2 and 13, 20, 26-$(CH_3)_3$), 1.29-1.26 (m, 12 Hz, 37, 38, 39, 37', 38', 39-CH_2), 0.90-0.86 (m, 6H, 40, 40'-CH_3); ^{13}C NMR (100 MHz, MeOD), δ 157.6 (11-C, 31-C), 157.0 (18-C, 31'-C), 156.0 (24-C, 5-C), 150.8 (6-C), 150.5 (4-C), 149.3 (33-C), 145.3 (33'-C), 138.8 (3-C), 135.9 (32-C), 135.7 (32'-C), 132.7 (27-C), 132.0 (27'-C), 127.7 (28-C), 127.0 (28'-C), 125.3 (2-C), 124.7 (7-C), 122.3 (1-C), 122.3 (30-C), 122.0 (30'-C), 121.4 (29, 29'-C), 119.2 (34-C), 118.8 (34'-C), 79.8, 79.6 and 78.6 (12, 19 and 25-C), 51.5 (35-C), 51.4 (35'-C), 49.4 (8-C), 46.5 (10, 14-C), 44.0 (17 and 21-C), 37.5 (23-C), 30.6 (37, 37'-C), 29.4 (22, 36, 36'-C), 27.4, 27.3 (9, 13, 15, 16, 20, 26-C), 25.4 (38, 38'-C), 22.1 (39, 39'-C), 12.9 (40, 40'); ^{19}F NMR (400MHz, MeOD), δ -74.6 (d, *J* = 707.2Hz, 6F-PF_6); MS (ES+) 1280 $[M]^+$, HRMS (ES+) $C_{60}H_{89}N_{13}O_6{}^{193}Ir$ requires 1280.6671 found 1280.6688.

6.5.4 Synthesis of $[Ir(L2)_2L6](CF_3CO_2)_4$ IrL2-L6

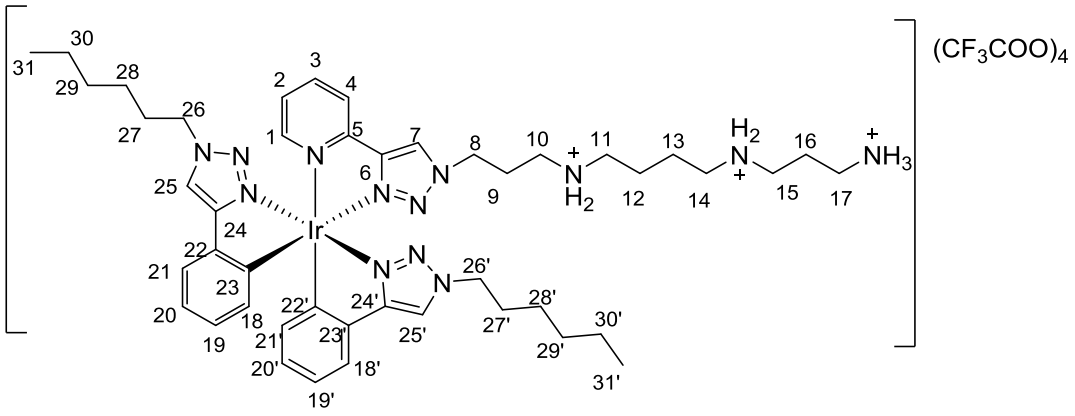

This was prepared from **$Ir(L2)_2L6.Boc$** (0.07 g, 0.03 mmol) was dissolved in 4M TFA in DCM and stirred at rt. for 18hr. The volatiles were removed and to give the product (0.04 g) as a pure. ^{1}H NMR (500 MHz, MeOD), δ 9.04 (s, 1H, 7-CH), 8.35 (d, *J* = 5.8 Hz, 2H, 25, 25'-CH), 8.19 (d, *J* = 7.9 Hz, 1H, 1-CH), 8.05 (d, *J* = 7.5 Hz, 2H, 3, 4-CH), 7.52 (d, *J* = 7.5 Hz, 1H, 21-CH), 7.46 (d, *J* = 7.5 Hz, 1H, 21'-CH), 7.36 (ddd, *J* = 7.9, 6.4 Hz, 1H, 2-CH), 6.97 (ddd, *J* = 8.3, 7.2Hz, 20-CH), 6.89 (ddd, 7.9, 7.2 Hz, 1H, 20'-CH), 6.81(ddd, *J* = 8.3, 7.4 Hz, 19-CH), 6.71 (ddd, *J* = 8.3, 7.4 Hz, 1H, 19'-CH), 6.24 (d, *J* = 7.7 Hz, 1H, 18-CH), 6.19 (d, *J* = 7.4 Hz, 1H, 18'-CH), 4.64 (t, 7.1 Hz, 2H, 8-CH_2), 4.36 (t, *J* = 6.7 Hz, 4H, 26, 26'-CH_2), 3.15 (t, *J* = 7.6 Hz, 2H, 17-CH_2), 3.12-3.06 (m, 6H, 10, 11, 14-CH_2), 3.01 (t, *J* = 7.5 Hz, 2H, 15-CH_2), 2.38-2.34 (m, 2H, 9-CH_2), 2.13-2.07 (m, 2H, 16-CH_2), 1.90-1.86 (m, 4H, 12, 13-CH_2), 1.80-1.78 (m, 4H, 27, 27'-CH_2), 1.31-1.26 (m, 10H, 28, 28', 29, 29', 30-CH_2), 1.21-1.16 (m, 2H, 30'-CH_2), 0.91-0.86 (m, 6H, 31, 31'-CH_3); ^{13}C NMR (125 MHz, MeOD), δ 155.9 (5-C), 152.2 (3-C), 151.6 (22, 22'), 146.1 (6-C), 142.5 (24, 24'-C), 140.3 (4-C), 134.1 (18-C), 133.4 (18'-C), 128.3 (19-C), 126.5 (19'-C), 123.7 (7-C), 123.5 (2-C), 123.3 (20-C),122.8 (21-C), 121.7 (20'-C), 120.2 (21'-C), 120.5 (1-C), 118.2 (25, 25'-C), 52.8 (26, 26'-C), 47.3 (8-C), 45.8 (17-C), 44.7 (10, 11-C), 43.3 (14-C), 36.2 (15-C), 32.0 (27, 27'-C), 28.2 (12-C), 26.8 (28, 28'-C), 25.7 (9-C), 24.2 (16-C), 22.9 (13-C), 21.3 (13-C), 21.1 (29, 29'-C), 21.1 (30, 30'-C), 14.2 (31, 31'-C); ^{19}F NMR (500MHz, MeOD), δ -76.9 (s, 3F-CF_3CO_2); MS (ES+) 980 $[M]^+$, HRMS (ES+) $C_{45}H_{65}N_{13}{}^{193}Ir$ requires 980.5102 found 980.5115.

6.5.5 Synthesis of $[Ir(L2)_2(L10.Boc)]PF_6$ $Ir(L2)_2L10.Boc$

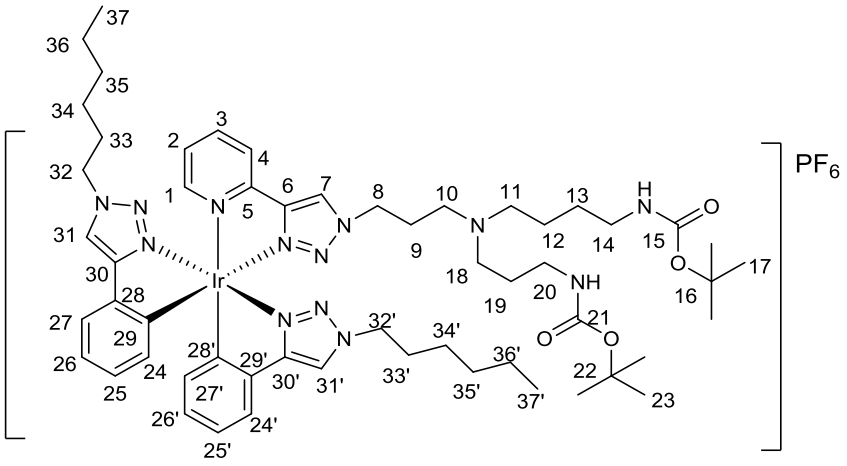

This was prepared from **$[Ir(L2)_2Cl]_2$** dimer (0.10 g, 0.07 mmol) and **L10.Boc** (0.08 g, 0.16 mmol) were dissolved in MeOH and then followed by KPF_6 (0.0288g, 0.157mmol) according to the method B and after work up gave product as a crude (0.14 g). Crude was purified by RP-HPLC method A, R_t = 30 min to give (0.07 g) as a pure product. ^{1}HNMR (500 MHz, MeOD), δ 9.05 (s, 1H, 7-CH), 8.36 (d, *J* = 3.1 Hz, 2H, 31, 31'-CH), 8.20 (d, *J* = 7.8 Hz, 1H, 1-CH), 8.07 (d, *J* = 7.6 Hz, 1H, 4-CH), 8.03 (d, *J* = 5.5 Hz, 1H, 3-CH), 7.52 (d, *J* = 7.3 Hz, 1H, 27-CH), 7.47 (d, *J* = 7.6 Hz, 1H, 27'-CH), 7.36 (ddd, *J* = 7.9, 6.1 Hz, 1H, 2-CH), 6.97 (ddd, *J* = 8.1, 7.5 Hz, 1H, 26-CH), 6.90 (ddd, *J* = 8.2, 7.4 Hz, 1H, 26'-CH), 6.81 (ddd, *J* = 8.5, 7.5 Hz, 1H, 25-CH), 6.73 (ddd, *J* = 8.4, 7.5 Hz, 1H, 25'-CH), 6.26 (d, *J* = 7.5 Hz, 1H, 24-CH), 6.18 (d, *J* = 7.8 Hz, 1H, 24'-CH), 4.63-4.61 (m, 2H, 8-CH_2), 4.36 (t, *J* = 6.8 Hz, 4H, 32, 32'-CH_2), 3.27-3.24 (m, 2H, 14-CH_2), 3.12-3.06 (m, 8H, 10, 11, 18, 20-CH_2), 2.41-2.40 (m, 2H, 9-CH_2), 1.89-1.86 (m, 4H, 12, 13-CH_2), 1.82-1.81 (m, 2H, 19-CH_2), 1.67-1.65 (m, 2H, 33-CH_2), 1.54-1.51 (m, 2H, 33'-CH_2), 1.44 (s, 18H, 17, 23-$(CH_3)_3$), 1.31-1.26 (m, 12H, 34, 34', 35, 35', 36, 36'), 0.90-0.81 (m, 6H, 37, 37'-CH_3); ^{13}C NMR (126 MHz, MeOD), δ 158.8 (28-C), 158.4 (28'-C), 152.2 (3-C), 151.6 (5-C), 150.8 (6-C), 146.5 (7-C), 143.2 (29, 29'-C), 140.4 (4-C), 137.2 (30, 30'-C), 134.2 (24-C), 133.3 (24'-C), 129.2 (25-C), 128.4 (25'-C), 126.6 (2-C), 124.7 (8-C), 123.8 (26-C), 123.4 (26'-C), 123.2 (27-C), 123.0 (27'-C), 122.9 (1-C), 120.6 (31-C), 120.3 (31'-C), 80.6 (16-C), 80.0 (22-C), 54.0 (18-C), 53.0 (32-C), 52.8 (32'-C), 51.9 (20-C), 51.4 (14-C), 49.9 (8-C), 40.2 (10-C), 38.2 (11-C), 32.1 (34-C), 23.0 (34'-C), 30.9 (12, 13, 33, 33'-C), 28.8 (17, 23-C), 25.5 (35-C), 24.9 (35'-C), 23.6 (19-C), 23.5 (9-C), 21.9 (36, 36'-C), 14.3 (37, 37'-C); ^{19}F NMR (500MHz, MeOD), δ -64.4 (s, 3F-py); MS (ES+) 1180 $[M]^+$, HRMS (ES+) $C_{55}H_{81}N_{13}O_4{}^{193}Ir$ requires 1180.6180 found 1180.6164.

6.5.6 Synthesis of $[Ir(L2)_2L10](CF_3CO_2)_4$ $Ir(L2)_2L10$

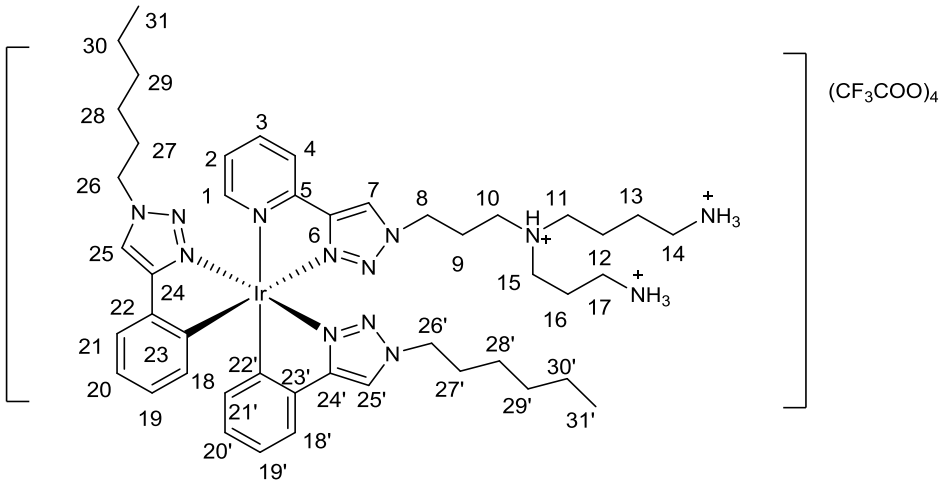

$Ir(L2)_2L10.Boc$ (0.04 g, 0.03 mmol) was dissolved in 4M TFA in DCM and stirred at rt. for 18hr. The volatiles were removed, and the crude solid was purified by RP-HPLC method A, R_t = 23 min to yield (0.025 g) as a pure product. ^{1}H NMR (500 MHz, MeOD), δ 9.03 (s, 1H, 7-CH), 8.31 (s, 1H, 25-CH), 8.30 (s, 1H, 25'-CH), 8.18 (d, *J* = 7.7 Hz, 1H,1-CH), 8.04 (ddd, *J* = 5.1, 4.7, 1.5 Hz, 2H, 3, 4-CH), 7.52 (d, *J* = 7.5 Hz, 1H, 21-CH), 7.4 (d, *J* = 7.4 Hz, 1H, 21'-CH), 7.35 (ddd, *J* = 7.3, 6.5, 1.2 Hz, 1H, 2-CH), 6.97 (ddd, *J* = 8.2, 7.3, 0.9 Hz, 1H, 20-CH), 6.90 (ddd, *J* = 7.9, 7.3, 0.9 Hz, 1H, 20'-CH), 6.81 (ddd, *J* = 8.3, 7.5, 1.3 Hz, 1H, 19-CH), 6.72 (ddd, *J* = 7.8, 7.3, 1.3 Hz, 1H, 19'-CH), 6.27 (d, *J* = 7.5 Hz, 1H, 18-CH), 6.18 (d, *J* = 7.2 Hz, 1H, 18'-CH), 4.57 (t, *J* = 7.0 Hz, 2H, 8-CH_2), 4.38-4.34 (m, 4H, 26, 26'-CH_2), 3.30- 3.24 (m, 4H, 14, 17-CH_2), 3.18 (t, *J* = 7.9 Hz, 2H, 10-CH_2), 3.05 (t, *J* = 7.3 Hz, 2H, 11-CH_2), 3.00 (t, *J* = 7.5 Hz, 2H, 15-CH_2), 2.47-2.41 (m, 2H, 9-CH_2), 2.15-2.09 (m, 2H, 16-CH_2), 1.91-1.81 (m, 4H, 12, 13-CH_2), 1.77-1.71 (m, 4H, 27, 27'-CH_2), 1.32-1.28 (m, 6H, 28, 28', 29-CH_2), 1.27-1.25 (m, 4H, 29', 30-CH_2), 1.21-1.19 (m, 2H, 30'-CH_2), 0.91-0.85 (m, 6H, 31,31'-CH_3); ^{19}F NMR (500MHz, MeOD), δ -64.5 (s, 3F-py), -76.9 (s, 3F-CF_3CO_2); MS (ES+) 980 $[M]^+$, HRMS (ES+) $C_{45}H_{65}N_{13}{}^{193}Ir$ requires 980.5115 found 980.5115.

6.5.7 $[Ir(L1)_2(L8.Boc)]PF_6$ $Ir(L1)_2L8.Boc$

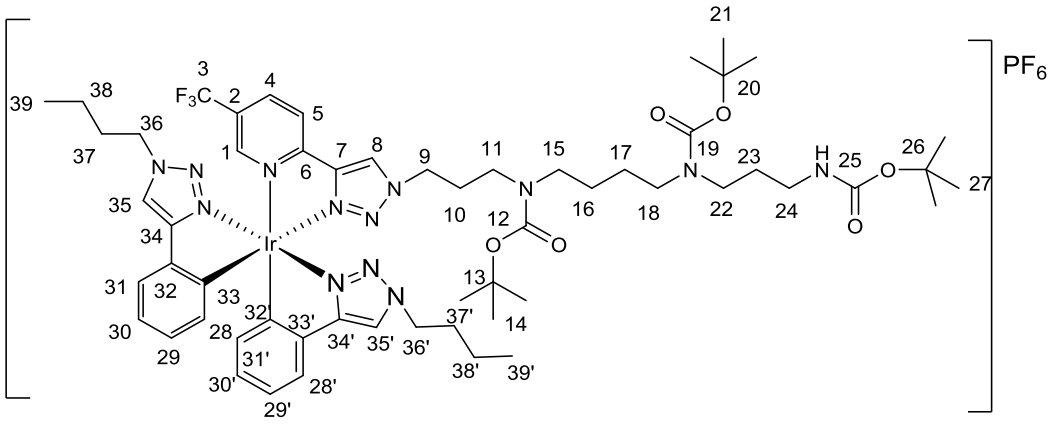

This was prepared from **$[Ir(L1)_2Cl]_2$** dimer (0.1 g, 0.08 mmol) and **L8.Boc** (0.12 g, 0.18 mmol) and KPF_6 (0.03 g, 0.17 mmol) according to method B and after work up gave a yellow sold. The residue was purified through alumina, eluting with 5% MeOH in DCM (0.09 g, 69 %) and then purified by RP-HPLC method A, R_t = 38 min to yield (0.05g) as a pure product. ^{1}H NMR (500 MHz, MeOD), δ 9.19 (s br,1H, 1-CH), 8.41 (s, 2H, 35, 35'-CH), 8.38-8.34 (m, 2H, 4, 5-CH), 8.26 (s,1H, 8-CH), 7.55 (d, *J* = 7.4 Hz, 1H, 31-CH),7.36 (d, *J* = 7.7 Hz, 1H, 31'-CH), 6.88 (ddd, *J* = 8.0, 7.4, 1.0 Hz, 1H, 30-CH), 6.78 (ddd, *J* = 8.3, 7.2, 0.9 Hz, 1H, 30'-CH), 6.74 (ddd, *J* = 8.5, 8.0, 1.2 Hz, 1H, 29-CH), 6.62 (ddd, *J* = 8.0, 7.7, 1.3 Hz, 1H, 29'-CH), 6.12 (d, *J* = 7.8 Hz, 1H, 28-CH), 6.09 (d, *J* = 7.7 Hz, 1H, 28'-CH), 4.41 (t, *J* = 6.8 Hz, 2H, 9-CH_2), 4.25 (t, *J* = 6.9 Hz, 4H, 36, 36'-CH_2), 3.12-3.08 (m, 8H, 11, 15, 18, 22), 2.92 (t, *J* = 6.7 Hz, 2H, 24-CH_2), 2.08-2.04 (m, 2H, 10-CH_2), 1.78-1.70 (m, 4H, 37, 37'-CH_2), 1.58-1.57 (m, 2H, 23-CH_2), 1.33 (d, *J* = 6.3 Hz, 31H, 16, 17-CH_2, 14, 21, 27-$(CH_3)_3$), 1.35-1.22 (m, 4Hz, 38, 38'-CH_2), 0.94-0.89 (m, 6H, 39, 39'-CH_3); ^{13}C NMR (125 MHz, MeOD), δ 161.2 (12-C), 161.0 (19, 25-C), 158.7 (6-C), 158.2 (7-C), 149.7 (32, 32'-C) 148.6 (8-C), 145.7 (34-C), 142.0 (34'-C), 137.7 (35, 35'-C),137.2 (33-C), 136.9 (33'-C), 134.0 (28, 28'-C), 129.4 (29, 29'-C), 128.5 (29, 29'-C), 128.3 (2-C), 124.1 (1-C), 123.5 (30, 30'-C), 123.4 (3-C), 123.2 (4, 5-C), 122.9 (35, 35'-C), 120.8 (31, 31'-C), 120.4 (31, 31'-C), 81.2 (13, 20-C), 80.9 (26-C), 52.7 (36-C), 52.6 (36'-C), 51.0 (9-C), 48.2 (11-C), 46.1(15-C), 44.9 (18, 22-C), 38.9 (24-C), 33.1(16,17-C), 32.9 (37, 37'-C), 28.9 (10-C), 26.7 (14, 21, 27-C), 28.7 (23-C), 20.5 (38-C), 20.4 (38'-C), 13.7 (39-C), 13.2 (39'-C); ^{19}F NMR (500MHz, MeOD), δ -64.5 (s, 3F-py); MS (ES+) 1292 $[M]^+$, HRMS (ES+) $C_{57}H_{80}N_{13}O_6F_3{}^{193}Ir$ requires 1292.5984 found 1292.5936.

6.5.8 Synthesis of $[Ir(L1)_2L8](CF_3COO)_4$ $Ir(L1)_2L8$

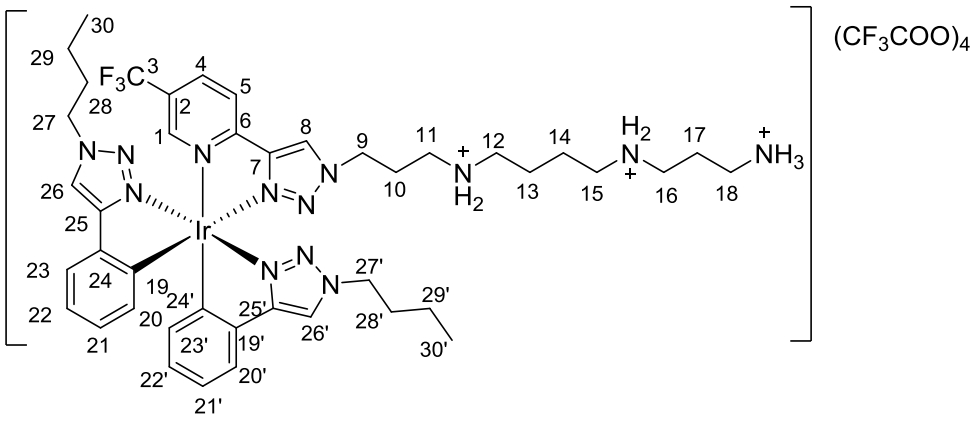

$Ir(L1)_2L8.Boc$ (0.04 g, 0.027 mmol) was dissolved in 4M TFA in DCM and stirred at rt. for 18hr. The volatiles were removed to produce the product (0.03 g) without further purification. ^{1}H NMR (500MHz, MeOD), δ 9.21 (s br,1H, 1-CH), 8.43 (s, 2H, 26, 26'-CH), 8.36 (d, *J* = 1.8 Hz, 2H, 4, 5-CH), 8.25 (s,1H, 8-CH), 7.55 (d, *J* = 7.3 Hz, 1H, 23-CH), 7.47 (d, *J* = 7.2 Hz, 1H, 23'-CH), 7.01 (ddd, *J* = 7.8, 7.3 Hz, 1H, 22-CH), 6.91 (ddd, *J* = 8.2, 7.1, 0.7 Hz, 1H, 22'-CH), 6.87 (ddd, *J* = 8.4, 7.5, 1.0 Hz, 1H, 21-CH), 6.74 (ddd, *J* = 8.4, 7.5, 1.2 Hz, 1H, 21'-CH), 6.24 (d, *J* = 7.4 Hz, 1H, 20-CH), 6.19 (d, *J* = 7.4 Hz, 1H, 20'-CH), 4.69-4.66 (m, 2H, 9-CH_2), 4.37 (t, *J* = 7.0 Hz, 4H, 27, 27'-CH_2), 3.16-3.13 (m, 2H, 28-CH_2), 3.10-3.06 (m, 4H, 11, 12-CH_2), 3.02 (t, *J* = 7.5 Hz, 2H, 18-CH_2), 2.40-2.34 (m, 2H, 10-CH_2), 2.13-2.2.07 (m, 4H, 15, 16-CH_2), 1.90-1.84 (m, 2H, 28'-CH_2), 1.80-1.79 (m, 2H, 17-CH_2), 1.34-1.25 (m, 8H, 13, 14, 29, 29' -CH_2), 0.92 (m, 6H, 30, 30'-CH_3); ^{13}C NMR (125 MHz, MeOD), δ 162.4 (q, *J* = 38.2Hz, CF_3CO_2), 158.7 (6-C), 158.3 (25, 25'-C), 155.2 (7-C), 149.4 (2-C), 148.6 (8-C), 145.5 (24-C), 141.9 (24'-C), 137.8 (26 or 26'-C), 137.2 (19-C), 137.0 (19'-C), 134.0 (20-C), 133.3 (20'-C), 129.4 (21-C), 128.3 (21'-C), 125.8 (1-C), 124.2 (22 or 22'-C), 123.5 (23, 23'-C), 123.4 (3-C), 123.3 (22 or 22'-C), 122.9 (26 or 26'-C), 52.7 (27-C), 52.6 (27'-C), 49.5 (9-C), 46.5 (11,12-C), 44.0 (28-C), 37.8 (18-C), 33.0 (15, 28'-C), 27.5 (10-C), 24.4 (16, 17-C), 24.2 (13, 14-C) 20.5 (29-C), 20.4 (29'-C), 13.6 (30-C), 13.5 (30'-C); ^{19}F NMR (500MHz, MeOD), δ -64.5 (s, 3F-py), -77.1 (s, 3F-CF_3CO_2); MS (ES+) 992 $[M]^+$, HRMS (ES+) $C_{42}H_{56}N_{13}F_3{}^{193}Ir$ requires 992.4395 found 992.4363.

6.5.9 Synthesis of $[Ir(L1)_2(L9.Boc)](PF_6)$ $Ir(L1)_2L9.Boc$

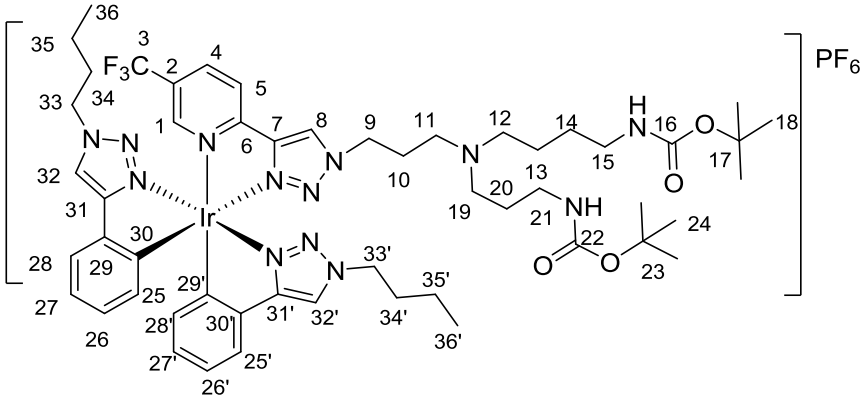

This was prepared from $[Ir(L1)_2Cl]_2$ dimer (0.1 g, 0.08 mmol), **L9.Boc** (0.12 g, 0.11 mmol) and KPF_6 (0.03 g, 0.18 mmol) according to method B and after work up gave a yellow sold. The residue was purified through alumina, eluting with 5% MeOH in DCM (0.07g, 69 %); ^{1}H NMR (AV-400MHz, MeOD), δ 9.22 (s,1H, 1-CH), 8.44 (d, *J* = 1.1 Hz, 2H, 4, 5-CH), 8.39 (s br, 32, 32'-CH), 8.24 (s, 1H, 8-CH), 7.56 (d, *J* = 7.0 Hz, 1H, 28-CH),7.49 (d, *J* = 7.6 Hz, 1H, 28'-CH), 7.02 (ddd, *J* = 7.9, 7.5 Hz, 1H, 27-CH), 6.92 (ddd, *J* = 8.0, 7.5 Hz, 1H, 27'-CH), 6.87 (ddd, *J* = 8.1, 7.5, 0.8 Hz, 1H, 26-CH), 6.76 (ddd, *J* = 8.1, 7.5, 1.0 Hz, 1H, 26'-CH), 6.25 (d, *J* = 7.4 Hz, 1H, 25-CH), 6.17 (d, *J* = 7.6 Hz, 1H, 25'-CH), 4.71-4.65 (m, 2H, 9-CH_2), 4.38 (t, *J* = 6.8 Hz, 4H, 33, 33'-CH_2), 3.29-3.25 (m, 2H, 11-CH), 3.15-3.06 (m, 4H, 12, 19-CH_2), 2.47-2.39 (m, 2H, 15-CH_2), 1.91-1.84 (m, 6H, 10, 34, 34'-CH_2), 1.71-1.63 (m, 2H, 20-CH_2), 1.56-1.49 (m, 2H, 13-CH_2), 1.44 (s, 20H, 14-CH, 18, 24-$(CH_3)_3$), 1.38-1.25 (m, 4H, 35, 35'-CH_2), 0.93 (m, 6H, 36, 36'-CH_3); ^{13}C NMR (100 MHz, MeOD), δ 156.8 (16 and 22-C), 155.3 (29, 29'-C), 149.6 (1-C), 148.7 (8-C), 145.9 (5-C), 142.1 (6-C), 138.0 (4-C), 137.1 (7-C), 134.2 (25or 25'-C), 133.4 (25or 25'-C),129.6 (26 or 26'-C), 129.1 (26 or 26'), 124.4 (27 and 27'), 123.6 (28, 28'-C), 123.0 (3-C), 54.1 (12, 19-C), 52.9 (33 and 33'-C), 52.12 (11-C), 50.2 (9-C), 40.4 (17-C), 38.4 (23-C), 33.0 (34, 34'-C), 28.8 (18, 24-C), 28.2 (14-C), 25.6 (10-C), 25.1 (15-C), 22.0 (20-C), 20.7 (35-C), 20.6 (35'-C), 13.8 (36-C), 13.7 (36'-C); ^{19}F NMR (400MHz, MeOD), δ -64.1(s, 3F-py); MS (ES+) 1192 $[M]^+$, HRMS (ES+) $C_{52}H_{72}N_{13}O_4F_3{}^{193}Ir$ requires 1192.5431 found 1192.5412.

6.5.10 Synthesis of $[Ir(L1)_2L9](CF_3COO)_4$ $Ir(L1)_2L9$

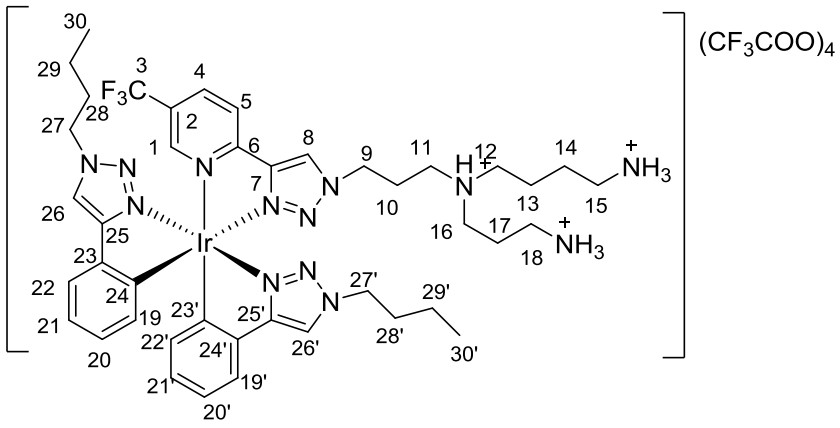

$Ir(L1)_2L9.Boc$ (0.05 g, 0.03 mmol) was dissolved in 4M TFA in DCM and stirred rt for 18hr. The volatiles were removed and the crude solid was purified by RP-HPLC method A, R_t = 24.9 min (0.03 g) as pure product. ^{1}H NMR (500 MHz, MeOD), δ 9.25 (s, 1H, 1-CH), 8.43 (d, *J* = 8.5 Hz, 1H, 4-CH), 8.40 (d, *J* = 8.5 Hz, 1H, 5-CH), 8.34 (d, *J* = 2.7 Hz, 26, 26'-CH), 8.24 (s, 1H, 8-CH), 7.54 (d, *J* = 7.4 Hz, 1H, 22-CH), 7.47 (d, *J* = 7.4 Hz, 1H, 22'-CH), 7.00 (ddd, *J* = 8.3, 7.5 Hz, 1H, 21-CH), 6.90 (ddd, *J* = 8.0, 6.9 Hz,1H, 21'-CH), 6.85 (ddd, *J* = 8.4, 7.5, 1.0 Hz, 1H, 20-CH), 6.74 (ddd, *J* = 8.2, 7.6, 1.1 Hz, 1H, 20'-CH), 6.25 (d, *J* = 7.5 Hz, 1H, 19-CH), 6.28 (d, *J* = 7.5 Hz, 1H, 19'-CH), 4.65 (t, *J* = 6.4 Hz, 2H, 9-CH_2), 4.36 (t, *J* = 6.9 Hz, 4H, 27, 27'-CH_2), 3.35-3.32 (m, 4H,11, 12-CH_2), 3.31-3.27 (m, 2H,17-CH_2), 3.04 (t, *J* = 7.2 Hz, 2H, 15-CH_2), 3.00 (t, *J* = 7.4Hz, 2H, 18-CH_2), 2.47-2.46 (m, 2H, 13-CH_2), 2.16-2.10 (m, 2H, 18-CH_2), 1.90-1.80 (m, 4H, 28, 28'-CH_2), 1.76-1.70 (m, 2H, 14-CH_2), 1.35-1.30 (m, 2H, 29-CH_2), 1.29-1.23 (m, 2H, 29'-CH_2), 0.95-0.89 (m, 6H, 30, 30'-CH_3): ^{13}C NMR (126 MHz, MeOD), δ 161.8 (q, *J* = 38.3Hz, CF_3CO_2), 158.7, 158.3 (23, 23'-C), 155.3 (6-C), 149.5 (2-C), 148.7 (8-C), 145.5 (25-C), 145.6 (25'-C), 142.1(5-C), 137.9 (4-C), 137.2 (7-C), 134.1 (19 or 19'-C), 133.3 (19 or 19'-C), 129.4 (20 or 20'-C), 128.5 (20 or 20'-C), 128.4 (1-C), 124.2 (5-C), 123.5 (22, 22'-C), 123.4 (3-C), 123.3 (21 or 21'-C), 122.9 (21 or 21'-C),120.8 (26 or 26'-C), 120.5 (26 or 26'-C), 53.7 (16-C), 52.7 (27 and 27'-C), 52.6 (27 and 27'-C), 51.1 (11, 12-C), 50.1 (9-C), 37.7 (18-C), 32.9 (28, 28'-C), 25.5 (13-C), 25.1 (18-C), 23.1 (14-C), 21.8 (29 or 29'-C), 20.4 (29, 29'-C), 13.6 (30-C), 13.5 (30'-C); ^{19}F NMR (500MHz, MeOD), δ -64.5(s, 3F-py), -76.8 (s, 3F-CF_3CO_2); MS (ES+) 992 $[M]^+$, HRMS (ES+) $C_{42}H_{56}N_{13}F_3{}^{193}Ir$ requires 992.4376 found 992.4363.

6.5.11 Synthesis of $[Ir(L2)_2(L8.Boc)](PF_6)$ $Ir(L2)_2L8.Boc$

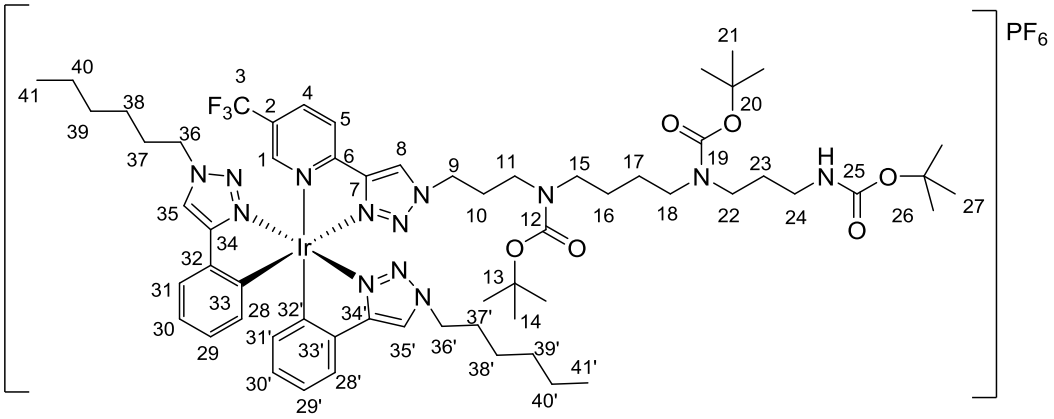

This was prepared from **$[Ir(L2)_2Cl]_2$** dimer (0.07 g, 0.05 mmol), **L8.Boc** (0.08 g, 0.12 mmol) and KPF_6 (0.02 g, 0.12 mmol) according to method B and fter work up gave the product as crude (0.14 g). Crude was purified by column chromatography using elute (95%DCM: 5%MeOH) and then change to 100 % MeOH to give the product (0.13 g, 84 %). ^{1}H NMR (500 MHz, MeOD), δ 9.18 (s, 1H, 1-CH), 8.40 (d, *J* = 4.3 Hz, 2H, 4, 5-CH), 8.35 (s, 2H, 35, 35'-CH), 8.25 (s, 1H, 8-CH), 7.54 (d, *J* = 7.2 Hz, 1H, 31-CH), 7.46 (d, *J* = 6.8 Hz, 1H, 31'-CH), 7.00 (ddd, *J* = 7.9, 7.1 Hz, 1H, 30-CH), 6.90 (ddd, *J* = 7.7, 7.1 Hz, 1H, 30'-CH), 6.85 (ddd, *J* = 7.9, 7.5, 0.9 Hz, 1H, 29-CH), 6.73 (ddd, *J* = 8.3, 7.5, 0.9 Hz, 1H, 29'-CH), 6.23 (d, *J* = 7.5 Hz, 1H, 28-CH), 6.20 (d, *J* = 7.7 Hz, 1H, 28'-CH), 4.53 (t, *J* = 6.5 Hz, 2H, 9-CH_2), 4.36 (t, *J* = 6.8 Hz, 4H, 36, 36'-CH_2), 3.25-3.18 (m, 8H, 11, 15, 18, 22-CH_2), 3.02 (t, *J* = 6.8 Hz, 2H, 24-CH_2), 2.20-2.17 (m, 2H, 10-CH_2), 1.90-1.86 (m, 4H, 16,17-CH_2), 1.70-1.67 (m, 2H, 23-CH_2), 1.44 (d, *J* = 8.4 Hz, 31H, 14, 21, 27, 37, 37'-CH_3), 1.30-1.26 (m, 12H, 38, 39, 40-CH_2), 0.88-0.86 (m, 6H, 41, 41'-CH_3). ^{13}C NMR (125 MHz, MeOD), δ 161.6 (q, *J* = 25.1 Hz, 3-C), 155.4 (32, 32'-C), 151.3 (6-C), 148.6 (8-C), 147.2 (2-C), 142.6 (34, 34'-C), 137.8 (4-C), 133.9 (28, 28'-C), 129.4 (29-C), 128.5 (29'-C), 124.2 (31-C), 123.5 (31'-C), 123.4 (30-C), 123.2 (30'-C), 122.9 (5-C), 120.8 (35-C), 120.4 (35'-C), 81.2, 80.9, 80.0 (13, 19, 25-C), 53.0 (36-C), 52.8 (36'-C), 50.2 (9-C), 48.0 (11-C), 46.8 (15-C), 38.6 (24-C), 32.1 (40, 40'-C), 32.0 (16, 17-C), 30.8 (10, 23-C), 28.8 (14, 21, 27-C), 26.9 (39, 39'-C), 18.7 (37-C), 17.2 (37'-C), 14.2 (41, 41'-C); ^{19}F NMR (500MHz, MeOD), δ -64.2 (s, 3F-py); MS (ES+) 1348 $[M]^+$, HRMS (ES+) $C_{46}H_{64}N_{13}F_3{}^{193}Ir$ requires 1348.6621found 1348.6562.

6.5.12 Synthesis of [Ir (L2)$_2$(L8)](CF$_3$COO)$_4$ Ir(L2)$_2$L8

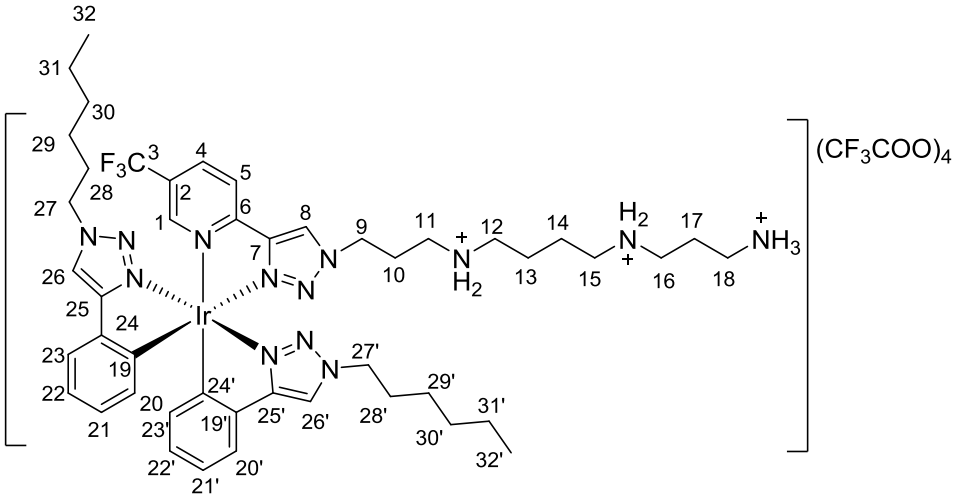

Ir(L2)$_2$L8.Boc (0.05 g, 0.03 mmol) was dissolved in 4M TFA in DCM and stirred at rt. for 18hr. The volatiles were removed to produce the product (0.04 g) without further purification. ^{1}H NMR (500 MHz, MeOD), δ 9.22 (s br,1H, 1-CH), 8.43 (d, *J* = 8.4 Hz, 2H, 4, 5-CH), 8.39 (s, 1H, 26-CH), 8.37 (s,1H, 26`-CH), 8.25 (s, 1H, 8-CH), 7.56 (dd, *J* = 7.3, 0.9 Hz, 1H, 23-CH), 7.47(d, *J* = 7.5, 0.8 Hz, 1H, 23'-CH), 7.02 (ddd, *J* = 8.6, 7.4, 0.9 Hz, 1H, 22-CH), 6.91 (ddd, *J* = 7.8, 7.4, 0.8 Hz, 1H, 22'-CH), 6.86 (ddd, *J* = 8.0, 7.5, 1.3 Hz, 1H, 21-CH), 6.73 (ddd, *J* = 8.2, 7.6, 1.2Hz, 1H, 21'-CH), 6.24 (d, *J* = 7.3 Hz, 1H, 20-CH), 6.19 (d, *J* = 7.3 Hz, 1H, 20'-CH), 4.68 (t, *J* = 6.3 Hz, 2H, 9-CH$_2$), 4.37 (t, *J* = 6.7 Hz, 4H, 27, 27'-CH$_2$), 3.16-3.12 (m, 2H, 11-CH$_2$), 3.10-3.06 (m, 2H, 12-CH$_2$), 3.02 (t, *J* = 7.5 Hz, 4H, 28, 28'-CH$_2$), 2.37 (t, *J* = 7.4 Hz, 2H, 15-CH$_2$), 2.10 (t, *J* = 7.3, 2H, 18-CH$_2$), 1.90-1.87(m, 6H, 29, 29', 10-CH$_2$), 1.79 (s br, 4H, 13, 14-CH$_2$), 1.31-1.27 (m, 14H, 15, 16, 17, 30, 30`, 31, 31`-CH$_2$), 0.94-0.90 (m, 6H, 32, 32'-CH$_3$); ^{13}C NMR (125 MHz, MeOD), δ 161.7 (q, *J* = 38.4Hz, CF$_3$CO$_2$), 158.7 (25-C), 158.3 (25'-C), 156.0 (6-C), 155.2 (7-C), 149.4 (2-C), 148.6 (8-C), 145.5 (24-C), 141.9 (24'-C), 137.8 (4-C), 137.2 (19-C), 137.0 (19'-C), 134.01 (20-C), 133.3 (20'-C), 129.4 (21-C), 128.5 (21'-C), 128.3 (1-C), 124.2 (3-C), 123.5 (23-C), 123.4 (23'-C), 123.3 (22, 22'-C), 120.8 (26-C),120.4 (26'-C), 53.1 (27-C), 52.8 (27'-C), 50.1 (45.8), 48.8 (11, 12-C), 37.8 (18-C), 32.1 (29-C), 32.0 (29'-C), 30.8 (13, 14-C), 26.9 (30-C), 26.8 (30'-C), 25.4 (15-C), 24.2 (16-C), 23.5 (28, 28'-C), 23.5 (31, 31'-C), 27.5 (10-C), 25.5 (17-C), 24.2 (13, 14-C) 13.6 (30-C), 14.2 (32, 32'-C); ^{19}F NMR (500MHz, MeOD), δ -64.1 (s, 3F-py), -

77.3 (s, 3F-CF_3CO_2); MS (ES+) 1048 $[M]^+$, HRMS (ES+) $C_{46}H_{64}N_{13}F_3{}^{193}Ir$ requires 1048.5026 found 1048.4989.

6.5.13 Synthesis of $[Ir(L2)_2(L9.Boc)]PF_6$ Ir(L2)$_2$L9.Boc

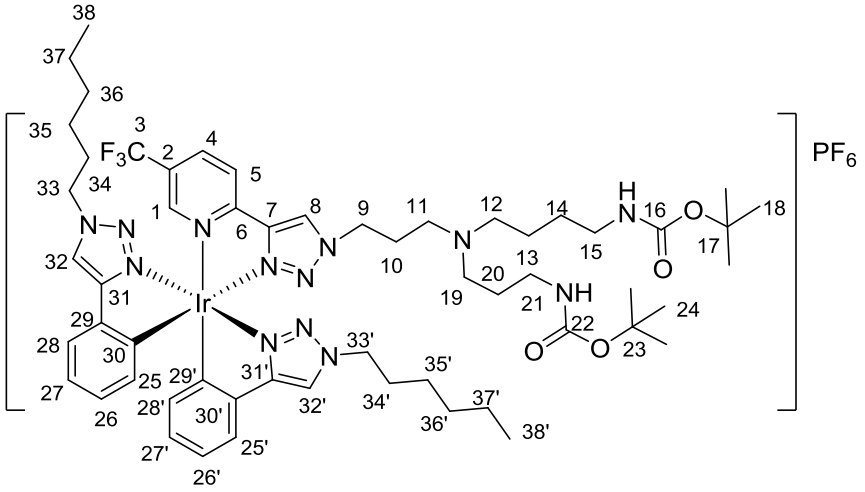

This was prepared from $[Ir(L2)_2Cl]_2$ dimer (0.05 g, 0.04 mmol), **L9.Boc** (0.05 g, 0.09 mmol) and KPF_6 (0.02 g, 0.09 mmol) according to the method B and after work up gave a solid crude with yield (0.12 g). Crude was purified by column chromatography using elute (95%DCM: 5%MeOH) and then change to 100% MeOH to obtain the product (0.08 g, 80 %). ^{1}H NMR (500MHz, MeOD), δ 9.24 (s, 1H, 1-CH), 8.45 (s, 2H, 32, 32'-CH), 8.41 (d, *J* = 2.4 Hz, 1H, 4-CH), 8.25 (s, 1H, 8-CH), 7.57 (d, *J* = 6.6 Hz, 1H, 28-CH), 7.49 (d, *J* = 6.7 Hz, 1H, 28'-CH), 7.40(d, *J* = 7.5 Hz, 1H, 5-CH), 7.03 (ddd, *J* = 8.5, 7.5, 0.9 Hz, 1H, 27-CH), 6.93 (ddd, 8.4, 7.8, 0.7 Hz, 1H, 27'-CH), 6.86 (ddd, *J* = 7.8, 7.5, 1.1 Hz, 1H, 26-CH), 6.76 (ddd, *J* = 8.3, 8.1, 1.1Hz, 1H, 26'-CH), 6.26 (d, *J* = 7.6 Hz, 1H, 25-CH), 6.17 (d, *J* = 7.4 Hz, 1H, 25'-CH), 4.67-4.64 (m, 4H, 33, 33'-CH_2), 4.40-4.36 (m, 2H, 9-CH_2), 3.26-3.24 (m, 2H,15-CH_2), 3.15-3.06 (m, 4H, 11, 21-CH_2), 2.43-2.42 (m, 2H, 12-CH_2), 2.18-2.09 (m, 2H, 19-CH_2), 1.92-1.88 (m, 2H, 10-CH_2), 1.83-1.81 (m, 2H, 20-CH_2), 1.67-1.66 (m, 4H, 13, 14-CH_2),1.44 (s br, 22H, 34, 34'-CH_2, 18, 24-CH_3), 1.32-1.28 (m, 12H, 35, 35', 36, 36', 37, 37' -CH_2), 0.96-0.86 (m, 6H, 38, 38'-CH_3); ^{13}C NMR (125 MHz, MeOD), δ 158.7 (29, 29'-C), 158.3 (6-C), 157.7 (7-C), 149.5 (2-C), 146.2 (31-C), 145.4 (31'-C), 137.9 (8-C), 137.2 (30-C), 137.0 (30'-C),134.8 (32 or 32'-C), 133.2 (25, 25-C), 128.0 (26, 26'-C), 124.3 (1-C), 123.6(3-C), 123.3 (32 or 32'-C), 122.7 (27, 27'-C), 120.8 (28-C), 120.5 (28'-C), 120.3 (4, 5-C), 52.9 (21-C), 51.9 (9-C), 50.9 (33, 33'-C), 50.1 (15-C), 40.3 (11-C), 38.2 (12-C), 36.6 (19-C), 31.1 (34, 34'-C), 30.8 (35, 35'-C), 25.5 (36, 36'-C), 24.9 (20-C), 23.6 (13-C), 23.5 (14-C), 21.9

(37, 37'-C); ^{19}F NMR (500MHz, MeOD), δ -64.0 (s, 3F-py); MS (ES+) 1248 $[M]^+$, HRMS (ES+) $C_{56}H_{80}N_{13}O_4{}^{193}Ir$ requires 1248.6033 found 1248.6038.

6.5.14 Synthesis of $[Ir(L2)_2\ L9]\ (CF_3COO)_4$ $Ir(L2)_2L9$

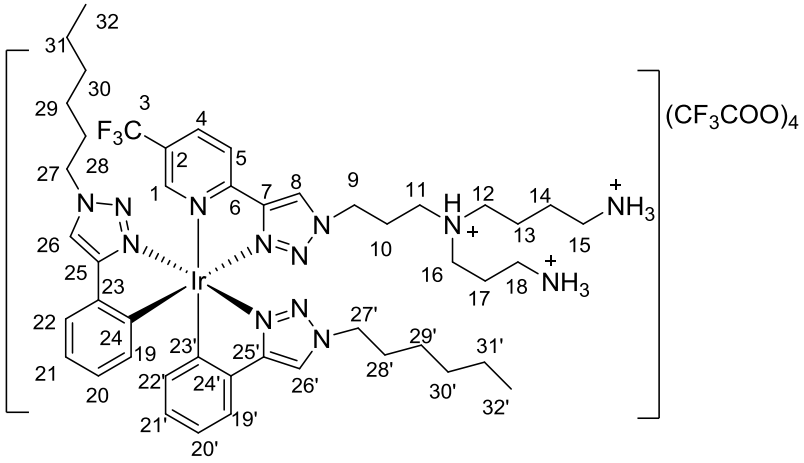

$Ir(L2)_2L9.Boc$ (0.07g, 0.05 mmol) was dissolved in 4M TFA in DCM and stirred at rt. for 18hr. The volatiles were removed to produce the product (0.075g). RP-HPLC method A, tR = 24.3 min to produce (0.04 g) as a pure product. ^{1}H NMR (500 MHz, MeOD), δ 9.24 (s, 1H, 1-CH), 8.44 (s, 2H, 26, 26'-CH), 8.40 (d, *J* = 7.2 Hz, 1H, 5-CH), 8.38 (d, *J* = 4.5 Hz, 1H, 4-CH), 8.25 (s, 1H, 8-CH), 7.56 (d, *J* = 7.6 Hz, 1H, 22-CH), 7.48 (d, *J* = 7.4 Hz, 1H, 22'-CH), 7.03 (ddd, *J* = 8.2, 7.1 Hz, 1H, 21-CH), 6.79 (ddd, *J* = 7.4, 7.1 Hz, 1H, 21'-CH), 6.86 (ddd, *J* = 8.5, 7.6 Hz, 1H, 20-CH), 6.74 (ddd, *J* = 8.5, 6.8 Hz, 1H, 20'-CH), 6.25 (d, *J* = 7.4 Hz, 1H, 19-CH), 6.16 (d, *J* = 7.4 Hz, 1H, 19'-CH), 4.65 (t, *J* = 6.8 Hz, 2H, 9-CH_2), 4.39-4.36 (m, 4H, 27, 27'-CH_2), 3.18 (t, *J* = 6.1 Hz, 2H, 15-CH_2), 3.04-2.97 (m, 6H, 11, 12, 18-CH_2), 2.66-2.64 (m, 2H, 10-CH2), 2.10-2.06 (m, 2H, 17-CH_2), 1.90-1.88 (m, 4H, 13, 14-CH_2), 1.81 (m, 4H, 28, 28'-CH_2), 1.74-1.72 (m, 4H, 29, 29'-CH_2), 1.32-1.17 (m, 8H, 30, 30', 31, 31'-CH_2), 0.90-0.79 (m, 6H, 32, 32'-CH_3); ^{13}C NMR (126 MHz, MeOD), δ 161 (q *J* = 38.2Hz, CF_3CO_2), 159.0 (6-C), 157.6 (23, 23'-C), 156.3 (7-C), 148.7 (1-C), 148.4 (25, 25'-C), 146.5 (8-C), 137.3 (7-C), 136.4 (24, 24'-C), 134.8 (26-C), 134.6 (26'-C), 134.1 (19-C), 133.2 (19'-C), 128.0 (20-C), 125.8 (21, 21'-C), 123.5 (3-C), 122.9 (20'-C), 120.8 (22-C), 120.1 (22'-C), 118.5 (5-C),117.1 (4-C), 53.1 (27-C), 52.8 (27'-C), 51.1 (9-C), 50.1 (15-C), 39.9 (18-C), 37.7 (11, 12-C), 32.3 (17-C), 32.0 (30, 30'-C), 31.1 (13-C), 30.8 (28, 28'-C), 25.5 (31, 31'-C), 25.1 (10-C), 23.6 (29, 29'-C), 21.8 (14-C), 14.3 (32-C), 14.2 (32'-C); ^{19}F NMR (500MHz, MeOD), δ -63.6 (s, 3F-py), -76.1 (s, 3F-CF_3CO_2); MS (ES+) 1048 $[M]^+$, HRMS (ES+) $C_{46}H_{64}N_{13}F_3{}^{193}Ir$ requires 1048.5012 found 1048.4989.

6.5.15 Synthesis of $[Ir(L4)_2(L6.Boc)]PF_6$ $Ir(L4)_2L6.Boc$

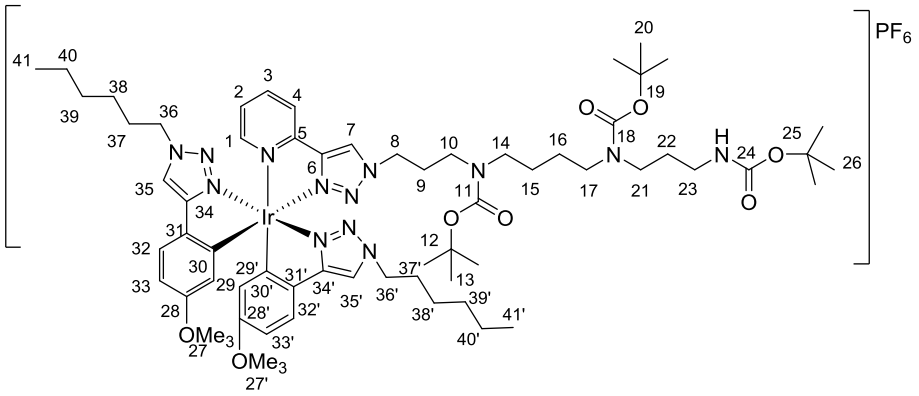

This was prepared from **$[Ir(L4)_2Cl]_2$** dimer (0.05 g, 0.03 mmol), **L6.Boc** (0.05 g, 0.07 mmol) and KPF_6 (0.01g, 0.07 mmol) according to method B and after work up gave product (0.12 g) as a crude. The crude was purified by RP-HPLC method A, in tR = 35 min to yield (0.08 g) of product. ^{1}H NMR (500 MHz, MeOD), δ 8.99 (s, 1H, 7-CH), 8.17 (d, *J* = 3.8 Hz, 1H, 1-CH), 8.14 (s, 2H, 35, 35'-CH), 8.09 (d, *J* = 5.1 Hz, 1H, 4-CH), 8.04 (t, *J* = 6.9 Hz, 1H, 3-CH), 7.43 (d, *J* = 8.2 Hz, 1H, 32-CH), 7.38 (d, *J* = 8.2 Hz, 1H, 32'-CH), 7.35 (d, *J* = 6.2 Hz, 1H, 2-CH), 6.54 (dd, *J* = 4.1, 2.2 Hz, 1H, 33-CH), 6.47 (dd, *J* = 4.1, 2.5 Hz, 1H, 33'-CH), 5.76 (d, *J* = 2.3Hz, 1H, 29-CH), 5.72 (d, *J* = 1.7 Hz, 1H, 29'-CH), 4.48 (s br, 2H, 8-CH_2), 4.32 (t, *J* = 6.9 Hz, 4H, 36, 36'-CH_2), 3.60 (s, 3H, 27-CH_3), 3.57 (s, 3H, 27'-CH_3), 3.23-3.16 (m, 8H, 10,14, 17, 21-CH_2), 3.04 (t, *J* = 6.7 H, 2H, 23-CH_2), 2.16-2.14 (m, 2H, 9-CH_2), 1.85-1.83 (m, 4H, 37, 37'-CH_2), 1.70-1.68 (m, 2H, 22-CH_2), 1.45 (d, *J* = 8.8 Hz, 31H, 15, 16-CH_2, 13, 20, 26-CH_3), 1.29 (s br, 12H, 38, 38', 39, 39', 40, 40'-CH_2), 0.89-0.87 (m, 6H, 41, 41'-CH_3); ^{13}C NMR (100MHz, MeOD), δ 160.9 (28-C), 160.2 (28'-C), 158.9 (31-C), 158.3 (31'-C), 155.8 (5-C), 152.3 (4-C), 151.9 (6-C), 149.0 (34-C), 145.5 (34'-C), 140.4 (3-C), 130.3 (30-C), 130.2 (30'-C), 126.8 (2-C), 126.2 (7-C), 124.5 (32-C), 123.9 (32'-C), 122.9 (1, 35-C), 120.4 (35'-C) 119.7 (29, 29'-C), 108.3 (33-C), 107.9 (33'-C), 81.3 (12-C), 81.1 (19-C), 80.1 (25-C), 55.3 (27, 27'-C), 53.0 (36-C), 52.9 (36'-C), 50.9 (8-C), 47.8 (10-C), 46.2 (14-C), 45.4 (17-C), 44.3 (21-C), 39.1 (23-C), 32.3 (9, 37, 37'-C), 31.2 (15, 16, 38, 38'-C), 29.0 (22-C) 28.9 (13, 20, 26-C), 26.9 (39, 39'-C), 23.6 (40, 40'-C), 14.5 (41, 41'-C); MS (ESI^+), 1340 $[M]^+$; HRMS (ES+) $C_{62}H_{93}N_{13}O_8{}^{193}Ir$ requires 1340.6907 found 1340.6899.

6.5.16 Synthesis of [Ir(L4)$_2$(L6)] (CF$_3$COO)$_4$ Ir(L4)$_2$L6

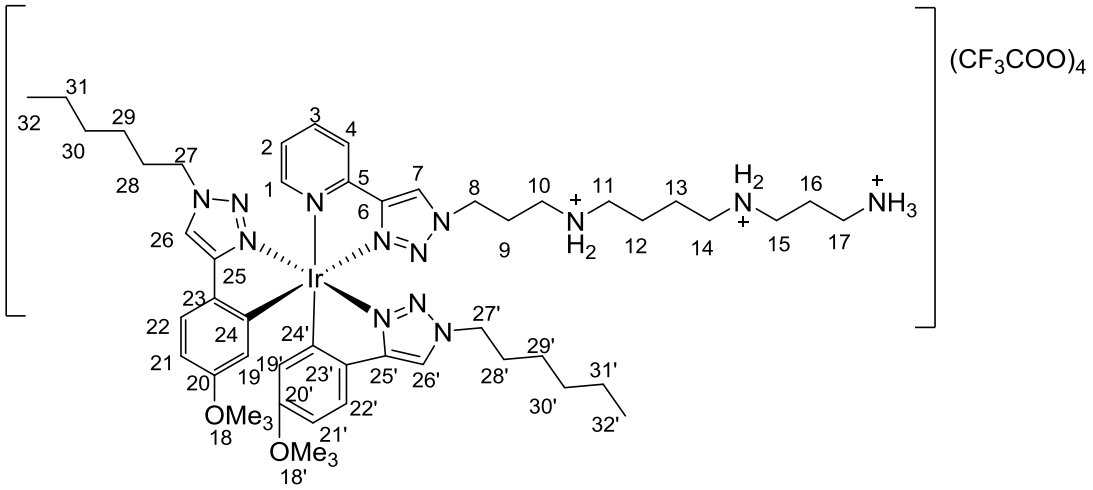

Ir(L4)$_2$L6.Boc (0.04 g, 0.026 mmol) was dissolved in 4M TFA in DCM and stirred at t rt. for 18hr. The volatiles were removed to produce the product (0.043 g) without further purification. ^{1}H NMR (500MHz, MeOD), δ 9.03 (s, 1H, 7-CH), 8.20-8.18 (m, 3H, 1, 26, 26'-CH), 8.08 (d, *J* = 5.3 Hz, 1H, 4-CH), 8.04 (t, *J* = 8.4 Hz, 1H, 3-CH), 7.45 (d, *J* = 8.4 Hz, 1H, 22-CH), 7.40 (d, *J* = 8.2 Hz, 22'-CH), 7.37 (t, *J* = 6.2 Hz, 1H, 2-CH), 6.57 (dd, *J* = 8.1, 2.3 Hz, 1H, 21-CH), 6.50 (dd, *J* = 8.3, 2.3 Hz, 1H, 21'-CH), 5.75 (d, *J* = 5.7, 2.3 H, 1H, 18-CH), 5.69 (d, *J* = 2.3 Hz, 1H, 18'-CH), 4.64 (t, *J* = 7.3 Hz, 2H, 8-CH$_2$), 4.33 (t, *J* = 4.8 Hz, 4H, 27, 27'-CH$_2$), 3.60 (s, 3H, 19-CH$_3$), 3.58 (s, 3H, 19-CH$_3$), 3.15 (t, *J* = 7.3 Hz, 2H, 17-CH$_2$), 3.09-3.07 (m, 6H, 10, 11, 15-CH$_2$), 3.02 (t, *J* = 6.6 Hz, 2H, 14-CH$_2$), 2.37-2.36 (m, 2H, 9-CH$_2$), 2.12-2.11 (m, 2H, 16-CH$_2$), 1.86-1.83 (m, 4H, 12, 13-CH$_2$), 1.79 (s br, 4H, 28, 28'-CH$_2$), 1.34-1.24 (m, 12H, 29, 29', 30, 30', 31, 31'-CH$_2$), 0.89-0.87 (m, 6H, 32, 32'-CH$_3$); ^{13}C NMR (125 MHz, MeOD), δ 160.8 (20-C), 160.1 (20'-C), 158.7 (23-C), 158.3 (23'-C), 152.2 (4-C), 151.6 (5-C), 150.7 (6-C), 148.6 (25-C), 145.2 (25'-C), 140.3 (3-C), 130.2 (24-C), 130.0 (24'-C), 126.8 (2-C), 126.4 (7-C), 124.4 (22-C), 123.7 (22'-C), 122.9 (1-C), 121.7 (26-C), 120.1 (18-C), 119.3 (18'-C), 116.9 (26'-C), 108.3 (21-C), 107.9 (21'-C), 55.2 (19-C), 55.1 (19'-C), 52. 9 (27-C), 52.7 (27'-C), 49.8 (8-C), 48.5 (17-C), 48.2 (15-C), 45.8 (10, 11-C), 37.8 (14-C), 32.2 (29-C), 32.1 (29'-C), 31.1 (12, 13-C), 27.5 (30-C), 26.9 (30-C), 27.5 (30'-C), 25.3 (9, 16-C), 24.3 (28-C), 24.2 (28'-C), 23.4 (31, 31'-C), 14.3 (32, 32'-C); ^{19}F NMR (500MHz, MeOD), δ -77.3 (s, 3F-CF$_3$CO$_2$); MS (ESI$^+$), 1040 [M]$^+$; HRMS (ES+) $C_{47}H_{69}N_{13}O_2{}^{193}Ir$ requires 1040.5326 found 1040.65326.

6.5.17 Synthesis of $[Ir(L4)_2(L8.Boc)]PF_6$ $Ir(L4)_2L8.Boc$

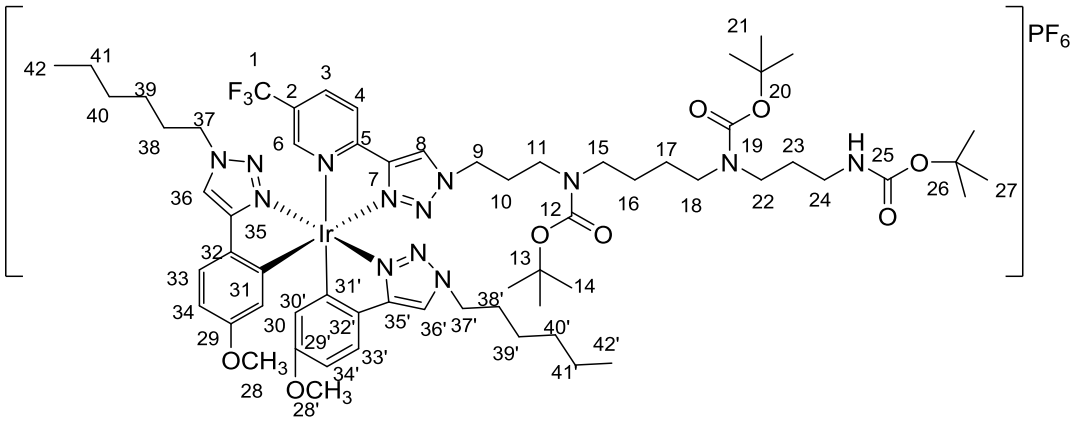

$[Ir(L4)_2Cl]_2$ dimer (0.05 g, 0.03 mmol), **L8.Boc** (0.05 g, 0.07 mmol) and KPF_6 (0.01 g, 0.07 mmol) according to method B and after work up gave as a yellow sold. The residue was purified through alumina, eluting with (70:30) MeOH /DCM (0.09 g, 80 %) and then purified by RP-HPLC method A, R_t = 38 min to produce (0.04 g) of product as a pure; ^{1}H NMR (500MHz, MeOD), δ 9.19 (s, 1H, 6-C), 8.38 (d, *J* = 8.3 Hz, 1H, 3-C), 8.31 (s, 1H, 8-CH), 8.18 (d, *J* = 5.7 Hz,1H, 4-CH), 7.74 (d, *J* = 8.3 Hz, 1H, 36-CH), 7.46 (d, *J* = 8.3 Hz, 1H, 33-CH), 7.39 (d, *J* = 8.2 Hz, 1H, 33'-CH), 6.99 (d, *J* = 8.7 Hz, 1H, 36'-CH), 6.56 (dd, 8.4, 2.4 Hz, 1H, 34-CH), 6.49 (dd, *J* = 8.3, 2.3 Hz, 1H, 34'-CH), 5.76 (d, *J* = 2.3 Hz, 1H, 30-CH), 5.72 (d, *J* = 2.1 Hz, 1H, 30'-CH), 4.52-4.50 (m, 2H, 9-CH_2), 4.34-4.32 (m, 4H, 37, 37'-CH_2), 3.61 (s, 3H, 28-CH_3), 3.58 (s, 3H, 28'-CH_3), 3.23-3.21 (m, 8H, 11, 15, 18, 22-CH_2), 3.04 (t, *J* = 6.7 Hz, 2H, 24-CH_2), 2.17 (s br, 2H, 10-CH_2), 1.86-1.84 (m, 4H, 16, 17-CH_2), 1.71-1.69 (m, 2H, 23-CH_2), 1.46 (d, *J* = 9.0 Hz, 31H, 38, 38'-CH_2, 14, 21, 27-CH_3), 1.32-1.30 (m, 12H, 39, 39', 40, 40', 41, 41'-CH_2), 0.88-0.86 (m, 6H, 42, 42'-CH_3); ^{13}C NMR (125 MHz, MeOD), δ 160.9 (32-C), 160.2 (32'-C), 158.1 (5-C), 155.4 (7-C), 149.3 (2-C), 147.9 (35, 35'-C), 144.2 (29, 29'-C), 137.8 (4-C), 130.0 (31, 31'-C), 128.0 (6, 36-C), 124.6 (33-C), 123.9 (33'-C), 120.1 (30-C), 119.6 (30'-C), 119.4 (3-C), 115.3 (36'-C), 108.6 (34-C), 108.1 (34'-C), 81.2, 80.9, 79.9 (13, 20, 26-C), 55.3 (28-C), 55.2 (28'-C), 53.0 (37-C), 52.8 (37'-C), 51.4 (9-C), 47.8 (11,12-C), 45.6 (18, 22-C), 39.0 (24-C), 32.2, 32.1 (39, 39'-C), 31.2 (10-C), 31.0 (16, 17-C), 30.1 (23-C), 28.8 (38, 38', 14, 21, 27-C), 27.2 (40-C), 27.0 (40'-C), 23.5 (41-C), 23.4 (41'-C), 14.3 (42, 42'-C); ^{19}F NMR (500MHz, MeOD), δ -64.4 (s, 3F-py); MS (ESI^+), 1408 $[M]^+$; HRMS (ES+) $C_{63}H_{92}N_{13}O_8F_3{}^{193}Ir$ requires 1408.6824 found 1408.6773.

6.5.18 [Ir(L4)$_2$(L8)] (CF$_3$COO)$_4$ Ir(L4)$_2$L8

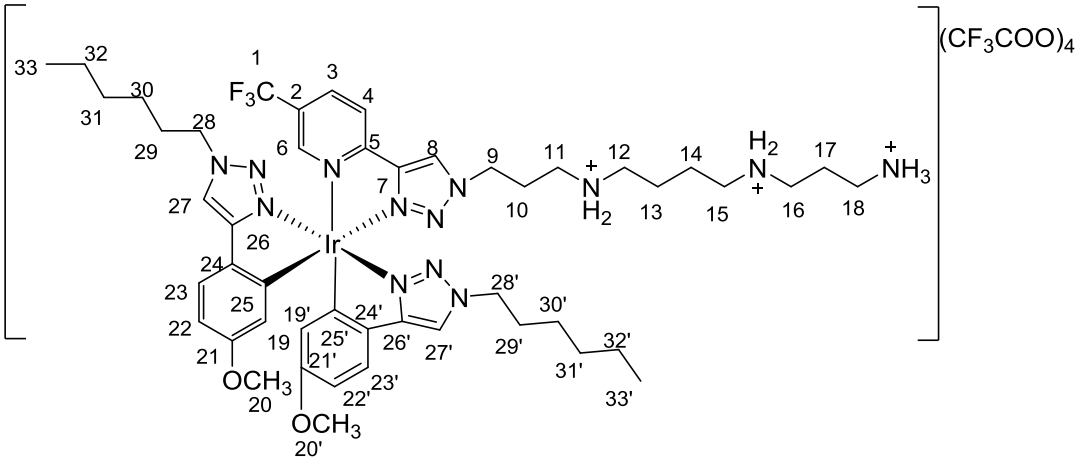

Ir(L4)$_2$L8.Boc (0.03 g, 0.02 mmol) was dissolved in 4M TFA in DCM and stirred at rt. for 18hr. The volatiles were removed to produce the product (0.034g) without further purification. ^{1}H NMR (500MHz, MeOD), δ 9.18 (s, 1H, 6-CH), 8.41 (s, 2H, 27, 27'-CH), 8.31 (s, 1H, 8-CH), 8.21 (d, *J* = 8.4 Hz, 2H, 3, 4-CH), 7.51 (d, *J* = 8.3 Hz, 23-CH), 7.42 (d, *J* = 8.3 Hz, 1H, 23'-CH), 6.63 (dd, *J* = 8.3, 2.5 Hz, 1H, 22-CH), 6.53 (d, *J* = 8.4, 2.5 Hz, 1H, 22'-CH), 5.77 (d, *J* = 2.4 Hz, 1H, 19-CH), 5.70 (d, *J* = 2.4 Hz, 1H, 19'-CH), 4.68 (t, *J* = 7.4 Hz, 2H, 9-CH$_2$), 4.37-4.32 (m, 4H, 28, 28'-CH$_2$), 3.63 (s, 3H, 20-CH$_3$), 3.60 (s, 3H, 20'-CH$_3$), 3.16-3.12 (m, 4H, 11, 12-CH$_2$), 3.09 (t, *J* = 6.8 Hz, 4H, 15, 16-CH$_2$), 3.04 (t, *J* = 7.1 Hz, 2H, 18-CH$_2$), 2.43-2.37 (m, 2H, 10-CH$_2$), 2.15-2.09 (m, 2H, 17-CH$_2$), 1.88-1.82 (m, 8H, 13, 14, 29, 29'-CH$_2$), 1.30-1.26 (m, 12H, 30, 30', 31, 31', 32, 32'-CH$_2$), 0.91-0.80 (m, 6H, 33, 33'-CH$_3$); ^{13}C NMR (125 MHz, MeOD), δ 162.4 (21, 21'-C), 159.1 (5-C), 158.1 (24, 24'-C), 157.5 (7-C), 150.2 (2-C), 149.1 (8-C), 135.8 (27, 27'-C), 133.3 (25-C), 131.7 (25'-C), 127.8 (6-C), 123.8 (23-C), 122.9 (23'-C), 123.4 (3-C), 120.8 (19-C), 119.4 (19'-C), 118.2 (4-C), 110.7 (22-C), 106.8 (22'-C), 55.0 (20, 20'-C), 52.7 (28-C), 52.1 (28'-C), 50.8 (9-C), 47.5 (11, 12-C), 45.9 (15,16-C), 35.5 (18-C), 32.1 (30, 30'-C), 30.9 (13, 14-C), 27.8 (17-C), 26.9 (31, 31'-C), 25.8 (10-C), 23.3 (29, 29'-C), 22.4 (32, 32'-C), 14.1 (33, 33'-C); ^{19}F NMR (500MHz, MeOD), δ -64.4 (s, 3F-py), -76.8 (s, 3F-CF$_3$CO$_2$); MS (ESI$^+$), 1108 [M]$^+$; HRMS (ES+) C$_{48}$H$_{68}$N$_{13}$O$_2$F$_3$^{193}Ir requires 1108.5211 found 1108.5200.

6.5.19 [Ir(L12)$_2$(L8.Boc)]PF$_6$ Ir(L12)$_2$L8.Boc

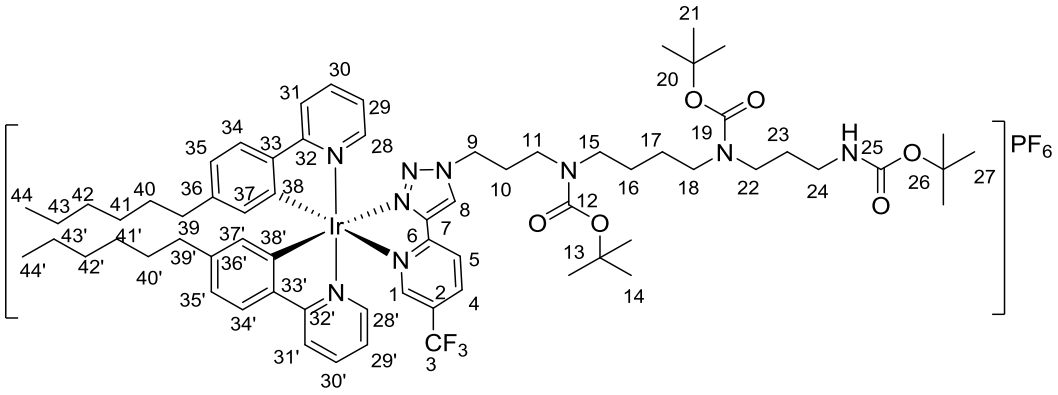

This was prepared from **[Ir(L12)$_2$Cl]$_2$** dimer (0.02 g, 0.01 mmol), **L8.Boc** (0.02 g, 0.03 mmol) and KPF_6 (0.01g, 0.03 mmol) according to method B and after work up gave the product as a crude (0.06 g). Crude was purified by RP-HPLC method A, tR = 39 min to give (0.025 g) as a pure of product. ^{1}H NMR (500 MHz, MeOD), δ 9.21 (s, 1H, 1-CH), 8.44 (m, 2H, 28, 28'-CH), 8.08 (s, 1H, 8-CH), 8.07(d, *J* = 4.9Hz, 1H, 31-CH), 8.05(d, *J* = 4.7 Hz, 1H, 31'-CH), 7.88 (dd, *J* = 7.0, 1.4 Hz, 1H, 34-CH), 7.85(dd, *J* = 7.0, 1.5 Hz, 1H, 34'-CH), 7.79 (d, *J* = 5.7 Hz, 1H, 4-CH), 7.74 (d, *J* = 7.8 Hz, 1H, 29-CH), 7.66 (d, *J* = 7.8 Hz, 1H, 29'-CH), 7.65-7.63 (m, 1H, 5-CH), 7.10 (ddd, *J* = 8.1, 6.8, 1.4 Hz, 30-CH), 7.04 (ddd, *J* = 7.1, 6.7, 1.3 Hz, 30'-CH), 6.91 (dd, *J* = 7.8, 1.6 Hz, 1H, 35-CH), 6.80 (dd, *J* = 8.1, 1.6 Hz, 1H, 35'-CH), 6.14 (d, *J* = 1.3 Hz, 1H, 37-CH), 6.09 (d, *J* = 1.3 Hz, 1H, 37'-CH), 4.54 (t, *J* = 7.1 Hz, 2H, 9-CH$_2$), 3.24-3.20 (m, 6H, 11, 15, 18-CH$_2$), 3.17-3.14 (m, 2H, 22-CH$_2$), 3.05 (t, *J* = 6.7 Hz, 2H, 24-CH$_2$), 2.44-2.33 (m, 4H, 39, 39'-CH$_2$), 2.22-2.18 (m, 2H, 10-CH$_2$), 1.37-1.68 (m, 2H, 23-CH$_2$), 1.45 (d, *J* = 8.1 Hz, 31H, 16, 17-CH$_2$, 14, 21, 27-CH$_3$), 1.43 (s br, 4H, 40, 40'-CH$_2$), 1.20-1.12 (m, 12H, 41, 41', 42, 42', 43, 43'-CH$_2$), 0.85 (t, *J* = 7.1 Hz, 6H, 44, 44'-CH$_3$); ^{13}C NMR (126 MHz, MeOD), δ 169.7 (32-C), 169.3 (32-C), 159.9 (33-C), 159.1 (33-C), 157.5 (6-C), 151.2 (38-C), 150.9 (38'-C),150.1 (4-C), 150.3 (2-C), 148.7 (5-C), 148.4 (8-C), 148.2 (7-C), 142.0 (36-C), 141.8 (36'-C), 139.4 (28-C), 132.8 (37-C), 132.6 (37'-C), 127.8 (1-C), 126.0 (34-C), 125.4 (34'-C), 125.1 (35-C), 124.6 (28'-C), 124.1 (35'-C), 123.7 (29, 29'-C), 123.6 (3-C), 120.6 (30-C), 120.4 (30'-C), 81.8, 81.3, 81.0 (13, 20, 26-C) 51.2 (9-C), 48.2 (11, 15-C), 47.8 (11-C), 46.6 (18-C), 44.5 (22-C), 39.1 (24-C), 36.8 (39-C), 36.7 (39'-C), 32.7 (16, 17, 23-C), 31.7 (40-C), 31.9 (40'-C), 29.6 (10, 41, 41'-C), 26.9 (40-C), 28.8 (14, 21, 27-C), 28.7 (43, 43'-C), 23.5 (42, 42'-C), 14.4 (44-C), 14.3 (44'-C); ^{19}F NMR (500MHz, MeOD), δ -64.3 (s, 3F-py); MS (ES+) 1370 [M]$^+$, HRMS (ES+) $C_{67}H_{92}N_9F_3{}^{193}Ir$ requires 1368.6764 found 1368.6752.

6.5.20 [Ir(L12)$_2$(L9)] (CF$_3$COO)$_4$ Ir(L12)$_2$L8

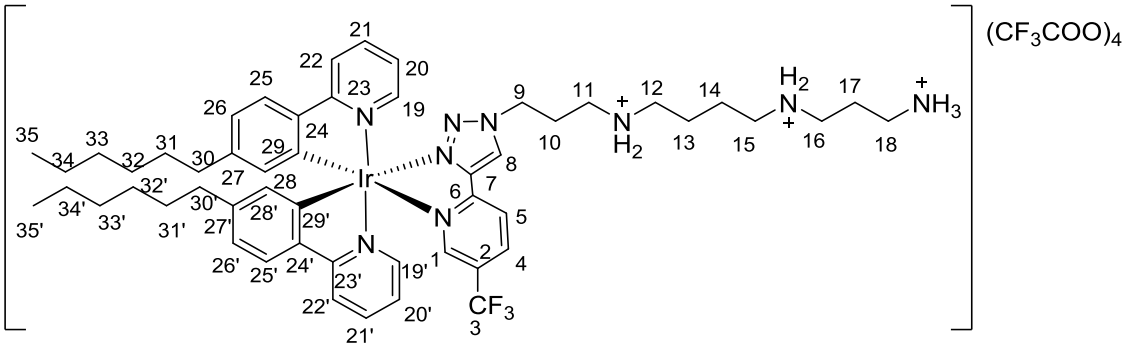

Ir(L12)$_2$L8.Boc (0.02g, 0.01 mmol) was dissolved in 4M TFA in DCM and stirred at rt. for 18hr. The volatiles were removed and the crude solid was dissolved in water, and then dried by freeze drying to produce (0.03g) as pure product. ^{1}H NMR (500 MHz, MeOD), δ 9.28 (s, 1H, 1-CH), 8.49-8.47 (m, 2H, 19, 19'-CH), 8.09-8.07 (m, 3H, 8, 22, 22'-CH), 7.90 (dd, *J* = 8.9, 1.4 Hz, 1H, 25-CH), 7.86 (dd, *J* = 8.8, 1.4 Hz, 1H, 25'-CH), 7.79 (d, *J* = 5.6 Hz, 1H, 4-CH), 7.76 (d, *J* = 8.1 Hz, 1H, 21-CH), 7.69 (d, *J* = 5.7 Hz, 1H, 5-CH), 7.65 (d, *J* = 8.2 Hz, 1H, 21'-CH), 7.10 (ddd, *J* = 7.6, 6.6, 1.4 Hz, 1H, 20-CH), 7.05 (ddd, *J* = 7.5, 6.7, 1.3 Hz, 1H, 20'-CH), 6.93 (dd, *J* = 7.9, 1.5 Hz, 1H, 26-CH), 6.79 (dd, *J* = 7.9, 1.6 Hz, 1H, 26'-CH), 6.11 (d, *J* = 1.4 Hz, 1H, 28-CH), 6.06 (d, *J* = 1.4 Hz, 1H, 28'-CH), 4.67 (t, *J* = 7.3 Hz, 2H, 9-CH$_2$), 3.15 (t, *J* = 7.7 Hz, 2H, 18-CH$_2$), 3.10-3.06 (m, 6H, 11, 12, 15-CH$_2$), 3.02 (t, *J* = 7.5 Hz, 2H, 16-CH$_2$), 2.44-2.30 (m, 4H, 13, 14-CH$_2$), 2.13-2.07 (m, 2H, 10-CH$_2$), 1.80-1.78 (m, 6H, 17, 30, 30'-CH$_2$), 1.38-1.26 (m, 8H, 31, 31', 32, 32'-CH$_2$), 1.20-1.12 (m, 8H, 33, 33', 34, 34'-CH$_2$), 0.85 (t, *J* = 6.9 Hz, 6H, 35, 35'-CH$_3$); ^{13}C NMR (126 MHz, MeOD), δ 168.9 (24-C), 168.2 (24'-C), 154.5 (6-C), 153.7 (23, 23'-C), 149.9 (4-C), 149.4 (5-C), 149.3 (2-C), 148.5 (29-C), 148.1 (29'-C), 147.1 (8-C), 145.1 (7-C), 142.1 (27-C), 142.0 (27'-C), 138.9 (25-C), 138.7 (25'-C), 137.4 (19'-C), 132.1 (28-C), 131.8 (28'-C), 125.2 (1-C), 124.6 (21-C), 123.8 (21'-C), 123.5 (20, 20'-C), 123.3 (3, 19-C), 122.9 (26, 26'-C), 119.8 (22-C), 119.6 (22'-C), 49.5 (9-C), 47.4 (11, 16-C), 45.0 (12, 18-C), 37.0 (15-C), 36.1 (13-C), 35.9 (14-C), 31.9 (33, 33'-C), 31.3 (32-C), 31.1 (32'-C), 28.9 (31-C), 28.6 (31'-C), 26.6 (17-C), 24.5 (10-C), 23.4 (30, 30'-C), 22.8 (34, 34'-C), 13.6 (35, 35'-C); ^{19}F NMR (500MHz, MeOD), δ -65.0 (s, 3F-py) -76.3 (s, 3F-CF$_3$CO$_2$); MS (ES+) 1066 [M]$^+$, HRMS (ES+) $C_{53}H_{70}N_8F_3{}^{193}Ir$ requires 1066.5190 found 1066.5148.

6.5.21 $[Ir(L12)_2(L9.Boc)](PF_6)$ $Ir(L12)_2L9.Boc$

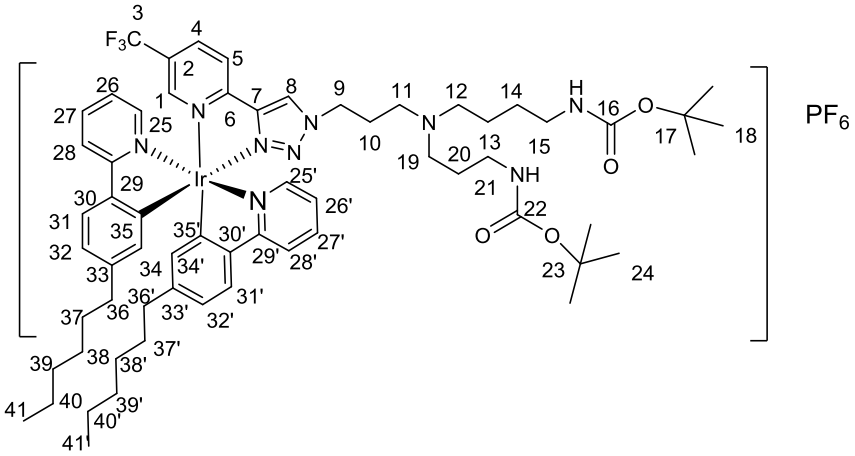

This was prepared from **$[Ir(L12)_2Cl]_2$** dimer (0.06 g, 0.04 mmol), **L9.Boc** (0.06 g, 0.017 mmol) and KPF_6 (0.01 g, 0.017mmol) according to method B and after work up gave the product as a crude (0.11g). Crude was purified by RP-HPLC method A, tR = 38 min to give (0.06 g) as a pure of product. ^{1}H NMR (500 MHz, MeOD), δ 9.32 (s, 1H, 1-CH), 8.51(d, *J* = 8.4 Hz, 1H, 25-CH), 8.47 (d, *J* = 8.4 Hz, 1H, 25'-CH), 8.09-8.06 (m, 3H, 8, 28, 28'-CH), 7.88 (t, *J* = 8.6, 7.7 Hz, 2H, 31, 31'-CH), 7.80 (d, *J* = 5.4 Hz, 1H, 4-CH), 7.73 (d, *J* = 7.9 Hz, 1H, 5-CH), 7.69-7.67 (m, 2H, 27, 27'-CH), 7.11 (d, *J* = 6.4 Hz, 1H, 26-CH), 7.06 (t, *J* = 6.5 Hz, 1H, 26'-CH), 6.90 (d, *J* = 7.5 Hz, 1H, 32-CH), 6.80 (d, *J* = 7.9 Hz, 1H, 32'-CH), 6.10 (s, 1H, 34-CH), 6.07 (s, 1H, 34'-CH), 4.67 (t, *J* = 6.8 Hz, 2H, 9-CH_2), 3.27-3.20 (m, 2H, 11-CH_2), 3.14-3.11(m, 6H, 12, 15, 21-CH_2), 2.35-2.25 (m, 6H, 10, 19, 20-CH_2), 1.85-1.80 (m, 2H, 13-CH_2), 1.69-1.63 (m, 2H, 14-CH_2), 1.44 (d, *J* = 1.9 Hz, 22H, 36, 36'-CH_2, 18, 24-CH_3), 1.22-1.19 (m, 16H, 37, 37', 38, 38', 39,39', 40, 40'-CH_3), 0.85 (t, *J* = 6.8 Hz, 6H, 41, 41'-CH_3); ^{13}C NMR (125 MHz, MeOD), δ 169.7 (29-C), 169.0 (29'-C), 154.5 (6, 35, 35'-C), 150.2 (4-C), 150.0 (2-C), 147.8 (5-C), 147. 0(30-C), 146.7 (30'-C), 146.8 (8-C), 145.8 (7-C), 142.9 (33-C), 142.8 (33'-C), 139.7 (28-C), 139.3 (28'-C), 138.3 (25-C), 132.8 (34-C), 132.6 (34'-C), 126.1 (1-C), 125.4 (31-C), 124.6 (31'-C), 124.3 (27-C), 124.1 (27'-C), 123.8 (32, 32'-C), 120.7 (26-C), 120.4 (26'-C), 80.5 (17-C), 80.1 (23-C), 51.9 (15-C), 50.9 (11-C), 50.3 (9-C), 36.9 (12-C), 36.7 (19, 21-C), 32.7 (37, 37'-C), 32.1 (38, 38'-C), 29.7 (36-C), 29.4 (36'-C), 28.8 (18, 24-C), 28.0 (14-C), 25.4 (20-C), 24.9 (10-C), 23.6 (39, 39', 40, 40'-C), 21.9 (13-C), 14.4 (41, 41'-C); ^{19}F NMR (500MHz, MeOD), δ -64.4 (s, 3F-py); MS (ES+) 1270 $[M]^+$, HRMS (ES+) $C_{62}H_{84}N_9O_4F_3{}^{193}Ir$ requires 1268.6290 found 1268.6228.

6.5.22 [Ir(L12)$_2$(L9)] (CF$_3$COO)$_4$ Ir(L12)$_2$L9

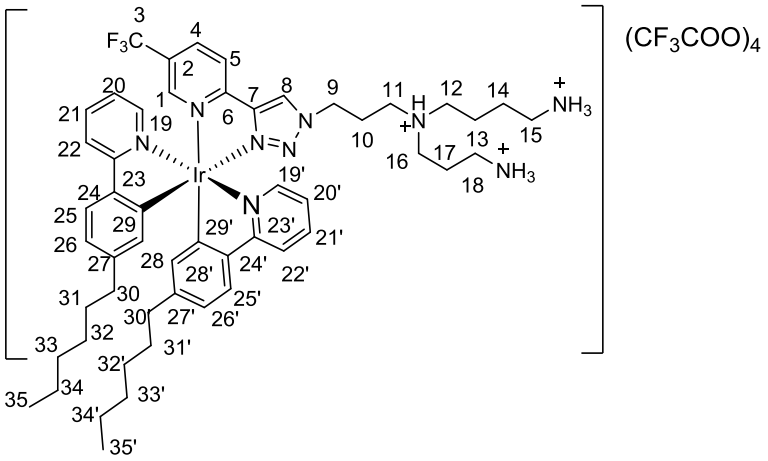

Ir(L12)L9.Boc (0.03 g, 0.02 mmol) was dissolved in 4M TFA in DCM and stirred at rt. for 18hr. The volatiles were removed, and the crude solid was and then dried by freeze drying to produce (0.04 g) as pure product. ^{1}H NMR (500 MHz, MeOD), δ 9.22 (s,1H, 1-CH), 8.39 (d, *J* = 8.3 Hz, 1H, 19-CH), 8.34 (d, *J* = 7.7 Hz, 1H, 19'-CH), 7.95-7.93 (m, 3H, 8, 22, 22'-CH), 7.75 (ddd, 8.4, 7.5, 2.2 Hz, 2H, 25, 25'-CH), 7.68 (d, *J* = 5.6 Hz, 1H, 4-CH), 7.61 (d, *J* = 7.8 Hz, 1H, 21-CH), 7.55 (d, *J* = 6.0 Hz, 1H, 5-CH), 7.53 (d, *J* = 8.0 Hz, 1H, 21'-CH), 6.99 (t, *J* = 6.7Hz, 1H, 20-CH), 6.93 (t, *J* = 6.8 Hz, 1H, 20'-CH) 6.78 (d, *J* = 8.0Hz, 1H, 26-CH), 6.67(d, *J* = 8.0 Hz, 1H, 26'-CH), 5.98 (s, 1H, 28-CH), 5.95 (s, 1H, 28'-CH), 4.54 (t, *J* = 7.2 Hz, 2H, 9-CH$_2$), 3.19-3.15 (m, 2H, 11-CH$_2$), 3.11-3.08 (m, 2H, 12-CH$_2$), 2.92 (t, *J* = 7.1 Hz, 2H, 15-CH$_2$), 2.88 (t, *J* = 7.3 Hz, 2H, 18-CH$_2$), 2.33-2.23 (m, 2H, 16-CH$_2$), 2.29-2.15 (m, 4H, 30, 30'-CH$_2$), 2.00 (s br, 2H, 10-CH$_2$), 1.71-1.70 (m, 2H, 17-CH$_2$), 1.64-1.58 (m, 2H, 13-CH$_2$), 1.31-1.20 (m, 6H, 14, 31, 31'-CH$_2$), 1.10-1.01 (m, 12H, 32, 32', 33, 33', 34, 34'-CH$_2$), 0.73 (t, *J* = 6.9 Hz, 6H, 35, 35'-CH3); ^{13}C NMR (125 MHz, MeOD), δ 169.7 (23-C), 169.0 (23'-C), 162.6 (q, *J* = 34.1 Hz, $CF_3CO_2^-$), 157.8 (6-C), 154.6 (24, 24'-C), 148.9 (2-C), 148.1 (5-C), 147.8 (4-C),147.5 (29-C), 147.3 (29'-C), 142.9 (27-C), 142.8 (27'-C), 139.7 (25-C), 139.4 (25'-C), 138.3 (19'-C), 137.3 (7-C), 132.8 (28-C), 132.6 (28'-C), 129.1(1-C), 124.6 (21, 21'-C), 124.3 (3-C), 124.1 (26, 26'-C), 123.7 (19-C), 121.8 (20-C), 121.1 (20'-C), 120.6 (22-C), 120.4 (22'-C), 53.6 (12-C), 51.1 (11-C), 51.0 (16-C), 50.3 (9-C), 38.5 (18-C), 37.7 (15-C), 36.9 (30-C), 36.7 (30'-C), 32.1 (32-C), 31.9 (32'-C), 29.7 (13, 33-C), 29.4 (14, 33'-C), 25.5 (31-C), 25.1 (31'-C), 23.6 (16-C), 21.8 (10, 34, 34'-C), 21.2 (17-C), 14.4 (35, 35'-C); ^{19}F NMR (500MHz, MeOD), δ -64.8 (s, 3F-py), -76.8 (s, 3F-CF_3CO_2); MS (ES+) 1068 $[M]^+$, HRMS (ES+) $C_{52}H_{68}N_9F_3{}^{193}Ir$ requires 1068.5189 found 1068.5179.

6.5.23 $[Ir(L1)_2(L15.Boc)]PF_6$ $Ir(L1)_2L15.Boc$

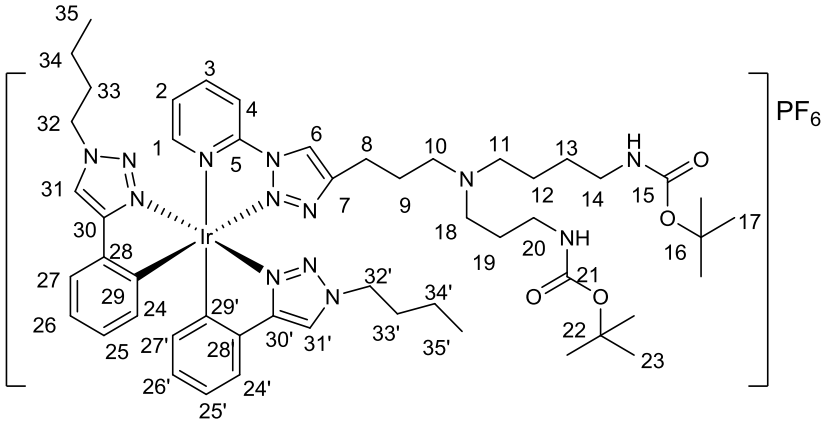

This was prepared from **$[Ir(L1)_2Cl]_2$** dimer (0.08 g, 0.59 mmol), **L15.Boc** (0.07g, 0.13 mmol) and KPF_6 (0.02 g, 0.13 mmol) according to method B and after work up gave the product as a crude (0.11 g). Crude was purified by RP-HPLC method A, tR = 29 min to give (0.05g) as a pure product. ^{1}H NMR (500 MHz, MeOD), δ 9.05 (s, 1H, 6-CH), 8.34 (d, *J* = 6.7 Hz, 2H, 31, 31'-CH), 8.20 (d, *J* = 7.8 Hz, 1H, 1-CH), 8.06 (d, *J* = 7.6 Hz, 1H, 4-CH), 8.02 (d, *J* = 4.6 Hz, 1H, 3-CH), 7.51 (d, *J* = 7.4 Hz, 27-CH), 7.47 (d, *J* = 7.5 Hz, 1H, 27'-CH), 7.35 (ddd, *J* = 7.8, 6.8, 1.0 Hz, 1H, 2-CH), 6.96 (ddd, *J* = 8.1, 7.4, 0.9 Hz, 1H, 26-CH), 6.89 (ddd, *J* = 8.1, 7.5, 0.9Hz, 1H, 26'-CH), 6.81(ddd, *J* = 8.2, 7.5, 1.2 Hz, 1H, 25-CH), 6.73 (ddd, *J* = 8.3, 7.5, 1.2 Hz, 1H, 25'-CH), 6.26 (d, *J* = 7.4 Hz, 1H, 24-CH), 6.18 (d, *J* = 7.3 Hz, 1H, 24'-CH), 4.62 (t, *J* = 5.8 Hz, 2H, 14-CH_2), 4.36 (t, *J* = 5.8 Hz, 4H, 32, 32'-CH_2), 3.24 (t, *J* = 7.7 Hz, 2H, 8-CH_2), 3.11 (t, *J* = 6.8 Hz, 6H, 10, 11, 20-CH_2), 2.44-2.38 (m, 2H, 18-CH_2), 1.92-1.79 (m, 8H, 9, 19, 12, 13-CH_2), 1.71-1.63 (m, 2H, 33-CH_2), 1.55-1.50 (m, 2H, 33'-CH_2), 1.44 (s, 18H, 17, 23-CH_3), 1.37-1.19 (m, 4H, 34, 34'-CH_2), 0.96-0.88 (m, 6H, 35, 35'-CH_3), ^{13}C NMR (126 MHz, MeOD), δ 159.0 (28-C), 158.6 (28'-C), 152.3 (3-C), 151.7 (5-C), 150.9 (7-C), 146.6 (29-C), 143.3 (29'-C), 140.5 (4-C), 137.3 (30, 30'-C), 134.3 (24-C), 133.5 (24'-C), 129.3 (25-C), 128.6 (25'-C), 127.0 (2-C), 126.8 (6-C), 123.9 (26-C), 123.5 (27-C), 123.3 (26'-C), 123.0 (27'-C), 123.1 (1-C), 120.7 (31-C), 120.4 (31'-C), 80.6, 80.1 (16, 22-C), 54.1 (10-C), 53.0 (11-C), 52.8 (32-C), 52.8 (32'-C), 51.2 (8-C), 50.9 (14-C), 40.4 (20-C), 38.4 (18-C), 33.2 (19-C), 28.9 (17, 23-C), 28.2 (33, 33'-C), 25.6 (9-C), 25.1 (12-C), 22.1 (13-C), 20.6 (34, 34'-C), 31.8 (35, 35'-C); MS (ES+) 1124 $[M]^+$, HRMS (ES+) $C_{51}H_{73}N_{13}O_4{}^{193}Ir$ requires 1124.5549 found 1124.5538.

6.5.24 [Ir(L1)(L15)] $(CF_3COO)_4$ $Ir(L1)_2L15$

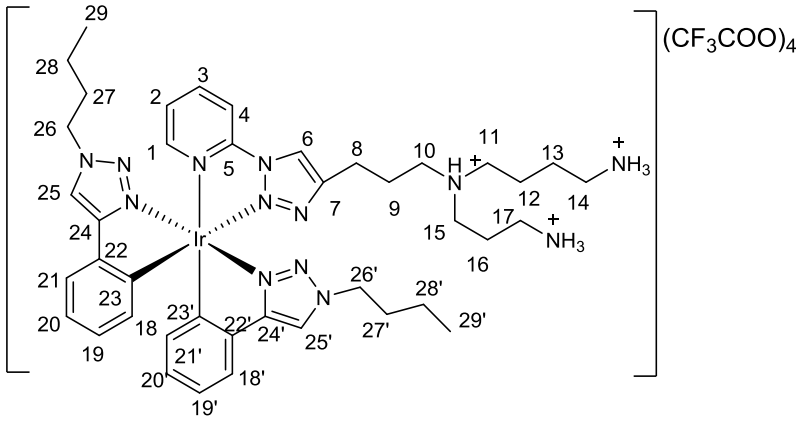

$Ir(L1)_2$15.Boc (0.02 g, 0.015 mmol) was dissolved in 4M TFA in DCM and stirred at rt. for 18hr. The volatiles were removed, and the crude solid was dissolved in water, and then dried by freeze drying to produce (0.025 g) as pure product. ^{1}H NMR (500 MHz, MeOD), δ 9.12 (s, 1H, 6-CH), 8.30 (d, *J* = 4.6 Hz, 1-CH), 8.28 (s, 2H, 25, 25'-CH), 8.19 (ddd, *J* = 8.8, 8.3, 1.4 Hz, 1H, 3-CH), 7.93 (d, *J* = 5.3 Hz, 1H, 4-CH),7.44 (d, *J* = 6.1Hz, 1H, 2-CH), 7.14 (d, *J* = 7.3 Hz, 1H, 21-CH), 7.37 (d, *J* = 6.9 Hz, 1H, 21'-CH), 6.88 (ddd, *J* = 7.8, 7.5 Hz, 1H, 20-CH), 6.81 (ddd, *J* = 7.5, 7.9 Hz, 1H, 20'-CH), 6.71(ddd, *J* = 8.4, 7.3, 1.2 Hz, 1H, 19-CH), 6.64 (ddd, *J* = 8.7, 6.4, 1.1 Hz, 1H, 19'-CH), 6.09 (d, *J* = 7.5 Hz, 1H, 18-CH), 6.01 (d, *J* = 7.4 Hz, 1H, 18'-CH), 4.26 (t, *J* = 7.0 Hz, 4H, 26, 26'-CH_2), 3.18-3.17 (m, 4H, 14, 17-CH_2), 3.07-3.05 (m, 2H, 8-CH), 2.98-2.91 (m, 4H, 10,11-CH_2), 2.87 (t, *J* = 7.3 Hz, 2H, 15-CH_2), 2.19-2.15(m, 4H, 12, 13-CH_2), 1.91-1.83 (m, 6H, 16, 27, 27'-CH_2), 1.77-1.70 (m, 2H, 9-CH_2), 1.35-1.24 (m, 4H, 28, 28'-CH_2), 0.96-0.90 (m, 6H, 29, 29'-CH_3); ^{13}C NMR (125 MHz, MeOD), δ 158.8 (22, 22'-C), 154.6 (5-C), 152.7 (7-C), 151.6 (4-C), 143.1 (3-C), 137.3 (24 , 24'-C), 133.9 (18-C), 133.2 (18'-C), 129.3 (19-C), 128.6 (19'-C), 126.2 (2-C), 125.8 (6-C), 124.3 (20-C), 123.9 (20'-C), 123.7 (21-C), 123.6 (21'-C), 120.8 (25-C), 120.6 (25'-C), 114.9 (1-C), 53.8 (8-C) 53.0 (14,17-C), 52.7 (26, 26'-C), 40.1 (10-C), 37.9 (11-C), 33.1 (27, 27'-C), 23.7 (12-C), 23.6 (15-C), 23.4 (13-C) 22.3 (9-C), 22.1(16-C), 22.0 (9-C), 20.5 (28, 28'-C), 13.6 (29, 29'-C); ^{19}F NMR (500MHz, MeOD), δ -77.2 (s, 3F-CF_3CO_2); MS (ES+) 924 $[M]^+$, HRMS (ES+) $C_{41}H_{57}N_{13}{}^{193}Ir$ requires 924.4540 found 924.4489.

6.5.25 $[Ir(ppy)_2(L5.Boc)]PF_6$ $Ir(ppy)_2L5.Boc$

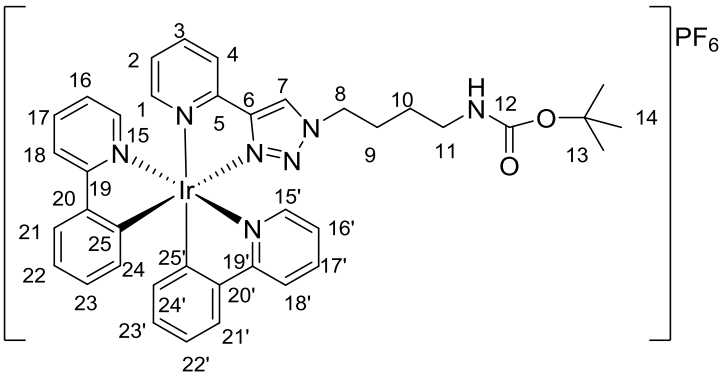

$[Ir(ppy)Cl]_2$ dimer (0.01 g, 0.01 mmol) and **L5.Boc** (0.06 g, 0.02 mmol) and KPF_6 (0.004 g, 0.021 mmol) were dissolved in MeOH (4 mL) and heated in the microwave for 1hr at 110ºC. after work up the yellow solid was obtained and yield (0.05 g, 80 %). ^1H NMR (400MHz, CD_2Cl_2), δ 8.92 (s, 1H,7-CH), 8.23 (d, *J* = 7.9 Hz, 1H, 1-CH), 7.99 (ddd, *J* = 8.5, 7.6, 1.5 Hz, 3H, 3, 15, 15'-CH), 7.76 (ddd, *J* = 8.3, 6.1, 1.5 Hz, 3H, 4, 18, 18',-CH), 7.64 (ddd , *J* = 9.1, 7.0, 0.8 Hz, 1H, 17, 17'-CH), 7.52 (d, *J* = 5.40 Hz, 1H, 21-CH), 7.50 (ddd , *J* = 7.8, 6.6, 1.3 Hz, 1H, 21'-CH), 7.01 (ddd, *J* = 7.7, 6.5, 1.2 Hz, 1H, 2-CH), 6.94 (dd, *J* = 7.1, 5.9 Hz, 2H, 16, 16'-CH), 6.91 (ddd, *J* = 6.8, 6.7, 1.1 Hz, 1H, 23-CH), 6.83 (ddd , *J* = 7.7, 7.4, 1.1 Hz, 22-CH) , 6.78 (ddd, *J* = 8.1, 7.5, 1.3 Hz, 1H, 22'-CH), 6.68 (ddd, *J* = 8.1, 7.6, 1.3 Hz, 1H, 23'-CH), 6.20 (dd, *J* = 7.7, 0.8 Hz, 1H, 24-CH), 6.14 (dd, *J* = 7.1, 0.8 Hz, 1H, 24'-CH), 4.39 (t, *J* = 7.2 Hz, 2H, 8-CH_2), 2.29-2.27 (m, 2H, 11-CH_2), 1.80-1.78 (m, 2H, 9-CH_2), 1.31-1.29 (m, 2H, 10-CH_2), 1.30 (s, 9H, 14-$(CH_3)_3$; ^{13}C NMR (100MHz, CD_2Cl_2), δ 169.8 (19-C), 169.1 (19'-C), 158.0 (12-C), 151.4 (1-C), 151.4 (15-C), 150.8 (15'-C), 149.9 (20-C), 147 (20'-C), 145.4 (17-C), 145.3 (17'-C), 140 (6-C), 139.4 (7-C), 132.9 (24-C), 132.7 (24'-C), 131.4 (22-C), 130.6 (22'-C), 130.3 (23-C), 128.5 (23'-C), 127.7 (21-C), 127.4 (21'-C), 125.9 (25-C), 125.4 (25'-C), 124.5 (18-C), 124.0 (18'-C), 123.7 (2-C), 120.8 (16-C), 120.6 (16'-C), 80.0 (13-C), 52.9 (8-C), 40.3 (11-C), 28 (14-C), 27 (10-C), 24 (9-C); MS(ES) *m/z* 820 $[M]^+$; HRMS (ES+) $C_{38}H_{39}N_7O_2{}^{191}Ir$ require 816.2740 found 816.2771.

6.5.26 [Ir(ppy)$_2$(L5)] (CF$_3$COO)$_4$ Ir(ppy)$_2$L5

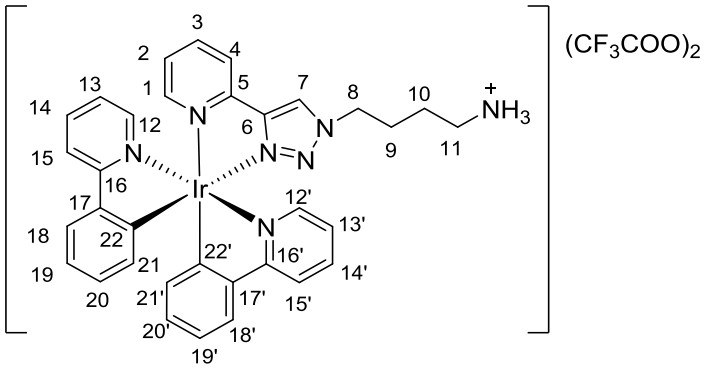

Ir(ppy)$_2$L5.Boc (0.03 g, 0.03 mmol) was dissolved in 4M TFA in DCM and stirred at rt. for 18hr. The volatiles were removed to produce the product (0.03 g) without further purification. ^{1}H NMR (500MHz, MeOD), δ 9.12 (s, 1 H, 7-CH), 8.29 (d, *J* = 7.9 Hz, 1 H, 1-CH), 8.08 - 8.16 (m, 3 H, 3, 12, 12'-CH), 7.86 - 7.93 (m, 3 H, 4, 15, 15'-CH), 7.83 (d, *J* = 7.5 Hz, 1 H, 18-CH), 7.75 (d, *J* = 7.3 Hz, 2H, 14, 14'-CH), 7.65 (d, *J* = 5.8 Hz, 1H, 18'-CH), 7.44 (ddd, *J* = 7.9, 6.8, 0.8 Hz, 2H, 13, 13'-CH), 7.12 (ddd, *J* = 7.6, 6.6, 1.1 Hz, 1H, 2-CH), 7.07 (ddd, *J* = 7.1, 6.7, 1.2 Hz, 1H, 19-CH), 6.95 (ddd, *J* = 8.4, 7.7, 0.9 Hz, 1H, 19'-CH), 6.90 (ddd, *J* = 8.4, 7.5, 1.1 Hz, 1H, 20-CH), 6.80 (ddd, *J* = 8.1, 7.4, 1.1 Hz, 1H, 20'-CH), 6.29 (d, *J* = 7.1 Hz, 1H, 21-CH), 6.26 (d, *J* = 7.6 Hz, 1H, 21'-CH), 4.55 (t, *J* = 7.4 Hz, 2H, 8-CH$_2$), 2.96 (t, *J* = 7.2 Hz, 2H, 11-CH$_2$), 2.04 (m, 2H, 9-CH$_2$), 1.71-1.67 (m, 2H, 10-CH$_2$); ^{13}C NMR (125 MHz, MeOD), δ 169.8 (16-C), 169.2 (16'-C), 163.1 (q, *J* = 38.3 Hz, CF$_3$CO$_2$), 150.8 (17, 17'-C), 150.5 (15, 15'-C), 147.5(5 and 6-C), 145.4 (22 and 22'-C), 140.9 (3 and 4-C) 139.5 (12, 12'-C), 131.5 (21 or 21'-C), 130.6 (20 or 20'-C), 127.8 (20 or 20'-C), 125.9 (13 or 13'-C), 125.4 (13 or 13'-C), 124.4 (7-C), 124.1 (18,18'-C), 123.9 (2-C), 123.7 (14, 14'-C), 120.9 (1-C, 19'-C), 120.7 (19-C), 52.5 (8-C), 39.8 (11-C), 27.7 (9-C), 25.4 (10-C); ^{19}F NMR (500MHz, MeOD), δ 76.8 (s, 3F-CF$_3$CO$_2$); MS m/z (ES+) 717 [M]$^+$; HRMS (ES+) C$_{33}$H$_{31}$N$_7$^{193}Ir requires 718.2288 found 718.2270.

Chapter 7

7 References

1. A. E. Pegg, *IUBMB Life*, 2009, **61**, 880-894.
2. D. M. Morgan, *Mol. Biotechnol.*, 1999, **11**, 229-250.
3. R. J. Bergeron, J. S. McManis, W. R. Weimar, K. Schreier, F. Gao, Q. Wu, J. Ortiz-Ocasio, G. R. Luchetta, C. Porter and J. T. Vinson, *J. Med. Chem.*, 1995, **38**, 2278-2285.
4. G. Karigiannis and D. Papaioannou, *Eur. J. Org. Chem.*, 2000, **2000**, 1841-1863.
5. P. M. Cullis, R. E. Green, L. Merson-Davies and N. Travis, *Chem. Biol.*, 1999, **6**, 717-729.
6. S.-Q. Xie, Q. Li, Y.-H. Zhang, J.-H. Wang, Z.-H. Mei, J. Zhao and C.-J. Wang, *Apoptosis*, 2011, **16**, 27-34.
7. A. Pegg and P. McCann, *Am. J. Physiol., Cell Physiol.*, 1982, **243**, C212-C221.
8. O. Phanstiel, N. Kaur and J.-G. Delcros, *Amino acids*, 2007, **33**, 305-313.
9. J.-M. Barret, A. Kruczynski, S. Vispé, J.-P. Annereau, V. Brel, Y. Guminski, J.-G. Delcros, A. Lansiaux, N. Guilbaud and T. Imbert, *Cancer Res.*, 2008, **68**, 9845-9853.
10. A. J. Palmer and H. M. Wallace, *Amino acids*, 2010, **38**, 415-422.
11. E. Redgate, S. Boggs, A. Grudziak and M. Deutsch, *J. Neuro-Oncol.*, 1995, **25**, 167-179.
12. C. W. Porter, R. J. Bergeron and N. J. Stolowich, *Cancer Res.*, 1982, **42**, 4072-4078.
13. T. Uemura, D. E. Stringer, K. A. Blohm-Mangone and E. W. Gerner, *Am. J. Physiol. Gastrointest. Liver Physiol.*, 2010, **299**, G517-G522.
14. E. Agostinelli, M. Marques, R. Calheiros, F. Gil, G. Tempera, N. Viceconte, V. Battaglia, S. Grancara and A. Toninello, *Amino acids*, 2010, **38**, 393-403.
15. K. Igarashi and K. Kashiwagi, *Biochem. J.*, 1999, **344**, 633.
16. D. Soulet, L. Covassin, M. Kaouass, R. Charest-Gaudreault, M. Audette and R. Poulin, *Biochem. J.*, 2002, **367**, 347.
17. C. F. Higgins, *Annu. Rev. Cell Biol.*, 1992, **8**, 67-113.
18. P. De Camilli, K. Takei and P. S. McPherson, *Curr. Opin. Neurobiol.*, 1995, **5**, 559-565.
19. G. J. Doherty and H. T. McMahon, *Annu. Rev. Biochem.*, 2009, **78**, 857-902.
20. G. Rudnick, *Annu Rev Physiol*, 1986, **48**, 403-413.
21. S. A. Mousavi, L. Malerød, T. Berg and R. Kjeken, *Biochem. J.*, 2004, **377**, 1.
22. K. Simons and D. Toomre, *Nat. Rev. Mol. Cell Biol*, 2000, **1**, 31.
23. R. V. Stan, *Biochim. Biophys. Acta*, 2005, **1746**, 334-348.
24. L. Pelkmans, T. Bürli, M. Zerial and A. Helenius, *Cell*, 2004, **118**, 767-780.
25. L. Pelkmans, D. Püntener and A. Helenius, *Science*, 2002, **296**, 535-539.
26. M. Bastiani and R. G. Parton, *J. Cell. Sci.*, 2010, **123**, 3831-3836.
27. M. Belting, K. Mani, M. Jönsson, F. Cheng, S. Sandgren, S. Jonsson, K. Ding, J.-G. Delcros and L.-Å. Fransson, *J. Biol. Chem.*, 2003, **278**, 47181-47189.
28. M. Belting, S. Persson and L.-Å. Fransson, *Biochem. J.*, 1999, **338**, 317.

29. M. Belting, L. Borsig, M. M. Fuster, J. R. Brown, L. Persson, L.-Å. Fransson and J. D. Esko, *Proc. Natl. Acad. Sci. U.S.A.*, 2002, **99**, 371-376.
30. K. Ding, S. Sandgren, K. Mani, M. Belting and L.-Å. Fransson, *J. Biol. Chem.*, 2001, **276**, 46779-46791.
31. A. A. Abdulhussein and H. M. Wallace, *Amino acids*, 2014, **46**, 655-660.
32. Z. Guo and P. Sadler, *Academic Press: San Diego, CA, USA*, 2000, **49**, 183-306.
33. H. Wallace and A. Fraser, *Amino acids*, 2004, **26**, 353-365.
34. A. Hegmans, Y. Qu, L. R. Kelland, J. D. Roberts and N. Farrell, *Inorg. Chem.*, 2001, **40**, 6108-6114.
35. C. Manzotti, G. Pratesi, E. Menta, R. Di Domenico, E. Cavalletti, H. H. Fiebig, L. R. Kelland, N. Farrell, D. Polizzi and R. Supino, *Clin. Cancer Res.*, 2000, **6**, 2626-2634.
36. R. Poulin, R. Casero and D. Soulet, *Amino acids*, 2012, **42**, 711-723.
37. S.G.Phillips, PhD Thesis, University of Leicester, 2014.
38. K. Harris and P. Sultan, *Neuropharmacology*, 1995, **34**, 1387-1395.
39. R. Jahn and T. C. Südhof, *J. Neurochem.*, 1993, **61**, 12-21.
40. R. Blumenthal, M. J. Clague, S. R. Durell and R. M. Epand, *Chem. Rev.*, 2003, **103**, 53-70.
41. T. C. Südhof and R. Jahn, *Neuron*, 1991, **6**, 665-677.
42. T. C. Südhof, *Annu. Rev. Neurosci.*, 2004, **27**, 509-547.
43. B. Ceccarelli, W. Hurlbut and A. Mauro, *J. Cell Biol.*, 1973, **57**, 499-524.
44. W. J. Betz and G. S. Bewick, *Science*, 1992, **255**, 200-203.
45. B. Ceccarelli, W. Hurlbut and A. Mauro, *J. Cell Biol.*, 1972, **54**, 30-38.
46. R. Fesce, F. Grohovaz, F. Valtorta and J. Meldolesi, *Trends Cell Biol*, 1994, **4**, 1-4.
47. J. R. Morgan, G. J. Augustine and E. M. Lafer, *Neuromolecular medicine*, 2002, **2**, 101-114.
48. K. M. Harris and R. J. Weinberg, *Cold Spring Harb Perspect Biol*, 2012, **4**, a005587.
49. A. L. Hodgkin and A. F. Huxley, *J. Physiol.*, 1952, **117**, 500-544.
50. J. Del Castillo and B. Katz, *J. Physiol.*, 1954, **124**, 560-573.
51. A. Dani and B. Huang, *Curr. Opin. Neurobiol.*, 2010, **20**, 648-652.
52. A. J. Cochilla, J. K. Angleson and W. J. Betz, *Annu. Rev. Neurosci.*, 1999, **22**, 1-10.
53. L. Loew and L. Simpson, *Biophys. J.*, 1981, **34**, 353-365.
54. J. Lichtman and R. Wilkinson, *J. Physiol.*, 1987, **393**, 355-374.
55. M. Ramaswami, K. Krishnan and R. B. Kelly, *Neuron*, 1994, **13**, 363-375.
56. T. A. Ryan and S. J. Smith, *Neuron*, 1995, **14**, 983-989.
57. S. J. Stafford, S. L. Shorte and J. G. Schofield, *Biosci. Rep.*, 1993, **13**, 9-17.
58. J. Heuser, Q. Zhu and M. Clarke, *J. Cell Biol.*, 1993, **121**, 1311-1327.
59. T. A. Vida and S. D. Emr, *J. Cell Biol.*, 1995, **128**, 779-792.
60. J. Angleson, A. Cochilla, G. Kilic, I. Nussinovitch and W. Betz, *Nat. Neurosci.*, 1999, **2**, 440.
61. T. A. Ryan, H. Reuter, B. Wendland, F. E. Schweizer, R. W. Tsien and S. J. Smith, *Neuron*, 1993, **11**, 713-724.
62. A. C. Brumback, J. L. Lieber, J. K. Angleson and W. J. Betz, *Methods*, 2004, **33**, 287-294.
63. T. Lang, I. Wacker, J. Steyer, C. Kaether, I. Wunderlich, T. Soldati, H.-H. Gerdes and W. Almers, *Neuron*, 1997, **18**, 857-863.
64. R. Heim and R. Y. Tsien, *Curr. Biol.*, 1996, **6**, 178-182.

65. V. Marra, J. J. Burden, F. Crawford and K. Staras, *Nat. Protoc.*, 2014, **9**, 1337.
66. B. Valeur and M. N. Berberan-Santos, *Molecular fluorescence: principles and applications*, John Wiley & Sons, 2012.
67. J. Demas, *Anal. Chem.*, 1991, **63**, 829A-837A.
68. C. H. Yang, Y. M. Cheng, Y. Chi, C. J. Hsu, F. C. Fang, K. T. Wong, P. T. Chou, C. H. Chang, M. H. Tsai and C. C. Wu, *Angew. Chem.*, 2007, **119**, 2470-2473.
69. E. Baranoff, J.-H. Yum, M. Graetzel and M. K. Nazeeruddin, *J. Organomet. Chem.*, 2009, **694**, 2661-2670.
70. C.-Y. Li, C. Su, H.-H. Wang, P. Kumaresan, C.-H. Hsu, I.-T. Lee, W.-C. Chang, Y. S. Tingare, T.-Y. Li and C.-F. Lin, *Dyes Pigm.*, 2014, **100**, 57-65.
71. A. Vogler and H. Kunkely, *Coord. Chem. Rev.*, 2000, **200**, 991-1008.
72. J. R. Farrell, G. J. Kerins, K. L. Niederhoffer, L. A. Crandall and C. Ziegler, *J. Organomet. Chem.*, 2016, **813**, 41-45.
73. J. R. Farrell, C. Becker, D. P. Lavoie, J. L. Shaw and C. J. Ziegler, *J. Organomet. Chem.*, 2004, **689**, 1122-1126.
74. S. Ranjan, S.-Y. Lin, K.-C. Hwang, Y. Chi, W.-L. Ching, C.-S. Liu, Y.-T. Tao, C.-H. Chien, S.-M. Peng and G.-H. Lee, *Inorg. Chem.*, 2003, **42**, 1248-1255.
75. P. J. Giordano, S. M. Fredericks, M. S. Wrighton and D. L. Morse, *J. Am. Chem. Soc.*, 1978, **100**, 2257-2259.
76. M. Obata, A. Kitamura, A. Mori, C. Kameyama, J. A. Czaplewska, R. Tanaka, I. Kinoshita, T. Kusumoto, H. Hashimoto and M. Harada, *Dalton Trans.*, 2008, 3292-3300.
77. S. Clède, F. Lambert, C. Sandt, Z. Gueroui, M. Réfrégiers, M.-A. Plamont, P. Dumas, A. Vessières and C. Policar, *Chem.Comm.*, 2012, **48**, 7729-7731.
78. M. Wolff, L. Munoz, A. François, C. Carrayon, A. Seridi, N. Saffon, C. Picard, B. Machura and E. Benoist, *Dalton Trans.*, 2013, **42**, 7019-7031.
79. S. Clède, F. Lambert, R. Saint-Fort, M. A. Plamont, H. Bertrand, A. Vessières and C. Policar, *Chem. Eur. J.*, 2014, **20**, 8714-8722.
80. H. V. Ching, X. Wang, M. He, N. Perujo Holland, R. Guillot, C. Slim, S. Griveau, H. C. Bertrand, C. Policar and F. Bedioui, *Inorg. Chem.*, 2017, **56**, 2966-2976.
81. B. S. Uppal, R. K. Booth, N. Ali, C. Lockwood, C. R. Rice and P. I. Elliott, *Dalton Trans.*, 2011, **40**, 7610-7616.
82. A. Boulay, A. Seridi, C. Zedde, S. Ladeira, C. Picard, L. Maron and E. Benoist, *Eur. J. Inorg. Chem.*, 2010, **2010**, 5058-5062.
83. T. U. Connell, D. J. Hayne, U. Ackermann, H. J. Tochon-Danguy, J. M. White and P. S. Donnelly, *J. Label. Compd. Radiopharm.*, 2014, **57**, 262-269.
84. E. Wolcan, G. Torchia, J. Tocho, O. Piro, P. Juliarena, G. Ruiz and M. Féliz, *J.Chem.Soc, Dalton Trans*, 2002, 2194-2202.
85. M. Felici, P. Contreras-Carballada, J. M. Smits, R. J. Nolte, R. M. Williams, L. De Cola and M. C. Feiters, *Molecules*, 2010, **15**, 2039-2059.
86. S. Ladouceur, D. Fortin and E. Zysman-Colman, *Inorg. Chem.*, 2011, **50**, 11514-11526.
87. D. L. Davies, F. Lelj, M. P. Lowe, K. S. Ryder, K. Singh and S. Singh, *Dalton Trans.*, 2014, **43**, 4026-4039.
88. H. J. Bolink, L. Cappelli, E. Coronado, M. Grätzel, E. Ortí, R. D. Costa, P. M. Viruela and M. K. Nazeeruddin, *J. Am. Chem. Soc.*, 2006, **128**, 14786-14787.
89. K. Hasan, A. K. Bansal, I. D. Samuel, C. Roldán-Carmona, H. J. Bolink and E. Zysman-Colman, *Sci. Rep.*, 2015, **5**, 12325.

90. S. Ladouceur, D. Fortin and E. Zysman-Colman, *Inorganic chemistry*, 2010, **49**, 5625-5641.
91. K. K.-W. Lo, J. S.-W. Chan, L.-H. Lui and C.-K. Chung, *Organometallics*, 2004, **23**, 3108-3116.
92. M. S. Lowry, W. R. Hudson, R. A. Pascal and S. Bernhard, *J. Am. Chem. Soc.*, 2004, **126**, 14129-14135.
93. L. Donato, P. Abel and E. Zysman-Colman, *Dalton Trans.*, 2013, **42**, 8402-8412.
94. J. Truong, K. B. Spilstead, G. J. Barbante, E. H. Doeven, D. J. Wilson, N. W. Barnett, L. C. Henderson, J. M. Altimari, S. C. Hockey and M. Zhou, *Analyst*, 2014, **139**, 6028-6035.
95. T. U. Connell, J. M. White, T. A. Smith and P. S. Donnelly, *Inorg. Chem.*, 2016, **55**, 2776-2790.
96. E. Kerr, E. H. Doeven, G. J. Barbante, C. F. Hogan, D. J. Bower, P. S. Donnelly, T. U. Connell and P. S. Francis, *Chem. Sci.*, 2015, **6**, 472-479.
97. K. K.-W. Lo, *Acc. Chem. Res.*, 2015, **48**, 2985-2995.
98. X. Wang, J. Jia, Z. Huang, M. Zhou and H. Fei, *Chem. Eur. J.*, 2011, **17**, 8028-8032.
99. P. G. Sammes and G. Yahioglu, *Nat. Prod. Rep.*, 1996, **13**, 1-28.
100. D. J. Stufkens and A. Vlček Jr, *Coord. Chem. Rev.*, 1998, **177**, 127-179.
101. V. Fernandez-Moreira, F. L. Thorp-Greenwood and M. P. Coogan, *ChemComm*, 2010, **46**, 186-202.
102. A. Amoroso, M. Coogan, J. Dunne and V. Fern, *Chem. Commun*, 2007, **3066**.
103. M. Wrighton and D. L. Morse, *J. Am. Chem. Soc.*, 1974, **96**, 998-1003.
104. K. K. W. Lo, C. K. Chung and N. Zhu, *Chem. Eur. J.*, 2003, **9**, 475-483.
105. K. K.-W. Lo, W.-K. Hui, D. C.-M. Ng and K.-K. Cheung, *Inorg. Chem.*, 2002, **41**, 40-46.
106. A. Boulay, S. Laine, N. Leygue, E. Benoist, S. Laurent, L. Vander Elst, R. N. Muller, B. Mestre-Voegtle and C. Picard, *Tetrahedron Lett.*, 2013, **54**, 5395-5398.
107. K. K.-W. Lo, M.-W. Louie, K.-S. Sze and J. S.-Y. Lau, *Inorg. Chem.*, 2008, **47**, 602-611.
108. B. S. Chhikara, D. Mandal and K. Parang, *J. Med. Chem.*, 2012, **55**, 1500-1510.
109. X.-y. Wang, A. Del Guerzo and R. H. Schmehl, *J. Photochem. Photobiol.*, 2004, **5**, 55-77.
110. D. L. Ma, H. Z. He, K. H. Leung, D. S. H. Chan and C. H. Leung, *Angew. Chem. Int. Ed.*, 2013, **52**, 7666-7682.
111. R. Schibli, R. Schwarzbach, R. Alberto, K. Ortner, H. Schmalle, C. Dumas, A. Egli and P. A. Schubiger, *Bioconjugate Chem.*, 2002, **13**, 750-756.
112. K. A. Stephenson, S. R. Banerjee, T. Besanger, O. O. Sogbein, M. K. Levadala, N. McFarlane, J. A. Lemon, D. R. Boreham, K. P. Maresca and J. D. Brennan, *J. Am. Chem. Soc.*, 2004, **126**, 8598-8599.
113. A. Coleman, C. Brennan, J. G. Vos and M. T. Pryce, *Coord. Chem. Rev.*, 2008, **252**, 2585-2595.
114. A. Seridi, M. Wolff, A. Boulay, N. Saffon, Y. Coulais, C. Picard, B. Machura and E. Benoist, *Inorg. Chem. Commun.*, 2011, **14**, 238-242.
115. C. Fernandes, J. Correia, L. Gano, I. Santos, S. Seifert, R. Syhre, R. Bergmann and H. Spies, *Bioconjugate Chem.*, 2005, **16**, 660-668.
116. A. Yazdani, N. Janzen, L. Banevicius, S. Czorny and J. F. Valliant, *Inorg. Chem.*, 2015, **54**, 1728-1736.

117. T. S. Pitchumony, L. Banevicius, N. Janzen, J. Zubieta and J. F. Valliant, *Inorg. Chem.*, 2013, **52**, 13521-13528.
118. Y. You and W. Nam, *Chem. Soc. Rev.*, 2012, **41**, 7061-7084.
119. S. Ladouceur and E. Zysman-Colman, *Eur. J. Inorg. Chem.*, 2013, **2013**, 2985-3007.
120. B. Aranda, P. Aguirre, S. A. Moya, M. Bonneau, J. G. Williams, L. Toupet, M. Escadeillas, H. Le Bozec and V. Guerchais, *Polyhedron*, 2015, **86**, 120-124.
121. K. K.-W. Lo, S. P.-Y. Li and K. Y. Zhang, *New J. Chem.*, 2011, **35**, 265-287.
122. F. L. Thorp-Greenwood, R. G. Balasingham and M. P. Coogan, *J. Organomet. Chem.*, 2012, **714**, 12-21.
123. M. Yu, Q. Zhao, L. Shi, F. Li, Z. Zhou, H. Yang, T. Yi and C. Huang, *ChemComm*, 2008, 2115-2117.
124. K. K. W. Lo, K. Y. Zhang, S. K. Leung and M. C. Tang, *Angew.Chem.*, 2008, **120**, 2245-2248.
125. W. H.-T. Law, L. C.-C. Lee, M.-W. Louie, H.-W. Liu, T. W.-H. Ang and K. K.-W. Lo, *Inorg. Chem.*, 2013, **52**, 13029-13041.
126. K. K. W. Lo, K. Y. Zhang, C. K. Chung and K. Y. Kwok, *Chem. Eur. J.*, 2007, **13**, 7110-7120.
127. K. K.-W. Lo, P.-K. Lee and J. S.-Y. Lau, *Organometallics*, 2008, **27**, 2998-3006.
128. M. Felici, P. Contreras-Carballada, Y. Vida, J. M. Smits, R. J. Nolte, L. De Cola, R. M. Williams and M. C. Feiters, *Chem. Eur. J.*, 2009, **15**, 13124-13134.
129. J. M. Haider, R. M. Williams, L. De Cola and Z. Pikramenou, *Angew. Chem. Int. Ed.*, 2003, **42**, 1830-1833.
130. A. Baschieri, S. Muzzioli, V. Fiorini, E. Matteucci, M. Massi, L. Sambri and S. Stagni, *Organometallics*, 2014, **33**, 6154-6164.
131. T. U. Connell, J. James, A. R. White and P. S. Donnelly, *Chem. Eur. J.*, 2015, **21**, 14146-14155.
132. H. Kobayashi, M. Ogawa, R. Alford, P. L. Choyke and Y. Urano, *Chem. Rev.*, 2009, **110**, 2620-2640.
133. K. Sakata, T. Fukuchi-Shimogori, K. Kashiwagi and K. Igarashi, *Biochem. Biophys. Res. Commun.*, 1997, **238**, 415-419.
134. B. Klenke, M. Stewart, M. P. Barrett, R. Brun and I. H. Gilbert, *J. Med. Chem.*, 2001, **44**, 3440-3452.
135. T. Antony, W. Hoyer, D. Cherny, G. Heim, T. M. Jovin and V. Subramaniam, *J. Biol. Chem.*, 2003, **278**, 3235-3240.
136. I. Otto Phanstiel, H. L. Price, L. Wang, J. Juusola, M. Kline and S. M. Shah, *J. Org. Chem.*, 2000, **65**, 5590-5599.
137. A. Muth, M. Madan, J. J. Archer, N. Ocampo, L. Rodriguez and O. Phanstiel IV, *J. Med. Chem.*, 2014, **57**, 348-363.
138. P. G. Wuts and T. W. Greene, Wiley-Interscience New York:, Editon edn., 2007.
139. V. V. Rostovtsev, L. G. Green, V. V. Fokin and K. B. Sharpless, *Angew.Chem.*, 2002, **114**, 2708-2711.
140. C. W. Tornøe, C. Christensen and M. Meldal, *J. Org. Chem.*, 2002, **67**, 3057-3064.
141. H. C. Kolb, M. Finn and K. B. Sharpless, *Angew. Chem. Int. Ed.*, 2001, **40**, 2004-2021.
142. V. O. Rodionov, S. I. Presolski, D. Díaz Díaz, V. V. Fokin and M. Finn, *J. Am. Chem. Soc.*, 2007, **129**, 12705-12712.

143. M. Ahlquist and V. V. Fokin, *Organometallics*, 2007, **26**, 4389-4391.
144. B. F. Straub, *ChemComm*, 2007, 3868-3870.
145. V. O. Rodionov, V. V. Fokin and M. Finn, *Angewandte Chemie*, 2005, **117**, 2250-2255.
146. L. Liang and D. Astruc, *Coord. Chem. Rev.*, 2011, **255**, 2933-2945.
147. R. Guezguez, K. Bougrin, K. El Akri and R. Benhida, *Tetrahedron Lett.*, 2006, **47**, 4807-4811.
148. P. Appukkuttan, W. Dehaen, V. V. Fokin and E. Van der Eycken, *Org. Lett.*, 2004, **6**, 4223-4225.
149. M. S. Singh, S. Chowdhury and S. Koley, *Tetrahedron*, 2016, **72**, 5257-5283.
150. H. S. Beckmann and V. Wittmann, *Org. Lett.*, 2007, **9**, 1-4.
151. C. O. Kappe and E. Van der Eycken, *Chem. Soc. Rev.*, 2010, **39**, 1280-1290.
152. E. Haldón, M. C. Nicasio and P. J. Pérez, *Org. Biomol. Chem.*, 2015, **13**, 9528-9550.
153. J. D. Crowley, P. H. Bandeen and L. R. Hanton, *Polyhedron*, 2010, **29**, 70-83.
154. N. Fischer, E. D. Goddard-Borger, R. Greiner, T. M. Klapötke, B. W. Skelton and J. r. Stierstorfer, *J. Org. Chem.*, 2012, **77**, 1760-1764.
155. D. F. Taber, R. E. Ruckle Jr and M. J. Hennessy, *J. Org. Chem.*, 1986, **51**, 4077-4078.
156. G. T. Potter, G. C. Jayson, G. J. Miller and J. M. Gardiner, *J. Org. Chem.*, 2016, **81**, 3443-3446.
157. P. T. Nyffeler, C.-H. Liang, K. M. Koeller and C.-H. Wong, *J. Am. Chem. Soc.*, 2002, **124**, 10773-10778.
158. A. K. Pandiakumar, S. P. Sarma and A. G. Samuelson, *Tetrahedron Lett.*, 2014, **55**, 2917-2920.
159. W. Fischer and J. P. Anselme, *J. Am. Chem. Soc.*, 1967, **89**, 5284-5285.
160. R. Heck and J. Nolley Jr, *J. Org. Chem.*, 1972, **37**, 2320-2322.
161. D. Milstein and J. Stille, *J. Am. Chem. Soc.*, 1978, **100**, 3636-3638.
162. E. Negishi, A. O. King and N. Okukado, *J. Org. Chem.*, 1977, **42**, 1821-1823.
163. K. Sonogashira, Y. Tohda and N. Hagihara, *Tetrahedron Lett.*, 1975, **16**, 4467-4470.
164. Y. Hatanaka and T. Hiyama, *Synlett*, 1991, **1991**, 845-853.
165. M. Sarmah, M. Mondal, S. B. Gohain and U. Bora, *Catal. Commun.*, 2017, **90**, 31-34.
166. C. W. Gallop, M.-T. Chen and O. Navarro, *Org. Lett.*, 2014, **16**, 3724-3727.
167. H. Dieck and F. Heck, *J. Organomet. Chem.*, 1975, **93**, 259-263.
168. L. Cassar, *J. Organomet. Chem.*, 1975, **93**, 253-257.
169. X. Li, B. Zhang, Z. G. Xi, S. Luo and J. P. Cheng, *Adv. Synth. Catal.*, 2010, **352**, 416-424.
170. Q. Zhu, L. Liao, G. Cheng, W. Yang, Y. Deng, D. Yang, S. Yoon, Y. Jung, I. Kim and M. Nayak, *Modern Research in Catalysis*, 2017, **6**, 121.
171. K. Sonogashira, *Pergamon Press, New York*, 1991, **3**, 521.
172. S. Thorand and N. Krause, *J. Org. Chem.*, 1998, **63**, 8551-8553.
173. S. Takahashi, Y. Kuroyama, K. Sonogashira and N. Hagihara, *Synthesis*, 1980, **1980**, 627-630.
174. G. W. Kabalka, L. Wang, V. Namboodiri and R. M. Pagni, *Tetrahedron Lett.*, 2000, **41**, 5151-5154.
175. M. Erdélyi and A. Gogoll, *J. Org. Chem.*, 2001, **66**, 4165-4169.
176. R. Chinchilla and C. Nájera, *Chem. Soc. Rev.*, 2011, **40**, 5084-5121.

177. A. Soheili, J. Albaneze-Walker, J. A. Murry, P. G. Dormer and D. L. Hughes, *Org. Lett.*, 2003, **5**, 4191-4194.
178. M. Kosugi, K. Sasazawa, Y. Shimizu and T. Migita, *Chem. Lett.*, 1977, **6**, 301-302.
179. M. M. Heravi, E. Hashemi and F. Azimian, *ChemInform*, 2014, **45**.
180. P. Espinet and A. M. Echavarren, *Angew. Chem. Int. Ed.*, 2004, **43**, 4704-4734.
181. V. Farina and B. Krishnan, *J. Am. Chem. Soc.*, 1991, **113**, 9585-9595.
182. V. Farina, S. R. Baker, D. A. Benigni and C. Sapino Jr, *Tetrahedron Lett.*, 1988, **29**, 5739-5742.
183. Y. Yamamoto, Y. Azuma and H. Mitoh, *Synthesis*, 1986, **1986**, 564-565.
184. M. Fujita, H. Oka and K. Ogura, *Tetrahedron Lett.*, 1995, **36**, 5247-5250.
185. S. Gronowitz, P. Björk, J. Malm and A.-B. Hörnfeldt, *J. Organomet. Chem.*, 1993, **460**, 127-129.
186. T. E. Barder, S. D. Walker, J. R. Martinelli and S. L. Buchwald, *J. Am. Chem. Soc.*, 2005, **127**, 4685-4696.
187. G. Kennedy and A. D. Perboni, *Tetrahedron Lett.*, 1996, **37**, 7611-7614.
188. A. F. Littke and G. C. Fu, *Angew. Chem. Int. Ed.*, 2002, **41**, 4176-4211.
189. A. F. Abdel-Magid, K. G. Carson, B. D. Harris, C. A. Maryanoff and R. D. Shah, *J. Org. Chem.*, 1996, **61**, 3849-3862.
190. B. T. Cho and S. K. Kang, *Tetrahedron*, 2005, **61**, 5725-5734.
191. C. Pollard and D. C. Young, *J. Org. Chem.*, 1951, **16**, 661-672.
192. M. Whiting, J. C. Tripp, Y.-C. Lin, W. Lindstrom, A. J. Olson, J. H. Elder, K. B. Sharpless and V. V. Fokin, *J. Med. Chem.*, 2006, **49**, 7697-7710.
193. B. Chattopadhyay, C. I. R. Vera, S. Chuprakov and V. Gevorgyan, *Org. Lett.*, 2010, **12**, 2166-2169.
194. M. B. Harisha, M. Nagaraj, S. Muthusubramanian and N. Bhuvanesh, *RSC Advances*, 2016, **6**, 58118-58124.
195. B. Japelj, S. Rečnik, P. Čebašek, B. Stanovnik and J. Svete, *J. Heterocycl. Chem.*, 2005, **42**, 1167-1173.
196. M. Meldal and C. W. Tornøe, *Chem. Rev.*, 2008, **108**, 2952-3015.
197. J. H. Boyer and E. Miller Jr, *J. Am. Chem. Soc.*, 1959, **81**, 4671-4673.
198. R. Sun, H. Wang, J. Hu, J. Zhao and H. Zhang, *Org. Biomol. Chem.*, 2014, **12**, 5954-5963.
199. T. Sasaki, K. Kanematsu and M. Murata, *J. Org. Chem.*, 1971, **36**, 446-449.
200. G. Colombano, C. Travelli, U. Galli, A. Caldarelli, M. G. Chini, P. L. Canonico, G. Sorba, G. Bifulco, G. C. Tron and A. A. Genazzani, *J. Med. Chem.*, 2009, **53**, 616-623.
201. S. I. Fukuzawa, E. Shimizu and S. Kikuchi, *ChemInform*, 2008, **39**.
202. S. Jindabot, K. Teerachanan, P. Thongkam, S. Kiatisevi, T. Khamnaen, P. Phiriyawirut, S. Charoenchaidet, T. Sooksimuang, P. Kongsaeree and P. Sangtrirutnugul, *J. Organomet. Chem.*, 2014, **750**, 35-40.
203. A. Kolarovic, M. Schnürch and M. D. Mihovilovic, *J. Org. Chem.*, 2011, **76**, 2613-2618.
204. Q. Zhang, X. Wang, C. Cheng, R. Zhu, N. Liu and Y. Hu, *Org. Biomol. Chem.*, 2012, **10**, 2847-2854.
205. I. Stengel, A. Mishra, N. Pootrakulchote, S.-J. Moon, S. M. Zakeeruddin, M. Grätzel and P. Bäuerle, *J. Mater. Chem.*, 2011, **21**, 3726-3734.
206. M. H. Elnagdi, M. S. Moustafa, S. M. Al-Mousawi, R. A. Mekheimer and K. U. Sadek, *Mol. Divers.*, 2015, **19**, 625-651.
207. H. Takeda and O. Ishitani, *Coord. Chem. Rev.*, 2010, **254**, 346-354.

208. K. K. W. Lo, K. Y. Zhang and S. P. Y. Li, *Eur. J. Inorg. Chem.*, 2011, **2011**, 3551-3568.
209. B. Schulze and U. S. Schubert, *Chem. Soc. Rev.*, 2014, **43**, 2522-2571.
210. P. Wu and V. V. Fokin, *Aldrichimica Acta*, 2007, **40**, 7-17.
211. M. Rodgers and P. Armentrout, *Int. J. Mass spectrom.*, 1999, **185**, 359-380.
212. T. L. Mindt, H. Struthers, L. Brans, T. Anguelov, C. Schweinsberg, V. Maes, D. Tourwé and R. Schibli, *J. Am. Chem. Soc.*, 2006, **128**, 15096-15097.
213. D. Urankar, B. Pinter, A. Pevec, F. De Proft, I. Turel and J. Košmrlj, *Inorg. Chem.*, 2010, **49**, 4820-4829.
214. J. T. Fletcher, S. E. Walz and M. E. Keeney, *Tetrahedron Lett.*, 2008, **49**, 7030-7032.
215. Z. K. Reeder, A. M. Adler and K. M. Miller, *Tetrahedron Lett.*, 2016, **57**, 206-209.
216. E. Baggaley, J. A. Weinstein and J. G. Williams, *Coord. Chem. Rev.*, 2012, **256**, 1762-1785.
217. J. D. Knoll, B. A. Albani and C. Turro, *Acc. Chem. Res.*, 2015, **48**, 2280-2287.
218. A. J. McConnell, C. S. Wood, P. P. Neelakandan and J. R. Nitschke, *Chem. Rev.*, 2015, **115**, 7729-7793.
219. M. H. Keefe, R. V. Slone, J. T. Hupp, K. F. Czaplewski, R. Q. Snurr and C. L. Stern, *Langmuir*, 2000, **16**, 3964-3970.
220. T. Hosseinnejad, F. Ebrahimpour-Malmir and B. Fattahi, *RSC Advances*, 2018, **8**, 12232-12259.
221. S. Záliš, C. J. Milne, A. El Nahhas, A. M. Blanco-Rodríguez, R. M. van der Veen and A. Vlček Jr, *Inorg. Chem.*, 2013, **52**, 5775-5785.
222. W.-K. Chu, C.-C. Ko, K.-C. Chan, S.-M. Yiu, F.-L. Wong, C.-S. Lee and V. Roy, *Chem. Mater.*, 2014, **26**, 2544-2550.
223. S. M. Fredericks, J. C. Luong and M. S. Wrighton, *J. Am. Chem. Soc.*, 1979, **101**, 7415-7417.
224. J. M. Villegas, S. R. Stoyanov, W. Huang and D. P. Rillema, *Inorg. Chem.*, 2005, **44**, 2297-2309.
225. B. López and L. Loeb, *J. Chil. Chem. Soc.*, 2004, **49**, 83-87.
226. B. B. Hueholt, W. Xu, M. Sabat, B. DeGraff and J. Demas, *J Fluoresc*, 2007, **17**, 522-527.
227. S. Bullock, A. J. Hallett, L. P. Harding, J. J. Higginson, S. A. Piela, S. J. Pope and C. R. Rice, *Dalton Trans.*, 2012, **41**, 14690-14696.
228. W. K. Lo, G. S. Huff, J. R. Cubanski, A. D. Kennedy, C. J. McAdam, D. A. McMorran, K. C. Gordon and J. D. Crowley, *Inorg. Chem.*, 2015, **54**, 1572-1587.
229. H. C. Bertrand, S. Clède, R. Guillot, F. Lambert and C. Policar, *Inorg. Chem.*, 2014, **53**, 6204-6223.
230. B. M. Suijkerbuijk, B. N. Aerts, H. P. Dijkstra, M. Lutz, A. L. Spek, G. van Koten and R. J. K. Gebbink, *Dalton Trans.*, 2007, 1273-1276.
231. S. Sprouse, K. King, P. Spellane and R. J. Watts, *J. Am. Chem. Soc.*, 1984, **106**, 6647-6653.
232. Y. Chi and P.-T. Chou, *Chem. Soc. Rev.*, 2010, **39**, 638-655.
233. I. M. Dixon, J.-P. Collin, J.-P. Sauvage, L. Flamigni, S. Encinas and F. Barigelletti, *Chem. Soc. Rev.*, 2000, **29**, 385-391.
234. M. Nonoyama, *Bull. Chem. Soc. Jpn.*, 1974, **47**, 767-768.
235. F. O. Garces and R. J. Watts, *Inorg. Chem.*, 1990, **29**, 582-584.

236. S. Bettington, M. Tavasli, M. R. Bryce, A. S. Batsanov, A. L. Thompson, H. A. Al Attar, F. B. Dias and A. P. Monkman, *J. Mater. Chem.*, 2006, **16**, 1046-1052.
237. B. Beyer, C. Ulbricht, D. Escudero, C. Friebe, A. Winter, L. González and U. S. Schubert, *Organometallics*, 2009, **28**, 5478-5488.
238. A. B. Tamayo, S. Garon, T. Sajoto, P. I. Djurovich, I. M. Tsyba, R. Bau and M. E. Thompson, *Inorg. Chem.*, 2005, **44**, 8723-8732.
239. R. D. Costa, P. M. Viruela, H. J. Bolink and E. Ortí, *J. Mol. Struct.*, 2009, **912**, 21-26.
240. A. Kumar, S.-S. Sun and A. J. Lees, *Coord. Chem. Rev.*, 2008, **252**, 922-939.
241. C.-H. Yang, M. Mauro, F. Polo, S. Watanabe, I. Muenster, R. Fröhlich and L. De Cola, *Chem. Mater.*, 2012, **24**, 3684-3695.
242. C. Fan, Y. Li, C. Yang, H. Wu, J. Qin and Y. Cao, *Chem. Mater.*, 2012, **24**, 4581-4587.
243. D. Xia, B. Wang, B. Chen, S. Wang, B. Zhang, J. Ding, L. Wang, X. Jing and F. Wang, *Angew. Chem. Int. Ed.*, 2014, **53**, 1048-1052.
244. D. L. Davies, M. P. Lowe, K. S. Ryder, K. Singh and S. Singh, *Dalton Trans.*, 2011, **40**, 1028-1030.
245. S. Jung, Y. Kang, H. S. Kim, Y. H. Kim, C. L. Lee, J. J. Kim, S. K. Lee and S. K. Kwon, *Eur. J. Inorg. Chem.*, 2004, **2004**, 3415-3423.
246. S. Lamansky, P. Djurovich, D. Murphy, F. Abdel-Razzaq, H.-E. Lee, C. Adachi, P. E. Burrows, S. R. Forrest and M. E. Thompson, *J. Am. Chem. Soc.*, 2001, **123**, 4304-4312.
247. K. K.-W. Lo, C.-K. Chung, T. K.-M. Lee, L.-H. Lui, K. H.-K. Tsang and N. Zhu, *Inorg. Chem.*, 2003, **42**, 6886-6897.
248. C. Adachi, M. A. Baldo, M. E. Thompson and S. R. Forrest, *J. Appl. Phys.*, 2001, **90**, 5048-5051.
249. D. K. Rayabarapu, B. M. J. S. Paulose, J. P. Duan and C. H. Cheng, *Adv. Mater.*, 2005, **17**, 349-353.
250. Y. You and S. Y. Park, *Dalton Trans.*, 2009, 1267-1282.
251. P. Alam, I. R. Laskar, C. Climent, D. Casanova, P. Alemany, M. Karanam, A. R. Choudhury and J. R. Butcher, *Polyhedron*, 2013, **53**, 286-294.
252. V. Balzani, N. Sabbatini and F. Scandola, *Chem. Rev.*, 1986, **86**, 319-337.
253. P. Chen and T. J. Meyer, *Chem. Rev.*, 1998, **98**, 1439-1478.
254. A. Kumar, S.-S. Sun and A. J. Lees, in *Photophysics of Organometallics*, Springer, Editon edn., 2009, pp. 37-71.
255. V. F. Moreira, *Design, synthesis and application of luminescent rhenium complexes in cell imaging*, Cardiff University (United Kingdom), 2008.
256. W. B. Connick, A. J. Di Bilio, M. G. Hill, J. R. Winkler and H. B. Gray, *Inorganica Chim. Acta*, 1995, **240**, 169-173.
257. H. Tsubaki, S. Tohyama, K. Koike, H. Saitoh and O. Ishitani, *Dalton Trans.*, 2005, 385-395.
258. X. Michalet, F. Pinaud, L. Bentolila, J. Tsay, S. Doose, J. Li, G. Sundaresan, A. Wu, S. Gambhir and S. Weiss, *science*, 2005, **307**, 538-544.
259. H. van der Salm, A. B. Elliott and K. C. Gordon, *Coord. Chem. Rev.*, 2015, **282**, 33-49.
260. P. A. Scattergood and P. I. Elliott, *Dalton Trans.*, 2017, **46**, 16343-16356.
261. C. B. Anderson, A. B. Elliott, C. J. McAdam, K. C. Gordon and J. D. Crowley, *Organometallics*, 2013, **32**, 788-797.

262. A. W.-T. Choi, M.-W. Louie, S. P.-Y. Li, H.-W. Liu, B. T.-N. Chan, T. C.-Y. Lam, A. C.-C. Lin, S.-H. Cheng and K. K.-W. Lo, *Inorg. Chem.*, 2012, **51**, 13289-13302.
263. K. K.-W. Lo and J. S.-Y. Lau, *Inorg. Chem.*, 2007, **46**, 700-709.
264. R. Gao, D. G. Ho, B. Hernandez, M. Selke, D. Murphy, P. I. Djurovich and M. E. Thompson, *J. Am. Chem. Soc.*, 2002, **124**, 14828-14829.
265. Y. Han, H.-T. Cao, H.-Z. Sun, G.-G. Shan, Y. Wu, Z.-M. Su and Y. Liao, *J. Mater. Chem. C*, 2015, **3**, 2341-2349.
266. H. J. Park, J. N. Kim, H.-J. Yoo, K.-R. Wee, S. O. Kang, D. W. Cho and U. C. Yoon, *J. Org. Chem.*, 2013, **78**, 8054-8064.
267. J. L. Rodríguez-Redondo, R. D. Costa, E. Ortí, A. Sastre-Santos, H. J. Bolink and F. Fernández-Lázaro, *Dalton Trans.*, 2009, 9787-9793.
268. S. Ladouceur, K. N. Swanick, S. Gallagher-Duval, Z. Ding and E. Zysman-Colman, *Eur. J. Inorg. Chem.*, 2013, **2013**, 5329-5343.
269. M. Mydlak, C. Bizzarri, D. Hartmann, W. Sarfert, G. Schmid and L. De Cola, *Adv. Funct. Mater.*, 2010, **20**, 1812-1820.
270. Y. Zhao, J. Tang, H. Zhang and Y. Ma, *Eur. J. Inorg. Chem.*, 2014, **2014**, 4843-4851.
271. A. M. Brouwer, *Pure Appl. Chem.*, 2011, **83**, 2213-2228.
272. K. Nakamaru, *Bull. Chem. Soc. Jpn.*, 1982, **55**, 2697-2705.
273. K. Suzuki, A. Kobayashi, S. Kaneko, K. Takehira, T. Yoshihara, H. Ishida, Y. Shiina, S. Oishi and S. Tobita, *Phys. Chem. Chem. Phys.*, 2009, **11**, 9850-9860.
274. M. P. Coogan, V. Fernández-Moreira, J. B. Hess, S. J. Pope and C. Williams, *New J. Chem.*, 2009, **33**, 1094-1099.
275. A. Amoroso, R. Arthur and M. Coogan, *New J. Chem*, 2008, **32**, 1097.
276. S. Sinn, B. Schulze, C. Friebe, D. G. Brown, M. Jäger, E. Altuntaş, J. Kübel, O. Guntner, C. P. Berlinguette and B. Dietzek, *Inorg. Chem.*, 2014, **53**, 2083-2095.
277. C. D. Sunesh, G. Mathai and Y. Choe, *ACS Appl. Mater. Interfaces*, 2014, **6**, 17416-17425.
278. H.-T. Cao, G.-G. Shan, Y.-M. Yin, H.-Z. Sun, Y. Wu, W.-F. Xie and Z.-M. Su, *Dyes Pigm.*, 2015, **113**, 655-663.
279. M. K. Nazeeruddin, R. Wegh, Z. Zhou, C. Klein, Q. Wang, F. De Angelis, S. Fantacci and M. Grätzel, *Inorg. Chem.*, 2006, **45**, 9245-9250.
280. F. De Angelis, S. Fantacci, N. Evans, C. Klein, S. M. Zakeeruddin, J.-E. Moser, K. Kalyanasundaram, H. J. Bolink, M. Grätzel and M. K. Nazeeruddin, *Inorg. Chem.*, 2007, **46**, 5989-6001.
281. J. Ohata, F. Vohidov, A. Aliyan, K. Huang, A. A. Martí and Z. T. Ball, *Chem.Comm.*, 2015, **51**, 15192-15195.
282. S. J. Pope, L. Groves, C. Schotten, J. Beames, J. Platts, D. Browne, S. Coles and P. Horton, *Chem. Eur. J.*, 2017.
283. A. Ionescu, E. I. Szerb, Y. J. Yadav, A. M. Talarico, M. Ghedini and N. Godbert, *Dalton Trans.*, 2014, **43**, 784-789.
284. S.-C. Lo, C. P. Shipley, R. N. Bera, R. E. Harding, A. R. Cowley, P. L. Burn and I. D. Samuel, *Chem. Mater.*, 2006, **18**, 5119-5129.
285. R. Kaliszan, 1987, **60**.
286. G. Cimpan, M. Hadaruga and V. Miclaus, *J. Chromatogr. A*, 2000, **869**, 49-55.
287. A. Pyka, *J. Liq. Chromatogr. Relat. Technol.*, 2009, **32**, 723-731.
288. W. Jiang, Y. Gao, Y. Sun, F. Ding, Y. Xu, Z. Bian, F. Li, J. Bian and C. Huang, *Inorg. Chem.*, 2010, **49**, 3252-3260.

289. L. J. Waters, Y. Shahzad and J. Stephenson, *Eur. J. Pharm. Sci.*, 2013, **50**, 335-340.
290. H. van De Waterbeemd and B. Testa, *Permeability, Absorption, and Bioavailability*, 2009, 3.
291. S. S. Zoghbi, K. B. Anderson, K. J. Jenko, D. A. Luckenbaugh, R. B. Innis and V. W. Pike, *J. Pharm. Sci.*, 2012, **101**, 1028-1039.
292. S. Halbach, *Arch. Toxicol.*, 1990, **64**, 315-319.
293. C. Hansch, A. Leo, D. Hoekman and D. Livingstone, *Exploring QSAR: hydrophobic, electronic, and steric constants*, American Chemical Society Washington, DC, 1995.
294. W. J. Lambert, *J. Chromatogr. A*, 1993, **656**, 469-484.
295. E. Rutkowska, K. Pajak and K. Jóźwiak, *Acta Pol Pharm*, 2013, **70**, 3-18.
296. S. K. Poole and C. F. Poole, *J. Chromatogr. B*, 2003, **797**, 3-19.
297. G. A. Wagnieres, W. M. Star and B. C. Wilson, *Photochem. Photobiol.*, 1998, **68**, 603-632.
298. V. Fernández-Moreira, F. L. Thorp-Greenwood and M. P. Coogan, *ChemComm.*, 2010, **46**, 186-202.
299. T. Wilson, *Academic Press: London, etc*, 1990, **426**, 1-64.
300. W. Denk, J. H. Strickler and W. W. Webb, *Science*, 1990, **248**, 73-76.
301. V. Gautam, J. Drury, J. M. Choy, C. Stricker, H.-A. Bachor and V. R. Daria, *Biomed. Opt. Express*, 2015, **6**, 4027-4036.
302. J. D. Slinker, A. A. Gorodetsky, M. S. Lowry, J. Wang, S. Parker, R. Rohl, S. Bernhard and G. G. Malliaras, *J. Am. Chem. Soc.*, 2004, **126**, 2763-2767.
303. A. P. Krapcho and C. S. Kuell, *Synth. Commun*, 1990, **20**, 2559-2564.
304. A. Q. Siddiqui, L. Merson-Davies and P. M. Cullis, *J. Chem. Soc. Perkin Trans. I*, 1999, 3243-3252.
305. L.-C. Campeau and K. Fagnou, *Chem. Soc. Rev.*, 2007, **36**, 1058-1068.

Chapter 8

8 Appendix

8.1 HPLC

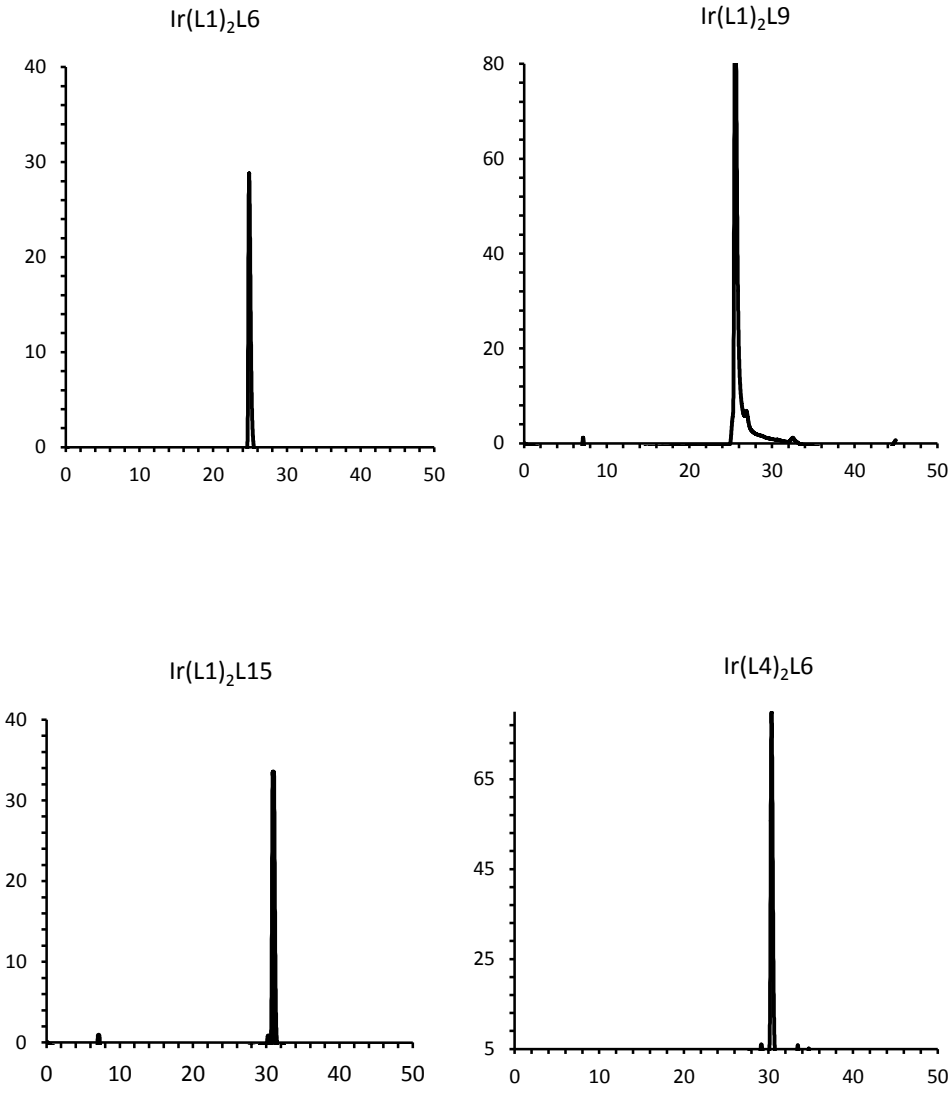

$Ir(L12)_2L9$

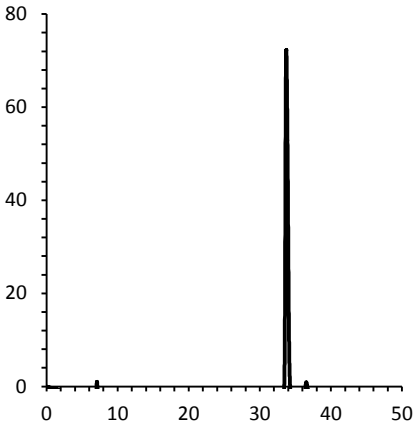

$Ir(L2)_2L8$

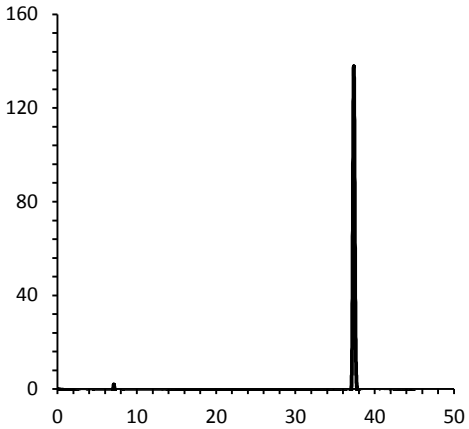

$Ir(L2)_2L9.Boc$

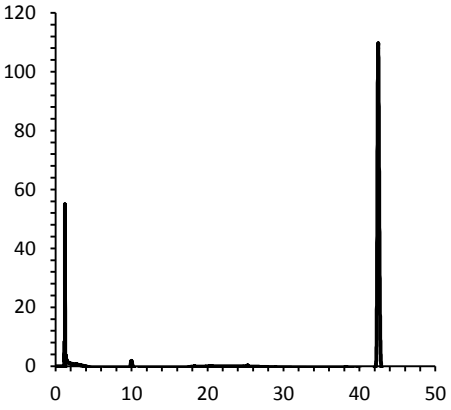

ReL14.L16

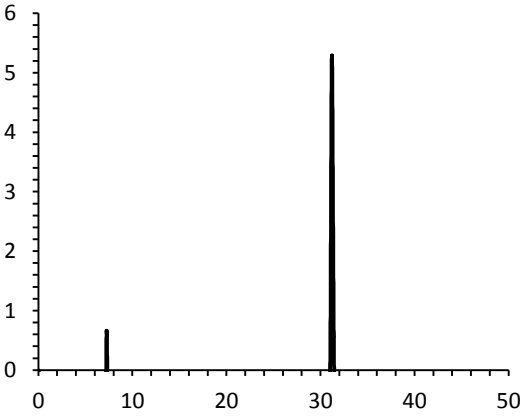

ReL6.Boc.L17

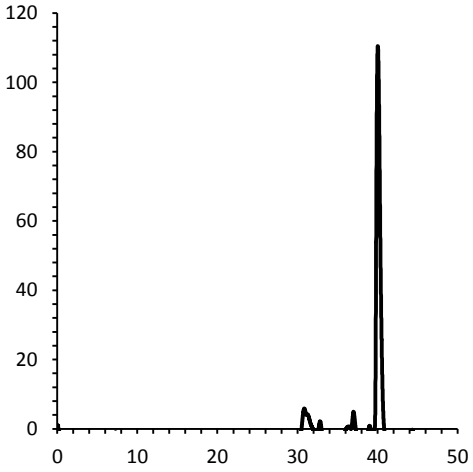

ReL6.L17

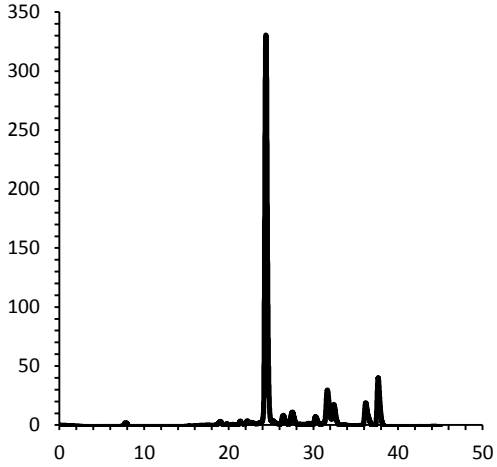

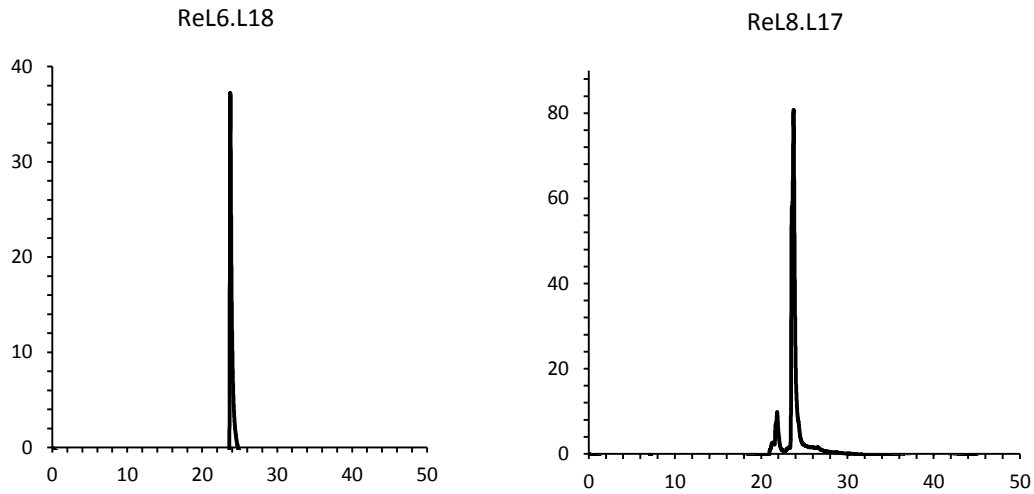

8.2 X-Ray crystallography

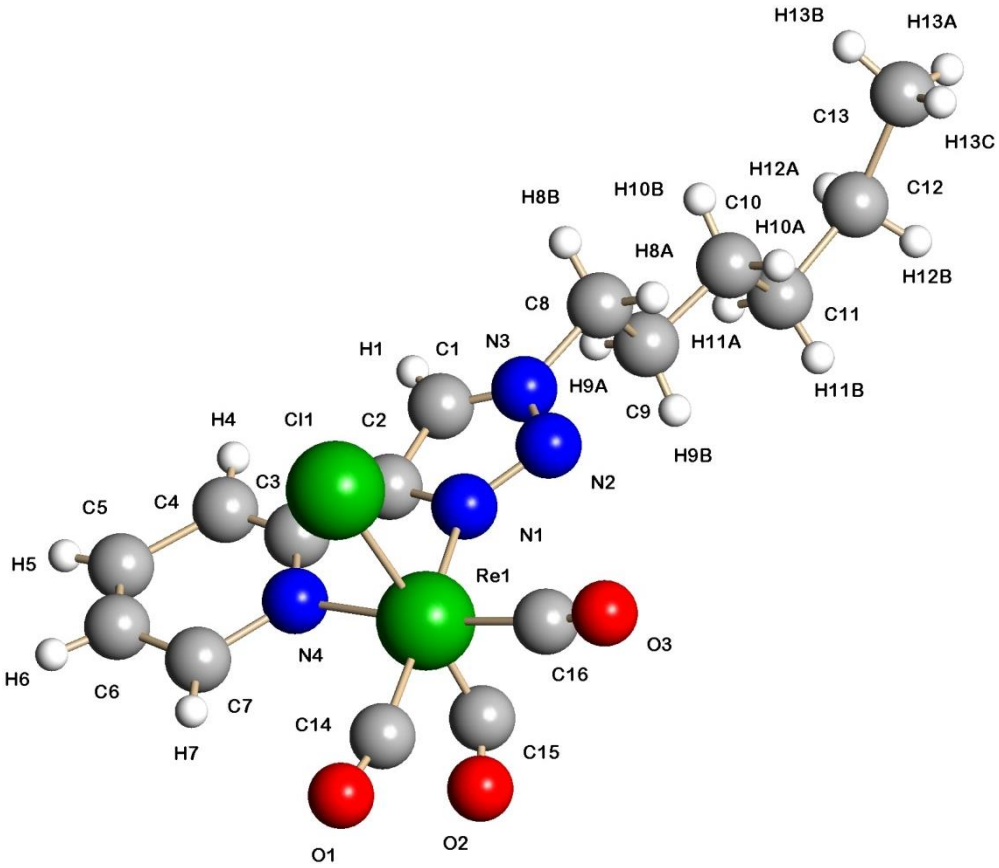

Fig.8.1: X- Ray Crystal structure of **ReL3** show ball and stick diagrams

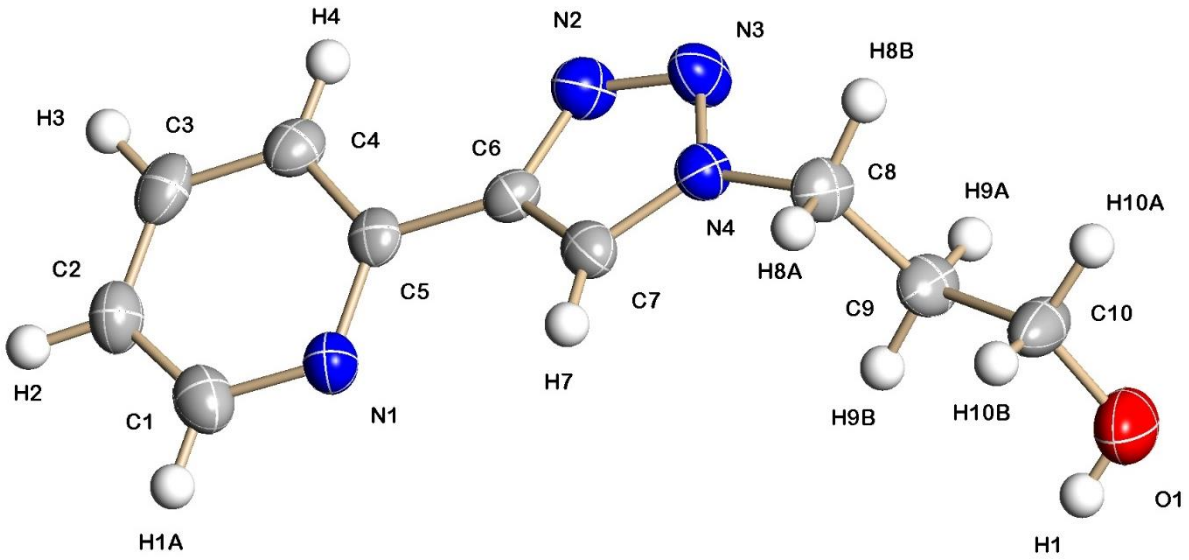

Figure 8.2: X- Ray Crystal structure of **2.8** show 50% displacement ellipsoids, There is intermolecular hydrogen bonding; R1 = 0.0806, wR2 = 0.1874

Table 8.1. Crystal data and structure refinement for 2.8

Identification code	16063	
Empirical formula	C10 H12 N4 O	
Formula weight	204.24	
Temperature	150(2) K	
Wavelength	0.71073 Å	
Crystal system	Monoclinic	
Space group	P2(1)/c	
Unit cell dimensions	a = 5.534(2) Å	α= 90°.
	b = 12.007(5) Å	β= 100.694(14)°.
	c = 15.059(7) Å	γ = 90°.
Volume	983.2(7) $Å^3$	
Z	4	
Density (calculated)	1.380 Mg/m^3	
Absorption coefficient	0.095 mm^{-1}	

F(000)	432
Crystal size	0.44 x 0.13 x 0.11 mm^3
Theta range for data collection	2.18 to 24.99°.
Index ranges	-6<=h<=6, -14<=k<=14, -17<=l<=16
Reflections collected	5037
Independent reflections	1716 [R(int) = 0.1387]
Completeness to theta = 24.99°	99.1 %
Absorption correction	Empirical
Max. and min. transmission	0.969 and 0.457
Refinement method	Full-matrix least-squares on F^2
Data / restraints / parameters	1716 / 0 / 136
Goodness-of-fit on F^2	0.889
Final R indices [I>2sigma(I)]	R1 = 0.0806, wR2 = 0.1874
R indices (all data)	R1 = 0.1447, wR2 = 0.2111
Largest diff. peak and hole	0.746 and -0.322 e.$Å^{-3}$

Table 8. 2. Atomic coordinates (x 10^4) and equivalent isotropic displacement parameters ($Å^2$x 10^3) for **2.8**. U(eq) is defined as one third of the trace of the orthogonalized U^{ij} tensor.

	x	y	z	U(eq)
O(1)	4920(6)	-811(3)	2121(3)	60(1)
N(1)	1502(7)	5666(3)	1801(3)	36(1)
N(2)	-2499(7)	3427(3)	754(3)	40(1)
N(3)	-1815(7)	2437(3)	534(3)	42(1)
N(4)	632(7)	2427(3)	675(2)	32(1)
C(1)	1449(9)	6747(4)	2025(3)	43(1)
C(2)	-557(9)	7430(4)	1800(3)	40(1)
C(3)	-2691(10)	6969(4)	1323(3)	41(1)
C(4)	-2723(8)	5855(4)	1079(3)	37(1)
C(5)	-567(8)	5230(3)	1320(3)	30(1)
C(6)	-456(8)	4058(3)	1042(3)	29(1)
C(7)	1534(8)	3414(3)	999(3)	34(1)
C(8)	1998(8)	1420(4)	538(3)	39(1)
C(9)	2452(9)	699(4)	1386(3)	40(1)
C(10)	4302(9)	-233(4)	1308(3)	48(1)

Table 8.3: Bond lengths [Å] and angles [°] for **2.8**

O(1)-C(10)	1.394(5)
O(1)-H(1)	0.8200
N(1)-C(1)	1.342(5)
N(1)-C(5)	1.342(5)
N(2)-N(3)	1.308(5)
N(2)-C(6)	1.364(5)
N(3)-N(4)	1.331(5)
N(4)-C(7)	1.342(5)
N(4)-C(8)	1.461(5)
C(1)-C(2)	1.371(6)
C(1)-H(1A)	0.9300
C(2)-C(3)	1.379(6)
C(2)-H(2)	0.9300
C(3)-C(4)	1.385(6)
C(3)-H(3)	0.9300
C(4)-C(5)	1.399(6)
C(4)-H(4)	0.9300
C(5)-C(6)	1.472(6)
C(6)-C(7)	1.357(6)
C(7)-H(7)	0.9300
C(8)-C(9)	1.525(6)
C(8)-H(8A)	0.9700
C(8)-H(8B)	0.9700
C(9)-C(10)	1.536(6)
C(9)-H(9A)	0.9700

C(9)-H(9B)	0.9700
C(10)-H(10A)	0.9700
C(10)-H(10B)	0.9700
C(10)-O(1)-H(1)	109.5
C(1)-N(1)-C(5)	117.2(4)
N(3)-N(2)-C(6)	108.9(3)
N(2)-N(3)-N(4)	107.5(3)
N(3)-N(4)-C(7)	110.4(3)
N(3)-N(4)-C(8)	121.5(4)
C(7)-N(4)-C(8)	127.9(4)
N(1)-C(1)-C(2)	124.8(5)
N(1)-C(1)-H(1A)	117.6
C(2)-C(1)-H(1A)	117.6
C(1)-C(2)-C(3)	117.7(4)
C(1)-C(2)-H(2)	121.2
C(3)-C(2)-H(2)	121.2
C(2)-C(3)-C(4)	119.5(5)
C(2)-C(3)-H(3)	120.2
C(4)-C(3)-H(3)	120.2
C(3)-C(4)-C(5)	118.7(5)
C(3)-C(4)-H(4)	120.6
C(5)-C(4)-H(4)	120.6
N(1)-C(5)-C(4)	122.1(4)
N(1)-C(5)-C(6)	116.7(4)
C(4)-C(5)-C(6)	121.2(4)
C(7)-C(6)-N(2)	107.4(4)
C(7)-C(6)-C(5)	129.4(4)

N(2)-C(6)-C(5)	123.1(4)
N(4)-C(7)-C(6)	105.7(4)
N(4)-C(7)-H(7)	127.2
C(6)-C(7)-H(7)	127.2
N(4)-C(8)-C(9)	111.1(4)
N(4)-C(8)-H(8A)	109.4
C(9)-C(8)-H(8A)	109.4
N(4)-C(8)-H(8B)	109.4
C(9)-C(8)-H(8B)	109.4
H(8A)-C(8)-H(8B)	108.0
C(8)-C(9)-C(10)	110.9(4)
C(8)-C(9)-H(9A)	109.4
C(10)-C(9)-H(9A)	109.4
C(8)-C(9)-H(9B)	109.4
C(10)-C(9)-H(9B)	109.4
H(9A)-C(9)-H(9B)	108.0
O(1)-C(10)-C(9)	110.7(4)
O(1)-C(10)-H(10A)	109.5
C(9)-C(10)-H(10A)	109.5
O(1)-C(10)-H(10B)	109.5
C(9)-C(10)-H(10B)	109.5
H(10A)-C(10)-H(10B)	108.1

Symmetry transformations used to generate equivalent atoms:

Table 8.4: Anisotropic displacement parameters ($Å^2 x\ 10^3$) for **2.8**. The anisotropic displacement factor exponent takes the form:

	U^{11}	U^{22}	U^{33}	U^{23}	U^{13}	U^{12}
O(1)	78(3)	42(2)	58(3)	-3(2)	3(2)	9(2)
N(1)	39(2)	30(2)	38(3)	0(2)	8(2)	1(2)
N(2)	37(2)	42(2)	42(3)	-7(2)	7(2)	4(2)
N(3)	38(3)	37(2)	50(3)	-11(2)	6(2)	1(2)
N(4)	34(2)	32(2)	31(2)	-2(2)	7(2)	2(2)
C(1)	54(3)	38(3)	37(3)	-2(2)	13(2)	-5(2)
C(2)	49(3)	30(2)	45(3)	0(2)	16(3)	4(2)
C(3)	54(3)	37(3)	35(3)	11(2)	16(3)	10(2)
C(4)	43(3)	40(3)	27(3)	0(2)	6(2)	7(2)
C(5)	37(3)	30(2)	25(3)	4(2)	12(2)	-1(2)
C(6)	27(2)	34(2)	27(3)	3(2)	6(2)	4(2)
C(7)	39(3)	33(3)	30(3)	1(2)	7(2)	-4(2)
C(8)	39(3)	39(3)	40(3)	-6(2)	10(2)	9(2)
C(9)	48(3)	38(3)	34(3)	-9(2)	7(2)	10(2)
C(10)	68(4)	39(3)	32(3)	-5(2)	-5(3)	17(3)

Table 8.5: Hydrogen coordinates (x 10^4) and isotropic displacement parameters ($Å^2$x 10^3)

for **2.8**.

	x	y	z	U(eq)
H(1)	5545	-380	2521	91
H(1A)	2877	7054	2358	51
H(2)	-481	8178	1963	48
H(3)	-4099	7402	1167	49
H(4)	-4149	5530	761	44
H(7)	3180	3615	1160	40
H(8A)	3562	1626	382	47
H(8B)	1078	997	39	47
H(9A)	910	373	1476	48
H(9B)	3080	1159	1907	48
H(10A)	3593	-745	832	58
H(10B)	5774	86	1148	58

Table 8.6. Torsion angles [°] for **2.8**.

C(6)-N(2)-N(3)-N(4)	-0.2(5)
N(2)-N(3)-N(4)-C(7)	0.7(5)
N(2)-N(3)-N(4)-C(8)	176.9(4)
C(5)-N(1)-C(1)-C(2)	0.1(7)
N(1)-C(1)-C(2)-C(3)	1.3(7)
C(1)-C(2)-C(3)-C(4)	-1.1(7)
C(2)-C(3)-C(4)-C(5)	-0.4(7)
C(1)-N(1)-C(5)-C(4)	-1.7(6)
C(1)-N(1)-C(5)-C(6)	177.3(4)
C(3)-C(4)-C(5)-N(1)	1.9(7)
C(3)-C(4)-C(5)-C(6)	-177.1(4)
N(3)-N(2)-C(6)-C(7)	-0.4(5)
N(3)-N(2)-C(6)-C(5)	178.4(4)
N(1)-C(5)-C(6)-C(7)	-18.1(7)
C(4)-C(5)-C(6)-C(7)	161.0(5)
N(1)-C(5)-C(6)-N(2)	163.4(4)
C(4)-C(5)-C(6)-N(2)	-17.5(6)
N(3)-N(4)-C(7)-C(6)	-1.0(5)
C(8)-N(4)-C(7)-C(6)	-176.9(4)
N(2)-C(6)-C(7)-N(4)	0.9(5)
C(5)-C(6)-C(7)-N(4)	-177.8(4)
N(3)-N(4)-C(8)-C(9)	-86.8(5)
C(7)-N(4)-C(8)-C(9)	88.7(5)
N(4)-C(8)-C(9)-C(10)	-168.9(4)
C(8)-C(9)-C(10)-O(1)	173.3(4)

Table 8.7: Hydrogen bonds for 2.8 [Å and °].

D-H...A	d(D-H)	d(H...A)	d(D...A)	<(DHA)
O(1)-H(1)...N(1)#1	0.82	2.16	2.917(5)	153.2

Symmetry transformations used to generate equivalent atoms:

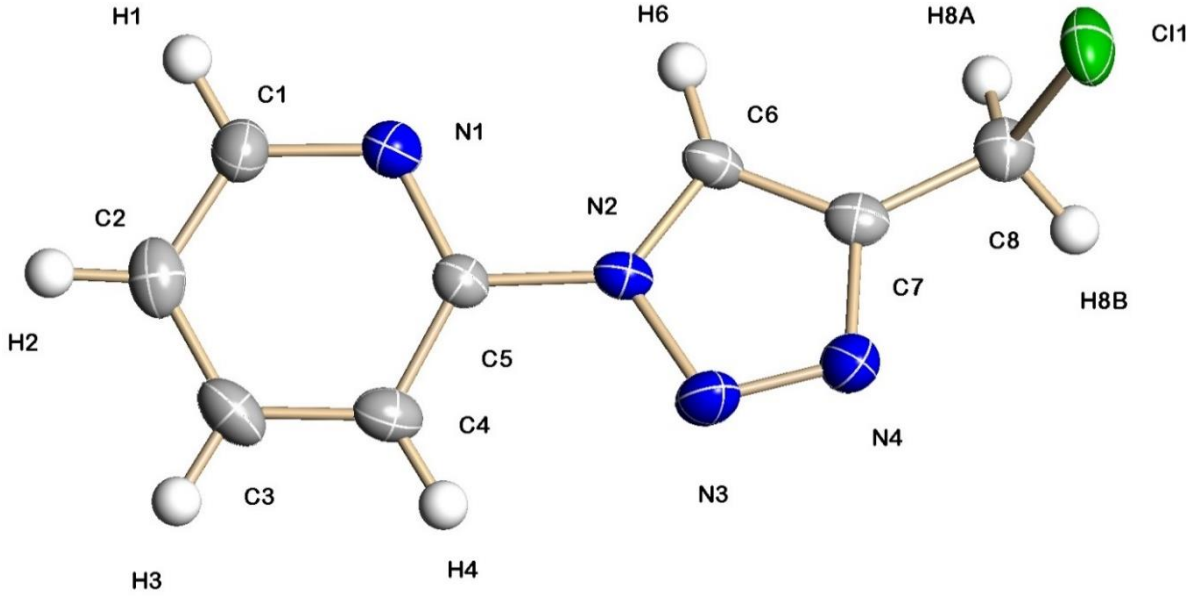

Figure 8.2: X- Ray Crystal structure of inverse pyridyl triazole **2.13.** Figure show 50% displacement ellipsoids. R1 = 0.0565, wR2 = 0.1196

Table 8.8: Crystal data and structure refinement for 2.13.

Identification code	**17099**
Empirical formula	**C8 H7 Cl N4**
Formula weight	**194.63**
Temperature	**150(2) K**
Wavelength	**0.71073 Å**
Crystal system	**Triclinic**

Space group	**P-1**	
Unit cell dimensions	**a = 5.5909(14) Å**	**□= 84.826(5)°.**
	b = 7.4813(19) Å	**□= 87.806(4)°.**
	c = 10.772(3) Å	**□ = 72.268(5)°.**
Volume	**427.39(19) Å^3**	
Z	**2**	
Density (calculated)	**1.512 Mg/m^3**	
Absorption coefficient	**0.399 mm^{-1}**	
F(000)	**200**	
Crystal size	**0.34 x 0.25 x 0.02 mm^3**	
Theta range for data collection	**1.90 to 25.99°.**	
Index ranges	**-6<=h<=6, -9<=k<=9, -13<=l<=13**	
Reflections collected	**3330**	
Independent reflections	**1656 [R(int) = 0.0506]**	
Completeness to theta = 25.99°	**98.7 %**	
Absorption correction	**Empirical**	
Max. and min. transmission	**0.894 and 0.409**	
Refinement method	**Full-matrix least-squares on F^2**	
Data / restraints / parameters	**1656 / 0 / 118**	
Goodness-of-fit on F^2	**0.935**	
Final R indices [I>2sigma(I)]	**R1 = 0.0565, wR2 = 0.1196**	
R indices (all data)	**R1 = 0.0821, wR2 = 0.1294**	
Largest diff. peak and hole	**0.348 and -0.283 e.Å^{-3}**	

Table 8.9: Atomic coordinates (x 10^4) and equivalent isotropic displacement parameters ($Å^2$x 10^3) for **2.13**. U(eq) is defined as one third of the trace of the orthogonalized U^{ij} tensor.

	x	y	z	U(eq)
Cl(1)	3668(2)	2271(1)	296(1)	40(1)
N(1)	1894(5)	1207(4)	6039(2)	32(1)
N(2)	42(4)	2880(3)	4214(2)	24(1)
N(3)	-2015(5)	3757(4)	3508(2)	35(1)
N(4)	-1187(5)	4271(4)	2417(2)	35(1)
C(1)	1688(6)	575(5)	7235(3)	33(1)
C(2)	-563(7)	903(5)	7876(3)	36(1)
C(3)	-2740(6)	1947(5)	7276(3)	36(1)
C(4)	-2604(6)	2615(4)	6044(3)	31(1)
C(5)	-252(6)	2207(4)	5486(3)	24(1)
C(6)	2154(6)	2845(4)	3561(3)	26(1)
C(7)	1378(6)	3734(4)	2419(3)	26(1)
C(8)	2851(6)	4168(4)	1312(3)	31(1)

Table 8.10: Bond lengths [Å] and angles [°] for **2.13**.

Cl(1)-C(8)	1.807(3)
N(1)-C(5)	1.335(4)
N(1)-C(1)	1.346(4)
N(2)-C(6)	1.345(4)
N(2)-N(3)	1.360(3)

N(2)-C(5)	1.438(4)
N(3)-N(4)	1.315(3)
N(4)-C(7)	1.367(4)
C(1)-C(2)	1.377(4)
C(1)-H(1)	0.9500
C(2)-C(3)	1.379(5)
C(2)-H(2)	0.9500
C(3)-C(4)	1.382(4)
C(3)-H(3)	0.9500
C(4)-C(5)	1.383(4)
C(4)-H(4)	0.9500
C(6)-C(7)	1.364(4)
C(6)-H(6)	0.9500
C(7)-C(8)	1.492(4)
C(8)-H(8A)	0.9900
C(8)-H(8B)	0.9900
C(5)-N(1)-C(1)	115.8(3)
C(6)-N(2)-N(3)	110.4(2)
C(6)-N(2)-C(5)	129.4(2)
N(3)-N(2)-C(5)	120.1(2)
N(4)-N(3)-N(2)	106.7(2)
N(3)-N(4)-C(7)	109.3(2)
N(1)-C(1)-C(2)	123.6(3)
N(1)-C(1)-H(1)	118.2
C(2)-C(1)-H(1)	118.2
C(1)-C(2)-C(3)	119.0(3)
C(1)-C(2)-H(2)	120.5

C(3)-C(2)-H(2)	120.5
C(2)-C(3)-C(4)	119.0(3)
C(2)-C(3)-H(3)	120.5
C(4)-C(3)-H(3)	120.5
C(3)-C(4)-C(5)	117.4(3)
C(3)-C(4)-H(4)	121.3
C(5)-C(4)-H(4)	121.3
N(1)-C(5)-C(4)	125.2(3)
N(1)-C(5)-N(2)	114.3(3)
C(4)-C(5)-N(2)	120.6(3)
N(2)-C(6)-C(7)	105.6(3)
N(2)-C(6)-H(6)	127.2
C(7)-C(6)-H(6)	127.2
C(6)-C(7)-N(4)	107.9(3)
C(6)-C(7)-C(8)	130.6(3)
N(4)-C(7)-C(8)	121.5(3)
C(7)-C(8)-Cl(1)	111.2(2)
C(7)-C(8)-H(8A)	109.4
Cl(1)-C(8)-H(8A)	109.4
C(7)-C(8)-H(8B)	109.4
Cl(1)-C(8)-H(8B)	109.4
H(8A)-C(8)-H(8B)	108.0

Symmetry transformations used to generate equivalent atoms:

Table 8.11: Anisotropic displacement parameters ($Å^2 x\ 10^3$) for **2.13**. The anisotropic displacement factor exponent takes the form:

	U^{11}	U^{22}	U^{33}	U^{23}	U^{13}	U^{12}
Cl(1)	60(1)	35(1)	24(1)	-4(1)	7(1)	-11(1)
N(1)	28(2)	35(2)	30(2)	-3(1)	2(1)	-7(1)
N(2)	19(1)	25(1)	29(1)	-5(1)	1(1)	-6(1)
N(3)	23(2)	39(2)	38(2)	5(1)	-2(1)	-6(1)
N(4)	31(2)	35(2)	34(2)	5(1)	1(1)	-5(1)
C(1)	36(2)	32(2)	28(2)	0(1)	0(2)	-7(2)
C(2)	52(2)	34(2)	28(2)	-4(2)	2(2)	-23(2)
C(3)	35(2)	41(2)	37(2)	-12(2)	13(2)	-18(2)
C(4)	25(2)	32(2)	37(2)	-12(2)	1(2)	-8(1)
C(5)	24(2)	23(2)	25(2)	-6(1)	2(1)	-9(1)
C(6)	18(2)	35(2)	28(2)	-11(1)	2(1)	-7(1)
C(7)	25(2)	21(2)	34(2)	-7(1)	1(1)	-7(1)
C(8)	36(2)	28(2)	30(2)	-4(1)	0(2)	-10(2)

Table 8.12. Hydrogen coordinates (x 10^4) and isotropic displacement parameters ($Å^2$x 10^3) for **2.13**.

	x	y	z	U(eq)
H(1)	3177	-137	7662	40
H(2)	-614	418	8719	43
H(3)	-4313	2203	7702	43
H(4)	-4068	3327	5599	37
H(6)	3835	2312	3838	32
H(8A)	4404	4375	1593	37
H(8B)	1850	5342	844	37